Green Energy and Technology

Luc Avérous
Eric Pollet *Editors*

Environmental Silicate Nano-Biocomposites

Springer

Green Energy and Technology

For further volumes:
http://www.springer.com/series/8059

Luc Avérous · Eric Pollet
Editors

Environmental Silicate Nano-Biocomposites

Springer

Editors
Luc Avérous
LIPHT-ECPM
University of Strasbourg
67087 Strasbourg
France

Eric Pollet
LIPHT-ECPM
University of Strasbourg
67087 Strasbourg
France

ISSN 1865-3529 ISSN 1865-3537 (electronic)
ISBN 978-1-4471-4101-3 ISBN 978-1-4471-4108-2 (eBook)
DOI 10.1007/978-1-4471-4108-2
Springer London Heidelberg New York Dordrecht

Library of Congress Control Number: 2012938634

Printed on acid-free paper

Springer is part of Springer Science+Business Media (www.springer.com)

Contents

Chapter 1
Green Nano-Biocomposites

Luc Avérous and Eric Pollet

Abstract The last two decades have seen the development of an alternative chemistry, a green chemistry, which intends to reduce the human impact on the environment. The polymers are obviously involved into this tendency and numerous biodegradable plastics are now processed for a wide range of applications such as packaging, leisure, agriculture, and biomedical. Some of these polymers combine renewability and biodegradability, such as polylactide, polyhydroxyalkanoate, and the polysaccharides. However, even if a lot of commercial products are now available, their properties (mechanical properties, moisture sensitivity …) have to be enhanced to be really competitive with the conventional petroleum-based plastics. One of the most promising answers to overcome these weaknesses is the elaboration of nano-biocomposites, namely the dispersion of nano-sized filler into a biodegradable matrix. This introductory chapter intends to briefly highlight some recent studies and developments on nano-biocomposites systems mainly based on nanoclay.

1.1 Introduction

Biodegradable materials have raised great interest since sustainable development policies tend to expand with the growing concern for the environment. These green materials bring a significant contribution to the sustainable development in view of the wider range of disposal options at low environmental impact.

L. Avérous (✉) · E. Pollet
LIPHT-ECPM, EAc(CNRS) 4379, Université de Strasbourg,
25 rue Becquerel, 67087 Strasbourg Cedex 2, France
e-mail: luc.averous@unistra.fr

L. Avérous and E. Pollet (eds.), *Environmental Silicate Nano-Biocomposites*,
Green Energy and Technology, DOI: 10.1007/978-1-4471-4108-2_1,

For instance, biodegradable polymers have been the topic of many researches. They can be mainly classified as agro-polymers (polysaccharides, proteins…) and biodegradable polyesters [polyhydroxyalkanoates, poly(lactic acid)…]. Unfortunately, for certain applications, these polymers cannot be fully competitive with conventional thermoplastics since some of their properties are too weak. Therefore, to extend their applications, they have been formulated and associated with nano-sized fillers which could bring a wide range of improved properties (stiffness, permeability, crystallinity, thermal stability…).

The resulting "nano-biocomposites" open a new materials topic and have been the subject of many recent publications. This chapter is dedicated to this novel class of materials.

1.2 Main Advantages of Nano-Biocomposites

The biodegradable polymers are an elegant and innovating answer to replace conventional and durable petroleum-based products. They fit with a real sustainable development approach in connection with some of the main principles of the green chemistry.

However, to obtain suitable and competitive materials, some of their properties (mechanical resistance, water sensitivity…) have to be enhanced. Consequently, even if the potentials of these materials have been pointed out, until now, they are not widely used to replace non-degradable plastics. The common approach to tune their behaviors consists of the elaboration of multiphase materials e.g., blends [1–3] or composites [4–8].

A new class of composite materials based on the incorporation of nanosized fillers (nanofillers) has been investigated [9–16]. Depending on the nanofiller, nanocomposites could exhibit drastic modifications in their properties, as improved mechanical and barrier properties, and higher transparency [10, 17–22]. Such properties enhancements rely both on the nanofiller geometry and on surface (interface) area. The corresponding specific surface area may attain 600–800 m^2/g when the filler is homogeneously dispersed and exfoliated (in the case of the montmorillonite nanoclay).

The nanofillers can be classified depending on their aspect ratio and geometry, such as

(i) layered (e.g., montmorillonite),
(ii) spherical (e.g., silica),
(iii) acicular (e.g., whiskers, sepiolite, and carbon nanotubes).

At present, the most intensive studies are focused on layered silicates, such as montmorillonite (MMT), due to their availability, versatility, and respectability towards the environment and health.

A wide range of nano-biocomposites (nanocomposites based on biodegradable matrix) [23] have been elaborated with different biodegradable matrices such as

PCL [18, 24–28], PLA [29–34], PHA [35, 36], or with agro-polymers [37–40] such as starch or chitosan, and have demonstrated that nano-biocomposites elaboration could be a powerful strategy to overcome the conventional drawbacks of biodegradable polymers.

1.3 Elaboration Protocol of Nano-Biocomposites

Depending on the processing conditions and on the polymer/nanofiller affinity, different morphologies can be obtained. These morphologies can be divided in three distinct main categories, (i) microcomposites, (ii) intercalated nanocomposites, and (iii) exfoliated nanocomposites [9–11].

- For microcomposites, the polymer chains have not penetrated into the interlayer spacing and the clay particles are aggregated. In this case, the designation as nanocomposite is abusive.
- In the intercalated structures, the polymer chains have diffused between the platelets leading to a d_{001} (interspacing) increase.
- In the exfoliated state, the clay layers are individually delaminated and homogeneously dispersed into the polymer matrix.

Intermediate dispersion states are often observed i.e., intercalated-exfoliated structures.

This classification does not take into account the dispersion multi-scale structures, such as percolation phenomenon, preferential orientation of the clay layers… [10].

The nanofiller incorporation into the polymer matrix can be carried out with three main techniques [9], (i) the in situ polymerization, (ii) the solvent intercalation, or (iii) the melt intercalation process.

1.3.1 In-situ Polymerization Process

In this method, layered silicates are swollen into a monomer solution. Then, the monomer polymerization is initiated and propagated. The molecular weight increases, leading to a d_{001} increase and sometimes to an almost fully exfoliated morphology for some studied systems [10]. However, for some agro-polymers, since the chains are synthesized during the plant growth and are then extracted from the plants, this technique cannot be used to prepare these nano-biocomposites.

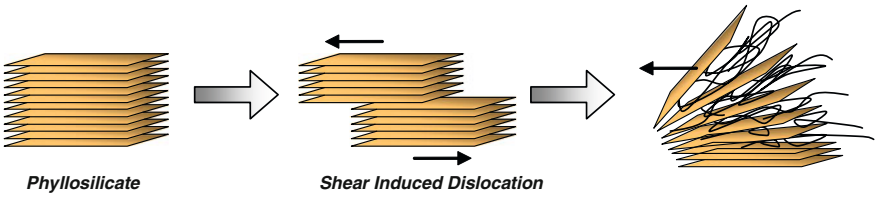

Fig. 1.1 Mechanism leading to clay exfoliation under shearing. (Adapted from Dennis et al., reproduced with kind permission from ©Elsevier [42])

1.3.2 Solvent Intercalation Process

This elaboration process is based on a solvent system in which the polymer is soluble and the silicate layers are swellable. The polymer is first dissolved in an appropriate solvent. In parallel, the clay (organo-modified or not) is swollen and dispersed into the same solvent or another one to obtain a miscible solution. Both systems are pooled together leading to a polymer chains intercalation. Then, the solvent is evaporated to obtain nanocomposite materials. Nevertheless, for non-water-soluble polymers, this process involves the use of large amount of organic solvents, which is environmentally unfriendly and cost prohibitive. Moreover, a small amount of solvent may remain in the final product at the polymer/clay interface creating lower interfacial interaction between the polymer and the clay surfaces [41]. Thus, this technique is mainly used in academic studies. Since some polysaccharides such as chitosan, pectin and some proteins present high thermal or thermo-mechanical degradations, the solvent process has been extensively used to produce polysaccharide/clay and protein/clay hybrid materials.

1.3.3 Melt Intercalation Process

Both the polymer and the clay are introduced simultaneously into a melt mixing device (extruder, internal mixer…). According to Dennis et al. [42], in addition to the polymer/nanofiller affinity, two main processing parameters favor the nano-dispersion of the nanoclay. These parameters, which are the driving force of the intercalation-exfoliation of the nanofiller by the matrix, are (i) the residence time and (ii) the shearing.

For MMT, the shearing is necessary to induce the platelets delamination from the clay tactoids (Fig. 1.1). The extended residence time is needed to allow the diffusion of polymer chains into the interlayer gallery and then to obtain an exfoliated morphology.

This simple process has extensively been used to prepare nano-biocomposite materials. Nevertheless, the thermal or thermo-mechanical inputs can lead to partial degradation of molecular chains. Moreover, the high residence time needed

to enhance the nanofiller dispersion favors the matrix degradation. Therefore, it is necessary to balance the process parameters to minimize the molecular chain degradation and to obtain a well exfoliated or/and dispersed morphology.

1.4 Nano-Biocomposites Based on Agro-Polymers

Most of the studies on nano-biocomposites based on agro-polymers have been developed with polysaccharide matrices.

1.4.1 Nano-Biocomposites Based on Polysaccharides

A recent review [43] presents the state of the art of nano-biocomposites based on the polysaccharides/nanoclay system. These nano-hybrid materials mainly differ from conventional nanocomposites due to their high hydrophilic character. Consequently, mainly microcomposite morphologies are reached with the dispersion of the common commercially available hydrophobic organo-modified nanoclays, such as Cloisite®-based MMT. On the opposite, exfoliated structures are sometimes obtained with highly hydrophilic nanofillers, such as "natural" sodium MMT.

Because of the high thermal sensitivity of the carbohydrate chains, solvent intercalation process is often required or used for the nano-biocomposites elaboration. This strategy allows an efficient nanoclay exfoliation in various matrices, e.g. starch and chitosan. Nevertheless, since this process is cost and time prohibitive, it may be not adapted for an industrial scale-up. Instead, the melt blending elaboration process appears as a better option to produce polysaccharide-based nano-biocomposites. However, plasticizer incorporation is often needed to melt the carbohydrate-based matrix and to limit its thermal degradation. According to the reported studies, these plasticizers greatly affect the nano-hybrid morphology with the establishment of strong hydrogen interactions with the nanofillers, which perturb the clay platelets intercalation/exfoliation process. Consequently, these nano-hybrids display mainly intercalated structures at high plasticizer content. To overcome this limitation and reach exfoliation, an organo-modification of the clay surface with hydrophilic surfactants, such as carbohydrate surfactants, has been proposed and tested to modify the nanofiller polarity and thus the clay/matrix affinity [44]. Such nano-hybrid materials display improved mechanical reinforcement, higher thermal stability and barrier properties, and lower moisture sensitivity.

However, although a significant amount of studies has already been performed on various aspects of polysaccharide nano-biocomposites, more research still remains to understand the complex plasticizer/matrix/nanofiller interactions and their influence on the resulting morphology and materials properties. Indeed, it is known that high plasticizer content leads to inhomogeneous materials (e.g. plasticized starch with high glycerol content). Until now, no attention has been paid to

the nanofiller influence on such phase separation and on the resulting nano-structuration. Thus, future investigations will have to include advanced characterization techniques to fully understand the complex interfacial behavior between the components of such multiphasic systems [43].

New nanocomposites have been recently elaborated from needle-shaped nanofillers (e.g., sepiolite, palygorskite…) [45–48]. Compared to more conventional layered silicates, they present substantial differences, namely their aspect ratio and their surface properties (silanol groups located at the nanofiller surface) and thus could permit the elaboration of innovative polysaccharide-based nano-hybrid materials with extended properties.

These polysaccharides/nanoclays materials seem to be a valid answer to produce low-cost, highly competitive, and pioneering environmentally friendly materials. Moreover, since people are more and more concerned about sustainable development as the global needs and the prices of the fossil resources increase, such agro-based materials now represent an interesting option to replace conventional fossil resource-based plastics. Thanks to the agro-polymers intrinsic characteristics and improved properties brought by the nanofillers, these materials could present a wide range of applications, such as packaging, agriculture devices, or even for biomedical applications with some developments based on the biocompatibility of these materials.

1.4.2 Nano-Biocomposites Based on Proteins

Although less studied than polysaccharides, proteins (soybean proteins, gluten, zein, casein, gelatin…) have long and traditionally been used as raw materials. Proteins are renewable and fully biodegradable polymers without toxic release. However, serious concerns remain regarding their high water sensitivity and their low mechanical properties. To overcome these strong issues, the development of nano-biocomposites has started since the last decade. Nano-biocomposites based on protein/nanoclay systems are for instance developed for the controlled release of active agents, e.g., as antimicrobial. A series of plant protein-based clay nano-biocomposites have been studied and have shown many aspects of enhancement of material performance [49–54]. Various advanced material characterization technologies have been applied not only to examine the property improvement, but also to explore the interactions between protein matrix and nanoparticles, the dispersion status of nanoparticles, the macromolecular motions of matrix, the nanoclay effect to each component of protein system, and the phase structures of the whole protein matrices [55, 56].

However, the great majority of the studies are devoted to the influence of filler content on mechanical properties, with only few articles concerning other properties such as barrier properties.

Unmodified clays which are naturally hydrophilic and thus compatible with proteins seem to be fully appropriate for the preparation of protein-based nano-biocomposites displaying both a good level of clay dispersion and a low

environmental impact. The rather good dispersion/exfoliation of layered silicates should lead to the formation of a nano-structure limiting the diffusion of small gas molecules, and thus to a significant decrease of permeability towards gases (oxygen, water vapor) and aroma compounds. Although nanoclays are well dispersed, the resulting improvement of barrier properties is quite moderate and does not exceed a two-fold reduction in case of water vapor, and the same effect or even no effect in case of O_2 and CO_2. The addition of nanoclays also leads to a significant improvement of material performance in terms of mechanical properties under uniaxial tensile or dynamic tests [51–54].

These nano-hybrids materials could also provide new additional functionalities such as UV protection or controlled delivery of active agents. Finally, these nano-biocomposites should find a wide range of fields for packaging, agriculture and biomedical applications.

1.5 Nano-Biocomposites Based on Biodegradable Polyesters

A recent review [57] presents the state of the art of biopolyester/clay nano-biocomposites. This review has clearly demonstrated that different parameters such as elaboration route, polymer/clay affinity and clay content can affect the structure and the nano-biocomposites properties. These latter can consequently be tuned as desired by controlling the parameters previously mentioned. It has to be noted that the high reinforcing effect is generally limited to small clay amounts (<6 wt%) and is reached for exfoliated state, which is not so trivial to obtain. Indeed, although the more convenient clays to obtain delaminated platelets into biopolyesters appear to be those matching the matrix polarity, i.e. clay with organo-modifier bearing at least one hydroxyl group, structure also depends on the elaboration process. Considering PLA and PCL matrices, nano-biocomposites with highly exfoliated clays can be obtained thanks to a well-controlled in situ polymerization process whereas the melt and/or solvent intercalation methods lead to more aggregated structures. Thus, for some biopolyester matrices like PHA [58], aliphatic or aromatic polyesters, exfoliated state was not reported or clearly demonstrated. Eventually, temperature sensitivity of some biopolyesters can also prevent good clay delamination and properties enhancement [57].

In the case of good delamination and dispersion of clays, the mechanical properties, thermal stability, biodegradability and barrier properties were generally improved [57].

Finally, these nano-biocomposites present concurrent improvement in various material properties at very low filler content with no more inconvenience in the elaboration since conventional processing techniques can be used.

Nano-biocomposites usefulness is no longer in question and more and more reports are focused on applicative aspects in the environment, packaging, agriculture devices, biomedical fields, etc. Moreover, since industrials were concerned about sustainable developments, production cost of biodegradable polymers goes on

decreasing which will allow strong developments of multiphase materials, such as the nano-biocomposites. Therefore, these materials will be technically and financially competitive towards synthetic polymer-based nanocomposites. Then, this new class of material opens a new dimension for plastic industry.

Future research should address some actual issues such as the difficulty to exfoliate the clay with some biopolyester matrixes (e.g., PHA). Further works should furnish valuable insight into new methods of nano-biocomposites design to establish new approaches to tailor novel nano-architectures.

1.6 Conclusion

The properties of the biodegradable polymers (mechanical properties, moisture sensitivity, permeability…) have to be enhanced to be really competitive with the conventional plastics (PE, PP, PS, PVC…). One of the most promising answers to overcome these weaknesses is the elaboration of nano-biocomposites, namely the dispersion of nano-sized filler into a biodegradable matrix.

Several advanced material characterization technologies have been applied not only to examine the property improvement, but also to explore the interactions between the biodegradable matrix and the nanoparticles, dispersion status of nanoparticles, molecular motions, and phase structures of the whole biomatrices.

Finally, the nano-biocomposites present concurrent improvement in various material properties at very low filler content with no more inconvenient in the elaboration since conventional plastic processing can be used. Nano-biocomposites usefulness is no longer in question and more and more reports are focused on applicative aspects in the environment, packaging, leisure, agriculture devices, biomedical fields….

References

1. Averous L, Fringant C (2001) Association between plasticized starch and polyesters: processing and performances of injected biodegradable systems. Polym Eng Sci 41(5):727–734
2. Averous L, Moro L, Dole P, Fringant C (2000) Properties of thermoplastic blends: starch-polycaprolactone. Polymer 41(11):4157–4167
3. Buchanan CM, Gedon SC, White AW, Wood MD (1992) Cellulose acetate butyrate and poly(hydroxybutyrate-co-valerate) copolymer blends. Macromolecules 25(26):7373–7381
4. Curvelo AAS, De Carvalho AJF, Agnelli JAM (2001) Thermoplastic starch-cellulosic fibers composites: preliminary results. Carbohydr Polym 45(2):183–188
5. Mohanty AK, Misra M, Drzal LT (2002) Sustainable bio-composites from renewable resources: opportunities and challenges in the green materials world. J Polym Environ 10(1–2):19–26
6. Wollerdorfer M, Bader H (1998) Influence of natural fibres on the mechanical properties of biodegradable polymers. Ind Crop Prod 8(2):105–112
7. Averous L, Boquillon N (2004) Biocomposites based on plasticized starch: thermal and mechanical behaviours. Carbohydr Polym 56(2):111–122

8. Averous L, Halley PJ (2009) Biocomposites based on plasticized starch. Biofuels Bioproducts Biorefining-Biofpr 3(3):329–343
9. Alexandre M, Dubois P (2000) Polymer-layered silicate nanocomposites: preparation, properties and uses of a new class of materials. Mater Sci Eng R-Rep 28(1):1–63
10. Sinha Ray S, Okamoto M (2003) Polymer/layered silicate nanocomposites: a review from preparation to processing. Prog Polym Sci 28(11):1539–1641
11. Vaia RA, Giannelis EP (1997) Polymer melt intercalation in organically-modified layered silicates: model predictions and experiment. Macromolecules 30(25):8000–8009
12. Cho JW, Paul DR (2001) Nylon 6 nanocomposites by melt compounding. Polymer 42(3):1083–1094
13. Giannelis EP (1996) Polymer layered silicate nanocomposites. Adv Mater 8(1):29–35
14. Krishnamoorti R, Vaia RA, Giannelis EP (1996) Structure and dynamics of polymer-layered silicate nanocomposites. Chem Mater 8(8):1728–1734
15. Lebaron PC, Wang Z, Pinnavaia TJ (1999) Polymer-layered silicate nanocomposites: an overview. Appl Clay Sci 15(1–2):11–29
16. Thostenson ET, Ren Z, Chou TW (2001) Advances in the science and technology of carbon nanotubes and their composites: a review. Compos Sci Technol 61(13):1899–1912
17. Gain O, Espuche E, Pollet E, Alexandre M, Dubois P (2005) Gas barrier properties of poly(ε-caprolactone)/clay nanocomposites: influence of the morphology and polymer/clay interactions. J Polym Sci Pt B-Polym Phys 43(2):205–214
18. Gorrasi G, Tortora M, Vittoria V, Pollet E, Alexandre M, Dubois P (2004) Physical properties of poly(ε-caprolactone) layered silicate nanocomposites prepared by controlled grafting polymerization. J Polym Sci Pt B-Polym Phys 42(8):1466–1475
19. Chivrac F, Pollet E, Averous L (2007) Nonisothermal crystallization behavior of poly(butylene adipate-co-terephthalate)/clay nano-biocomposites. J Polym Sci Pt B-Polym Phys 45(13):1503–1510
20. Picard E, Gerard JF, Espuche E (2008) Water transport properties of polyamide 6 based nanocomposites prepared by melt blending: on the importance of the clay dispersion state on the water transport properties at high water activity. J Membr Sci 313(1–2):284–295
21. Picard E, Vermogen A, Gerard JF, Espuche E (2007) Barrier properties of nylon 6-montmorillonite nanocomposite membranes prepared by melt blending: Influence of the clay content and dispersion state. Consequences on modelling. J Membr Sci 292(1–2):133–144
22. Peprnicek T, Kalendova A, Pavlova E, Simonik J, Duchet J, Gerard JF (2006) Poly(vinyl chloride)-paste/clay nanocomposites: Investigation of thermal and morphological characteristics. Polym Degrad Stabil 91(12):3322–3329
23. Chivrac F, Kadlecova Z, Pollet E, Averous L (2006) Aromatic copolyester-based nano-biocomposites: Elaboration, structural characterization and properties. J Polym Environ 14(4):393–401
24. Messersmith PB, Giannelis EP (1993) Polymer-layered silicate nanocomposites: In situ intercalative polymerization of ε-Caprolactone in layered silicates. Chem Mat 5(8):1064–1066
25. Lepoittevin B, Pantoustier N, Devalckenaere M, Alexandre M, Kubies D, Calberg C, Jerome R, Dubois P (2002) Poly(e-caprolactone)/clay nanocomposites by in situ intercalative polymerization catalyzed by dibutyltin dimethoxide. Macromolecules 35(22):8385–8390
26. Jimenez G, Ogata N, Kawai H, Ogihara T (1997) Structure and thermal/mechanical properties of poly(ε-caprolactone)-clay blend. J Appl Polym Sci 64:2211–2220
27. Lepoittevin B, Devalckenaere M, Pantoustier N, Alexandre M, Kubies D, Calberg C, Jerome R, Dubois P (2002) Poly (ε-caprolactone)/clay nanocomposites prepared by melt intercalation: mechanical, thermal and rheological properties. Polymer 43(14):4017–4023
28. Lepoittevin B, Pantoustier N, Devalckenaere M, Alexandre M, Calberg C, Jerome R, Henrist C, Rulmont A, Dubois P (2003) Polymer/layered silicate nanocomposites by combined intercalative polymerization and melt intercalation: a masterbatch process. Polymer 44(7):2033–2040

29. Paul MA, Alexandre M, Degee P, Calberg C, Jerome R, Dubois P (2003) Exfoliated polylactide/clay nanocomposites by in situ coordination-insertion polymerization. Macromol Rapid Commun 24(9):561–566
30. Paul MA, Delcourt C, Alexandre M, Degee P, Monteverde F, Rulmont A, Dubois P (2005) (Plasticized) polylactide/(organo-)clay nanocomposites by in situ intercalative polymerization. Macromol Chem Phys 206(4):484–498
31. Ogata N, Jimenez G, Kawai H, Ogihara T (1997) Structure and thermal/mechanical properties of poly(L-lactide)-clay blend. J Polym Sci Pt B-Polym Phys 35:389–396
32. Paul MA, Alexandre M, Degee P, Henrist C, Rulmont A, Dubois P (2002) New nanocomposite materials based on plasticized poly(L-lactide) and organo-modified montmorillonites: thermal and morphological study. Polymer 44(2):443–450
33. Pluta M, Galeski A, Alexandre M, Paul MA, Dubois P (2002) Polylactide/montmorillonite nanocomposites and microcomposites prepared by melt blending: structure and some physical properties. J Appl Polym Sci 86(6):1497–1506
34. Sinha Ray S, Maiti P, Okamoto M, Yamada K, Ueda K (2002) New polylactide/layered silicate nanocomposites. 1. Preparation, characterization, and properties. Macromolecules 35(8):3104–3110
35. Maiti P, Batt CA, Giannelis EP (2007) New biodegradable polyhydroxybutyrate/layered silicate nanocomposites. Biomacromolecules 8:3393–3400
36. Sanchez-Garcia MD, Gimenez E, Lagaron JM (2008) Morphology and barrier properties of nanobiocomposites of poly(3-hydroxybutyrate) and layered silicates. J Appl Polym Sci 108(5):2787–2801
37. Fischer S, De Vlieger J, Kock T, Batenburg L, Fischer H (2001) "Green" nano-composite materials—new possibilities for bioplastics. In: Materials research society symposium—proceedings, pp 628–661
38. Park HM, Li X, Jin CZ, Park CY, Cho WJ, Ha CS (2002) Preparation and properties of biodegradable thermoplastic starch/clay hybrids. Macromol Mater Eng 287(8):553–558
39. Park HM, Lee WK, Park CY, Cho WJ, Ha CS (2003) Environmentally friendly polymer hybrids Part I mechanical, thermal, and barrier properties of thermoplastic starch/clay nanocomposites. J Mater Sci 38(5):909–915
40. Chiou BS, Yee E, Glenn GM, Orts WJ, Wood DF, Imam SH (2004) Biopolymer nanocomposites containing native wheat starch and nanoclays. In: ACS national meeting book of abstracts. vol 1
41. Jin YH, Park HJ, Im SS, Kwak SY, Kwak S (2002) Polyethylene/clay nanocomposite by in situ exfoliation of montmorillonite during Ziegler-Natta polymerization of ethylene. Macromol Rapid Commun 23(2):135–140
42. Dennis HR, Hunter DL, Chang D, Kim S, White JL, Cho JW, Paul DR (2001) Effect of melt processing conditions on the extent of exfoliation in organoclay-based nanocomposites. Polymer 42(23):9513–9522
43. Chivrac F, Pollet E, Avérous L (2009) Progress in nano-biocomposites based on polysaccharides and nanoclays. Mater Sci Eng R: Reports 67(1):1–17
44. Chivrac F, Pollett E, Schmutz M, Averous L (2008) New approach to elaborate exfoliated starch-based nanobiocomposites. Biomacromolecules 9(3):896–900
45. Bilotti E, Fischer HR, Peijs T (2008) Polymer nanocomposites based on needle-like sepiolite clays: Effect of functionalized polymers on the dispersion of nanofiller, crystallinity, and mechanical properties. J Appl Polym Sci 107(2):1116–1123
46. Bokobza L, Burr A, Garnaud G, Perrin MY, Pagnotta S (2004) Fibre reinforcement of elastomers: nanocomposites based on sepiolite and poly(hydroxyethyl acrylate). Polym Int 53(8):1060–1065
47. Duquesne E, Moins S, Alexandre M, Dubois P (2007) How can nanohybrids enhance polyester/sepiolite nanocomposite properties? Macromol Chem Phys 208(23):2542–2550
48. Chivrac F, Pollet E, Schmutz M, Averous L (2010) Starch nano-biocomposites based on needle-like sepiolite clays. Carbohyd Polym 80(1):145–153

49. Kumar P, Sandeep KP, Alavi S, Truong VD, Gorga RE (2010) Preparation and characterization of bio-nanocomposite films based on soy protein isolate and montmorillonite using melt extrusion. J Food Eng 100(3):480–489
50. Kumar P, Sandeep KP, Alavi S, Truong VD, Gorga RE (2010) Effect of type and content of modified montmorillonite on the structure and properties of bio-nanocomposite films based on soy protein isolate and montmorillonite. J Food Sci 75(5):N46–N56
51. Guilherme MR, Mattoso LHC, Gontard N, Guilbert S, Gastaldi E (2010) Synthesis of nanocomposite films from wheat gluten matrix and MMT intercalated with different quaternary ammonium salts by way of hydroalcoholic solvent casting. Compos A Appl Sci Manuf 41(3):375–382
52. Olabarrieta I, Gallstedt M, Ispizua I, Sarasua J-R, Hedenqvist MS (2006) Properties of aged montmorillonite-wheat gluten composite films. J Agric Food Chem 54(4):1283–1288
53. Sothornvit R, Rhim J-W, Hong S-I (2009) Effect of nano-clay type on the physical and antimicrobial properties of whey protein isolate/clay composite films. J Food Eng 91(3):468–473
54. Tunc S, Angellier H, Cahyana Y, Chalier P, Gontard N, Gastaldi E (2007) Functional properties of wheat gluten/montmorillonite nanocomposite films processed by casting. J Membr Sci 289(1–2):159–168
55. Zhang X, Do MD, Dean K, Hoobin P, Burgar IM (2007) Wheat-gluten-based natural polymer nanoparticle composites. Biomacromolecules 8(2):345–353
56. Dean K, Yu L (2005) Biodegradable protein-nanoparticles composites. In: Smith R (ed) Biodegradable polymers for industrial applications. Woodhead Publishing Ltd, Cambridge, pp 289–312
57. Bordes P, Pollet E, Averous L (2009) Nano-biocomposites: Biodegradable polyester/nanoclay systems. Prog Polym Sci 34(2):125–155
58. Bordes P, Pollet E, Bourbigot S, Averous L (2008) Structure and properties of PHA/clay nano-biocomposites prepared by melt intercalation. Macromol Chem Phys 209(14):1473–1484

Chapter 2
Biodegradable Polymers

Luc Avérous and Eric Pollet

Abstract In the recent years, bio-based and biodegradable products have raised great interest since sustainable development policies tend to expand with the decreasing reserve of fossil fuel and the growing concern for the environment. These polymers bring a significant contribution to the sustainable development in view of the wider range of disposal options with minor environmental impact. As a result, the market of these environmentally friendly materials is in rapid expansion, 10–20 % per year. Consequently, biodegradable polymers are the topics of much research. Biodegradable polymers can be mainly classified as agro-polymers (starch, chitin, protein…) and biodegradable polyesters [polyhydroxyalkanoates, poly(lactic acid)…]. These latter, also called biopolyesters, can be synthesized from fossil resources but main productions are obtained from renewable resources. This chapter intends to present these polymers regarding the synthesis, the structure, properties and their applications.

2.1 Introduction

Increasing concern exists today about the preservation of our ecological systems. Most of today's synthetic polymers are produced from petrochemicals and are not biodegradable. Persistent polymers generate significant sources of environmental pollution, harming wildlife when they are dispersed in nature. For example, the disposal of non-degradable plastic bags adversely affects sea-life. It is widely

L. Avérous (✉) · E. Pollet
LIPHT-ECPM, EAc(CNRS) 4379, Université de Strasbourg,
25 rue Becquerel, 67087 Strasbourg Cedex 2, France
e-mail: luc.averous@unistra.fr

L. Avérous and E. Pollet (eds.), *Environmental Silicate Nano-Biocomposites*,
Green Energy and Technology, DOI: 10.1007/978-1-4471-4108-2_2,

accepted that the use of long-lasting polymers in products with a short life-span, such as engineering applications, packaging, catering, surgery, and hygiene, is not adequate. Moreover, incineration of plastic waste presents environmental issues as well since it yields toxic emissions (e.g., dioxin). Material incineration is also limited due to the difficulties to find accurate and economically viable outlets. In addition, plastic recycling shows a negative eco-balance due to the necessity, in nearly all cases, to wash the plastic waste as well as the energy consumption during the recycling process phases (waste grinding and plastic processing). As plastics represent a large part of the waste collection at the local, regional, and national levels, institutions are now aware of the significant savings that compostable or biodegradable materials would generate. For these different reasons, reaching the conditions of conventional plastic replacements by degradable polymers, particularly for short-term applications (packaging, agriculture…), is of major interest to the society as a whole, from the plastic industries to the citizens.

The potential of biodegradable polymers has been recognized for a long time since they could be an interesting way to overcome the limitation of the petrochemical resources in the future. The fossil fuel and gas could be partially replaced by green agricultural resources, which would also participate in the reduction of CO_2 emissions [1]. However, till now, biodegradable polymers have not found extensive applications in industries to largely replace conventional plastic materials, reasons being their high production costs and sometimes their underperformed properties.

2.1.1 Renewability and Sustainable Development

Renewability is linked to the concept of sustainable development. The UN World Commission on "Environment and Development in Our Future" defines sustainability as the development which meets the needs of the present time without compromising the ability of future generations to meet their own needs. According to Narayan [1], the manufactured products must be designed and engineered from "conception to reincarnation", the so-called "cradle-to-grave" approach. The use of annually renewable biomass must be understood in a complete carbon cycle. The carbon cycle is a complex process by which carbon is exchanged between the four main reservoirs of carbon on the planet i.e., the lithosphere (e.g., limestone), the biosphere (plant and animal), the hydrosphere (e.g. bicarbonate dissolved in the oceans), and the atmosphere (CO_2). Recent human activities (burning fossil fuel and massive deforestation) lead to an important imbalance in the carbon cycle with a huge and rapid release of CO_2 to the atmosphere, which cannot be fully compensated by the photosynthesis activity and the dissolution in the oceans. It results in a large accumulation of CO_2 in the atmosphere, which contributes to the global warming. People are now aware that efforts have to be made to re-balance the carbon cycle by reducing the amount of CO_2 production. Part of the carbon cycle re-balancing concept is based on the development and manufacture of products based on renewable and biodegradable resources. By collecting and

composting biodegradable plastic wastes, we can generate much-needed carbon-rich compost: humus materials. These valuable soil inputs can go back to the farmland and "reinitiate" the carbon cycle. Then, the plants growth contributes to reducing CO_2 atmospheric accumulation through photosynthesis activity. Besides, composting is an increasing key point to maintain the sustainability of agricultural systems by reducing the consumption of chemical fertilizers.

2.1.2 Biodegradability and Compostability

According to ASTM standard D-5488-94d and European norm EN 13432, "biodegradable" means "capable of undergoing decomposition into carbon dioxide, methane, water, inorganic compounds, and biomass". The predominant mechanism is the enzymatic action of microorganisms, which can be measured by standard tests over a specific period of time, reflecting available disposal conditions. There are different media (liquid, inert, or compost medium) to analyze biodegradability. Compostability is material biodegradability using compost medium. Biodegradation is the degradation of an organic material caused by biological activity (biotic degradation), mainly microorganisms' enzymatic action. The end-products are CO_2, new biomass, and water (in the presence of oxygen, i.e. aerobic conditions) or methane (in the absence of oxygen, i.e., anaerobic conditions), as defined in the European Standard EN 13432-2000. Depending on the type of standard to follow (ASTM or EN), different composting conditions (humidity and temperature cycle) must be realized to determine the compostability level [2]. Therefore, the comparison of the results obtained from different standards seems to be difficult or impossible. We must also take into account the amount of mineralization as well as the nature of the residues (commonly called "by-products") left after biodegradation [3]. The accumulation [4] of contaminants with toxic residues can cause plant growth inhibition. The key issue is to determine the environmental toxicity level for these by-products, which is known as eco-toxicity [5]. Some general rules enable the determination of the biodegradability evolution. For example, an increase in parameters such as the hydrophobicity, the macromolecules molecular weights, and the crystallinity or the size of crystalline domains decreases the biodegradability [6].

2.1.3 Biodegradable Polymers Classifications

Biodegradable polymers represent a growing field [7–9]. A vast number of biodegradable polymers (e.g. cellulose, chitin, starch, polyhydroxyalkanoates, polylactide, polycaprolactone, collagen and other polypeptides…) have been synthesized or are formed in natural environment during the growth cycles of

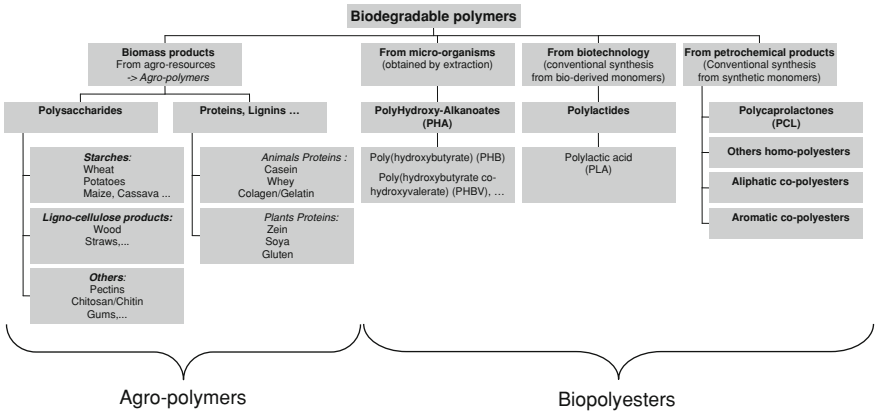

Fig. 2.1 Classification of the main biodegradable polymers

organisms. Some microorganisms and enzymes capable of degrading such polymers have been identified [7, 10].

Different classifications of various biodegradable polymers have been proposed. We propose to classify the biodegradable polymers according to their synthesis process (Fig. 2.1): (i) polymers from biomass such as agro-polymers from agro-resources (e.g., starch or cellulose), (ii) polymers obtained by microbial production such as the polyhydroxyalkanoates (PHAs), (iii) polymers conventionally and chemically synthesized from monomers obtained from agro-resources, e.g., the polylactic acid (PLA), and (iv) polymers obtained from fossil resources. Only the first three categories (i–iii) are obtained from renewable resources.

We can further classify these biodegradable polymers into two main categories: the agro-polymers (category i) and the biodegradable polyesters or biopolyesters (categories ii–iv).

2.2 Agro-Polymers

Main agro-polymers presented in this chapter are the polysaccharides and the proteins. They are often used to elaborate multiphase materials.

2.2.1 Polysaccharides

Polysaccharides are the most abundant macromolecules in the biosphere. These complex carbohydrates constituted of glycosidic bonds are often one of the main structural elements of plants and animals exoskeleton (cellulose, carrageenan,

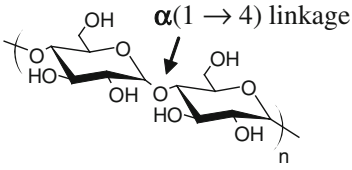

Fig. 2.2 Amylose chemical structure

chitin…). The polysaccharides presented in this chapter are starch, chitin, chitosan, and pectins, successively.

2.2.1.1 Starch

Starch is mainly extracted from cereals (wheat, corn, rice…) and from tubers (potatoes, manioc…). It is stocked in seeds or roots and represents the main plant energy reserve.

Native Starch Structure

Depending on the botanical origin of the plant, starch granules can have different shapes (sphere, platelet, polygon…) and size (from 0.5 to 175 μm). These granules are composed of two α-D-glucopyranose homopolymers, the amylose and the amylopectin. Their proportions in the granules depend directly on the botanical source [11]. In addition, starch also contains, in much smaller proportions, other compounds such as proteins, lipids and minerals.

The amylose is mainly a linear polysaccharide composed of D-glucose units linked by α(1→4) linkages (Fig. 2.2). These chains are partially ramified with some α(1→6) linkages. Depending on the botanical source and the extraction process, amylose molecular weight varies from 10^5 to 10^6 g.mol^{-1} with a polydispersity ranging from 1.3 to 2.1 [12–14]. The amylose chains show a single- or double-helical conformation with a rotation on the α(1→4) linkage [15].

Amylopectin is the main starch component and has the same monomeric unit as amylose. It shows 95 % α(1→4) linkages and 5 % α(1→6) linkages (Fig. 2.3). These latter are found every 24–79 glucose units [16] and bring to the amylopectin a highly branched structure. Consequently, the amylopectin structure and organization can be seen as a grape with pending chains (Fig. 2.3) [17].

The starch granule organization consists in alternation of crystalline and amorphous areas leading to a concentric structure [18]. The amorphous areas are mainly constituted of amylose chains and amylopectin branching points. The crystalline parts are mainly composed of amylopectin side chains. Some co-crystalline structures with amylose chains have been also identified [19, 20]. Four allomorphic starch structures exist [19]. Depending on the botanical origin, starch granules present a crystallinity varying from 20 to 45 %.

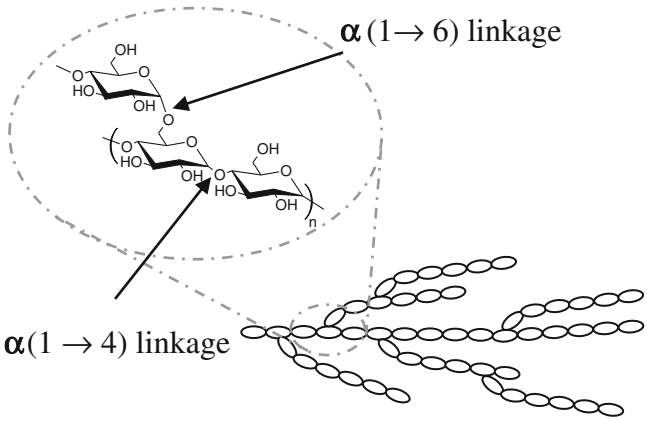

Fig. 2.3 Amylopectin chemical and grape structure (From Hizukuri, reproduced with kind permission from ©Elsevier 2011 [17])

Plasticized Starch: Elaboration and Properties

Because of numerous intermolecular hydrogen bonds existing between the chains, the melting temperature (T_m) of starch is higher than its degradation temperature [21, 22]. Consequently, to elaborate a plastic-like material, it is necessary to introduce high water content or/and some non-volatile plasticizers (glycerol, sorbitol,…) which decrease the glass transition temperature (T_g) and the T_m [23, 24]. These plasticized materials are currently named "thermoplastic starch" or "plasticized starch". To be transformed, the starch granular structure has to be disrupted. The disruption can be obtained either by a solvent-casting process or by a melting process where starch and plasticizers are mixed under thermo-mechanical treatment.

Solvent-assisted disruption of starch granules is mostly carried out with water. At ambient temperature, starch remains insoluble in water and keeps its granular structure. The increase of water temperature induces an irreversible swelling process named "gelatinization". During gelatinization, the amylose is well solubilized, the granular semi-crystalline structure disappears, and the granules swell rapidly. This phenomenon occurs at a given temperature defined as "gelatinization temperature" (T_{gel}) which depends on the starch botanical origin [25–27]. To obtain a quite full starch solubilization, hot DMSO is often used as a solvent. Then, this solvent can be volatilized under vacuum and heat.

The starch melting process is often carried out in association with plasticizers to obtain a homogeneous molten phase. During the thermo-mechanical process, e.g., extrusion, different and successive phenomena occur (Fig. 2.4) [28].

The disruption of starch granules being dependent on the specific mechanical energy provided during processing, this material could be described as a "thermo-mechanical-plastic" material [29, 30].

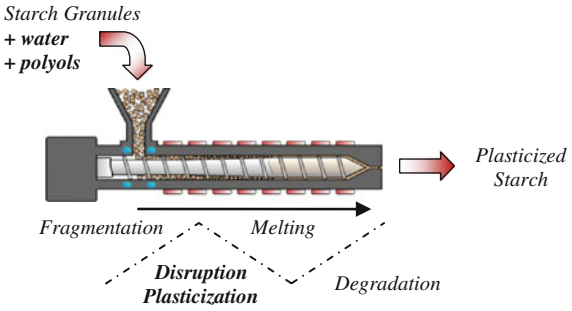

Fig. 2.4 Schematic representation of the starch extrusion process

During processing, amylose and amylopectin degradation occurs and this phenomenon is obviously dependent on the thermal and mechanical energy brought to the system. Numerous studies were conducted to determine the degradation mechanism and to understand the contribution of each parameter [31–38].

Since starch is a hydrophilic material, water is the best plasticizer [24, 39–41]. Nevertheless, the water content and thus the plasticized starch properties are strongly dependent on the storage conditions (temperature and atmosphere relative humidity). This drawback is partially solved with the use of less volatile plasticizers, which present lower plasticization efficiency. These compounds (polyols), bearing hydroxyl groups, can interact with the starch chains through hydrogen bonds. Glycerol is the most common plasticizer [42–45], but numerous other polyols, such as sorbitol [46], xylitol [47], fructose [48], glucose, [49], and glycols [50], can also be used as plasticizers. Nevertheless, these plasticizers are more hydrophilic than starch and are also sensitive to the relative humidity.

Depending on the plasticizer content, starch may display one or two relaxations, corresponding to a homogeneous or multiphasic material. Some authors [44, 51] have demonstrated that a phase separation occurs for glycerol content higher than 27 wt% on dry-basis. The corresponding second relaxation (named β) is consistent with the glycerol glass transition and occurs around -50 to -70 °C. This secondary transition is dependent on the glycerol concentration and more particularly on the 'free' glycerol [52, 53]. The main relaxation (named α) is attributed to the plasticized starch T_g and this temperature decreases when the glycerol content increases from 0 to 25 wt% [54].

Several studies were also performed in order to highlight the different interactions taking place in water/glycerol/starch multiphasic systems and to determine the influence of the water content at equilibrium [44, 55]. The results have shown that the higher the water content, the lower the T_g of plasticized starch.

The great influence of water and glycerol contents on starch properties has also been highlighted by the "so-called" anti-plasticization effect [46, 54]. For example, with glycerol content below 12 wt%, a remarkable behavior occurs, leading to the hardening of the material.

The mechanical properties of plasticized starch evolve with time due to molecular reorganization, which is dependent on processing protocol and storage

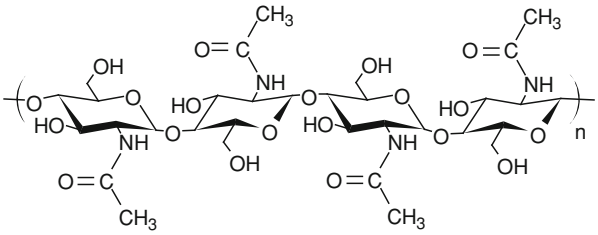

Fig. 2.5 Chitin chemical structure

conditions. When the samples are stored below the T_g, the samples will undergo physical ageing with material densification [56]. When $T > T_g$, the samples will retrograde with a crystallinity increase [57]. The physical ageing is observed for materials with plasticizer content lower than 25 wt% [22, 58]. This phenomenon induces hardening and a decrease in the strain at break. The retrogradation takes place after the amylose crystallization and concerns the amylopectin crystallization. This phenomenon is slow since it lasts for more than a month [52, 59] and induces a strong variation of mechanical properties [20, 60–62]. Thus, even if these two phenomena are different, both of them induce internal stresses in the material, which lead to embrittlement characterized by a stiffness increase correlated to a decrease in the strain at break.

2.2.1.2 Chitin and Chitosan

Chitin is the second most abundant agro-polymer produced in nature after cellulose. It appears in nature as ordered crystalline microfibrils forming structural components in the exoskeleton of arthropods or in the cell walls of fungi and yeasts [63, 64]. It is an acetylated polysaccharide composed of *N*-acetyl-D-glucosamine groups linked by $\beta(1\rightarrow4)$ linkages (Fig. 2.5). From chitin, chitosan is obtained by deacetylation.

Depending on the source, chitin occurs in two allomorphic forms named α and β [65]. A third allomorphic structure γ has also been reported, but it seems to be a variant of the α form [66].These two structures are organized in crystalline sheets where a number of intra-sheet hydrogen bonds tightly hold them. The α form presents some inter-sheets hydrogen bonds. Such a feature is not found for the β form, which is consequently more prone than the α form to water swelling [67, 68]. Like cellulose, the semi-crystalline structure of chitin microfibrils can be treated with acid to produce whisker-shaped nanofillers which can be incorporated into polymers to elaborate nano-hybrid materials [69, 70]. Contrary to chitin, chitosan is not widespread in nature. It is found in some mushrooms (zygote fungi) and in the termite queen's abdominal wall. It is industrially obtained by partial and controlled chitin deacetylation [71]. Its chemical structure, represented in Fig. 2.6,

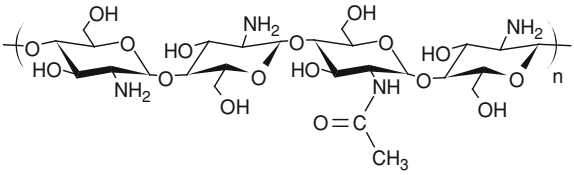

Fig. 2.6 Chitosan chemical structure

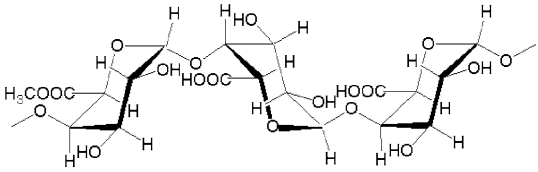

Fig. 2.7 Pectin chemical structure

is a random linear chaining of N-acetyl-D-glucosamine units (acetylated unit) and D-glucosamine (deacetylated unit) linked by $\beta(1\rightarrow4)$ linkages.

Thanks to its amino group and compared to chitin, chitosan shows some particular properties. In acid conditions, when the amino groups are protonated, it becomes a water soluble polycation. Some polysaccharides like carrageenan can have a polyelectrolyte behavior, but these agro-polymers are mainly polyanions [72]. The chitosan is characterized by its acetylation degree and by its molecular weight. These last parameters influence its viscosity and solubility. Depending on the source (shrimp, crab, mushrooms…), industrial chitosan has molecular weight varying from 5,000 to 1,000,000 $g.mol^{-1}$ and acetylation degrees from 2 to 60 %.

In solid state, chitosan is a semi-crystalline polymer. Its morphology has been investigated and many allomorphs have been described, depending on its acetylation degree, on the distribution of the acetyl groups along the carbohydrate chain, and on the chitosan preparation procedure [73, 74].

Chitosan can be plasticized with glycerol to obtain a kind of thermoplastic material like, for instance, plasticized starch [75].

2.2.1.3 Pectin

Pectin is a linear macromolecule constituted of $\alpha(1\rightarrow4)$-linked D-galacturonic acid (Fig. 2.7). This monomer unit could be partially replaced by $\alpha(1\rightarrow2)$-linked L-rhamnose leading to a new structure named rhamnogalacturonan I. A third pectin structural type is rhamnogalacturonan II, which is a less frequent, but complex and highly branched polysaccharide [76].

In nature, around 80 % of the galacturonic acid carboxyl groups are esterified with methanol. This proportion depends on the extraction conditions. Since the ratio of esterified/non-esterified galacturonic acid determines the behavior of pectin in food applications, pectins are classified as high- or low-ester pectins [77]. The non-esterified galacturonic acid units can be either free acid or salts, with

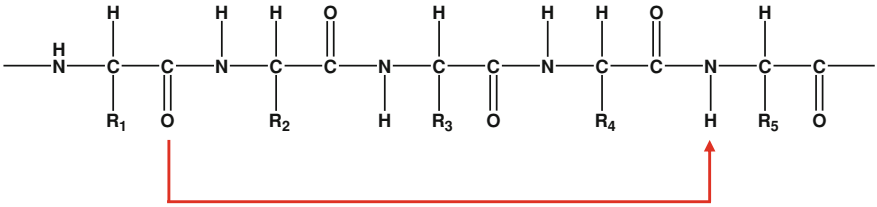

Fig. 2.8 Protein chemical structure. Hydrogen bonds interaction between the amino-acids (*arrow*)

sodium, potassium, or calcium as the counter ion. The partially esterified pectin salts are named pectinates. If the degree of esterification is below 5 %, the salts are called pectates.

2.2.2 Proteins

Proteins are agro-polymers. They are an important renewable resources produced by animals, plants, and bacteria. The term "protein" comes from the Greek, *proteios*, for "primary, first and foremost". A certain number of proteins have received much attention as biodegradable polymers but few have led to actual industrial scale-up due to the high production cost and the low product performance. In terms of potential sources, soy protein, corn protein (zein…) and wheat proteins (gluten…) are among the main plant proteins. Casein, collagen protein or gelatin, and keratin are important animal proteins. Lactate dehydrogenase, chymotrypsin, and fumarase constitute the main bacterial proteins.

Most proteins consist of linear polymers built from a series of up to 20 different amino acids (Fig. 2.8). The side chains of the standard amino acids have a great variety of chemical structures and properties. It is the combined effect of all of the amino acid side chains that determines the final 3D structure and the chemical reactivity. Most proteins fold into unique 3D structures. Biochemists often refer to four distinct aspects of a protein's structure [78]:

- Primary structure: the amino acid sequence (Fig. 2.8).
- Secondary structure: regularly repeating local structures stabilized by hydrogen bonds (Fig. 2.8) such as the alpha helix or the beta sheet. Different zones with various secondary structures can be present in the same protein.
- Tertiary structure: the overall shape of a single protein molecule; the spatial relationship of the secondary structures to another. Tertiary structure is generally stabilized by nonlocal interactions with the formation of a hydrophobic core. The tertiary structure is what controls the basic function of the protein.
- Quaternary structure: the structure formed by numerous proteins, which function as a single protein complex.

Proteins can be classified according to the shape and solubility as fibrous, globular, or membrane [78]. Fibrous proteins tend to have relatively simple, regular linear structures. Globular proteins are roughly spherical. The polypeptide chain is compactly folded so that hydrophobic amino acid side chains are in the interior of the molecule and hydrophilic side chains are on the outside exposed to the solvent. They are very soluble in aqueous media. Membrane proteins are found in association with various membrane systems of cells. For interaction with the non-polar phase within membranes, membrane proteins have hydrophobic amino acid side chains oriented outwards. They are mainly insoluble in aqueous media.

Proteins can be processed with the same kinds of approaches developed for starch-based materials, e.g., formulation with plasticizers, cross-linkers….

2.2.2.1 Soybean Proteins

Typically soybean proteins contain 38–42 % crude protein, 16–20 % triglycerides, and around 33 % carbohydrates, on dry basis. Soy proteins are the isolated proteins from soybean. It is made of dehulled, defatted soybean meal. Dehulled and defatted soybeans are processed into three kinds of high protein commercial products: soy flour, concentrates, and isolates. More recently, Soy proteins have been the subject of studies regarding the health effects of soy protein consumption. Soy protein contains phytoestrogens and some studies suggest that high levels of phytoestrogens may increase the risk of certain forms of cancer. Then, these proteins could be rather developed for non-food applications in the future [79].

2.2.2.2 Corn Proteins

Proteins form about 9 % of the dry weight of corns. They are mainly composed of zein (a highly hydrophobic protein, soluble in alcohols), glutelin (soluble in aqueous alkaline solutions), albumins, and globulins.

Zein comprises about 40 % of the total kernel protein on dry basis. It is one of the few cereal proteins extracted in a relatively pure form and is a unique and complex biopolymer. Zein comes from the alcohol soluble protein of corn, classified as a prolamin. It is the principle storage protein of corn and constituting 45–80 % of endosperm protein. Zein is a mixture of proteins varying in molecular weight and solubility, which can be separated by differential solubility to give four related zeins named α, β, γ and δ [78]. Commercial zein is made up of α-zein, which is by far the most abundant, accounting for around 70 % of the total. The molecular weight of zein is between 9,600 and 44,000 $g.mol^{-1}$.

The cost of purified zein is €15–50 per kg depending on the grade and purity. The cost and also its poor water resistance are two main issues of this protein to find a large range of applications.

2.2.2.3 Wheat Gluten

Wheat gluten is a protein carbohydrate complex of which proteins are the major component. Two main fractions are present. Gliadin is soluble in neutral 70 % ethanol, made of single chain polypeptides with an average molecular weight of 25,000–100,000 $g.mol^{-1}$ by intramolecular disulphide bonds. The second fraction is glutenin, which is an alcohol-insoluble fraction consisting of gliadin-like subunits stabilized by intermolecular disulphide bonds in large aggregates with molecular weight greater than 100,000 $g.mol^{-1}$. Thus, the term "gliadin" defines a group of proteins extracted from gluten by 70 % ethanol. Gliadins and glutenins are present in almost equivalent quantities in wheat gluten and have comparable amino acid compositions, with high concentrations in glutamine and proline. The amount, size distribution, and macromolecular architecture of glutenins and gliadins greatly influence the rheological, processing, mechanical, and physicochemical properties of the gluten [80]. Wheat protein-based materials has greatly attracted attention during the two last decades and some material applications have already been found for them [81]. Some targeted areas are molded objects for interior use such as toys, leather imitation for office products (covers), design articles and pieces of furniture….

2.2.2.4 Casein

Caseins are animal proteins and are commonly found in mammalian milk, making up 80 % of the proteins in cow milk and between 60 and 65 % of the proteins in human milk. Casein molecular weight is between 1,000 and 20,000 $g.mol^{-1.}$ Caseins include four different types. Casein is the predominant phosphoprotein and is characterized by an open, random coil structure. By treating acid-precipitated caseins with alkali solution, caseinates are produced. Both caseins and caseinates form transparent films from aqueous solutions without any treatment based on hydrogen bonds [82]. Caseins have shown to be useful in a great number of fields such as adhesives, controlled releases, and biomedical applications.

2.2.2.5 Gelatin

Gelatin is a natural material based on animal proteins. It is derived from collagen, which is elongated fibrils and mostly found in fibrous tissues such as tendon, ligament, and skin. It is also abundant in cornea, cartilage, bone, blood vessels, gut, and intervertebral disc. Gelatin is commonly used for biomedical applications due to its biodegradability and biocompatibility in physiological environments, in contact with living tissues [83]. Two different types of gelatin can be produced depending on the method in which collagen is pretreated, prior to the extraction process. Alkaline process targets the amide groups of asparagines and glutamine and hydrolyzes them into carboxyl groups, thus converting many of these residues

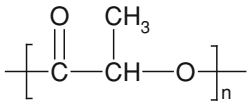

Fig. 2.9 Chemical structure of poly(lactic acid) (PLA)

to aspartate and glutamate. In contrast, acidic pre-treatment does little to affect the amide groups and the gelatin processed with an alkaline pre-treatment is electrically different in nature from acidic-processed gelatin. Gelatin has shown to be useful in a great number of fields such as adhesives, and pharmaceutical and biomedical applications.

2.3 Biodegradable Polyesters

We distinguish biobased (PLA, PHA…) and non-renewable polyesters (PCL, PBSA, PBAT…) in the following.

2.3.1 Polyesters Based on Agro-Resources

Some biobased polyesters are now largely available like PLA and PHAs, with different industrial productions.

2.3.1.1 Poly(Lactic Acid)

Lactic acid is a chiral molecule existing as two stereoisomers, L- and D-lactic acid which can be produced by different ways, i.e., biologically or chemically synthesized [84].

In the first case, lactic acid is obtained by fermentation of carbohydrates by lactic bacteria belonging mainly to the genus *Lactobacillus*, or fungi [85, 86]. This fermentative process requires a bacterial strain but also a carbon source (carbohydrates), a nitrogen source (yeast extract, peptides…), and mineral elements to allow the growth of bacteria and the production of lactic acid. The lactic acid as-formed exists almost exclusively as L-lactic acid and leads to poly(L-lactic acid) (PLLA) with low molecular weight by polycondensation reaction (Fig. 2.9). However, Moon et al. [87, 88] have proposed an alternative solution to obtain higher molecular weight PLLA by polycondensation route.

In contrast, the chemical process could lead to various ratio of L- and D-lactic acid. The chemical reactions, leading to the formation of a cyclic dimer, the lactide, as an intermediate step to the production of PLA, could lead to long macromolecular chains with L- and D-lactic acid monomers. This mechanism of

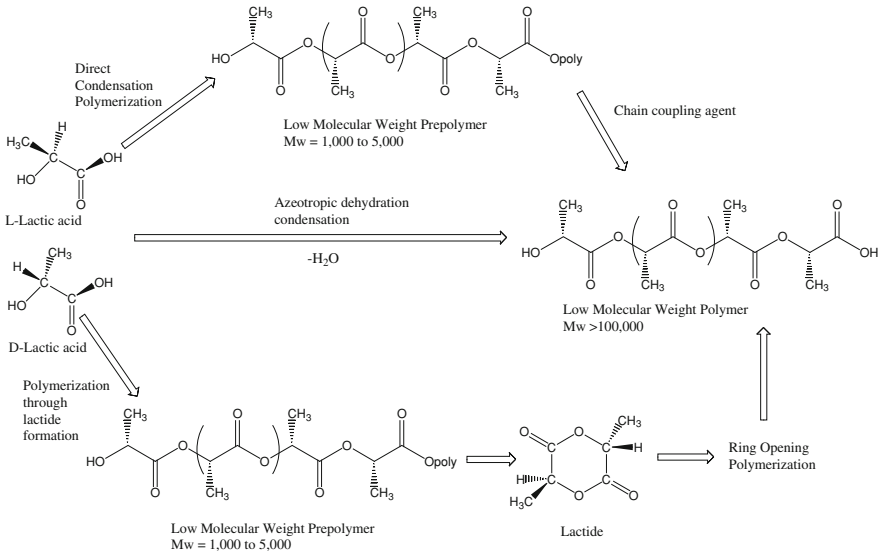

Fig. 2.10 Chemical structure of PLA and Synthesis methods for obtaining high molecular weight (Adapted from Averous. With kind permission from ©Elsevier 2011 [84])

ring-opening polymerization (ROP) from the lactide explains the formation of two enantiomers. This ROP route has the advantage of reaching high molecular weight (Fig. 2.10) and of allowing the control of PLA final properties by adjusting the proportions and the sequencing of L- and D-lactic acid units [7, 85, 89, 90].

At present, due to its large availability on the market and its relatively low price [91–94], PLA shows one of the highest potential among biopolyesters, particularly for packaging [92, 94] and medical applications. For instance, Cargill has developed processes that use corn and other feedstock to produce different PLA grades (NatureWorks®) [93, 95]. In this company, the actual production is estimated to be 140,000 tons/year. Presently, it is the highest and worldwide production of biodegradable polyester. Its price is lower than 2€/kg. Different companies such as Mitsui Chemicals (Japan), Mitsubishi (Japan), Shimadzu (Japan), Futerro (Total/Galactic—Belgium), Purac (Netherland), Teijin (Japan), and Zhejiang Hisun Biomaterials (China) produced different PLA products with a wide range of L/D ratios. PLA consumption is only around 200,000 tons/year. At present, only ~30 % of lactic acid is used for PLA production. Thus, this biopolymer presents a high potential for development.

Commercially available, we can find 100 % PLLA which present a high crystallinity (C-PLA) and also copolymers of PLLA and poly(D,L-lactic acid) (PDLLA) which are rather amorphous (A-PLA) [95–97].

Properties of PLA, as well as other polymers, depend on their molecular characteristics as well as ordered structures such as crystalline thickness, crystallinity, spherulite size, morphology, and degree of chain orientation.

The physical properties of polylactide are related to the enantiomeric purity of lactic acid stereo-copolymers. Homo-PLA is a linear macromolecule having a molecular architecture that is determined by its stereo-chemical composition. PLA can be produced totally amorphous or up to 40 % crystalline. PLA resins containing more than 93 % of L-lactic acid are semi-crystalline. But, PLA with 50–93 % L-lactic acid is completely amorphous. Therefore, the L/D ratio induces or restrains polymer crystallinity. Both meso- and D-lactides induce twists in a very regular poly(L-lactide) architecture. Macromolecular imperfections are responsible for the decrease in both the rate and extent of PLLA crystallization. Practically most PLA are made up of L-and D,L-lactide copolymers since PLA production contains often some meso-lactide impurities.

Depending on the preparation conditions, poly(L-lactide) crystallizes into different forms [84]. The α-form exhibits a well-defined diffraction pattern. This structure is more stable than the β-structure, with a T_m at 185 °C compared to 175 °C for the β-structure. This latter can be formed at a high draw ratio and high drawing temperature [28]. The γ-form is found by epitaxial crystallization. It has been observed that a blend with equivalent PLLA and PDLA contents gives stereo-complexation (racemic crystallite) of both polymers. This stereo-complex gives mechanical properties higher than those of pure PLLA or PDLA and a high T_m equal to 230 °C. Literature reports different density data for PLA. Mainly, crystalline parts give a density of 1.29 compared to 1.25 for the amorphous material.

PLA is a slowly crystallizing polymer similar to PET. The PLA crystallization kinetics have been extensively studied. As PET, PLA can be oriented by processing. Chain orientation increases the mechanical strength of PLLA plastics. If orientation is performed at low temperature, the resulting PLLA has enhanced modulus without a significant increase in crystallinity. To determine crystallinity levels by DSC, the value, most often referred in the literature concerning the PLA melt enthalpy at 100 % crystallinity, is 93 J/g [98].

Crystallization of the thermally crystallizable but amorphous PLA can be initiated by annealing at temperatures between 75 °C and T_m. The annealing of crystallizable PLA copolymers often produces two melting peaks. Different hypothesis have been presented. Some authors [99] found double melting points in PLLA polymers and attributed them to the slow rates of crystallization and recrystallization.

The typical T_g of PLA ranges from 50 to 80 °C while the T_m ranges from 130 to 180 °C. For instance, enantiomerically pure PLA is a semi-crystalline polymer with a T_g of 55 °C and a T_m of 180 °C. For semi-crystalline PLA, the T_m is a function of the different processing parameters and the initial PLA structure. T_m increases with the molecular weight (Mw) until a maximum value. Besides, the crystallinity decreases with increasing Mw. T_g is also determined by the proportion of the different types of lactide. T_m depends on the presence of meso-lactide in the structure which produces a T_m reduction [84].

PLA can be plasticized using oligomeric lactic acid (o-LA) [98], citrate ester [100], or low molecular weight polyethylene glycol (PEG) [98, 101–103]. The effect of plasticization increases the chain mobility and then favors the PLA

organization and crystallization. After plasticization, a crystallinity ranging between 20 and 30 % is obtained.

PLA presents a medium water and oxygen permeability level [94, 104] comparable to polystyrene [105]. These different properties associated with its tunability and its availability favor its actual developments in different packaging applications (trays, cups, bottles, films…) [92, 94, 95]. McCarthy (1999) [106] showed that A-PLA presents a soil degradation rate much slower compared to e.g., PBSA. PLA is presumed to be biodegradable although the role of hydrolytic versus enzymatic depolymerization in this process remains open to debate [107]. Regarding biodegradation in compost, adequate conditions are only found in industrial units with a high temperature (above 50 °C) and a high relative humidity (RH%) to promote chain hydrolysis. According to Tuominen et al. (2002) [108], PLA biodegradation does not exhibit any eco-toxicological effect.

2.3.1.2 Polyhydroxyalkanoates

PHAs are a family of intracellular biopolymers synthesized by many bacteria as intracellular carbon and energy storage granules. PHAs are mainly produced from renewable resources by fermentation. A wide variety of prokaryotic organisms [109, 110] accumulate PHA from 30 to 80 % of their cellular dry weight. Biotechnological studies revealed that PHB is produced under balanced growth conditions when the cells become limited for an essential nutrient but are exposed to an excess of carbon [111]. Depending on the carbon substrates and the metabolism of the microorganism, different monomers, and thus (co)polymers, could be obtained [112]. Besides, PHAs are considered as biodegradable and thus suitable for e.g., short-term packaging, and also considered as biocompatible in contact with living tissues and can be used for biomedical applications (e.g., drug encapsulation, tissue engineering…). PHA can be degraded by abiotic degradation, i.e., simple hydrolysis of the ester bond without requiring the presence of enzymes to catalyze this hydrolysis. During the biodegradation process, the enzymes degrade the residual products till final mineralization (biotic degradation).

PHAs are generally classified into short-chain-length PHA (sCL-PHA) and medium-chain-length PHA (mCL-PHA) by the different number of carbons in their repeating units. For instance, sCL-PHAs contain 4 or 5 carbons in their re-peating units, while mCL-PHAs contain 6 or more carbons in the repeating units. The term mCL was coined because the number of carbons in the monomers roughly corresponds to those of medium-chain-length carboxylic acids. PHA nomenclature and classification may still evolve as new structures continue to be discovered. The main biopolymer of the PHA family is the poly hydroxybutyrate homopolymer (PHB), but also different poly(hydroxybutyrate-co-hydroxyalkanoates) copolyesters exist such as poly(hydroxybutyrate-co-hydroxy valerate) (PHBV), poly(hydroxybutyrate-co-hydroxyhexanoate) (PHBHx),

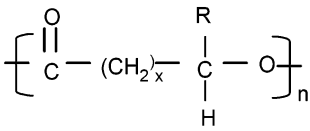

Fig. 2.11 Generic chemical structure of the polyhydroxyalkanoates

Table 2.1 Main PHAs homopolymer structures based on the Fig. 2.11

Chemical name	Abbreviation	x value	R group
Poly(3-hydroxypropionate)	P(3HP)	1	Hydrogen
Poly(3-hydroxybutyrate)	P(3HB)	1	Methyl
Poly(3-hydroxyvalerate)	P(3HV)	1	Ethyl
Poly(3-hydroxyhexanoate) or poly (3-hydroxycaproate)	P(3HHx) or P(3HC)	1	Propyl
Poly(3-hydroxyhexanoate)	P(3HH)	1	Butyl
Poly (3-hydroxyoctanoate)	P(3HO)	1	Pentyl
Poly (3-hydroxynonanoate)	P(3HN)		Hexyl
Poly(3-hydroxydecanoate)	P(3HD)	1	Heptyl
Poly(3-hydroxyundecanoate) or	P(3HUD)or P(3HUd)	1	Octyl
Poly(3-hydroxydodecanoate)	P(3HDD) or P(3HDd)	1	Nonyl
Poly(3-hydroxyoctadecanoate)	P(3HOD) or P(3HOd)	1	Pentadecanoyl
Poly(4-hydroxybutyrate)	P(4HB)	2	Hydrogen
Poly(5-hydroxybutyrate)	P(5HB)	2	Methyl
Poly(5-hydroxyvalerate)	P(5HV)	3	Hydrogen

Table 2.2 Main PHA abbreviations

Conventional abbreviations (short)	Full abbreviations	Structures
PHB	P(3HB)	Homopolymer
PHV	P(3HV)	Homopolymer
PHBV	P(3HB-co-3HV)	Copolymer
PHBHx	P(3HB-co-3HHx)	Copolymer
PHBO	P(3HB-co-3HO)	Copolymer
PHBD	P(3HB-co-3HD)	Copolymer
PHBOd	P(3HB-co-3HOd)	Copolymer

poly(hydroxybutyrate-co-hydroxyoctanoate) (PHBO), and poly(hydroxybutyrate-co-hydroxyoctadecanoate) (PHBOd) (Tables 2.1, 2.2).

Figure 2.11 shows the generic formula for the PHAs where x is 1 or higher, and R can be either hydrogen or hydrocarbon chains of up to around C16 in length. The main members of the PHA homopolymer family are presented in Table 2.1.

A wide range of PHA homopolymers and copolymers have been produced, in most cases at laboratory scale. A few of them have attracted industrial interest and were commercialized in the past decade.

Copolymers of PHAs vary in the type and proportion of monomers, and are typically random in sequence. Poly(3-hydroxybutyrate-*co*-3-hydroxyvalerate) or

Table 2.3 Main PHA commercial productions

Company	Country	Trade name	PHA	Pilot/industrial scale
PHB industrial/ copersucar	Brazil	Biocycle	PHB, PHBV	Pilot/ind. (?)
Biomatera	Canada	Biomatera	PHBV	Pilot scale
PolyFerm Canada	Canada	VersaMer PHA	PHBV and copolymers	Pilot scale
Tianan	China	Enmat	PHBV	Ind.
Tianjin & DSM	China	GreenBio	PHB—copolymers based on 3 and 4HB	Pilot/ind. (?)
Tianzhu	China	Tianzhu	PHBHx	Pilot scale
Biomer	Germany	Biomer	PHB, PHBV	Pilot scale
Bio-On	Italy	Minerv PHA	PHB, PHBV	Pilot scale
Kaneka	Japan	Kaneka	PHBHx	Pilot/ind. (?)
DaniMer/Meredian	US	?	Copolymers	Pilot/ind. (?)
Telles (Metabolix/ ADM)	US	Mirel	Copolymer	Ind.

P(3HB-*co*-3HV) is based on a random arrangement of two monomers with R = methyl and with R = ethyl. Poly(3-hydroxybutyrate-*co*-3-hydroxyhexanoate) consists of two monomers with R = methyl and propyl. Some examples of homo and copolymers are shown in Table 2.2.

PHB is a highly crystalline polyester (above 50 %) with a high melting point, T_m=173–180 °C, compared to the other biodegradable polyesters. The T_g is around 5 °C. The homopolymer shows a narrow window for the processing conditions. To ease the transformation, PHB can be plasticized with citrate ester. In contrast, PHBV copolymer processing is easier. Material properties can be tailored by varying the HV content. An increase of the HV content induces an increase in impact strength and decreases in T_m and T_g [113], crystallinity [114], water permeability [114], and tensile strength [115]. Besides, PHBV properties can evolve when plasticization occurs, e.g., with citrate ester (triacetin) [115, 116]. PHAs, like the PLAs, are sensitive to processing conditions. Under extrusion, we obtain rapid decreases in viscosity and molecular weight due to macromolecular chain cleavage by increasing the shear level, the temperature, and/or the residence time [117]. Regarding the biodegradable behavior, the kinetic of enzymatic degradation is variable according to the crystallinity, the structure [6, 118], and then to the processing history [119]. Bacterial copolyesters biodegrade faster than homopolymers [120] and synthetic copolyesters [121].

Table 2.3 shows that PHA production is shared among a great numbers of companies. Worldwide, more than 24 companies are known to be engaged in PHA production and applications. Compared to PLA, the world production of PHA is lower, largely less than 50,000 tons/year. But, it is difficult to have a precise idea

because there is a wide gap between the (press) announcements and the true production. Only the production capacities are published.

The story of PHA industrial production is very long and starts in the 1950s. In the seventeenth, Zeneca (formerly ICI) produced several tons of PHA copolymers under the trade name Biopol®. In the nineteenth, Zeneca UK produced P(3HB-*co*-3HV) in a pilot plant by bacterial fermentation using a mixture of glucose and propionic acid. In 1996, Zeneca sold its Biopol business to Monsanto, who continued the investigations started by Zeneca to produce PHA from genetically-modified crops. Monsanto commercially produced Biopol® P(3HB-*co*-3HV) with HV contents reaching 20 % by means of fermentation. The production was ceased at the end of 1999. Metabolix bought Biopol® assets in 2001. In 2007, Metabolix and Archer Daniels Midland (ADM) formed a joint venture, Telles, to produce PHAs under the trade name Mirel. ADM started in 2010 to build a first plant in Clinton, Iowa (US), which was expected to produce 50,000 tons of resin per year. This joint venture stopped in January 2012. Metabolix has developed production of PHA from genetically-modified crops, and announced in 2010 that it had completed a field trial of genetically engineering of tobacco into PHA biobased polymers. This company has also declared that, in greenhouse trials, switchgrass plants engineered using multi-gene expression technology can produce significant amounts of PHA bioplastics from leaf tissues.

Different small companies currently produce bacterial PHA. For instance, PHB Industrial (Brazil) produces PHB and PHBV (HV = 12 %) with 45 % crystallinity, from sugar cane molasses [118]. Biocycle® production is planned to be 4,000 tons/year, and then to be extended to 14,000 tons/year. In 2004, Procter & Gamble (US) and Kaneka Corporation (Japan) announced a joint development agreement for the completion of R&D leading to the commercialization of Nodax®, a large range of polyhydroxybutyrate-*co*-hydroxyalkanoates (PHBHx, PHBO, PHBOd) [122]. Although the industrial large-scale production was planned with a target price around 2€/kg, the Nodax® development stopped in 2006 [123]. In 2007 Meredian Inc. purchased P&G's PHA technology. Meredian plans to produce over 270,000 tons annually in connection with DaniMer. Tianan, a Chinese company also announced to increase the capacity from the current 2,000 tons to 10,000 tons/year. The Dutch chemical company DSM announced to invest in a PHA plant together with a Chinese bio-based plastics company—Tianjin Green Bio-Science Co. The company will start up the production of PHA with an annual capacity of 10,000 tons. The Japanese company Kaneka planned to start the production of 50,000 tons/year of PHBHx in 2011.

The production of PHA is intended to replace synthetic non-degradable polymers for a wide range of applications [123]: packaging, agriculture, leisure, fast-food, hygiene as well as medicine and biomedical [112, 124] since PHA is biocompatible.

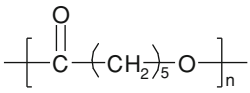

Fig. 2.12 Chemical structure of Polycaprolactone (PCL)

2.3.2 Petroleum-Based Polyesters

A large number of biodegradable polyesters are based on petroleum resources, obtained chemically from synthetic monomers [89–93, 95, 96]. According to the chemical structures, we can distinguish polycaprolactone, aliphatic copolyesters, and aromatic copolyesters. All these polyesters are soft at room temperature.

2.3.2.1 Polycaprolactone

Figure 2.12 gives the chemical structure of poly(ε-caprolactone) (PCL).

It is usually obtained by ROP of ε-caprolactone in the presence of metal alkoxides (aluminium isopropoxide, tin octoate…) [89, 90, 121]. PCL is widely used as a PVC solid plasticizer or for polyurethane applications, as polyols. But, it finds also some applications based on its biodegradable character in domains such as biomedicine (e.g. drugs controlled release) and environment (e.g. soft compostable packaging). Different commercial grades were produced by Solvay (CAPA®), which has sold this activity to Perstorp (Sweden), by Dow Chemical (Tone®) and by Daicel (Celgreen®). PCL shows a very low T_g (−61 °C) and a low T_m (65 °C), which could be a handicap in some applications. Therefore, PCL is generally blended [52, 107, 125, 126] or modified (e.g., copolymerisation, cross-linking [127]). Tokiwa et al. [128] have discussed the hydrolysis of PCL and biodegradation by fungi. They have shown that PCL can easily be enzymatically degraded. According to Bastioli [107], the biodegradability can be clearly claimed but the homopolymer hydrolysis rate is very low.

2.3.2.2 Aliphatic Copolyesters

A large number of aliphatic copolyesters based on petroleum resources are biodegradable copolymers. They are obtained by the combination of diols such as 1,2-ethanediol, 1,3-propanediol or 1,4-butadenediol, and of dicarboxylic acids like adipic, sebacic or succinic acid. Showa Highpolymer (Japan) has developed a large range of polybutylene succinate (PBS) obtained by polycondensation of 1,4-butanediol and succinic acid. Anqing Hexing Chemical Co (China) also commercializes this aliphatic polyester.

Figure 2.13 gives the chemical structure of polybutylene succinate/adipate (PBSA). It is obtained by addition of adipic acid to 1,4-butanediol and succinic acid polycondensation. These copolymers are commercialized under the Bionolle®

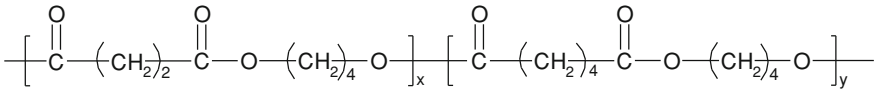

Fig. 2.13 Chemical structure of poly(butylene succinate adipate) (PBSA)

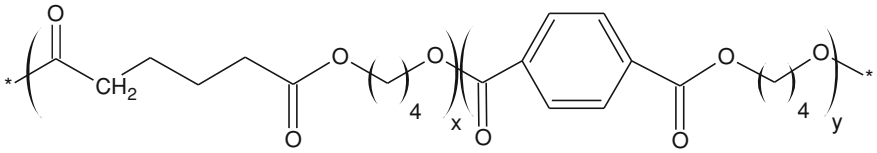

Fig. 2.14 Chemical structure of poly(butylene adipate-co-terephthalate)

trademark [95]. Ire Chemical (Korea) commercialized exactly the same kind of copolyesters under EnPol® trademark. Skygreen®, a product from SK Chemicals (Korea), is obtained by polycondensation of 1,2-ethanediol, 1,4-butadenediol with succinic and adipic acids [129]. Nippon Shokubai (Japan) also commercializes such aliphatic copolyester (Lunare SE®). The properties of these copolyesters depend on the structure [130] i.e., the combination of diols and diacids used. The biodegradability of these products depends also on the structure. The addition of adipic acid, which decreases the crystallinity [131], tends to increase the compost biodegradation rate [132]. According to Ratto et al. [133], the biodegradation results demonstrate that, while PBSA is inherently biodegradable, the addition of starch filler can significantly improve the rate of degradation.

2.3.2.3 Aromatic Copolyesters

Compared to totally aliphatic copolyesters, aromatic copolyesters are often based on terephthalic acid. For instance, Fig. 2.14 gives the chemical structure of poly(butylene adipate-*co*-terephthalate) (PBAT).

BASF, DuPont, and Novamont have commercialized aromatic copolyesters under Ecoflex® [95], Biomax®, and Origo-Bi® trademarks, respectively. Biomax® shows a high terephthalic acid content which modifies some properties such as the T_m (200 °C). However, according to Muller et al. [130], an increase of terephthalic acid content tends to decrease the degradation rate. The production of Eastar Bio® from Eastman Chemical was stopped some years ago. This activity has been sold to Novamont, which now produces Origo-Bi®.

Ecoflex® biodegradation had been analyzed by Witt et al. [134]. They concluded that there is no indication of environmental risk (ecotoxicity) when aliphatic–aromatic copolyesters of the Ecoflex®-type are introduced into composting processes.

2.4 Conclusion

Biodegradable polymers have been the topics of many studies for the last two decades. The development of these polymers (10–20 % per year) is a significant contribution to sustainable development in view of the wider range of disposal option at lower environmental impact.

Legislative attention able to properly address this issue could become a further incentive to the development of biodegradable products and maximize the environmental, social, and industrial benefits. The success of such highly innovative products is linked to the achievement of high quality standards. In this domain, quality mainly means environmental quality. Standards such as European EN 13432:2000 on the compostability and biodegradability norms at international level are now in place to partially control this bio-value.

References

1. Narayan R (2001) Drivers for biodegradable/compostable plastics and role of composting in waste management and sustainable agriculture. Orbit J 1(1):1–9
2. Steinbuchel A (2003) Biopolymers, general aspects and special applications, vol 10. Wiley-VCH, Weinheim
3. Avella M, Bonadies E, Martuscelli E (2001) European current standardization for plastic packaging recoverable through composting and biodegradation. Polym Test 20(5):517–521
4. Van Tuil R, Fowler P, Lawther M, Weber CJ (2000) Properties of biobased packaging materials, biobased packaging materials for the food industry: status and perspectives. KVL, Frederiksberg
5. Fritz J, Link U, Braun R (2001) Environmental impacts of biobased/biodegradable packaging. Starch 53(3–4):105–109
6. Karlsson S, Albertsson A-C (1998) Biodegradable polymers and environmental interaction. Polym Eng Sci 38(8):1251–1253
7. Kaplan DL, Mayer JM, Ball D, McCassie J, Allen AL, Stenhouse P (1993) Fundamentals of biodegradable polymers. In: Ching C, Kaplan DL, Thomas EL (eds) Biodegradable polymers and packaging. Technomic Pub Co, Lancaster, pp 1–42
8. Van de Velde K, Kiekens P (2002) Biopolymers: overview of several properties and consequences on their applications. Polym Test 21(4):433–442
9. Rouilly A, Rigal L (2002) Agro-materials: a bibliographic review. J Macromol Sci Part C Polym Rev C42(4):441–479
10. Chandra R, Rustgi R (1998) Biodegradable polymers. Prog Polym Sci 23(7):1273–1335
11. Guilbot A, Mercier C (1985) The polysaccharides. In: Aspinall GO (ed) Molecular biology, vol 3. Academic Press Incorporation, New York, pp 209–282
12. Della Valle G, Buleon A, Carreau PJ, Lavoie PA, Vergnes B (1998) Relationship between structure and viscoelastic behavior of plasticized starch. J Rheol 42(3):507–525
13. Colonna P, Mercier C (1984) Macromolecular structure of wrinkled- and smooth-pea starch components. Carbohydr Res 126(2):233–247
14. Hizukuri S, Takeda Y, Yasuda M (1981) Multibranched nature of amylose and the action of debranching enzymes. Carbohydr Res 94(2):205–213
15. Hayashi A, Kinoshita K, Miyake Y, Cho CH (1981) Conformation of amylose in solution. Polym J 13(6):537–541

16. Zobel HF (1988) Molecules to granules: a comprehensive starch review. Starch-Starke 40(2):44–50
17. Hizukuri S (1986) Polymodal distribution of the chain lengths of amylopectins, and its significance. Carbohydr Res 147(2):342–347
18. Jenkins PJ, Donald AM (1995) The influence of amylose on starch granule structure. Int J Biol Macromol 17(6):315–321
19. Van Soest JJG, Hulleman SHD, De Wit D, Vliegenthart JFG (1996) Crystallinity in starch bioplastics. Ind Crop Prod 5(1):11–22
20. Van Soest JJG, Essers P (1997) Influence of amylose-amylopectin ratio on properties of extruded starch plastic sheets. J Macromol Sci Part A-Pure Appl Chem 34(9):1665–1689
21. Jang JK, Pyun YR (1986) Effect of moisture content on the melting of wheat starch. Starch-Starke 48(2):48–51
22. Shogren RL (1992) Effect of moisture content on the melting and subsequent physical aging of cornstarch. Carbohydr Polym 19(2):83–90
23. Swanson CL, Shogren RL, Fanta GF, Imam SH (1993) Starch-plastic materials-preparation, physical properties, and biodegradability (a review of recent USDA research). J Environ Polym Deg 1(2):155–166
24. Tomka I (1991) Thermoplastic starch. Adv Exp Med Biol 302:627–637
25. Cooke D, Gidley MJ (1992) Loss of crystalline and molecular order during starch gelatinisation: origin of the enthalpic transition. Carbohydr Res 227:103–112
26. Stevens DJ, Elton GAH (1971) Thermal properties of the starch/water system. Part I. Measurement of heat of gelatinisation by differential scanning calorimetry. Starch-Starke 23(1):8–11
27. Genkina NK, Wikman J, Bertoft E, Yuryev VP (2007) Effects of structural imperfection on gelatinization characteristics of amylopectin starches with A- and B-type crystallinity. Biomacromolecules 8(7):2329–2335
28. Averous L (2004) Biodegradable multiphase systems based on plasticized starch: a review. J Macromol Sci Part C-Polym Rev 44(3):231–274
29. Ollett AL, Parker R, Smith AC, Miles MJ, Morris VJ (1990) Microstructural changes during the twin-screw extrusion cooking of maize grits. Carbohydr Polym 13(1):69–84
30. Martin O, Averous L, Della Valle G (2003) In-line determination of plasticized wheat starch viscoelastic behavior: impact of processing. Carbohydr Polym 53(2):169–182
31. Della Valle G, Boche Y, Colonna P, Vergnes B (1995) The extrusion behaviour of potato starch. Carbohydr Polym 28(3):255–264
32. Vergnes B, Villemaire JP, Colonna P, Tayeb J (1987) Interrelationships between thermomechanical treatment and macromolecular degradation of maize starch in a novel rheometer with preshearing. J Cereal Sci 5:189
33. Orford PD, Parker R, Ring SG (1993) The functional properties of extrusion-cooked waxy-maize starch. J Cereal Sci 18(3):277–286
34. Sagar AD, Merrill EW (1995) Starch fragmentation during extrusion processing. Polymer 36(9):1883–1886
35. Baud B, Colonna P, Della Valle G, Roger P (1999) Macromolecular degradation of extruded starches measured by HPSEC-MALLS. In: Colonna P, Guilbert S (eds) Biopolymer science food and non food applications. Les Colloques de l'INRA, Paris, pp 217–221
36. Wang SS, Chiang WC, Yeh AI, Zhao B, Kim IH (1989) Kinetics of phase transition of waxy corn starch at extrusion temperatures and moisture contents. J Food Sci 54(5):1298–1301
37. Davidson VJ, Paton D, Diosady LL, Larocque G (1984) Degradation of wheat starch in a single screw extruder: characteristics of extruded starch polymers. J Food Sci 49(2): 453–458
38. Davidson VJ, Parker R, Diosady LL, Rubin LT (1984) A model for mechanical degradation of wheat starch in a single-screw extruder. J Food Sci 49(4):1154–1169
39. Zeleznak KJ, Hoseney RC (1987) The glass transition in starch. Cereal Chem 64(2): 121–124

40. Kalichevsky MT, Jaroszkiewicz EM, Ablett S, Blanshard JMV, Lillford PJ (1992) The glass transition of amylopectin measured by DSC, DMTA and NMR. Carbohydr Polym 18(2):77–88
41. Van Soest JJG, Knooren N (1997) Influence of glycerol and water content on the structure and properties of extruded starch plastic sheets during aging. J Appl Polym Sci 64(7): 1411–1422
42. Forssell P, Mikkila J, Suortti T, Seppala J, Poutanen K (1996) Plasticization of barley starch with glycerol and water. J Macromol Sci Part A-Pure Appl Chem 33(5):703–715
43. Hulleman SHD, Kalisvaart MG, Janssen FHP, Feil H, Vliegenthart JFG (1999) Origins of B-type crystallinity in glycerol-plasticised, compression-moulded potato starches. Carbohydr Polym 39(4):351–360
44. Lourdin D, Coignard L, Bizot H, Colonna P (1997) Influence of equilibrium relative humidity and plasticizer concentration on the water content and glass transition of starch materials. Polymer 38(21):5401–5406
45. Van Soest JJG, De Wit D, Tournois H, Vliegenthart JFG (1994) The influence of glycerol on structural changes in waxy maize starch as studied by Fourier transform infra-red spectroscopy. Polymer 35(22):4722–4727
46. Gaudin S, Lourdin D, Forssell PM, Colonna P (2000) Antiplasticisation and oxygen permeability of starch-sorbitol films. Carbohydr Polym 43(1):33–37
47. Lourdin D, Della Valle G, Colonna P (1995) Influence of amylose content on starch films and foams. Carbohydr Polym 27(4):261–270
48. Kalichevsky MT, Blanshard JMV (1993) The effect of fructose and water on the glass transition of amylopectin. Carbohydr Polym 20(2):107–113
49. Ollett AL, Parker R, Smith AC (1991) Deformation and fracture behaviour of wheat starch plasticized with glucose and water. J MaterSci 26(5):1351–1356
50. Shogren RL, Swanson CL, Thompson AR (1992) Extrudates of cornstarch with urea and glycols: structure/mechanical property relations. Starch-Starke 44(9):335–338
51. Lourdin D, Ring SG, Colonna P (1998) Study of plasticizer-oligomer and plasticizer-polymer interactions by dielectric analysis: maltose-glycerol and amylose-glycerol-water systems. Carbohydr Res 306(4):551–558
52. Averous L, Moro L, Dole P, Fringant C (2000) Properties of thermoplastic blends: starch-polycaprolactone. Polymer 41(11):4157–4167
53. Lourdin D, Bizot H, Colonna P (1997) Correlation between static mechanical properties of starch-glycerol materials and low-temperature relaxation. Macromol Symp 114:179–185
54. Lourdin D, Bizot H, Colonna P (1997) "Antiplasticization" in starch-glycerol films? J Appl Polym Sci 63(8):1047–1053
55. Godbillot L, Dole P, Joly C, Roge B, Mathlouthi M (2006) Analysis of water binding in starch plasticized films. Food Chem 96(3):380–386
56. Thiewes HJ, Steeneken PAM (1997) The glass transition and the sub-Tg endotherm of amorphous and native potato starch at low moisture content. Carbohydr Polym 32(2): 123–130
57. Lu TJ, Jane JL, Keeling PL (1997) Temperature effect on retrogradation rate and crystalline structure of amylose. Carbohydr Polym 33(1):19–26
58. Appelqvist IAM, Cooke D, Gidley MJ, Lane SJ (1993) Thermal properties of polysaccharides at low moisture: 1—An endothermic melting process and water-carbohydrate interactions. Carbohydr Polym 20(4):291–299
59. Averous L, Fauconnier N, Moro L, Fringant C (2000) Blends of thermoplastic starch and polyesteramide: processing and properties. J Appl Polym Sci 76(7):1117–1128
60. Van Soest JJG, Borger DB (1997) Structure and properties of compression-molded thermoplastic starch materials from normal and high-amylose maize starches. J Appl Polym Sci 64(4):631–644
61. Van Soest JJG, De Wit D, Vliegenthart JFG (1996) Mechanical properties of thermoplastic waxy maize starch. J Appl Polym Sci 61(11):1927–1937

62. Van Soest JJG, Hulleman SHD, De Wit D, Vliegenthart JFG (1996) Changes in the mechanical properties of thermoplastic potato starch in relation with changes in B-type crystallinity. Carbohydr Polym 29(3):225–232
63. Campbell NA, Reece JB, Mitchell LG (1999) Biology, 5th edn. Addison Wesley Longman, Menlo Park
64. Rinaudo M (2006) Chitin and chitosan: Properties and applications. Prog Polym Sci 31:603–632
65. Rudall KM, Kenchington W (1973) The chitin system. Biol Rev 40:597–636
66. Atkins EDT (1985) Conformation in polysaccharides and complex carbohydrates. J Biosci 8:375–387
67. Minke R, Blackwell J (1978) The structure of a-chitin. J Mol Biol 120:167–181
68. Gardner KH, Blackwell J (1975) Refinement of the structure of b-chitin. Biopolymers 14:1581–1595
69. Lu Y, Weng L, Zhang L (2004) Morphology and properties of soy protein isolate thermoplastics reinforced with chitin whiskers. Biomacromolecules 5(3):1046–1051
70. Paillet M, Dufresne A (2001) Chitin whisker reinforced thermoplastic nanocomposites. Macromolecules 34(19):6527–6530
71. Peter MGPI (2002) Chitin and Chitosan from Fungi. In: Steinbüchel A (ed) Biopolymers, vol 6., Polysaccharides IIWiley-VCH, Weinheim, pp 123–157
72. Shahidi F, Arachchi JKV, Jeon YJ (1999) Food applications of chitin and chitosan. Trends Food Sci Technol 10(2):37–51
73. Ogawa K (1991) Effect of heating an aqueous suspension of chitosan on the crystallinity and polymorphs. Agric Biol Chem 55(9):2375–2379
74. Ogawa K, Yui T, Miya M (1992) Dependence on the preparation procedure of the polymorphism and crystallinity of chitosan membranes. Biosci Biotech Biochem 56:858–862
75. Epure V, Griffon M, Pollet E, Averous L (2011) Structure and properties of glycerol-plasticized chitosan obtained by mechanical kneading. Carbohyd Polym 83(2):947–952
76. Thakur BR, Singh RK, Handa AK (1997) Chemistry and uses of pectin—a review. Crit Rev Food Sci Nutr 37(1):47–73
77. May CD (1990) Industrial pectins: Sources, production and applications. Carbohydr Polym 12(1):79–99
78. Zhang L, Zeng M (2008) Proteins as sources of materials. In: Belgacem M, Gandini A (eds) Monomers polymers and composites from renewable resources. Elsevier, Amsterdam, pp 479–493
79. Zhang JW, Chen F (2010) Development of novel soy protein-based polymer blends. Green Polym Chem: Biocatal Biomater 1043:45–57
80. Domenek S, Morel MH, Guilbert S (2004) Wheat gluten based biomaterials: environmental performance, degradability and physical modifications. Roy Soc Ch 295:443–446
81. Guillaume C, Gontard N, Guilbert S (2011) New packaging materials based on renewable resources: properties, applications, and prospects. In: Aguilera JM, Simpson R, Welti-Chanes J, Bermudez Aguirre D, Barbosa-Canovas G (eds) Food Engineering Interfaces. Springer, New York, pp. 619–630
82. Arvanitoyannis I, Psomiadou E, Nakayama A (1996) Edible films made from sodium caseinate, starches, sugars or glycerol.1. Carbohyd Polym 31(4):179–192
83. Ofokansi K, Winter G, Fricker G, Coester C (2010) Matrix-loaded biodegradable gelatin nanoparticles as new approach to improve drug loading and delivery. Eur J Pharm Biopharm 76(1):1–9
84. Averous L (2008) Polylactic acid: synthesis, properties and applications. In: Belgacem N, Gandini A (eds) Monomers, oligomers, polymers and composites from renewable resources. Elsevier, Amsterdam, pp 433–450
85. Garlotta D (2001) A literature review of poly(lactic acid). J Polym Environ 9(2):63–84
86. Wee Y-J, Kim J-N, Ryu H-W (2006) Biotechnological production of lactic acid and its recent applications. Food Technol Biotechnol 44(2):163–172

87. Moon SI, Lee CW, Miyamoto M, Kimura Y (2000) Melt polycondensation of L-lactic acid with Sn(II) catalysts activated by various proton acids: a direct manufacturing route to high molecular weight poly(L-lactic acid). J Polym Sci Part A: Polym Chem 38(9):1673–1679
88. Moon S-I, Lee C-W, Taniguchi I, Miyamoto M, Kimura Y (2001) Melt/solid polycondensation of L-lactic acid: an alternative route to poly(L-lactic acid) with high molecular weight. Polymer 42(11):5059–5062
89. Okada M (2002) Chemical syntheses of biodegradable polymers. Prog Polym Sci (Oxford) 27(1):87–133
90. Albertsson A-C, Varma IK (2002) Aliphatic polyesters: synthesis, properties and applications. Adv Polym Sci 157:1–40
91. Vert M, Schwarch G, Coudane J (1995) Present and future of PLA polymers. J Macromol Sci Pure Appl Chem A32(4):787–796
92. Sinclair RG (1996) The case for polylactic acid as a commodity packaging plastic. J Macromol Sci—Pure Appl Chem 33(5):585–597
93. Lunt J (1998) Large-scale production, properties and commercial applications of polylactic acid polymers. Polym Degrad Stabil 59(1–3):145–152
94. Auras R, Harte B, Selke S (2004) An overview of polylactides as packaging materials. Macromol Biosci 4(9):835–864
95. Steinbuchel A, Doi Y (2002) Biopolymers: polyesters III—applications and commercial products, vol 4. Wiley-VCH, Weinheim
96. Bigg DM (1996) Effect of copolymer ratio on the crystallinity and properties of polylactic acid copolymers. J Eng Appl Sci 2:2028–2039
97. Perego G, Cella GD, Bastioli C (1996) Effect of molecular weight and crystallinity on poly(lactic acid) mechanical properties. J Appl Polym Sci 59(1):37–43
98. Martin O, Avérous L (2001) Poly(lactic acid): plasticization and properties of biodegradable multiphase systems. Polymer 42(14):6209–6219
99. Yasuniwa M, Iura K, Dan Y (2007) Melting behavior of poly(L-lactic acid): Effects of crystallization temperature and time. Polymer 48(18):5398–5407
100. Labrecque LV, Kumar RA, Dave V, Gross RA, McCarthy SP (1997) Citrate esters as plasticizers for poly(lactic acid). J Appl Polym Sci 66(8):1507–1513
101. Jacobsen S, Fritz HG (1999) Plasticizing polylactide—the effect of different plasticizers on the mechanical properties. Polym Eng Sci 39(7):1303–1310
102. Kranz H, Ubrich N, Maincent P, Bodmeier R (2000) Physicomechanical properties of biodegradable poly(D,L-lactide) and poly(D,L-lactide-co-glycolide) films in the dry and wet states. J Pharm Sci 89(12):1558–1566
103. Ljungberg N, Andersson T, Wesslen B (2003) Film extrusion and film weldability of poly(lactic acid) plasticized with triacetine and tributyl citrate. J Appl Polym Sci 88(14):3239–3247
104. Van Tuil R, Fowler P, Lawther M, Weber CJ (2000) Properties of biobased packaging materials. In: Biobased packaging materials for the food industry—status and perspectives. KVL, Frederiksberg, pp 8–33
105. Lehermeier HJ, Dorgan JR, Way JD (2001) Gas permeation properties of poly(lactic acid). J Membrane Sci 190(2):243–251
106. McCarthy SP, Ranganthan A, Ma W (1999) Advances in properties and biodegradabilility of co-continuous, immiscible, biodegradable, polymer blends. Macromol Symp 144:63–72
107. Bastioli C (1998) Biodegradable materials—present situation and future perspectives. Macromol Symp 135:193–204
108. Tuominen J, Kylma J, Kapanen A, Venelampi O, Itävaara M, Seppälä J (2002) Biodegradation of lactic acid based polymers under controlled composting conditions and evaluation of the ecotoxicological impact. Biomacromolecules 3(3):445–455
109. De Koning GJM (1993) Prospects of bacterial poly[(R)-3-hydroxyalkanoates]. Eindhoven University of Technology, Eindhoven
110. Madison LL, Huisman GW (1999) Metabolic engineering of poly(3-hydroxyalkanoates): from DNA to plastic. Microbiol Mol Biol Rev 63(1):21–53

111. Doi Y (1990) Microbial polyesters. Wiley, New York
112. Zinn M, Witholt B, Egli T (2001) Occurrence, synthesis and medical application of bacterial polyhydroxyalkanoate. Adv Drug Deliver Rev 53(1):5–21
113. Amass W, Amass A, Tighe B (1998) A review of biodegradable polymers: Uses, current developments in the synthesis and characterization of biodegradable polyesters, blends of biodegradable polymers and recent advances in biodegradation studies. Polym Int 47(2):89–144
114. Shogren R (1997) Water vapor permeability of biodegradable polymers. J Environ Polym Degr 5(2):91–95
115. Kotnis MA, O'Brien GS, Willett JL (1995) Processing and mechanical properties of biodegradable poly(hydroxybutyrate-co-valerate)-starch compositions. J Environ Polym Degr 3(2):97–105
116. Shogren RL (1995) Poly(ethylene oxide)-coated granular starch-poly(hydroxybutyrate-co-hydroxyvalerate) composite materials. J Environ Polym Degr 3(2):75–80
117. Ramkumar DHS, Bhattacharya M (1998) Steady shear and dynamic properties of biodegradable polyesters. Polym Eng Sci 38(9):1426–1435
118. El-Hadi A, Schnabel R, Straube E, Müller G, Henning S (2002) Correlation between degree of crystallinity, morphology, glass temperature, mechanical properties and biodegradation of poly(3-hydroxyalkanoate) PHAs and their blends. Polym Test 21(6):665–674
119. Parikh M, Gross RA, McCarthy SP (1998) The influence of injection molding conditions on biodegradable polymers. J Inject Molding Technol 2(1):30
120. Dos Santos Rosa D, Calil MR, Fassina Guedes CdG, Rodrigues TC (2004) Biodegradability of thermally aged PHB, PHB-V, and PCL in soil compostage. J Polym Environ 12(4):239–245
121. Chiellini E, Solaro R (1996) Biodegradable polymeric materials. Adv Mater 8(4):305–313
122. Noda I, Green PR, Satkowski MM, Schechtman LA (2005) Preparation and properties of a novel class of polyhydroxyalkanoate copolymers. Biomacromolecules 6(2):580–586
123. Philip S, Keshavarz T, Roy I (2007) Polyhydroxyalkanoates: biodegradable polymers with a range of applications. J Chem Technol Biotechnol 82(3):233–247
124. Williams SF, Martin DP, Horowitz DM, Peoples OP (1999) PHA applications: addressing the price performance issue I. Tissue engineering. Int J Biol Macromol 25(1–3):111–121
125. Bastioli C, Cerutti A, Guanella I, Romano GC, Tosin M (1995) Physical state and biodegradation behavior of starch-polycaprolactone systems. J Environ Polym Degr 3(2):81–95
126. Bastioli C (1998) Properties and applications of Mater-Bi starch-based materials. Polym Degrad Stab 59(1–3):263–272
127. Koenig MF, Huang SJ (1994) Evaluation of crosslinked poly(caprolactone) as a biodegradable, hydrophobic coating. Polym Degrad Stab 45(1):139–144
128. Tokiwa Y, Suzuki T (1977) Hydrolysis of polyesters by lipases. Nature 270(5632):76–78
129. Lee S-R, Park H-M, Lim H, Kang T, Li X, Cho W-J, Ha C-S (2002) Microstructure, tensile properties, and biodegradability of aliphatic polyester/clay nanocomposites. Polymer 43(8):2495–2500
130. Muller R-J, Witt U, Rantze E, Deckwer W-D (1998) Architecture of biodegradable copolyesters containing aromatic constituents. Polym Degrad Stab 59(1–3):203–208
131. Yokota Y, Marechal H (1999) Processability of biodegradable poly(butylene) succinate and its derivates. A case study. In: Biopolymer conference, Wurzburg, Germany, 24 Feb 1999
132. Fujimaki T (1998) Processability and properties of aliphatic polyesters, 'Bionolle', synthesized by polycondensation reaction. Polym Degrad Stab 59(1–3):209–214
133. Ratto JA, Stenhouse PJ, Auerbach M, Mitchell J, Farrell R (1999) Processing, performance and biodegradability of a thermoplastic aliphatic polyester/starch system. Polymer 40(24):6777–6788
134. Witt U, Einig T, Yamamoto M, Kleeberg I, Deckwer W-D, Muller R-J (2001) Biodegradation of aliphatic-aromatic copolyesters: evaluation of the final biodegradability and ecotoxicological impact of degradation intermediates. Chemosphere 44(2):289–299

Chapter 3
Clays and Clay Minerals as Layered Nanofillers for (Bio)Polymers

Faïza Bergaya, Maguy Jaber and Jean-François Lambert

Abstract This introductory chapter presents the most relevant structural, physical, and chemical properties of clay minerals for the formation of nanocomposites with polymers. The general principles of silicates classification are outlined in order to better understand the structures of the various types of clay minerals as phyllosilicates. Cation exchange capacity (CEC), surface area, porosity, and rheological properties of clay minerals are briefly discussed. The physico-chemical properties of clay mineral layers, including the reactivity at the edges surfaces, are introduced together with their consequences for the various mechanisms of clay-polymer interactions. The chapter closes on a brief presentation of synthetic clay minerals and a general introduction to clay polymer nanocomposites.

3.1 Introduction

Silicate nano-biocomposites which constitute the topic of this book are a class of hybrid materials combining organic and inorganic components at the nanometer scale. The vast majority of the literature on biopolymers nanocomposites uses

F. Bergaya (✉)
Centre de Recherche sur la Matière Divisée (CRMD) UMR 6619 CNRS,
Université d'Orléans, 1b rue de la Férollerie, 45071 Orléans Cedex 02, France
e-mail: f.bergaya@cnrs-orleans.fr

M. Jaber · J.-F. Lambert
Laboratoire de Réactivité de Surface (LRS) UMR 7197 CNRS,
University Paris 6, Case Courrier 178, UPMC, 4 Pl. Jussieu,
75252 Paris Cedex 05, France
e-mail: maguy.jaber@upmc.fr

J.-F. Lambert
e-mail: jean-francois.lambert@upmc.fr

L. Avérous and E. Pollet (eds.), *Environmental Silicate Nano-Biocomposites*,
Green Energy and Technology, DOI: 10.1007/978-1-4471-4108-2_3,

clays or clay minerals as the inorganic component, and it is therefore worthy to describe and classify in detail these inorganic materials in order to better understand the nanocomposites. In this chapter, we will start with a description at the structural level; since many clay minerals are a particular variety of silicates, we will first be concerned with silicates classification.

3.2 From Silicates to Clay Minerals

3.2.1 The Structural Variability of Silicates

Silicates are the largest class of natural minerals (about 30 % of all known minerals) making up the Earth's crust or lithosphere. Indeed the lithosphere is called in geochemistry the "sial" because silicon and aluminium oxides constitute a large majority of its material. Their structural study has always been the object of much interest and there are famous classical books devoted to silicates science [1–7].

The basic chemical unit of silicates is the (SiO_4)-based tetrahedral anion. Formally, the central silicon ion has an oxidation number of +IV and the oxygens of –II, so that an isolated silicate anion would bear a negative charge of −4: $(SiO_4)^{4-}$. This species is in fact the completely deprotonated form corresponding to silicic acid, H_4SiO_4, and actually exists in dilute, basic aqueous solutions.

However, the chemistry of silicates is much richer than that because of their tendency to give rise to *indirect catenation* by condensation of the tetrahedral units. This means that they can build simple or complex skeletons by sharing siloxane bridges (Si–O-Si) between different tetrahedral units (a few silicates contain edge-sharing units but they are something of a mineralogical oddity). The simplest instance of catenation is the formation of the disilicate anion (Fig. 3.1).

It can immediately be seen that condensation can proceed further, because there remain several "dangling" oxygens on each tetrahedron.

Silicates are classified according to the connectivity of these arrangements of tetrahedra (Fig. 3.2). In nesosilicates, the condensation stops at the stage of discrete units. In inosilicates ("chain silicates"), infinite 1-dimensional (1D) chains of tetrahedra (or of cycled tetrahedra) are observed. In phyllosilicates (from the Greek $\phi\upsilon\lambda\lambda o\nu$, "leaf"), condensation occurs in two directions to give infinite sheets of tetrahedra, but is limited in the direction perpendicular to the sheets. Finally, in tectosilicates (Greek $\tau\varepsilon\kappa\tau\omega\nu$, "carpentar"), the tetrahedra are fully condensed by their four corners in a lattice extending over the 3 directions of space. Tectosilicates include both feldspars and zeolites as well as many other structural types with which we shall no longer be concerned.

A very general feature of silicates is the easy substitution of the Si^{4+} by the Al^{3+} cation. Both are similar in size—but not in charge: obviously, if one Al^{3+} occupies the place of one Si^{4+}, the structure will be short of one positive charge to compensate the negative charges of the O^{2-} anions, and a localized negative charge

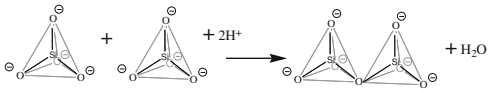

Fig. 3.1 Simple catenation: the formation of the disilicate anion

1. Nesosilicates

(isolated SiO_4 tetrahedra) ex. Grenat

2. Inosilicates

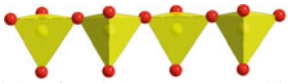

(single or multiple chains of tetrahedra) ex. pyroxene (illustration), amphibole

4. Cyclosilicates
(rings of silica) – ex. tourmaline, cordierite, not illustrated

5. Phyllosilicates

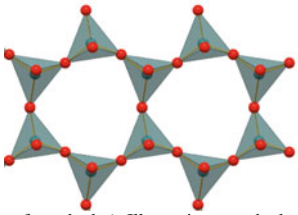

(bidimensionnal layers of tetrahedra). Illustration: tetrahedral sheet of smectite clay

6. Tectosilicates

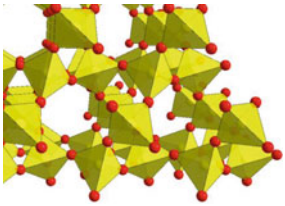

(three-dimensional structures). Illustration: part of the structure of quartz

Fig. 3.2 Tetrahedral arrangements and silicates classification

will be present at the point of substitution. These localized charges are of paramount importance in the chemistry of aluminosilicates.

Among these different silicates arrangements, the structures built from the simplest units are generally well crystallized, in opposite to the more complicated bidimensional phyllosilicates which are solids with imperfect crystalline organization. The latter structures form the basis for the best known clay minerals family existing abundantly in soils all over the world, namely, cationic clay minerals. A precise description of cationic clay minerals structure will be found in Sect. 3.3, including the reason why they are called "cationic": it will be seen that they consist in 2D layers bearing a net negative charge which is

compensated by an equivalent number of "exchangeable cations" located between the layers. A caveat is in order here. While cationic clay minerals are silicates, there also exist anionic clay minerals which have a completely different chemical composition, based on different structural units (e.g. Al-containing octahedra) and are electrostatically "reversed"—with layers bearing a net positive charge, separated by compensating anions. They are usually known as layered double hydroxides (LDH) and their best-known representative is the mineral hydrotalcite [8–11]. Because they are not the main focus of the other chapters of this book, and because they are non-silicate oxides, they will not be studied further here.

3.2.2 Clay Science

Clays have been used intuitively since the beginning of technological societies as base materials by potters but their accurate scientific classification and important fundamental studies, denominated rather recently as 'Clay Science' [12, 13], started only about one century ago. In fact, clay science is a young discipline [14] which started with the visual macroscopic observations of clays in soils by geologists, followed by the chemical and structural analysis of clay minerals by mineralogists and finally by other several physico-chemical determinations by different scientists. The study of their properties is in constant progress, following the constant development of the techniques.

The term of "clays" was used to designate a cheap raw material by different users before it was assigned a well-defined scientific meaning and it is not surprising that it has different connotations depending on the application. They are designed as clay materials or as clay minerals according to whether they are considered by industrials or by scientific researchers. In principle, clays should be distinguished from clay minerals [15]. This distinction has been clearly defined by the Nomenclature Committee (NC) of the Association Internationale Pour l'Etude des Argiles (AIPEA). This international NC is composed by clay scientists coming from ten different countries whose aim is to deliberate on the definitions of clay science terms in order to homogenize as far as possible the used language between scientists of different disciplines and coming from different countries. Their major published recommendations are (i) to describe a "clay" in terms of macroscopic properties by the following definition: *it is a naturally occurring material composed primarily of fine-grained minerals, which is generally plastic at appropriate water contents and will harden when dried or fired* and (ii) to use the "clay mineral" term to designate the crystallographic structures of the minerals which composed a clay. Simply, natural clay consists of one (or several) clay mineral(s) mixed with other associated minerals or amorphous phases considered in principle as impurities. However, this distinction is not always clearly made in many papers which use well-defined clay minerals but will refer to them as "clays" for short [15].

Historically, the criterion of particle size as a macroscopic property has been used by geologists to define clay materials. They defined the "clay fraction" as

fine-grained materials with a maximum particle size (or, rather, an equivalent spherical diameter) ≤2 μm. Later different size limits have been fixed depending on the disciplines. Particle size limits used by different communities vary from 1 (for colloid scientists) up to 4 μm (for engineers) [16]. Nowadays, it is not considered as good practice any more to set a well-defined size limit to clay minerals [15], although the particles must definitely be small enough to form colloidal dispersions in water.

3.2.3 Clay and Clay Mineral Purification

The size criterion remains useful as a practical recipe for clay purification however: according to Stokes's law [17] particles with different sizes will sediment at different rates in water, and the finest clay mineral fraction can thus be obtained by centrifugation at the laboratory scale, even though industrialists use other methods such as sonication to separate large quantities of clays for practical reasons.

The available commercial clay materials are often raw clays. They usually contain embarrassing impurities such as carbonates, cristobalite, feldspars, quartz, organic matter, iron hydroxides… In fact, natural clays are very abundant and clay deposits are spread all over the world (North Africa, Europe, Russia, China, USA…). They are available in big quantities and most deposits are commercialized. Most clay minerals form where rocks are in contact with water, air, or steam. They form from preexisting minerals by dissolution-reprecipitation. The soil solution concentration of Si and Al from the weathering of volcanic rock is one of the most important factors determining the type of clay minerals which will be formed. Extensive alteration of rocks to clay minerals can produce relatively pure clay mineral deposits that are of economic interest and are used for drilling muds and in ceramics. In addition to the weathering process, some clay minerals are formed by hydrothermal activity. Clay deposits may be formed at places as residual deposits in soil, but thick deposits usually are formed as the result of a secondary sedimentary deposition process after they have been eroded and transported from their original location of formation.

Primary clays, mostly kaolins, are located at the site of formation. The bentonites form mainly from alteration of pyroclastic and/or volcanoclastic rocks. Extensive deposits, linked to large eruptions, have formed repeatedly in the past. Bentonites are generally formed by diagenetic or hydrothermal alteration, favoured by fluids that leach alkali elements and by high Mg^{2+} content. Smectite composition is partly controlled by parent rock chemistry. Bentonite deposits may display variations in layer charge and these correlate with physical properties. Unfortunately, clay minerals obtained from the same deposit may show some variability in the properties in different parts of the deposit. They differ by their composition and the nature of the impurities.

For fundamental studies and for some applications, purified clay mineral fractions are needed. Besides sedimentation fragmentation, which has already been

mentioned, several other treatments are aimed e.g. at eliminating iron oxide impurities by selective dissolution. The recommended procedures to obtain pure clay mineral samples are reported in more details by Carrado et al. [18]. However, the complexity of purification processes of raw clays is an incentive for researchers to synthesize cationic clay minerals de novo. Synthetic clay minerals are of course more expensive than natural clays but their advantage is that they can be obtained as pure phases in a single step in many cases, thus bypassing the purification steps. For applications where a very high purity is required, an argument can be made for the use of synthetic clay minerals (presented further in Sect. 3.7).

3.3 Phyllosilicates Classification

3.3.1 General Principles

The most salient structural feature of cationic clay minerals is that they are layered (they are phyllosilicates). We have explained the origin of this layered morphology in the previous Sect. 3.2.1: tetrahedral silicate units condense in 2D to form sheets connected by Si–O–Si bridges. The reader will easily be convinced that no matter the mode of connection, each tetrahedron will then still have one "dangling" $Si–O^-$ (or Si–OH in case of protonation) moiety directed perpendicular to the layer. These groups have a significant tendency towards further condensation. There are indeed "pure" phyllosilicates composed only of tetrahedral units such as magadiite [19–22], kenyaite [21, 22], kanemite [21, 23], etc., but a common feature of their reactivity is that stacked layers have a tendency to "stick" together if not prevented from doing so, initiating a transition to tectosilicates and decreasing the surface available to interact with other molecules. This is probably the reason why these silicates have been little used in the field of nanocomposite materials so far.

Phyllosilicates of the clay minerals family, on the other hand, contain other units in addition to the sheets of tetrahedra which are denoted as "T" sheets. Octahedral, or "O" sheets, are formed by the juxtaposition of $(MO_4(OH)_2)$ or $(MO_2(OH)_4)$ polyhedra, where the central cation can be Li^+, Mg^{2+}, Fe^{2+}, Fe^{3+}, Al^{3+}… These cations, being somewhat larger than Si^{4+}, normally prefer the higher coordination they achieve in octahedra (6 neighbours) relative to tetrahedra (4 neighbors). Al^{3+} is "borderline" and can accommodate tetrahedral as well as octahedral coordination. By a quirk of geometry, the oxygens exposed on the surface of an octahedral (O) sheet are almost exactly in register with the terminal Si–O exposed by a tetrahedral (T) sheet, so that T–O condensation can occur. The result of this condensation is called a "layer" (Fig. 3.3).

All the clay minerals are composed either of TO or of TOT layers. Each tetrahedron [XO_4 unit where X is either Si^{4+} or Al^{3+}] shares three basal oxygen atoms at the corners with three other tetrahedral units, to give a hexagonal

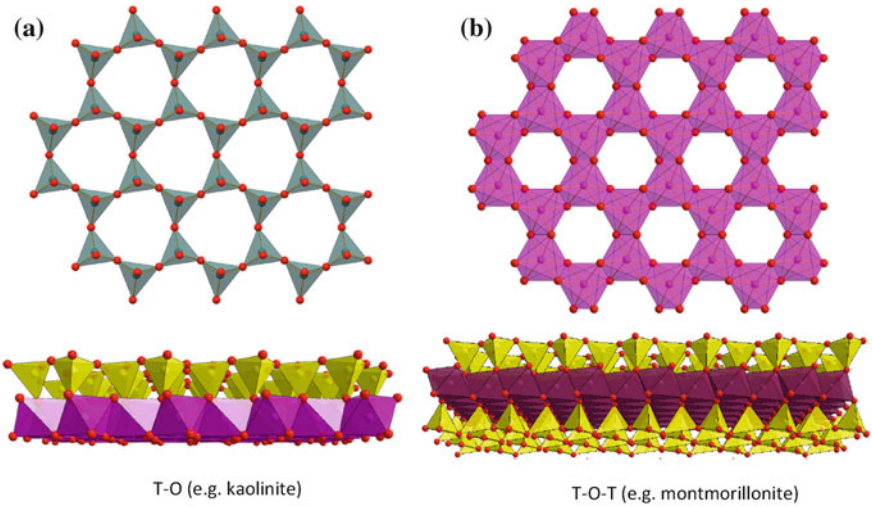

Fig. 3.3 T (**a**) and O (**b**) sheets and their assembly in TO and TOT layers

arrangement of tetrahedra, and the remaining one with an octahedron of the O sheet. This hexagonal arrangement leads to a 2D sheet along *a, b* crystallographic direction. In each octahedron [MO_4 $(OH)_2$ unit] M can be either a trivalent (such as Al^{3+}), a divalent (such as Mg^{2+}) or a monovalent (Li^{+}) ion. The central site of the octahedron may also be vacant. The octahedral sheet, also of (pseudo) hexagonal symmetry, is formed by connection of each octahedron with its neighbours through edges sharing. These sheet structures, described in more details by Brigatti et al. [24], with the elementary units as well as their assembly in TO and TOT layers are shown in Fig. 3.3. The TO and TOT layers are also called "1:1" and "2:1" types because one octahedral sheet is linked to one tetrahedral sheet, or sandwiched between two tetrahedral sheets, respectively.

Within this general structural framework, the phyllosilicates are subdivided in nine clay minerals groups (Table 3.1) which are detailed below. This classification in groups is based on the molecular-level order and does not allow predicting the larger-scale morphologies.

A first and important feature of this classification is the distinction between trioctahedral and dioctahedral clay mineral species according the occupancy of the octahedral sheets. The trioctahedral sites are completely occupied by dications such as Mg^{2+} while 2/3 of the dioctahedral sites are occupied by trications such as Al^{3+} ion leaving the third octahedral site empty. The number of positive charges is obviously the same in both cases (6 per 3 octahedral units, distributed as $2 \times 3+$, or $3 \times 2+$), but it may be confusing to the beginner that dioctahedral clay minerals contain mostly trivalent cations, while trioctahedral clay minerals contain divalent cations.

In a second step, clay minerals classification is based on the layer charge. In view of the many possibilities for cation substitution, this parameter can vary continuously between almost zero (neutral layers) and highly negative values

Table 3.1 The nine groups of phyllosilicates

Group	Name
I	The TO kaolinite and serpentine group
II	The TOT pyrophyllite and talc group
III	The TOT smectite group
IV	The TOT vermiculite group
V	The TOT true (flexible) micas and brittle micas group
VI	The TOT chlorite group
VII	The interstratified clay minerals group
VIII	The TOT sepiolite and palygorskite group
IX	The TO allophane and imogolite group

(down to 2 negative charges per formula unit). Some of the theoretically envisageable substitution patterns are not possible because of unfavorable local energetics: for instance, "Löwenstein's rule" [25, 26] states that no two adjacent tetrahedra can be simultaneously substituted by Al^{3+}.

Dioctahedral pyrophyllite and trioctahedral talc, considered as the "heading files" of the TOT family, have neutral layers. Therefore there is no need for the presence of compensating cations to insure electroneutrality; the interlayer spaces are empty and the layers are held together by van der Waals interactions. For the derived clay mineral groups, increasing degrees of isomorphic substitutions can occur in the T and/or O sheets of the layers. In the octahedral sheet, high charge cations are substituted by cations with a charge lower by one, e.g. Al^{3+} by Mg^{2+}, Fe^{2+} or Mg^{2+} by Li^{+}. Similarly in the tetrahedral sheet, Si^{4+} is substituted essentially by Al^{3+} (other tetrahedral substitutions for instance by Fe^{3+} have been proposed in some cases but often remain controversial). The layers become negatively charged. Tetrahedral substitutions generate localized layer charges, while the charges generated by octahedral substitutions are "smeared" out by the T sheets on both sides and may be considered as "delocalized" (their effect is similar to that of a constant density of negative charge on the layer surface).

To maintain global electric neutrality, the negative charges of the layer are counterbalanced by an equal amount of positive charges provided by cations located in the "interlayer space". The variable negative charge amount from 0 (neutral) up to 2 per formula unit of the layers is, as stated above, a criterion for the classification of the tri- and di-octahedral groups of the phyllosilicates. The negative layers, and compensating cations, alternate in a stacking in the *c* crystallographic direction.

This means that the 2D layers can be separated from each other relatively easily, and the volume included between two successive layers, whatever its content, is called the "interlayer space" as previously mentioned (the term "gallery" or "intergallery space" was formerly used synonymously but has to be discarded). A macroscopic analogy would be a cake such as a 'mille-feuille' where

the layers of pastry are continuous but only loosely connected to each other, or maybe a pile of paper sheets.

3.3.2 The Nine Groups of Clay Minerals

Among the nine classically recognized groups, only three different clay minerals groups (kaolinite, smectite and sepiolite) will be considered in more details because of their widespread occurrence and frequent use in clay polymer nanocomposite studies.

3.3.2.1 Group I: The TO Kaolinite and Serpentine Group

These phyllosilicates, composed of only two sheets, have an almost zero layer charge. The best-known species of the first subgroup are kaolinite and halloysite (both dioctahedral). At the mesoscopic level (the level observable for example with an optical microscope), kaolinite clearly exhibits a planar morphology by forming hexagonal flakes but halloysite forms spheroidal aggregates. As indicated by the examples of halloysite and chrysotile, the 2D connectivity of the layers does not guarantee that platelets will form at the upper organizational level: structural constraints in the layers may cause them to curl and adopt different morphologies. In the serpentine group, the best-known species is probably trioctahedral chrysotile which forms rolled-up cylinders.

The interactions of these initially non-swelling TO clay minerals and more particularly kaolinite, with biopolymers have been investigated chiefly in studies of bioflocculants, based on chitosan, starch and pectin, or produced by bacteria. Other applications include the formation of composite superabsorbent hydrogel. Besides, interest for kaolinite has surged in another related field, namely clay-polymer nanocomposites (CPN) used in the rubber industry: it constitutes a cheaper filler than the more commonly used montmorillonite (Mt), and while it does not swell in water it can be "preswollen" by different compounds due to its particular structure as described further (in Sect. 3.6). Although rarely considered, serpentine has also been used as filler of polypropylene more recently [27].

3.3.2.2 Group II: The TOT Pyrophyllite and Talc Group

These non-swelling TOT phyllosilicates without isomorphous substitution, and therefore uncharged, correspond only to two clay mineral species which are of course called the same name as the group, pyrophyllite (dioctahedral) and talc (trioctahedral). The latter has been used with several polymers such as polylactic acid (PLA) [28], polypropylene (PP) [29], cellulose [30]….

3.3.2.3 Group III: The TOT Smectite Group

In this group the layer charge varies from 0.2 to 0.6 per half unit cell. The morphology of TOT planar layers of smectites is 2D, like that of "smectic" liquid crystals: both names come from the Greek *σμηκτικος*, whose initial meaning is "cleaning earth". Smectites are also known as "swelling clays" because of their behavior in water. Montmorillonite (Mt) which is the most widely used in nanocomposites and in particular as filler in CPN, belongs to this group. Mt is the major component of the commercial bentonites. Hectorite is a dioctahedral smectite whose octahedral layers contain Mg^{2+} ions partly substituted with Li^{+}, and Laponite® is a trade name for a variety of synthetic hectorites. Saponite is also a trioctahedral smectite with Mg^{2+} in the O sheets, but the substitution in this case is observed in the tetrahedral sheet (Al^{3+} for Si^{4+}). Beidellite is a dioctahedral smectite with Al^{3+} in the O sheet, and there are many other minerals containing other cations, such as the iron-containing nontronite. Smectites are particularly important in the nanocomposites technology, and the intercalation properties of clay minerals (detailed in Sect. 3.6) have been mostly assessed on this group.

3.3.2.4 Group IV: The TOT Vermiculite Group

These TOT phyllosilicates have a more limited swelling ability as compared to the smectites group. This is due to their higher layers charge which varies from 0.6 to 0.9 per half unit cell. The most frequent vermiculite species are trioctahedral.

3.3.2.5 Group V: The TOT True (Flexible) Micas and Brittle Micas Group

For these TOT phyllosilicates, the charge of the layers is higher than the charge of the vermiculite group and varies from 0.9 to 2 per half unit cell for these two micas groups. The most common mica, i.e. *illite* is subject of controversy in the literature, considered either as a species of the true mica group (lying at the borderline with vermiculite as regards the degree of substitution) or as a separate group [31–33]. Illite is thought to be a mineral derived from smectite dehydration, progressing from montmorillonite to beidellite to illite [34]. This probably explains the occurrence in nature of interstratified smectite-illite layers presented further (cf. group VII).

3.3.2.6 Group VI: The TOT Chlorite Group

This group is currently considered as belonging to TOT phyllosilicates [24, 35], although it has a rather particular structure: the TOT layers, bearing a net negative charge, alternate with a single octahedral sheet bearing a positive charge in the

interlayer space. In other words, instead of isolated compensating cations in the interlayer, one has a continuous, polymerized sheet similar to the octahedral sheets already defined in Fig. 3.3 and isomorphous to brucite $Mg(OH)_2$ or gibbsite. Yet alternatively, chlorites could be viewed as regular interstratifications (see following paragraph) of cationic and anionic clay mineral layers. Trioctahedral chlorites are the most common where both the TOT and the interlayer sheet are trioctahedral, but other combinations also exist [24].

3.3.2.7 Group VII: The Interstratified Clay Minerals Group

The term of *interstratified* mineral is used to designate a lamellar material where different types of layers may be found in the stacking. It is a common phenomenon which may be considered as an intergrowth of different types of layers along the ***c*** axis (i.e. along the stacking direction). In fact, different combinations occur in nature between all the previous TO and/or TOT groups, in a regular or irregular manner, leading to different kinds of more complex layer types. For example irregular illite–smectite (I–S) are often encountered in mineralogy, where the particles contain variable proportions of swelling and non-swelling interlayers [36]; one also finds kaolinite-smectite (K–S) systems which consist of an alternating irregular layer sequence of kaolinite (TO) layers with smectite (TOT) layers. These combinations are called irregular interstratified clay minerals. However, when the succession of different layers occurs in a regular manner, a specific name is generally attributed to this interstratified stacked sequence [37] as for example rectorite which consists of a regular ordered succession of dioctahedral smectite and illite layers and may be symbolized as I–S-I–S.

It should be noticed that a 'filling interstratification' occurs when the smectite particles contain interlayers of different thicknesses due to different degrees of cations hydration (one water layer, two water layers… [38]). As will be seen in more detail in Sect. 3.5.4, the interlayers then have different thicknesses. This filling interstratification should not be confused with the above mentioned structural interstratification of mixed layers systems. In some cases, interstratified phases [39–41] may be observed with alternance of zero, one, two or three water pseudo-layers between the TOT layers (strata).

3.3.2.8 Group VIII: The TOT Sepiolite and Palygorskite Group

This TOT group shows a layer-fibrous structure. In opposition to all the previously mentioned groups which have continuous tetrahedral and octahedral sheets, this group has a discontinuous octahedral sheet between 2D tetrahedral sheets that are continuous, but exhibit regular inversions of tetrahedron orientation along one crystallographic direction (*b*). In fact lath-like fragments of TOT structures extend along the *c* axis, being connected by siloxane bridges (Fig. 3.4).

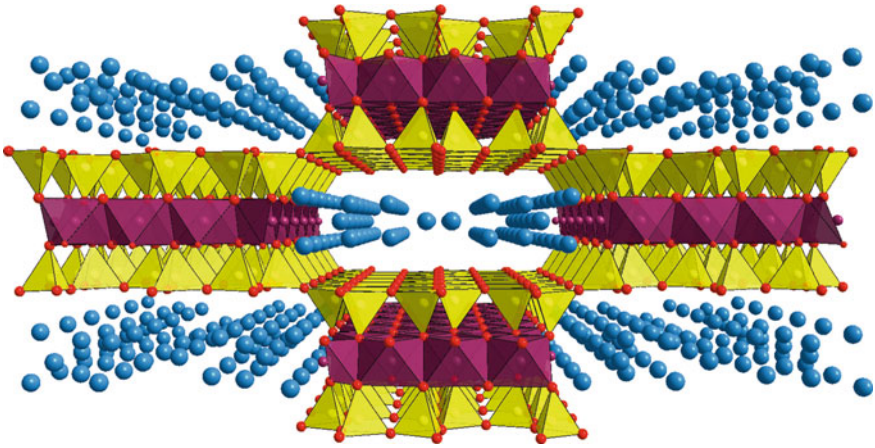

Fig. 3.4 Sepiolite and Palygorskite structures

As can be seen in the figure, this results in the existence of linear channels filled with compensating cations and water molecules. The two representative species are trioctahedral sepiolite and dioctahedral palygorskite, which also differ by their unit cell dimension, larger for sepiolite than for palygorskite, leading to larger channels. A recent study showed that intermediate compositions exist between these two species [42]. The name "attapulgite" which was given by de Lapparent [43] to a clay mineral discovered in fullers'earth from Attapulgus in USA, has sometimes been used as synonymous with palygorskite and is still largely used in industry. Since connections in the direction perpendicular to the layers are assured in part by covalent bonds (Si-O-Si), minerals of this group cannot present the phenomenon of swelling. Despite the scarce occurrence of commercial deposits and the absence of swelling properties, sepiolites are the most recently used fillers in CPN. Sepiolite-based biopolymers nanocomposites are also drawing increased attention because their particular morphology allows obtaining nanocomposites with interesting properties [44].

3.3.2.9 Group IX: The TO Allophane and Imogolite Group

These alumino-silicates belong to the TO group at least as regards short-range order and are frequently found together in soils derived from volcanic ash. Both are very poorly crystalline minerals, being X-ray amorphous. Allophane should actually be considered as a group since its composition is highly variable. The allophane structure remains somewhat hypothetical but it is known to consist in fibrous tubes which are formed by "curling up" of the layers to form 3–5 nm rings. The structure of imogolite has been originally proposed by Cradwick et al. [45] and consists in 2 nm aluminosilicate tubes which extend to a few μm in length;

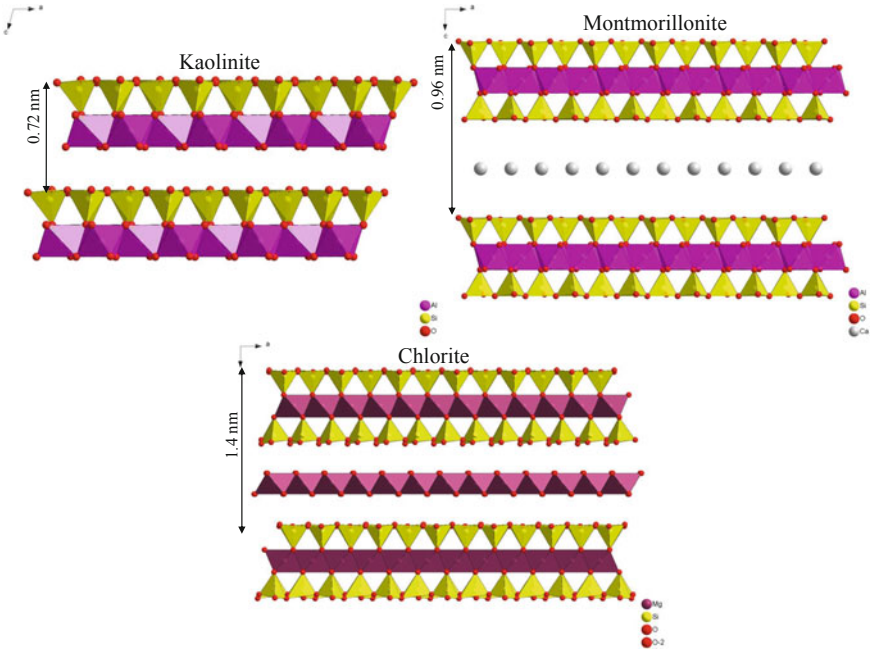

Fig. 3.5 Main phyllosilicates groups with their basal distances (d_{001}) as a recognition criterion

they exhibit an empty internal space diameter of 1 nm. In fact, these minerals are natural nanotubes and if they have not been the object of very much research in nanotechnology, it is only because the word "nanotubes" has been coined for another category of materials (carbon nanotubes). Recently, this group of minerals has attracted renewed interest as it has been shown that imogolite-like materials can be synthesized in large quantities [46], and double walled Al–Ge imogolite-like nanotubes have been described. It is hoped that they could constitute a cheaper alternative to carbon nanotubes in some application [47].

3.3.3 Basal Distance as a Recognition Criterion

The previously described groups can be more or less recognized using their basal distances (d_{001}) as a criterion (Fig. 3.5), a rough method that is often used due to its ease of implementation. Caution is in order however in interpreting the results.

The TO groups are characterized by a basal distance of about 0.7 nm for kaolinite. Halloysite is a hydrated kaolinite where water molecules form a single layer in the interlayer space. The thickness of such a "water layer", roughly equivalent to the size of a water molecule, is a little under 0.3 nm so that halloysite

has a d_{001} of (0.7 + 0.3 =) 1.0 nm. As regards allophane and imogolite, they are poorly crystalline materials and have rather broad and weak XRD peaks, at about 0.3 nm for allophane.

The TOT groups exhibit basal distances of 1 and 1.4 nm for the mica and chlorite groups respectively. For the sepiolite and palygorskite group the basal distance is 1.2 nm. In the case of smectites the basal distances are variable according to the hydration state. The most typical value is a little over 1.2 nm corresponding to one water layer between the clay mineral layers but the observed value depends on several factors, (i) the nature of the interlayer cation which can have a higher or lower affinity for water; (ii) the water activity, i.e. the relative water pressure and (iii) the pretreatment to which the sample has been submitted. It is important to be careful in interpreting X-ray diffractograms of a clay mineral sample: a d_{001} peak at 1.0 nm does not necessarily indicate the presence of mica, but might correspond to a fully dehydrated smectite. In the latter case, equilibration in an atmosphere with high relative water pressure would result in an increase of d_{001}, while a mica sample would not be affected.

For the interstratified groups the situation is more complex, except for regular interstratified layers where the high distance observed corresponds to the sum of the layer thicknesses in the repeating unit.

3.4 Variable Geometric Organization at Different Scales

The organization of native clay minerals can be represented by a simple scheme showing three successive levels at different scales, aggregates, particles and layers in decreasing order of size [15, 35]. These three levels of organization may also be identified when the clay minerals are dispersed in a solvent (water or other polar solvents): in that case they form pastes, then gels, then dispersions upon addition of increased amounts of solvent to the dry solid.

3.4.1 Organization from the Millimeter to the Nanometer Scale

At the macroscopic level, clay minerals are structured as millimetric-size aggregates built from a number of flat micrometer size particles sometimes called *platelets* (the term "tactoids" which is sometimes used should be discouraged). "Aggregation" used in opposition to "dispersion" should be used to designate the organisation of the clay mineral particles at the macroscopic level (micrometer to millimeter scale). The aspect ratio (average ratio of the width to the thickness of the particles) ranges from about 5–30 for smectites, but might exceed 100 when clay mineral layers are completely separated (see below).

In water dispersion, particles and even single layers can be associated in different ways depending on solution conditions, especially on the pH value and ionic

strength. Individual platelets may aggregate in different geometries. Face-to-face aggregation is the most frequent arrangement, but edge-to-edge and edge-to-face also occur. Extended edge-to-face agglomerates are often called "cardhouse" structures. This organization of the clay minerals is important for the understanding of their swelling and rheological properties.

Many factors can induce a strong tendency of clay mineral particles to aggregate. A high concentration of clay mineral particles will of course favor aggregation. Other experimental parameters characteristic of the dispersing liquid phase are the concentration of ionized salts which is expressed as the ionic strength, or the presence of surfactants and organic polymers. The nature of the compensating cations is another parameter of paramount importance. Cations with small radius such as Li^+ are strongly hydrated and known to induce the dispersion of the aggregates into individual nanoparticles. The aggregation of clay mineral particles is also linked to other factors characteristic of the clay mineral structure (and thus of the nature of the solid phase) such as the charge heterogeneity or the redox state of iron (Fe^{2+} or Fe^{3+}).

Extensive aggregation may result in the visual observation of flocculation (or coagulation; both terms are synonymous). Flocculation may be followed by sedimentation, or remain at the level of a stable dispersion.

Vigorous mechanical agitation of the system is generally needed to increase the dispersion of a clay mineral/water system, even in conditions (such as low clay mineral concentration) when dispersion is favored. Several other techniques are also used to reach the final dispersion state such as ultrasonification.

3.4.2 Organization at the Nanometric Scale

The individual particles which constitute the units of organization at the micrometric scale are stackings of a limited number of the layers that constitute the basic elements of organization in the crystallographic description (Sects. 3.3.1 and 3.3.2 above). A particle may be composed of as little as 2–5 stacked layers. This number can be higher depending on the environmental conditions (pressure, temperature, pH and ionic strength of the dispersion medium) and on the considered clay mineral. The reader will recall that layer stacking occurs along the crystallographic *c* axis giving rise to periodicity in this direction. It must be mentioned that successive layers in the stacking (i.e., in the same particle) may be differently oriented in the *a* and *b* directions, a state called "turbostratic". This is another consequence of the strong bonding anisotropy in clay minerals.

The separation of individual layers from the stacking is not an all-or-nothing situation. It has already been mentioned that interlayer spaces between the planar faces of two adjacent layers may contain in addition to the compensating cations variable amounts of intercalated water molecules according to water activity. In aqueous dispersion, many more water molecules enter the interlayer which necessarily leads to increasing separation of two successive layers. As long as

there is a significant interaction between two layers with some crystallographic orientation maintained, this separation is called *delamination*. At some point, no further interaction occurs between the delaminated units (isolated layers or stackings of a few layers), which become independently mobile in the liquid phase. The phenomenon is then called *exfoliation* [35, 48]. Even if a large degree of delamination is obtained in a dilute clay mineral dispersion, drying will usually be accompanied by a strong tendency to restacking.

3.4.3 *Effect of the Organization State on the Available Surface Area*

It is easy to calculate the specific surface area (SSA) of a fully delaminated clay mineral (consisting in individual layers). The exact result will depend somewhat on the lateral size extension of the layers and on the layer composition, but theoretical values in the order of 700–800 m^2/g are typically obtained for TOT clay minerals. These should be considered as the maximum value that can be obtained if the clay mineral layers retain their structural integrity.

Experimentally measured values of the SSA (usually by low temperature N_2 isotherms adsorption on dried powder samples) are considerably lower, typically by an order of magnitude [49]. This is because the N_2 molecules used as probes cannot access the interlayer spaces, but only the external surface of the individual platelets. There is then an obvious relationship between the observed SSA and the degree of stacking/delamination of the clay mineral layers. For instance, if all the particles consisted of 2-layer stackings, half of the basal layer surfaces would be unavailable for N_2 physisorption, and neglecting again the lateral surface, the SSA would be reduced by a factor of 2 with respect to its maximum value. In the same way, the SSA values measured for dried Mt particle would correspond to stackings of a few tens of layers. This reasoning is oversimplified however and due to structural defects and cracks, the observed experimental value could be higher, up to about 100 m^2/g.

Compared to Mt and kaolinite, sepiolite and palygorskite (attapulgite) have a particular fibrous morphology with the occurrence of channels accessible to N_2 molecules: the 3D connected structure of the layers prevents them from collapsing upon dehydration and the channels remain open to the N_2 molecules. Among the phyllosilicates, sepiolites have the highest BET surface area as it can reach about 300 m^2/g, and this explains why they are often used as industrial adsorbents.

The nitrogen SSA can then provide information on the stacking state of clay mineral layers into platelets. It must of course be understood that what will be estimated is the stacking in the dry clay mineral samples that are used for measurements. The stacking of the same clay mineral dispersed in a solvent may be less extensive, as the necessary drying step will cause some restacking of separate platelets.

3.5 Important Physico-Chemical Properties of Phyllosilicates

Surface area, porosity and cation exchange capacity (CEC) are among the most relevant properties of clay minerals. The first two properties depend on the accessible surface deduced from the geometric organisation as described above. If one wants to understand the reactivity of clay minerals, the chemical heterogeneity of their exposed surfaces should also be examined. These parameters will be successively discussed in Sects. 3.5.1–3.5.4 below.

3.5.1 Surface Area

We have had a first look at specific surface area (SSA) in Sect. 3.4.3. Phyllosilicates can be roughly classified into three groups on the basis of their typical SSA values. The first group presenting very low SSA values (less than 10 m^2/g) includes kaolinite; the second group includes montmorillonites and vermiculites, with SSA values between 10 and 150 m^2/g; and finally the last group including illite and sepiolite presents SSA values higher than 150 m^2/g. However the nature of the clay mineral does not allow more than an order of magnitude prediction of the SSA since this value depends on such factors as the nature of the exchangeable cations, the particle size, the presence of cracks and other defects, and even the drying conditions. For example Laponite can reach SSA values as high as about 400 m^2/g which would correspond to an average of two layers per particle; and for kaolinites, values spanning a range from 30 to a value as low as 3 m^2/g can be obtained depending on the degree of organization [49].

The above discussion referred to experimental results obtained from low-temperature nitrogen physisorption, which is the most common characterization technique applied to solid materials. It can provide a quantitative measurement of the surface exposed to the gas. This is most commonly estimated by applying the BET treatment (Brunauer-Emmet-Teller) to the physisorption data at relatively low relative N_2 pressures ($P/P^\circ = 0–0.4$). As we have explained, this method will give access only to the external surface of the platelets. The total surface area (maximum theoretical values) is the sum of the external and internal surface area (i.e., the part corresponding to surfaces inaccessible to gaseous N_2 molecules) [50].

The internal surface corresponds to the basal surface of the layers that are "stuck" together within a secondary particle. While invisible to N_2, it can be made available to the adsorption of other molecules that have the power to prop the layers apart. One of the best-known of such molecules is ethylene glycol monoethyl ether (EGME) (glycerol may also work in the same way). EGME molecules have a strong tendency to form a single dense layer on each basal plane, where each molecule occupies a space of 0.44 nm^2. In other words EGME forms a bilayer in the interlayer space of clay minerals (one monolayer on each of the basal planes that limit the interlayer), and simple geometrical modelling shows that this

should manifest as a XRD basal distance at 1.77 nm; therefore adsorption is easy to check, and since the density of the EGME monolayers is known the total surface area can be estimated from the adsorbed amount. Historically, EGME adsorption [51] was among the first classical methods used for internal surface area determination. Unsurprisingly, the view of EGME adsorption presented above is somewhat idealized. More careful studies have shown that its retention depends on the type of compensating cation and on the layer charge density [52]. In practice, this method is still useful, but mostly to provide semi-quantitative comparisons or indicate tendencies in series of swelling clay mineral samples [53].

Another molecule that can be used in the same way as EGME because it also induces swelling is methylene blue (MB), used in the laboratory for "MB-titration" [54]. Note that there also exists a very rough version of this method, mostly applied in the field, and called the "MB-spot", where the amount of swelling clay minerals in a sample is evaluated from the intensity of a blue spot due to MB adsorption.

Of course many other molecules will adsorb on clay minerals, but in many cases this will be due to chemical interactions with specific surface sites (chemisorption). Water for example will distinguish between more or less hydrophilic surface groups and cannot be readily used for total surface measurements.

3.5.2 Porosity

We have already mentioned cases such as sepiolite where the clay mineral structure encloses empty pores of well-defined shapes and sizes. It is of course a very general problem in inorganic materials characterization to determine the "porous volume" and the pore size distribution. According to the IUPAC recommendations, the following terms should be used: micropores (for pore diameter <2 nm), mesopores ($2\ \text{nm} \leq \text{diameter} \leq 40$ nm) and macropores (diameter ≥ 40 nm). Except for the special case of sepiolites, micropores will be found in clay minerals only when cracks are present, or when special treatments such as "Al pillaring" are used to prop the layers apart without filling the interlayers. Mesopores on the other hand will always be formed, at least between different particles (interparticle mesopores) with geometries that depend on the aggregation mode of individual platelets. Thus, lenticular pores are often observed on TEM images of natural clay minerals. These pores can be open and accessible, or closed. They depend on the chemistry of the clay mineral layer and particularly on the type of exchangeable cation, but also on the experimental conditions of sample preparation such as air- or freeze-drying [55].

While microscopy is satisfactory in providing direct visualisation, it does not constitute a practical method for systematic pore size characterization. As the reader probably knows, it is much more customary to evaluate pore sizes from the same technique that was used for SSA measurement, namely, N_2 physisorption. In fact, a single nitrogen adsorption isotherm contains information on condensation in the micropores, on the exposed external surface area, and in the mesopores. The detailed analysis of adsorption isotherms has been the object of much work which

is well described in the literature [56, 57]. A critical comparison of the many techniques of porosity characterization, may be found in the monograph by Rouquerol et al. [58]. One of the most widely used treatments is the BJH (Barclay-Joyner-Halenda) method based on Kelvin's equation of capillary condensation which relates the equivalent pore size and the relative pressure of condensation. This treatment will provide a distribution of porous volume as a function of mesopores size, but some degree of training is necessary to evaluate the significance of the results obtained.

For the measurement of macroporous volumes, the main technique has long been mercury intrusion. It is not without problems of its own since mercury is probably able to deform the geometry of the smaller pores during their invasion [59].

3.5.3 Cation Exchange Capacity

We have explained in Sect. 3.3.1 why most clay structures must retain a significant number of exchangeable cations to maintain electroneutrality. The amount of cations retained is a direct consequence of the stoichiometric layers composition and therefore characteristic of the considered clay mineral. The cation exchange capacity (CEC) is simply defined as the number of cationic charges retained by a fixed mass of the clay mineral sample, generally either 1 or 100 g. Therefore it is commonly expressed as (meq/g) or (meq/100 g), where "meq" stands for "milliequivalents". It can be evaluated by different standardized methods listed in Ref. [60]. Most of these rely on the phenomenon of ion exchange from aqueous solutions, and necessitate the complete replacement of the initial exchangeable cations by added 'index' or displacing cations which ideally (i) should not be present initially in the sample, (ii) should have a high affinity for the clay mineral phase so that the replacement of the initial cations is quantitative. For instance, little-hydrated cations such as Cs^+, NH_4^+ and Sr^{2+} are often used to displace the original cations but the best displacing cations are not easy to predict. Usually for smectites, there is a preference for larger inorganic cations over the smaller ones, and for cations with higher valence. In dioctahedral smectites with beidellitic character, the tetrahedral substitutions which induce the CEC have been estimated through an exchange of the original cations by NH_4^+, followed by the IR observation of the resulting ammonium-saturated clay minerals [61]. Copper-polyamine complexes (e.g. $[Cu(EDA)_3]^{2+}$ where (EDA) is ethylenediamine) also used as index cations, show some advantages (like irreversible exchange…) in comparison to other classical methods and may be assessed in the laboratory by different methods (volumetric or photometric titration…) [62, 63]. In general, it is difficult to quantitatively measure the composition of the solid sample after ion exchange, and it will be easier to evaluate the amount of exchanged cations from the depletion in the liquid phase.

Organic cations such as methylene blue (MB) are widely used for a rough estimation of the amount of swelling clay minerals in pure samples, but this may lead to confusion as the MB method is also used for the estimation of total surface

area (see above). The CEC can also be determined by XRD of the clay mineral after exchange with alkylammonium ions [64], but this method usually leads to underestimate the CEC value by 10–20 %.

In general, CEC values can be measured empirically not only for pure minerals but also for complex mixtures and this is indeed done e.g. by soil scientists. The additives used in nanocomposite synthesis on the other hand are generally composed of relatively pure clay minerals. The CEC will mostly be due to the smectite contents, and the layer charge of smectites can be deduced from the chemical structural formula. Typical CEC values are 80–120 meq/100 g for smectites, 150 meq/100 g for vermiculites, 3–15 meq/100 g for kaolinites, 20–30 meq/100g for palygorskite, and 10–40 meq/100 g for the "clay nanotubes" allophane and imogolite.

The CEC is an important parameter of clay minerals because it is the chief determiner of adsorption by electrostatic interaction. It represents the maximum amount of cations that can be retained electrostatically by the clay mineral lattice. Electrostatic adsorption is of course first and foremost manifested in cation exchange equilibria, e.g. the exchange of the originally present sodium cations by index cesium cations, that we have previously mentioned, would be denoted by the reaction scheme:

$$Na^{+}_{clay} + Cs^{+}_{aq} = Cs^{+}_{clay} + Na^{+}_{aq}$$

(in this equation the subscripts "aq" and "clay" refer to the aqueous solution and solid clay mineral phases respectively).

Exchange reactions can be treated thermodynamically like any other chemical reactions, and in particular equilibrium constants (K_{eq}) can be defined for them.

Cation exchange reactions show interesting selectivities depending on the ion size, its hydration state, etc., as already hinted earlier. The nature of the cations involved is not sufficient to predict exchange equilibria; what matters is the interaction between the cations and the matrix. For instance, potassium ions, whose radius exactly fits the size of the ditrigonal cavities in the tetrahedral sheets at the surface of illite and micas, are rather selectively retained.

Obviously the existence of a CEC can play an important role in the interaction with polymers. The presence of positively ionized groups on the polymer is a favorable factor for adsorption on smectites since the electrostatic interaction with negatively charged layers will provide a driving force for polymer retention. However in the case of bulky organic molecules, adsorption is more complicated than a simple ion exchange and usually falls into the category of intercalation, which will be discussed later (Sect. 3.6).

While the CEC is a defining parameter of a clay mineral, it can actually be modified by applying a rather simple procedure in which clay minerals are first exchanged with small cations (generally Li^{+}) and heated between 200 and 300 °C. This thermal treatment leads to an (almost) irreversible migration of the small cations into vacant positions of the octahedral sheets (if any). Any migrated cation will correspondingly decrease the CEC: this is called the Hofmann-Klemen or "HK" effect [65].

3.5.4 Swelling and Rheology

Rheology is important to better control clay mineral nanocomposites synthesis and also for many of their applications. Therefore it is important to consider the rheological properties of raw clay minerals in the present chapter, especially in water dispersions.

One of the particularities of clay-based materials, actually, is that a continuous variation can be observed starting from completely dehydrated clay minerals (water content of the system = 0 %) and going to highly diluted aqueous dispersions (water content of the system close to 100 %).

When progressively adding water to a dehydrated clay mineral, the first phenomenon one encounters is swelling. This is typical enough of smectites and has provided their alternate name of "swelling clays", and we have already mentioned the phenomenon in Sects. 3.3.3 and 3.4.2. To recall it briefly, the first water molecules form discrete layers in the interlayer space, and are included in the crystallographic periodicity of the clay mineral. Swelling can thus be described at the molecular level, but it has a macroscopic counterpart: a large increase in volume upon water addition as compared to the dry solid, with the progressive formation of gel-like phases. At the same time, the interparticle porosity is starting to fill with water. To give an order of magnitude, the gel volume may reach values of 25–30 mL per 10 g of clay mineral [66]. While the first steps of swelling are discrete intercalation of crystallographically ordered water pseudo-layers and manifest as discontinuous jumps of the d_{001} spacing [67], when more water is added, swelling turns into a continuous phenomenon (osmotic swelling). The "osmotic transition" (OT) corresponds to the transition from a hydrated powder to a paste. The clay mineral/water system remains in the form of a gel up to rather high water contents, superior to 90 weight % of water. It still appears as a gel when containing amounts of clay mineral of the order of 10 % for Mt, and as low as 3 % for Laponite. Upon further water addition, another threshold is observed: the sol-gel transition (SGT), where aggregates are separated from each other. Finally, in even more dilute dispersions (about 3 % for Mt), a local osmotic transition (LOT) happens where individual particles are desolidarized from each other [68]. An intermediate organization of smectite dispersions as nematic liquid crystals can sometimes be observed in the gel region [69, 70].

Most clay mineral/water systems will go through the same succession of stages described above, but there are some quantitative and qualitative differences. The layer charge density and nature of the compensating cations are important: for example, fully Na^+-exchanged montmorillonites can swell extensively. In kaolinite minerals, when water is added, layers become free to slide alongside each other so that the morphology of the stacking goes from "columnar" to "zigzag".

These changes in organization of water/clay mineral systems translate into a complex rheological behavior [38]. At low smectite concentrations dispersions with almost Newtonian properties are observed, changing into a Bingham plastic behavior at higher clay mineral concentrations. The rheology of clay mineral

dispersions is a classical subject in colloid science and data on these systems are used to test models of solid/solute interactions. A more detailed treatment of clay mineral dispersions rheology is presented in Ref. [35].

3.6 Intercalation and Other Mechanisms of Clay Interface Reactivity

Intercalation deserves a paragraph of its own because this phenomenon is highly typical of layered materials. In fact, it is the epitome of soft chemistry ("chimie douce") reactions: in intercalation reactions, the layers are pushed apart in gentle conditions, giving very conspicuous increases of one crystallographic parameter (**c** in most clay minerals) while the other two are unchanged because each individual layer remains intact. Another way to view this phenomenon is to consider that the intercalating species build their own customized porosity by spreading the layers apart. This is in contrast with solids having 3D connected porous networks such as zeolites and mesoporous silicas where the pore size is fixed. One common point however is confinement: species in the interlayer space will have very specific local chemical environment, and orientation, which may affect their reactivity. The porous network, or the interlayer space, may actually be considered as a nanoreactor allowing specific influences such as specific reaction catalysis.

Intercalation in clay minerals is a vast research domain. It can involve both inorganic and organic species and can occur from vapor, solutions, polymer melts or in the solid state (from solid mixtures of the clay mineral and the intercalating species). The latter two procedures may be considered as belonging to "green" chemistry, since they avoid the use of polluting organic solvent.

It should be obvious then that intercalation phenomena are of primordial importance when studying clay mineral/polymers reactivity. However intercalation has an even broader scope and therefore we will briefly summarize the main types of intercalation reactions in clay minerals, before treating the case of non-intercalative adsorption. A general question may be asked: what is the driving force for intercalation? In other words, what is the initial intercalation mechanism? Indeed, a given species will enter the interlayer region only if it has a favorable interaction either with something that is already there, or with the basal surface of the layers.

3.6.1 Intercalation by Ion Exchange

3.6.1.1 Ion Exchange in Organoclays

Modified bentonites called bentones are marketed in large amounts and they constitute an example of "organoclays". This is a category of composite materials in which the intercalation of organic molecules into clay minerals strongly

modifies their properties, for instance changing them from hydrophilic to hydrophobic. There are several recent reviews of the field of organoclays [71–73].

Bentones are in fact clay minerals intercalated with various alkylammonium cations, generally from water solutions, and in this case the main, or at least the initial adsorption mechanism is ion exchange. Alkylammonium-intercalated clay minerals are often stabilized by the formation of regular, quasi-crystalline arrangements of alkyl chains in the interlayer, which have been the object of a vast amount of early crystallographic work [71, 74, 75]. But the success of the crystallographic approach should not obscure the fact that other types of intercalated chain behaviors are possible. The advent of characterization techniques more sensitive to local order and mobility (such as solid-state NMR [76]) has revealed that liquid-like structures with high organizational disorder may be formed in some cases [77], especially when the interlayer density of alkylammonium chains is rather low.

3.6.1.2 "Pillaring" as an Irreversible Intercalation

In a particular type of ion exchange, the pristine compensating cations may be replaced by bulky inorganic polycations or "pillars". These species are known to form in well-defined conditions from solutions containing aluminum, iron, and a few other related metals. The best-known (and the first investigated) example is the so-called "Keggin" ion, whose formula is actually $[Al_{13}O_4(OH)_{24}(H_2O)_{12}]^{7+}$ but which is called "Al_{13}" for short. Here the driving force for intercalation is the favorable electrostatic interaction with the strongly charged polycations. However simple calcination of the "Al_{13}"-intercalated smectites will lead to a modification of the interaction between the pillars and the clay mineral layers, and to irreversible fixation of the pillars. The mechanism of this "pillaring" process is not completely understood [78] and may be different according to the type of smectite—in some cases it involves covalent bond formation [79]. Anyway, the resulting "pillared clays", sometimes abbreviated as PILC, are useful as adsorbents and catalysts [78, 80, 81] because the pillars maintain permanent pore opening without blocking the whole interlayer space, allowing access to the open microporosity (and also providing new surface sites with interesting reactivity on the pillars themselves [82]).

3.6.2 Intercalation by Coordinative Bond Formation (Ion–Dipole Interaction)

We have already discussed the progressive hydration of clay minerals and indicated that in its early stages it consists in the formation of discrete water layers (Sects. 3.4.2 and especially 3.5.4), and thus can be followed by XRD. We will mention it again here to address the question of the driving force for water intercalation.

In the interlayer space, water molecules interact most strongly with the compensating cations. The first molecules will enter the coordination sphere or

"inner sphere" of the cations, to form coordinative bonds. For instance, in the "2-water layers" Na^+-vermiculite, each sodium is surrounded by six water ligands in an octahedral geometry [83, 84]. Further water molecules will not be able to directly bind to the cation form, but they may still form H-bonds with ligands in the first sphere; the adsorption mechanism will then be called "outer-sphere adsorption".

This adsorption mechanism influences the chemical reactivity of the intercalated species. The cation-ligand interactions results in weakening the O–H bond and therefore in increased acidity. Indeed, intercalated water has a much higher acidity compared to free water in the solution, comparable to coordinated water in dissolved metal complexes.

Other polar molecules such as alcohols may interact with compensating cations in much the same way as water does. For instance, methanol, which contains a single hydroxyl group as opposed to the two OH of water, was studied in [85] and three types of interaction could be distinguished. The first methanol molecules to adsorb are linked by cation-dipole interaction (which is another way to look at coordinative bonds), the following ones form hydrogen bonds between each other in the interlayer space and even with the siloxanes of the basal clay mineral surface (and perhaps also with the residual inner sphere waters). Finally, a third population of methanol molecules simply fill up the interparticle porosity and are located out of the interlayers. Similar phenomena probably occur with other polar solvents.

3.6.3 Intercalation by Covalent Bond Formation

Intercalation can also occur by grafting reactions, i.e., by covalent bonds formation. The condensation of reactive groups such as alcohol functions with the hydroxyl groups of the octahedral sheets of kaolinite has been reported [86]. In that case electrostatic interactions do not play a significant role because neither the intercalated molecule nor the clay mineral surface bear electrostatic charges, and the intercalation mechanism implies the formation of C–O–Al covalent links. It is often observed that kaolinite layers have to be "pre-swollen" by molecules such as DMSO, which are not themselves grafted to the layers but probably intercalated by dipolar mechanisms.

3.6.4 Reactivity at Edge Surfaces: Chemical Anisotropy

3.6.4.1 Origins of Chemical Heterogeneity

The extreme anisotropy of clay minerals induces an important chemical heterogeneity of their surfaces. Even though the aspect ratio may be high, the clay mineral layers are of course not really infinitely extended in 2D and do not exceed

a fraction of micrometer in width. Their interruption along the a and b axis generates "edge surfaces" which are quite different from the basal layer surfaces.

The basal surfaces actually are chemically rather inert, chiefly exposing unreactive Si–O–Si (siloxane) groups [87]. Their interaction with the outside world is mediated by their permanent negative charge arising from isomorphous substitutions. They are called "permanent" because they depend only on the sheets composition and remain unmodified as long as the clay mineral structure is intact. In particular when contacted with an aqueous solution they are insensitive to the pH in a large range of values.

Quite different is the situation on the edges. The interruption of the lattice generates strongly reactive species whose valence is saturated, generally by reaction with water. For instance cutting the siloxane bridges in the tetrahedral sheets will not result in exposed dangling oxygens, or oxides, but rather in silanols: terminal Si–OH. In the same way, interrupting the octahedral sheets will cause the appearance of various groups, e.g. if the octahedral cations are Mg^{2+} one may get bridging $(Mg)_2OH$, but also terminal Mg-OH_2 where exposed Mg^{2+} complete their coordination sphere with one water molecule. It is essential to realize that these edge groups will have a variable charge induced by their amphoteric behavior and depending on the pH and ion strength of the solution, just as the surface groups of a divided oxide or hydroxide such as SiO_2 or $Mg(OH)_2$. For instance at very low pH, the Si–OH can react with a proton, giving Si-OH_2^+; the edges will thus develop a net positive charge. Conversely, at high pH they will be deprotonated by reaction with a hydroxide giving Si–O^- and the edges will develop a negative charge.

3.6.4.2 Chemical Heterogeneity and CEC Values

A first consequence is that the total CEC will be the sum of the permanent CEC (due to isomorphous lattice substitution) and a pH-dependent contribution due to the amphoterous reactions of edge groups. In smectites, the ratio of the edge/permanent surface charge is small but significant, between 10 and 20% to give an order of magnitude [88]. In other clay minerals such as kaolinite, the edge contribution is actually dominant in the CEC since (i) the isomorphic substitution in the layers, and thus the permanent charge, is negligible, and (ii) because of extensive layers stacking, the area of the edge surfaces exceeds that of the basal surfaces. However "excess CEC" only appears in basic solutions when the edges are negatively charged. In other conditions they may be positively charged, which contributes to explain the otherwise puzzling retention of anions by clay minerals.

As a second consequence, clay minerals have intrinsic acid–base properties and a clay mineral dispersion will behave as a buffer solution. For example, aqueous dispersions of smectites have pH values of about 7.5 (Mt) or up to 10 (Laponite).

3.6.4.3 Point of Zero Charge Versus Isoelectric Point

Like any other amphoteric surface, the edge surface of the clay mineral layers may be characterized by a "point of zero charge", PZC (or "point of zero net protonic charge", PZNPC). This is the pH for which positively charged groups will be present in exactly the same number as negatively charged ones and it is measured by simple protonic titration. For montmorillonite edge surfaces, the PZC has been reported to be 6.5 [89]. The PZC is often confused with the isoelectric point (IEP) which is obtained from electrophoretic mobility measurement. The IEP is defined as the pH at which a particle will not migrate in an applied electric field. Since electrophoretic migration depends on the overall charge of the particle (plus a few "solidary" water layers), a given clay mineral may well not have an IEP (because the particle will always keep a net negative charge due to a strong isomorphic substitution) while its edges have a perfectly well-defined PZC.

3.6.4.4 Chemical Heterogeneity and Specific Adsorption

The reactivity of clay mineral edges goes beyond the formation of pH-dependent surface charge and some edge groups are able to participate in H-bonding or to act as a ligand for Lewis acids, both of which abilities are very limited on the basal planes of the clay mineral layers. In other words there are specific adsorption sites on the edges, i.e., surface groups that are able to take part in adsorption mechanisms involving some degree of recognition of the adsorbed molecule. In opposition, electrostatic adsorption is non-specific in that it only depends on the electric charges of the partners. This phenomenon of specific adsorption is sometimes evident in gas adsorption at low temperature. The measurement of surface area as mentioned in Sect. 3.4.3 and 3.5.1 relies on the supposition of non-specific physisorption over the whole exposed geometric area. However careful measurements of Ar or N_2 adsorption isotherms at low pressure indicate that these species first adsorb on specific sites such as ditrigonal cavities next to Al substitutions [90] but also sites with high Brönsted acidity such as found on the edges, before covering the remaining surface by physisorption.

When dealing with the adsorption of polymers from a solution, the same kind of behavior may be predicted: the polymer molecules will probably react very differently (and adsorb along a different mechanism) on the edge surface and on the basal surface.

3.6.5 Putting It All Together: Clay Minerals/Biopolymers Interaction

In spite of the simplified picture presented above for organoclays formation from alkylammonium solutions, when organic molecules are contacted with smectites, the intercalation mechanism may be different from ion exchange. Neutral organic

molecules can form complexes with the interlayer cations in the same way as described in Sect. 3.6.2 for small polar molecules, and more generally they can displace water by establishing the same kind of interactions as it does with the clay mineral. This will concern molecules such as alcohols or aldehydes that are not easily protonated but can nevertheless be intercalated in the clay mineral interlayer [91]. Interactions such as H bonds, ion–dipole interaction, charge transfer and van der Waals forces may all play a role. Furthermore, in addition to the enthalpic contribution to the driving force for interaction (the sum of all the clay mineral/polymer interaction enthalpies), a significant entropic contribution should be present although its sign is not clear. Indeed, while the configuration entropy of the polymer will probably decrease upon immobilization in the interlayer (negative contribution), the intercalation of a single polymer molecule will displace many interlayer molecules, giving rise to a positive contribution.

Finally, nature is never as simple as we would wish. In practical cases, several different types of interaction might be at play in a single system, For instance, OH-functionalized alkylammonium cations may be intercalated chiefly by ion exchange, but nevertheless show a "tethering" effect of the OH groups onto the basal planes [92]. The exploration of clay mineral/polymers interaction mechanisms, and of their effect on polymer organization, is still in its infancy and will necessitate a concerted research effort combining many different experimental characterization techniques as well as the fast developing power of computational chemistry.

The existence of positive charges on the polymer chain (such as in polylysine) is certainly a factor leading to intercalation since it will provide a driving force (cation exchange). Many uncharged polymers are able to directly intercalate within pristine clay minerals provided they are sufficiently polar, especially hydrophilic polymers which include polyethylene oxides (PEO) [93] and polyesters such as PLA [94], but also polyvinyl alcohol (PVA [95]). Some polypeptides or proteins such as gelatin [96] may also be intercalated and more details will of course be provided in the following chapters of the present book.

Intercalation of non-ionic polymers from aqueous solutions can be enhanced if the starting clay mineral is delaminated. However, it is often observed that the basal distance of the resulting intercalates is not very large: the thickness of the interlayer space corresponds at most to one or two linear macromolecule chains.

In fact even the distinction between intercalation and edge adsorption may become blurred when long chains interact with clay minerals particles. Not only can polymers, including biopolymers, be adsorbed on the external surface of the particles as well as intercalated; the two possibilities may indeed coexist for a single chain, simultaneously showing amorphous loops in the interaggregates porosity with part of the polymer tails intercalated in the interlayer space. These intercalated tails may even exhibit more crystalline domains due to the effect of nanoconfinement as in the model of Vaia et al. [97]. More such studies are needed to understand the structure and mobility of adsorbed polymer chains.

Recent updates on clay minerals/polymers interaction was presented by Ruiz-Hitzky et al. [98] and by Lagaly [71], to whom we refer the interested reader for further details.

3.7 Synthetic Clay Minerals

Natural clays have a major advantage for large-scale industrial applications including composite materials manufacture: they are cheap, as they are found in easily exploited mineral deposits. However clays consist in mixtures of different minerals with variable contents of the clay minerals that are the active component useful for composite materials synthesis. Depending on the purity desired for a given application purification procedures may be needed to obtain well-crystallized clay minerals with controlled composition and properties, inducing additional costs. Furthermore it is an unfortunate fact of life that natural deposits become depleted by overexploitation, including some of those that were the source for original clay mineral types. There are good reasons then to develop methods of clay mineral synthesis from other materials. So far, synthetic clay minerals remain too expensive for all but the highest-value applications, although technically they can be used as raw materials for composites manufacture [99–101]. However economical parameters may change in the future, and at any rate de novo synthesis of clay minerals is useful for small-scale laboratory studies where researchers attempt to rationalize the effect of changes in clay minerals structural properties on the final properties of the nanocomposites.

This field has been the object of much effort from mineralogists and materials scientists and critical reviews have been published [102, 103]. Most often, synthetic clay minerals are crystallized in hydrothermal conditions (from 150 to 450 °C under pressures up to 1500 bar) from gel phases containing sources of the various composing elements (Si from colloidal amorphous silica or TEOS, Al from Al_2O_3, $Al(OH)_3$, or $NaAlO_2$, Na from the latter and/or from NaOH…). The duration of the synthesis has to be carefully controlled since the desired clay mineral may not be the thermodynamically stable product. A lot of empirical information and "recipes" are available. For instance, it is often helpful to work in a medium containing "mineralizing agents" such as the fluoride ion. Their exact role in clay minerals synthesis process is the object of much ongoing research.

Trioctahedral clay minerals are relatively easy to synthesize. Hectorite and saponite belong to this class with Mg^{2+} ions in the octahedral sheet; Mg oxides are then added to the starting materials. The first commercial synthetic clay mineral is called Laponite, and currently marketed by Rockwood Additives. It is in fact a synthetic hectorite with very small particle size (the particles are disks with a 30 nm diameter) which easily exfoliates and gives rise to colloidal dispersions and gels.

Dioctahedral clay minerals such as montmorillonite are more difficult to obtain synthetically, especially with a satisfying degree of crystalline order.

Organically modified natural clays or clay minerals (organoclays), as well as synthetic clay minerals, are also available commercially at relatively low cost at least for the former. They may be used with profit to facilitate access to the interlayers in polymer composite syntheses because they are "pre-swollen": the layers are already separated by the intercalation of monomeric, but sometimes rather bulky, organic species. The most common organic swelling agents are mixtures of long-chain alkylammonium ions. They constitute the basis of commercial organoclays which are sometimes manufactured in full-scale production units. A non-exhaustive list of commercial organoclays can be found in our recent review on the subject [73].

3.8 Clay Minerals as Fillers of Clay Polymer Nanocomposites

Among the different types of clay minerals, the 2:1 charged phyllosilicates belonging to the smectites family are the minerals most widely involved in the preparation of nano-biocomposites. Nature has not awaited us to create its own nano-biocomposites, actually.

The interaction of clay minerals with biopolymers takes place spontaneously in soils. As these silicates are abundant components of soils, they are often associated with different biopolymers, e.g, proteins, polysaccharides, fulvic and humic acids, and lignosulfonates [104]. The role of those naturally occurring clay-biopolymer systems is crucial in soil science because the stability and the biodegradation of these biopolymers are determined by the protective effect of the clay mineral on the polymer. Sodium-montmorillonite appears as the most interesting smectite clay for nano-biocomposite preparations, due to its tendency to swell in the presence of water (Sect. 3.5.4). This feature favors the exfoliation of the layer silicates, therefore facilitating the access of some biopolymers, at least the hydrophilic ones, to the interlayer space of the clay mineral. However, other clay minerals such as kaolinite and fibrous clay minerals such as sepiolite and palygorskite [105], can constitute the inorganic counterparts or inorganic partners associated to molecular or polymeric organic species, a subject investigated for a long time.

Considering classical industrial applications, the latter types of clay minerals have been largely employed in fields as different as cellulose-based paper fabrication that uses kaolinite as a filling and coating agent [106] or in the clarification of wine, vinegar and cider using fibrous clays (such as sepiolite) due to its strong tendency to associate proteins in dispersion [107].

In our time of "green" chemistry, clays are particularly attractive as starting materials to be used as fillers in the formulation of various products based on polymers matrices. They are not harmful to human health; indeed they may have curative properties and are sometimes used in pharmaceutical preparations. For instance the oral drug, sold in pharmacy under the trade name of 'Smecta™, [108] is a natural montmorillonite. Clays also benefit from a positive image in the opinion, which certainly facilitates their marketability.

Historically, the first reason to add nanoclay fillers to polymers was simply to reduce costs as compared to previously used fillers such as calcium carbonates. It took a long time before realizing that these cheap materials could also be smart materials. The first instance of a nanoclay hybrid material was probably the synthesis of a nylon 6-clay hybrid [109] which had excellent thermal and mechanical properties and was later commercialized by Toyota.

It has appeared many times that the addition of a few percent of clay minerals incorporated in CPN is enough to provide spectacular improvements as compared to the properties of the raw polymer, or to gain new properties not seen in the neat polymer alone. This kind of research is particularly developed in the field of elastomers. Several books, book chapters and other reviews have already been dedicated to the synthesis and properties of CPN [98, 110–116]. They show both the richness of the field and the huge potential for progress in our scientific understanding. The present book will fill a void by focusing on clays and clay minerals-biopolymers nanocomposites, where the opportunities are just as promising—and the open questions as challenging.

References

1. Marshall CE (1949) The colloid chemistry of silicates minerals. Cornell University Press, Ithaca
2. Eitel W (1954) The physical chemistry of silicates. University of Chicago Press, Chicago
3. Eitel W (1964–1976) Silicate science, vol I-VIII. Academic Press, New York
4. Iler RK (1955) The colloid chemistry of silica and silicates. Cornell University Press, New York
5. Iler RK (1979) The chemistry of silica. Solubility, polymerization, colloid and surface properties and biochemistry. Wiley, New York
6. Hauser EA (1955) Silicic science. D Van Nostrand Co, Inc., New York
7. Liebau F (1985) Structural chemistry of silicates. Structure, bonding, and classification. Springer, Heidelberg
8. Rives V (ed) (2001) Layered double hydroxides: present and future. Nova Science Publishers, New York
9. Duan X, Evans DG (eds) (2006) Layered double hydroxides. Springer, Heidelberg
10. Forano C, Hibino T, Leroux F, Taviot-Guého C (2006) Layered double hydroxides. In: Bergaya F, Theng BKG, Lagaly G (eds). Handbook of Clay Science. Developments of Clay Science, vol 1. Elsevier, Amsterdam, pp 1021–1096
11. Choy J-H, Choi S-J, Oh J-M, Park T (2007) Clay minerals and layered double hydroxides for novel biological applications. Appl Clay Sci 26:122–132
12. Veniale F (1992) Clay science, facts and perspectives, opening lecture. In: Paper presented at the proceedings of the Mediterranean clay meeting 1992, Lipari
13. Konta J (2000) Clay science at the threshold of the new millennium: a look at the history and present trends. Acta Universitatis Carolinae-Geologica 44:11
14. Bergaya F, Lagaly G, Beneke K (2006) History of clay science: a young discipline. In: Bergaya F, Theng BKG, Lagaly G (eds) Handbook of clay science. Developments of clay science, vol 1. Elsevier, Amsterdam, pp 1163–1181
15. Bergaya F, Lagaly G (2006) General introduction: clays, clay minerals and clay science. In: Bergaya F, Theng BKG, Lagaly G (eds) Handbook of clay science. Developments of clay science, vol 1. Elsevier, Amsterdam, pp 1–18

16. Moore DM, Reynolds RC Jr (1997) X-ray diffraction and the identification and analysis of clay minerals. Oxford University Press, Oxford
17. Stokes G (1851) On the effect of the internal friction of fluids on the motion of pendulums. Trans Camb Phil Soc 9:8–106
18. Carrado KA, Decarreau A, Petit S, Bergaya F, Lagaly G (2006) Synthetic clay minerals and purification of natural clays. In: Bergaya F, Theng BKG, Lagaly G (eds) Handbook of clay science. Developments of clay science, vol 1. Elsevier, Amsterdam, pp 1–18
19. Lagaly G, Beneke K, Weiss A (1975) Magadiite and H-magadiite. I. Sodium magadiite and some of its derivatives. Am Miner 60(7-8):642–649
20. Lagaly G, Beneke K, Weiss A (1975) Magadiite and H-magadiite. II. H-magadiite and its intercalation compounds. Am Miner 60(7–8):650–658
21. Almond GG, Harris RK, Franklin KR (1996) A ^{23}Na NMR study of hydrous layered silicates. J Mater Chem 6(5):843–847
22. Almond GG, Harris RK, Franklin KR (1997) A structural consideration of kanemite, octosilicate, magadiite and kenyaite. J Mater Chem 7(4):681–687
23. Apperley DC, Hudson MJ, Keene MTJ, Knowles JA (1995) Kanemite ($NaHSi_2O_5.3H_2O$) and its hydrogen-exchanged form. J Mater Chem 5(4):577–582
24. Brigatti F, Galan E, Theng BKG (2006) Structures and mineralogy of clay minerals. In: Bergaya F, Theng BKG, Lagaly G (eds) Handbook of clay science. Developments of clay science, vol 1. Elsevier, Amsterdam, pp 19–86
25. Löwenstein W (1954) The distribution of aluminium in the terahedra of silicates and aluminates. Am Miner 39:92–96
26. Gonzalez-Gallardo S, Jancik V, Delgado-Robles AA, Moya-Cabrera M (2011) Cyclic alumosiloxanes and alumosilicates: exemplifying the loewenstein rule at the molecular level. Inorg Chem 50(10):4226–4228
27. Tan S, Tincer T (2011) Preparation and characterization of polypropylene/serpentine. J Appl Polym Sci 121:846–854
28. Battegazzore D, Bocchini S, Frache A (2011) Crystallization kinetics of poly(lactic acid)-talc composites. Express Polym Lett 5(10):849–858
29. Fowlks AC, Narayan R (2010) The effect of maleated polylactic acid (PLA) as an interfacial modifier in PLA-Talc composites. J Appl Polym Sci 118(5):2810–2820
30. Cuba-Chiem LT, Huynh L, Ralston J, Beattie DA (2008) In situ particle film ATR FTIR spectroscopy of carboxymethyl cellulose adsorption on talc: binding mechanism, pH effects, and adsorption kinetics. Langmuir 24(15):8036–8044
31. Brindley GW, Brown G (1980) Crystal structure of clay minerals and their X ray identification. Mineralogical Society, London
32. Rieder M, Cavazzini G, D'Yakonov YS, Frank-Kamenetskii VA, Gottardi G, Guggenheim S, Koval PV, Muller G, Neiva AMR, Radoslovich EW, Robert J-L, Sassi FP, Takeda H, Weiss Z, Wones DR (1998) Nomenclature of the micas. Clays Clay Miner 46(5):486–495
33. Meunier A, Velde B (2004) Illite. Origins, evolution and metamorphism. Springer, Berlin
34. Brigatti MF, Guggenheim S (2002) Mica crystal chemistry and the influence of pressure, temperature, and solid solution on atomistic models. In: Mottana A, Sassi FP, Thompson JB, Guggenheim S (eds) Micas: crystal chemistry and metamorphic petrology. Mineralogical Society of America, Washington, pp 1–97
35. Bergaya F, Jaber M, Lambert JF (2011) Clays and clay minerals—Chapter 1. In: Galimberti M (ed) Rubber clay nanocomposites. Science, technology and application. Wiley, Chichester
36. Altaner S, Ylagan RF (1997) Comparison of structural models of mixed-layer illite/smectite and reaction mechanisms of smectite illitization. Clays Clay Miner 45(4):517–533
37. Bailey SW (1982) Nomenclature for regular interstratifications. Am Miner 67:394–398
38. Lagaly G (2006) Colloid clay science. In: Bergaya F, Theng BKG, Lagaly G (eds) Handbook of Clay Science. Developments of Clay Science, vol 1. Elsevier, Amsterdam, pp 141–246
39. Michot LJ, Bihannic I, Pelletier M, Rinnert E, Robert JL (2005) Hydration and swelling of synthetic Na-saponites: influence of layer charge. Am Mineral 90(1):166–172

40. Ferrage E, Lanson B, Sakharov BA, Drits VA (2005) Investigation of smectite hydration properties by modeling experimental X-ray diffraction patterns: Part I. Montmorillonite hydration properties. Am Miner 90(8–9):1356–1374
41. Ferrage E, Tournassat C, Rinnert E, Lanson B (2005) Influence of pH on the interlayer cationic composition and hydration state of Ca-montmorillonite: analytical chemistry, chemical modelling and XRD profile modelling study. Geochem Cosmochem Acta 69(11): 2797–2812
42. Garcia-Romero E, Suarez M (2010) On the chemical composition of sepiolite and palygorskite. Clays Clay Miner 58(1):1–20
43. de Lapparent J (1935) Sur un constituent essentiel des terres à foulon. Acad Sci 201: 481–483
44. Yang H, Peng Z, Zhou Y, Zhao F, Zhang J, Cao X, Hu Z (2011) Preparation and performances of a novel intelligent humidity control composite material. Energy Build 43(2–3):386–392
45. Cradwick PD, Wada K, Russell JD, Yoshinaga N, Masson CR, Farmer VC (1972) Imogolite, a hydrated aluminum silicate of tubular structure. Nature Phys Sci 240:187–199
46. Levard C, Rose J, Masion A, Doelsch E, Borschneck D, Olivi L, Dominici C, Grauby O, Woicik JC, Bottero JY (2008) Synthesis of large quantities of single-walled aluminogermanate nanotube. J Am Chem Soc 130(18):5862
47. Maillet P, Levard C, Larquet E, Mariet C, Spalla O, Menguy N, Masion A, Doelsch E, Rose J, Thill A (2010) Evidence of double-walled Al-Ge imogolite-like nanotubes. A cryo-TEM and SAXS investigation. J Am Chem Soc 132(4):1208–1218
48. Bergaya F, Lagaly G (2011) Intercalation processes of layered minerals—Chapter 7. In: Brigatti MF, Mottana A (eds). Layered mineral structure and their application in advanced technologies, vol 11. European Mineralogical Union Notes in Mineralogy
49. Aparicio P, Perez-Bernal JL, Galan E, Bello MA (2004) Kaolin fractal dimension. Comparison with other properties. Clay Miner 39(1):75–84
50. Annabi-Bergaya F, Cruz MI, Gatineau L, Fripiat JJ (1979) Adsorption of alcohols by smectites I. Distinction between internal and external surfaces. Clay Miner 14:249–258
51. Eltantawy IM, Arnold PW (1974) Ethylene glycol sorption by homoionic montmorillonites. J Soil Sci 25:99–110
52. Chiou CT, Rutherford DW (1997) Effects of exchanged cation and layer charge on the sorption of water and EGME vapors on montmorillonite clays. Clays Clay Miner 45:867–880
53. Tiller KG, Smith LH (1990) Limitations of EGME retention to estimate the surface area of soils. Aust J Soil Res 28:1–26
54. Yukselen Y, Kaya A (2008) Suitability of methylene blue test for surface area, cation exchange capacity and swell potential determination of clayey soils. Eng Geol 102:38–45
55. Bergaya F (1995) The meaning of surface area measurements of clays and pillared clays. J. Por. Mat. 2:91–96
56. Rouquerol J, Rodriguez-Reinoso F, Sing KSW, Unger KK (1994) Characterization of porous solids III. Proceedings of the IUPAC Symposium Elsevier Science, Amsterdam
57. Michot LJ, Villieras F (2006) Surface area and porosity. In: Bergaya F, Theng BKG, Lagaly G (eds) Handbook of Clay Science. Developments of Clay Science, vol 1. Elsevier, Amsterdam, pp 965–978
58. Rouquerol F, Rouquerol J, Sing K (1999) Adsorption by powders and porous solids. Principles, methodology and applications. Academic Press, San Diego
59. Julve D, Ramos J, Perez J, Menendez M (2011) Analysis of mercury porosimetry curves of precipitated silica, as an example of compressible porous solids. J Non-Cryst Sol 357(4): 1319–1327
60. Bergaya F, Lagaly G, Vayer M (2006) Cation and anion exchange. In: Bergaya F, Theng BKG, Lagaly G (eds) Handbook of Clay Science. Developments of Clay Science, vol 1. Elsevier, Amsterdam, pp 979–1001
61. Chourabi B, Fripiat JJ (1981) Determination of tetrahedral substitutions and interlayer surface heterogeneity from vibrational spectra of ammonium in smectites. Clays Clay Miner 29:260–268

62. Bergaya F, Vayer M (1997) CEC of clays: measurement by adsorption of a copper ethylenediamine complex. Appl Clay Sci 12(3):275–280
63. Ammann L, Bergaya F, Lagaly G (2005) Determination of the cation exchange capacity of clays with copper complexes revisited. Clay Min. 40(4):441–453
64. Lagaly G (1994) Layer charge determination by alkyl ammonium. In: Mermut AR (ed) Layer charge charactersitics of 2:1 silicate clay minerals. The Clay Minerals Society, Boulder, pp 2–46
65. Hofmann U, Klemen R (1950) Verlust der Austauschfähigkeit von Lithiumionen an Bentonit durch Erhitzung. Z Anorg Allg Chem 262:95–99
66. Christidis GE, Blum AE, Eberl DD (2006) Influence of layer charge and charge distribution of smectites on the flow behaviour and swelling of bentonites. Appl Clay Sci 34:125–138
67. Norrish K (1954) The swelling of montmorillonite. Disc. Faraday Soc. 18:120–134
68. Benna M, Kbir-Ariguib N, Clinard C, Bergaya F (2001) Static filtration of purified sodium bentonite clay suspensions. Effect of clay content. Appl Clay Sci 19:103–120
69. Michot LJ, Baravian C, Bihannic I, Maddi S, Moyne C, Duval JFL, Levitz P, Davidson P (2009) Sol-gel and isotropic/nematic transitions in aqueous suspensions of natural nontronite clay. Influence of particle anisotropy. 2. Gel structure and mechanical properties. Langmuir 25(1):127–139
70. Michot LJ, Bihannic I, Maddi S, Baravian C, Levitz P, Davidson P (2009) Sol-gel and isotropic/nematic transitions in aqueous suspensions of natural nontronite clay. Influence of particle anisotropy. 1. Features of the I/N Transition. Langmuir 24:3127–3139
71. Lagaly G, Ogawa M, Dekany I (2006) Clay mineral organic interaction. In: Bergaya F, Theng BKG, Lagaly G (eds) Handbook of Clay Science. Developments of Clay Science, vol 1. Elsevier, Amsterdam, pp 309–377
72. de Paiva LB, Morales AR, Valenzuela Diaz FR (2008) Organoclays: properties, preparation and applications. Appl Clay Sci 42(1–2):8–24
73. Bergaya F, Jaber M, Lambert JF (2011) Organophilic clay minerals—Chapter 2. In: Galimberti M (ed) Rubber clay nanocomposites. Science, technology and application. Wiley, Chichester
74. Lagaly G (1976) Kink-block and gauche-block structures of bimolecular films. Angewandte Chemie-International Edition in English 15(10):575–586
75. Lagaly G, Beneke K (1991) Intercalation and exchange reactions of clay minerals and non-clay layer compounds. Colloid Polym Sci 269:1198–1211
76. Wang L-Q, Liu J, Exarhos GJ, Flanigan KY, Bordia R (2000) Conformation heterogeneity and mobility of surfactant molecules in intercalated clay minerals studied by solid-state NMR. J Phys Chem B 104(13):2810–2816
77. Vaia RA, Teukolsky RK, Giannelis EP (1994) Interlayer structure and molecular environment of alkylammonium layered silicates. Chem Mater 6:1017–1022
78. Bergaya F, Aouad A, Mandalia T (2006) Pillared clays and clay minerals. In: Bergaya F, Theng BKG, Lagaly G (eds) Handbook of Clay Science. Developments of Clay Science, vol 1. Elsevier, Amsterdam, pp 393–421
79. Plee D, Borg F, Gatineau L, Fripiat JJ (1985) High-resolution solid-state aluminum-27 and silicon-29 nuclear magnetic resonance study of pillared clays. J Am Chem Soc 107: 2362–2369
80. Gil A, Gandía LM, Vicente MA (2000) Recent advances in the synthesis and catalytic applications of pillared clays. Catal Rev—Sci Eng 42:145–212
81. Gil A, Korili SA, Vicente MA (2008) Recent advances in the control and characterization of the porous structure of pillared clay catalysts. Catal Rev Sci Eng 50(2):153–221
82. Lambert JF, Poncelet G (1997) Acidity in pillared clays: origin and catalytic manifestations. Top Catal 4:43–56
83. Hougardy J, Stone WEE, Fripiat JJ (1976) NMR-study of adsorbed water.1. Molecular orientation and protonic motions in 2-layer hydrate of a Na vermiculite. J Chem Phys 64(9):3840–3852

84. Laperche V, Lambert JF, Prost R, Fripiat JJ (1989) High-resolution solid-state NMR of exchangeable cations in the interlayer surface of a swelling mica- Na-23, Cd-111, and Cs-133 vermiculites. J Phys Chem 94(25):8821–8831
85. Annabi-Bergaya F, Cruz MI, Gatineau L, Fripiat JJ (1979) Adsorption of alcohols by smectites III. Nature of the bonds. Clay Miner 14:225–237
86. Tunney JJ, Detellier C (1993) Interlamellar covalent grafting of organic units on kaolinite. Chem Mater 5(6):747–748
87. Bleam WE (1993) Atomic theory of phyllosilicates: quantum chemistry, statistical, mechanics, electrostatic theory, and crystal chemistry. Rev Geophys 31:51–73
88. Tournassat C, Neaman A, Villieras F, Bosbach D, Charlet L (2003) Nanomorphology of montmorillonite particles: estimation of the clay edge sorption site density at low pressure gas adsorption and AFM observations. Am Miner 88:1989–1995
89. Tombácz E, Szekeres M (2004) Surface charge heterogeneity of kaolinite in aqueous suspension in comparison with montmorillonite. Appl Clay Sci 34:105–124
90. Michot LJ, Villieras F (2002) Assessment of surface energetic heterogeneity of synthetic Na-saponites. The role of layer charge. Clay Min 37(1):39–57
91. Beall GW, Goss M (2005) Self-assembly of organic molecules on montmorillonite. Appl Clay Sci 27:179–186
92. Paul DR, Zeng QH, Yu AB, Lu GQ (2005) The interlayer swelling and molecular packing in organoclays. J Colloid Interface Sci 292:462–468
93. Aranda P, Ruiz-Hitzky E (1992) Poly(ethylene oxide) intercalation materials. Chem Mater 4(6):1395–1403
94. Krishnamachari P, Zhang J, Lou J, Yan J, Uitenham L (2009) Biodegradable poly(lactic acid)/clay nanocomposites by melt intercalation: a study of morphological, thermal, and mechanical properties. Int J Polym Anal Charact 4:336–350
95. Sengwa RJ, Sankhla S, Choudhary S (2009) Dielectric characterization of solution intercalation and melt intercalation poly(vinyl alcohol)-poly(vinyl pyrrolidone) blend-montmorillonite clay nanocomposite films. Indian J Pure Appl Phys 48(3):196–204
96. Fernandes FM, Ruiz AI, Darder M, Aranda P, Ruiz-Hitzky E (2009) Gelatin-clay bio-nanocomposites: structural and functional properties as advanced materials. J Nanosci Nanotechnol 9(1):221–229
97. Vaia RA, Ishii H, Giannelis EP (1993) Synthesis and properties of 2-dimensional nanostructures by direct intercalation of polymer melts in layered silicates. Chem Mater 6:1694–1696
98. Ruiz-Hitzky E, Darder M, Aranda P (2005) Functional biopolymer nanocomposites based on layered solids. J Mater Chem 15:3650–3662
99. Da Silva C, Haidar B, Vidal A, Miehé-Brendlé J, Le Dred R, Vidal L (2005) Preparation of EPDM/synthetic montmorillonite nanocomposites by direct compounding. J Mater Sci 40:1813–1815
100. Utracki LA, Sepehr M, Boccaleri E (2007) Synthetic, layered nanoparticles for polymeric nanocomposites WNCO. Polym Adv Technol 18(1):1–37
101. Sharma S, Komarneni S (2009) Synthesis and characterization of synthetic mica-bionanocomposites. Appl Clay Sci 42(3–4):553–558
102. Kloprogge JT, Komarneni S, Amonette JE (1999) Synthesis of smectites clay minerals: a critical review. Clays Clay Miner 57(5):529–554
103. Zhang D, Zhou C-H, Lin C-X, Tong D-S, Yu W-H (2010) Synthesis of clay minerals. Appl Clay Sci 50(1):1–11
104. Theng BKG (1979) Formation and properties of clay-polymer complexes. Elsevier, New York
105. Singer A, Huang PM (1989) Adsorption of humic acid by palygorskite and sepiolite. Clay Miner 24(3):561–564
106. Murray HH, Kogel JE (2005) Engineered clay products for the paper industry. Appl Clay Sci 29(3–4):199–206
107. Robertson RHS (1957) Sepiolite—a versatile raw material. Chem Ind 46:1492–1495

108. Yao-Zong Y, Shi-Rong L, Delvaux M (2004) Comparative efficacy of dioctahedral smectite (Smecta (R)) and a probiotic preparation in chronic functional diarrhoea. Digest Liver Dis 36(12):824–828
109. Usuki A, Kojima Y, Kawasumi M, Okada A, Fukushima Y, Kurauchi T, Kamigaito O (1993) Synthesis of nylon 6-clay hybrid. J Mater Res 8(5):1179–1184
110. Pinnavaia TJ, Beall GW (eds) (2001) Polymer-clay nanocomposites. Wiley, Chichester
111. Biswas M, Sinha Ray S (2001) Recent progress in synthesis and evaluation of polymer-montmorillonite nanocomposites. Adv Polym Sci 135:167–221
112. Sinha Ray S, Okamoto M (2003) Polymer/layered silicate nanocomposites: a review from preparation to processing. Prog Polym Sci 28:1539–1641
113. Sanchez C, Julian B, Belleville P, Popall M (2005) Applications of hybrid organic–inorganic nanocomposites. J Mater Chem 15:3559–3592
114. Chen B, Evans JRG, Greenwell HC, Boulet P, Coveney PV, Bowden AA, Whiting A (2007) A critical appraisal of polymer-clay nanocomposites. Chem Soc Rev 37:568–594
115. Carrado KA, Bergaya F (eds) (2007) Clay-based polymer nanocomposites (CPN). CMS workshop lectures series, vol 14. The Clay Minerals Society, Boulder
116. Ruiz-Hitzky E, Darder M, Aranda P, Ariga K (2010) Advances in biomimetic and nanostructured biohybrid materials. Adv Mater 22(3):323–336

Chapter 4
Polylactide/Clay Nano-Biocomposites

Masami Okamoto

Abstract Polymer/layered filler nano-composites (PLFNCs) offer remarkably improved mechanical and various other properties with low inorganic filler loading. The major development in this field has been carried out over last one and half decades. However we are far from the goal in terms of understanding the mechanisms of the enhancement effect in the nano-composites. Continued progress in nanoscale controlling, as well as an improved understanding of the physicochemical phenomena at the nanometer scale, have contributed to the rapid development of novel PLFNCs. This chapter presents recent advances in biodegradable polylactide (PLA)-based nano-composites with the primary focus of recent advances from basic science to technology.

4.1 Introduction

Increased importance of renewable resources for raw materials and recyclability or biodegradability of the material at the end of its useful life is demanding a shift from petroleum-based synthetics to agro-based materials in industry applications. Increased social awareness of environmental problems posed by the non-degradable, non-recyclable contents of products is forcing product manufacturers to enhance the biodegradable content, which is in favor of switching to biomaterials [1].

M. Okamoto (✉)
Advanced Polymeric Nanostructured Materials Engineering,
Graduate School of Engineering, Toyota Technological Institute,
2-12-1 Hisakata, Tempaku, Nagoya 468 8511, Japan
e-mail: okamoto@toyota-ti.ac.jp

L. Avérous and E. Pollet (eds.), *Environmental Silicate Nano-Biocomposites*,
Green Energy and Technology, DOI: 10.1007/978-1-4471-4108-2_4,

On these backgrounds, there is an urgent need to develop renewable source based environmental benign polymeric materials (biopolymers [2]). Such materials would not involve the use of toxic or noxious components in their manufacture, and could allow to composting to naturally occurring degradation products.

In today's commercial venues, biopolymers have proven to be relatively expensive and available only in small quantities. This has led to limitations on application to date. However, there are signs that this is changing, with increasing environmental awareness and more stringent legislation regarding recyclability and restrictions on waste disposal. Cargill Dow has a polylactide (PLA) in production (Natureworks as a trade name). Metabolix has been working on polyhydroxyalkanoate (PHA) (Biopol as a trade name) [2].

Thus, the increasing applications of the various intrinsic properties of biopolymers, coupled with the knowledge on how such properties can be improved to achieve the compatibility with thermoplastics processing, manufacturing, and end-use requirements, has fueled technological and commercial interest in biopolymers.

Of particular interest are the recently developed nano-composites consisting of a polymer and layered silicate because they often exhibit remarkably improved mechanical and various other properties [3] when compared with pure polymer or conventional composites (both micro- and macro-composites). A primary progress in polymer/layered filler nano-composites (PLFNCs), a Nylon 6/layered silicate hybrid [4] reported by Toyota Central Research & Development Co. Inc. (TCRD), was successfully prepared by in situ polymerization of ε-caprolactam in a dispersion of montmorillonite (MMT). The silicate can be dispersed in liquid monomer or a solution of monomer. It has also been possible to melt-mix polymers with layered silicates, avoiding the use of organic solvents. The latter method permits the use of conventional processing techniques such as injection molding and extrusion. The extensive literatures in nano-composite research are covered in the recent reviews [5–7]. The study on nano-composites has gained greater momentum. This new class of materials is now being introduced in structural applications, such as gas barrier film, flame retardant product, and other load-bearing applications [8].

This chapter is intended to highlight the biodegradable PLA-based nano-composites with the primary focus on nano-structure control and processing operation with the aim of plastics having nano-pores. Development of PLA-based nano-composite is one of the latest evolutionary technologies of the polymeric composite through a pioneering effort by Okamoto et al. [9, 10].

4.2 Nano-Structure Development

4.2.1 Melt Intercalation

Since the possibility of direct melt intercalation was first demonstrated [11], melt intercalation has become a preparation of the intercalated polymer/layered silicate

nano-composites (PLSNCs). This process involves annealing, statically or under shear, a mixture of the polymer and organically modified layered fillers (OMLFs) above the softening point of the polymer. During annealing, the polymer chains diffuse from the bulk polymer melt into the nano-galleries between the layered fillers.

In order to understand the thermodynamic issue associated with the nano-composites formation, Vaia and Giannelis [12, 13] have applied mean-field statistical lattice model and found conclusions based on the mean field theory nicely agreed with the experimental results. The entropy loss associated with confinement of a polymer melt is not prohibited to nanocomposite formation because an entropy gain associated with the layer separation balances the entropy loss of polymer intercalation, resulting in a net entropy change near to zero. Thus, from the theoretical model, the outcome of nano-composite formation via polymer melt intercalation depends on energetic factors, which may be determined from the surface energies of the polymer and OMLF.

Nevertheless, we have often faced the problem that the nano-composite shows fine and homogeneous distribution of the nano-particles in the polymer matrix [e.g., poly(L-lactide)] without a clear peak shift of the mean interlayer spacing of the (001) plane as revealed by wide-angle X-ray diffraction (WAXD) analysis [14]. Furthermore we sometimes encounter a decreasing of the interlayer spacing compared with that of pristine OMLF, despite very fine dispersion of the silicate particles. For this reason, information on the structure of the surfactant (intercalant)-polymer interface is necessary to understand the intercalation kinetics that can predict final nano-composite morphology and overall materials properties [15–18].

4.2.2 Nano-Composite Structure

Figure 4.1 shows the results of transmission electron microscope (TEM) bright field images of PLA-based nano-composites, in which dark entities are the cross section of intercalated MMT layers.

The organically modified MMT content in all nano-composites was 4 wt%. The MMT-based OMLFs were prepared with octadecylammonium ($C_{18}H_3N^+$) (MMT-$C_{18}H_3N^+$), octadecyltrimethylammonium ($C_{18}(CH_3)_3N^+$) (MMT-$C_{18}(CH_3)_3N^+$) and dioctadecyldimethylammonium ($2C_{18}(CH_3)_2N^+$) (MMT-$2C_{18}(CH_3)_2N^+$). From the TEM images, it becomes clear that there are some intercalated-and-stacked silicate layers in the nano-composites. Yoshida et al. estimate the form factors obtained from TEM images, i.e. average value of the particle length (L), of the dispersed particles and the correlation length (ξ) between them [18]. From the WAXD patterns, the crystallite size (D) of intercalated stacked silicate layers of each nano-composite is calculated by using Scherrer equation. The calculated value of D ($\cong$thickness of the dispersed particles) and other parameters for each nano-composite are presented in Table 4.1.

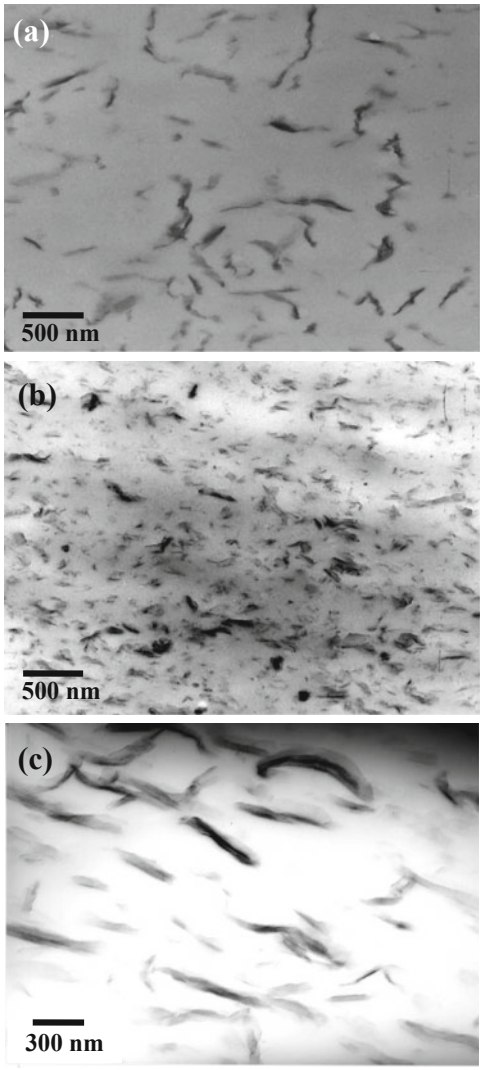

Fig. 4.1 Bright filed TEM images of PLA-based nanocomposites prepared with **a** MMT-$C_{18}H_3N^+$, **b** MMT-$C_{18}(CH_3)_3N^+$ and **c** MMT-$2C_{18}(CH_3)_2N^+$. The *dark* entities are the cross section and/or face of intercalated-and-stacked silicate layers and the *bright* areas are the matrix. Reprinted from [15], © 2006, Wiley–VCH

For PLA/MMT-$C_{18}(CH_3)_3N^+$, L and D are in the range of 200 ($\pm$25) and 10.7 nm, respectively. On the other hand, PLA/MMT-$C_{18}H_3N^+$ exhibits large value of L (450 $\pm$ 200 nm) with large level of stacking of the silicate layers ($D \sim$ 21 nm). ξ value of the PLA/MMT-$C_{18}(CH_3)_3N^+$ (80 $\pm$ 20 nm) is lower than the value of PLA/MMT-$C_{18}H_3N^+$ (260 $\pm$ 140 nm), suggesting that the intercalated layers are more homogeneously and finely dispersed in case of PLA/MMT-$C_{18}(CH_3)_3N^+$. The number of the stacked individual silicate layers ($\equiv D/d_{(001)} + 1$) is 5 for PLA/MMT-$C_{18}(CH_3)_3N^+$ and ξ value of this nano-composite is one order of magnitude lower compared with those of PLA/MMT-$C_{18}H_3N^+$ and

Table 4.1 Form factors of three nano-composites obtained from WAXD and TEM observations

Nano-composites	PLA/MMT-$C_{18}H_3N^+$	PLA/MMT-$C_{18}(CH_3)_3N^+$	PLA/MMT-$2C_{18}(CH_3)_2N^+$
d_{001}/nm	3.03	2.85	2.95
Δ Opening/nm	0.72	0.879	0.45
Final layer opening/nm	2.07	1.89	1.99
D/nm	20.9	10.73	14.71
$(D/d_{001}) + 1$	7.9	4.8	6.0
L/nm	450 ± 200	200 ± 25	655 ± 121
ξ/nm	260 ± 140	80 ± 20	300 ± 52

Reprinted with permission from [15] © 2006, Wiley–VCH

PLA/MMT-$2C_{18}(CH_3)_2N^+$, suggesting that intercalated silicate layers are more homogeneously and finely dispersed.

Although the (initial) interlayer opening of MMT-$C_{18}(CH_3)_3N^+$ at 1.011 nm is smaller than MMT-$C_{18}H_3N^+$ at 1.350 nm and MMT-$2C_{18}(CH_3)_2N^+$ at 1.540 nm, the intercalation of the PLA in these different OMLFs gives almost same basal spacing after preparation of the nano-composites. Note that the existence of sharp Bragg peak in PLA-based nano-composites after melt extrusion clearly indicates that the dispersed silicate layers still retain an ordered structure after melt extrusion [15].

In Table 4.1 are summarized the layer expansion after preparation (=Δ opening) of three nanocomposites, or after subtraction of the initial layer opening. For same MMT with different intercalants [e.g., comparison between MMT-$C_{18}(CH_3)_3N^+$ and MMT-$2C_{18}(CH_3)_2N^+$], the layer expansion of the former (0.879 nm) exhibits large value compared with that of the later (0.45 nm) in PLA-based nano-composites. In other words, the smaller interlayer opening caused by the configuration with small tilt angle [$\alpha = 22.9°$ for $C_{18}(CH_3)_3N^+$ [15]] promotes the large amount of the intercalation of the polymer chains. Accordingly, PLA/MMT-$C_{18}(CH_3)_3N^+$ exhibits finer dispersion of the nano-fillers compared with PLA/MMT-$2C_{18}(CH_3)_2N^+$ and PLA/MMT-$C_{18}H_3N^+$ as discussed before (see Fig. 4.1).

One more interesting feature is the absolute value of Δ opening. According to the molecular modeling, the width and thickness of one single PLA chain are 0.76 and 0.58 nm (see Fig. 4.2). This may suggest that the polymer chains could not penetrate into galleries in case of MMT-$2C_{18}(CH_3)_2N^+$ when we compare the apparent interlayer expansion (=Δ opening).

Now it is necessary to understand the meaning of the interlayer expansion in the intercalated nano-composites. As discussed before, we have to take the interdigitated layer structure into consideration. This structure may suggest that the different orientation angle could be adopted when the polymer chains penetrate into the galleries, giving a decrease of the basal spacing after intercalation. At the same time, this structure apparently provides a balance between the polymer penetration and different orientation angle of the intercalants. That is, we have to pay attention to the polymer chains intercalation into the galleries from the result of the change

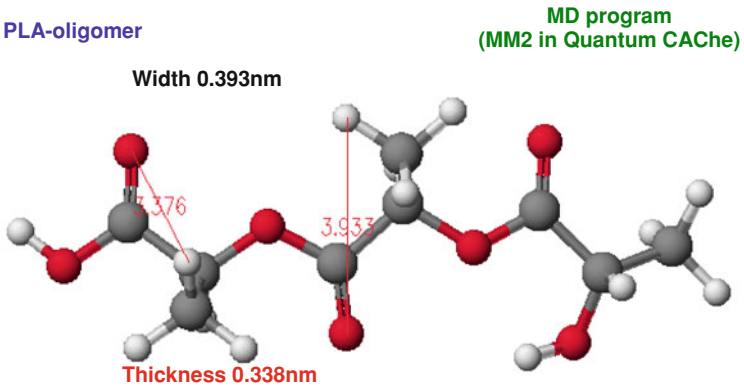

Fig. 4.2 Molecular dimensions of PLA-backbone using the molecular dynamics program (MM2 in Quantum CAChe) in consideration of van der Waales radii. Optimization of structure is based on minimization of the total energy of the molecular system

of the basal spacing as revealed by WAXD. Presumably the penetration of the polymer chain is prevented or reduced by the steric-limitation of the configuration with large value of α [e.g. $\alpha = 40.1°$ for MMT-2$C_{18}(CH_3)_2N^+$]. Accordingly, we sometimes observe small interlayer expansion and encounter a decrease of the interlayer spacing after melt intercalation. As seen in Table 4.1, the initial interlayer opening depends on the interlayer expansion (=Δ opening) after melt intercalation. The smaller initial opening leads to the larger interlayer expansion, and gives almost same final interlayer opening. This feature has been observed in the results of other nano-composites prepared with different OMLFs intercalated with varying surfactants [19]. From this result, the entropic contribution of the intercalants, which leads to the entropy gain associated with the layer expansion after intercalation of the small molecules and/or polymer chains, may not be significant due to the interdigitated layer structure. Presumably the penetration takes place by pressure drop within the nano-galleries, a nano-capillary action, generated by the two platelets.

As reported in the literature [17], the pressure drop (Δp) into the nano-galleries, which makes the polymer penetration more difficult, should be discussed. The estimated pressure difference ($\sim$24 MPa) is much larger than the shear stress ($\sim$0.1 MPa) during melt compounding [17]. This suggests that shear stress has little effect on the delamination (exfoliation) of the layer. This reasoning is consistent with the intercalated structure reported by so many nano-composite researchers, who can prepare only intercalated (not exfoliated) nano-composites via simple melt extrusion technique [5]. A novel compounding process is currently in progress. Solid-state shear processing may be an innovative technique to delaminate the layered fillers [20].

4.3 Control of Nano-Structure Properties

4.3.1 Flocculation Control and Modulus Enhancement

Most of the nano-composite researchers obdurately believe that the preparation of completely exfoliated structure is the ultimate target for better overall properties. However, these significant improvements are not observed in every nano-composite systems, including systems where the silicate layers are near to exfoliated [21]. While from the barrier property standpoint, the development of exfoliated nano-composites is preferred always. On the other hand, Nylon 6-based nano-composite systems are completely different from other nano-composite systems as discussed [3, 8].

In Fig. 4.3, Okamoto summarized the clay content dependence of dynamic storage modulus (G') of various types of nano-composites obtained under temperature well below T_g of the matrices. Einstein coefficient (k_E) derived by using Halpin and Tai's theoretical expression modified by Nielsen is shown in the Figure, and represents the aspect ratio (L_{filler}/d_{filler}) of dispersed MMT particles without intercalation. From Fig. 4.3, it is clearly observed that poly(butylene succinate)(PBS)-based nano-composites (PBSCNs) show very high increment in G′ compared to other nano-composites having same content of clay in the matrix. N6CNs are well-established exfoliated Nylon 6-based nano-composites.

PLACNs are established intercalated-and-flocculated PLA-based nano-composites, while PBSCNs are intercalated-and-extended flocculated nano-composites systems [22, 23]. Due to the strong interaction between hydroxylated edge–edge groups, the MMT particles are some time flocculated in the polymer matrix. As a result of this flocculation the length of the MMT particles increases enormously and hence overall aspect ratio. For the preparation of high molecular weights PBS, di-isocyanate [OCN-(C_6H_{12})-NCO] type end-groups are generally used as a chain extender. These isocyanate end group chain extenders make urethane bonds with hydroxy terminated low molecular weight PBS, and each high molecular weights PBS chain contain two such kinds of bonds. These urethane type bonds lead to the strong interaction with silicate surface by forming hydrogen bonds and hence strong flocculation.

This behavior can be explained with the help of classical rheological theory of suspension of conventional filler reinforced systems. According to this theory [24], the rotation of filler is possible when volume fraction of clay $\phi_{filler} < \phi_{critical} \cong (\text{aspect ratio})^{-1}$. All PBSCNs studied here follow this relation except PBSCN4 (MMT = 3.6 wt%), in which $\phi_{filler} \gg (\text{aspect ratio})^{-1}$. For this reason in PBSCN4 rotation of dispersed intercalated with flocculated stacked silicate layers is completely hindered and only translational motion is available, and hence show very high modulus. This behavior is clearly observed in dynamic storage modulus measurements under molten state [22]. In case of N6CN3.7 (MMT = 3.7 wt%) we can see same high increment in G' as well as PBSCNs. The development of the

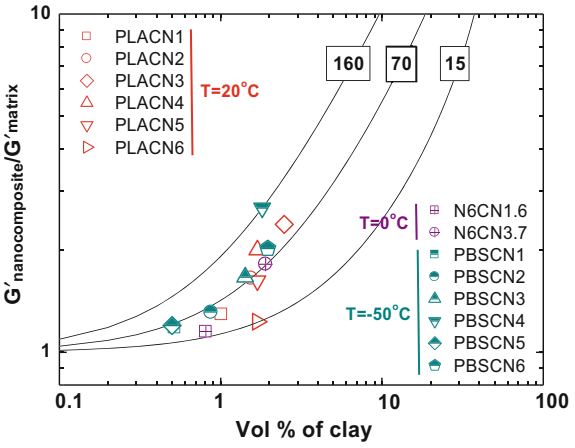

Fig. 4.3 Plots of $G'_{nanocomposite}/G'_{matrix}$ versus vol.% of MMT for various nano-composites. The Einstein coefficient k_E is shown with the number in the *box*. The *lines* show the calculated results from Halpin and Tai's theory with various k_E

flocculated structure is observed even though N6CNs are well-established exfoliated nano-composite systems.

4.3.2 Linear Viscoelastic Properties

The measurement of rheological properties of the PLFNCs under molten state is crucial to gain a fundamental understanding of the nature of the processability and the structure–property relationship for these materials.

Dynamic oscillatory shear measurements of polymeric materials are generally performed by applying a time dependent strain of $\gamma(t) = \gamma_o \sin(\omega t)$ and the resultant shear stress is $\sigma(t) = \gamma_o[G' \sin(\omega t) + G'' \cos(\omega t)]$, with $G'$and G'' being the storage and loss modulus, respectively.

Generally, the rheology of polymer melts strongly depends on the temperature at which measurement is carried out. It is well known that for the thermo-rheological simplicity, isotherms of storage modulus ($G'(\omega)$), loss modulus ($G''(\omega)$) and complex viscosity [$|\eta^*|(\omega)$] can be superimposed by horizontal shifts along the frequency axis:

$$b_T G'(a_T w, T_{ref}) = b_T G'(\omega, T);$$

$$b_T G''(a_T w, T_{ref}) = b_T G''(\omega, T)$$

$$|\eta^*|(a_T w, T_{ref}) = |\eta^*|(\omega, T)$$

where a_T and b_T are the frequency and vertical shift factors, and T_{ref} is the reference temperature. All isotherms measured for pure polymer and for various nano-composites can be superimposed along the frequency axis.

In case of polymer samples, it is expected, at the temperatures and frequencies at which the rheological measurements were carried out, the polymer chains should be fully relaxed and exhibit characteristic homo-polymer-like terminal flow behavior (i.e. curves can be expressed by a power-law of $G' \propto \omega^2$ and $G'' \propto \omega$).

To date, the melt state linear dynamic oscillatory shear properties of various kinds of nano-composites have been examined for a wide range of polymer matrices including Nylon 6 with various matrix molecular weights [25], polystyrene (PS) [26], PS-polyisoprene (PI) block copolymers [27, 28], poly(ε-caprolactone) (PCL) [29], PLA [30, 31], PBS [22, 32], and so on [33].

The linear dynamic viscoelastic master curves for the neat PLA and various PLA-based nano-composites (PLACNs) are shown in Fig. 4.4 [31]. The linear dynamic viscoelastic master curves were generated by applying time–temperature superposition principle and shifted to a common temperature T_{ref} using both frequency shift factor a_T and modulus shift factor b_T. The moduli of the nano-composites increase with increasing clay loading at all frequencies ω. At high ωs, the qualitative behavior of $G'(\omega)$ and $G''(\omega)$is essentially same and unaffected with frequencies. However, at low frequencies $G'(\omega)$ and $G''(\omega)$increase monotonically with increasing clay content. In the low frequency region, the curves can be expressed by power-law $G'(\omega)$of $\propto \omega^2$ and $G''(\omega) \propto \omega$ for neat PLA, suggesting that this is similar to those of the narrow M_w distribution homopolymer melts. On the other hand, for $a_T < 5$ rad s^{-1}, viscoelastic response (particularly $G'(\omega)$) for all the nano-composites displays significantly diminished frequency dependence as compared to the matrices. In fact, for all PLACNs, G′(ω) becomes nearly independent at low $a_T\omega$ and exceeds $G''(\omega)$, characteristic of materials exhibiting a pseudo-solid like behavior [33]. The terminal zone slopes values of both neat PLA and PLACNs are estimated at lower $a_T\omega$ region (<10 rad s^{-1}), and are presented in Table 4.2.

The lower slope values and the higher absolute values of the dynamic moduli indicate the formation of "spatially-linked" structure in the PLACNs under molten state [27]. Because of this structure or highly geometric constraints, the individual stacked silicate layers are incapable of freely rotating and hence by imposing small $a_T\omega$, the relaxations of the structure are prevented almost completely. This type of prevented relaxation due to the highly geometric constraints of the stacked and intercalated silicate layers leads to the presence of the pseudo-solid like behavior as observed in PLACNs. This behavior probably corresponds to the shear-thinning tendency, which strongly appears in the viscosity curves ($a_T\omega < 5$ rad s^{-1}) ($|\eta^*|$ vs. $a_T\omega$). Such feature strongly depended on the shear rate in the dynamic measurement because of the formation of the shear-induced alignment of the dispersed MMT particles [34].

The temperature dependence frequency shift factor (a_T, Williams–Landel–Ferry type [35]) used to generate master curves shown in Fig. 4.4 are shown in Fig. 4.5.

The dependence of the frequency shift factors on the silicate loading suggests that the temperature-dependent relaxations process observed in the viscoelastic

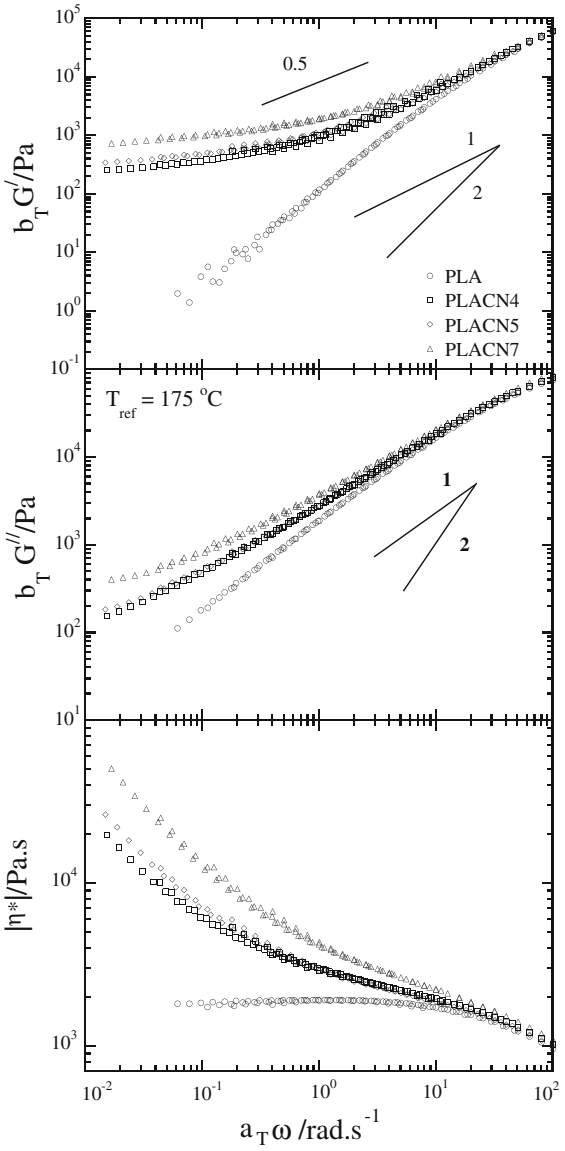

Fig. 4.4 Reduced frequency dependence of storage modulus, loss modulus and complex viscosity of neat PLA and various nanocomposites (PLACNs). Reprinted from [31], © 2003, Elsevier Science

Table 4.2 Terminal slopes of G′ and G″ versus $a_T\omega$ for PLA and various PLACNs

System	G′	G″
PLA	1.3	0.9
PLACN4	0.2	0.5
PLACN5	0.18	0.4
PLACN7	0.17	0.32

Reprinted from [31], © 2003, Elsevier Science

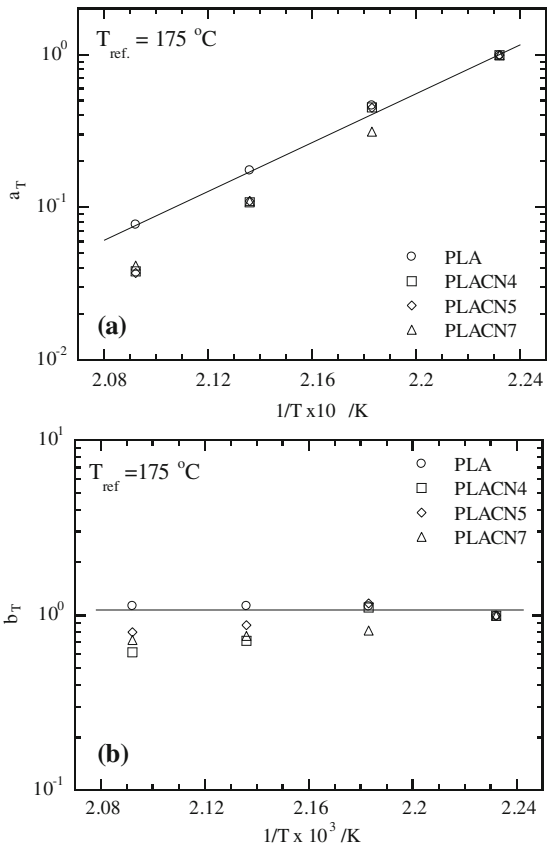

Fig. 4.5 **a** Frequency shift factors a_T and **b** modulus shift factor b_T as a function of temperature. Reprinted from [31], © 2003, Elsevier Science

measurements are somehow affected by the presence of the silicate layers [33]. In case of Nylon 6-based nano-composite, where occurs the hydrogen-bonding on the already formed hydrogen-bonded molecule to the silicate surface, the system exhibits large value of flow activation energy near one order higher in magnitude compared with that of neat Nylon 6 [36].

The shift factor b_T shows large deviation from a simple density effect, it would be expected that the values would not vary far from unity [35]. One possible explanation is an internal structure development occurring in PLACNs during measurement (shear process). The alignment of the silicate layers probably supports for PLFNC melts to withstand the shear force, thus lead to the increase in the absolute values of $G'(\omega)$ and $G''(\omega)$.

Galgali et al. [37] have also shown that the typical rheological response in nano-composites arises from frictional interactions between the silicate layers and not due to the immobilization of confined polymer chains between the silicate layers. These authors have also shown a dramatic decrease in the creep compliance for the PP-based nano-composite with 9 wt% of MMT. They showed a dramatic

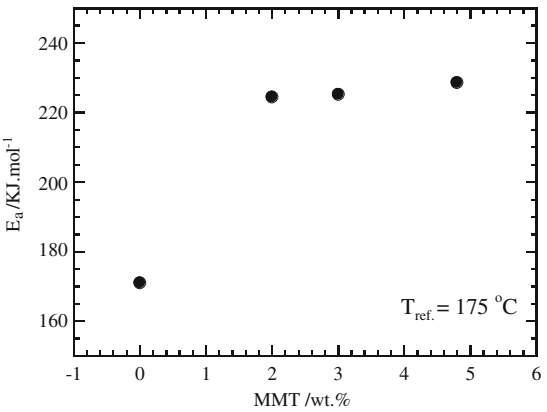

Fig. 4.6 Flow activation energy of pure PLA and various PLA-based nano-composites as a function of MMT content. Reprinted from [38], © 2003 Wiley–VCH Verlag GmbH & Co

three-order of magnitude drop in the zero shear viscosity beyond the apparent yield stress, suggesting that the solid-like behavior in the quiescent state is a result of the percolated structure of the layered silicate.

Figure 4.6 represents the MMT content dependent (wt%) flow activation energy (E_a) of pure PLA and various PLACNs obtained from Arrhenius fit of master curves [38]. It is clearly observed that E_a value significantly increased with nano-composite containing 3 wt% of MMT and then almost comparable with increasing MMT content. This result indicates that in presence of MMT, it is very difficult for the materials to flow. This behavior also ascribed to the formation of spatially linked structure in nano-composite under molten state.

4.3.3 Elongational Flow and Strain-Induced Hardening

Okamoto et al. [39] first conducted elongation test of PP-based nano-composites under molten state at constant Hencky strain rate, $\dot{\varepsilon}_0$ using an elongation flow optorheometry [40] and also they attempted to control the alignment of the dispersed silicate layers with nanometer dimensions of an intercalated PP-based nano-composites under uniaxial elongational flow.

Figure 4.7 shows double-logarithmic plots of transient elongational viscosity (η_E) against time (t) observed for PLA-based nano-composite (PLACN) (MMT = 4 wt%) at 170 °C with different Hencky strain rates ($\dot{\varepsilon}_0$) ranging from 0.01 to 1 s^{-1} [38]. We observed a very strong tendency of *strain-induced hardening* in the nano-composite melt. In the early stage, η_E gradually increases with t but almost independent of $\dot{\varepsilon}_0$, which is generally called the *linear region* of the viscosity curve. After a certain time, t_{η_E} which is called the *up-rising* time (marked with the upward arrows in Fig. 4.7a), strongly dependent on $\dot{\varepsilon}_0$, we see rapid upward deviation of η_E from the curves of the linear region. Authors reported very low shear viscosity of pure PLA which is the main reason for this, because

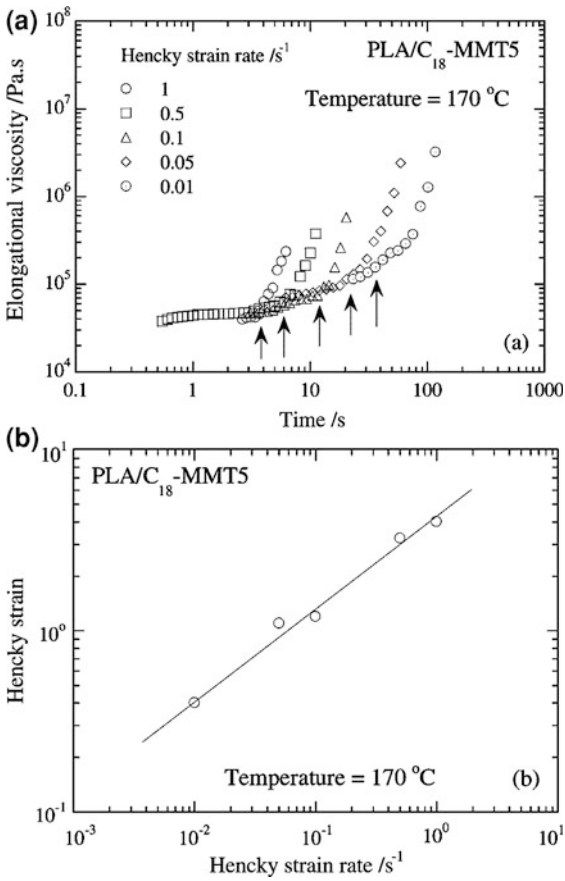

Fig. 4.7 **a** Time variation of elongational viscosity for PLA-based nano-composite (MMT = 4 wt%) melt at 170 °C; **b** Strain rate dependence of up-rising Hencky strain. Reprinted from [38], © 2003 Wiley–VCH Verlag GmbH & Co

minimum viscosity range of the instrument was greater than 10^4 Pa s. However, it was confirmed that neither strain-induced hardening in elongation nor rheopexy in shear flow took place in case of pure PLA having same molecular weights and polydispersity as the nano-composite.

As in PP-based nano-composite systems, the extended Trouton rule, $3\eta_0(\dot{\gamma};t) \cong \eta_E(\dot{\varepsilon}_0;t)$, also does not hold for PLACN melts, as opposed to the melt of pure polymers. These results indicate that in case of PLACN, the flow induced internal structural changes also occur in elongation flow [39], but the changes are quite different from shear flow. The strong rheopexy observed in shear measurements for PLA-based nano-composite at very slow shear rate reflects the fact that the shear-induced structural change involved a process with an extremely long relaxation time.

Regarding elongation-induced structure development, Fig. 4.7b shows Hencky strain rate dependence of the up-rising Hencky strain $(\varepsilon_{\eta_E}) = \dot{\varepsilon}_0 \times t_{\eta_E}$ taken for PLACN at 170 °C. The ε_{η_E} increases systematically with the $\dot{\varepsilon}_0$. The lower the value of $\dot{\varepsilon}_0$, the smaller is the value of ε_{η_E}. This tendency probably corresponds to the rheopexy of PLACN under slow shear flow.

4.4 Physicochemical Phenomena

4.4.1 Biodegradability

Another most interesting and exciting aspect of nano-composite technology is the significant improvements of biodegradability of some biodegradable polymers after nano-composites preparation with OMLS. Aliphatic polyesters are among the most promising materials for the production of environmentally friendly biodegradable plastics. Biodegradation of aliphatic polyester is well known and relies upon some bacteria degrade them by producing enzymes, which attack and degrade the polymer. Tetto et al. [41] first reported some results about the biodegradability of nano-composites based on PCL, where authors found that the PCL-based nano-composites showed improved biodegradability compared to pure PCL. According to them, the improved biodegradability of PCL after nano-composites formation may be due to the catalytic role of the OMLS in the biodegradation mechanism. But still it is unclear how the clay increases the biodegradation rate of PCL.

Recently, Sinha et al. [42–44] first reported the biodegradability of neat PLA and PLA-based nano-composites prepared with trimethyl octadecylammonium modified MMT (MMT-$C_{18}(CH_3)_3N^+$) with detailed mechanism. The used compost was prepared from food waste and tests were carried out at temperature of 58 $\pm$ 2 °C. Figure 4.8a shows the real picture of the recovered samples of neat PLA and nano-composite (MMT = 4 wt%) from compost with time. The decreased molecular weight M_w and residual weight percentage R_w of the initial test samples with time are also reported in Fig. 4.8b. The biodegradability of neat PLA is significantly enhanced after nano-composite preparation. Within 1 month, both the variations of M_w and extent of weight loss are almost same level for both PLA and nano-composite. However, after 1 month, a sharp change occurs in weight loss of nano-composite, and within 2 months, it is completely degraded in compost. The degradation of PLA in compost is a complex process involving four main phenomena, namely: water absorption, ester cleavage and formation of oligomer fragments, solubilization of oligomer fragments, and finally diffusion of soluble oligomers by bacteria [45]. Therefore, the factor which increases the hydrolysis tendency of PLA ultimately controls the degradation of PLA. The presence of terminal hydroxylated edge groups of the silicate layers may be one of the responsible factors for this behavior. In case of PLA-based nano-composite, the stacked ($\sim$4 layers) and intercalated silicate layers are homogeneously dispersed in the PLA matrix (from TEM image [44]) and these hydroxy groups start heterogeneous hydrolysis of the PLA matrix after absorbing water from compost. This process takes some time to start. For this reason, the weight loss and degree of hydrolysis are almost the same for PLA and nano-composite up to 1 month (see Fig. 4.8b). However, after 1 month there is a sharp weight loss in case of nano-composite compared to that of PLA. That means 1 month is a critical value to start heterogeneous hydrolysis and due to this type of hydrolysis matrix becomes very small fragments and disappear in compost. This assumption was confirmed by

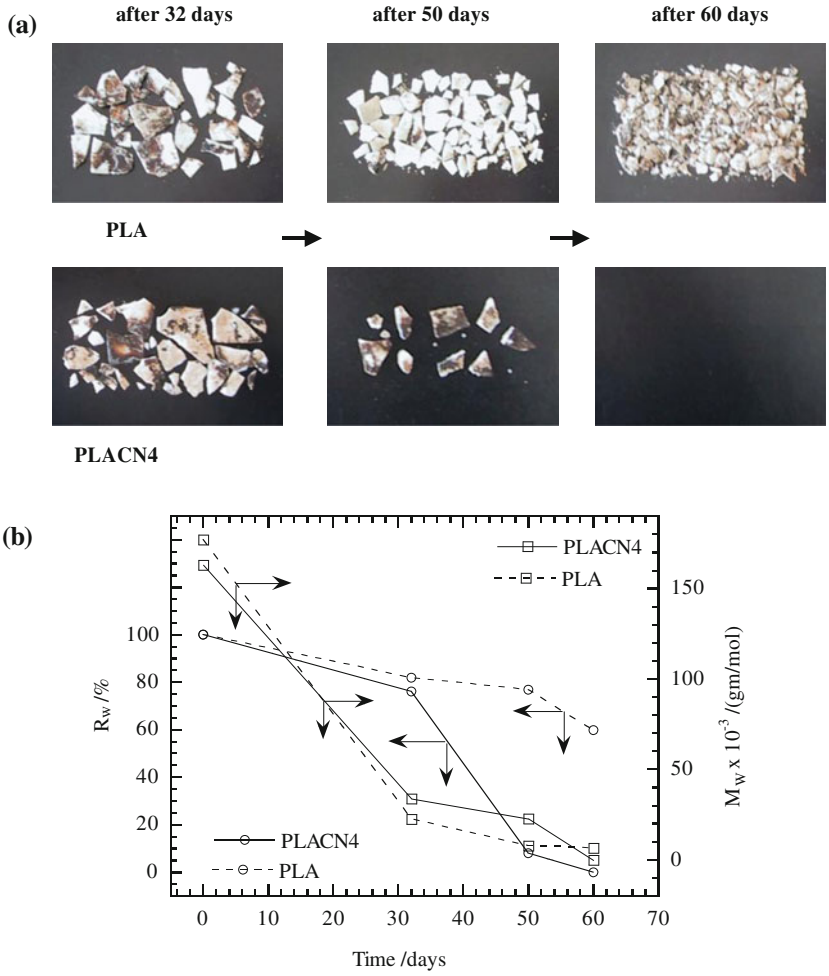

Fig. 4.8 **a** Real picture of biodegradability of neat PLA and PLA-based nano-composite recovered from compost with time. Initial shape of the crystallized samples was $3 \times 10 \times 0.1$ cm^3. **b** Time dependence of residual weight, R_w and of matrix, M_w of PLA and PLACN4 under compost at 58 ± 2 °C. Reprinted from [42], © 2002 American Chemical Society

conducting same type of experiment with PLACN prepared by using $2C_{18}(CH_3)_2N^+$ modified *syn*-FH which has no terminal hydroxylated edge group. In this case, the degradation tendency was almost the same as for neat PLA [43].

Authors also conducted respirometric test to study degradation of the PLA matrix in compost environment at 58 ± 2 °C. For this test the compost was made from bean-curd refuse, food waste, and cattle feces. Unlike weight loss, which reflects the structural changes in the test sample, CO_2 evolution provides an indicator of the ultimate biodegradability of PLA in PLA-based nano-composite [prepared with $qC_{14}(OH)$ modified *syn*-FH], i.e. mineralization, of the samples.

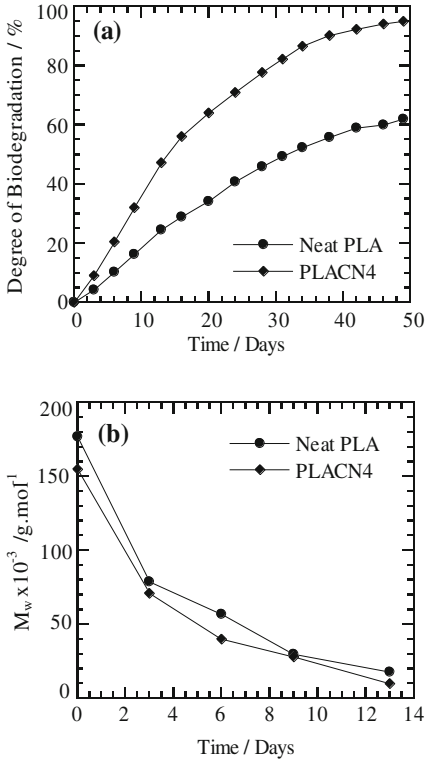

Fig. 4.9 **a** Degree of biodegradation (i.e. CO_2 evolution), and **b** time-dependent change of matrix M_w of neat PLA and PLA-based nano-composite (syn-FH = 4wt%) under compost at 58 ± 2 °C. Reprinted from [43], © 2004 Wiley–VCH

Figure 4.9 shows the time dependence of the degree of biodegradation of neat PLA and nano-composite, indicating that the biodegradability of PLA in the nano-composite is enhanced significantly. The presence of OMLF may thus cause a different mode of attack on the PLA component, which might be due to the presence of hydroxy groups. Details regarding the mechanism of biodegradability are presented in relevant literature [43, 44].

K. Okamoto and M. Okamoto also investigated biodegradability of neat PBS before and after nano-composites preparation with three different types of OMLF. They used alkylammonium or alkylphosphonium salts for the modification of pristine layered silicates, and these surfactants are toxic for microorganisms [32].

4.4.2 Photodegradation

Hiroi et al. [46] first reported the photodegradability of neat PLA and corresponding PLA-based nano-composite prepared by using organically modified layered titanate (HTO) as a new nano-filler. One of the features of this material is its photocatalytic

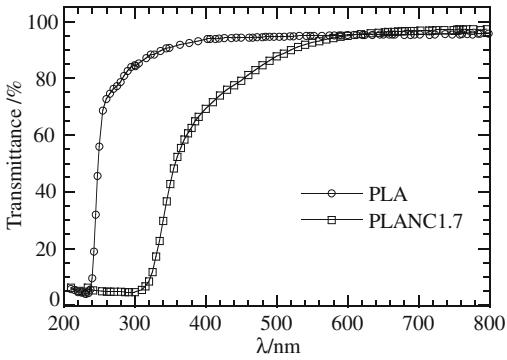

Fig. 4.10 UV/Vis transmission spectra of neat PLA and nano-composite (PLANC1.7). Reprinted from [46], © 2004 Wiley–VCH

reactivity, such as titania (TiO_2). The photocatalytic reactions of anatase-TiO_2, such as evolution of hydrogen gas from water or oxidative degradation of organic compounds, have attracted intense research interest because of their possible application to the conversion of solar energy into chemical energy [47].

Figure 4.10 shows the UV/vis transmission spectra of pure PLA and nano-composite (PLANC1.7: HTO = 1.7 wt%). The spectra show that the VIS region ($>\sim 400$ nm) is changed with increasing absorbency by the presence of titanate layers compared with neat PLA. For UV wavelengths, there is strong absorption up to 320 nm, resulting in 0 % transmittance. This significant change in the spectra may indicate occurrence of the photodegradation of PLA matrix. To confirm this, some preliminary experiments were conducted on photodegradation of PLA-based nano-composites under sunshine weathermeter at 60 °C. After 300 h, there was no change in the nature of sample surfaces of neat PLA, however, the surface color of nano-composite samples altered to yellow and/or light brown. Table 4.3 shows the GPC measurement of recovered samples from the test.

The drop in M_w accompanied with broadening of M_w/M_n indicates that the enhancement of degradation of PLA in the titanate-filled system has occurred.

4.5 Foam Processing Using Supercritical CO_2

4.5.1 PLA-Based Nano-Composite

PLA-based nano-composites have already been shown to exhibit a tendency toward strong strain-induced hardening. This strain-induced hardening behavior is an indispensable characteristic for foam processing due to its capacity to withstand the stretching force experienced during the latter stages of bubble growth. On the basis of this result, the first successful nano-composite foam, processed by using supercritical (sc)-CO_2 as a physical foaming agent, appeared through a pioneering effort by Okamoto et al. [9, 10].

Table 4.3 GPC results of sample recovered from weathermeter after 300 h

Samples	$M_w \times 10^{-3}$ (g/mol)	M_w/M_n	M_w/M_w^{oa}
PLA	198	1.53	0.94
PLANC1.7	93.7	1.89	0.68
PLANC3.9	86.3	1.86	0.76

Reprinted from [46], © 2004, Wiley–VCH
[a] M_w^o is molecular weight before test

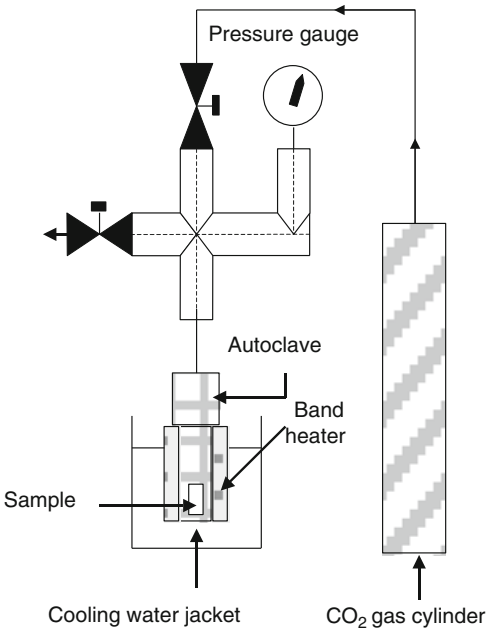

Fig. 4.11 Schematic representation of autoclave set-up. Reprinted with permission from [10], © 2002, Society of Plastic Engineers

A small amount of nano-fillers in the polymer matrix serves as nucleation sites to facilitate the bubble nucleation during foaming. Novel nano-composite foams based on the combination of new nano-fillers and sc-CO_2 lead to a new class of materials. The process consists of four stages: (1) saturation of CO_2 in the sample at desired temperature, (2) cell nucleation when the release of CO_2 pressure started (supersaturated CO_2), (3) cell growth to an equilibrium size during the release of CO_2, and (4) stabilization of cell via cooling process of the foamed sample. The setup of autoclave used in the study is shown in Fig. 4.11.

Figure 4.12 shows the typical scanning electron microscope (SEM) images of the fracture surfaces of the PLA-based nano-composite (PLA/MMT-ODA) and neat PLA without MMT foamed at a temperature range of 100–140 °C under the different isobaric saturation conditions (14, 21 and 28 MPa) [48].

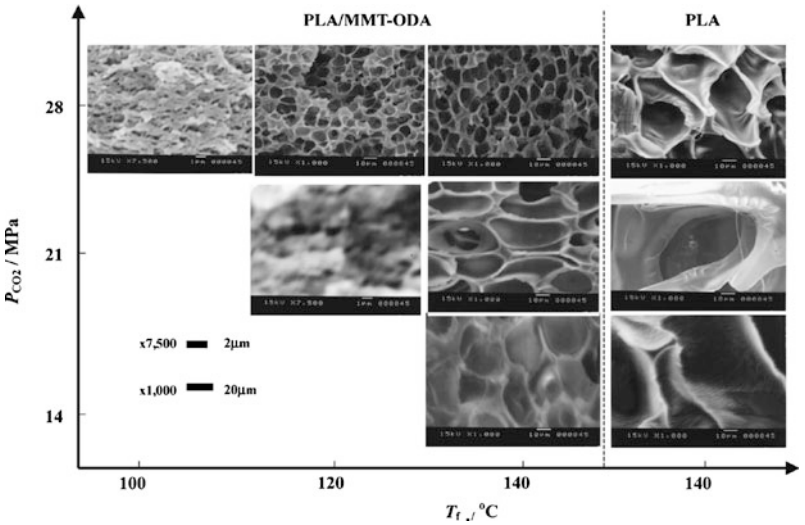

Fig. 4.12 Typical results of SEM images of the fracture surfaces of PLA/MMT-ODA and neat PLA foamed at temperature range of 100–140 °C under different isobaric saturation condition (14, 21 and 28 MPa). Reprinted from [48], © 2006, Elsevier Science

All foams exhibit nicely the closed-cell structure. It must be noted here that homogeneous cells were formed in case of nano-composite foams, while neat PLA foams show rather non-uniform cell structure having large cell size. The nano-composite foams show smaller cell size (d) and larger cell density (N_c) compared with neat PLA foam, suggesting that the dispersed silicate particles act as nucleating sites for cell formation [9].

For both foam systems, the calculated distribution functions of cell size from SEM images are presented in Fig. 4.13. The nano-composite foams nicely obeyed the Gaussian distribution. In case of PLA/ODA foamed at 150 °C under high pressure of 24 MPa, we can see that the width of the distribution peaks, which indicates the dispersity for cell size, became narrow and is accompanied by finer dispersion of silicate particles.

Obviously, with decreasing saturation pressure condition ($\sim$140 °C and 14 MPa), both foams exhibit large cell size due to the low supply of CO_2 molecules, which can subsequently form a small population of cell nuclei upon depressurization. The incorporation of MMT induces heterogeneous nucleation because of a lower activation energy barrier compared with homogeneous nucleation [49]. However, the competition between homogeneous and heterogeneous nucleation is no longer discernible.

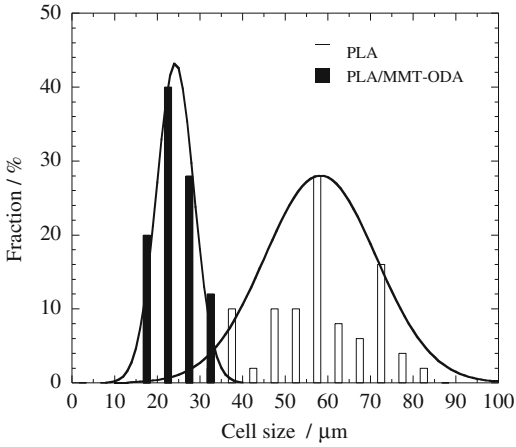

Fig. 4.13 Typical example for cell size distribution of foamed PLA/MMT-ODA and neat PLA in experiment at 150 °C under 24 MPa. Average values d in μm and variances σ_d^2 in μm^2 in the Gaussian fit through the data are 24.2 and 19.1 for PLA/MMT-ODA foam and 58.3 and 171.0 for PLA foam. Reprinted from [48], © 2006, Elsevier Science

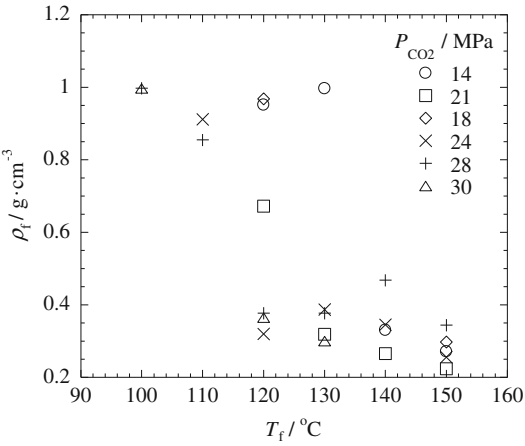

Fig. 4.14 Foaming temperature dependence of mass density for PLA/MMT-ODA foamed under different CO_2 pressure condition. Reprinted from [48], © 2006, Elsevier Science

4.5.2 Temperature Dependence of Cellular Structure

The dependence of the foam density (ρ_f) at the T_f under different CO_2 pressure is shown in Fig. 4.14. Throughout the whole CO_2 pressure range, the mass density of PLA/MMT-ODA foams remains constant value at low foaming temperature (T_f) range and abruptly decreases beyond a certain T_f, and then attains a minimum constant value up to 150 °C again. From the above results, it can be said that such behavior of mass density evolution is due to the competition between the cell nucleation and the cell growth.

At the low T_f range ($\sim$110 °C), in which a large supply of CO_2 molecules are provided, the cell nucleation is dominant, while at the high T_f, ($\sim$140 °C), the cell growth and the coalescence of cells are prominent due to low viscosity of the

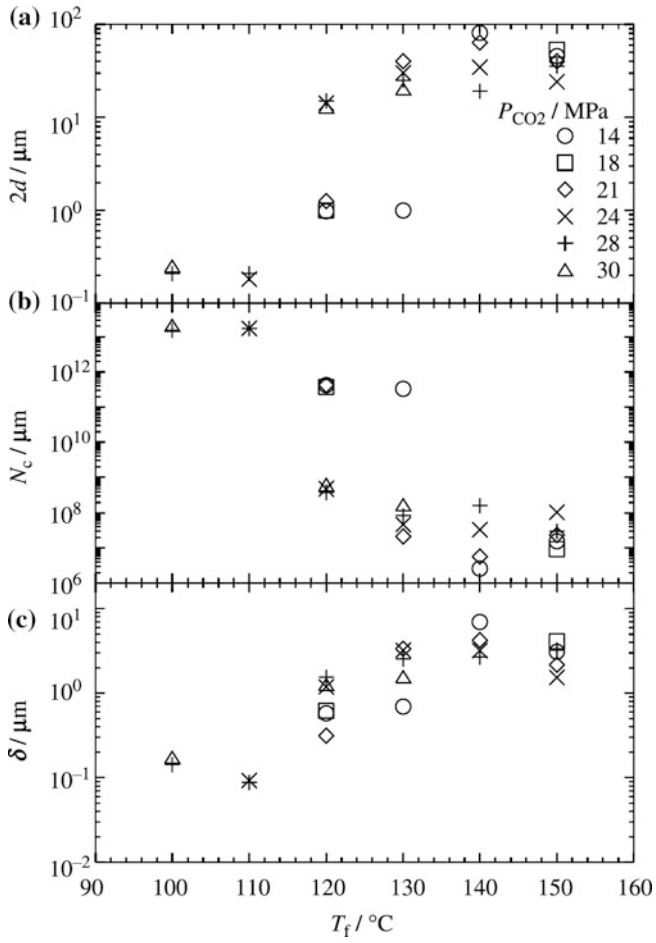

Fig. 4.15 Foaming temperature dependence of **a** cell size, **b** cell density and **c** mean cell wall thickness under different CO_2 pressure condition. Reprinted from [48], © 2006, Elsevier Science

systems compared with the low T_f range ($\sim$110 °C). This behavior clearly appears in the plots of the cell size ($\cong 2d$), the cell density (N_c), and the mean cell wall thickness (δ) versus T_f under various pressure conditions, respectively.

As seen in Fig. 4.15, with increasing T_f all nano-composite foams show an increasing tendency of $2d$ and/or δ and attain a maximum. On the other hand, the temperature dependence of N_c shows opposite behavior compared with the tendency of $2d$ due to the cell growth and coalescence. Both $2d$ and N_c affect the mass density of the foams.

Using the glass transition temperature (T_g) depressions (corresponding to ΔT_g), the authors reconstructed plots of ρ_f versus $T_f + \Delta T_g$ from the data of Fig. 4.14. The results are shown in Fig. 4.16. All the data, including neat PLA and different

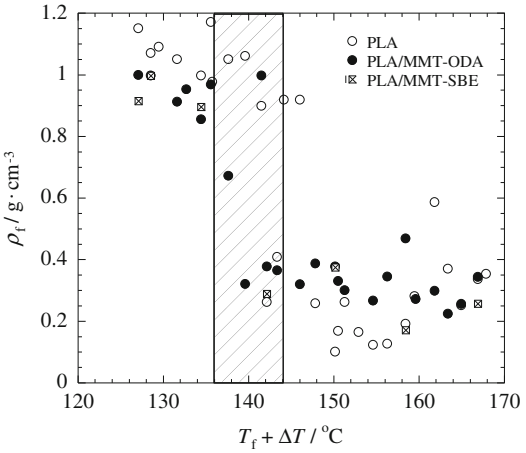

Fig. 4.16 Plot of mass density for PLA/MMT-ODA, PLA/MMT-SBE and neat PLA versus reduced foaming temperature ($T_f + \Delta T_g$). The critical temperature (140 ± 4 °C) is *shaded*. Reprinted from [48], © 2006, Elsevier Science

type of PLA-based nano-composites (PLA/MMT-SBE), nicely conform to a reduced curve with $\rho_f \sim 1.0 \pm 0.1$ g cm^{-3} at $T_f + \Delta T_g < 140 \pm 4$ °C (nano-cellular region), whereas ρ_f values approach around 0.3 ± 0.15 g cm^{-3} as reduced temperature ($T_f + \Delta T_g$) increased well above 150 °C (microcellular region). The critical temperature is thus 140 ± 4 °C, above which the cell growth prevails. Below the critical temperature, the cell nucleation dominates and the cell growth are suppressed due to the high modulus and viscosity as revealed by the temperature dependence of strage, $G'(\omega)$ and loss, $G''(\omega)$ moduli ($G' = 162$ MPa and viscosity component; $G''/\omega \cong 2$ MPa s at 140 °C).

Figure 4.17 shows temperature-reduced plots of $2d$, N_c and δ versus $T_f + \Delta T_g$. The all data nicely conform to a reduced curve like Fig. 4.16. Interestingly, when they used both T_g and the melting temperature (T_m) [50] depressions to conduct superposition, they have recognized that the reduced curve is nicely constructed but there is no significant difference compare with the case of $T_f + \Delta T_g$. This indicates that T_g depression is important in optimizing foam processing condition but T_m depression is not a significant factor for processing because the T_f range is still below T_m after CO_2 saturation.

In Fig. 4.18, the relations between $2d$ and N_c, and δ and $2d$ are shown. The relation nicely obeys in Eqs. (4.1) and (4.2).

$$N_c = 10^4 \frac{3\left[1 - \left(\rho_f/\rho_p\right)\right]}{4\pi \mathrm{d}^3} \tag{4.1}$$

$$\delta = d\left(1/\sqrt{1 - \left(\rho_f/\rho_p\right)} - 1\right) \tag{4.2}$$

where ρ_p and ρ_f are the mass density pre-foamed and post-foamed samples, respectively.

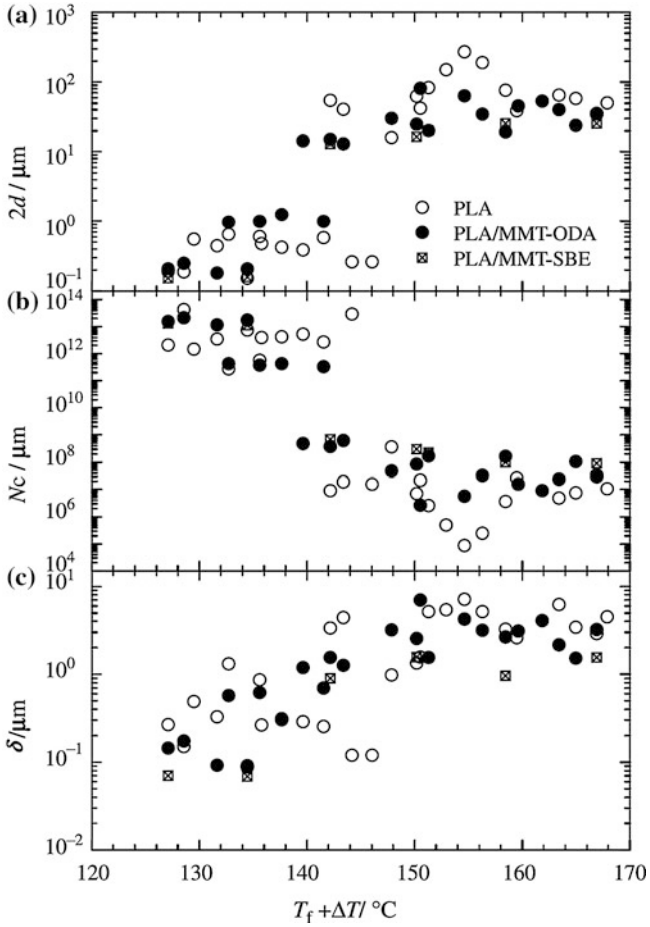

Fig. 4.17 Temperature-reduced plots of **a** 2d, **b** N_c and **c** δ versus $T_f + \Delta T_g$ for PLA/MMT-ODA, PLA/MMT-SBE and neat PLA. Reprinted from [48], © 2006, Elsevier Science

But the deviation occurs beyond the value of $N_c \sim 10^{12}$cell cm^{-3} for panel (a) and below $2d \sim 1$ μm for panel (b). The downward and upward deviations indicate that the heterogeneous cell distribution mechanism due to the rigid crystalline phases in the PLA matrix is caused by high degree of the crystallinity (∼49 wt%) under the low foaming temperature range (∼100 °C).

As seen in Fig. 4.19, the PLACN foams exhibit the heterogeneous cell distribution. The PLA foam reduces the value of N_c accompanied by the large value of δ compared with that of PLACN foams. In case of PLACN foams, the controlled structure of the PLACN foams is from microcellular ($2d \cong 30$ μm and $N_c \cong 3.0 \times 10^7$cells cm^{-3}) to nano-cellular ($2d \cong 200$ nm and $N_c \cong 2.0 \times 10^{13}$cells cm^{-3}).

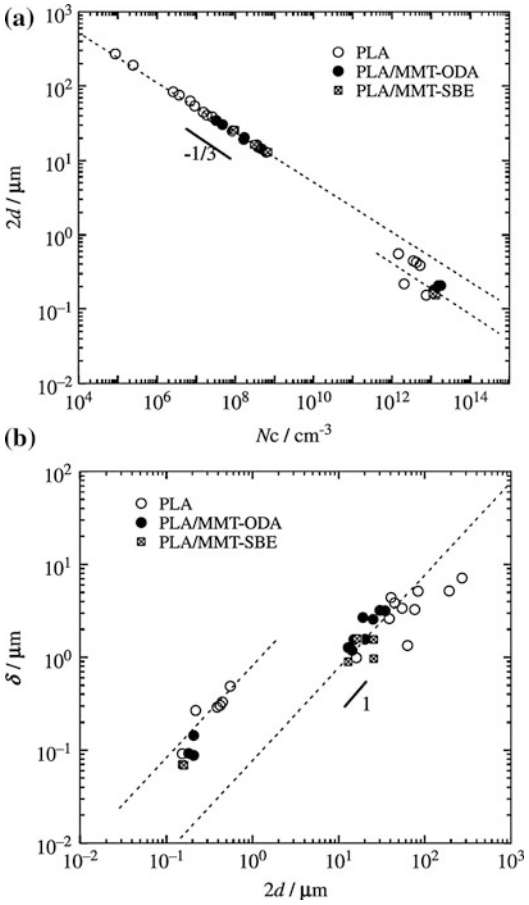

Fig. 4.18 Relation between **a** cell size versus cell density and **b** cell wall thickness versus cell size for all foams. Reprinted from [48], © 2006, Elsevier Science

4.5.3 CO_2 Pressure Dependence

At high pressure, both homogeneous and heterogeneous nucleation mechanisms may appear to be of comparable significance. All systems demonstrate that N_c increases systematically with increasing CO_2 pressure in the low T_f region ($\sim$100–120 °C). For PLA/MMT-ODA foams, the system suggests that the heterogeneous nucleation is favor at high pressure condition. The cell nucleation in the heterogeneous nucleation system such as PLA/MMT-ODA foams took place in the boundary between the matrix and the dispersed MMT (nano-filler) particles. Accordingly, the cell size decreases without individual cell coalescence for PLA/MMT-ODA and neat PLA systems as seen in Fig. 4.19. To clearly investigate whether the addition of internal surfaces of the dispersed nano-clay may hinder CO_2 diffusion by creating a more tortuous diffusive pathway [18], they conducted the characterization of the interfacial tension between bubble and matrix was conducted by using the modified classical nucleation theory [49].

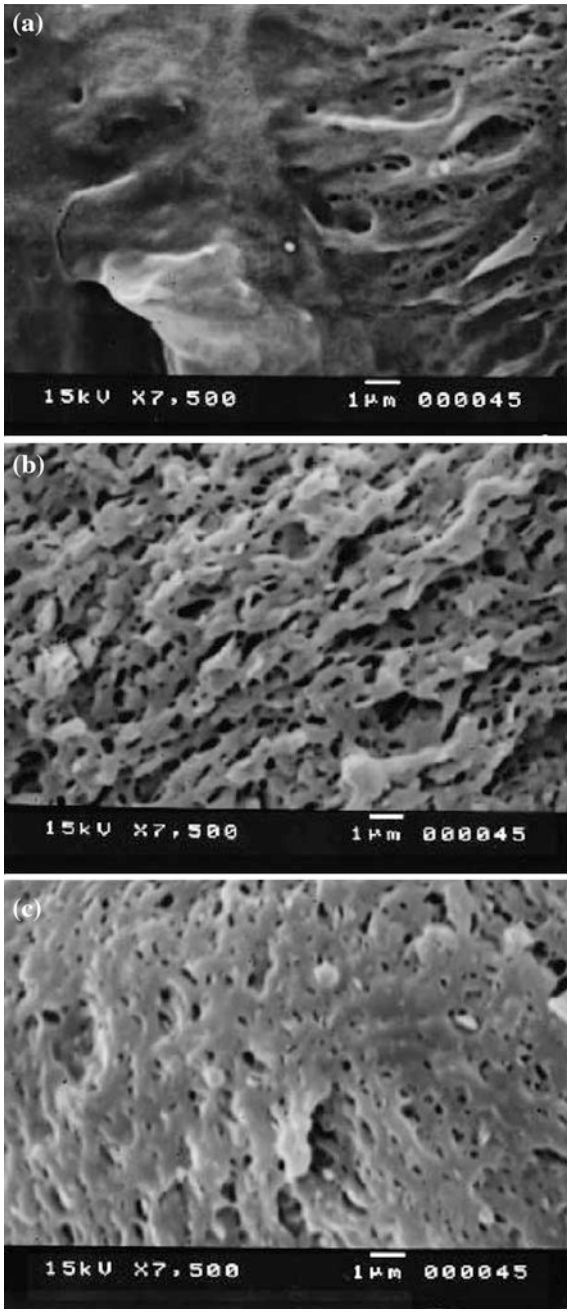

Fig. 4.19 SEM images of the fracture surfaces of **a** neat PLA, **b** PLA/MMT-ODA and **c** PLA/MMT-SBE foamed at 100 °C under 28 MPa. Reprinted from [48], © 2006, Elsevier Science

Table 4.4 Characteristic interfacial parameters of two systems

	T_f/°C	$\gamma S(\theta)^{1/3}$/mJ/m^2	$S(\theta)$	θ/°
PLA/CO_2	110	7.43		
PLA/MMT-ODA/CO_2		6.65	0.717	107.3
PLA/CO_2	120	7.08		
PLA/MMT-ODA/CO_2		5.38	0.439	85.3

Reprinted from [48], © 2006, Elsevier Science

According to the theory proposed by Suh and Colton, the rate of nucleation of cells per unit volume ($\dot{N}$) can be written as

$$\dot{N} \sim Cf \exp\left[\frac{-16\pi\gamma^3 S(\theta)}{3(\Delta P_{CO2})^2 k_B T}\right] \tag{4.3}$$

where C is the concentration of CO_2 and/or the concentration of heterogeneous nucleation sites, f is the collision frequency of CO_2, γ is the interfacial tension between bubble and matrix, $S(\theta)$ is the energy reduction factor for the heterogeneous nucleation (i.e., PLA/MMT-ODA), ΔP_{CO2} is the magnitude of the pressure quench during depressurization, k_B is the Boltzmann constant, and T is absolute temperature.

The theoretical cell density is given by

$$N_{theor} = \int_0^t \dot{N} dt \tag{4.4}$$

where t is the foaming time that takes approximately 3 s. Assuming no effect of the coalescence of cell on the value of N_c, the interfacial tension of the systems can be calculated using Eqs. (4.3) and (4.4), i.e., the slope of the plots (N_c, vs. $1/\Delta P_{CO2}$). The characteristic parameters of two systems are shown in Table 4.4.

The interfacial tension of PLA/MMT-ODA and neat PLA are 6.65 mJ m^{-2} and 7.43 mJ m^{-2} at 110 °C, respectively. These estimated γ values are in good agreement with that of other poly(methyl methacrylate) (PMMA)-CO_2 system ($\sim$10 mJ m^{-2}) [51]. PLA/MMT-ODA system has a low value compared to that of neat PLA. This trend reflects the relative importance of heterogeneous nucleation, which dominates over homogeneous one in the event that the amount of CO_2 available for bubble nucleation is limited because of a lower activation energy barrier, as mentioned before. That is, in the heterogeneous nucleation (PLA/MMT-ODA), we have to take the reduction of the critical energy into consideration because of the inclusion of nucleants, which is a function of the PLA-gas-nanoclay contact angle (θ) and the relative curvature (W) of the nucleant surface to the critical radius of the nucleated phase [52]. In case of $W \geq 10$, the energy reduction factor $S(\theta)$ can be express by

$$S(\theta) = (1/4)(2 + \cos\theta)(1 - \cos\theta)^2 \tag{4.5}$$

In case of homogeneous nucleation $S(\theta)$ is unity ($\theta = 180°$). The obtained values of the contact angle are 107.3° at 110 °C and 85.3° at 120 °C. The estimated reduction factor [$S(\theta) = 0.4$–0.7] was not so small when compared with the other nano-filler [e.g., carbon nanofiber, $S(\theta) = 0.006$] [53]. However, experimentally, nano-clay particles lead to an increase in N_c.

For PLA/MMT-SBE foams prepared under the condition with low T_f ($\sim$100–110 °C) and high pressure ($\sim$28 MPa), the nano-composite foams exhibit no significant difference in N_c compared with PLA/MMT-ODA foams. This reasoning is consistent with the large value of W in both systems.

4.5.4 TEM Observation

To confirm the heterogeneous nucleation and the feature of the nanocellular in the foam processing, TEM observation of the cell wall in the PLA/MMT-ODA foam were performed.

Figure 4.20 shows TEM micrograph for the structure of the cell wall foamed at 100 °C under 28 MPa. Interestingly, the grown cells having a diameter of $\sim$200 nm are localized along the dispersed nano-clay particles in the cell wall. In other words, the dispersed nano-filler particles act as nucleating sites for cell formation and the cell growth occurs on the surfaces of the MMTs, i.e., the cellular structure is oval-faced morphology rather than spherical cellular structures for high T_f condition ($\sim$140 °C). In Fig. 4.20, in addition to the nano-cellular structure formation, a lamellar pattern beside the nano-clay (MMT) particles is observed. This behavior appears to arise from the formation of the α-phase of the PLA crystal in the presence of nano-clay particles [54]. This is a unique observation of the epitaxial crystallization of PLA grown up from MMT (clay) surfaces due to the nucleation effect of the dispersed nano-clays.

4.5.5 Mechanical Properties of Nano-Composite Foams

Figure 4.21 shows the relation of relative modulus (K_f/K_p) against relative density (ρ_f/ρ_p) of neat PLA and PLA-based nano-composite foams, taken in the directions parallel (a) and perpendicular (b) to the flow, respectively.

To clarify whether the modulus enhancement of the nano-composite foams was reasonable, authors applied the following Eq. (4.6) proposed earlier by Kumar and Weller [55] to estimate relative moduli with various foam density:

$$\frac{K_f}{K_p} = \left(\frac{\rho_f}{\rho_p}\right)^4 - \left(\frac{\rho_f}{\rho_p}\right)^2 + \left(\frac{\rho_f}{\rho_p}\right) \tag{4.6}$$

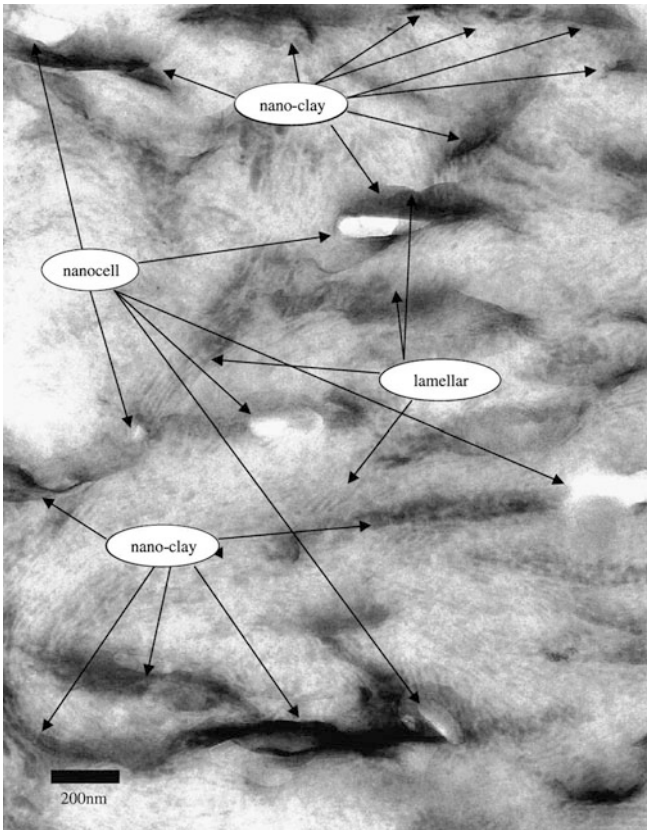

Fig. 4.20 TEM micrograph for the structure of PLA/MMT-ODA cell wall foamed at 100 °C under 28 MPa. Reprinted from [48], © 2006, Elsevier Science

where K_p and K_f are the modulus of pre-foamed and post-foamed samples, respectively. The solid line in the figure represents the fit with Eq. (4.6). The neat PLA foam does not show any difference between two moduli [(a) and (b)]. On the other hand, for nano-composite foams, the relative moduli exhibit a large value compared with the theoretical one. The dispersed MMT particles in the cell wall align along the thickness direction of the sample. In other word, the MMT particles arrange due to the biaxial flow of material during foaming. The MMT particles seem to act as a secondary cloth layer to protect the cells from being destroyed by external forces. In the directions perpendicular to the flow, the relative modulus of PLA/MMT-ODA and PLA/MMT-SBE foams appear higher than the predicted value even through at same relative mass density in the range of 0.7–0.85 (Fig. 4.21a). This upward deviation suggests that the small cell size with large cell density enhances the material property as predicted by Weaire and Fu [56]. This may create the improvement of mechanical properties for polymeric foams through polymeric nano-composites.

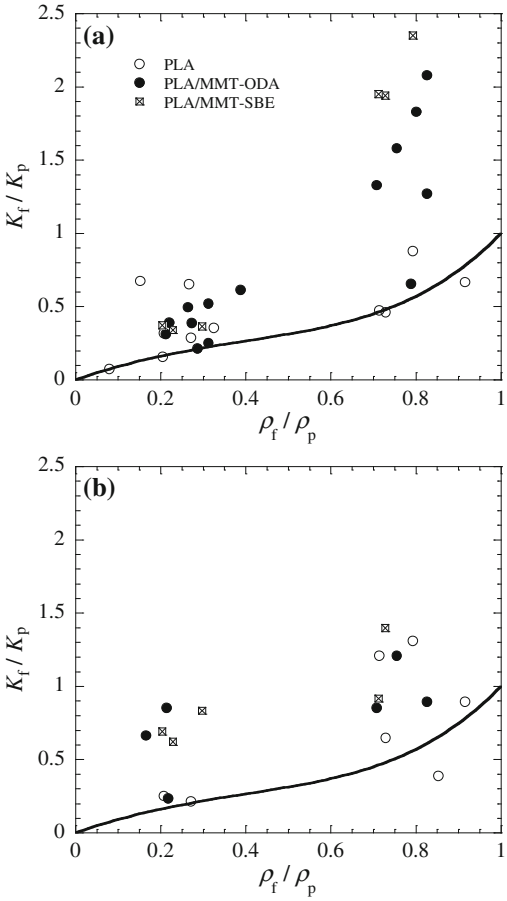

Fig. 4.21 The relation of relative modulus (K_f/K_p) against relative density (ρ_f/ρ_p) of neat PLA and PLA-based nano-composite foams, taken in the directions parallel (**a**) and perpendicular (**b**) to the flow

4.6 Fabrication of Porous 3-D Structure

The preparation of the porous three-dimensional (3-D) structure from a PLA-based nano-composite foam via enzymatic degradation is a new concept towards the analysis of the biodegradation of foams. The biodegraded nano-composite foam provide a porous 3-D scaffold and the pore size is determined by controlling the degradation time using proteinase-K as an effective degrading catalyst [57, 58].

The enzymatic degradation of PLLA in the presence of proteinase-K, which is extracted from protease in a fungus called *Tritirachium album* in 1974 [59]. This enzyme has a molecular weight of 18,500 ± 500, an isoelectric point of 8.9 and a pH optimum activity range between 7.5 and 12.0 [60]. Proteinase-K preferentially degrades PLLA over poly(D-lactide). The degradation rate significantly increases with reducing %L content from 100 to 92 % in PLLA, suggesting the crystalline order dominates enzymatic degradation [61].

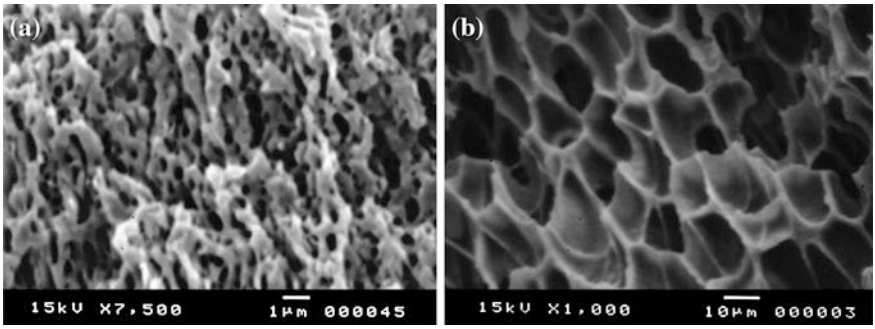

Fig. 4.22 SEM images of the fracture surface (cross section) of the PLA-based nano-composite foams: **a** nanocellular and **b** microcellular. Reprinted from [57], © 2008, Elsevier Science

4.6.1 Enzymatic Degradation of PLA foams

Figure 4.22 shows the SEM images of the PLA nano-composite (cross-section) foams at 100 and 120 °C (before degradation).

The foams exhibited closed-cell structure and homogeneous nano- (Fig. 4.22a) and micro-cellular (Fig. 4.22b) distribution, suggesting that the dispersed silicate particles act as nucleating sites for cell formation [48]. The morphological parameters are summarized in Table 4.5.

In case of PLLACN5 foamed at 100 °C under high pressure of 28 MPa, the foam shows smaller cell size ($d \sim 165 \pm 7$ nm) and larger cell density ($N_c \sim 383 \times 10^{10}$ cell cm^{-3}) compared with that of PLA nano-composite foamed at 120 °C. At low foaming temperature (100 °C), the nano-composite foam exhibits nanocellular structure, while foam prepared at 120 °C shows rather large cell structure having low cell density (microcellular).

Figure 4.23 shows the time variation of the weight (μg/mm^2) and normalized weight losses (%) of microcellular having different χ_c (crystallinity) during the enzymatic degradation with a χ_c of 44.4 % in the PLA nano-composite bulk. The weight losses increases linearly with degradation time (t) over a period of 400 h (corresponding to 84 wt% degradation), regardless of χ_c in the PLA matrix.

A clear induction period is observed, which is the onset time until start of the weight loss in the specimen as compared with prefoamed nano-composite sample. Figure 4.24 compares the time variation of weight loss of nanocellular structure having high χ_c value of 54.5 % [58].

The degradation mechanism of the nano-composite foams, the linear degradation rate is estimated from the slope (d[weight loss]/dt) in the linear regime, as indicated by the solid line in Figs. 4.23 and 4.24, and is plotted as a function of the initial χ_c of the sample prior to hydrolysis in Fig. 4.25. The enzymatic degradation of neat PLLA ($M_w = 3 \times 10^5$) with high χ_c values and pre-foamed PLA nano-composite (bulk) are compared in this plot [62].

Table 4.5 Morphological parameters of nano-composite foams

Parameters	Nanocellular	Microcellular
ρ_f/g cm^{-3a}	1.01	0.32
d/μm	0.165 ± 0.072	7.55 ± 2.50
$N_c \times 10^{-8}$/cell cm^{-3}	38300	3.81
δ/μm	0.23	1.55

Reprinted from [57], © 2008, Elsevier Science
[a] ρ_p for PLLACN5 is 1.2620 g cm^{-3}

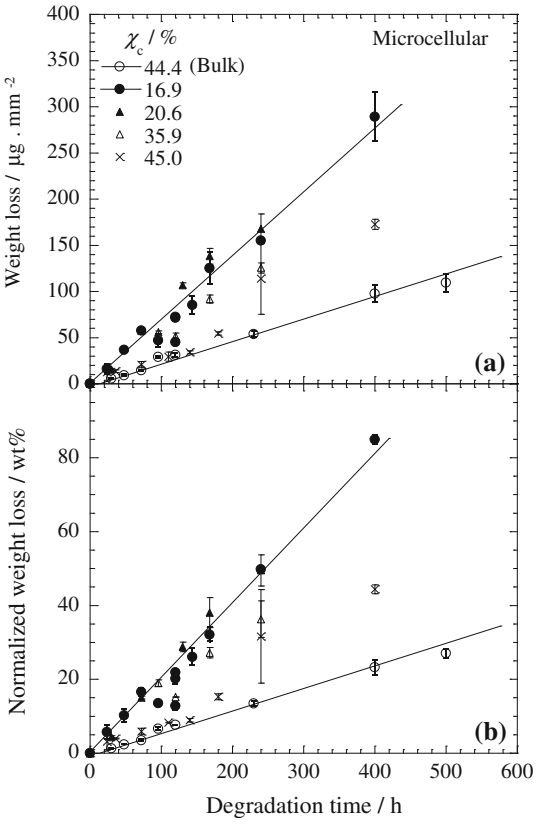

Fig. 4.23 **a** Weight loss and **b** normalized weight loss of microcellular having different χ_c with that of bulk data ($\chi_c = 44.4$ %) for comparison [58] during the enzymatic degradation. The *solid lines* are calculated by linear regression. Reprinted from [57], © 2008, Elsevier Science

For both bulk and neat PLA, the degradation rate slightly decreases with increasing initial $_c$ in the range of 0–30 % and abruptly decreases beyond 30 %. The dispersed MMT layers have almost no effect on the acceleration of the degradation rate with the nano-composite bulk and in the foam state This observation suggests that the linear degradation rate of the foams is affected by the initial value of χ_c as well as PLA nano-composite (and neat PLA) degradation [58]. The enzymatic hydrolysis of PLLA matrix proceeds preferentially at disordered amorphous region

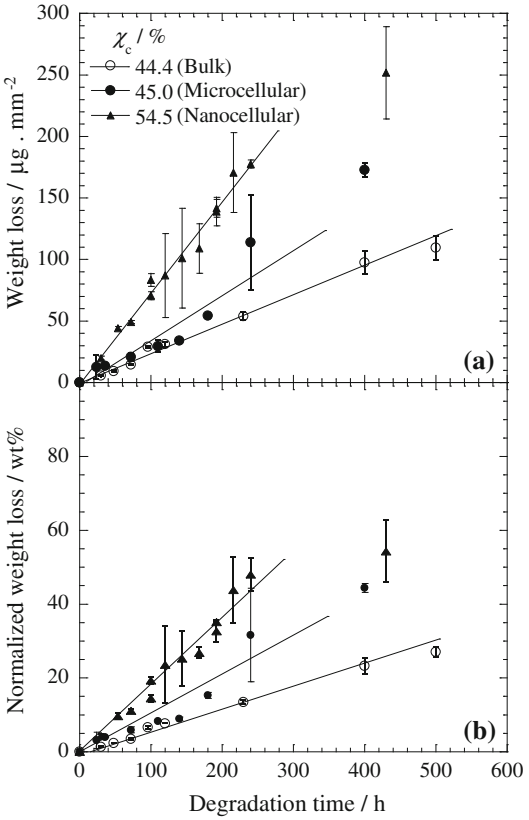

Fig. 4.24 **a** Weight loss and **b** normalized weight loss of nano-composite bulk, microcellular and nanocellular foams during the enzymatic degradation. The *solid lines* are calculated by linear regression. Reprinted from [57], © 2008, Elsevier Science

on the sample surface rather than on the restricted amorphous domains, which are located between the crystalline lamellae in the spherulites [62].

4.6.2 Microcellular versus Nanocellular

The enzymatic degradation of matrix PLLA proceeds through a surface erosion mechanism [59, 62–64]. In this process, the enzyme cannot diffuse into the film bulk. However, in the case of foams having cellular structure, the enzyme can contact with a lot of polymer chains at the cell wall surface compared with that of pre-foamed sample. In Figs. 4.24 and 4.25, the linear degradation rate of the nanocellular is about two times higher than that of microcellular with same crystallinity. The accelerated enzymatic degradation in the foam is caused by the large surface area inside the nanocellular structure. From Table 4.5, the calculated value of the specific surface area (3.3×10^5 mm^2) is two times higher than that of microcellular (1.7×10^5 mm^2). Obviously, both the difference of the degradation

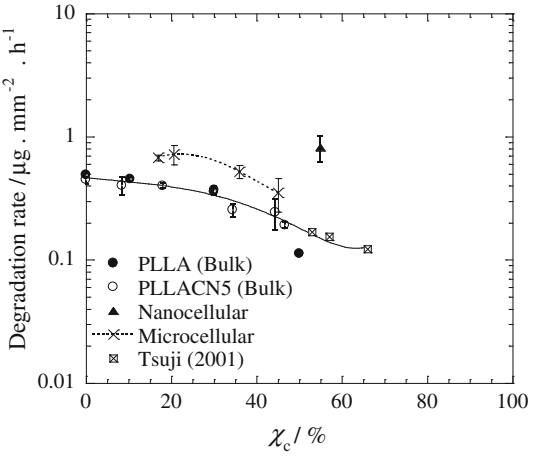

Fig. 4.25 Semi-logarithmic plots of linear degradation rates (μg/mm^2 h) of neat PLA bulk, nano-composite bulk, microcellular and nanocellular versus initial χ_c. Previous results on PLA (bulk) with high χ_c values are reproduced from [62]. Reprinted from [57], © 2008, Elsevier Science

rate and the difference of the surface area inside the cell structure are almost the same level for both cellular structures. This trend reflects the relative importance of the surface erosion in the enzymatic degradation of PLA matrix, as mentioned above. This feature is also assigned to the observation in water uptake data (Fig. 4.26).

The nanocellular appears to uptake water much more than both microcellular and bulk. During the first 250 h, the water absorption of the foams increases continuously to attain 30 % for microcellular and 50 % for nanocellular. Beyond 300 h, the water uptake remains almost constant, presumably due to the saturation caused by the morphology development after enzymatic degradation. That is, the water can more easily penetrate into the foam. In contrast, PLA nano-composite bulk shows very hydrophobic behavior with less than 2 % of absorbed water during the degradation period. The nanocelluar takes up large amount of water compared with that of microcellular, which leads to the swelling of the foam, and thus facilitate the enzymatic degradation of matrix PLA as compared with the bulk sample. The content of absorbed water greatly determines the enzymatic degradability [58].

4.6.3 Morphological Changes During Enzymatic Degradation

Figure 4.27 shows the surface and the cross-section morphologies of the microcellular with $\varkappa_c = 16.9$ % (Fig. 4.27a–c) recovered after enzymatic degradation for 400 h (corresponding to 84 wt% degradation), regardless of $\varkappa_c$ in the matrix of the microcellular samples.

For comparison, the morphologies of the nanocellular $\varkappa_c = 54.5$ % (Fig. 4.27d–f) and bulk sample $\varkappa_c = 44.4$ % recovered after enzymatic

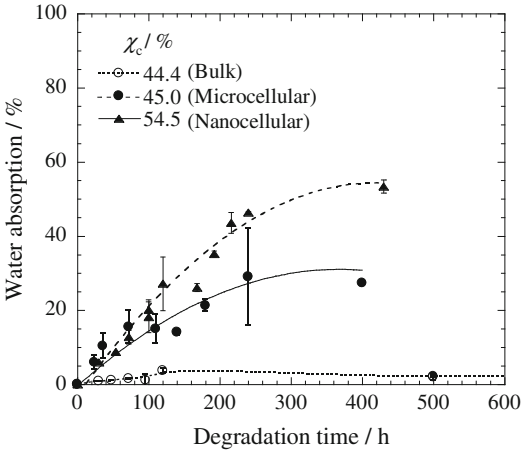

Fig. 4.26 Water absorption changing of nano-composite bulk, microcellular and nanocellular during the enzymatic degradation at 37 °C. Reprinted from [57], © 2008, Elsevier Science

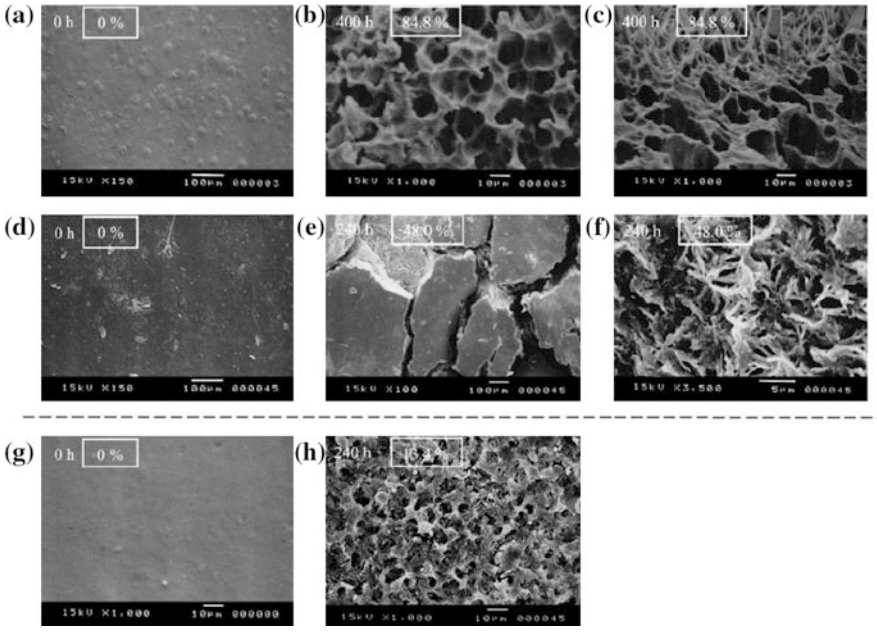

Fig. 4.27 Typical results of SEM images of the cross section and the surface of microcellular (**a**–**c**), nanocellular (**d**–**f**) and nano-composite bulk (**g**, **h**) after enzymatic degradation for different time (240 and 400 h). The weight loss (in %) of each specimen is shown by the number in the *box*. **c** and **f** are the cross sectional images. The remaining are the surface images. Reprinted from [57], © 2008, Elsevier Science

degradation for 240 h (Fig. 4.27g and h) were also investigated by using SEM. For the microcellular sample, a lot of pores appeared on the surface after degradation for 400 h with the diameter of ~15 μm and are polygon cell structure in shape. Interestingly, in the cross sections, the fibrillar structure with diameter of ~1–2 μm is generated on the thick cell wall ($\delta \sim 1.6$ μm) with some entanglement, suggesting that the amorphous region in the cell wall has been predominantly degraded. In contrast, the surfaces of both nanocellular and bulk samples are smooth before degradation (Fig. 4.27d and g). In the bulk sample, a lot of pores are generated on the surface after degradation up to 120 h and the pores with diameter of ~3 μm are spherical in shape with circular interconnections (Fig. 4.27h) and similar reports are available [65, 66]. These holes resulted from the degradation of the swollen (amorphous) region by the enzymatic attacks [67]. On the other hand, for the nanocellular sample, there is a great tendency to generate the skin-layer (~100 μm thickness) with cracked surface and hence more rapid fragmentation on the surface (Fig. 4.27e). No significant change, such as pore formation, on the surface during degradation up to 240 h suggests that the core part of the foam underwent significant hydrolysis during this period. This indicates that the cell structure allows the PLA chains to become susceptible to enzymatic hydrolysis. This speculation is supported by the water uptake behavior of the nano-foam. Figure 4.27h presents the morphological change of the cross-section in the nanocellular after enzymatic degradation for 240 h (corresponding to 48 wt% degradation). The interesting feature is the formation of some flower-like structure [68] as a remaining scaffold in the core part, reflecting a spherulite of the crystallized PLA. After the restricted amorphous region has been degraded, the porous 3-D scaffold left the core part in the nano-foam. This morphology of the PLA crystals is enhanced with degradation up to 240 h. The structure with a diameter size of 10 mm observed by SEM is in good agreement with the average diameter of the spherulite developed in the sample by annealing at 100 °C before degradation [54]. The generation of the porous 3-D structure is completely different from the enzymatic degradation of bulk sample, where the morphology of the core parts remains unchanged during degradation because of the surface erosion mechanism. Thus, the degraded nanocellular provides the porous 3-D scaffold and the pore size is determined by controlling the degradation time using proteinase-K as an effective degrading agent.

4.6.4 Distribution of Pores and Molecular Weight

Mercury porosimetry represents a very powerful tool in determining the pore size distribution of small and/or large pores that are not visible in the SEM observation. In Fig. 4.28, the results of the pore size distribution are summarized for different degradation time taken for 0, 120 and 240 h with the y-axis corresponding to the pore number fraction. In the nanocellular, the appearances of main peaks are observed at

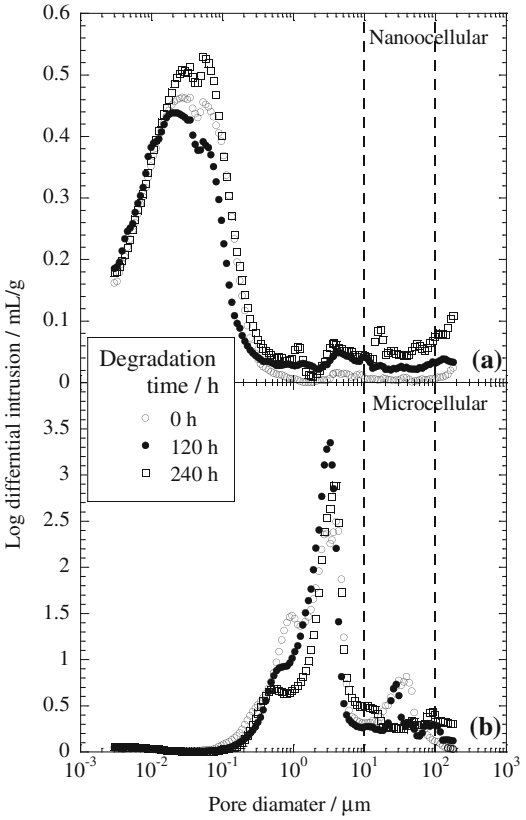

Fig. 4.28 Pore size distribution of **a** nanocellular and **b** microcellular after enzymatic degradation for different time intervals. The *dashed lines* represent the pore size range of 10–100 μm. Reprinted from [57], © 2008, Elsevier Science

40–50 nm range, which remains almost constant in the range of the degradation proceeded, whereas the appearance of small peak around 10–100 mm size is enhanced with increasing degradation time. For the microcellular, the appearances of main peaks are observed around pore size range of 3–4 μm with a small remnant shoulder around 1 μm (before degradation). As seen in nanocellular degradation, the microcellular produces pore size of 10–100 μm accompanied with a decrease of the size around 1 μm range, as the degradation takes place**.** Thus, the combination of initial cellular structure and controlling the degradation time offers 3-D pore size tuning from nano to micrometer.

Table 4.6 summarizes the results of the foamed PLA molecular characteristics, i.e., $\varkappa_c$ and molecular weight of the residual sample after degradation. After a weight loss of 49.6 %, the residual microcellular shows no change in M_w. The little decrease in M_w in the core part of the nanocellular is observed beyond degradation of 192 h ($M_w = 98.6 \times 10^3$ g mol^{-1}, $M_w/M_n = 3.04$) (weight loss in 30.1 %). At the same time, a small increase in $_c$ appears due to the preferential enzymatic degradation in the restricted amorphous region,

Table 4.6 Change in χ_c and M_w of residual nano-composite foams recovered after degradation

Samples	Before degradation			After degradation		
	χ_c/%	$M_w \times 10^{-3}$/g mol^{-1}	M_w/M_n	χ_c/%	$M_w \times 10^{-3}$/g mol^{-1}	M_w/M_n
Microcellular	16.9	113	1.71	21.9 (t = 240 h)	117	1.75
	45.0	113	1.71	47.1 (t = 240 h)	116	1.90
				46.9 (t = 400 h)	113	2.46
Nanocellular	54.5	121	1.70	63.1 (t = 192 h)	98.6	3.04

Reprinted from [57], © 2008, Elsevier Science

leaving a crystalline residue. This is in agreement with the characteristics of enzymatic degradation of bulk PLA [58, 62, 63], i.e., a sample weight loss without molecular weight decrease.

4.7 Porous Ceramic Materials via Nano-Composite

A new route for the preparation of porous ceramic material from thermosetting epoxy/MMT nano-composite was first demonstrated by Brown et al. [69]. This route offers attractive potential for diversification and application of the PLFNCs. Okamoto and coworkers have reported the elaboration on novel porous ceramic material via burning of the PLA-based nano-composite containing 3.0 wt% inorganic MMT [70]. The SEM image of fracture surface of porous ceramic material prepared from simple burning of the PLACN in a furnace up to 950 °C is shown in Fig. 4.29. After complete burning, as seen in the figure, the nano-composite becomes a white mass with porous structure. The bright lines in the SEM image correspond to the edge of the stacked silicate layers. In the porous ceramic material, the silicate layers form a cards-house structure, which consist of the large plates having length of ~1000 nm and thickness of ~30–60 nm. This implies that the further stacked platelet structure is formed during burning. The material exhibits the open-cell type structure having 100–1000 nm diameter void, BET surface area of 31 $m^2\ g^{-1}$ and low density of porous material of 0.187 g ml^{-1} estimated by the buoyancy method. The BET surface area value of MMT is 780 m^2/g and that of the porous ceramic material is 31 $m^2\ g^{-1}$, which suggests that about 25 MMT platelets are stacked together.

When MMT is heated above 700 °C (but below 960 °C) first all OH groups are eliminated from the structure and thus MMT is decomposed into a non-hydrated aluminosilicate. This transformation radically disturbs the crystalline network of the MMT, and resulting diffraction pattern is indeed often typical of an amorphous (or non-crystalline) phase. The estimated rough value of compression modulus (K) is in

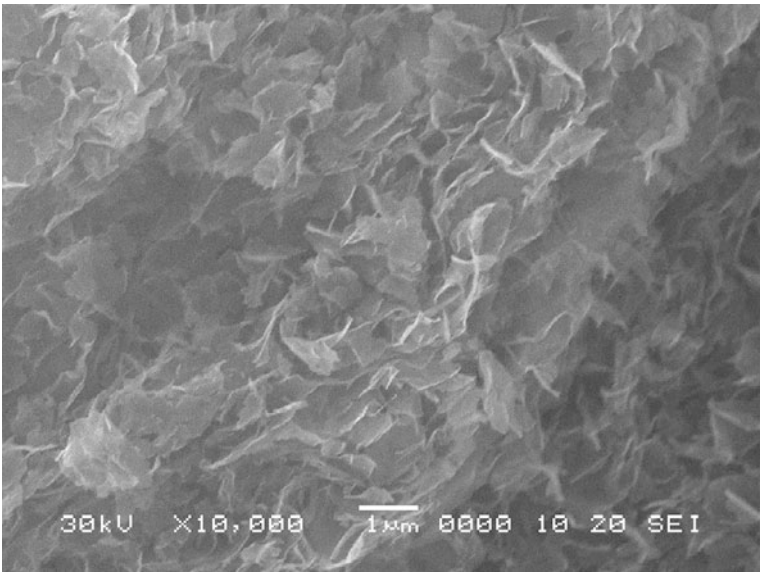

Fig. 4.29 SEM image of porous ceramic material after coated with platinum layer ($\sim$10 nm thickness). Reprinted from [70], © 2002 American Chemical Society

the order of $\sim$1.2 MPa, which is five orders of magnitude lower than the bulk modulus of MMT ($\sim 10^2$ GPa) [3]. In the stress–strain curve, the linear deformation behavior is nicely described in the early stage of the deformation, i.e., the deformation of the material closely resembles that of ordinary polymeric foams [71]. This open-cell type porous ceramic material consisting of the cards-house structure is expected to provide the strain recovery and excellent energy dissipation mechanism after unloading in the elastic region up to 8 % strain, probably each plate bend like leaf spring. This porous ceramic material is a new material possessing feature of elastic and very lightweight. This new route for the preparation of porous ceramic material via burning of nano-composites can be expected to pave the way for much broader range of applications of the PLSNCs. This porous ceramic material closely relates an excellent insulator property for flame retardant of PLFNCs [3]. The flame behavior must derive from the morphological control of the shielding properties of the graphitic clay created during polymer ablation.

4.8 Future Prospects

Development of the PLFNCs is one of the latest evolutionary steps of the polymer technology. The PLFNCs offer attractive potential for diversification and application of conventional polymeric materials. Some of PLFNCs are already commercially available and applied in industrial products.

Biodegradable polymers based nano-composites and foams have a great deal of future promise for potential applications as high-performance biodegradable materials. These are entirely new types of materials based on plant and nature materials. When disposed of in compost, these are safely decomposed into CO_2, water, and humus through the activity of microorganisms. The CO_2 and water will become corn or sugarcane again through plant photosynthesis. Undoubtedly, there unique properties originated from the controlled nano-structure paves the way to much broader range of applications (already commercially available through Unitika Ltd., Japan), and open a new dimension for plastics and composites. The major impact will be at least a decade away and will be a major stepping stone towards a greener and sustainable environment.

References

1. Smith R (2005) Biodegradable polymer for industrial applications. CRC Press, New York
2. Johnson RM, Mwaikambo LY, Tucker N (2003) Biopolymer. Rapra Review Report No 159. Rapra Technology Ltd., London, 148 pp
3. Okamoto M (2003) Polymer/layered silicate nanocomposites. Rapra Review Report No 163. Rapra Technology Ltd., London, 166 pp
4. Usuki A, Kojima Y, Okada A, Fukushima Y, Kurauchi T, Kamigaito O (1993) Swelling behavior of montmorillonite cation exchanged for ω-amino acids by ε-caprolactam. J Mater Res 8:1174–1178
5. Sinha Ray S, Okamoto M (2003) Polymer/layered silicate nanocomposites: a review from preparation to processing. Prog Polym Sci 28:1539–1641
6. Gao F (2004) Clay/polymer composites: the story. Mater Today 7:50–55
7. Okada A, Usuki A (2006) Twenty years of polymer-clay nanocomposites. Macromol Mater Eng 291:1449–1476
8. Okamoto M (2006) Recent advances in polymer/layered silicate nanocomposites: an overview from science to technology. Mater Sci Tech 22(7):756–779
9. Okamoto M, Nam PH, Maiti M, Kotaka T, Nakayama T, Takada M, Ohshima M, Usuki A, Hasegawa N, Okamoto H (2001) Biaxial flow-induced alignment of silicate layers in polypropylene/clay nanocomposite foam. Nano Lett 1:503–505
10. Nam PH, Okamoto M, Maiti P, Kotaka T, Nakayama T, Takada M, Ohshima M, Hasegawa N, Usuki A (2002) Foam processing and cellular structure of polypropylene/clay nanocomposites. Polym Eng Sci 42:1907–1918
11. Vaia RA, Ishii H, Giannelis EP (1993) Synthesis and properties of two-dimensional nanostructures by direct intercalation of polymer melts in layered silicates. Chem Mater 5:1694–1696
12. Vaia RA, Giannelis EP (1997) Lattice model of polymer melt intercalation in organically-modified layered silicates. Macromolecules 30:7990–7999
13. Vaia RA, Giannelis EP (1997) Polymer melt intercalation in organically-modified layered silicates: model predictions and experiment. Macromolecules 30:8000–8009
14. Hiroi R, Sinha Ray S, Okamoto M, Shiroi T (2004) Organically modified layered titanate: a new nanofiller to improve the performance of biodegradable polylactide. Macromol Rapid Commun 25:1359–1364
15. Yoshida O, Okamoto M (2006) Direct melt intercalation of polylactide chains into nano-galleries: interlayer expansion and nanocomposite structure. Macromol Rapid Commun 27: 751–757

16. Sinha Ray S, Yamada K, Okamoto M, Ueda K (2003) Biodegradable polylactide/montmorillonite nanocomposites. J Nanosci Nanotech 3:503–510
17. Yoshida O, Okamoto M (2006) Direct melt intercalation of polymer chains into nano-galleries: interdigitated layer structure and interlayer expansion. J Polym Eng 26:919–939
18. Sinha Ray S, Yamada K, Okamoto M, Ogami A, Ueda K (2003) New polylactide/layered silicate nanocomposites. 3. High-performance biodegradable materials. Chem Mater 15: 1456–1465
19. Saito T, Okamoto M, Hiroi R, Yamamoto M, Shiroi T (2006) Intercalation of diphenyl sulfide into nanao-galleries and preparation of poly(p-phenylenesulfide)-based nano-composites Macromol Mater Eng 291:1367–1374
20. Saito T, Okamoto M, Hiroi R, Yamamoto M, Shiroi T (2006) Dealmination of organically modified layered filler via solid-state processing. Macromol Rapid Commun 27:1472–1475
21. Chen JS, Poliks MD, Ober CK, Zhang Y, Wiesner U, Giannelis EP (2002) Study of the interlayer expansion mechanism and thermal–mechanical properties of surface-initiated epoxy nanocomposites. Polymer 43:4895–4904
22. Sinha Ray S, Okamoto K, Okamoto M (2003) Structure-property relationship in biodegradable poly(butylenes succinate)/layered silicate nanocomposites. Macromolecules 36:2355–2367
23. Okamoto K, Sinha Ray S, Okamoto M (2003) New poly(butylenes succinate)/layered silicate nanocomposites. 2. Effect of organically modified layered silicates on structure, properties, melt rheology, and biodegradability. J Polym Sci Part B Polym Phys 41:3160–3172
24. Utracki LA (1990) Polymer alloys and blends: thermodynamics and rheology. Hasser Publishers, New York
25. Fornes TD, Yoon PJ, Keskkula H, Paul DR (2001) Nylon 6 nanocomposites: the effect of matrix molecular weight. Polymer 42:9929–9940
26. Hoffman B, Dietrich C, Thomann R, Friedrich C, Mulhaupt R (2000) Morphology and rheology of polystyrene nanocomposites based upon organoclay. Macromol Rapid Commun 21:57–61
27. Ren J, Silva AS, Krishnamoorti R (2000) Linear viscoelasticity of disordered polystyrene − polyisoprene block copolymer based layered-silicate nanocomposites. Macromolecules 33:3739–3746
28. Mitchell CA, Krishnamoorti R (2002) Rheological properties of diblock copolymer/layered-silicate nanocomposites. J Polym Sci Part B Polym Phys 40:1434–1443
29. Lepoittevin B, Devalckenaere M, Pantoustier N, Alexandre M, Kubies D, Calberg C, Jerome R, Dubois P (2002) Poly(ε-caprolactone)/clay nanocomposites prepared by melt intercalation: mechanical, thermal and rheological properties. Polymer 43:4017–4023
30. Sinha Ray S, Maiti P, Okamoto M, Yamada K, Ueda K (2002) New polylactide/layered silicate nanocomposites. 1. Preparation, characterization, and properties. Macromolecules 35: 3104–3110
31. Sinha Ray S, Yamada K, Okamoto M, Ueda K (2003) New polylactide/layered silicate nanocomposites. 2. Concurrent improvements of material properties, biodegradability and melt rheology. Polymer 44:857–866
32. Okamoto K, Sinha Ray S, Okamoto M (2003) New poly(butylene succinate)/layered silicate nanocomposites. ii. Effect of organically modified layered silicates on structure, properties, melt rheology, and biodegradability. J Polym Sci Part B Polym Phys 41:3160–3172
33. Krishnamoorti R, Yurekli K (2001) Rheology of polymer layered silicate nanocomposites. Curr opin Colloid Interface Sci 6:464–470
34. Okamoto M, Taguchi H, Sato H, Kotaka T, Tatayama H (2000) Dispersed structure and rheology of lipophilized-smectite/toluene suspensions. Langmuir 16:4055–4058
35. Williams ML, Landel RF, Ferry JD (1955) The temperature dependence of relaxation mechanisms in amorphous polymers and other glass-forming liquids. J Amer Chem Soc 77:3701–3707
36. Nam PH (2001) The structure and properties of intercalated polypropylene/clay nanocomposites. Master thesis, Toyota Technological Institute

37. Galgali G, Ramesh C, Lele A (2001) A rheological study on the kinetics of hybrid formation in polypropylene nanocomposites. Macromolecules 34:852–858
38. Sinha Ray S, Okamoto M (2003) Biodegradable polylactide and its nanocomposites: opening a new dimension for plastics and composites. Macromol Rapid Commun 24:815–840
39. Okamoto M, Nam PH, Maiti P, Kotaka T, Hasegawa N, Usuki A (2001) A house of cards structure in polypropylene/clay nanocomposites under elongational flow. Nano Lett 1:295–298
40. Kotaka T, Kojima A, Okamoto M (1997) Elongational flow opto-rheometry for polymer melts—1. construction of an elongational flow opto-rheometer and some preliminary results. Rheol Acta 36:646–656
41. Ratto JA, Steeves DM, Welsh EA, Powell BE (1999) A study of polymer claynanocomposites for biodegradable applications. ANTEC'99, 1628–1632
42. Sinha Ray S, Okamoto M, Yamada K, Ueda K (2002) Polylactide-layered silicate nanocomposite: a novel biodegradable material. Nano Lett 2:1093–1096
43. Sinha Ray S, Yamda K, Ogami A, Okamoto M, Ueda K (2002) New polylactide/layered silicate nanocomposite: nanoscale control over multiple properties. Macromol Rapid Commun 23:943–947
44. Sinha Ray S, Yamada K, Okamoto M, Ueda K (2003) Melt rheology and foam processing. Macromol Mater Eng 288:936–944
45. Liu JW, Zhao Q, Wan CX (2001) Research progresses on degradation mechanism in vivo and medical applications of polylactic acid. Space Medicine Medical Eng 14:308
46. Hiroi R, Sinha Ray S, Okamoto M, Shiroi T (2004) Organically modified layered titanate: a new nanofiller to improve the performance of biodegradable polylactide. Macromol Rapid Commun 25:1359–1364
47. Fujishima A, Honda K (1972) Electrochemical photolysis of water at a semiconductor electrode. Nature 238:37–38
48. Ema Y, Ikeya M, Okamoto M (2006) Foam processing and cellular structure of polylactide-based nanocomposites. Polymer 47:5350–5359
49. Colton JS, Suh NP (1987) The nucleation of microcellular thermoplastic foam with additives: part i: theoretical considerations. Polym Eng Sci 27:485–492
50. Takada M (2004) Crystallization control and foam processing of semi-crystalline polymers via supercritical CO_2. PhD thesis, Kyoto University
51. Goel SK, Beckman EJ (1994) Generation of microcellular polymeric foams using supercritical carbon dioxide. i: effect of pressure and temperature on nucleation. Polym Eng Sci 34:1137–1147
52. Fletcher NH (1958) Size effect in heterogeneous nucleation. J Chem Phys 29:572–576
53. Shen J, Zeng C, Lee LJ (2005) Synthesis of polystyrene–carbon nanofibers nanocomposite foams. Polymer 46:5218–5224
54. Nam JY, Sinha SR, Okamoto M (2003) Crystallization behavior and morphology of biodegradable polylactide/layered silicate nanocomposite. Macromolecules 36:7126–7131
55. Kumar V, Weller JE (1991) Microcellular polycarbonate .1. Experiments on bubblenucleation and growth. ANTEC'91, 1401–1405
56. Weaire D, Fu TL (1988) The mechanical behavior of foams and emulsions. J Rheol 32: 271–284
57. Bitou M, Okamoto M (2008) Fabrication of porous 3-D structure from poly(L-lactide)-based nano-composite foams. Effect of foam structure on enzymatic degradation. Polym Deg Stab 93:1081–1087
58. Bitou M, Okamoto M (2007) Fabrication of porous 3-D structure from poly(L-lactide)-based nano-composite foam via enzymatic degradation. Int Polym Process 22:446–454
59. Williams DF (1981) Enzymatic hydrolysis of polyactic acid. Eng Med 10:5–7
60. Ebeling W, Hennrich N, Klockow M, Metz H, Orth HD, Lang H (1974) Proteinase K from *Tritirachium album* limber. Eur J Biochem 47:91–97
61. Reeve MS, McCarthy SP, Downey MJ, Gross RA (1994) Polylactide stereochemistry: effect on enzymic degradability. Macromolecules 27:825–831

62. Tsuji H, Miyauchi S (2001) Poly(L-lactide): VI effects of crystallinity on enzymatic hydrolysis of poly(L-lactide) without free amorphous region. Polym Degrad Stab 71:415–424
63. Iwata T, Doi Y (1998) Morphology and enzymatic degradation of poly(L-lactic acid) single crystals. Macromolecules 31:2461–2467
64. Abe H, Doi Y, Hori Y, Hagiwara T (1997) Compatibilizing effect of maleic anhydride functionalized sebs triblock elastomer through a reaction induced phase formation in the blends of polyamide 6 and polycarbonate: 2. Mechanical properties. Polymer 39:59–78
65. Li S, Girard A, Garreau H, Vert M (2001) Enzymatic degradation of polylactide stereocopolymers with predominant D-lactyl contents. Polym Degrad Stab 71:61–67
66. Cai Q, Shi G, Bei J, Wang S (2003) Enzymatic degradation behavior and mechanism of poly(lactide-co-glycolide) foams by trypsin. Biomaterials 24:629–638
67. Fukuda N, Tsuji H, Ohnishi Y (2002) Physical properties and enzymatic hydrolysis of poly(L-lactide)–$CaCO_3$ composites. Polym Degrad Stab 78:119–127
68. Wang CH, Fan KR, Hsiue GH (2005) Enzymatic degradation of PLLA-PEOz-PLLA triblock copolymers. Biomaterials 26:2803–2811
69. Brown JM, Curliss DB, Vaia RA (2000) Proceedings of PMSE, Spring Meeting, San Francisco, CA, p 278
70. Sinha Ray S, Okamoto K, Yamada K, Okamoto M (2002) Novel porous ceramic material via burning of polylactide/layered silicate nanocomposite. Nano Lett 2:423–425
71. Gibson LJ, Ashby MF (1988) Cellular solids. Pergamon Press, Oxford, p 8

Chapter 5
PCL/Clay Nano-Biocomposites

Samira Benali and Philippe Dubois

Abstract Poly(ε-caprolactone) is a biopolyester synthesized from fossil resources with interesting biodegradable properties. However, for certain applications, this biopolymer cannot be fully competitive with conventional thermoplastics since some of its properties appear too weak. The association of PCL with nano-sized fillers allows for significantly improving a large range of properties. The most reported nano-fillers in poly(ε-caprolactone)-based materials are represented by organo-modified clays more likely leading to one of the most widely investigated families of nano-biocomposites. This chapter is dedicated to this novel class of materials with a special focus set on the relationships between the production process, the extent of nano-filler dispersion and the thermo-mechanical properties, e.g., crystallinity and stiffness, of the related nano-biocomposites.

5.1 Introduction

Poly(ε-caprolactone) (PCL) is recognized not only as a biodegradable and non-toxic material but exhibits also a unique compatibilizing ability with a great variety of other polymers that can result in improved or modified properties [1]. These properties allow considering PCL for use in many applications, from biomedical to commodity polymer blends. PCL can be obtained by anionic, cationic

S. Benali (✉)
Centre d'Innovation et de Recherche en Matériaux Polymères CIRMAP,
Service des Matériaux Polymères et Composites (SMPC), Université de Mons-UMONS,
Place du Parc, 20, 7000 Mons, Belgium
e-mail: samira.benali@umons.ac.be

P. Dubois
CIRMAP, SMPC, Université de Mons-UMONS, Place du Parc, 20, 7000 Mons, Belgium

L. Avérous and E. Pollet (eds.), *Environmental Silicate Nano-Biocomposites*,
Green Energy and Technology, DOI: 10.1007/978-1-4471-4108-2_5,

or coordinated ring-opening polymerization (ROP) of ε-caprolactone (CL), enzymatic or radical polymerization [2]. PCL is a semi-crystalline polymer with a very low glass transition temperature T_g (~ -60 °C) and a relatively low melting temperature (~ 60 °C).

Nanocomposites consist in the incorporation of small amounts (usually less than 10 wt%) of nano-sized fillers into a polymer matrix. Among nanofillers, clays offer a great potential when combined within polymers [3]. No exhaustive list of clays will be presented here. This chapter is focused on two types of clays studied for the preparation of PCL-based nanocomposites: (i) layered silicate clays and (ii) needle-like clays. Bergaya [4] indicates that the two main features leading to the interest of these clays are: (1) their common availability, and (2) their amazing properties.

This chapter concentrates on nanocomposites for which PCL is the main matrix. PCL/starch blends, where PCL is a minor component as well as nanocomposites where PCL is used as minor compatibilizer for clay dispersion in non biopolymer-like matrices (such as styrene-acrylonitrile copolymers [5, 6] or chlorinated polyethylene [7–10]) are beyond the scope of this chapter.

5.2 Clays Studied with PCL/Clay Nanocomposites

5.2.1 Layered Silicate Clays

The most common layered silicate used for the preparation of PCL/clay nanocomposites is montmorillonite [3, 4].

Montmorillonite is a 2:1 phyllosilicate or smectite clay consisting of an octahedral sheet of alumina sandwiched between two opposing tetrahedral sheets of silica, negatively charged due to isomorphic substitution of a part of the trivalent aluminum cations for divalent cations such as Fe^{2+} or Mg^{2+} (see Fig. 3.4). The isomorphic substitution within the layers generates negative charges that are counterbalanced by alkali or alkaline earth cations situated in the interlayer. In order to render these hydrophilic phyllosilicates more organophilic, the hydrated cations of the interlayer can be exchanged with cationic surfactant such as alkylammoniums or imidazoliums. The modified clay being organophilic, and therefore more compatible with organic polymers, is largely studied for enhancing PCL properties.

5.2.2 Needle-Like Clays

Brigatti et al. [11] define sepiolite and attapulgite (or palygorskite) also as phyllosilicate clays with two-dimensional tetrahedral sheet. However, they differ from layered silicates in that they lack continuous octahedral sheets. Their structure

Table 5.1 Main clays studied within PCL/clay nanocomposites

Clay	Shape	Origin	References
Fluorohectorite	Mica-type layered silicate	Semi-synthetic	[21]
Bentonite (montmorillonite)	2:1 layered silicate	Natural cationic clay	[1, 7, 13, 14, 21, 25–32, 34–41, 43, 45, 46, 49, 50, 53–78]
Maghnite (partially protonated montmorillonite)	–	–	[23, 79]
Fluoromica	–	Synthetic cationic silicate	[80–82]
Magadiite	–	–	[83]
Sepiolite	Needle-like silicate	Natural clay	[16, 17]
Attapulgite	–		[18–20]

can be considered to contain ribbons of a 2:1 phyllosilicate structure, each ribbon being linked to the next one through inversion of SiO_4 tetrahedra along a set of Si–O bonds. These ribbons extend parallel to the X-axis and have an average width along Y of three linked pyroxene-like (magnesio-silicate) single chains in sepiolite and two linked chains in attapulgite (see Fig. 3.3). Chain phyllosilicates have a fibrous morphology with channels running parallel to the fiber length. The structural characteristics of these needle-like clays, with the presence of small channels, are responsible for their absorption and adsorption properties and the derived standard applications.

5.2.3 State of Art

For the last two decades, PCL clay nanocomposites based on layered and needle-like clays have been leading to more than 150 publications. The main clays studied in the literature are summarized in Table 5.1. Scientific community has dedicated the largest part of studies for the montmorillonite-based PCL nanocomposites. The same interest for montmorillonite is confirmed for a lot of other polymer-based nanocomposites (for reviews, see [3, 12, 13]). In case of ε-caprolactone (CL), the possible swelling of the clay interlayer galleries by this monomer, actually liquid at room temperature, followed by readily initiated ROP that induces excellent layered silicate nanoplatelets dispersion, allows to understand why PCL/lamellar clay nanocomposites have received significant attention.

Numerous studies have also focused on PCL/clay nanocomposite preparation by direct melt blending within the molten PCL matrix. Due to the low polarity of PCL,

Table 5.2 Alkylammonium cations frequently studied for the preparation of PCL/organoclay nanocomposites

Substituents of quaternary ammonium cations	Abbreviation	Formula
Dimethyl, benzyl, hydrogenated tallow	2MBHT	$(CH_3)_2\ CH_2\phi N^+(HT)$
Dimethyl, dihydrogenated tallow	2M2HT	$(CH_3)_2(HT)N^+(HT)$
Dimethyl, hydrogenated tallow, 2-ethylhexyl	2MHTL8	$(CH_3)_2C_8H_{17}N^+(HT)$
Distearyl, dimethyl	DS2MA	$(CH_3)_2N^+((CH_2)_{17}CH_3)_2$
Methyl, tallow, bis-2-hydroxyethyl	MT2EtOH	$(CH_3)_2(CH_2CH_2OH)_2N^+(T)$
Hexadecyltrimethyl	HD3MA	$C_{16}H_{33}N^+(CH_3)_2$
Stearyl, trimethyl	STAB	$CH_3(CH_2)_{17}N^+(CH_3)_3$
Tetraoctyl	TOA	$[CH_3(CH_2)_7]_4N^+$

polymer intercalation can only be reached if the clay minerals are previously surface-modified by exchange of the native alkaline counterions with organic cations like, e.g., alkylammonium cations [14]. The most frequently investigated alkylammonium cations for producing PCL/organoclay nanocomposites are shown in Table 5.2.

Two needle-like silicates have also been studied with PCL matrix. Sepiolite is a layered hydrated magnesium silicate characterized by a specific surface area higher than in layered phyllosilicates [15]. Fukushima et al. [16] have presented a comparative study between organo-modified layered silicate/PCL and unmodified sepiolite/PCL by melt blending and Duquesne et al. [17] have compared PCL nanocomposites using either natural sepiolite, sepiolite organo-modified by γ-aminopropyltriethoxysilane or sepiolite surface-grafted with PCL chains. Both studies highlight the interesting potential of sepiolite for the enhancement of PCL properties with the possibility to use the clay either as-received or after PCL grafting. Liu et al. [18, 19] studied the effect of attapulgite [4], another needle-like clay, onto the PCL properties. They showed that attapulgite can be used as an efficient nucleating agent [18] and they characterized the rheological behavior of the PCL/attapulgite nanocomposites [19]. PCL/attapulgite nanocomposites have also been recently synthesized by a combination of controlled ROP and "click" chemistry [20].

5.3 PCL/Clay Nanocomposite Preparation

PCL/clay nanocomposites can be produced using one of the four following preparation methods: (i) in situ polymerization of CL monomer, which consists in swelling the clay in the liquid monomer prior to its catalyzed polymerization, (ii) solvent casting route by swelling the clay and dissolving the PCL polymer in a common solvent, (iii) melt intercalation method based on the melt processing of the polymer/clay mixture and (iv) the PCL/clay masterbatch strategy, which consists in the preparation of PCL/clay premix (with high clay content) by in situ polymerization of CL in presence of hydroxylated ammonium surface-modified clays allowing for the grafting of PCL chains onto the clay surface (*PCL-grafted* "*nanohybrid*" *masterbatch*).

5.3.1 In Situ Polymerization Method

The production of PCL/clay nanocomposites by in situ polymerization of CL is largely reported starting from organo-modified layered silicate clays. The process consists in the addition of a layered silicate into CL prior to polymerization. The monomer intercalates into the clay galleries and, under appropriate conditions, polymerizes via ROP. The platelets are separated/expanded from each other by the action of the polymerization reaction, resulting eventually in exfoliation of the clay nanoplatelets within the so-formed PCL matrix [3]. The ability of CL to delaminate and disperse the layered silicate in the polymerization medium is related to a number of factors, including the exchange capacity of the silicate clays, the polarity of the medium, and the chemical nature of the interlayer cations [1, 21, 22].

Messersmith et al. were the first to report on the intercalative polymerization of CL by thermal activation at 170 °C in the presence of montmorillonite exchanged with Cr^{3+} cations [21]. Later, Haouas et al. [23] proposed a study demonstrating, by using solid state NMR characterization, that during the in situ formation of PCL/Maghnite (a partially protonated natural montmorillonite) nanocomposites, the grafting of the polyester chains onto the layered silicates took place from Brønsted/Lewis acidic sites located at the clay interface. Unlike the in situ polymerization of CL initiated by protonic acid without clay [24], no linear dependence of the PCL molecular weight on the carboxylic acid was observed in the presence of this acidic montmorillonite. Interestingly enough, Kubies et al. [25] reported on a convenient route to control the in situ intercalative polymerization of CL initiated by metal alkoxides such as dibutyltin(IV) dimethoxide ($Bu_2Sn(OMe)_2$) or catalyzed by tin(II) octoate ($Sn(Oct_2)$) directly in presence of organo-modified clays. Dubois et al. [25–33] reported the effect of the nature of the catalyst/initiator on both the molecular parameters of the PCL (molar mass and polydispersity) and the degree of clay exfoliation, when in situ polymerization was combined with hydroxyl-containing ammonium cations or not. Various metal alkoxides, either preformed (e.g. $Bu_2Sn(OMe)_2$) or formed 'in situ' by reaction of a metal catalyst (e.g. $Sn(Oct_2)$ or triethylaluminium ($AlEt_3$)) with alcohol-bearing ammonium modifiers were investigated. More recently, Chrissafis et al. [31] used a titanium (IV) butoxide as catalyst with nonfunctional alkylammonium modifier and Tarkin-Tas et al. [32] reported the effect of montmorillonite exchanged with an alkyl imidazolium ion bearing hydroxyl groups and activated by tin octoate for the preparation of exfoliated PCL/clay nanocomposites and its impact on crystallinity and thermal stability of the polyester matrix. Through all studies, it was demonstrated that the presence of hydroxyl groups "ionically" anchored at the clay surface in combination with a controlled coordination-insertion ROP process, allows for the formation of tethered polyester chains and largely favored the exfoliation of clay nanoplatelets.

Table 5.3 Reported routes of CL ring-opening polymerization in presence of specific organo-modified clays

Clay	Intercalative polymerization route	Ion exchanger	References
Fluorohectorite	Thermal activation	Cr^{3+}	[21]
Fluoromica	Thermal activation	Alkyl chain ammonium	[81, 82]
Montmorillonite	Thermal activation	Protonated 12-aminododecanoic acid	[1, 61, 64, 70, 84]
–	Sn-based catalyzed activation	Alkyl chain ammonium	[14, 29, 58, 68, 84]
–	–	Hydroxyalkyl chain ammonium	[14, 26, 28, 29, 68, 69, 84]
–	–	Hydroxyalkyl chain imidazolium	[32]
–	$AlEt_3$ catalyzed activation	Hydroxyalkyl chain ammonium	[26, 30]
–	Titanium (IV) butoxide catalyzed activation	Alkyl chain ammonium	[31]
–	Microwave activation	Hydroxyalkyl chain ammonium	[34, 35]

Another method described by Liao et al. [34, 35] can be pointed out as well, in which PCL/clay nanocomposites were prepared using hydroxyl-bearing organo-modified clay via microwave-assisted in situ ROP of CL, using tin octoate as catalyst and montmorillonite modified with MT2EtOH as initiator.

Table 5.3 summarizes the different routes reported in the literature for ring-opening polymerization of CL conducted in the presence of organo-modified clays.

As far as needle-like clays are concerned, Duquesne et al. prepared PCL/sepiolite nanohybrids by ROP of CL and in situ PCL anchoring onto sepiolite surface. These nanohybrids were synthesized from the aminopropyl functionalized sepiolite, the primary amino functions behaving as initiation sites for the ROP of CL catalyzed by $Sn(Oct)_2$.

5.3.2 Solvent Intercalation Method

This method consists in exfoliating the layered silicate clays into single nanolayers using a solvent where PCL is soluble. Owing to the weak forces (van der Waals interactions mainly) that stack the layers together in organo-modified clays, adequate solvent can readily swell and disperse the layered silicates. The solubilized polymer chains then adsorb onto the delaminated sheets and when the solvent is evaporated (or the mixture precipitated), the sheets reassemble, sandwiching the polymer chains to form, in the best case, an ordered multilayer structure [3]. The main interest in PCL is inherent to its biodegradable aspect, so environmentally

friendly preparations have been favored. Accordingly, organic solvent casting method is far less developed for PCL nanocomposites with the exception of a few scientific papers. An early paper, written by Jimenez et al. in 1996 [36] can be pointed out. It reports on a casting method used for the production of PCL-based biodegradable nanocomposites using a montmorillonite surface-modified with DS2MA ammonium cations. The composites were prepared by dissolving PCL in hot chloroform in presence of a given amount of the so-modified clay, then vaporizing the solvent to obtain homogeneous films. More recently, the preparation of PCL/exfoliated organoclay nanocomposites in presence of 50 % (v/v) solution of dichloromethane and dimethylformamide have been reported by Ludueña et al. [37].

5.3.3 Melt Intercalation Method

The melt intercalation method is based on polymer processing in molten state. Obviously, this method is highly preferred by industrials [38]. Indeed, in the context of sustainable development, melt intercalation is considered to be of the utmost importance as encountering ecological and economic requirements. Concerning phyllosilicate clays, the intercalation of a polymer inside a surface-modified layered silicate while the polymer is in its molten state is driven by enthalpic factors [3]. The likely good dispersion of clays into the PCL depends on a lot of parameters. First, the electrostatic interactions between natural silicate layers are very strong. Thus before compounding with PCL, pristine clays have to be modified in order to facilitate the dispersion of the clay nanoplatelets [39–41]. However, it is not always possible to prepare well dispersed nanocomposites, even though the interactions between matrix polymer and organic modifier are favorable. In other words, optimized mixing conditions should be applied for obtaining a fairly good dispersion to improve material properties, but unfortunately, it seems that such a systematic study has not been undertaken yet to optimize the melt processing of PCL/clay nanocomposites. Therefore, even if the objective is to exfoliate as much as possible the nanoclay into the PCL matrix, in practice, this is not often fully achieved. Most of the time, good dispersion means coexistence of individually spread clay nanolayers together with remaining small clay stacks and relatively good improvement of properties. Table 5.4 summarizes different mixing conditions as reported in the literature.

Some authors have chosen to use supercritical carbon dioxide ($scCO_2$) to prepare PCL/clay nanocomposites. $scCO_2$ has attracted much attention because the eco-friendly, chemically inert, inexpensive and non-flammable carbon dioxide has a potential to be an alternative to substitute organic solvents to reduce environmental pollution. Furthermore, this unique solvent combines several interesting properties, such as low viscosity or high diffusivity [6]. The preparation of PCL/clay nanocomposites by melt intercalation of PCL in $scCO_2$ was performed at 8.5 and 30.8 MPa of CO_2, a much lower temperature than T_m of PCL. These high pressures of CO_2 could assist melting of PCL because of the presence of CO_2-carbonyl groups interactions [42]. Shieh et al. [43] reported on the efficient intercalation of PCL in organo-modified layered silicate as performed in $scCO_2$.

Table 5.4 Mixing conditions for producing melt intercalated PCL/clay nanocomposites

Clay	Process	Mixing conditions	References
OMMT[a]	Mini-max molder	100 °C; 10′; 120 rpm	[39]
–	Twin-roll mill	130 °C; 10′	[28–30, 40, 41, 49, 58, 59]
–	Twin rotary roller-mixer	120 °C; 5′; 50 rpm	[71]
–	Internal mixer	100 °C; 12′; 100 rpm	[59]
–	–	70 °C; 3′; 80 rpm	[90]
–	–	80 °C; 15′; 50 rpm	[72]
–	–	80 °C; 15′; 65 rpm	[53]
–	–	90 °C; 5′; 40 rpm	[76]
–	–	140 °C; 250 rpm	[75]
–	–	75 °C; 5′; 60 rpm	[60]
–	Twin screw Extruder	60 °C; 60 rpm	[74]
Magadiite	Press	160 °C; 30′, 70 MPa	[83]
Sepiolite	Internal mixer	75 °C; 5′; 60 rpm	[16]
–	Twin-screw mini-extruder	80 °C; 10′	[17]

[a] *OMMT* Organo-modified montmorillonite

5.3.4 Masterbatch Method

A polymer/clay masterbatch is a premix of polymer and clay with a high content in inorganic fraction. These concentrated clay premixes are particularly appreciated in industry because of their easier use/handling with classical polymer manufacturing, avoiding the contact with volatile powders. In the same time, polymer/clay masterbatches can allow a pre-dispersion/pre-destructuration of the clay nanoparticles into the polymer favoring a fine distribution/dispersion of the clay after redispersion into the host polymer at low content.

Pucciariello et al. [44] reported the use of a clay organo-modified by 12-aminolauric acid (OMONT) to prepare OMONT/PCL composition with 30 wt% of inorganics by in situ polymerization of CL by thermal activation. Finally, this highly concentrated OMONT/PCL composite was redispersed into high-molecular weight PCL matrix.

An interesting two-step route to polymer/layered silicate nanocomposites was reported. This process, that is the ‘PCL-grafted clay nanohybrid masterbatch’ technique, consists in combining a ‘grafting-from’ intercalative controlled polymerization followed by a melt delamination process. In the first step, organo-modified clay is prepared by ion exchange of sodium cations naturally present in montmorillonite (MMT) with an adequate amount of hydroxylated alkylammonium cations. Then, the silicate layers are delaminated by catalyzed ROP of CL directly initiated from this adequately organo-modified filler surface. Finally, the resulting polyester-grafted high content organoclay nanohybrids are used as masterbatches and are dispersed in commercial polymeric matrices by melt blending. These masterbatches offer a great potential to disperse organoclay into a large range of commercial polymers known to be miscible with PCL.

Lepoittevin et al. [45] and Pollet et al. [46] investigated such PCL-grafted clay nanohybrid masterbatches with 32 wt% of inorganic into PCL matrix [45] and 36 wt% of inorganic into poly(butylene succinate) (PBS) or poly(butylene adipate-*co*-butylene terephthalate) (P(BA-co-BT) [46]. Both stiffness and thermal stability of the PCL-based nanocompositions as obtained from the PCL-clay masterbatch were significantly improved with respect to a microcomposite directly prepared by melt intercalation. However, Pollet et al. [46] noted poor results in terms of mechanical property enhancement as a result of the immiscibility between PCL and either PBS or P(BA-co-BT).

With acicular clays, Chen et al. [20] prepared a PCL/attapulgite nanocomposite by combination of controlled ROP and "click" chemistry. First, the chlorine-bearing attapulgite was prepared by the self-assembly of 3-chloropropyltrimethoxysilane from the surface of attapulgite. Then, the terminal chlorines of modified attapulgite were substituted with azido groups. As the second step, linear propargyl-terminated PCLs were synthesized by controlled ROP of CL in toluene with $Sn(Oct)_2$. Finally, the azido-terminated attapulgite was reacted with propargyl-terminated PCL by "click" chemistry to form highly concentrated PCL-attapulgite masterbatches.

5.4 PCL/Clay Nanocomposite Morphological Characterization

Because of their high aspect ratio, the clays have a great potential to enhance polymer properties if the filler is well dispersed into the polymer matrix. In order to achieve the clay dispersion into PCL matrix allowing to increase the clay/polymer interfacial areas to enhance PCL properties, the literature describes the different approaches developed in Sect. 5.3. And, as with other polymers, the clay exfoliation degree within PCL is a function of the composite processing parameters [38, 47]. In order to correlate the material microstructure with their processing and properties, it is fundamental to characterize the clay dispersion degree. With PCL/clay nanocomposites, authors used a set of tools well-known by materials scientists, (1) transmission electron microscopy (TEM) (2) X-ray diffraction (XRD) (3) atomic force microscopy (AFM) (4) differential scanning calorimetry (DSC) and (5) rheological techniques. Their use, by scientific community to determine the clay dispersion, is dependent on the clays and the availability of the tools. Advantages and drawbacks of each technique, to characterize the degree of clays dispersion into polymers have been largely discussed in the literature [3, 4, 47, 48]. In this chapter, focus is made onto the study of the clay dispersion into PCL with (i) smectite clays and (ii) needle-like clays.

5.4.1 Layered Silicate Clay Dispersion

Depending on the nature of the (organo) clay used and the preparation method, different structures of PCL/layered silicate nanocomposites, as with all polymer/

layered silicate (see review [3]), can be obtained: (i) a microcomposite, (ii) an intercalated nanocomposite or (iii) an exfoliated nanocomposite. Two complementary techniques are mainly used to characterize those structures. X-ray diffraction (XRD) is used to identify microcomposites (no shift of the diffraction peak) or intercalated structures (shift of the diffraction peak towards lower angle value) [3]. In the case of exfoliated structure, no more diffraction peaks are visible in the XRD patterns and transmission electronic spectroscopy (TEM) or atomic force microscopy (AFM) is then used to characterize the nanocomposite morphology. Many authors concluded to intercalated or exfoliated structure from morphological characterization. In practical, PCL/clay nanocomposite investigation leads often to an intercalated-exfoliated intermediate organization. In order to give a global view of both the best dispersion degree obtained in function of the nanocomposites preparation and the enhanced properties targeted, Table 5.5 gathers the most important works studying the structure-properties relationship.

Some studies were performed to better quantify the clay nanoplatelets dispersion degree within PCL/clay nanocomposites [47, 49–51]. Miltner et al. [50] demonstrated that three techniques are able to provide a direct and truly quantitative assessment of the nanofiller dispersion state. These methods allow paying attention to their sensitivity to the different length scales and physico-chemical aspects of the nanocomposite morphology.

They are based on (i) *dynamic rheometry measurement,* which indicates the formation of a percolating silicate network, but authors explain that the presence of this network formation cannot be by itself an evidence of an exfoliated structure. (ii) *secant modulus measurement* is considered more sensitive to the extent of silicate dispersion, but as it depends on the overall structure of the nanocomposite it may be influenced by phenomena such as an alteration of crystallinity or a processing-induced filler orientation. (iii) C_p^{excess} *approach*, obtained by the 'excess' measurement of the heat capacity, recorded during quasi-isothermal crystallization experiments, and caused by reversible melting and crystallization phenomena on the timescale of the imposed temperature modulation. The magnitude of this 'excess' heat capacity C_p^{excess} can be related to the nanofillers dispersion state.

5.4.2 Needle-Like Clays Dispersion

In addition to smectites, other silicate clays such as sepiolite or attapulgite are used to prepare PCL/clay nanocomposites. PCL not only interacts with the external surface of needle like silicate, but it can also penetrate into the structural tunnels of the mineral. TEM is the tool that is used by different authors [16, 17] to see the structure of materials at almost an atomic level.

AFM and TEM imaging allows a direct visual observation of the silicate dispersion within a polymer matrix; however, for a reliable qualitative evaluation of the nanofillers dispersion state, care should be taken to image truly representative areas of the sample, preferably at different magnifications.

Table 5.5 Main works studying the structure-properties relationship of PCL/clay nanocomposites

Clay type	Organo-modifier type	Process	Structure evaluation	Assessed structure	Targeted properties	References
MMT	No	Solvent casting	XRD and TEM	Disordered stacks	Crystallization, thermal degradation, biodegradation	[54]
OMMT	DS2MA	Solvent casting	WAXS and SAXS	Intercalated	Crystallization, DMA	[36]
–	MT2EtOH	Microwave-assisted in situ polymerization	XRD and TEM	Exfoliated	DMA	[35]
–	–	Solvent casting	XRD and TEM	Disordered intercalates	Crystallization, rheology, tensile testing, biodegradation	[77]
–	–	Melt intercalation	XRD and TEM	Semi-intercalated, semi-exfoliated	Tensile testing, thermal degradation, crystallization, rheology, impact strength,	[37, 40, 41]
–	–	–	–	Intercalated	Crosslinked material, crystallization, rheology, foaming, compression testing	[76]
–	–	–	XRD	Fine dispersed state	Transport properties, tensile testing	[59]
–	–	–	–	Intercalated	Crystallization	[56]
–	–	–	–	–	Biodegradation	[60]
–	2M2HT	Melt intercalation	XRD and TEM	Intercalated	Crystallization	[53]
–	2MBHT	Melt intercalation	XRD and TEM	Intercalated	Crystallization, tensile and flexural testing	[49]
–	2MHTL8	Solvent casting	XRD	Intercalated	Thermal degradation, tensile testing, DMA, Rheology	[52, 57, 91]
–	Protonated amino acid	In situ polymerization	XRD and nucleating action	Intercalated and exfoliated	Barrier properties crystallization	[1, 52, 86]

(continued)

Table 5.5 (continued)

Clay type	Organo-modifier type	Process	Structure evaluation	Assessed structure	Targeted properties	References
–	Dimethylamino-terminated CL	Melt intercalation	XRD and TEM	Intercalated	Tensile testing, DMA, crystallization	[71]
–	Imidazolium	In situ polymerization	XRD and TEM	Exfoliated	Thermal degradation, crystallization, DMA	[32]
–	Hydroxyl-bearing ammonium	In situ polymerization	XRD	Intercalated and exfoliated	Tensile properties, DMA, transport properties, crystallization kinetics	[69, 84, 89]
–	Biosurfactant	Melt intercalation	XRD and SEM fractured surface	Irregular distribution	DMA, crystallization, thermal degradation	[72]
–	PCL-grafted masterbatch	Solvent casting	XRD	Intercalated	Transport properties, tensile properties, DMA, crystallization	[47, 65]
–	STAB	$scCO_2$ intercalation	XRD	Intercalated	Thermal degradation, crystallization, DMA	[43]
–	Various surfactants	Melt intercalation	XRD and TEM,	From intercalated to exfoliated	Rheology, calorimetry, flexural testing	[50]
Fluoromica	HD3MA and dodecylamine hydrochloride	In situ polymerization	XRD	Intercalated	Crystallization	[80, 81]

Table 5.6 Sample shape used with PCL/clay nanocomposite studies

Clay type	Process	Shape sample for measuring PCL/clay nanocomposite	References
MMT	Solvent casting	Thin film (e < 1 mm)	[36, 54]
OMMT	In situ polymerization	Solid masterbatch	[5, 8–10]
–	–	Bulk	[31]
–	–	Powder	[30, 32, 42, 47, 68, 79, 86]
–	–	Compression-molding: thin film (e < 1 mm)	[16, 34, 35, 81, 85, 88]
–	–	Compression molding: thick film (e > 1 mm)	[26]
–	Solvent casting	Thin film (e < 1 mm)	[36, 37, 56, 77]
–	Solvent intercalation	Fibre (Electrospinning)	[57]
–	$scCO_2$ intercalation	Casting thin film (e < 1 mm)	[43]
–	–	Powder masterbatch	[6, 7]
–	Melt intercalation	Compression-molding: thick film (e > 1 mm)	[7, 28, 29, 40, 45, 50, 64]
–	–	Compression-molding: thin film (e < 1 mm)	[16, 56, 60, 72]
–	–	Injection-molding: Dumbbell-shaped (e = 3 mm)	[49, 59, 71, 74, 75]
–	–	Foam	[44, 76]
–	–	Extruded (string)	[53, 55, 80]
–	–	Extruded (pellet)	[48]
Attapulgite	In situ polymerization and click-chemistry	Powder	[22]
–	Melt intercalation	Compression-molding: thick film (e > 1 mm)	[19]
–	Solvent casting	Thin film	[18]
Sepiolite	Melt intercalation	Compression-molding: thick film (e > 1 mm)	[16, 17]

5.5 Influence of Nanocomposite Production Technique

Before studying the possible enhanced properties of polymer/clay nanocomposites, another fundamental factor has to be considered. Indeed, depending on the processes used for producing the nanocomposites, some clay orientation can be induced. This orientation can be interesting for some properties, e.g., gas transport, or prejudicial for others, e.g., mechanical behavior. Moreover, PCL being a semi-crystalline material, the preparation method can also influence on the degree of crystallinity of the polymer matrix as well as on the size and perfection of the crystallites.

Concerning PCL/clay nanocomposites, all literature references have been classified in Table 5.6 in function of the process and sample shape used for

measuring PCL/clay nanocomposites. Five different shapes were reported (1) solid bulk from in situ polymerization or melt intercalation (2) powder (after solvent precipitation or using $scCO_2$) (3) thin films (thickness: $e < 1$ mm) or thick films (thickness: $e < 1$ mm) by compression-molding or injection-molding, (4) fibbers or (5) foams.

5.6 PCL/Clay Nanocomposite Properties

PCL/clay nanocomposite properties have been widely studied. It is worth noting that in this contribution Chap. 9 gives important information about the permeability properties of PCL/clay nanocomposites while their biodegradation behavior is addressed in Chap. 16. Table 5.5 lists other main properties studied in the literature. Amongst those properties, this subsection aims to discuss, more specifically, the crystallization behavior and mechanical properties of PCL/layered silicate nanocomposites. Mechanical properties of crystalline polymers depend on the morphology, structure of the crystals and the degree of crystallization. Furthermore, the crystalline morphology is strongly affected by the presence of the clay particles and the extent of their dispersion throughout the polyester matrix. Similarly, the nature of the clay surface organomodifiers can play a highly significant role on the course of polymer crystallization as well as the process used to prepare the samples. As far as PCL is concerned as matrix, apart from promising mechanical properties, PCL-based nanocomposites exhibit also very interesting structural features as well as crystallization behavior.

5.6.1 Crystalline Behavior of PCL/Clay Nanocomposites

The study of polymer crystallization close to an inorganic surface is of particular importance, especially when the filler has a large surface area, such as in nanocomposites. In fact, it has been found that the inorganic surface may favor nucleation and crystal growth or development of a different crystalline structure and/or morphology [52]. Such effects are important because the ultimate properties of the materials (e.g., mechanical and thermal) are greatly modified. So, in order to control the property enhancement by clay incorporation, the knowledge of the thermal behavior and crystallization kinetics of PCL, especially before tensile test samples, are advisable. During crystallization of the polymer matrix, the silicate layers can both act as non-crystallizable barriers, that disturb or completely stop crystal growth, or can hinder the polymer chain motion, necessary for the crystallization [53].

With PCL/OMMT obtained by in situ polymerization, Pucciarello et al. [52] studied the isothermal kinetics of a series containing from 6 to 44 wt% in inorganics. They noted that the most enhanced thermal properties are obtained for

exfoliated nanocomposites with smaller crystallites—observed by light microscopy—with respect to those of neat PCL. In contrast, for intercalated nanocomposites, crystallites have an irregular, non-spherulitic shape that is attributed to the interruption of the crystallite growth in the vicinity of the large tacto. So, authors concluded that the presence of OMMT does not prevent PCL from crystallizing in a spherulitic morphology, but when the OMMT content increases, the crystallization becomes slower, especially at higher temperatures and for intercalated nanocomposites. This delay can be explained by the fact that the nanoclay acts as nucleating agents for PCL but little or negatively affects the linear growth rate of PCL spherulites. Later, Tarkin-Tas et al. [32] studied the PCL/exfoliated silicate layer nanocomposite obtained by in situ polymerization of ε-CL from hydroxyl-containing ammonium cations used to organomodify the clay. The focus to the PCL crystallization behavior highlighted that the PCL degree of crystallinity increases with increasing clay content—i.e. from 51 to 69 % for 5 wt% of inorganics. The authors explained that highly exfoliated structure increases the surface area but with virtually all chains bound to the surfaces. This led to a pre-organization of the chains near the platelets that enhanced nucleation and increased the degree of crystallinity with increasing clay content.

Concerning the solvent intercalation method, Jimenez et al. [36] prepared an intercalated PCL/organoclay nanocomposite starting from the polymer in chloroform solution. These authors also reported that a small amount of clay seemed to serve as a PCL nucleating agent, whereas a large amount of it has the opposite effect. On the other hand, Ludueña et al. [37] prepared clay nanocomposites with high dispersion state, both in melt intercalation and in presence of 50 % (v/v) solution in CH_2Cl_2/DMF, and have shown that the degree of crystallinity remained almost unchanged up to 10 wt% of inorganics. And this observation was achieved whatever the preparation method. However, more recently, Wu et al. [54] dispersed Na^+-MMT in DMF to prepare PCL nanocomposites by solvent casting. They indicated that the crystallization behavior of PCL depends on the balance between the nucleating effect and the suppression of the PCL segment mobility. Polarizing microscopy imaging, applied to study the MMT on the spherulite dimensions, has shown that the spherulites became gradually smaller upon increasing the clay content and convert into lamellar crystals for 4 wt% of inorganics.

As far as melt intercalated PCL/clay nanocomposites are concerned, non-isothermal crystallization experiments on PCL have been described. Lepoittevin et al. [41] reported a decrease of X_c with organoclay content. With the work of Homminga et al. [53], the addition of low MMT quantities leads to an increase of nucleating sites but this trend is reversed when the MMT concentration is sufficiently high to hinder the process of crystal growth. In the same trend, Chen et al. [49] studied the crystallinity of PCL/clay nanocomposites with clay loading from 1.7 to 59 wt% prepared by melt processing and authors also concluded that the crystallinity of PCL was increased when the organoclay loading was low, and it was decreased with higher clay loading. On the other side, Di et al. [55] investigated the isothermal crystallization behavior of PCL/clay nanocomposites,

with clay concentration ranging from 0.1 to 10 wt%. A theoretical description of the effects of nanoclay on the crystallization phenomenon has been carried out. This work showed that the very well dispersed organoclay platelets acted as nucleating agents in PCL matrix, reducing the crystallization half-time $t_{1/2}$. In the same way, Ludueña et al. [56] have shown the correlation between polymer/clay compatibility—i.e. the dispersion state—and the crystallization rate. The nanocomposite with the less dispersed clay produced the highest spherulitic growth rate with respect to the neat matrix at the same undercooling degree.

5.6.2 Mechanical Properties

PCL is a ductile polymer able to sustain large deformations. Unfortunately, the elastic modulus is rather low making it useless for any application that requires higher rigidity. Thus, the addition of filler can contribute to improve its stiffness.

Mechanical properties of PCL are highly dependent on both of the crystalline state—i.e. of the thermal history—and of the measurements of mechanical properties. So, the comparison of values measured by different groups is rendered difficult. It is therefore only possible to depict general trends in mechanical behavior. The following section reports some representative results mostly depending on the method of preparation of the PCL/clay nanocomposites. It is worth noting that almost no work has been reported on the mechanical properties of PCL/clay (nano)composites as produced by in situ polymerization. One illustration can be found in the works performed by Chrissafis et al. [31]. However no detailed investigation on the structure of the so-produced compositions was provided making difficult the interpretation of the results. Interestingly enough, in situ polymerization has been combined to melt intercalation for producing higher performance nanocomposite materials (*vide infra*: masterbatch process).

Solvent intercalation method

With solvent intercalation method, Ludueña et al. [37] have shown that adequate selection of the solvent/polymer/organoclay system is needed to lead to significant improvement of the stiffness of the resulting materials. When dimethylformamide (DMF), a good dispersant of montmorillonite organomodified with MT2EtOH is added to dichloromethane, larger Young's moduli are measured with increase by 47 % compared to neat PCL for a dispersion in 50/50 v/v CH_2Cl_2/DMF while no stiffness improvement is observed with CH_2Cl_2 alone, for PCL loaded with 5 wt% of the organoclay. Here again, a slight decrease in elongation at break, from 668 to 445 %, is observed when dispersing 5 wt% of organoclay. Upon increasing the organoclay loading above 5 wt%, the composite stiffness is however not improved while ultimate properties are strongly decreased, indicating some limitation of the solvent intercalation method for preparation of stiff and ductile PCL/clay nanocomposites. Marras et al. [57] have also prepared PCL/2MHTL8-modified montmorillonite nanocomposites by solvent intercalation method, using

Table 5.7 Tensile properties of PCL before and after filling with 3 wt% of layered silicate by melt blending at 130 °C

Sample	Young's modulus (in MPa)	Elongation at break ε_b (in %)	Stress at break σ_b (in MPa)
PCL	216 ± 5	745 ± 43	37 ± 2
PCL/MMT	200 ± 9	715 ± 44	35 ± 3
PCL/MMT-2M2HT	282 ± 9	528 ± 58	26 ± 3
PCL/MMT-2MHTL8	280 ± 10	530 ± 58	26 ± 3
PCL/MMT-MT2EtOH	272 ± 16	560 ± 62	25 ± 3

dichloromethane and sonication to insure the clay dispersion and ended up with a intercalated structure, even if partial exfoliation cannot be excluded. The recovered PCL nanocomposite films (1, 3, 5, 9 and 15 wt% of organoclay) show a small but significant increase in Young's modulus during tensile testing (12 for 3 wt% of organoclay and 29 % for 5 wt% of organoclay) while experiencing a steady decrease in ductility (going from 702 % of elongation at break for the pure PCL sample down to 494 % for the 15 wt% organoclay nanocomposite) and in tensile strength.

Melt intercalation method

Concerning melt intercalation method, better improvement in mechanical properties—i.e. larger increase in stiffness—has been obtained. The effect of the content and nature of the clay on the mechanical properties of the PCL (nano)composites by tensile testing have been studied in the literature [13, 40, 41, 58] and the major results are summarized in Table 5.7. The presence of a tiny amount of filler—i.e. as low as 3 wt% in inorganics—allows to increase the elastic modulus from 216 MPa for unfilled PCL to around 280 MPa for intercalated nanocomposites obtained with organo-modified clays. It is worth pointing out that increasing the clay content enhances the material stiffness (Fig. 5.1). For instance, an elastic modulus as high as 399 MPa has been measured for a PCL nanocomposite filled with 10wt% of MMT-MT2EtOH, attesting for an almost twofold increase of the material rigidity. By contrast, the microcomposites obtained from non-modified clays (MMT) show rather a constant value of Young's modulus with clay content. The mechanical properties of these microcomposites and unfilled PCL remain in the same range.

For filler contents below 5 wt%, PCL retains a good ductility with an elongation at break only slightly reduced and higher than 550 %. The stress at break, which represents the ultimate strength that the material can sustain before breaking, decreases with clay concentration but remains maintained at an acceptable level. All these observations show that PCL nanocomposites present a high stiffness while retaining a good ductility at least up to a filling level of 5 wt%. Above this threshold, a drastic loss in ultimate tensile properties is observed.

Later, Di et al. [59] have also investigated mechanical properties from tensile tests of PCL/MMT-MT2EtOH and PCL/MMT-M2HT nanocomposites prepared

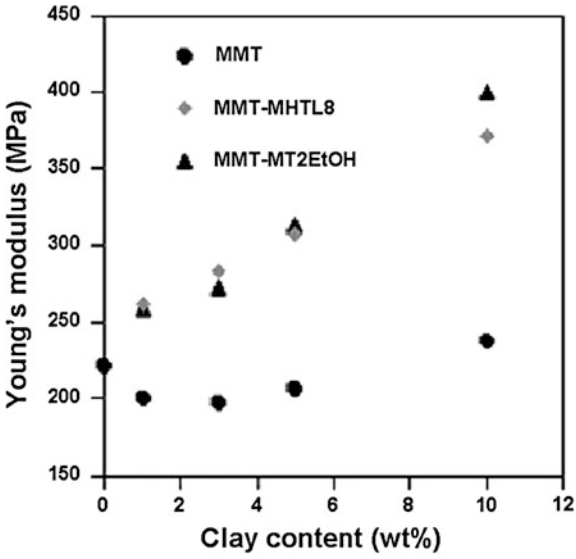

Fig. 5.1 Evolution of Young's modulus with clay content for composite samples prepared with MMT, MMT-2MHTL8 and MMT-MT2EtOH (adapted from Pollet and Dubois 2003 [13])

by melt intercalation method. The presence of 2 wt% of organoclay content allows to increase the elastic modulus from 174 MPa for unfilled PCL to around 246 MPa for very well dispersed nanocomposites obtained with MMT-MT2EtOH. This increase of more than 41 % of modulus is taken to a decrease of elongation at break of less than 10 %—i.e. from 804 to 718 %. The use of MMT-M2HT led to intercalated structure with an increase of modulus of only 12 %—from 174 to 196 MPa with 2 wt% of organoclay content—and a decrease of ultimate properties of more than 25 %—from 804 to 604 %. For filler contents of 10 wt %, PCL retains a good ductility with an elongation at break at 588 %.

Chen et al. [49] also prepared PCL/clay composites with three type of clay—i.e. MMT, MMT-2M2HT, MMT-2MBHT—and clay loading from 1.7 to 59 wt% by melt-processing. The presence of clay in PCL increased tensile strength, tensile modulus and elongation at break for clay loading typically lower (<10 wt% of inorganic). Results showed that nanocomposites with more exfoliation give greater property enhancement. Taking sample, MMT-2M2HT containing 4.2 wt% of platelets, the tensile strength, Young's modulus and elongation at break were increased from 17 to 31 MPa, 439 to 655 MPa and 165 to 522 %, respectively.

Masterbatch method

As previously described, melt intercalation of preformed polymers and in situ intercalative polymerization represent the most commonly used techniques to prepare polymer/clay nanocomposites. Both techniques display their own advantages. The major advantage of the melt blend intercalation is its easiness of

processing since it only requires the addition of the filler during the extrusion/kneading process, without making any important change on the industrial production line. On the other hand, the in situ polymerization process allows to obtain exfoliated nanocomposites (when using the appropriate functionalized organo-modified clay), displaying much enhanced properties.

Accordingly, a two-step method, named masterbatch process, has been approached for the preparation of PCL layered silicate nanocomposites by combining the in situ intercalative polymerization and the melt blend intercalation process. In such a process, a highly filled (organomodified) clay PCL is first prepared by in situ intercalation polymerization of ε-CL, followed by its addition as a masterbatch that is blended with the molten, polyester matrix. As will be shown, this method permits to prepare PCL-based nanocomposites with a high degree of exfoliation which cannot be achieved by direct mixing of PCL and clay.

Lepoittevin et al. [45] and Pollet et al. [13] compared the mechanical properties measured for the PCL/MMT nanocomposites (obtained by the two-step masterbatch process) and for the microcomposites prepared by direct melt blending of PCL and MMT under the same thermal and processing conditions. The difference in properties observed for the two series of composites is the expression of the difference in their morphology.

The elastic modulus is improved from 217 MPa for unfilled PCL up to 365 MPa for the nanocomposites (filled with 10 wt% MMT) prepared by the masterbatch process. In contrast, the microcomposites prepared by direct melt blending with MMT showed only very limited increase in stiffness.

All the PCL nanocomposites originated from the masterbatches remain rather ductile, with an elongation at break higher than 300 %. The stress at break slightly drops when the clay content is increased but remains at an acceptable level. Similar observations have been reported for the two organomodified clays (MMT-2MHTL8 and MMT-MT2EtOH), showing increased stiffness and preserved ultimate tensile properties.

5.7 Conclusions

Aliphatic polyester layered silicate nanocomposites based on poly(ε-caprolactone) (PCL) have been prepared by different processes with different clays.

Since the main interest in PCL is inherent to its biodegradable aspect, organic solvent casting method is far less interesting for the preparation of PCL nanocomposites. So, other processing routes—i.e. in situ polymerization, melt intercalation and masterbatch methods—were preferred. It has been demonstrated that melt blending with organo-modified clay such as MMT-2M2HT, MMT-2MHTL8 or MMT-MT2EtOH, yields intercalated nanocomposites with the possibility of partial exfoliation. Even at low organo-clay content, substantial improvement of mechanical performances has been noticed. However, melt blending of natural montmorillonite with PCL leads to microphase separated compositions.

As an alternative, in situ intercalative polymerization of ε-caprolactone directly in between the silicate layers was also approached. In this way, intercalated nanocompositions could be obtained even with "unmodified" MMT. Furthermore, exfoliated nanocomposites have been recovered starting from MMT-MT2EtOH, thus a montmorillonite surface-modified by ammonium cations bearing two primary hydroxyl functions. Such morphology resulted from the direct grafting of the growing polyester chains onto the hydroxyl functionalized silicate layers. As expected the clay delamination confers an additional effect in the improvement of the materials properties, in comparison with intercalated nanocompositions obtained by melt blending.

Studies noted that improvement in clay exfoliation leads to a large increase in the stiffness of the materials with only a small decrease of ductility, at least at filler content lower than 10 wt%.

Different works showed that the very well dispersed organoclay platelets acted as nucleating agents in crystallization of the PCL matrix at low loading.

Interestingly enough, both synthetic pathways have been successively combined to each other, via the so-called masterbatch process. It consists of producing first a highly filled clay/PCL nanocomposition by in situ polymerization and then dispersing it within preformed PCL matrix by melt blending. Either intercalated (with MMT) or partially intercalated/partially exfoliated (with MMT-MT2EtOH) nanocomposites have been prepared with much improved mechanical and thermal properties.

Stiffness of the PCL nanocomposites was significantly improved compared to microcomposites directly prepared by melt intercalation. This process presents major advantages since it allows preparing intercalated nanocomposites (or even exfoliated structures) with a high molecular weight polymer matrix. Furthermore, this synthetic pathway permits to bring compatibility between the inorganic filler and the polymer matrix by anchoring PCL chains on the clay surface. This strategy has been extended to polymers known for being miscible with PCL (such as poly(vinyl chloride) [45], styrene-acrylonitrile copolymers [5, 6] or chlorinated polyethylene [7–10]).

Finally, by its easiness of processing (simple addition of the filler during the extrusion process), the masterbatch process presents a good potential for further industrial applications.

References

1. Messersmith PB, Giannelis EP (1995) Synthesis and barrier properties of poly(ε-caprolactone)-layered silicate nanocomposites. J Polym Sci Part A: Polym Chem 33:1047–1057
2. Albertsson AC (2002) Degradable aliphatic polyesters. Adv Polym Sci 157:1–179
3. Dubois P (2000) Polymer-layered silicate nanocomposites: preparation, properties and uses of a new class of materials. Mater Sci Eng R 28:1–63
4. Bergaya F, Theng BKG, Lagaly G (2006) Handbook of clay science. Developments in Clay Science Editor, Oxford
5. Benali S, Olivier A, Brocorens P et al (2008) Fire and gas barrier properties of poly(styrene-co-acrylonitrile) nanocomposites using polycaprolactone/clay nanohybrid based-masterbatch. Adv Mater Sci Eng 11. doi:10.1155/2008/394235

6. Urbanczyk L, Calberg C, Benali S et al (2008) Poly(caprolactone)/clay masterbatches prepared in supercritical CO_2 as efficient clay delamination promoters in poly(styrene-co-acrylonitrile). J Mater Chem 18:4623–4630
7. Urbanczyk L, Calberg C, Stassin F et al (2008) Synthesis of PCL/clay masterbatches in supercritical carbon dioxide. Polymer 49:3979–3986
8. Benali S, Peeterbroeck S, Brocorens P et al (2008) Chlorinated polyethylene nanocomposites using PCL/clay nanohybrid masterbatches. Eur Polym J 44:1673–1685
9. Broekaert C, Peeterbroeck S, Benali S et al (2007) Chlorinated polyethylene/layered silicate nanocomposites: poly(ε-caprolactone)-based "masterbatch" approach. Eur Polym J 43: 4160–4168
10. Brocorens P, Benali S, Broekaert C et al (2008) Microscopic morphology of chlorinated polyethylene-based nanocomposites synthesized from poly(ε-caprolactone)/clay masterbatches. Langmuir 24:2072–2080
11. Brigatti MF, Galan E, Theng BKG (2006) Structures and mineralogy of clay minerals. In: ES Ltd Handbook of clay science. Elsevier Science, Oxford
12. Sinha Ray S, Okamoto M (2003) Polymer/layered silicate nanocomposites: a review from preparation to processing. Prog Polym Sci 28:1539–1641
13. Pollet E, Paul M-A, Dubois P (2003) New aliphatic polyester layered silicate nanocomposites. In: Chiellini E, Solaro R (eds) Biodegradable polymers and plastics. Klumer Academic, Plenum Publishers, New-York
14. Lepoittevin B, Pantoustier N, Devalckenaere M et al (2002) Poly(ε-caprolactone)/clay nanocomposites by in situ intercalative polymerization catalyzed by dibutyltin dimethoxide. Macromolecules 35:8385–8390
15. Tartaglione G, Tabuani D, Camino G et al (2008) PP and PBT composites filled with sepiolite: morphology and thermal behaviour. Compos Sci Technol 68:451–460
16. Fukushima K, Tabuani D, Camino G (2009) Nanocomposites of PLA and PCL based on montmorillonite and sepiolite. Mater Sci Eng C 29:1433–1441
17. Duquesne E, Moins S, Alexandre M et al (2007) How can nanohybrids enhance polyester/sepiolite nanocomposite properties? Macromol Chem Phys 208:2542–2550
18. Liu Q, Peng Z, Chen D (2007) Nonisothermal crystallization behavior of poly(ε-caprolactone)/attapulgite nanocomposites by DSC analysis. Polym Eng Sci 47:460–466
19. Liu Q, Chen D (2008) Viscoelastic behaviors of poly(ε-caprolactone)/attapulgite nanocomposites. Eur Polym J 44:2046–2050
20. Chen J, Wang H, Luo W et al (2010) Preparation of poly (ε-caprolactone)@attapulgite nanocomposites via a combination of controlled ring-opening polymerization and click chemistry. Colloid Polym Sci 288:173–179
21. Messersmith PB, Giannelis EP (1993) Polymer-layered silicate nanocomposites: in situ intercalative polymerization of ε-caprolactone in layered silicates. Chem Mater 5:1064–1066
22. Gardebien F, Gaudel-Siri A, Bredas J-L et al (2004) Molecular dynamics simulations of intercalated poly(ε-Caprolactone)-montmorillonite clay nanocomposites. J Phys Chem B 108:10678–10686
23. Haouas M, Harrane A, Belbachir M et al (2007) Solid state NMR characterization of formation of poly(ε-caprolactone)/maghnite nanocomposites by in situ polymerization. J Polym Sci Part B: Polym Phys 45:3060–3068
24. Mecerreyes D, Jérôme R, Dubois P (1999) Novel macromolecular architectures based on aliphatic polyesters relevance of the 'coordination-insertion' ring-opening polymerization. Adv Polym Sci 147:1–59
25. Kubies D, Pantoustier N, Dubois P et al (2002) Controlled ring-opening polymerization of ε-Caprolactone in the presence of layered silicates and formation of nanocomposites. Macromolecules 35:3318–3320
26. Lepoittevin B, Pantoustier N, Alexandre M et al (2002) Polyester layered silicate nanohybrids by controlled grafting polymerization. J Mater Chem 12:3528–3532
27. Lepoittevin B, Pantoustier N, Alexandre M et al (2002) Layered silicate/polyester nanohybrids by controlled ring-opening polymerization. Macromol Symp 183:95–102

28. Gorrasi G, Tortora M, Vittoria V et al (2003) Vapor barrier properties of polycaprolactone montmorillonite nanocomposites: effect of clay dispersion. Polymer 44:2271–2279
29. Viville P, Lazzaroni R, Pollet E et al (2003) Surface characterization of poly(ε-caprolactone)-based nanocomposites. Langmuir 19:9425–9433
30. Gain O, Espuche E, Pollet E et al (2004) Gas barrier properties of poly(ε-caprolactone)/clay nanocomposites: influence of the morphology and polymer/clay interactions. J Polym Sci Part B: Polym Phys 43:205–214
31. Chrissafis K, Antoniadis G, Paraskevopoulos KM et al (2007) Comparative study of the effect of different nanoparticles on the mechanical properties and thermal degradation mechanism of in situ prepared poly(ε-caprolactone) nanocomposites. Compos Sci Technol 67:2165–2174
32. Tarkin-Tas E, Goswami SK, Nayak BR et al (2008) Highly exfoliated poly(ε-caprolactone)/organomontmorillonite nanocomposites prepared by in situ polymerization. J Appl Polym Sci 107:976–984
33. Pollet E, Delcourt C, Alexandre M et al (2004) Organic-inorganic nanohybrids obtained by sequential copolymerization of ε-caprolactone and L,L -lactide from activated clay surface. Macromol Chem Phys 205:2235–2244
34. Liao L, Zhang C, Gong S (2007) Preparation of poly(ε-caprolactone)/clay nanocomposites by microwave-assisted in situ ring-opening polymerization. Macromol Rapid Commun 28:1148–1154
35. Liao L, Zhang C, Gong S (2007) Microwave-assisted synthesis and characterization of poly(ε-caprolactone)/montmorillonite nanocomposites. Macromol Chem Phys 208: 1301–1309
36. Jimenez G, Ogata N, Kawai H et al (1997) Structure and thermal/mechanical properties of poly(ε-caprolactone)-clay blend. J Appl Polym Sci 64:2211–2220
37. Ludueña LN, Alvarez VA, Vazquez A (2007) Processing and microstructure of PCL/clay nanocomposites. Mater Sci Eng A A460–A461:121–129
38. Bordes P, Pollet E, Avérous L (2009) Nano-biocomposites: biodegradable polyester/nanoclay systems. Prog Polym Sci 34:125–155
39. Kim SW, Jo WH, Lee MS et al (2001) Preparation of clay-dispersed poly(styrene-co-acrylonitrile) nanocomposites using poly(ε-caprolactone) as a compatibilizer. Polymer 42:9837–9842
40. Pantoustier N, Alexandre M, Degree P et al (2001) Poly(ε-caprolactone) layered silicate nanocomposites: effect of clay surface modifiers on the melt intercalation process. e-Polym 9
41. Lepoittevin B, Devalckenaere M, Pantoustier N et al (2002) Poly(.vepsiln.-caprolactone)/clay nanocomposites prepared by melt intercalation: mechanical, thermal and rheological properties. Polymer 43:4017–4023
42. Shieh Y-T, Lai J-G, Tang W-L (2008) Preparation of polyester/montmorillonite nanocomposites in supercritical CO_2. In: 235th ACS national meeting. American Chemical Society, New Orleans, United State
43. Shieh Y-T, Lai J-G, Tang W-L et al (2009) Supercritical CO_2 intercalation of polycaprolactone in layered silicates. J Supercrit Fluids 49:385–393
44. Pucciariello R, Villani V, Gorrasi G et al (2005) Phase behavior of blends of poly(ε-caprolactone) and a modified montmorillonite-poly(ε-caprolactone) nanocomposite. J Macromol Sci Phys B44:79–92
45. Lepoittevin B, Pantoustier N, Devalckenaere M et al (2003) Polymer/layered silicate nanocomposites by combined intercalative polymerization and melt intercalation: a masterbatch process. Polymer 44:2033–2040
46. Pollet E, Delcourt C, Alexandre M et al (2006) Transesterification catalysts to improve clay exfoliation in synthetic biodegradable polyester nanocomposites. Eur Polym J 42:1330–1341
47. Luo ZP, Koo JH (2008) Quantification of the layer dispersion degree in polymer layered silicate nanocomposites by transmission electron microscopy. Polymer 49:1841–1852
48. Gupta RK, Kennel E, Kim KJ (2010) Polymer nanocomposites handbook. CRC Press, Boca Raton

49. Chen B, Evans JRG (2006) Poly(ε-caprolactone)-clay nanocomposites: structure and mechanical properties. Macromolecules 39:747–754
50. Miltner HE, Watzeels N, Block C et al (2010) Qualitative assessment of nanofiller dispersion in poly(ε-caprolactone) nanocomposites by mechanical testing, dynamic rheometry and advanced thermal analysis. Eur Polym J 46:984–996
51. Chen B, Evans JRG (2006) Nominal and effective volume fractions in polymer-clay nanocomposites. Macromolecules 39:1790–1796
52. Pucciariello R, Villani V, Belviso S et al (2004) Phase behavior of modified montmorillonite-poly(ε-caprolactone) nanocomposites. J Polym Sci Part B: Polym Phys 42:1321–1332
53. Homminga D, Goderis B, Dolbnya I et al (2006) Crystallization behavior of polymer/montmorillonite nanocomposites. Part II. Intercalated poly(ε-caprolactone)/montmorillonite nanocomposites. Polymer 47:1620–1629
54. Wu T, Xie T, Yang G (2009) Preparation and characterization of poly(ε-caprolactone)/Na+-MMT nanocomposites. Appl Clay Sci 45:105–110
55. Di ME, Iannace S, Sorrentino L et al (2004) Isothermal crystallization in PCL/clay nanocomposites investigated with thermal and rheometric methods. Polymer 45:8893–8900
56. Luduena LN, Vazquez A, Alvarez VA (2008) Crystallization of polycaprolactone-clay nanocomposites. J Appl Polym Sci 109:3148–3156
57. Marras SI, Kladi KP, Tsivintzelis I et al (2008) Biodegradable polymer nanocomposites: the role of nanoclays on the thermomechanical characteristics and the electrospun fibrous structure. Acta Biomater 4:756–765
58. Pantoustier N, Lepoittevin B, Alexandre M et al (2002) Biodegradable polyester layered silicate nanocomposites based on poly(ε-caprolactone). Polym Eng Sci 42:1928–1937
59. Di Y, Iannac S, Sanguigno L et al (2005) Barrier and mechanical properties of poly(caprolactone)/organoclay nanocomposites. Macromol Symp 228:115–124
60. Fukushima K, Abbate C, Tabuani D et al (2010) Biodegradation trend of poly(ε-caprolactone) and nanocomposites. Mater Sci Eng C 30:566–574
61. Krishnamoorti R, Giannelis EP (1997) Rheology of end-tethered polymer layered silicate nanocomposites. Macromolecules 30:4097–4102
62. Giannelis EP (1998) Polymer-layered silicate nanocomposites: synthesis, properties and applications. Appl Organomet Chem 12:675–680
63. Ko MB (2000) One-pot synthesis of clay-dispersed poly(styrene-co-acrylonitrile) copolymer nanocomposite using poly(ε-caprolactone) as a compatibilizer. Korea Polym J 8:186–191
64. Krishnamoorti R, Giannelis EP (2001) Strain hardening in model polymer brushes under shear. Langmuir 17:1448–1452
65. Gorrasi G, Tortora M, Vittoria V et al (2002) Transport and mechanical properties of blends of poly(ε-caprolactone) and a modified montmorillonite-poly(ε-caprolactone) nanocomposite. J Polym Sci Part B: Polym Phys 40:1118–1124
66. Kwak S-Y, Oh KS (2003) Effect of thermal history on structural changes in melt-intercalated poly(ε-caprolactone)/organoclay nanocomposites investigated by dynamic viscoelastic relaxation measurements. Macromol Mater Eng 288:503–508
67. Pantoustier N, Alexandre M, Degee P et al (2003) Intercalative polymerization of cyclic esters in layered silicates: thermal vs. catalytic activation. Compos Interfaces 10:423–433
68. Calberg C, Jerome R, Grandjean J (2004) Solid-state NMR study of poly(ε-caprolactone)/clay nanocomposites. Langmuir 20:2039–2041
69. Karaman VM, Privalko EG, Privalko VP et al (2005) Stretching calorimetry studies of poly(ε-caprolactone)/organoclay nanocomposites. Polymer 46:1943–1948
70. Pucciariello R, Villani V, Guadagno L et al (2005) Equilibrium thermal behavior and morphology of organophilic montmorillonite/poly(ε-caprolactone) nanocomposites. J Polym Sci Part B: Polym Phys 44:22–32
71. Shibata M, Teramoto N, Someya Y et al (2007) Nanocomposites based on poly(ε-caprolactone) and the montmorillonite treated with dibutylamine-terminated ε-caprolactone oligomer. J Appl Polym Sci 104:3112–3119

72. Liao H-T (2008) A new application of biosurfactant for the preparation of polycaprolactone/layered silicate nanocomposites. Polym Eng Sci 48:1524–1531
73. Sasmal A, Sahoo D, Nanda R et al (2009) Biodegradable nanocomposites from maleated polycaprolactone/soy protein isolate blend with organoclay: preparation, characterization, and properties. Polym Compos 30:708–714
74. Campbell K, Qi S, Craig DQM et al (2009) Paracetamol-loaded poly(.vepsiln.-caprolactone) layered silicate nanocomposites prepared using hot-melt extrusion. J Pharm Sci 98:4831–4843
75. Labidi S, Azema N, Perrin D et al (2010) Organo-modified montmorillonite/poly(.vepsiln.-caprolactone) nanocomposites prepared by melt intercalation in a twin-screw extruder. Polym Degrad Stab 95:382–388
76. Liu H, Han C, Dong L (2010) Study of the biodegradable poly(.vepsiln.-caprolactone)/clay nanocomposite foams. J Appl Polym Sci 115:3120–3129
77. Singh NK, Das PB, Roy JK et al (2010) Nanoparticle-induced controlled biodegradation and its mechanism in poly(ε-caprolactone). ACS Appl Mater Interfaces 2:69–81
78. Hoidy WH, Ahmad MB, EaJ Al-Mulla et al (2010) Preparation and characterization of polyactic acid/polycaprolactone clay nanocomposites. J Appl Sci 10:97–106
79. Harrane A, Meghabar R, Belbachir M (2006) Kinetics of the ring opening polymerization of ε-caprolactone catalyzed by a proton exchanged montmorillonite clay. React Funct Polym 66:1696–1702
80. Kiersnowski A, Gutmann JS, Piglowski J (2007) Influence of organic modifiers on morphology and crystallization of poly(ε-caprolactone)/synthetic clay intercalated nanocomposites. J Polym Sci Part B: Polym Phys 45:2350–2367
81. Kiersnowski A, Kozak M, Jurga S et al (2004) Structure and crystallization behaviour of poly(ε-caprolactone)/clay intercalated nanocomposites. Polym Polym Compos 12:727–737
82. Kiersnowski A, Piglowski J (2004) Polymer-layered silicate nanocomposites based on poly(.vepsiln.-caprolactone). Eur Polym J 40:1199–1207
83. Mao Q, Schleidt S, Zimmermann H et al (2007) Molecular motion in surfactant layers inside polymer composites with synthetic magadiite. Macromol Chem Phys 208:2145–2160
84. Gorrasi G, Tortora M, Vittoria V et al (2004) Physical properties of poly(ε-caprolactone) layered silicate nanocomposites prepared by controlled grafting polymerization. J Polym Sci Part B: Polym Phys 42:1466–1475
85. Kim HB, Lee CH, Choi JS et al (2005) Preparation and rheological characteristics of poly(ε-caprolactone)/organoclay nanocomposites. J Ind Eng Chem (Seoul, Repub Korea) 11:769–772
86. Tortora M, Vittoria V, Galli G et al (2002) Transport properties of modified montmorillonite-poly(ε-caprolactone) nanocomposites. Macromol Mater Eng 287:243–249
87. Wang X-L, Huang F-Y, Zhou Y et al (2009) Nonisothermal crystallization kinetics of poly(ε-caprolactone)/montmorillonite nanocomposites. J Macromol Sci Part B Phys 48:710–722
88. Kiersnowski A, Dabrowski P, Budde H et al (2004) Synthesis and structure of poly(ε-caprolactone)/synthetic montmorillonite nano-intercalates. Eur Polym J 40:2591–2598
89. Pucciariello R, Villani V, Langerame F et al (2004) Interfacial effects in organophilic montmorillonite-poly(ε-caprolactone) nanocomposites. J Polym Sci Part B: Polym Phys 42:3907–3919
90. Marrazzo C, Di ME, Iannace S (2008) Conventional and nanometric nucleating agents in poly(ε-caprolactone) foaming: crystals vs. bubbles nucleation. Polym Eng Sci 48:336–344
91. Hong CH, Lee CH, Choi JS et al (2007) Rheological characteristics of solvent-cast poly(ε-caprolactone)/organoclay nanocomposite. Diffus Defect Data Part B 121–123:1455–1458

Chapter 6
PHA/Clay Nano-Biocomposites

David Plackett

Abstract Polyhydroxyalkanoates or PHAs were first observed in a laboratory in France in the 1920s and, since then, their creation as a form of energy storage in bacteria as well as their practical uses have been much studied. There has been increased interest in commercial production of PHAs in recent times and, over the past 10 years in particular, there have been various reports on solution-cast or melt-processed PHA/clay nano-biocomposites and their properties. In most studies, these nano-biocomposites exhibit intercalated or mixed exfoliated/intercalated morphologies. The use of plate-like clays as additives can lead to some enhancement in the mechanical and gas barrier properties of PHAs as well as increased thermal stability, although the effects depend significantly on clay type, clay organomodifer and process conditions. The influence of clay addition on PHA biodegradability has been either positive or negative according to the particular study. There has been very little research to date on the migration properties of PHA in the context of use in packaging and none yet in which PHA/clay nano-biocomposites have been the focus. If economic and technical challenges can be solved, PHAs should have a promising future in various uses ranging from packaging through to medicine and PHA/clay nano-biocomposites may also play a role in the future by providing a way for PHA material properties to be tuned according to the particular need.

D. Plackett (✉)
Department of Chemical and Biochemical Engineering,
Technical University of Denmark, DTU,
DK-2800 Kgs, Lyngby, Denmark
e-mail: dapl@kt.dtu.dk

L. Avérous and E. Pollet (eds.), *Environmental Silicate Nano-Biocomposites*,
Green Energy and Technology, DOI: 10.1007/978-1-4471-4108-2_6,

6.1 Introduction

In today's world, sustainability and innovation leading to sustainable economic growth are at the forefront of discussions in academe and in business circles. This is true not only in respect to new forms of renewable energy, such as wind, solar and biofuels, but also in relation to the wide range of materials and products on which modern societies depend. A new way of looking at materials, which includes sustainable sourcing and less dependence on fossil fuels, reduced greenhouse gas emissions in their production and use, and greater emphasis on recycling and reuse, has for example, been expressed in the cradle-to-cradle philosophy proposed by McDonough and Braungart [1]. Therefore, in parallel with developments in sustainable energy such as biofuels (i.e., bioethanol, biodiesel, and biogas) there is an increasing interest in bio-derived polymers and how the use of such materials, which are commonly also biodegradable or compostable, can contribute to a more sustainable future.

Polymers from non-fossil fuel sources are regarded as CO_2-neutral and have been the subject of academic study and commercialisation for several decades. However, this interest is now accelerating as questions about sustainability attract more attention from governments, NGOs and industry. The various types of polymer which are accessible from biomass are broadly outlined in Fig. 6.1, which shows how they may be divided into three categories depending upon how these polymers are sourced.

From a commercial perspective, biomass-derived polymers can be converted into useful bioplastics and bio-thermoset resins; however, with a few current exceptions, the latter are generally less well advanced in an industrial sense. As shown in Fig. 6.1, the biopolymers include an important family referred to as the polyhydroxyalkanoates (PHAs) which are often described as true biopolymers since they are produced in nature by living organisms (i.e., bacteria) rather than being derived from a bio-monomer, such as is the case for the polylactides (PLAs).

As described elsewhere, the investigation of PHAs has a long history and actually pre-dates the concept of macromolecules as developed by Staudinger et al. [2–4]. According to Chowdhury [5], the particles produced by certain bacteria under nutrient-limited conditions, and which we now know to be PHAs produced as a form of energy storage, were initially observed by Beijerinck as early as 1888. Landmark studies then took place in the 1920s in the laboratory of the French bacteriologist Maurice Lemoigne. At that time the composition of the materials produced in cells of *Bacillus megaterium* was identified and described as ether-insoluble lipids [5]. However, it took more years of research in Lemoigne's laboratory before the full nature and significance of PHA production in bacterial cells was uncovered [6–11] and it was not until the work of Stanier and Wilkinson and co-workers in the 1950s that the role of PHB granules as an intracellular food and energy reserve, produced in response to nutrient limitations in the bacterial growth environment, was understood. In 1958, Macrae and Wilkinson reported the production of polyhydroxybutyrate (PHB) as a function of glucose:nitrogen ratio in the feed medium and suggested a pathway for PHB synthesis [12]. In subsequent

Fig. 6.1 Categories of bio-derived polymers

Polymers extracted directly from biomass
1. Polysaccharides (starch, cellulose, chitin, gums)
2. Proteins (casein, zein, soy)
3. Lipids (triglycerides)

Polymers synthesized from bio-derived monomers
1. Polylactides
2. Other polyesters

Polymers synthesized by natural or GM organisms
1. Polyhydroxyalkanoates
2. Bacterial cellulose
3. Tunicate cellulose
4. Algal cellulose

Fig. 6.2 The general formula for polyhydroxyalkanoates (PHAs)

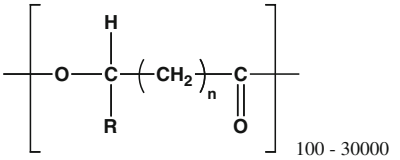

Polymer

n = 1	R = hydrogen	Poly(3-hydroxypropionate)
	R = methyl	Poly(3-hydroxybutyrate)
	R = ethyl	Poly(3-hydroxyvalerate)
	R = propyl	Poly(3-hydroxyhexanoate)
	R = pentyl	Poly(3-hydroxyoctanoate)
	R = nonyl	Poly(3-hydroxydodecanoate)
n = 2	R = hydrogen	Poly(4-hydroxybutyrate)
n = 3	R = hydrogen	Poly(5-hydroxyvalerate)

years, the discovery of a wide range of PHAs produced as a function of bacterial growth conditions was realised and the possibility of preparing various PHAs as a function of the substrate was first revealed by the work of De Smet et al. [13], in which *Pseudomonas oleovorans* was cultivated in n-octane and the resulting polymer was found to consist primarily of 3-hydroxyoctanoate units. The general formula of the PHAs is shown in Fig. 6.2.

Commercial development of PHAs extracted from bacterial cells started in the early 1980s when Imperial Chemical Industries Ltd. (ICI) began production of films and fibres from melt-processed PHA [14]. In this case, the product was a polyhydroxybutyrate-*co*-hydroxyvalerate (PHBV) copolyester containing randomly arranged units of [R]-3-hydroxybutyrate and [R]-3-hydroxyvalerate. The product, known as Biopol®, was transferred to Zeneca when ICI was split up in 1993 and then sold on to Monsanto in 1996. In 1998, the technology to manufacture Biopol® was acquired by the American company Metabolix and this company has until recently been developing a large-scale facility in the United

States for production of PHBV in cooperation with the Archer Daniels Midland Company (ADM). A summary of past and present companies worldwide with interests in PHA research and production is shown in Table 6.1.

Polymer nanocomposites have been of interest since the pioneering work in the laboratories of Toyota and collaborators in the 1980s, in which the potential enhancement in polymer properties at low nano-additive loadings was first recognised [16]. Fabrication of polymer nanocomposites can involve nanoparticles of various types, including lamellar, fibrillar, tubular, spherical and other shapes. In order to improve the mechanical and barrier properties of polymers, anisometric nanoparticles such as the lamellar type are preferred. In contrast, fibrillar nanoparticles typically improve rigidity and strength while spherical or other nanoparticles may be desirable if improved functional properties such as optical characteristics and electrical conductivity are targeted. Of the lamellar nanoparticles, layered silicates have been the most significant category from a research and development perspective.

As discussed in Chap. 3 and illustrated in Fig. 6.3, layered silicates, otherwise known as sheet silicates or phyllosilicates, are a large group of silicate minerals comprised of $[SiO_4]^{4-}$ tetrahedra linked together to form flat sheets with the composition $[Si_4O_{10}]$. The group consists of micas, chlorite, clays, talc and serpentine, which are soft minerals of variable but generally low density. Of these various minerals, it is the clays which have received the most attention as polymer nanofillers and a number of companies, such as those listed in Table 6.2, now have unmodified and organomodified clays available for purposes of polymer nanocomposite processing. The use of layered silicates as polymer nanofillers has been described in two recent texts [17, 18] and a number of review articles [19–23] as well as in one review focused only on biodegradable polymers [24].

The clays which have been developed and tested for use in nanocomposites consist of platelets which are typically one to a few nanometres (nm) in thickness and hundreds or even thousands of nm in length and width and, in this context, the term nanoclay is widely used. As discussed in the rest of this chapter, the use of nanoclays or other layered silicates in combination with PHAs has formed part of the international research activity on nano-biocomposites in recent years.

6.2 PHA/Clay Nanocomposites and their Properties

6.2.1 Rationale

Although commercial development of PHAs is now gaining increased attention, the widespread introduction of PHAs has been slow to occur for both technical and economic reasons. Apart from the question of cost, the most widely studied of the PHAs, PHB, has a narrow melt processing window above the melting point (Tm). At processing temperatures above this window, significant polymer degradation and therefore molecular weight reduction can be expected. This phenomenon has

Table 6.1 Companies past and present involved in PHA research and production (adapted from [15])

Company	Types of PHA	Production scale (tonnes/annum)	Period	Applications
ICI, UK	PHBV	300	1980s–1990s	Packaging
Chemie Linz, Austria	PHB	20–100	1980s	Packaging and drug delivery
P & G, USA	Several PHAs	Contract manufacturing	1980s–2005	Packaging
BASF, Germany	PHB, PHBV	Pilot scale (but never went into production)	1980s–2005	Blending with Ecoflex
btF, Austria	PHB	20–100	1990s	Packaging and drug delivery
Monsanto, USA	PHB, PHBV	Plant PHA production	1990s	Raw materials
Mitsubishi, Japan	PHB	10	1990s	Packaging
Jiangmen Biotech Ctr., China	PHBHHx	Unknown	1990s	Raw materials
Tianjin Northern Food, China	PHB	Pilot scale	1990s	Raw materials
Shantou Lianyi Biotech, China	Several PHAs	Pilot scale	1990s–2005	Packaging and medical
Telles (joint venture between Archer Daniels Midland and Metabolix), USA	Several PHAs	50,000	2009–present	Raw materials
Kaneka, Japan (with P & G)	Several PHAs	Unknown	1990s–present	Packaging
Biocycle, Brazil	PHB	100	1990s–present	Raw materials
Bio-On, Italy	PHA (unclear)	10,000	2008–present	Raw materials
Zhejiang Tian An, China	PHBV	2000	1990s–present	Raw materials
Yikeman, China	PHA (unclear)	3000	2008–present	Raw materials
Meredian, USA	Several PHA	10,000	2007–present	Raw materials
Tianan Biologic Material, China	PHBV	Unknown	2000–present	Raw materials
Jiang Su Nan Tian, China	PHB	Pilot scale	1990s–present	Raw materials
Shenzhen O'bioer, China	Several PHAs	Unknown	2004–present	Unclear
Tianjin Green Bio-science (+DSM), China	P3HB4HB	10,000	2004–present	Raw materials and packaging
Shandong Lukang, China	Several PHAs	Pilot scale	2005–present	Raw materials and medical
Biomer, Germany	PHB	Unknown	1990s–present	Packaging and drug delivery
Metabolix, USA	Several PHAs	Unknown	1980s–present	Packaging
Tepha, USA	Several PHAs	Unknown	1990s–present	Medical implants
Shenzhen Ecomann Biotechnology, China	PHB	Unknown	2009–present	Raw materials
Beijing Tianzhu Changyun, China	All types of PHA	Unknown	2002–present	Medical implants

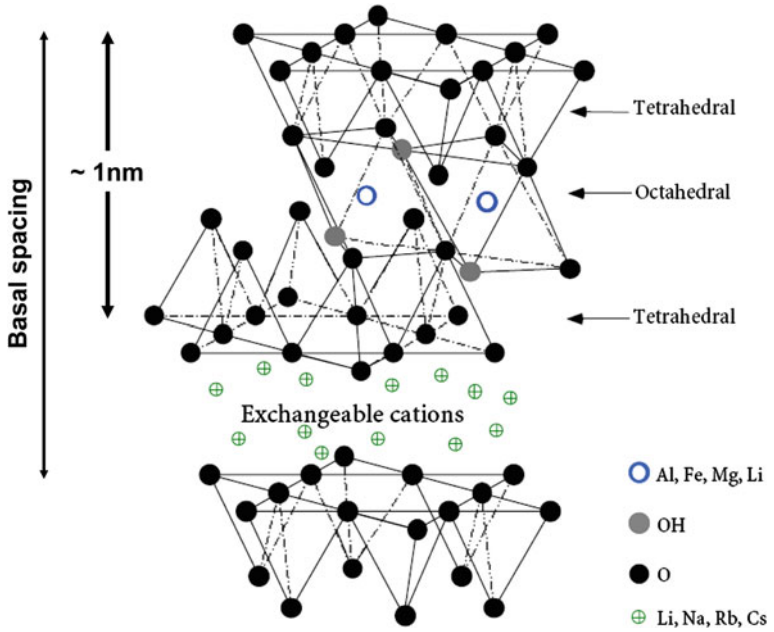

Fig. 6.3 Schematic showing the generalised structure of layered silicates

Table 6.2 Selected nanoclay suppliers and their product trade names

Company	Location	Product name
Southern Clay Products (Rockwood Specialties, Inc.)	USA	Cloisite® and Nanofil®
Nanocor/Amcol Int.	USA	Nanomer®
Nanobiomatters	Spain	Nanoter®
Elementis Specialties	USA	Bentone®
Laviosa Chimica Mineraria	Italy	Delite®
FCC Inc (Sino Holding Company)	China	Nanolin DK®

been explored and mechanisms for thermal degradation proposed [25–27]. Moreover, PHB is highly crystalline and suffers from high stiffness and brittleness when compared with conventional thermoplastics. PHBV offers some improvements since it is more flexible than PHB and also has a lower Tm, thereby allowing a broader window of processing temperatures. Blending together of different PHAs or blending of PHAs with other biopolymers has also been widely investigated as a way to obtain enhanced processing and product properties while maintaining biodegradability and biocompatibility [2–4]. An alternative approach and the main subject of this chapter is the formation of PHA nanocomposites to achieve significant improvements in material properties.

The use of layered silicates such as montmorillonite (MMT) clays to produce polymer nanocomposites has been extensively studied over the past 20 years and

the potential benefits of these materials have been widely documented [17–23]. As part of this research activity, the use of silicates to enhance the properties of bio-derived plastics such as thermoplastic starch, PLAs, PHAs and a variety of other biopolymers has been reported. In these cases, the advantages of forming nanocomposites include enhancements in mechanical properties, reduced gas permeability, greater fire resistance and modifications in biodegradability. Progress to date in research on PHA/layered silicate nanocomposites is discussed here in terms of various important material properties.

6.2.2 Mechanical Properties

Depending upon composition, PHAs display a wide variety of mechanical properties, ranging from those of the hard crystalline type to more elastic materials. As indicated by Sudesh et al. [28], the Young's modulus (3.5 GPa) and the tensile strength (43 MPa) of poly-3-hydroxybutyrate or P(3HB) are similar to those of isotactic polypropylene, but the extension at break (5 %) is much lower than that of polypropylene (400 %), which highlights one of the practical difficulties in using unmodified PHB. Various explanations for the brittleness of P(3HB) have been proposed, including the formation of cracks in the spherulites when cooling from the melt [29–31]. De Koning and Lemstra [32] also pointed out that embrittlement of P(3HB) can take place during storage after initial crystallisation from the melt and this can be addressed by use of annealing treatments.

Various approaches have been explored and developed in order to obtain PHAs which are less brittle. For example, nucleating agents can be added to the polymer melt during processing in order to speed up uniform crystal formation [33]. The manufacture of stretched films from ultra-high molecular weight P(3HB), produced using genetic engineering techniques, results in better mechanical properties with values for elongation at break, Young's modulus and tensile strength of 58 %, 1.1 GPa and 62 MPa, respectively [34, 35]. In addition to improvements through adjustments in PHA molecular weight, the introduction of HA comonomers (i.e., development of copolymers such as PHBV) has also proven fruitful with respect to less brittle PHA-based materials. Another example is the development of the Nodax™ copolymers (e.g., poly 3-hydroxybutyrate-*co*-3-hydroxyhexanoate) by Procter & Gamble, which sold the technology to Meredian, Inc. in 2007. In Table 6.3, mechanical properties reported for PHB and PHBV are compared with those of commercial plastics.

There have been various studies in which modification of the mechanical properties of PHAs by producing MMT clay-based nanocomposites has been investigated. Reports of this type can be broadly divided into those in which the nanocomposites were formed by solution casting and those in which melt processing was used. Comparison of results from the various studies reveals the expected trends in mechanical properties but is also complicated by differences in test methodology and the raw materials used. Furthermore, researchers have had a

Table 6.3 Indicative mechanical properties of PHB and PHBV in comparison to those of other bioplastics or synthetic plastics

Polymer[a]	Tensile strength (MPa)	Young's modulus (GPa)	Elongation at break (%)
PHB	40	1.7–3.5	3–6
PHBV	30–38	0.7–2.9	20
PLA	28–50	1.2–2.7	7–9
PCL	16	0.4	120–800
TPS	2.6	0.5–1.0[b]	47
PET	56	2.2	70–100
LDPE	10–15	0.2	300–500
PP	35–40	1.7	150
PS	12–50	1.6–3.1	3–4
PVC	10–60	0.3–2.4	12–32

PCL polycaprolactone, *TPS* thermoplastic starch, *PET* polyethylene terephthalate, *LDPE* low-density polyethylene, *PP* polypropylene, *PS* polystyrene, *PVC* polyvinyl chloride
Sources adapted from Refs. [28, 36–38]
[a] Values for individual polymer samples will vary according to a number of factors including polymer molecular weight, crystallinity and orientation, if produced as a film, as well as the mechanical testing conditions
[b] At low water contents (5-7 wt%)

tendency in some cases to report that mechanical properties are "improved" without really clarifying what this means in practice. For example, an increase in modulus in an already stiff and brittle material may not represent an improvement in a practical sense. The number of studies to date in which PHAs have been combined with layered silicates is still relatively limited and therefore the effects on mechanical properties in these materials can be shortly summarised.

In one of the first reported studies on PHB/MMT nanocomposites, Lim et al. [39] used solution casting and applied X-ray diffraction (XRD) and Fourier Transform Infra-Red (FTIR) spectroscopy to confirm that an intercalated structure had been formed. However, mechanical and rheological characterisation was not carried out at this stage. In a later study, Bruzaud and Bormaud investigated solution-cast combinations of PHBV with an organically modified MMT (OMMT) at loadings of 1, 2.5 and 5 %, the typical range in which the benefits of adding nanofillers are anticipated. In this work, tensile strength and modulus increased with increasing OMMT content and elongation at break decreased [40]. These researchers also applied the nanoindentation technique and discovered that moduli determined in this manner were similar to those from macro-scale testing. This finding was attributed to good dispersion of the OMMT at a nano-scale, such that the resulting films behaved as a homogeneous phase rather than a two-phase material. Nanoindentation also showed an increase in hardness with OMMT content and a hardness value at 5 % OMMT loading roughly twice that of unfilled PHBV.

For reasons to do with practical applications, there have been more research investigations on melt-processed PHA/layered silicates than solution-casting studies. As discussed, thermal instability can be a concern with PHAs and this will

not normally be a factor in solution-casting work. In one of the first reports on PHA melt processing with layered silicates, Choi et al. [41] melt compounded PHBV with Cloisite® 30B, an OMMT from Southern Clay Products (Gonzales, Texas), in a Brabender mixer. The OMMT additive was incorporated at 1–3 % by weight. In this case, the Young's modulus increased from 481 to 795 MPa by addition of 3 % OMMT and elongation at break showed a corresponding decrease from 8.5 to 5.6 %; however, tensile strength showed virtually no change. Dynamic mechanical analysis (DMA) has been used to explore the mechanical properties of PHB melt extruded with an OMMT or an organomodified synthetic fluoromica [42]. The storage modulus increased with clay content, showing a percentage increase from 13 to 40 % relative to unfilled PHB at the same temperature. There was also a difference between the modified fluoromica and the OMMT in terms of storage modulus and tan δ response as a function of temperature, which the authors assigned either to differences in nanofiller dispersion or to the likely greater adverse affect on PHB molecular weight in the presence of the OMMT. This observation is also referred to later in the section of this chapter which discusses thermal properties.

Parulekar et al. [43] prepared PHB in combination with an MMT modified with neopentyl (diallyl)oxy tri(dioctyl) pyrophosphate titanate and an epoxidised natural rubber toughening agent as an approach to overcoming the brittleness and fracture susceptibility of PHB. The purpose of adding the modified MMT was to compensate for the loss in modulus brought about by rubber addition and to provide materials suitable for structural applications. Clay nanofillers typically act as stress concentrators and can therefore reduce impact strength. Processing was carried out in a small-scale twin-screw extruder, which was followed by injection moulding of test specimens. Mechanical properties were assessed in terms of impact strength and storage modulus. The results confirmed the expected benefits and also showed that the modified MMT provided better impact strength while still improving the modulus when compared with the use of a commercial modified clay with much higher organomodifier loading. Botana et al. [44] investigated biodegradable composites prepared from PHB in combination with an unmodified MMT or Cloisite® 30B and carried out melt mixing in a Brabender Plasti-Corder®. These researchers discovered that there was some agglomeration of the OMMT and that the exfoliation/intercalation ratio in the nano-dispersed clay was insufficient to bring about an increase in tensile strength. However, some increase in Young's modulus was noted for the samples containing the MMTs, especially those in which Cloisite® 30B had been used. In research on poly(3-hydroxybutyrate-co-3-hydroxyhexanoate) or PHB-co-PHH (Nodax™) at up to 5 % clay loading, Zhang et al. [45] reported an increased elastic modulus but also pointed out that modulus and strength were not enhanced at higher clay loadings. Pavlidou and Papaspyrides stated that the exfoliation/intercalation ratio is the main factor determining the improvement in mechanical properties in nanocomposites [46]. Intercalation can ensure that the modulus is increased but it is generally the exfoliation/intercalation ratio which determines the influence of the nano-additive on tensile strength.

Table 6.4 Permeability properties of PHB and PHBV compared with those of other plastics

Polymer[a]	O_2 permeability at 23 °C, 0–50 % RH (ml mm m^{-2} day^{-1} atm^{-1})	Water vapour permeability at 23–38 °C, 50–90 % RH (g mm m^{-2} day^{-1})	CO_2 permeability at 23 °C, 0–50 % RH (ml mm m^{-2} day^{-1} atm^{-1})
PHB	2–10	1–5	3
PHBV	5–14	1–3	–
PLA	15–25	5–7	35–70
LLDPE/starch (60:40)	400	2–3	1120
PCL	20–200	300	–
LDPE	50–200	0.5–2	800–1000
PET	1–5	0.5–2	15–20
PP	50–100	0.2–0.4	200–400
PS	100–150	1–4	250–500
PVC	2–8	1–2	10–15

Sources adapted from Refs. [48–53]

Polymer abbreviations are as indicated in Table 6.3 with the addition that *LLDPE* = linear low-density polyethylene

[a] Values should be regarded as indicative only since measured values will depend on various factors such as polymer molecular weight, crystallinity and test conditions

6.2.3 Barrier Properties

Since one of the larger markets for PHAs could eventually be in food packaging, where there is now increasing interest in bio-derived plastics [47], the barrier properties of PHAs are also of some considerable importance. In this respect, oxygen and water vapour barrier properties, normally indicated through permeability measurements, are of interest and a summary of values reported in the literature for PHAs is presented in Table 6.4.

The demonstrated improvement in barrier properties by adding layered silicates and creating nanocomposites is a key factor driving interest in these materials. A common explanation for the effect of lamellar nanoparticles on oxygen permeability is the tortuosity effect, in which the presence of well-dispersed clay platelets increases the diffusion pathway of gas molecules through plastic films. Models such as those of Nielsen and Fricke have been developed to effectively model barrier effects based on the tortuous path concept [54]. A number of researchers have reported the influence of layered silicates on the permeability of PHAs. For example, Sanchez-Garcia et al. [48] used an organically modified kaolinite and an OMMT in melt-blended PHB nanocomposites in which polycaprolactone (PCL) was incorporated as a plasticiser. A 43 % decrease in oxygen permeability was observed in PHB or PHB/PCL blends containing 4 % nanoclay, when measured at 24 °C and 0 % RH. However, the values recorded did not fit widely used models, which the authors attributed to limitations in terms of accounting for polymer morphology, crystallinity, nanofiller platelet orientation,

matrix chemistry and the solubility of penetrants in the various components. In an earlier study from the same laboratory, Sanchez-Garcia et al. [49] found approximately 20 and 27 % reduction in oxygen permeability of PHB and PHBV films respectively when 5 % OMMT was incorporated.

6.2.4 Thermal Stability

The sensitivity of PHAs to thermal degradation at temperatures above the Tm has been an important factor hindering their application. The thermal properties of PHB and PHBV and the use of different approaches to improving thermal stability has been the focus of various studies [25–27, 55–58]. Thermal degradation of PHAs occurs mainly by a non-radical chain-scission reaction and is significant at temperatures over 200 °C. In general, as the HV content in a PHBV copolymer increases, the melting temperature decreases and there is greater scope for melt processing without excessive polymer degradation.

The effect of nano-additives on polymer degradation has been a recurring theme in research on melt processing of PHAs with MMTs. In principle, the dispersion of layered silicates should provide a mass barrier effect, resulting in reduced rate of diffusion of degradation products and therefore delayed thermal decomposition [39–41]. As an example, in one study using melt blending in a Brabender mixer for nanocomposite preparation, the addition of 1–3 % Cloisite® 30B to PHBV increased the degradation onset temperature [T_{onset} recorded in thermogravimetric analysis (TGA) experiments] from 252 to 263 °C [41], while in another study using a solvent-casting preparation method the addition of Cloisite® 15A at 5 % caused the temperature corresponding to 50 % weight loss in TGA to increase by 30 °C [40]. In the research of Lim et al. [39], 3, 6 or 9 % Cloisite® 25A was added to PHB prior to solvent casting into films. TGA analyses showed that T_{onset} for material with 3 % OMMT addition was slightly higher than that of unfilled PHB, whereas the T_{onset} was lower at the two higher OMMT loadings. The authors suggested that lower T_{onset} at higher clay loadings could be a consequence of clay particle agglomeration. Clay agglomerates may act as sites for heat accumulation and thereby trigger a faster start to thermal decomposition. In other words, clay agglomeration can act to reverse the conventional enhancement of thermal stability which would be expected [59]. Typically, the tendency towards clay aggregation increases as clay content increases [60]. Erceg et al. [61] found that 5 % OMMT was an upper loading limit with respect to increased thermal stability when Cloisite® 30B was used in combination with PHB. It has been suggested that aluminium Lewis acid sites in layered silicates may catalyse hydrolysis of ester linkages and this phenomenon, contributing to PHA degradation under various conditions, could also be more pronounced at higher clay loadings [61].

The influence of nanofiller type on PHA thermal stability has been studied. For example, although OMMT addition has been shown to increase the decomposition temperature, this may not be the case when an unmodified MMT is used, likely because of less efficient nanoclay dispersion in the latter case [42]. Further studies

have suggested that the organomodifiers present in OMMTs (e.g., quaternary ammonium ions) may have a strong catalytic influence on PHA degradation [62–64]. Bordes et al. [65] proposed that the quaternary ammonium ions could be converted to amines during melt processing and that the acidic protons or nucleophilic amines released could catalyse PHA chain scission. It is also possible that any fermentation residues still present in PHAs could act in synergy with quaternary ammonium ions to degrade PHB [63]. However, the exact mechanism for such degradation remains unexplained.

As pointed out in the study by Cabedo et al. [64], previously dried nanoclays could still release tightly-bound water which would have an adverse effect on PHA molecular weight. The kinetics of PHA thermal degradation in the presence of nanoclays has been studied by Erceg et al. [61, 66]. Other researchers have reported that a simple first-order kinetic model cannot be applied to describe isothermal degradation of PHB and PHB nanocomposites because there are likely to be a variety of different reaction mechanisms [67, 68]. As mentioned by Bordes et al. [65], full exfoliation of nanoclays in a twin-screw extruder normally requires high shear rates, which may also contribute to polymer degradation during processing of biopolyesters. El-Hadi et al. [31] noted that reductions in polymer molecular weight can lead to surface sticking during extrusion or injection moulding as well as increased crystallisation times. The work of Cabedo et al. in a bench-scale study also illustrated the variety of factors, such as atmosphere and clay type, which can influence PHBV molecular weight during melt processing with nanoclays [64].

6.2.5 Biodegradability

Biodegradation of PHAs has been widely studied under both aerobic and anaerobic conditions and in environments ranging from compost, sewage or soil through to fresh or salt water [2, 3, 50, 69–74]. In general, PHAs are more readily biodegradable than PLAs [28]. The process of PHA biodegradation involves extracellular PHA depolymerases, which are widespread in fungi and bacteria and can convert PHAs into monomers and soluble oligomers. These low-molecular weight products are subsequently metabolised into H_2O and CO_2 by intracellular depolymerase enzymes. The rate at which PHAs biodegrade is influenced by a wide variety of material factors including polymer composition, crystallinity, surface area and molar mass as well as by test environment conditions such as water content, temperature, pH, nutrient supply and microbial activity. More detailed information on PHA biodegradation can be found elsewhere [15, 28]. As a general rule, PHAs with higher degrees of crystallinity and higher molecular weights show reduced rates of biodegradation. In the case of PHBV, biodegradation has been observed to increase as the HV content increases under aerobic conditions [75]. Reports suggest that PHBV degrades more rapidly than PHB under aerobic conditions [76–78]. However, the opposite effect was reported by Abou-Zeid et al. [79, 80] when running tests under anaerobic conditions.

The biodegradability of PHAs containing layered silicates as nano-additives has been investigated with indications that biodegradation rate is decreased under such circumstances. Explanations vary but a tortuous path effect could impede penetration of microorganisms, restrict enzyme accessibility and reduce the rate of water ingress into test samples. An example of research in this field is the work of Wang et al. [81] in which the biodegradability of PHBV/OMMT in soil suspension decreased with increasing OMMT content. However, there are also reports indicating enhanced degradation rates in nanocomposites as, for example, in the study of titanate-modified clay as an additive in a toughened PHB matrix [43]. In this case, PHB and PHB compounded with an epoxidised natural rubber degraded at similar rates but faster than a combination of PHB with epoxidised natural rubber and maleated rubber. Incorporation of a titanate-modified clay in the latter case gave an increased biodegradation rate, albeit less than that of PHB or the PHB/natural rubber combination. The rate of biodegradation of PHB was also significantly enhanced when 2 % fluoromica was used as an additive [42]. As suggested by Sinha Ray et al. [82], albeit with reference to PLAs, it is possible that the terminal hydroxyl groups on clay edges could bind water in the test environment and act as active sites for ester hydrolysis, thereby speeding up the process of biodegradation. As noted by Parulekar et al. [43], the state of dispersion of nanoclays in a polymer matrix may also influence polymer chain fragmentation.

6.2.6 Migration

Given the potential for future increased use of bioplastics and bioplastic nanocomposites in commodity products such as food packaging, migration and associated safety issues are increasingly in focus. This issue is discussed in the scientific opinion on nanoscience and nanotechnology recently released by the European Food Safety Authority (EFSA) [83]. Although reports of specific migration studies on PHAs appear to be lacking, total migration from PHB into food simulants has been investigated and detected migrant levels found to be below recommended threshold values [84]. In regards to nanoparticle migration, there are very little data relating to migration of nanoparticles from any kind of biopolymer that might be used in food packaging [85]. Simon et al. [86] discussed nanoparticle migration from a theoretical viewpoint and concluded that only particles with a radius of about 1 nm should migrate. These authors also noted that such conditions would likely be met in the case of nanocomposites of silver with polyolefins such as low-density polyethylene (LDPE), high-density polyethylene (HDPE), and polypropylene (PP). It was also predicted that no appreciable migration would occur in the case of larger nanoparticles bound in polymer matrices with a relatively high dynamic viscosity such as polystyrene and polyethylene terephthalate. The question of nanoparticle migration from PHA films remains largely unaddressed but it will become necessary to obtain such information as and when PHA nanocomposites receive attention in respect to uses such as food packaging.

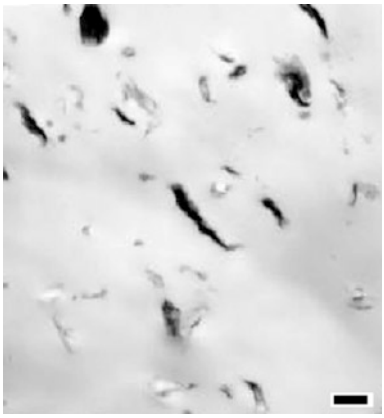

Fig. 6.4 Bright field transmission electron micrograph of a micro-injected sample of PHB containing 2.3 wt % dimethyl-octadecylamine-modified montmorillonite showing stacks of silicate layers dispersed in the polymer matrix. *Black scale bar* at *lower right* in the image = 500 nm. (Reprinted from Ref. [42] with kind permission © American Chemical Society (2007))

6.2.7 Morphology of PHA/Clay Nanocomposites

The main reason for improvements in properties in layered silicate nanocomposites relative to conventional composites is the increased interfacial interaction between the polymer matrix and the high aspect ratio nanofiller. Since the impact of adding layered silicates to polymers is highly dependent on the state of dispersion of these additives, many of the reports in the literature discuss sample morphology as determined by transmission electron microscopy (TEM), frequently in combination with XRD studies. Factors such as clay type, organomodifier and overall processing conditions can influence the final outcome in terms of clay dispersion and, in the case of melt extrusion, it is generally considered necessary to use a twin-screw machine with a minimum extruder barrel length-to-diameter ratio (l/d) of ~40 in combination with specific screw geometries [87]. A few examples of PHA/clay nanocomposite morphologies are cited below and in general it seems that mixed intercalated/exfoliated rather than totally exfoliated nanocomposites have been obtained.

Maiti et al. [42], as indicated by TEM evidence in Fig. 6.4, obtained well-ordered intercalated nanocomposites when melt processing PHB with OMMTs and, although the state of dispersion was not ideal, a storage modulus increase of 40 % and an increase in biodegradation rate relative to unfilled PHB was reported.

Bruzaud and Bourmaud applied XRD to investigate the morphology of PHBV which was solution cast in combination with Cloisite® 15A nanoclay from Southern Clay Products (Fig. 6.5) and concluded that an intercalated and/or exfoliated nanocomposite had been obtained [40].

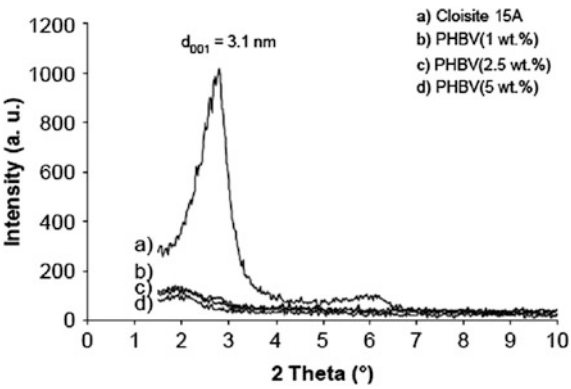

Fig. 6.5 Wide-angle X-ray scattering patterns for Cloisite® 15A (an OMMT from Southern Clay Products), and PHBV solvent-cast with Cloisite® 15A at three different loadings, providing evidence for predominant, if not complete, nanoclay exfoliation. (Reprinted from Ref. [40] with kind permission from ©Elsevier (2007))

Choi et al. [41] adopted a melt-processing method in which PHBV was compounded with Cloisite® 30B in a Brabender mixer and these authors used XRD and TEM to demonstrate that intercalated morphology was achieved. Parulekar et al. [43] claimed that well-defined exfoliated morphology was obtained when dispersing titanate-modified clay in a PHB toughened with epoxidised natural rubber and a maleated rubber and evidence was presented in terms of both TEM and melt rheological analysis. Similarly, Botana et al. [44] used XRD and TEM to confirm that an intercalated structure had been obtained when melt compounding PHB with Cloisite® 30B in a Brabender Plasti-Corder®. Sanchez-Garcia et al. [48] also utilised several different clays and compounded these nanofillers with PHB or PHB-PCL blends in a Brabender Plasti-Corder® internal mixer. In this case, processing with OMMTs led to significant PHB degradation but, somewhat surprisingly, enhanced crystallinity and barrier effects were noted when Nanoter® 2012 organomodified kaolinite clay (NanoBioMatters, Valencia, Spain) was used. In addition, these authors used SEM to distinguish the phases in the PHB-PCL blends and to provide indications of clay dispersion. In general, from XRD and TEM evidence in the literature it appears that well-dispersed PHB- or PHBV-based clay nanocomposites have been produced which exhibit intercalated or mixed intercalated/exfoliated morphology. However, unequivocal evidence for a fully exfoliated PHB/clay or PHBV/clay nanocomposite material is rarely found. As in other polymer nanocomposite systems and as discussed in this chapter, various property enhancements related to good nanoclay dispersion in PHA matrices have been presented in the literature.

6.3 Summary and Future Trends

PHAs are attracting increasing interest as a family of bio-derived thermoplastics with a variety of potentially interesting applications in areas such as packaging, composites (e.g., building materials, furnishing, automotive part), electronic components and medicine. Although knowledge regarding PHAs and their production has been

available for decades and various products have already been manufactured, there is now enhanced awareness of environmental issues and the need for renewable materials in the twenty-first century and, as a result, there is renewed momentum in terms of the development and use of these biopolyesters. Of the various potential applications, packaging is the largest commodity market and, for that reason, the processing and properties of PHAs have often been discussed in this context. The research on PHA/clay nanocomposites reported in the literature has confirmed that, as with other polymers, this technology should in principle allow PHA properties, whether mechanical-, barrier- or biodegradation-related, to be tuned according to specific needs. Even though PHA nanocomposites containing fully exfoliated clay nanoplatelets have been scarcely reported, evidence for positive enhancements in material properties are certainly available in the literature.

As with unfilled PHA-based products, the extent to which PHA/clay nanocomposites will be adopted in the future will depend upon both economics and technical issues and especially whether further advances can be made in respect to thermal stability during processing and less brittle materials. The recent announcements about new commercial developments in PHA production suggest that these concerns can be addressed and that there is a promising future for PHAs as part of the broader portfolio of commercial bioplastics. As reported recently [88], there is expected to be continued strong growth in this sector overall, even if output will remain a relatively small percentage of total plastics production. The need for renewably-derived plastics will continue and, in an interesting new development, customers can consider the availability of bio-polyethylene which, although naturally non-biodegradable, may now be produced from plant raw materials (e.g., sugar cane) and is attracting wide interest from plastic converters [89, 90].

It should be noted, as inferred previously, that PHAs reinforced with layered silicates have potential uses beyond the packaging industry in smaller but possibly higher value niches such as in medicine. As a recent example of research in this direction, Da Silva-Valenzuela et al. [91] investigated production of nanocomposite microcapsules containing one of two clays for the purposes of drug delivery. This work was built upon earlier suggestions regarding the suitability of PHB microspheres for medical applications [92]. PHB/clay films were cast from chloroform as solvent and microcapsules were produced by a solvent-mediated emulsification-diffusion technique [93]. Electron microscopy revealed the nanocapsules had a "nanoflower" or "hydrangea" morphology and the authors indicated that these microcapsules (Fig. 6.6) would be the subject of further investigations in respect to drug delivery applications [91].

The development of composite materials based on bio-resins (e.g., PLA, furans) for engineering applications is still very much in its infancy but there is commercial interest and this topic has already been the subject of several European Union research projects [e.g., BIOCOMP (http://www.biocomp.eu.com), WOODY (http://www.woodyproject.eu), and BIOSTRUCT (http://www.biostructproject.eu)]. The commercial interest in these cases is largely driven by the need to satisfy increasing customer demands for sustainable materials. In this respect, the use of clay nanofillers can also provide improvements in terms of flammability [94] and this

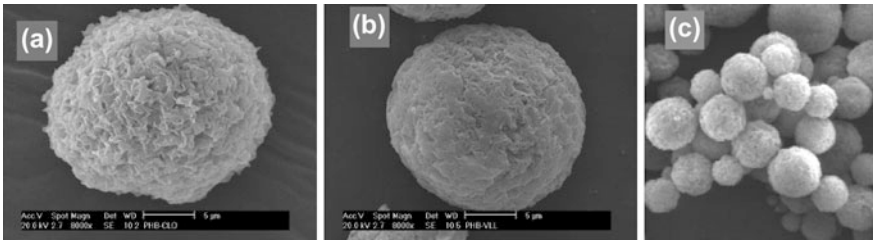

Fig. 6.6 Scanning electron micrographs of microcapsules prepared from PHB and either: **a** Cloisite® 20A (an OMMT from Southern Clay Products) or **b** a natural polycationic MMT. Indicated *scale bars* in **a** and **b** represent 5 μm. **c** shows the variation in microcapsule diameters, from 0.5 to 15 μm, which occurred when using either clay type. (Reprinted from Ref. [91] with kind permission ©Trans Tech Publications (2010))

advantage would also be applicable to PHA/clay nanocomposites if this should be a requirement. One of the few reports indicating future interest in this field has recently been released and, in this case, a PHBV/poly (butylene adipate-*co*-terephthalate) was successfully combined with a phosphorus-based additive and nanometric metal oxides in order to achieve improved fire retardancy [95]. Although this report did not include work on use of nanoclays, it does point to the interesting potential for further research and development in a field which, so far, has been barely studied.

6.4 Further Reading

Information about the latest commercial developments can be found through the websites of the PHA manufacturers (i.e., Metabolix, Meredian, Biocycle and others) as well as through the European Bioplastics Association (http://www.european-bioplastics.org). PHA nanocomposites are discussed in a recent book on multifunctional and nanoreinforced polymers for food packaging [96] and a review article published in 2009 provides an interesting overview of plant-derived biodegradable plastics which refers to the potential for future PHA production in genetically engineered plants [97]. An overview of the developing value chain for PHAs and PHA-based materials can be found in another recent review [98]. The basics of PHAs, including a discussion of manufacturing processes, are also available in a recent issue of Bioplastics magazine [99].

References

1. McDonough W, Braungart M (2002) Cradle to cradle—rethinking the way we make things. North Point Press, New York
2. Pollet E, Averous L (2011) Production, chemistry and properties of polyhydroxyalkanoates. In: Plackett D (ed) Biopolymers—new materials for sustainable films and coatings. Wiley, Chichester

3. Chodak I (2008) Polyhydroxyalkanoates: origin, properties and applications. In: Belgacem M, Gandini A (eds) Monomers, polymers and composites from renewable resources. Elsevier, Amsterdam
4. Lenz R, Marchessault RH (2005) Bacterial polyesters: biosynthesis, biodegradable plastics and biotechnology. Biomacromolecules 6:1–8
5. Chowdhury AA (1963) Poly-β-hydroxybuttersäure abbauende bakterien und exoenzym. Archiv für Mikrobiol 47:167–200
6. Lemoigne M (1923) Production of β-hydroxybutyric acid by certain bacteria of the B. subtilis group. Compt Rend 176:1761–1763
7. Lemoigne M (1924) Mechanism of the production of β-hydroxybutyric acid by the biochemical method. Compt Rend 178:1093–1095
8. Lemoigne M (1924) Production of β-hydroxybutyric acid by a bacterial process. Compt Rend 179:253–256
9. Lemoigne M (1925) The origin of β-hydroxybutyric acid obtained by bacterial process. Compt Rend 180:1539–1541
10. Lemoigne M (1927) Chemical origin of the products of dehydration and of polymerization of β-hydroxybutyric acid. Hydroxybutyric fermentation. Bull Soc Chim Biol 9:446–453
11. Hocking PJ, Marchessault RH (1994) Biopolyesters. In: Griffin GJL (ed) Chemistry and technology of biodegradable polymers. Blackie Academic and Professional, London
12. Macrae RM, Wilkinson JF (1958) Poly-β-hydroxybutyrate metabolism in washed suspensions of Bacillus cereus and Bacillus megaterium. J Gen Microbiol 19:210–222
13. De Smet MJ, Eggink G, Witholt B et al (1983) Characterization of intracellular inclusions formed by Pseudomonas oleovorans during growth on octane. J Bacteriol 154:870–878
14. Anderson AJ, Dawes EA (1990) Occurrence, metabolism, metabolic role, and industrial uses of polyhydroxyalkanoates. Microbiol Rev 54:450–472
15. Chen G-Q (2010) Plastics from bacteria: natural functions and applications. Springer, Berlin
16. Kojima Y, Usuki A, Kawasumi M et al (1993) Mechanical properties of nylon 6-clay hybrid. J Mater Res 8:1185–1189
17. Utracki L (2004) Clay-containing polymeric nanocomposites, vol 1. Rapra Technology Ltd, Shawbury
18. Utracki L (2004) Clay-containing polymeric nanocomposites, vol 2. Rapra Technology Ltd, Shawbury
19. Gianellis EP (1996) Polymer layered silicate nanocomposites. Adv Mater 8:29–35
20. Ray SS, Okamoto M (2003) Polymer/layered silicate nanocomposites: a review from preparation to processing. Prog Polym Sci 28:1539–1641
21. Hussain F, Hojjati M, Okamoto M (2006) Polymer-matrix nanocomposites, processing, manufacturing, and application: an overview. J Compos Mater 40:1511–1575
22. Utracki LA (2007) Synthetic, layered nanoparticles for polymeric nanocomposites (PNCs). Polym Adv Technol 18:1–37
23. Mittal V (2009) Polymer layered silicate nanocomposites: a review. Materials 2:992–1057
24. Okamoto M (2005) Biodegradable polymer/layered silicate nanocomposites: a review. In: Mallapragada SK, Narasimhan B (eds) Handbook of biodegradable polymeric materials and their applications, vol 1. American Scientific Publishers, Los Angeles
25. Grassie N, Murray EJ, Holmes PA (1984) Thermal degradation of poly(-(D)-β-hydroxybutyric acid): part 1—identification and quantitative analysis of products. Polym Degr Stab 6:47–61
26. Grassie N, Murray EJ, Holmes PA (1984) Thermal degradation of poly(-(D)-β-hydroxybutyric acid): part 2—changes in molecular weight. Polym Degr Stab 6:95–103
27. Grassie N, Murray EJ, Holmes PA (1984) Thermal degradation of poly(-(D)-β-hydroxybutyric acid): part 3—the reaction mechanism. Polym Degr Stab 6:127–134
28. Sudesh K, Abe H, Yoi D (2000) Synthesis, structure and properties of polyhydroxyalkanoates: biological polyesters. Prog Polym Sci 25:1503–1555
29. Barham PJ, Keller A (1986) The relationship between microstructure and mode of fracture in polyhydroxybutyrate. J Polym Sci B 24:69–77

30. Barham PJ, Parker P, Organ SJ (1992) Physical properties of poly(hydroxybutyrate) and copolymers of hydroxybutyrate and hydroxyvalerate. FEMS Microbiol Rev 103:289–298
31. El-Hadi A, Schnabel R, Straube E et al (2002) Correlation between degree of crystallinity, morphology, glass temperature, mechanical properties and biodegradation of poly(3-hydroxyalkanoate) PHAs and their blends. Polym Test 21:665–674
32. de Koning GJM, Lemstra PJ (1993) Crystallization phenomena in bacterial poly[(R)-3-hydroxybutyrate]. Embrittlement and rejuvenation. Polymer 34:4089–4094
33. Hänggi U (1995) Requirements on bacterial polyesters as future substitute for conventional plastics for consumer goods. FEMS Microbiol Rev 16:213–220
34. Kusaka S, Iwata T, Doi Y (1998) Microbial synthesis and physical properties of ultra-high-molecular weight poly[(R)-3-hydroxybutyrate]. J Macromol Sci Pure Appl Chem A 35: 319–335
35. Kusaka S, Iwata T, Doi Y (1999) Properties and biodegradability of ultra-high-molecular weight poly[(R)-3-hydroxybutyrate] produced by a recombinant *Escherichia coli*. Int J Biol Macromol 25:87–94
36. Khanna S, Srivastava AK (2005) Recent advances in microbial polyhydroxyalkanoates. Process Biochem 40:607–619
37. Philip S, Keshavarz T, Roy I (2007) Polyhydroxyalkanoates: biodegradable polymers with a range of applications. J Chem Technol Biotechnol 82:233–257
38. van Soest JJG, Benes K, de Wit D et al (1996) The influence of starch molecular mass on the properties of extruded thermoplastic starch. Polymer 37:3543–3552
39. Lim ST, Hyun YH, Lee CH et al (2003) Preparation and characterization of microbial biodegradable poly(3-hydroxybutyrate)/organoclay nanocomposite. J Mater Sci Lett 22: 299–302
40. Bruzaud S, Bourmaud A (2007) Thermal degradation and (nano)mechanical behaviour of layered silicate reinforced poly(3-hydroxybutyrate-*co*-3-hydroxyvalerate) nanocomposites. Polym Test 26:652–659
41. Choi WM, Kim TW, Park OO et al (2003) Preparation and characterization of poly(hydroxybutyrate-*co*-hydroxyvalerate)-organoclay nanocomposites. J Appl Polym Sci 90: 525–529
42. Maiti P, Batt CA, Gianellis EP (2007) New biodegradable polyhydroxybutyrate/layered silicate nanocomposites. Biomacromolecules 8:3393–3400
43. Parulekar Y, Mohanty AK, Imam SH (2007) Biodegradable nanocomposites from toughened polyhydroxybutyrate and titanate-modified montmorillonite clay. J Nanosci Nanotechnol 7:3580–3589
44. Botana A, Mollo M, Eisenberg P et al (2010) Effect of modified montmorillonite on biodegradable PHB nanocomposites. Appl Clay Sci 47:263–270
45. Zhang X, Lin G, Abou-Hussein R et al (2007) Some novel layered-silicate nanocomposites based on a biodegradable hydroxybutyrate copolymer. Eur Poly J 43:3128–3135
46. Pavlidou S, Papaspyrides CD (2008) A review on polymer-layered silicate nanocomposites. Prog Polym Sci 33:1119–1198
47. Kaeb H (2011) Bioplastics in packaging. Bioplastics 2:46–49
48. Sanchez-Garcia MD, Gimenez E, Lagaron JM (2008) Morphology and barrier properties of nanobiocomposites of poly(3-hydroxybutyrate) and layered silicates. J Appl Polym Sci 108:2787–2801
49. Sanchez-Garcia MD, Gimenez E, Lagaron JM (2007) Novel PET nanocomposites of interest in food packaging applications and comparative barrier performance with biopolyester nanocomposites. J Plast Film Sheet 23:133–148
50. Thellen C, Coyne M, Froio D et al (2008) A processing, characterization and marine biodegradation study of melt-extruded polyhydroxyalkanoate (PHA) films. J Polym Environ 16:1–11
51. Lange J, Wyser Y (2003) Recent innovations in barrier technologies for plastic packaging. Pack Tech Sci 16:149–158

52. Miguel O, Fernandez-Berridi MJ, Iruin JJ (1997) Survey on transport properties of liquids, vapors, and gases in biodegradable poly(3-hydroxybutyrate) (PHB). J Appl Polym Sci 64:1849–1859
53. Euaphantasate N, Prachayawasin P, Uasapon S et al (2008) Moisture sorption characteristic and their relative properties of thermoplastic starch/linear low density polyethylene film for food packaging. J Metal Mater Min 18:103–109
54. Nielsen LE (1967) Models for the permeability of filled polymer systems. J Macromol Sci (Chem) A1:929–942
55. Galego N, Rosza C (1999) Thermal decomposition of some poly(β-hydroxyalkanoates). Polym Int 48:1202–1204
56. He J, Cheung MK, Yu PH et al (2001) Thermal analyses of poly(3-hydroxybutyrate), poly(3-hydroxybutyrate-*co*-3-hydroxyvalerate), and poly(3-hydroxybutyrate-*co*-3-hydroxyhexanoate). J Appl Polym Sci 82:90–98
57. Aoyagi Y, Yamashita K, Doi Y (2002) Thermal degradation of poly[(R)-3-hydroxybutyrate], poly[ε-caprolactone] and poly[S-lactide]. Polym Degr Stab 76:53–59
58. Carrasco F, Dionisi D, Martinelli A et al (2006) Thermal stability of polyhydroxyalkanoates. J Appl Polym Sci 100:2111–2121
59. Lim ST, Hyun YH, Choi HJ et al (2002) Synthetic biodegradable aliphatic polyester/montmorillonite nanocomposites. Chem Mater 14:1839–1844
60. Yang Y, Zhu Z-K, Yin J et al (1999) Preparation and properties of hybrids of organo-soluble polyimide and montmorillonite with various chemical surface modification methods. Polymer 40:4407–4414
61. Erceg M, Kovacic T, Klaric I (2009) Poly(3-hydroxybutyrate) nanocomposites: Isothermal degradation and kinetic analysis. Thermochim Acta 485:26–32
62. Xie W, Gao Z, Pan W et al (2001) Thermal degradation chemistry of alkyl quaternary ammonium montmorillonite. Chem Mater 13:2979–2990
63. Hablot E, Bordes Pollet E et al (2008) Thermal and thermo-mechanical degradation of poly(3-hydroxybutyrate)-based multi-phase systems. Polym Degrad Stab 93:413–421
64. Cabedo L, Plackett D, Gimenez E et al (2009) Studying the degradation of polyhydroxybutyrate-*co*-valerate during processing with clay-based nanofillers. J Appl Polym Sci 112:3669–3676
65. Bordes P, Hablot E, Pollet E et al (2009) Effect of clay organomodifiers on degradation of polyhydroxyalkanoates. Polym Degrad Stab 94:789–796
66. Erceg M, Kovacic T, Sanja P (2010) Isothermal degradation of poly(3-hydroxybutyrate)/organically modified montmorillonite nanocomposites. Polym Compos 31:272–278
67. Kopinke F, Remmler M, Mackenzie K (1996) Thermal decomposition of biodegradable polyesters—I. Poly(β- hydroxybutyric acid). Polym Degrad Stab 52:25–38
68. Wu T-M, Hsu S-F, Shih Y-F et al (2008) Thermal degradation kinetics of biodegradable poly(3-hydroxybutyrate)/layered double hydroxide nanocomposites. J Polym Sci Part B 46:1207–1213
69. Yue L, Gross RA, McCarthy SP (1996) Composting studies of poly(β-hydroxybutyrate-co-β-hydroxyvalerate). Polym Degrad Stab 51:205–210
70. Savenkova L, Gercberga Z, Nikolaeva V et al (2000) Mechanical properties and biodegradation characteristics of PHB-based films. Process Biochem 35:573–579
71. Tsuji H, Suzuyoshi K (2002) Environmental degradation of biodegradable polyesters 1. Poly(ε-caprolactone), poly[[R]-3-hydroxybutyrate], and poly(L-lactide films) in controlled static seawater. Polym Degrad Stab 75:347–355
72. Tsuji H, Suzuyoshi K (2002) Environmental degradation of biodegradable polyesters 2. Poly(ε-caprolactone), poly[[R]-3-hydroxybutyrate], and poly(L-lactide films) in natural dynamic seawater. Polym Degrad Stab 75:357–363
73. Tsuji H, Suzuyoshi K, Tezuka Y et al (2003) Environmental degradation of biodegradable polyesters: 3. Effects of alkali treatment on biodegradation of poly(ε-caprolactone) and poly[[R]-3-hydroxybutyrate] films in controlled soil. J Polym Environ 11:57–65
74. Tsuji H, Suzuyoshi K (2003) Environmental degradation of biodegradable polyesters: IV. The effect of pores and surface hydrophilicity on the biodegradation of poly(ε-caprolactone) and poly[[R]-3-hydroxybutyrate] films in controlled seawater. J Appl Polym Sci 90:587–593

75. Renard E, Walls M, Guérin P et al (2004) Hydrolytic degradation of blends of polyhydroxyalkanoates and functionalized polyhydroxyalkanoates. Polym Degrad Stab 85:779–787
76. Mergaert J, Webb A, Anderson C et al (1993) Microbial degradation of poly(3-hydroxybutyrate) and poly(3-hydroxybutyrate-*co*-3-hydroxyvalerate) in soils. Appl Environ Microbiol 59:3233–3238
77. dos Santos RD, Calil MR, Fasina Guedes CDG et al (2004) Biodegradability of thermally aged PHB, PHB-V and PCL in soil compostage. J Polym Environ 12:239–245
78. Li Z, Lin H, Ishii N et al (2007) Study of enzymatic degradation of microbial copolyesters consisting of 3-hydroxybutyrate and medium-chain length 3-hydroxyalkanoates. Polym Degrad Stab 92:1708–1714
79. Abou-Zeid D, Müller R, Deckwer W (2001) Degradation of natural and synthetic polyesters under anaerobic conditions. J Biotechnol 86:113–126
80. Abou-Zeid D, Müller R, Deckwer W (2004) Biodegradation of aliphatic homopolyesters and aliphatic-aromatic copolyesters by anaerobic microorganisms. Biomacromolecules 5:1687–1697
81. Wang S, Song C, Chen G et al (2005) Characteristics and biodegradation properties of poly(3-hydroxybutyrate-*co*-3-hydroxyvalerate)/organophilic montmorillonite (PHBV/OMMT nanocomposite). Polym Degrad Stab 87:69–76
82. Ray SS, Yamada K, Okamoto M et al (2003) New polylactide/layered silicate nanocomposites. 5. Designing of materials with desired properties. Polymer 44:6633–6646
83. EFSA Scientific Committee (2011) Scientific opinion: guidance on the risk assessment of the application of nanoscience and nanotechnologies in the food and feed chain. EFSA J 9:2140
84. Bucci DZ, Tavares LBB, Sell I (2007) Biodegradation and physical evaluation of PHB packaging. Polym Test 26:908–915
85. de Azeredo HMC (2009) Nanocomposites for food packaging applications. Food Res Int 42:1240–1253
86. Simon P, Chaudhry Q, Bakos D (2008) Migration of engineered nanoparticles from polymer packaging to food—a physiochemical view. J Food Nutr Res 47:105–113
87. Dennis HR, Hunter DL, Chang D et al (2001) Effect of melt processing conditions on the extent of exfoliation in organoclay-based nanocomposites. Polymer 42:9513–9522
88. Shen L, Haufe J, Patel M (2009) Product overview and market projection of emerging bio-based plastics. PRO-BIP 2009: final report. University of Utrecht and European Bioplastics Association
89. Morschbacker A (2009) Bio-ethanol based ethylene. J Macromol Sci Part C Polym Rev 49:79–84
90. Morschbacker A (2010) Basics of bio-polyolefins. Bioplastics 5:52–55
91. da Silva-Valenzuela MDG, Wang SH, Wiebeck H et al (2010) Nanocomposite microcapsules from powders of polyhydroxybutyrate (PHB) and smectite clays. Mater Sci Forum 660–661:794–798
92. Shishatskaya EI, Voinova ON, Goreva AV et al (2008) Biocompatability of polyhydroxybutyrates microspheres: in vitro and in vivo evaluation. J Mater Sci Mater Med 19:2493–2502
93. Quintanar-Guerrero D, Fessi H, Alleman E et al (1996) Influence of stabilizing agents and preparative variables on the formation of poly(D,L-lactic acid) nanoparticles by an emulsification-diffusion technique. Int J Pharm 143:133–141
94. Gilman JW (1999) Flammability and thermal studies of polymer layered-silicate (clay) nanocomposites. Appl Clay Sci 15:31–49
95. Gallo E, Schartel B, Acierno D et al (2011) Flame retardant biocomposites: synergism between phosphinate and nanometric metal oxides. Eur Polym J 47:1390–1401
96. Plackett D, Siró I (2011) Polyhydroxyalkanoates (PHAs) for food packaging. In: Lagaron J-M (ed) Multifunctional and nanoreinforced polymers for food packaging. Wiley, Chichester
97. Mooney BP (2009) The second green revolution? Production of plant-based biodegradable plastics. Biochem J 418:219–232
98. Chen G-Q (2009) A microbial polyhydroxyalkanoates (PHAs) based bio- and materials-industry. Chem Soc Rev 38:2434–2446
99. Endres H-J, Siebert-Raths A (2011) Basics of PHAs. Bioplastics 3:42–45

Chapter 7
Poly(Butylene Succinate) and Poly[(Butylene Succinate)-co-Adipate] Nanocomposites

Vincent Ojijo and Suprakas Sinha Ray

Abstract In the recent years, biodegradable aliphatic polyesters-based composite materials have attracted substantial interest, primarily due to their sustainable production, use and end-life. This chapter discusses the preparation, characterisation, and properties of nanoclay-containing composites of biodegradable poly(butylene succinate) (PBS) and poly[(butylene succinate)-co-adipate] (PBSA). Various nanocomposite structures arising from the incorporation of layered silicate particles, both pristine and organically modified, into the neat PBS and PBSA matrices is critically reviewed. Good dispersion of the layered silicates, especially the organically modified layered silicates, tends to result in an improvement in a number of properties of the final nanocomposites: storage modulus, tensile modulus, gas barrier properties, degradability, and thermal stability, when compared with the neat polymers.

V. Ojijo
Division of Polymer Technology, Department of Mechanical Engineering,
Tshwane University of Technology, Pretoria 0001, South Africa

V. Ojijo · S. S. Ray (✉)
DST/CSIR Nanotechnology Innovation Centre,
National Centre for Nano-Structured Materials,
Council for Scientific and Industrial Research,
1-Meiring Naude Road, Brummeria,
Pretoria 0001, South Africa
e-mail: rsuprakas@csir.co.za

S. S. Ray
Department of Chemical Technology, University of Johannesburg,
Doornfontein, Johannesburg 2018, South Africa

L. Avérous and E. Pollet (eds.), *Environmental Silicate Nano-Biocomposites*,
Green Energy and Technology, DOI: 10.1007/978-1-4471-4108-2_7,

7.1 Introduction

In the recent years, biodegradable polymers (bio-polymers/bio-based polymers) have continued to attract a lot of interest; and due to a number of reasons, they find applications in packaging, agriculture, medicine, bags, sacks, and other areas [1–7]. Most importantly, they are recognised as part of the solution to the problem of environmental pollution arising from the use of non-biodegradable polymers especially in the packaging industry. Among the most attractive biodegradable polymers are polybutylene succinate (PBS) and its co-polymer, poly(butylene succinate-co-adipate) (PBSA). PBS and PBSA are both fully biodegradable polyesters and have some remarkable properties. Despite such advantages, PBS and PBSA, like some biopolymers, are more costly than conventional thermoplastics and may be unsuitable for practical use due their softness and poor gas barrier property, among other weaknesses. With this in mind, attempts have been made to improve the properties of these biopolymers in order to make them more competitive with the conventional non-biodegradable polymers. One such way of improving properties of these biopolymers is through the nanocomposite technology [8–18].

Nanocomposite technology involves the nano-scale dispersion, even at low levels (less than 5 %), of nano-sized fillers into a polymer matrix. The nano-fillers have very high surface area while some, especially non-spherical ones, have a high aspect ratio, which partly affect the final properties of the nanocomposites. Good dispersion of these nano-fillers, their high surface area and in some cases high aspect ratio, could potentially lead to improved properties of the nanocomposites. The improvement in quality is usually more than that of conventional micro and macro-composites for the same quantity of fillers. Among the nano-fillers that have these qualities and have been extensively used are the clays. These layered silicates have a high surfaces area, more than 700 m^2/g, and relatively high aspect ratios (e.g. 50–200). Apart from the improved properties arising from the addition of the layered silicates to biopolymers, the corresponding nanocomposites retain the biopolymer biodegradability, without any eco-toxicity, since the layered silicates are themselves eco-friendly.

Lee et al. [19] first prepared and characterised clay nanocomposites based on biodegradable aliphatic polymer (APES), which are closely related to PBSA. The nanocomposites showed higher tensile strengths when compared to the neat APES. Moreover, motivated by the successful preparation of polylactide/clay nanocomposites [20–22], Sinha Ray and co-workers [23, 24] first prepared PBS/clay nanocomposites with improved mechanical properties. Since then, a number of publications have appeared on both PBS/clay and PBSA/clay nanocomposites.

This chapter reviews the major development in the PBS/clay and PBSA/clay nanocomposites since the last decade. It discusses the various methods used to prepare the nanocomposites, their characterisation, properties and ultimately gives a conclusion and an outline of future prospects of these nanocomposites.

7.2 Synthesis, Structure and Properties of PBS and PBSA

PBS is a biodegradable aliphatic thermoplastic polyester which has a melting point of around 90–120 °C and a glass transition temperature which lies between –45 and –5 °C [25–30]. It is produced through condensation polymerization of a glycol, 1, 4-butanediol and an aliphatic dicarboxylic acid, succinic acid [25–27, 29, 31, 32]. The unit chemical structure of PBS is as shown in Fig. 7.1. However, due to the relatively low molecular weight, which makes it weak and brittle, chain extenders are to be used to increase its molecular weight [26, 33]. In their patent, Kawasaki and Kawakura [33] described the use of, among other chain extenders, hexamethylene diisocyanate (OCN–C_6H_{12}–NCO), in a coupling reaction between the polyester prepolymers. Each PBS chain consisted of 0.1–5 parts by weight of diisocyanate with 100 parts of aliphatic polyester prepolymer having a number average molecular weight of at least 5000. Relatively higher molecular weight chains were then achieved through the urethane bonds derived from the diisocyanate.

Apart from being strong, PBS has many interesting properties: biodegradability; melt processability; thermal and chemical resistance [2, 26, 34]. Their mechanical properties such as elongation at break and tensile strength are comparable with those of PP and LDPE while their crystallization behaviour is similar to that of polyethylene with well formed lamellar morphologies [30]. Because of its excellent processability, PBS can be processed in the field of textile into: melt blown; multifilament; monofilament; nonwoven; flat and split yarn and in the field of plastics into: injection moulded products; film; paper laminate; sheet and tape [26]. However, even though it has some excellent properties, which suggest potential applications, some of its other properties such as softness, gas barrier properties, etc. are frequently not adequate for a wide range of applications [34, 35]. Furthermore, it exhibits a lower biodegradation rate compared to its copolymers because of its high crystallinity [30, 36–38]. Therefore, different approaches have been used to improve the physical properties, extend the range of application, and increase the biodegradability of PBS for instance: copolymerization; physical blending; and the formation of a composite with organoclay. One example of such copolymers is PBSA.

PBSA is environmentally benign biodegradable thermoplastic polyester made of butylene succinate adipate random copolymer. It is chemically synthesized by polycondensation of 1, 4-butanediol with succinic and adipic acids [26, 36, 39–41]. The chemical structure of PBSA is as shown in Fig. 7.2.

Like PBS, it has good properties such as biodegradability, melt-processability and chemical resistance. It has been developed by various researchers in order to control the physical properties and rate of biodegradation. These studies have involved among others: thermal analysis [39, 42]; solubility and diffusion of carbon dioxide as a blowing agent into PBSA [43]; melt-rheology [44]; crystallization and morphology [45]; biodegradability [46–49]; etc.

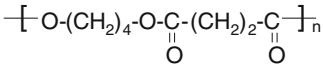

Fig. 7.1 Chemical structure of PBS. Reproduced from Ray, Okamoto and Okamoto with permission [35]

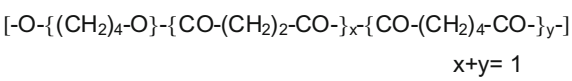

Fig. 7.2 Chemical structure of PBSA. Reproduced from Ray and Bousmina with permission [63]

The incorporation of adipate units within PBSA copolymer results into improved biodegradability compared to neat PBS [25, 48]; a fact that has been attributed to factors such as lower crystallinity [39] and polymer chain structure [36], among others. In a study by Hayase et al. [48], the NMR spectra of degradation products from PBSA indicated that the highly-enriched adipate units were more rapidly degraded than 1, 4-butanediol and succinate units. This seemed to be one of the reasons why PBSA biodegrades faster than PBS.

However, like PBS, the mechanical and other properties of PBSA, such as softness, gas-barrier and thermal stability of the neat polymer are often not sufficient for a wide range of end-use applications. Therefore, improvement in such properties has been explored through the addition of nano-particles into the neat polymers. In the recent years, a great interest has arisen in the formulation and association of biopolymers with nano-sized fillers, which could potentially result in a large range of improved properties and render the materials fully competitive with conventional thermoplastics. An example of these nano-particles is clay. The dispersion of nano-sized clay into a polymer matrix—forming polymer/clay nanocomposites—leads to a number of advantages compared to neat polymers and conventional composites.

7.3 Layered Silicate-Containing Nanocomposites of PBS and PBSA: Generalities

PBS/clay and PBSA/clay nanocomposites often exhibit enhanced properties even with the addition of a small amount of clay as compared to the conventional micro-scale composite materials. It is however, important for us to have a general understanding of the polymer/clay systems, *vis-à-vis*, clay types and structure; clay surface modification; and polymer–clay interaction and structure in order to understand how properties enhancement or lack thereof occurs. Therefore, a brief overview of the clay types, structure and surface modification is presented first, before a discussion of the polymer/clay nanocomposites.

Like in other systems, the types of clay normally used in PBS and PBSA/clay nanocomposites mainly fall under the family of 2:1 phyllosilicates [2, 9, 15, 16]. Table 7.1 summarises the commonly used layered silicates in PBS and PBSA/clay

Table 7.1 Commercial clays used in PBS and PBSA/clay nanocomposites and their characteristics

Commercial clays supplier/type/ designation	Organic modifier	Modifier conc. (meq/100 g)	d-spacing (Å)	References
Southern clay products (USA)				
Cloisite®10A (10A)-(MMT)	Dimethyl benzyl hydrogenated-tallow ammonium	125	19.2	[19, 58]
Cloisite®15A (C15A)-(MMT)	Dimethyl dihydrogenated-tallow ammonium	125	31.5	[63]
Cloisite®20A (C20A)-(MMT)	Dimethyl dihydrogenated-tallow ammonium	95	24.2	[87]
Cloisite®25A (C25A)-(MMT)	Dimethyl hydrogenated-tallow (2-ethylhexyl) quaternary ammonium methyl sulphate	95	21.8	[52, 56, 73, 88, 97, 98]
Cloisite®25A (C25A)-(MMT)	Twice modified with a coupling agents: (glycidoxypropyl) trimethoxysilane and (methacryloyloxypropyl) trimethoxy silane	–	–	[52, 73, 88]
Cloisite®30B (C30B)-(MMT)	Methyl bis(2-hydroxyethyl) (tallow alkyl) ammonium salt	90	18.7	[19, 58, 62–69, 72, 77]
Cloisite®30B (C30BM)-(MMT)	Twice modified with coupling agent: 1,6-diisocyanatohexan	90	29.4	[53, 58]
Cloisite®93A (C93A)-(MMT)	Methyl dihydrogenated-tallow ammonium	90	23.6	[63]
Kunimine Co., Japan				
Kunipia F -(MMT)	Cetyl trimethyl ammonium bromide (CTAB)	–	–	[76, 78]
	Cetyl pyridinium chloride (CPC)	–	20.7	[78, 83]
Kunipia F-MMT/Amine supplier: Tokyo Kasei Kogyo Co., Ltd. Japan	Dodecylamine (DA)	–	17.7	[80]
(ODA-MMT)	Octadecylamine (ODA)	–	18.2	[80]
(ALA-MMT)	12-aminolauric acid (ALA)	–	17.1	[80]
(LEA-MMT)	N-lauryldiethanolamine (LEA),	–	18.2	[80]
(HEA-MMT)	1-[N,N-bis(2-hydroxyethyl) amino]-2-propanol (HEA)	–	13.7	[80]

(continued)

Table 7.1 (continued)

Commercial clays supplier/type/ designation	Organic modifier	Modifier conc. (meq/100 g)	d-spacing (Å)	References
Nanocor Inc. (C_{18}-MMT)	Octadecylammonium cation	110	23.1	[23, 24, 35]
Hojun Yoko Co. (qC_{18}-MMT)	Octadecyltrimethylammonium cation	90	19.3	[24, 35, 85]
CO-OP Chemicals: Saponite (qC_{16}-SAP)	Hexadecyltributylphosphonium cation	86.6	18.7	[24, 35]
Sythetic Fluorine Mica (SOMASIF)	N- (coco alkyl)-N,N-[bis(2- hydroxyethyl)]-N-methylammonium cation	120	20.6	[70, 74, 101, 102]
Unicoop, Japan Synthetic fluorohectorites (FHTs)	Unmodified	–	10	[74]
Na-FHT MEE	Di poly(oxyethylene) alkyl methyl ammonium	120	20.6	[74]
Na-FHT MAE	Dimethyl dialkyl ammonium	–	36	[74]
Na-FHT MTE	Trioctyl methyl ammonium	–	24	[74]

nanocomposites: montmorillonite (MMT); saponite (SAP) and fluorohectorite (FHT). Structurally, the crystal lattice of the 2:1 phyllosilicates consists of layers made up of two tetrahedrally coordinated silicon atoms fused to an edge-shared octahedral sheet of either aluminium or magnesium hydroxide. These sheets arrange themselves to form stacks. The layer stacking leads to a regular Van der Waals gap between the platelets called the interlayer or the gallery. The MMT have a permanent layer negative charge due to the isomorphous substitution, generally in the octahedral sheet (typically from the substitution of low charge species such as Mn^{2+} for Al^{3+}). The FHT is crystallographically different from the MMT since its charge is due to the isomorphous substitution of Li^{+} for Mg^{2+}. The hydroxyl (OH) groups that are found in the octahedral sheets of MMTs are substituted by fluorine (F) in FHTs. However, in all the phyllosilicates, the global negative charge is counterbalanced by alkali and alkaline earth cations situated inside the galleries, which increases the clay hydrophilic characteristics. These clays are characterised by a moderate negative charge known as the exchange capacity (CEC), and is expressed in meq/100 g.

PBS and PBSA are hydrophobic polymers and hence do not have any affinity for the hydrophilic clay surfaces in their pristine form. Therefore, the surface of clay is modified with surfactants to enhance the clays hydrophobicity, and hence better interaction with the polymers. This is done through the exchange of the cations inside the galleries: K^{+}, Ca^{2+}, etc. with cationic surfactant such as primary, secondary, tertiary and quaternary alkyl-ammonium or alkyl-phosphonium. These organically modified clays are usually known as organoclays. Examples of the organic modifiers used in modification of clays in PBS and PBSA/clay nanocomposites as well as the exchange capacities are summarised in Table 7.1. The modification of clay surface leads to a drastic decrease of surface free energy, which eventually helps in improving wetting characteristics of the polymer matrix and results in a larger interlayer spacing [50]. The low surface energy leads to weaker forces between the layers, which might facilitate formation of the three thermodynamically feasible polymer/clay nanocomposite structures: intercalated; flocculated; and exfoliated [9, 12, 13, 35, 51].

These different nanocomposites structures are formed, depending on a number of factors; one being the surface polarities of polymer and clay. For instance, MMT has been modified by various surfactants as listed in Table 7.1, to give different organoclays with varying degrees of hydrophocity. For instance, methyl bis(2-hydroxyethyl) (tallow alkyl) ammonium salt surfactant has been used to prepare C30B organoclay. The surfactant on C30B has been found by various researchers to have favourable interactions with PBS and PBSA matrices, and hence forms the main organomodified clay used in preparation of nanocomposites based on PBS and PBSA (see Tables 7.2, 7.3).

The modification is generally done once, however, additional modification can be also carried out. Chen and Yoon [52] devised a new method of introducing additional functional groups to C25A organoclay. The twice-functionalised organoclay (TFC) was prepared by the reaction of (glycidoxypropyl)trimethoxy silane (GPS) or (methacryloyloxypropyl)trimethoxy silane (MPS) with the silanol

Table 7.2 Summary of reported methods used for the preparation for PBS/clay systems

Preparation technique	Polymer/clay system	References
In situ intercalative polymerisation	MMT-Cloisite 10A; and 30B. C30B modified again with urethane	[53, 58]
Solution intercalation	Polymer: PBS-(Bionolle# 1020) from Showa Denko, Japan. Clay: MMT (Kunipia F) from Kunimine Co., Japan:-Two organic modifiers: (i) cetyl pyridinium chloride (CPC) and (ii) cetyl trimethyl ammonium bromide (CTAB)	[78]
	Polymer: PBS-(Bionolle# 1001) from Showa Denko, Japan. Clay: MMT (Kunipia F) from Kunimine Co., Japan. Organic modifier: cetyl pyridinium chloride (CPC). Cured by dicumyl peroxide (DCP)	[83]
	Polymer: PBS-(Bionolle# 1020) from Showa Denko, Japan. Clay: MMT (Kunipia F) from Kunimine Co., Japan. Organic modifier: CTAB	[76]
Melt intercalation	Polymer: PBS-(Bionolle # 1020, hexamethylene diisocyanate chain extender used) from Showa Denko, Japan. Clay: C_{18}-MMT, from Nanocor	[23, 24, 35, 81]
	Polymer: PBS-(Bionolle # 1020, hexamethylene diisocyanate chain extender used) from Showa Denko, Japan Clay: (qC_{18}-MMT), from Hojun Yoko Co	[24, 35, 85]
	Polymer: PBS-(Bionolle # 1020, hexamethylene diisocyanate chain extender used) from Showa Denko, Japan Clay: Saponite (qC_{16}-SAP), from CO-OP Chemicals	[24, 35]
	PBS: obtained from Irae Chemical Co., Korea, Clay: C25A from Southern Clay Product Inc	[73, 88]
	Polymer: PBS-(Bionolle # 1020, hexamethylene diisocyanate chain extender used) from Showa Denko, Japan Clay: MMT (Kunipia F) from Kunimine Co., Japan; various amines used as modifiers, ODA, LEA, HEA and ALA	[80]
	Polymer: PBS-(Bionolle # 1003) from Showa HighPolymer, Japan Clay: MMT-C30B from Southern Clay Products, USA; and polycaprolactone (PCL)-grafted-C30B	[62]

groups on C25A as shown in Fig. 7.3. They reported better interfacial interaction between the TFC and PBSA than between C25A and PBSA. Recently, Hwang et al. [53] have also successfully modified organic clay C30B with the urethane 1, 6-diisocyanatohexane. They reported substantial improvement in interfacial interaction between the twice-modified clay (C30BM) and PBS matrix. The PBS/C30BM nanocomposite exhibited a higher degree of exfoliation as well as improvement in all the mechanical properties, including tensile strength, storage modulus, and elongation at break, compared with PBS, C10A, and C30B nanocomposites.

Table 7.3 Summary of reported methods used for the preparation for PBSA/clay systems

Preparation technique	Polymer/clay system	References
Solution intercalation	Polymer: biodegradable aliphatic polyester (BAP) from diols (1,4 butanediol and ethylene glycol) and dicarboxylic acids (succinic and adipic acid): Skygreen 2109 from Sunkyong Industries Korea Clay: MMT-C25A from Southern Clay Products	[56, 98]
Melt intercalation	Polymer: PBSA-(Bionolle # 3001) from Showa HighPolymer, Japan Clay: MMT-C30B from Southern Clay Products	[63–69, 72, 77, 87]
	Polymer: PBSA-(Bionolle # 3001) from Showa HighPolymer, Japan Clay: Synthetic Fluorine Mica (SOMASIF) (78)from CO-OP Chemicals	[101, 102]
	Polymer: PBSA obtained from Irae Chemical Co., Korea, Clay: C25A from Southern Clay Product Inc.; modified second time with glycidoxypropyl trimethoxy silane or (methacryloyloxypropyl)trimethoxy silane	[52]
	Polymer: Biodegradable aliphatic polyester (BAP) from diols (1,4 butanediol and ethylene glycol) and dicarboxylic acids (succinic and adipic acid): Skygreen 2109 from Sunkyong Industries Korea Clays: MMT-10A and 30B	[19]
	Polymer: PBSA-(Bionolle # 3001) from Showa HighPolymer, Japan Clay: MMT-C20A from Southern Clay Products	[87]
	Polymer: Synthetic BAP (Skygreen 2109) Skygreen 2109 from Sunkyong Industries Korea Clay: MMT-C25A from Southern Clay Products	[97, 98]
	Polymer: PBSA-(Bionolle # 3001) from Showa HighPolymer, Japan Clay: MMT-C93A from Southern Clay Products	[63]
	Polymer: PBSA-(Bionolle # 3001) from Showa HighPolymer, Japan Clay: MMT-15A from Southern Clay Products	[63]

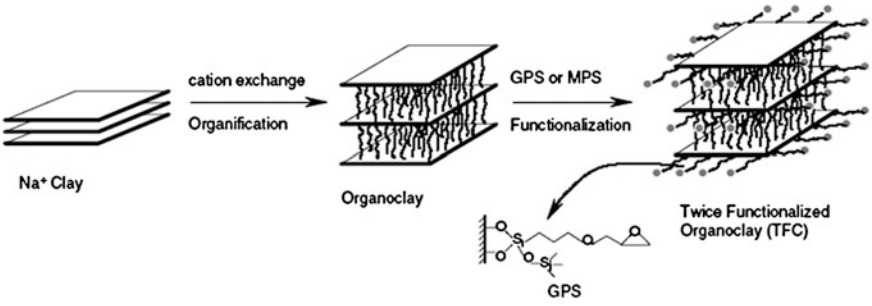

Fig. 7.3 Schematic diagrams for preparation of the twice-functionalized organoclay (TFC). Reproduced from Chen and Yoon, with kind permission from ©Wiley

7.4 Preparation Methods of Clay-Containing PBS and PBSA Nanocomposites

In general, three main techniques have been used in preparation of PBS and PBSA/clay nanocomposites: intercalation of polymer or pre-polymer from solution; in situ intercalative polymerization and melt intercalation. A summary of reported methods of preparation for PBS/clay and PBSA/clay systems is shown in Tables 7.2, 7.3, respectively. Judging by the number of publications reported, melt intercalation method has proven to be the preferred route probably due to its eco-friendliness since it avoids the use of chemicals.

7.4.1 Solution Intercalation

The method is based on a solvent system in which the polymer or pre-polymer is soluble and the silicate layers are swellable [54, 55]. Solvents such as water, chloroform or toluene are used to swell the silicate layers. It is well known that such layered silicates can be easily dispersed due to the weak forces that stack the layers together. Once the swelling is done, the polymer solution is then mixed with the layered silicate solution. The polymer chains intercalate, eject the solvent within the interlayer of the silicate and adsorb onto the silicate. When the solvent is evaporated, the intercalated structure remains, resulting into PBS/clay nanocomposites or PBSA/clay nanocomposites. In their work, Lim et al. [56] prepared, for the first time, biodegradable aliphatic polyester (Skygreen 2109) (BAP)/MMT nanocomposites, characterised them and studied thermal and rheological properties. The BAP were copolymers synthesised from diols (1,4 butanediol and ethylene glycol) and dicarboxylic acids (succinic and adipic). They dissolved different amounts of BAP into chloroform whereas; C25A organoclay was also dispersed in chloroform for 48 h. The chloroform from a mixture of both was then evaporated and the samples dried in vacuum for 24 h. These nanocomposites largely formed intercalated structures.

However, due to use of organic chemicals as solvent, some of which are toxic, lesser attempts have been made at preparing PBS and PBSA/clay nanocomposites through the solution intercalation method, as compared to melt intercalation.

7.4.2 The In Situ Intercalative Polymerization

During in situ intercalative polymerization, the layered silicate is swollen within the liquid monomer or a monomer solution so that the polymer formation can occur between the intercalated sheets [15, 54, 57]. Polymerization can be initiated either by heat or radiation, by diffusion of a suitable initiator or by an organic

initiator or catalyst fixed through cationic exchange inside the interlayer before the swelling step by the monomer.

Hwang et al. [53, 58] prepared PBS/MMT nanocomposites by in situ polymerization through direct esterification and polycondensation. These studies were geared towards understanding the role of urethane group, 1, 6 diisocyanatohexane, on the organoclay (C10A; C30B and C30BM), with regards to the structure and properties of the PBS/MMT nanocomposites. The nanocomposites revealed different extents of delaminated structures (depending on the clay surface modification). However, there seems to be less reported studies on in situ polymerization method of preparation of the nanocomposites. A lot of research seems to be concentrated on the advantageous melt intercalation technique.

7.4.3 Melt Intercalation

In this technique, the layered silicate is mixed with the polymer in the molten state. The process involves mixing the clay with the polymer and heating the mixture above the softening point of the polymer, statically or under shear [59, 60]. The formation of polymer/clay nanocomposites via polymer melt intercalation depends upon the thermodynamic interaction between the polymer and host silicate as well as transport of polymer chains from the bulk melt into the silicate interlayers [59, 61].The polymer needs to be sufficiently compatible with silicate layer surface. A range of nanocomposites with structures from intercalated to exfoliated can be obtained, depending on the degree of penetration of the polymer chains into the silicate galleries. This method has several advantages over the others. It is environmentally sound since no chemical is used. Secondly, it is compatible with the current industrial process, such as extrusion and injection moulding [59]. For these reasons therefore, the preparation route of choice for PBS and PBSA/clay nanocomposites have been prepared through melt intercalation (see Tables 7.2, 7.3).

For the first time, Sinha Ray et al. [23] reported the preparation, structure, and mechanical properties of PBS/C_{18}-MMT through melt intercalation. In a typical procedure, they first mixed the PBS pellets and C_{18}-MMT organoclay in a bag before melt-extruding at 150 °C to yield gray strands. The resulting strands were then pelletized and dried under vacuum at 75 °C for 7 h to remove any remaining moisture. These nanocomposites (PBSCNs) were then converted into sheets with thickness of 0.7–2 mm by pressing them at about 1.5 MPa at 135 °C for 3 min. The moulded pellets were then quickly quenched between glass plates and then annealed at 60 °C for 1.5 h to crystallize completely before being subjected to all measurements. The PBSCNs obtained showed stacked and intercalated structures as discussed in the characterisation section of this chapter. Subsequently, Sinha Ray and various co-workers [24, 35] used more or less the same melt-intercalation technique as aforementioned to prepare PBS-clay nanocomposites. The resulting nanocomposites had various kinds of structures: intercalated and extended flocculated, intercalated and flocculated, stacked intercalated and delaminated.

Several other researchers have used the melt intercalation method to process PBS-clay nanocomposites as listed in Table 7.2. For instance, Pollet et al. [62] used C30B to prepare a 3 wt% filled PBS-based nanocomposites by melt intercalation. The authors also tested three metal-based catalysts: dibutyltin dilaurate $Sn(Bu)_4$; titanium (IV) butoxide $Ti(OBu)_4$; and antimony (III) oxide Sb_2O_3 for their ability to promote transesterification between the ester functionalities of the PBS and the organoclay surface. The nanocomposites obtained had an intercalated structure, whereas, when catalyst was used, high level of clay platelet exfoliation was realised. They attributed the enhanced dispersion to transesterification reaction between the hydroxyl function of the organic modifier and the PBS chains. This interesting and original technique could allow for the preparation of nearly-exfoliated nanocomposites by the now popular method of melt intercalation. This could give it an edge as environmentally friendly and a one-pot industrial procedure for the preparation of nearly exfoliated PBS/clay nanocomposite.

Over the recent years, Sinha Ray and various co-workers have prepared PBSA-clay nanocomposites through melt intercalation technique [63–71]. These studies began by testing clays with different extents of hydrophobicity, and hence different levels of interaction between the surfactants with the polymer matrix [63]. In a typical experiment, three OMMTs were used: C15A; C93A; and C30B and different composite structures obtained: phase-separated; intercalated; and a coexistence of intercalated and exfoliated, depending on the polarity of the surfactants used to modify the montmorillonite. A higher degree of dispersion of the C30B clay was attributed to more favourable enthalpic interactions between the diols present in the C30B surfactant and the C = O groups present on the PBSA backbone. Hence, PBSA/C30B nanocomposite showed relatively better improvement in properties. Therefore, the subsequent studies by Sinha Ray and co-workers tended to dwell on PBSA/C30B nanocomposites and the sample preparation procedures were more or less the same as one already described.

Because of the strong interaction between the C30B surfactant and PBSA matrix, Eslami et al. [72]. employed melt intercalation technique to prepare PBSA/C30B nanocomposites as well. The nanocomposites structure showed individual clay layers and stacks of clay platelets uniformly dispersed in PBSA matrix. The extent of exfoliation was almost the similar, but slightly better than got by Sinha Ray et al. [63], described above.

Another interesting application of melt intercalation method to produce PBSA/C25A nanocomposites was shown by Chen and Yoon [52]. In their work, the C25A was twice-functionalised with two types of silane coupling agents: (glycidyloxypropyl)trimethoxy silane and (methacryloyloxypropyl)trimethoxy silane. They observed stacks of clay layers well-dispersed in the PBSA matrix with multiple ordered platelets. The higher degree of exfoliation of the silicate layers in the case of twice-functionalised organoclay as compared to C25A was attributed to two factors: the reaction between the end-groups of PBSA and the epoxy groups on the coupling agents; and the polar interaction between the ester groups in the coupling agents and PBSA.

7.5 Characterisation Techniques

It is well-established that the final properties of a nanocomposite are directly related to the dispersion characteristic and orientation of the silicate layers in the polymer matrix. As with other polymer/clay nanocomposites, the structural characterisation of PBS and PBSA/clay nanocomposites is centred around wide angle X-ray diffraction (WAXD) and transmission electron microscopy (TEM) [19, 23, 24, 35, 58, 62, 67, 72–74]. However, other techniques such as: small-angle X-ray scattering (SAXS) (66, 69); nuclear magnetic resonance (NMR) (39, 88); Fourier transform infrared spectroscopy (FT-IR) [52, 58, 75]; optical microscopy (OM) [45, 76]; scanning electron microscopy (SEM) [64, 66] have been used to quantify and qualify the dispersion of silicate layers in the polymer matrix as well as the molecular mobility and phase structure. In addition, high resolution-TEM combined with electron tomography [64] as well as focused ion beam (FIB)-tomography [77] have recently been used to study the dispersion of clays into the PBSA matrix. More recently, a unique morphology of dispersed clay particles in 3 wt% containing PBSA nanocomposite has been reported [65]. This was studied using FIB-surface delineation etching technique.

The WAXD technique allows a direct evidence of the intercalation of the polymer chains into the silicate galleries, however, little can be said about the spatial distribution of the silicate layers or any structural in-homogeneities in the polymer nanocomposite. On the other hand, TEM allows a qualitative understanding of the internal structure, spatial distribution of the various phases, and defect structure through a direct visualisation. Both the WAXD and the TEM have been the most applied techniques in characterisation of PBS and PBSA/clay nanocomposites. Sinha Ray et al. [23] first reported the intercalation of PBS into C_{18}-MMT clay interlayers, prepared through melt-compounding. Figure 7.4 shows the WAXD patterns of C_{18}-MMT, PBS/C_{18}-MMT nanocomposites (PBSCNs) and PBS matrix in the range of $2\theta = 1$ to 10°.

The mean interlayer distance of the (001) plane ($d_{(001)}$) for the C_{18}-MMT is 2.31 nm (at $2\theta \cong 3.82°$). For PBS nanocomposite containing 1.7 wt% (inorganic part) C_{18}-MMT (PBSCN1.7), a clear peak is observed at $2\theta \cong 2.82°$ and a very small peak is observed at $2\theta \cong 5.14°$, corresponding to (001) and (002) planes of the silicate layers dispersed in the PBS matrix. In the case of PBSCN2.8, both peaks became strong and are shifted toward the higher angles. The difference in the interlayer spacing between the C_{18}-MMT powder and that in PBSCNs after melt mixing is presumably due to the intercalation of the PBS chains into the silicate galleries. To visualise the clay dispersion, TEM bright-field image of the PBSCN2.8 was taken. The dark entities are the cross section of the stacked and intercalated organically modified silicate layers. Stacked and flocculated silicate layers were observed from the TEM images, which are randomly distributed in the PBS matrix. The size of some of the stacked-silicate layers appears to reach about 300–700 nm.

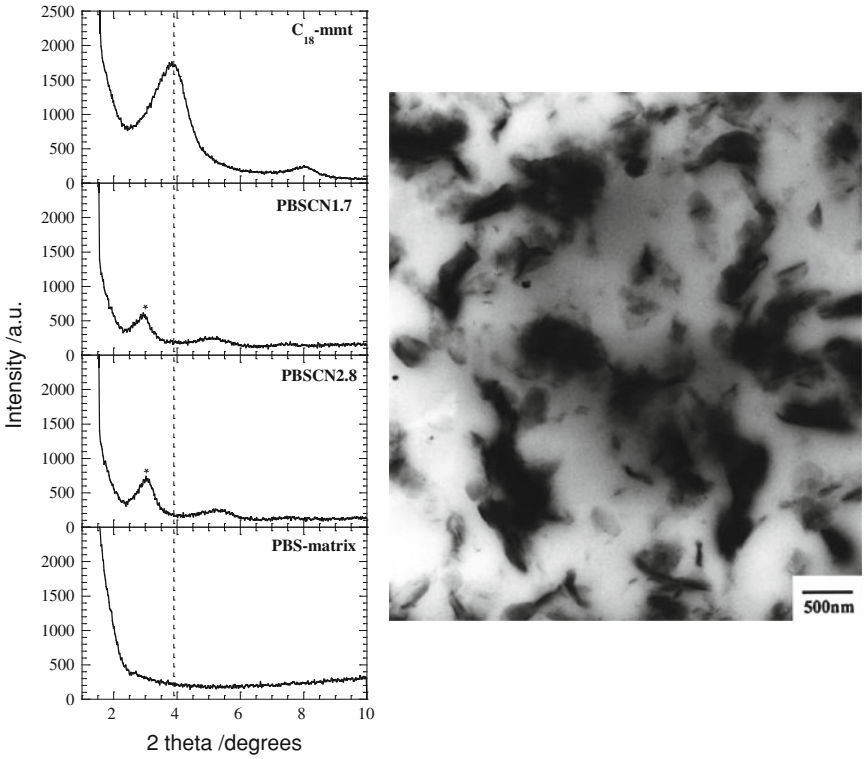

Fig. 7.4 WAXD patterns for C18-MMT, PBS nanocomposites with different clay loading and PBS, respectively; and TEM micrograph of PBSCN2.8. Reproduced from Sinha Ray et al. [23] with permission

In the study by Hwang et al. [58], WAXD and TEM were used to examine the degree of clay dispersion in the PBS/clay nanocomposites. In this case, MMT with different surface modifications were used to make the nanocomposite through in situ polymerization of PBS: C10A; C30B; and urethane modified C30B (C30BM). One of the reasons for surface modification using urethane was to increase the silicate basal spacing. Figure 7.5 shows the WAXD profiles indicating (A) the basal spacing of clays and (B) the intercalation spacing of the prepared nanocomposite samples. The basal spacing is 18.7 Å ($2\theta = 4.7°$) for C30B, 19.6 Å ($2\theta = 4.5°$) for C10A, and 29.4 Å ($2\theta = 3.0°$) for C30BM. The basal spacing was wider in C10A than in C30B due to the steric hindrance of benzene molecules between silicate layers. The reflection peak of $d_{(001)}$ in C30BM (urethane-modified clay) shifted to a lower diffraction angle at 3.0°, corresponding to a larger basal spacing than modified clays. The authors observed that the increased basal spacing reduced the level of silicate–silicate attraction between adjacent silicate layers, making it easier to penetrate the PBS matrix in silicate layers and to form a probable exfoliated structure. However, the WAXD patterns do not provide a

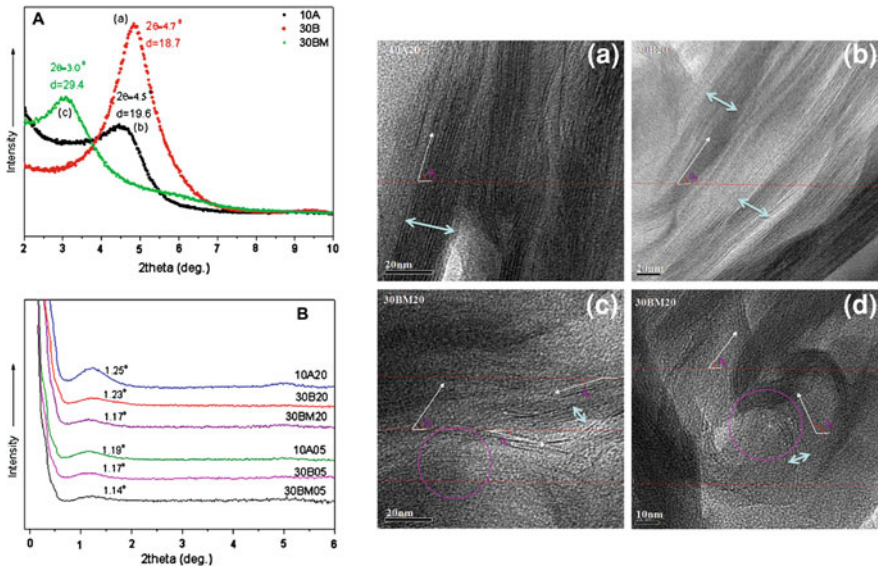

Fig. 7.5 WAXD profiles (**A**) of various clays: (*a*) 10A, (*b*) 30B, and (*c*) 30BM; WAXD profiles (**B**) of nanocomposites. The number after the clay designation denotes clay content, e.g. 10A20 = PBS/C10A nanocomposite with 2 wt% clay content and TEM micrographs of nanocomposites composed of (*a*) 10A20, (*b*) 30B20, (*c*) 30BM20, and (*d*) 30BM20 (at 10 nm resolution. Reproduced from Hwang et al. [58] with kind permission from ©Elsevier 2010

direct evidence of exfoliation. Therefore, the authors used TEM to visualise the clay dispersion in PBS matrix.

As observed in Fig. 7.5a, b (10A20 and 30B20, respectively), clay sheets were uniformly oriented with a complete layer stack containing an average of 14 and12 silicate sheets per bundle, respectively. The authors measured the orientation of clay stack/platelets with reference to an arbitrary horizontal line. In the case of 10A20 and 30B20, the clay layer orientation angle was fixed ($\theta_1 = 74°$, $\theta_2 = 60°$), resulting in images of complete MMT layer stacks with one side direction. On the other hand, Fig. 7.5c, d (30BM20) reveal significantly smaller bundles composed of only 3–4 randomly oriented silicate sheets. The clay layer angle had several values ($\theta_3 = 60°$, $\theta_4 = 14°$, $\theta_5 = 19°$) measured from an arbitrary horizontal line. In particular, an omni-directional angle of dispersed clay layer can be seen in neighbouring red circle areas in Fig. 7.5 c, d; the resulting clay sheets were largely exfoliated in the PBS matrix. This result indicates that the alkyl modifier in clay layers (10A and 30B) did not effectively disperse the clay sheet in the PBS matrix due to poorer affinity between the clay and alkyl modifier compared to urethane-modified clay. In the case of 30BM20 sample, the urethane-modified MMT nanocomposite yielded far superior clay exfoliation. They attributed this fact to better affinity between the clay and the urethane group and to wider d-spacing, which enabled PBS chains to penetrate the clay galleries.

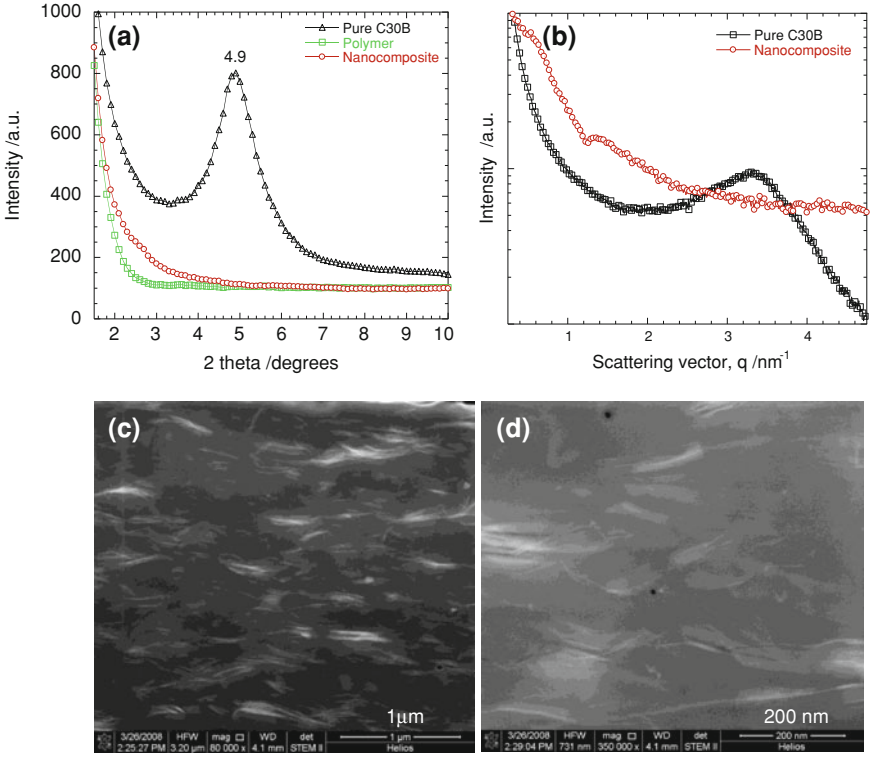

Fig. 7.6 **a** WAXD patterns of pure C30B powder, compression moulded pure PBSA and PBSA/C30B (4 wt%) nanocomposite samples (thickness ≈ 0.4 mm), **b** Normalised background subtracted SAXS patterns of pure C30B powder and compression moulded nanocomposite samples (thickness ≈ 0.4 mm), and HAADF-STEM images of the same nanocomposite at two different magnifications: **c** 80 k and **d** 350 k. Reproduced from Sinha Ray with permission [64]

However, the use of only WAXD and TEM to study the clay dispersion in polymer matrices may not at times result to conclusive clay dispersion analysis. The use of TEM for instance, has a serious drawback due to the fact that it projects three-dimensional (3-D) body on to two-dimensional (2-D) plane. The information along the thickness direction of the sample is only an accumulated one and this actually leads to the wrong conclusion about the degree of dispersion of silicate layers in the polymer matrix. A featureless WAXD results could also wrongly suggest a highly delaminated structure. This was illustrated by the studies on C30B organoclay dispersion in PBSA matrix as shown in Fig. 7.6a [64]. The featureless WAXD pattern for the nanocomposite suggests a highly delaminated structure. However, additional STEM (Fig. 7.6c, d) and SAXS (Fig. 7.6b) studies reveal a different scenario, bringing to question whether complete exfoliation is really possible.

From the high-annular-angle-dark-field scanning transmission electron microscopy (HAADF-STEM) images in Fig. 7.6c, d, we can see that most of the silicate layers are homogeneously dispersed in the PBSA matrix; however, stacking of some

silicate layers is still observable and this is more discernible at high magnification STEM images. Moreover, in the SAXS patterns in Fig. 7.6b, there was a sharp peak at scattering vector, $q = 1.39\ nm^{-1}$ for nanocomposite sample, indicating the presence of stacked and intercalated silicate layers in the PBSA matrix as observed in STEM images, a feature previously not visible. In a recent study, Bandyopadhyay and Sinha Ray [68] characterised the structure of PBSA/C30B nanocomposite containing 3 wt% clay (PBSANC3), by SAXS combined with bright-field TEM. They sought to show the exact mechanism of enhanced elongation at break in the case of nanocomposite. For cases with a densely packed system of particles, the positional ordering can develop a preferential orientation with respect to each other, especially for particles that are not spherical. The degree of orientation can be detected easily from the 2D SAXS patterns. An arc-profile is usually used to determine the orientation of crystals in a certain basal plane. Parts (a) and (b), respectively, of Fig. 7.7A represent the 2D SAXS patterns of PBSA and PBSANC3 before the tensile test. Similarly, the 2D SAXS patterns of PBSA and PBSANC3 after the tensile tests are shown in parts (c) and (d), respectively, of Fig. 7.7A.

From Fig. 7.7A neither (a) PBSA nor (b) PBSANC3 possesses any preferred orientation in the masked crystal plane. However, after the tensile test (parts (c) and (d)) both PBSA and PBSANC3 show scattering patterns similar to the oriented sample. The scaled normalized scattering profiles determined on the basis of the arc-mask against the orientation angle for all samples are presented in Fig. 7.7B. The figure shows that the moulded PBSA and PBSANC3 samples do not possess a specific orientation since the specific orientation remains constant throughout the range of orientation angle. However, after the tensile test the neat PBSA chains exhibit an orientation at ±90°. On the other hand, in the case of the PBSANC3, three intensity maxima appear (at ±90° and –2.4°) in the azimuthal scattering profile. The resultant profile after subtracting PBSA profile from the PBSANC3 profile confirms that –2.4° is due to the oriented dispersed clay particles in the PBSA matrix. The studies showed that the enhanced elongation at break in the case of nanocomposite is due to the orientation of the dispersed clay layers in the direction of the applied tensile force.

Recently, we have used, for the first time, FIB-tomography as a high-resolution 3D-technique to study the morphology of PBSA/C30B nanocomposites [77]. The 3D-tomography of a material using FIB/scanning electron microscopy cross beam system starts by cutting 2D- slices through the selected volume by milling steps and cross-section can be imaged by high-resolution SEM (see Fig. 7.8a). Then the 2D-images are aligned using cross correlation of reference markers and finally, computer reconstruction of 2D-images enables the 3D-morphology of the dispersed silicate layers in the polymer matrix (see Fig. 7.8b). For the preparation of cross sections using FIB, the Gallium ion beam is perpendicular to the sectioning plane of interest. To avoid damage, prior to the milling, the PBSANC film is sputter coated using PtPd alloy for 60 s at 40 mA current.

Figure 7.8 shows the dispersion of silicate layers in different planes. From the elemental analysis using X-ray (EDS analysis), Si, Al, Mg, and oxygen were mainly identified and from the elemental compositional analysis, the white

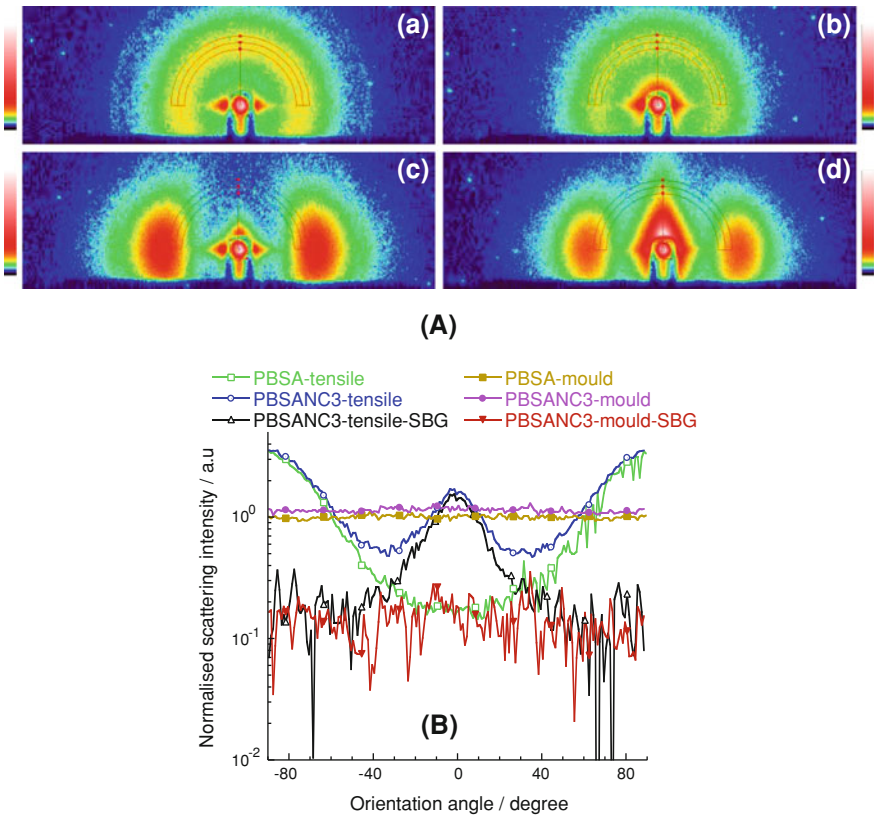

Fig. 7.7 (**A**) Two-dimensional small-angle X-ray scattering patterns: (*a*) PBSA before the tensile test, (*b*) PBSANC3 before the tensile test, (*c*) PBSA after the tensile test, and (*d*) PBSANC3 after the tensile test. SAXS samples were prepared from injection-molded bars along the elongation direction and for all samples; the contrast was kept at 53 during determination of the arc-profile. (**B**) The scaled normalized scattering profiles (determined on the basis of the arc-mask) against the orientation angle. Mold indicates molded sample; tensile indicates after tensile test; and SBG indicates background (here PBSA) subtracted. Reproduced from Bandyopadhyay and Sinha Ray [68], with permission

particles were found to be MMT, used for the preparation of PBSANC. It is clear from the images that silicate particles have platelet-like geometry, mostly intercalated, nicely oriented (particularly in the YZ- and XY-planes), and finely dispersed in the PBSA matrix. Moreover, the intercalated particles are mostly interconnected, forming network like geometry inside the PBSA matrix. In addition, as shown in Fig. 7.8b, it is clear from the reconstruction that the layered silicate particles are completely embedded within the PBSA matrix. This information is very crucial in understanding the overall integrity of the PBSANC and predicting its mechanical and other properties.

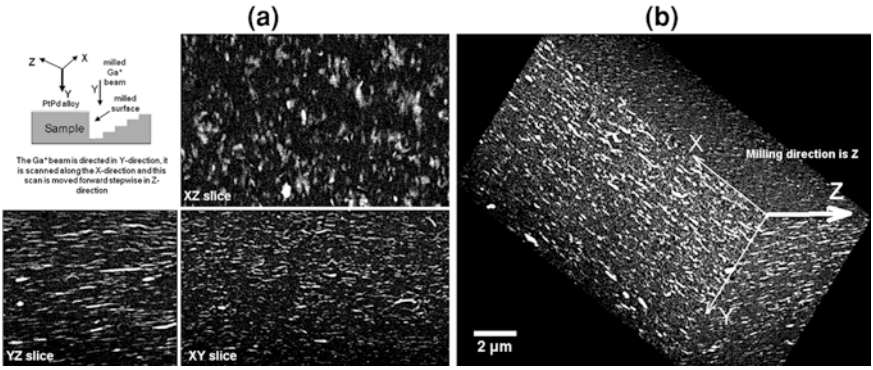

Fig. 7.8 **a** Cross-sectional view of the nanocomposite sample, in which three digital slices from different planes are displayed. XY slice is one of the original SEM image, while the XZ and YZ slices are virtual slices extracted digitally from the 3D-data set **b** 3D-representation of layered silicate dispersion (white parts) in PBSA matrix. The reconstructed volume after data processing was 14.85 × 8.55 × 9.51 μm3. 'Milling direction is Z' refers to the direction of slicing. Reproduced from Sinha Ray with permission [77]

7.6 Properties

The primary reason for the formation of PBS and PBSA/clay nanocomposites has always been to enhance certain properties in the neat polymers. The enhancement of properties in the nanocomposites arises mainly due to the interfacial interaction between the clay surfaces and PBS and PBSA matrices. These properties include: mechanical; thermal; gas barrier; and biodegradability.

7.6.1 Mechanical Properties

7.6.1.1 Dynamic Mechanical Analysis

The dynamic mechanical analysis (DMA) does reveal the amount of energy stored in the nanocomposite as elastic energy and the portion of the energy dissipated during mechanical strain. This is strongly dependent on the geometry of the sample and the level of clay dispersion, hence, the degree of interaction between the polymer matrix and the clay. The results are expressed by three main parameters: storage modulus (G' or E') corresponding to the elastic response to deformation; loss modulus (G'' or E'') corresponding to the viscous portion; and tanθ (G''/G'), useful in determining the occurrence of molecular mobility transition such as glass transition temperature (T_g).

Nanocomposites based on PBS and PBSA show better storage modulus than the neat polymers, and the extent of the improvement is dependent on clay interfacial interaction with the polymers, aspect ratio of the clay [24, 35], processing

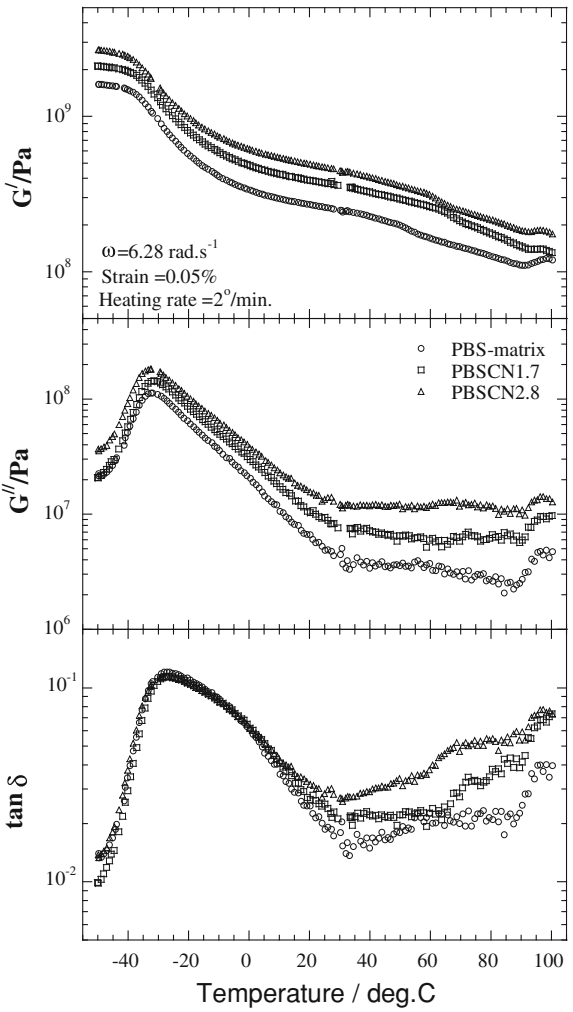

Fig. 7.9 Temperature dependence of G′, G″ and tan δ for PBSCNs and the corresponding PBS-matrix. Reproduced from Ray, Okamoto, Maiti and Okamoto [23], with permission

procedure [23] and the resultant nanocomposite structure [63, 78]. Sinha Ray et al. [23] performed DMA analysis on PBS/C_{18}-MMT under tension–torsion mode at a constant frequency (ω) of 6.28 rad/s with a strain amplitude of 0.05 %. Figure 7.9 shows the temperature dependence of G', G'' and tan δ of PBS/C_{18}-MMT nanocomposites (PBSCN1.7 and PBSCN2.8, for 1.7 and 2.8 wt% clay inorganic part, respectively) and the corresponding PBS matrix.

There was an improvement in storage moduli in all the temperature ranges for both of the PBSCNs. In the temperature range of–50 °C to–30 °C, there was 33 % increment in G' for PBSCN1.7 and 62 % for PBSCN2.8 as compared to the neat PBS. Also, between 30 and 100 °C, a higher degree of enhancement in G', was achieved for both of the PBSCNs, over that of neat PBS. At room temperature, the increment was 42 % for PBSCN1.7 and 82 % for PBSCN2.8. The reason for such

improvement in G' with temperature is the dominant role played by strong reinforcement effect of clay particles above T_g, when the material is soft. However, due to the low T_g (–30 °C) for PBS, the order of such improvement, below and above the T_g, is only marginally different. With an increase in the clay content, the nanocomposite becomes even stiffer, thus the better storage modulus.

On the other hand, the presence of clay particles in the PBS matrix does not lead to a big shift and broadening of the tan δ curves for both PBSCNs. There is, however, a large enhancement of tan δ and G'' for PBSCNs above T_g as compared to neat PBS caused by the large anisotropy of the clay particles due to flocculation.

The effect of PBS/clay nanocomposite structure on the dynamic mechanical properties has been illustrated by Shih et al. [78]. They prepared different classes of nanocomposites, with Kunipia F-MMT clay organically-modified by two surfactants: cetyl pyridium chloride (CPC) and trimethyl ammonium bromide (CTAB). Different clay contents were used, 1, 3 and 5 wt% and the nanocomposites coded PBS20; PBS20A01; PBS20A03; PBS20A05; for neat PBS and nanocomposites with 1, 3 and 5 wt% CTAB, respectively. Their findings showed that 3 wt% clay content produced a better clay dispersion than the aggregated nanocomposite structures obtained at 5 wt% loading. Consequently, the storage modulus and loss modulus were more enhanced for nanocomposites with 3 wt% clay content than those with 5 wt% clay content.

Apart from the presence of well-ordered intercalated structures, aspect ratio of clays has been shown to play an important role in the enhancement of dynamic mechanical properties [24, 35]. Sinha Ray et al. [35] prepared PBS/clay nanocomposites with two types of organoclays having different aspect ratios: C_{18}-MMT and qC_{16}-SAP. The C_{18}-MMT platelets had a length of –150 nm while those of qC_{16}-SAP had a length of –55 nm. The nanocomposites were designated PBSCN1, PBSCN2, PBSCN3 and PBSCN4 for PBS/C_{18}-MMT with clay content (inorganic part) of 1.5, 2.5, 4.0 and 5.5 wt%, respectively. On the other hand, PBSCN5 and PBSCN6 were PBS/qC_{16}-SAP with clay content (inorganic part) of 1.5 and 5.5 wt%, respectively. Figure 7.10 shows the temperature dependence of G' and G'' and their ratio, tan δ. In all the temperature range studied, the PBSCNs posted better G'' and G'' , as compared to the neat PBS. At room temperature for instance, the increment of G′ in PBSCNs over neat PBS was 18.5, 44, 82 and 248 % for PBSCN1, PBSCN2, PBSCN3 and PBSCN4, respectively. However, relatively weaker enhancements in G' in the case of PBS/qC_{16}-MMT nanocomposites as compared to those with C_{18}-MMT was exhibited. For PBSCN6, the increment in G' at room temperature was 128.6 %. This was much lower than the 248 % increment corresponding to PBSCN4, which had similar clay content. The difference in the degree of enhancement of G' has been attributed to the higher aspect ratio of the dispersed clay particles in PBSCN4 as compared to that of PBSCN6.

However, fewer studies have been reported on the dynamic mechanical properties of PBSA/clay nanocomposites. Sinha Ray and Bousmina [63] again showed that favourable interaction between the clay surface and the PBSA matrix helped improve mechanical properties, among them, storage modulus. Expectedly, there was enhancement of E' for all the nanocomposites over neat PBSA. At around T_g

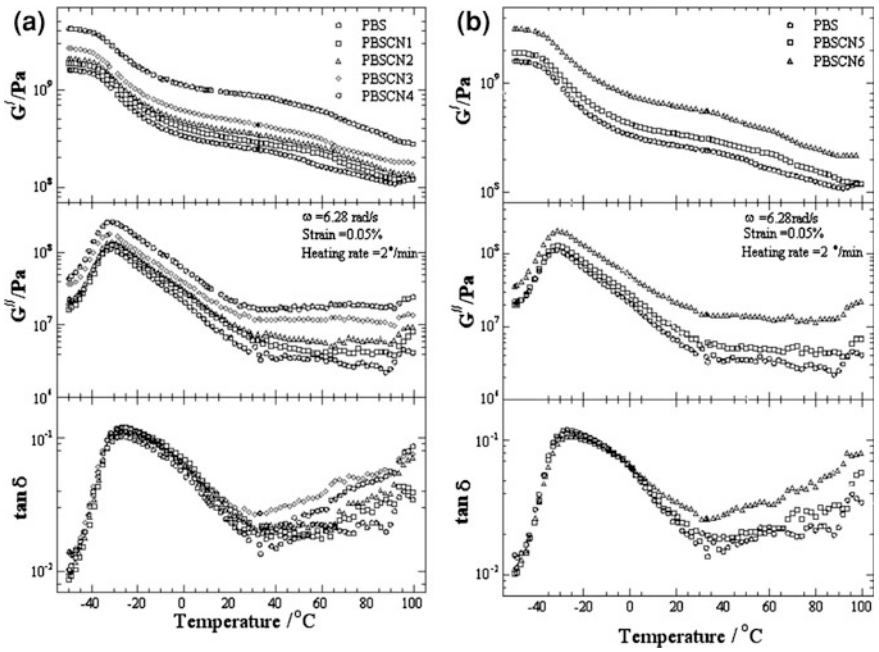

Fig. 7.10 **a** Temperature dependence of the storage modulus, loss modulus and their ratio, tan δ for PBS and various PBSCNs prepared with C18-MMT clay. **b** Temperature dependence of the storage modulus, the loss modulus and their ratio for PBS and various PBSCNs prepared with qC16-SAP clay. Reproduced from Ray, Okamoto and Okamoto [35] with permission

of PBSA, (–42 °C), the increment in E' was about 22 % for PBSA/C15A, 56 % for PBSA/C93A and 57 % for PBSA/C30B as compared to that of neat PBSA. It has previously been ascertained that C30B organoclay had better interactions with the PBSA matrix than C93A and C15A. This led to the obviously better enhancement of the storage modulus. On varying the clay content in PBSA/C30B system, Sinha Ray et al. [67] noted that, for all the nanocomposites, there was enhancement of E' and E'' as compared to neat PBSA. This is due to the intercalation of PBSA chains between C30B layers, which leads to chain immobilization and hence higher values of storage modulus. The stiffness increased with increasing clay content, hence the noted increased improvement in E' with addition of clay content. The increase in clay content increases internal friction between homogeneously dispersed intercalated silicate particles and hence the loss modulus, E''. T_g of the polymeric matrix was however, not affected significantly by the addition of C30B.

In conclusion, the dynamic mechanical properties of nanocomposites based on PBS and PBSA has been shown to be strongly dependent on the structure of the nanocomposite, processing procedure (like annealing or lack of annealing) and the clay type and content.

Table 7.4 Tensile properties of PBSA, PBSA/C25A, PBSA/TFC-GPS and PBSA/TFC-MPS [52]. Reproduced from Chen and Yoon with permission

Sample	Modulus (MPa)	Strength at break (MPa)	Elongation at break (%)
PBSA	163.5	15.6	408.0
PBSA/C25A2	222.1	18.6	439.5
PBSA/C25A5	251.0	18.7	442.5
PBSA/C25A10	248.7	17.5	428.0
PBSA/C25A15	234.0	17.2	380.5
PBSA/TFC-GPS2	226.2	20.0	430.5
PBSA/TFC-GPS5	249.3	20.9	447.0
PBSA/TFC-GPS10	283.8	20.6	419.0
PBSA/TFC-GPS15	381.8	20.4	361.0
PBSA/TFC-MPS2	244.3	20.9	605.0
PBSA/TFC-MPS5	261.7	18.5	438.0
PBSA/TFC-MPS10	296.2	18.2	417.5
PBSA/TFC-MPS15	342.3	17.3	416.5

7.6.1.2 Tensile Properties

Nanocomposites based on PBS and PBSA usually show vast improvement in tensile modulus, as compared to that of neat polymers, even with the addition of very low quantities of clay. Tensile strength and elongation at break could be occasionally improved with the addition of clay particles in polymer matrix, depending on the system under study. The changes in the tensile properties of the nanocomposites, whether improved or not, is dependent on, among other factors; the degree of dispersion of the silicate layers in polymer matrix, crystallinity, anisotropy and orientation of the dispersed clay particles.

Even though clays have much higher modulus (about 170 GPa [79]) than the polymers, the dramatic improvement in tensile modulus in nanocomposites over neat polymers at low clay concentrations may not be attributed simply to such high modulus of the clay particles. Interfacial interaction between the polymer matrix and the clay particle is necessary for the propagation of stress through the nanocomposite. Moreover, for effective stress/load transfer between polymer matrix and the clay particle, there needs to be a large surface area/volume ratio of the particles, which enhances the interfacial interaction. Therefore, for silicate layers with high aspect ratios, the surface area exposed to the polymer matrix is large and this significantly increases the modulus, even at low clay content. However, beyond percolation limit, extra clay particles lead to less dramatic improvement or even a reduction in modulus.

Chen and Yoon [52] tested the tensile properties of PBSA/C25A and PBSA/twice-functionalised organoclays (TFC) composites. Organoclays had been functionalised with silanes, GPS and MPS as described in Sect. 7.3 of this chapter. The tensile properties of the composites containing different amounts of clays are shown in Table 7.4. The tensile modulus of PBSA/C25A increased from 163.5 MPa to 251 MPa as the C25A content increased to 5 wt%. However, further

increase in clay content resulted in a reduction of tensile modulus. On the other hand, the modulus of PBSA/TFC-GPS and PBSA/TFC-MPS increased monotonically to 381.8 and 342.3 MPa, respectively, as the clay loading increased to 15 wt%. The authors attributed such enhancement in modulus to the resistance exerted by the clay itself as well as the orientation and the higher aspect ratio of the silicate layers, owing to the fine dispersion and strong interaction between TFC and PBSA.

For all the composites, the tensile strength was enhanced to a maximum value before decreasing, as clay content was increased. For PBSA/C25A, a maximum strength of 18.7 MPa was reached when the clay content was 5 wt%. For PBSA/TFC-GPS and PBSA/TFC-MPS, the maximum strength was 20.9 MPa, when the TFC-GPS content was 5 wt% and that of TFC-MPS was 2 wt%. Above these clay contents, which could be thought of as the percolation limits, the tensile strength began to reduce. The observation was ascribed to the agglomeration of the clay particles, since cracks are usually initiated on and propagated through the agglomerates to provoke failure of the specimen. Moreover, PBSA/TFC-GPS and PBSA/TFC-MPS had higher tensile strengths than PBSA/C25A, primarily due to the uniform dispersion of the clay particles.

The elongation at break for all the composites increased at a very low clay loading, but with further addition of clay, it decreased. However, regardless of the fact that PBSA/C25A had somewhat inferior degree of dispersion of clay particles as compared to PBSA/TFC-GPS and PBSA/TFC-MPS, its elongation at break was not very different from that of the two composites. The reason behind this phenomenon was subject to further research.

Sinha Ray and Bousmina [63] reported the tensile properties of three nanocomposites based on PBSA as shown in Fig. 7.11. There was an increase in the modulus after nanocomposite formation, and this was strongly dependent on the degree of dispersion of the silicate layers in the PBSA matrix. The higher degree of interfacial interaction between PBSA and C30B than with other organoclays led to higher modulus. The fine dispersion of the clay led to an increase in active surface area, which resulted in higher amount of stress transfer between the PBSA matrix and the clay particles.

However, the yield strength of PBSA did not improve with the addition of clay particles, regardless of the type of organoclay used in preparation of the nanocomposites. This observation could be due to the reduced crystallinity of the PBSA after nanocomposite formation.

The unique finding in the study was the improvement in elongation at break at 6 wt% loading for all the organoclays. The extent of the enhancement in elongation at break followed the order of favourable interaction between the organic modifier and the PBSA matrix. Again, the high degree of interaction between the 'CO' groups on the PBSA backbone and the diols in C30B led to PBSA/C30B posting the best elongation at break. Such interactions led to confinement of polymer chains inside the silicate layers. This in turn led to better transfer of energy in the PBSA/C30B nanocomposite and delayed crack formation in the specimens under applied stress.

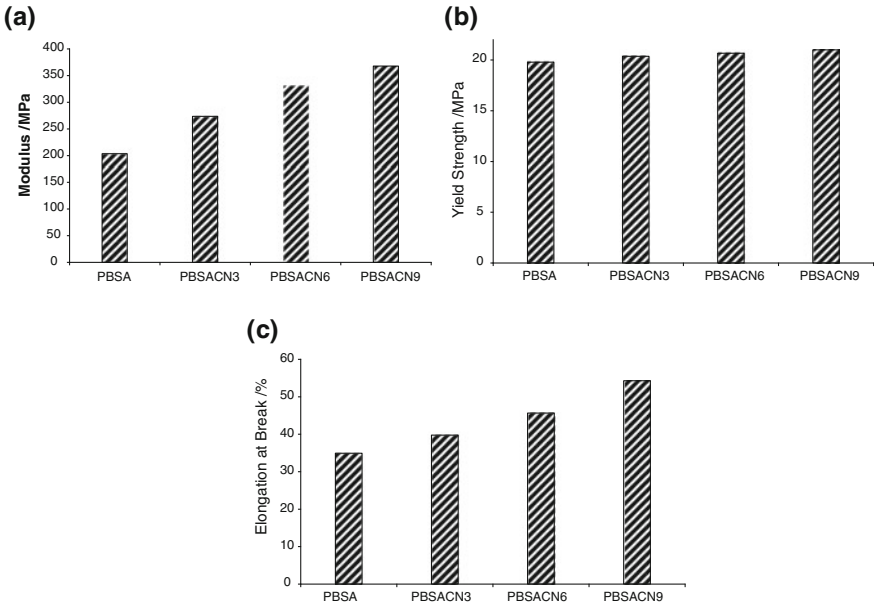

Fig. 7.11 Tensile properties of neat PBSA and various nanocomposites: **a** tensile Modulus, **b** tensile strength, and **c** elongation at break. Data are average of eight tests with a maximum error of 9 %. Reproduced from Ray and Bousmina with permission [63]

In a subsequent study, Sinha Ray et al. [67] varied the loading (3–9 wt%) of the clay particles in PBSA/C30B nanocomposites and tested its effect on tensile properties. Increasing clay content enhanced the modulus as well as the elongation at break. This was attributed to the high degree of dispersion of the intercalated silicate layers in the PBSA matrix. Even at 9 wt% clay loading, the TEM results had shown that the PBSA/C30B nanocomposite had well dispersed intercalated stacked and disordered and/or exfoliated silicate-layers. Another reason advanced is the effect of low value of modulus of PBSA itself. It is expected that with such low modulus as 200 MPa, addition of even small amount of clay would easily alter the value of the modulus.

The tensile strength improved slightly with addition of 3 wt% clay, but thereafter there was no more improvement. The filler/matrix interactions are also responsible for the increment, even though there was a possibility of lowered crystallinity for PBSA with addition of clay which could have had adverse effects on tensile strength. On the other hand, the elongation at break also improved with the increase in clay content. This unique finding was ascribed to the better interaction between organic modifier on C30B and the PBSA backbone, and shows that probably the percolation limit of the clay had not been reached.

In the same manner as in PBSA/clay nanocomposites, those based on PBS also display similar behaviour. The tensile properties of PBS/clay nanocomposites have been studied as a function of clay type [24, 58, 80], clay loading [58, 81, 82] and

Table 7.5 Mechanical properties of PBS and PBS nanocomposites. Reproduced and re-arranged from Hwang et al. [58] with permission

Sample	Modulus (MPa)	Strength at break (MPa)	Elongation at break (%)
PBS	385.5 (11.9)	32.2 (0.82)	180.5 (11.9)
PBS/C10A05	437.5 (16.3)	32.3 (0.57)	183.1 (5.7)
PBS/C10A10	390.2 (18.4)	48.5 (7.4)	362.3 (16.8)
PBS/C10A20	487.1 (39.6)	31.5 (0.77)	10.7 (2.41)
PBS/C30B05	386.0 (21.3)	40.5 (1.96)	261.4 (7.4)
PBS/C30B10	433.0 (28.1)	33.6 (1.03)	170.4 (2.9)
PBS/C30B20	442.1 (22.2)	30.6 (0.46)	80.1 (6.5)
PBS/C30BM05	385.2 (6.8)	54.3 (0.46)	401.5 (15.0)
PBS/C30BM10	424.6 (1.1)	55.4 (7.51)	435.6 (13.1)
PBS/C30BM20	408.9 (12.5)	46.3 (3.1)	370.4 (32.5)

Note values in parenthesis are standard deviations. 05, 10 and 20 are 0.5, 1 and 2 % clay loadings

nanocomposite preparation methods [62]. Someya et al. [80] studied tensile properties of PBS/clay nanocomposites prepared using Kunipia F-MMT, and four organoclays namely, DA-MMT, ODA-MMT, LEA-MMT, HEA-MMT and ALA-MMT. For all the clay types they used in preparation of PBS nanocomposites, there was a reduction in tensile strength at 3 wt% inorganic content. They also did not report tensile properties at lower inorganic loading for all the nanocomposites, save for PBS/LEA-MMT, and it could have been possible that there might have been an increase in tensile strength at a very low loading, before the noted reductions at 3 wt% loading, since this was the case with PBS/LEA-MMT. However, the modulus for all the nanocomposites increased as compared to that of neat PBS. The increase more or less followed the order of increasing degree of polymer intercalation, as measured by the difference in interlayer spacing of the clays in the nanocomposites. On the other hand, elongation at break for all the nanocomposites was less than that of neat PBS at the reported inorganic loading of 3 wt%. However, PBS/LEA-MMT showed a slight improvement in elongation at break at 1 wt% inorganic loading, while further increase in clay content systematically reduced the elongation at break. Even though the authors did not discuss it, this trend has been observed by others like Chen and Yoon [52] and Dean et al. [74] who also did not give direct reason for it.

Hwang et al. [58] also studied the effect of clay loading on tensile properties in three nanocomposites namely, PBS/C10A, PBS/C30B and PBS/C30BM, and the neat PBS. The third composite, PBS/C30BM was prepared from C30B clay that had been modified with urethane, 1, 6-diisocyanatohexane. This was primarily done to increase the interlayer spacing and favourable interaction between the polymer and the clay. Indeed, as shown in Table 7.5, it was noted that C30BM improved the tensile strength and elongation at break considerably as compared to C10A and C30B organoclays. The Young's modulus of PBS/C30BM was almost comparable with that of PBS/C30B. The improvement of elongation at break for most of the nanocomposites was attributed to the reinforcement effect due to clay rigidity.

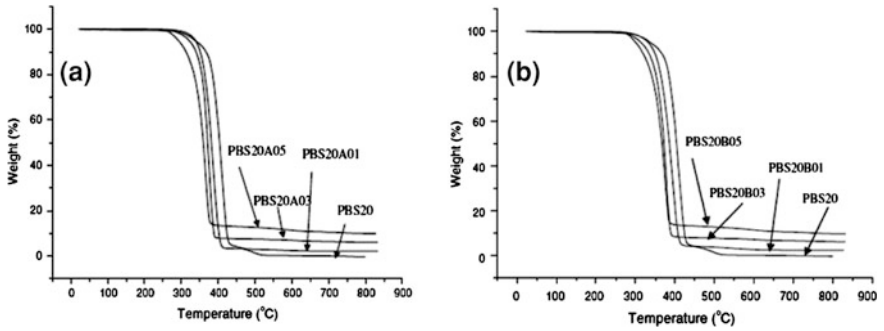

Fig. 7.12 TGA thermograms of (**a**) PBS/CTAB-MMT and (**b**) PBS/CPC-MMT. Reproduced from Shih et al. [78] with permission

However, unlike PBS/C10A and PBS/C30B, PBS/C30BM nanocomposite with 2 wt% clay content (PBS/C30BM20) was able to maintain the tensile strength and elongation at break without much deviation or reduction, witnessed with the first two nanocomposites. The results indicate that surface modification of clay to diminish micro-voids resulted in a fine dispersion of clay in the PBS matrix, and that adding urethane groups to clay surface increased the physical affinity between the clay and PBS.

7.6.2 Thermal Stability

The thermal stability of the PBS/clay and PBSA/clay nanocomposites has been studied through thermogravimetric analysis (TGA) by various researchers [39, 56, 58, 62, 63, 67, 78, 82]. The weight loss due to the formation of volatile products after degradation at high temperatures, either in inert gas atmosphere or air, is usually monitored as a function of temperature. For instance, Shih et al. [78] thermally degraded various nanocomposites based on PBS under nitrogen and studied how the clay type and content affected the thermal stability. In the study, two organoclays were used, CPC-MMT and CTAB-MMT. The content of clays were 1, 3 and 5 wt%. The neat PBS was coded PBS20, whereas PBS20A01, PBS20A03 and PBS20A05, were the PBS/CTAB-MMT nanocomposites with clay content of 1, 3 and 5 wt%, respectively. On the other hand, PBS20B01, PBS20B03 and PBS20B05 were the PBS/CPC-MMT nanocomposites with clay content of 1, 3 and 5 wt%, respectively. The TGA results are shown in Fig. 7.12. They reveal that the char yield of the nanocomposites were expectedly higher than that of neat PBS. The authors argued that the char yield, which is directly correlated to the potency of flame retardation, limit the production of gases, decrease the exothermicity of the pyrolysis reaction and inhibit the thermal conductivity of the burning material. Even though they did not report on the onset of degradation of the neat

Table 7.6 Thermogravimetric analysis data for clay and PBS nanocomposites. Reproduced from Hwang et al. [58] with permission

Sample	T_D^3(° C)[a]	Sample	T_D^3(° C)[a]
C10A	201.5	PBS	326.7
C30B	240.1	PBS/C10A20	338.7
C30BM	242.7	PBS/C30B20	342.1
		PBS/C30BM20	345.0

[a] Temperature at a weight reduction of 3 %

PBS and the nanocomposites, it is clear from the Fig. 7.12 that the nanocomposites had lower onset of degradation as compared to the neat PBS. This was probably due to the lower onset temperature of degradation associated with the organic modifiers on the organoclays.

Hwang et al. [58] made an interesting observation about a chain extender enhancing thermal stability of PBS/C30BM nanocomposite compared to PBS/C10A and PBS/C30B nanocomposites. From TGA results represented in Table 7.6, the C30BM clay, which had been modified by urethane, had a higher decomposition temperature for 3 % weight loss, $\left(T_D^3\right)$ than did C10A and C30B clays. This was attributed to the chemical covalent bonding between the silanol groups of the clay and the hydroxyl groups of the modifier (urethane), which in effect enhanced thermal stability of the PBS/C30BM nanocomposite. Therefore, it was noted that the urethane group did not act just as a chain extender, in which case the onset of thermal degradation would have been low, but covalently bonded with the silanol group of the clay. On the other hand, the C10A clay slightly improved the onset degradation temperature of the PBS/C10A nanocomposite as compared to that of neat PBS (see Table 7.6). Once again, this illustrates the dependence of thermal stability of the nanocomposites on the organic modifier used in the preparation of the organoclays.

Sinha Ray and co-workers have reported thermal stability of PBSA/clay nanocomposites as a function of clay type [63], clay loading [67], and atmosphere [70]. Sinha Ray and Bousmina [63] investigated the thermal stability of three nanocomposites namely, PBSA/C30B, PBSA/C93A and PBSA/C15A (with 6 wt% clay loading) as well as that of neat PBSA. Ultimately, PBSA/C30B showed higher thermal stability than the neat PBSA. The other organoclays only had marginal improvement in thermal stability with respect to that of the neat PBSA. The onset of degradation (at 3 % weight loss), as measured from the intersection of the tangent of the initial point and the inflection point, are 333.4 ± 0.7, 336.9 ± 1.9, 332.1 ± 1.5, and 328.2 ± 1.1 8 °C for neat PBSA, PBSA/C15A, PBSA/C93A, and PBSA/C30B nanocomposites, respectively. Even though these values seem to be close enough to each other, it is worthwhile to note that they reduced with increasing level of dispersion of silicate layers in the PBSA matrix. However, after at about 373 ± 1.8 °C, the thermal stability of the nanocomposites followed the opposite trend. The authors attributed this behaviour to the degree of

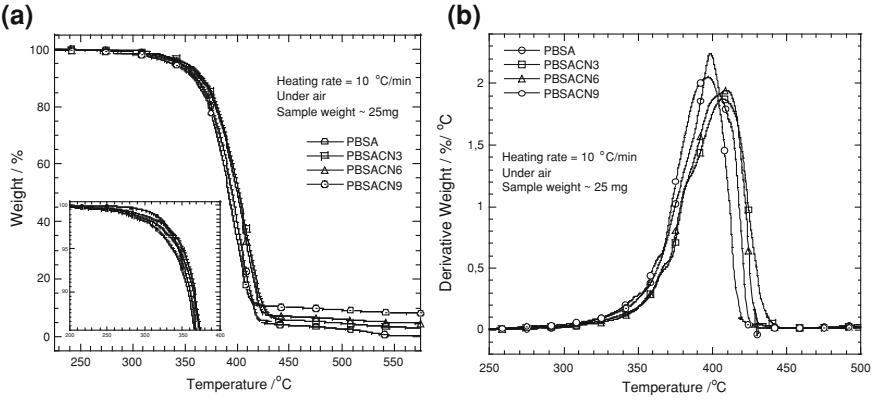

Fig. 7.13 **a** TGA traces of weight loss as a function of temperature of pure PBSA and three PBSACNs. **b** First derivative TGA (dTGA) curves of neat PBSA and three PBSACNs. Reproduced from Sinha Ray et al. [67], with permission

dispersion of clay particles in PBSA matrix. The high degree of silicates such as the one observed by the authors in PBS/C30B, enhances the ultimate thermal stability by the well dispersed clay particles acting as superior insulator and mass-transport barrier to the volatile products generated during thermal decomposition. Even though the authors did not carry out thermogravimetric analysis of the organoclays separately, a probable explanation for the observation made at the beginning of the thermal decomposition of the nanocomposites was presented. They argued that the stacked and intercalated silicate layers, associated with the PBSA/C15A and partly PBSA/C93A nanocomposites, by acting as superior insulator compared to the exfoliated silicate layers shifts the decomposition to a higher temperature. However, after certain degree of decomposition, this heat barrier effect would result in a reverse thermal stability. In other words, the stacked and intercalated silicate layers could hold accumulated heat that could be used as a heat source to accelerate the decomposition process, in conjunction with the heat flow supplied by outside heat source.

In a subsequent study, Sinha Ray et al. [67] sought to find out the effect of clay loading on the thermal stability of PBSA/C30B nanocomposites. Three different clay contents were used: 3, 6 and 9 wt%. The TGA traces of weight loss as a function of temperature are represented in Fig. 7.13. The onset of degradation at 3 % weight loss of neat PBSA and PBSACN3 is the same but as expected, systematically decreased upon further addition of C30B to the PBSACNs. In order to have a clearer difference in thermal stability of all the samples studied, the first derivative TGA (dTGA) curves of neat PBSA and the nanocomposites (see Fig. 7.13b). PBSA/C30B containing 3 wt% clay had the ultimate best thermal stability.

Between the temperatures ranges of 100–332 °C, all PBSACNs degrade at a slightly faster rate compared to the neat polymer (see inset of Fig. 7.13). This fact

could be attributed to the lower thermal stability of the alkyl ammonium modifiers used, which are known to undergo Hoffman degradation around 200 °C, even though the authors did not carry out separate thermogravimetric analysis of the clays. However, after 332 °C, PBSACN3 and PBSACN6 degrade at a much slower rate compared to that of PBSA; whereas, the degradation rate of PBSACN9 is higher than neat PBSA. This was noted by the authors as the most unexpected observation in the research because one of the most important property enhancement expected upon formation of nanocomposite is the retardation of the thermal degradation that is directly related to the amount of clay loading; such as the trend observed in Skygreen-2109/C25A nanocomposite by Lim et al. [56]. However, it could be argued that at higher particle loading, clay particles increasingly act as further heat source, especially at higher temperatures. Above 545 °C, only inorganic aluminosilicate is left in the nanocomposites, hence the noted slower degradation of all PBSACNs.

7.6.3 Gas Barrier Properties

Clays normally increase the barrier properties of nanocomposites by creating a tortuous path for the gas molecules to diffuse through. Like in other polymer/clay nanocomposites, the reduction in gas permeability for PBS and PBSA/clay nanocomposites is primarily dependent on the clay type and hence the degree of dispersion of the layered silicates [24, 74], their dimensions, which means their aspect ratio [35] and loading [81, 83]. According to the Nielsen model [84], platelets of length (L_{clay}) and width (D_{clay}) of the clay which are presumably dispersed parallel in a polymer matrix, and the tortuosity factor (τ) can be expressed as follows:

$$\tau = 1\left(L_{clay}/2D_{clay}\right)\phi_{clay} \tag{7.1}$$

where ϕ_{clay} is the volume fraction of dispersed clay particles. The relative permeability coefficient (P_{PCN}/P_P), where P_{PCN} and P_P are the permeability of nanocomposite and neat polymer is given by the following expression:

$$\frac{P_{PCN}}{P_P} = \frac{1}{1 + \left(L_{clay}/2D_{clay}\right)\phi_{clay}} \tag{7.2}$$

Okamoto et al. [24] compared the O_2 gas permeability coefficient of three nanocomposites: PBS/C_{18}-MMT, PBS/qC_{18}-MMT and PBS/qC_{16}-SAP, with that of the neat PBS. The O_2 permeability coefficients in (mL.mm/m^2.day.MPa) were 87.3, 42.2, 69.0 and 71.2 for PBS, PBS/C_{18}-MMT, PBS/qC_{18}-MMT and PBS/qC_{16}-SAP, respectively. It is evident that there was reduction in the gas permeability coefficient in the case of the nanocomposites. The validity of the relative permeability model was tested using PBS/C_{18}-MMT and found to be almost a match.

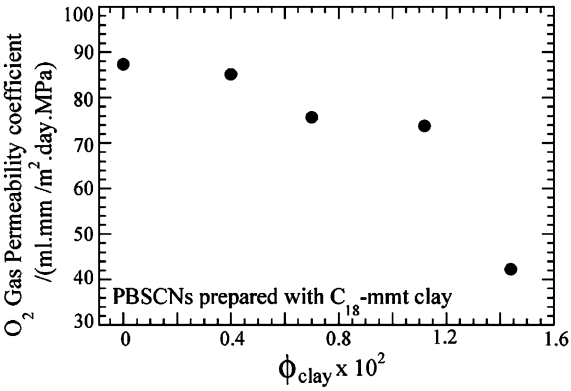

Fig. 7.14 O_2 gas permeability coefficient of various PBSCNs prepared with C18-MMT as a function of clay content. Reproduced from Sinha Ray et al. [35] with permission

The calculated relative permeability values for the PBS/C_{18}-MMT nanocomposite, based on $L_{clay} = 1721$ nm from TEM images, and $D_{clay} = 15.3$ nm, got from Scherrer's equation, was 0.55. On the other hand, the experimental value was 0.48. This was close enough to the one predicted by the model, but slightly less. This slight disparity was attributed to the fact that there was enhanced crystallinity due to the induced crystallization with clay particles acting as nucleating agents.

In a subsequent study by Sinha Ray et al. [35], the effect of clay loading on the gas permeability of the PBS/C_{18}-MMT was tested and the results are shown in Fig. 7.14. The gas permeability value systematically reduced with increasing clay content up to 1.1 vol% (2.8 wt%) and after that there was a sharp decrease in gas permeability with clay loading of 1.4 vol% (3.6 wt%). The authors attributed this observation to the sudden increase in aspect ratio of dispersed clay particles after clay content of 1.1 vol%. They argued that that strong flocculation of dispersed clay particles had occurred after 1.1 vol% clay loading, and that the percolation value of strong flocculation was situated between the values of MMT of 1.1 and 1.4 vol%. However, the same authors, Sinha Ray et al. [85] found out that, for the same ranges of clay loadings, the gas barrier in another nanocomposite, PBS/qC_{18}-MMT, did not significantly improve.

Little work has been reported on PBSA/clay nanocomposites gas barrier properties. However, Dean et al. [74] did note that clays enhance gas barrier properties and this depended on dispersion of clay in the polymer matrix. Even though neat FHT in the PBSA/FHT nanocomposite was poorly dispersed, the nanocomposite showed a remarkable improvement in gas barrier properties.

There was a 35 % reduction in oxygen permeation rate as shown in Table 7.7. The use of organoclays, FHT-MEE and FHT-MAE enhanced barrier properties substantially, at 53 and 42 % permeation rate reduction, respectively. The TEM images of the two nanocomposites had shown that the dispersion of their platelets was better than the rest. This led to a better gas barrier property. The improvement in gas barrier property was better in the case of PBSA/FHT-MEE and PBSA/FHT-MAE due to the better compatibility of these modified clays with PBSA, which led

Table 7.7 Oxygen permeability of neat PBSA and nanocomposites. Reproduced from Dean et al. [74], with permission

Sample	Film thickness (μm)	O_2 permeability (cc/[m^2 day])	Permeation rate (cc-mm/[m^2 day])
PBSA	265.0	155.8 ± 5.7	41.3 ± 0.4
PBSA/FHT	280.0	96.0 ± 0.2	26.8 % ± 0.1/35 % reduction
PBSA/FHT-MEE	277.5	70.6 ± 1.4	19.6 % ± 0.2/53 % reduction
PBSA/FHT-MAE	280.0	86.2 ± 0.2	24.1 % ± 0.1/42 % reduction
PBSA/FHT-MTE	280.0	94.7 ± 3.9	26.5 % ± 0.4/36 % reduction

to fine dispersion of the particles in the PBSA matrix. Through dynamic scanning calorimetry results, the authors were able to rule out the increased crystallinity being responsible for the noted reduction in gas permeability.

7.6.4 Biodegradability

One of the advantages of nanocomposite technology is that, generally, there is significant improvement in biodegradability of the nanocomposites after addition of organoclays. Some of the factors affecting the rate of biodegradation of neat polymers and their nanocomposites are molecular weight, melting point, crystallinity, barrier properties, etc. Even though only few reported studies on the degradation of PBS/clay and PBSA/clay nanocomposites are available, it forms an important aspect of these nanocomposites, since their use has primarily been motivated by their ease of biodegradability. Okamoto et al. [24] and Sinha Ray et al. [35] first reported biodegradability of neat PBS and its nanocomposites in two modes: under compost and under soil field. Under soil field, the biodegradability of PBS and nanocomposite exhibited rather lower extents of degradation, compared to the compost. Figure 7.15 shows the real pictures of samples recovered from compost after 35 days.

They had previously been composted at (58 ± 2) °C with soybean dust and effective micro-organisms. Before the composting, the soybean/effective micro-organisms mixture had been sealed and fermented for 20 days at open air temperature. Thereafter, compression-moulded samples, measuring (0.3 ± 0.02) cm in thickness, were clipped with a 35 mm slide holder and put into the compost. After 35 days, they were recovered, washed with distilled water and finally with methanol in an ultrasonic bath for 5 min. From Fig. 7.15, it is discernible that the nanocomposites had more cracks, indicating improved biodegradability. The cracks are important since they further hasten the degradation rate, by exposing more surfaces to the action of microbes. Notably, the extent of cracks depended on the type of organoclay used. The authors also noted that gas barrier properties of

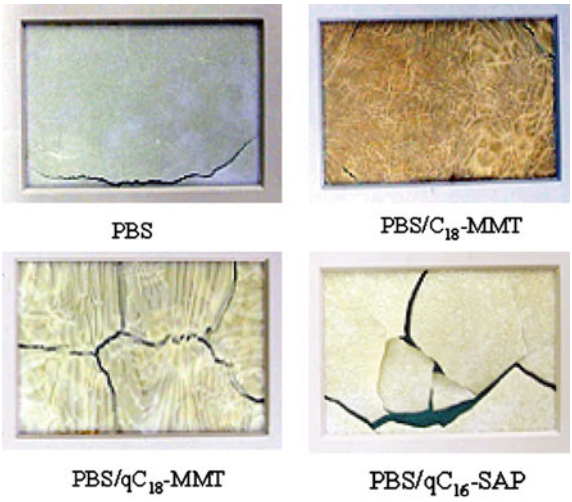

Fig. 7.15 Biodegradability of neat PBS and various nanocomposites sheet under compost. Reproduced from Okamoto et al. [24] with permission

the nanocomposites, had no role to play in the studied nanocomposites, as has been found in previous polylactide-based nanocomposites [86].

The authors also conducted gel permeation chromatography (GPC) measurements on the samples recovered from compost. The GPC results showed that the extent of molecular weight loss was almost the same for all the samples. This result indicated that the extent of hydrolysis of PBS in the pure state or organoclay-filled systems is the same in compost.

Apart from PBS/qC_{16}-SAP nanocomposite, the extent of degradation was not different for the other samples. The authors argued that this was an indication that MMT or alkylammonium cations had no effect on the biodegradation of PBS. On the other hand, the presence of alkylphosphonium surfactant seemed to accelerate the degradation of PBS. However, they could not elucidate on the exact mechanism of compost degradability of PBS at that time.

Recently, Shih and Wu [76] have studied the enzymatic degradation kinetics of PBS/clay nanocomposites. The use of enzymatic testing in evaluating rate of biodegradability was employed because it allows fast evaluation over a short period of time. They studied the degradation as a function of clay type (Kunipia-F MMT, and organoclay, CTAB-MMT) and clay content (1, 3, and 5 wt%). These formulations were coded PBS01, PBS0101, PBS0103, PBS0105, PBS01T01, PBS01T03 and PBS01T05, for neat PBS, PBS/MMT with 1, 3 and 5 wt%, and PBS/CTAB-MMT with 1, 3 and 5 wt%, respectively.

Figure 7.16 showed that the weight loss of PBS/MMT was slightly larger than that of pristine PBS. On the other hand, the weight loss of PBS/CTAB-MMT nanocomposites was about two to three times of pristine PBS. The authors attributed this enhancement of biodegradation rate for the nanocomposites to the nature of organic modifier or crystal morphology, but not because of clay. The CTAB modifier caused lower crystallinity in the nanocomposite and this was probably one

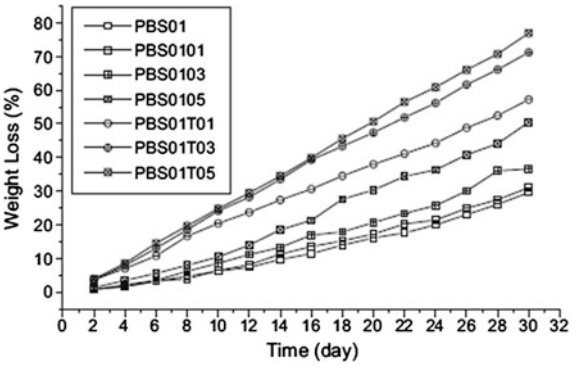

Fig. 7.16 Weight loss of samples after different periods of incubation. Re-produced from Shih and Wu [76] with permission

of the reasons for the enhancement of degradation rate. Another probable reason advanced by the authors was that the CTAB modifier could act as a catalyst of the hydrolytic degradation and hence further promote the rate of PBS degradation.

In the case of nanocomposite of a co-polyester, Skygreen-2109, Lee et al. [19] had first reported that its degradability depended on the gas permeability, even though they did not measure the permeability of the various nanocomposites studied. They compared the degradation of this aliphatic biodegradable polymer (APES) with its nanocomposites, APES/C10A and APES/C30B. The APES/C10A exhibited higher degree of degradation than the APES/C30B nanocomposites, even though APES/C30B had higher degree of intercalation of organoclays in the polymer matrix than APES/C10A. They attributed this to the fact that due to higher aspect ratio as a result of better dispersion of clay particles in APES/C30B, micro-organisms had to travel a longer distance to access parts of the polymer and hence the noted lower degradability.

7.7 Crystallisation

Crystallisation is an effective process of controlling the mechanical and other properties of both the neat polymers and their nanocomposites. It is therefore important that the process be understood well, especially during non-isothermal processes, which in fact is what happens during industrial processing of polymers and their nanocomposites. The crystallisation process is dependent on a number of factors including temperature, pressure and the cooling rate. The crystallization behaviour of PBS/clay and PBSA/clay nanocomposites has been studied both in isothermal [53] and non-isothermal conditions [71, 83, 87, 88]. From such studies, the kinetics of crystallisation process has been investigated through known models, namely: Avrami [89–91]; Ozawa [92] and mixed Avrami-Ozawa models [93].

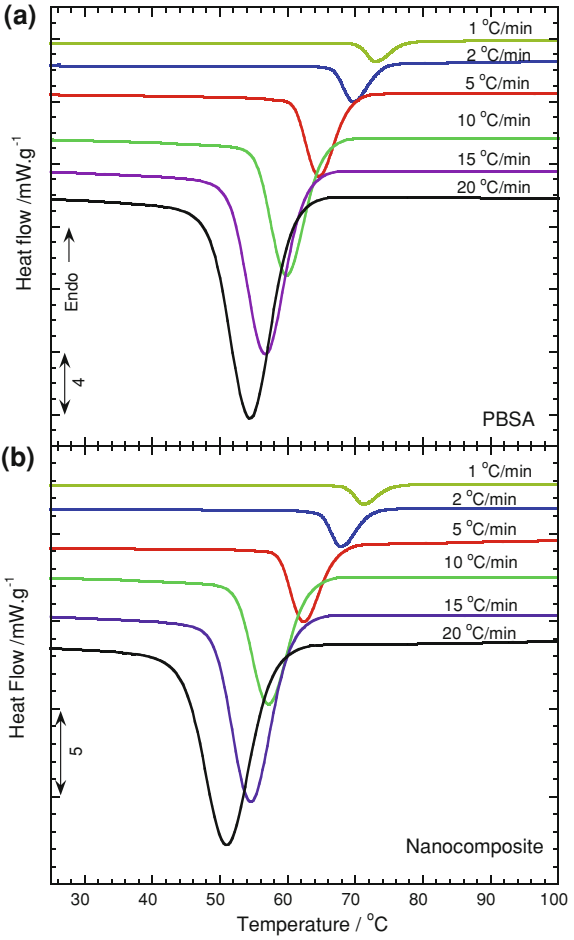

Fig. 7.17 The crystallisation exotherms of (**a**) neat PBSA and (**b**) the nanocomposite for non-isothermal crystallisation from the melt (at 150 °C) at six different cooling rates from 1 to 20 °C. Reproduced from Sinha Ray and Bousmina [71], with permission

In general, PBSA tends to have lower crystallinity as compared to PBS. Kuwabara et al. [94] made an interesting molecular mobility and phase structure observation on poly(butylene succinate-co- 20 % mol butylene adipate), [P(P(BS-co-20 mol% BA)] through solid state ^{13}C NMR measurements. They showed that BA units were excluded from the crystalline regions of the P(BS-co-20 mol% BA), but resided in the amorphous regions instead. This contributed to the lowering of the crystallinity of the co-polymer.

Sinha Ray and Bousmina [71] reported crystallisation behaviour of PBSA/OSFM nanocomposite (6 wt% organoclay content) as compared to that of neat PBSA. The study mainly dwelt on the kinetics of non-isothermal crystallisation process as a function of cooling rate. The crystallisation exothermic curves represented in Fig. 7.17 became wider and shifted to the lower temperature region as the cooling rate increased, for both neat PBSA and the nanocomposite. As the cooling rate was increased, the onset temperature (T_{on}) and peak temperature (T_p)

Table 7.8 Characteristic parameters of non-isothermal crystallisation from melt. Reworked from Sinha Ray and Bousmina [87] and Sinha Ray et al. [71], with permission

Sample	ϕ[a] °C.min^{-1}	T_{on}[b] °C	T_p[c] °C	ΔH_{en}[d] J.g^{-1}	ΔH_{en}[e] J g^{-1}	References
PBSA	1	84.2	73	66.13	92.0	[71, 87]
	2	81.2	69.6	63.5	91.1	
	5	80.2	64.7	62.4	79.5	
	10	71.7	60.0	60.8	78.9	
	15	67.6	56.7	60.1	77.1	
	20	66.6	54.5	57.0	73.5	
PBSA/OSFM	1	78.8	71.3	49.2	89.5	[71]
	2	76.6	67.8	51.2	88.3	
	5	73.5	62.4	53.0	78.5	
	10	69.0	57.2	53.7	77.3	
	15	66.9	54.7	54.0	76.8	
	20	64.9	50.9	54.7	72.7	
PBSA/C20A	1	83.0	74.0	45.4	–	[87]
	5	76.1	65.1	39.7	–	
	10	70.3	60.4	40.1	–	
	15	69.5	56.9	40.1	–	
	20	67.2	53.7	40.6	–	
PBSA/C30B	1	81.2	71.8	36.0	–	[87]
	5	73.4	62.5	39.0	–	
	10	69.5	57.3	39.6	–	
	15	68.4	53.6	40.3	–	
	20	66.5	50.9	40.4	–	

[a] ϕ is the cooling rate during non-isothermal crystallization from the melt
[b] T_{on} is the crystallization onset temperature
[c] T_p is the crystallization peak temperature
[d] ΔH_{ex} is the total heat of crystallization
[e] ΔH_{en} is the total heat of melting (the total heat of fusion of two melting peaks of PBSA evaluated from heating scans after non-isothermal crystallisation)

of crystallisation, heat of crystallisation (ΔH_{ex}), and the heat of fusion (ΔH_{en}), reduced (see Table 7.8).

This trend was similar for both the PBSA and the nanocomposite. This was attributed to the fact that as the cooling rate increased, little time was available for the PBSA to crystallise fully. However, unexpectedly, the onset temperature for crystallisation was higher in the case of neat PBSA than that of PBSA/OSFM nanocomposites. This shows that the nucleation role of the clay was inactive. Moreover, the degree of crystallinity of neat PBSA was higher than that of the nanocomposites (see Table 7.8).

The authors attributed this observation to the high level of dispersion of the OSFM, which hindered the local lamellar crystallisation, which in turn led to a decrease in crystallinity of the nanocomposite. Similar observation of such, not so usual results, were also made by Sinha Ray et al. [87]. They had investigated how the degree of intercalation affect crystallisation phenomenon in PBSA/C20A and PBSA/C30B nanocomposites. As shown in Table 7.8, for a particular cooling rate,

neat PBSA showed higher T_{on} and T_p values than the PBSA/C30B nanocomposites. Like in the case of PBSA/OSFM, the nucleating role of C30B was inactive. The PBSA/C30B had a higher level of dispersion of the silicate layers than PBSA/C20A, and this resulted in much lower crystallinity as compared to both the neat PBSA and PBSA/C20A nanocomposite (see Table 7.8).

The crystallisation kinetics of PBS/clay and PBSA/clay nanocomposites could be generalised by the Avrami, the Ozawa and a mixed Avrami–Ozawa, i.e. Liu models. Generally, time dependent Avrami model (Eq. 7.3) is applied in isothermal crystallisation process, while the Ozawa model [92] (Eq. 7.4) is applied to non-isothermal processes. On the other hand, Liu et al. [93] proposed a model which combined both Avrami and Ozawa models (Eq. 7.5). These models are represented by the equations below:

$$X_t = 1 - \exp(-Z_t t^n) \tag{7.3}$$

$$1 - X_T = \exp(-K(T)/\phi^m) \tag{7.4}$$

$$\ln \phi = \ln[F(T)] - a \cdot \ln t \tag{7.5}$$

where, X_t is the time dependent degree of crystallinity; Z_t is a modified, composite rate constant; the Avrami exponent n is a constant that depends on the nucleation mechanism and growth process; $K(T)$ is the Ozawa crystallisation rate constant and 'm' is the Ozawa exponent, which depends on the dimension of crystal growth; $F(T) = [K(T)/Z_t]^{1/m}$ refers to the cooling rate to reach a defined degree of crystallinity and a is the ratio of Avrami exponent to Ozawa exponent, i.e. $a = n/m$.

If the model is valid, a plot of $\ln[-\ln(1-X_t)]$ versus $\ln t$ results in a straight line from where the parameters can be determined. Sinha Ray and co-workers [71, 87] applied the Avrami model in non-isothermal crystallisation process for PBSA/OSFM, PBSA/C20A, PBSA/C30B and neat PBSA. The n and $\ln Z_t$ values are summarised in Table 7.9.

It should be however noted that in this case the Z_t and n did not possess the same physical meaning as original Avrami analysis for isothermal crystallisation, because temperature changes instantly in non-isothermal crystallisation. Rather, they were adjustable parameters used to fit experimental results and help analyse crystallisation kinetics. In comparison to neat PBSA, the modified Avrami analysis appeared to be more valid for PBSA/OSFM and PBSA/C30B nanocomposites. The linear portions of the $\ln[-\ln(1-X_t)]$ versus $\ln t$ plots for PBSA/OSFM and PBSA/C30B nanocomposites were almost parallel to each other (figures not shown) and shifted to a shorter time with increasing cooling rates, while PBSA/C20A nanocomposite was in between neat PBSA and the other two nanocomposites. This deviation is considered to be a result of the secondary crystallisation, which is caused by the spherulite impingement in the later stage. Therefore, for the four samples, the nucleation mechanism, crystal growth geometries for primary and secondary crystallisation at all cooling rates are completely different from each other.

In all the samples, the value of n decreased with an increase in cooling rate. Moreover, the values of n tended to be lower in the nanocomposites than in neat

Table 7.9 Kinetic parameters based on the Avrami equation melt. Reproduced and rearranged from Sinha Ray and Bousmina [87] and Sinha Ray et al. [71], with permission

Sample	ϕ[a] °C.min^{-1}	n[b] °C	ln Z_t[c] °C	$t_{1/2}$[d] J.g^{-1}	References
PBSA	1	6.29	–33.97	11.17	[71, 87]
	5	6.77	–28.44	3.10	
	10	5.72	–18.27	1.18	
	15	4.24	–11.98	0.72	
	20	4.25	–11.20	0.60	
PBSA/OSFM	1	3.56	–17.91	7.55	[71]
	2	3.91	–17.66	4.40	
	5	4.31	–16.78	2.22	
	10	4.03	–13.24	1.18	
	15	3.72	–10.99	0.82	
	20	3.73	–10.43	0.7	
PBSA/C20A	1	5.33	–28.04	9	[87]
	5	5.43	–20.51	2.2	
	10	3.45	–10.90	1	
	15	3.77	–11.32	0.86	
	20	3.76	–9.86	0.68	
PBSA/C30B	1	4.06	–21.0	9.4	[87]
	5	4.73	–17.96	2.2	
	10	4.28	–14.24	1.2	
	15	4.62	–14.13	0.98	
	20	4.33	–12.44	0.8	

[a] ϕ is the cooling rate during non-isothermal crystallization from the melt
[b] 'n' is the Avrami exponent
[c] Z_t is the growth factor
[d] $t_{1/2}$ is the crystallization half time

PBSA. The reduction in the value of n, as well as the lower crystallinity of nanocomposites when compared to neat PBSA (see Table 7.8), showed that the incorporation of the organoclay results in a deceleration of the kinetics of the non-isothermal crystallisation. However, the time required to reach 50 % crystallinity for PBSA ($t_{1/2}$), were generally higher than that of the nanocomposites (see Table 7.8). This unexpected observation was attributed to the dispersion of silicate layers in PBSA, which in turn offered surface area for crystals to start growing. However, due to the homogeneous dispersion of silicate layers especially in PBSA/OSFM and PBSA/C30B, the crystals were tightly bound and there was no chance of further impingement between themselves. Hence, the crystals grew more slowly and perfectly, in the case of nanocomposites, more so for PBSA/OSFM and PBSA/C30B. On the other hand, in the case of neat PBSA and to some extent PBSA/C20A, there was an impingement effect, i.e., the secondary crystallisation phenomenon, and hence the overall crystallisation growth rate is relatively higher.

However, for neat PBSA and PBSA/OSFM nanocomposite, the Ozawa model was not perfectly valid, except at certain temperatures. The authors argued that due

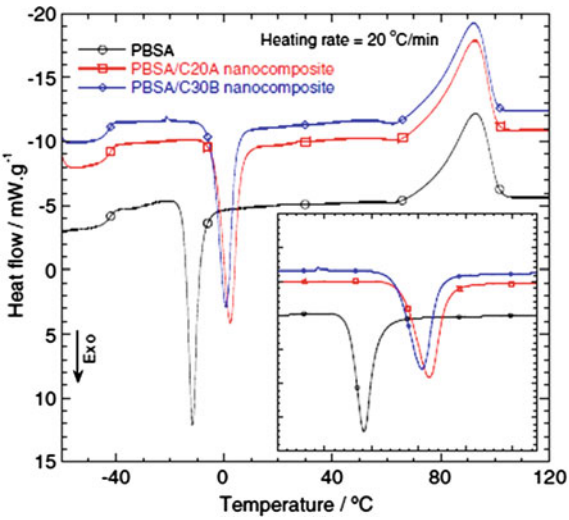

Fig. 7.18 DSC thermograms of melt-quenched samples of neat PBSA and two different nanocomposites. Reproduced from Sinha Ray et al. [87]

to the high level of intercalation of PBSA inside the silicate layers, secondary crystallisation effects were less important, just like in Avrami analysis.

On the other hand, the parameters for Liu model for PBSA, PBSA/OSFM, PBSA/C20A and PBSA/C30B were determined [71, 87]. The value of $F(T)$ and 'a' for the nanocomposites were generally higher than that of neat PBSA, more so for PBSA/C30B and PBSA/OSFM. This indicates the neat PBSA achieved a certain extent of crystallinity faster than the nanocomposites, an observation which supports the slower crystallisation kinetics of the nanocomposites already discussed.

To support crystallisation data, the spherulite growth behaviour of PBSA/OSFM and neat PBSA was observed by means of polarized optical microscopy (POM) [71] (figure not shown). It was observed that the nanocomposite spherulites are relatively larger and more perfectly grown than those of neat PBSA. Similar observation was made in the case of PBSA/C30B, whereas the spherulites sizes of PBSA/C20A were just slightly bigger than those of neat PBSA [87]. In case of the nanocomposites, more so, PBSA/OSFM and PBSA/C30B, the nucleating role of these organoclays was quite inactive. Such observations go counter the general understanding of the role of organoclays in polymer crystallisation.

To determine the effect of organoclay on cold crystallisation temperature of the PBSA matrix, Sinha Ray and co-workers [71, 87] did differential scanning calorimetry (DSC) studies of melt-quenched samples of neat PBSA and the nanocomposites. In a typical procedure, the samples inside aluminium pans were first annealed at 130 °C for 10 min to remove any previous thermal history and subsequently quenched in liquid nitrogen. The samples were then transferred to the DSC cell, which was previously set at –70 °C, as quickly as possible to measure the cold crystallisation temperature. Figure 7.18 shows the DSC thermograms of the melt-quenched samples of PBSA and PBSA/C20A and PBSA/C30B nanocomposites.

Well-defined T_g is observed for all the samples, and this was attributed to the removal of constraint provided by the crystallites in the initial material. There was a shift of the T_g of neat PBSA to higher temperature in the case of the PBSA/C30B nanocomposite, when compared to the PBSA/C20A nanocomposite, probably due to the favourable interactions between the PBSA matrix and the C30B surface. For all the samples, there was a single sharp exotherm. The single prominent exotherm indicates that for all samples the cold crystallization process takes place from a single homogeneous phase. However, the cold crystallisation peak temperature of neat PBSA (–11.8 °C) increased in the case of PBSA/C20A nanocomposite (0.7 °C), and even higher in the case of the PBSA/C30B nanocomposite (2.5 °C). Almost similar results were observed in the case of PBSA/OSFM (87), with the cold crystallisation peak temperature of –6.6 °C. More thermal energy is required to introduce crystallisation in the case of the nanocomposites. The results indicate that the nucleation role of C30B particles is less active than that of C20A particles for PBSA matrix crystallization. Similarly, the OSFM particles had an inactive role as nucleating agent. This again supports the previous conclusion that the crystal growth of PBSA in the case of PBSA/C30B and PBSA/OSFM nanocomposite is slower than for the neat PBSA matrix.

In the case of PBS/clay nanocomposites, isothermal and non-isothermal crystallisation kinetics, have been modelled by the Avrami [53] as well as Ozawa and modified Avrami equations [83]. Hwang et al. [53] carried out isothermal crystallisation analysis on PBS/C30B20 and PBS/C30BM20, with the 20 denoting clay content of 2 wt%. The C30BM organoclay was C30B organoclay, further modified with urethane. The PBS/C30B20 nanocomposite had a largely intercalated structure, whereas, the PBS/C30BM20 nanocomposites showed exfoliated structure. In a typical experimental procedure, the nanocomposites were first heated to 150 °C and held for 5 min to eliminate the thermal history. The samples were then cooled rapidly at 200 °C/min to the desired temperature between 80 and 90 °C and maintained at this temperature for 30 min. During crystallisation, exothermic heat flow was recorded as a function of time at different crystallisation temperatures. Then the crystallised samples were then cooled at 200 to 30 °C/min, before a second heat was carried out at a rate of 10 °C/min. The isothermal crystallisation kinetics was modelled using the Avrami equation. All of the samples had an Avrami exponent value n which ranged from 2.3 to 3.2, which the authors argued indicated spherulite growth from heterogeneous nucleation. The Avrami parameters for various crystallisation temperatures are represented in Table 7.10.

Increase of crystallisation temperature led to a systematic increase in the value of n, with corresponding decrease in the rate of crystallisation. The rate constant Z_t showed a very temperature-sensitive decrease in all the samples. The role of clay as a nucleating agent was illustrated by the shorter $t_{1/2}$ time for PBS/C30B than that of neat PBS and PBS/C30BM nanocomposite (see Table 7.10). In contrast, the $t_{1/2}$ for PBS/C30BM nanocomposite displaying delamination of clay particles was almost similar to those of neat PBS at the various crystallisation temperatures. The authors argued that this was because surface urethane modification of C30B organoclay which disturbed the PBS matrix in contact with inorganic groups, and

Table 7.10 The Avrami parameters for various crystallisation temperatures. Reproduced Hwang et al. [53] with permission

Sample	n	K	$t_{1/2}$ (s)
PBS-80	2.27	1.93 E-01	106
84	2.63	3.67 E-02	173
88	2.55	8.30 E-03	328
92	3.17	2.88 E-04	638
PBS/C30B-80	2.34	9.46 E-01	61
84	2.65	1.81 E-01	108
88	2.97	1.52 E-02	220
92	3.12	2.88 E-04	532
PBS/C30BM-80	2.25	1.93 E-01	100
84	2.38	3.09 E-02	182
88	2.26	8.40 E-03	319
92	2.92	3.52 E-04	615

hence there was a reduction in nucleation role, even though there existed a partial exfoliation in PBS/C30BM nanocomposite.

Shih et al. [83] studied the crystallisation phenomenon of cross-linked and uncross-linked PBS nanocomposites. The MMT used had been modified with cetyl pyridinium chloride (CPC): CPC/MMT, while the cross-linking of the nanocomposites had been achieved by curing using dicumyl peroxide (DCP). The nanocomposites derived were abbreviated PBSMC5 and PBSMC10, for PBS containing 5 and 10 wt% of the CPC, respectively. On the other hand, PBSDMC5 and PBSDMC10 were the abbreviations for the nanocomposites cured with DCP, with the numbers at the end representing wt% content of the DCP. PBS1D was the cross-linked PBS without any organoclay. From the DSC studies, (figures not shown), the initial temperature of crystallisation was decreased with the increasing cooling rate for all the samples. However, for cross-linked samples, the initial temperatures of crystallisation were lower than those of uncross-linked ones, at the same cooling rate. This implied that cross-linking hindered the rate of crystallisation.

The kinetics of crystallisation could not be modelled with the Ozawa equation, and this was attributed to the fact that the Ozawa model neglects secondary crystallisation. However, a modified Avrami equation adequately modelled the crystallisation kinetics. Generally, the crystallisation temperature, the modified Avrami rate constants and heat of crystallisation were decreased with the addition of organoclay at the same cooling rate for uncross-linked samples (PBS, PBSMC5 and PBSMC10). The $t_{1/2}$ was increased in the case of the nanocomposites, and hence the overall growth rate of the crystals was higher in the neat PBS than in the nanocomposites. Likewise, there was lower crystallinity in the nanocomposites than in the neat PBS. The lower crystallinity seen in the nanocomposite is because of the inability of polymers chains to be fully incorporated into growing crystalline lamella. This leads to the smaller crystallization rate, lower T_c and crystallinity.

On the other hand, the $t_{1/2}$ and the heat of crystallisation were larger in PBS1D than in the neat PBS. This was attributed to molecular motion of the polymer chain being possibly restrained by the network structure. The authors argued that the

larger crystallinity in PBS1D was possibly due to better alignment in the amorphous regions of PBS resulting from cross-linking. The shorter polymer chains created in the amorphous parts are easier to crystallise and thus partly contributed to the thickening of the already existing lamellae.

For the cross-linked PBSDMC5 and PBSDMC10 samples, the heat of crystallisation was reportedly decreased with the addition of organoclay, at the same cooling rate. This observation is in line with the ones already discussed above, about the general effect of organoclays on crystallinity of the polymer nanocomposites.

7.8 Melt Rheology

In order to understand the thermal processability of the PBS/clay and PBSA/clay nanocomposites, one needs information on the rheological behaviour of the nanocomposites under molten state. The rheological behaviour of the nanocomposites is strongly influenced by their nano-scale structure, the state of dispersion and interfacial characteristics. Therefore, information on rheological behaviour of the nanocomposites also helps in finding out the structure–property relationship. The rheological properties could be determined either through dynamic or steady shear measurements [95, 96].

7.8.1 Dynamic Oscillatory Shear

The dynamic oscillatory shear measurements of the polymeric materials are generally performed by applying a time dependent strain of $\gamma(t) = \gamma_o \sin(\omega t)$ and measuring the resultant shear stress $\sigma(t) = \gamma_o [G' \sin(\omega t) + G'' \cos(\omega t)]$, where G' and G'' are the storage modulus and loss modulus, respectively.

Okamoto et al. [24] conducted the dynamic oscillatory shear measurements on three nanocomposites: PBS/C_{18}-MMT; PBS/qC_{18}-MMT and PBS/qC16-SAP. Of the three nanocomposites, PBS/C18-MMT had a strongly flocculated structure. The master curves were generated by applying the time–temperature superposition principle and shifted to a T_{ref} of 120 °C (which had considered as the most representative of a typical processing temperature of PBS) with both a_T and the vertical shift factor (b_T). In Fig. 7.19, it can be seen that both the storage and loss moduli of all the nanocomposites increased monotonically at all frequencies as compared to that of neat PBS. In the higher frequency region (i.e. >10 rad $\cdot$ s^{-1}), the viscoelastic behaviour are the same, with the exception of the systematic increase in the modulus value. On the other hand, at low frequencies (<10 rad $\cdot$ s^{-1}), both storage and loss moduli show weak frequency dependence, meaning that there is a gradual change from liquid-like power-law region to solid-like behaviour, with the incorporation of clay. The terminal region slopes of both storage for neat PBS and the nanocomposites at low frequency values (<10 rad $\cdot$ s^{-1}) were: 1.7, 0.2, 9.25 and 0.3

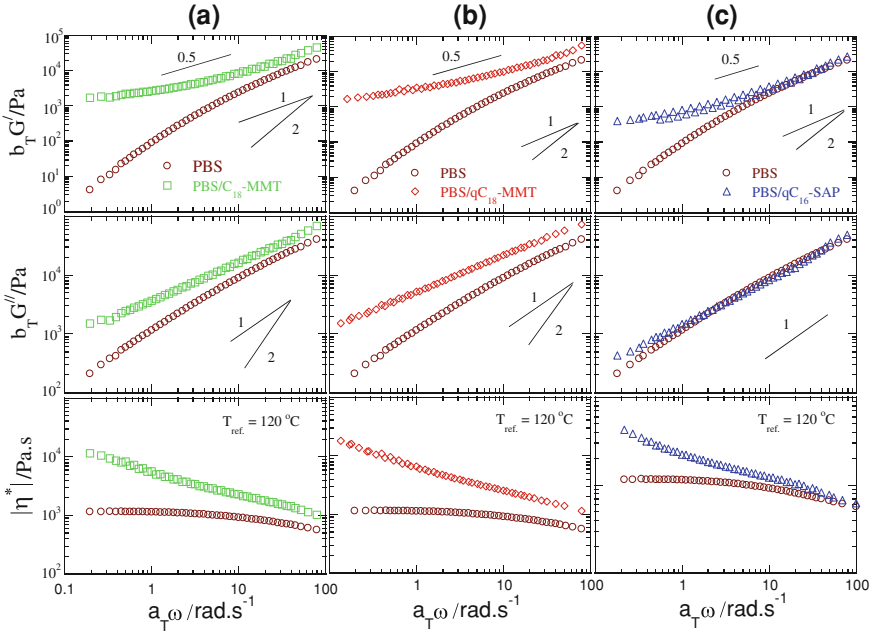

Fig. 7.19 Reduced-frequency dependence of G′(ω), G″(ω), and |η*|(ω) of neat PBS and various nanocomposites: **a** PBS/C18-MMT; **b** PBS/qC18-MMT and **c** PBS/qC16-SAP nanocomposites. Reproduced from Okamoto, Sinha Ray and Okamoto [24] with permission

for PBS, PBS/C_{18}-MMT, PBS/qC_{18}-MMT and PBS/qC_{16}-MMT, respectively. While for loss moduli they were: 1, 0.4, 0.6 and 0.7 for PBS, PBS/C_{18}-MMT, PBS/qC_{18}-MMT and PBS/qC_{16}-MMT, respectively. The lower slope values and the higher absolute values of the dynamic moduli implied the formation of spatially linked super-molecular structure, in the nanocomposites in molten state. There was a geometric constraint in the super-molecular structure; therefore, the individual stacked silicate layers were incapable of freely rotating (only translational motion is available). Hence, by imposing small frequency, $a_T\omega$, the relaxations of the structure were prevented almost completely. This type of prevented relaxation due to the highly geometric constraints of the stacked and intercalated silicate layers led to the presence of the solid-like behaviour as observed in nanocomposites. The degree of this prevented relaxation was greater for the PBS/C_{18}-MMT nanocomposite because of the presence of the strongly flocculated structure. On the other hand, as the clay content in the PBS/qC_{18}-MMT nanocomposite (PBSCNs) was later on increased from 2 to 5.4 % (80), the pseudo-solid-like behaviour became more pronounced, and at high clay content (5.4 wt%), the G' (ω) was almost independent of the frequency at low frequency values. Similar observation had previously been made by Sinha Ray et al. [23], when the inorganic part of clay content in PBS/C_{18}-MMT nanocomposite had been increased from 1.7 to 2.8 wt% and also when it was increased from 1.07 to 3.6 wt% [35].

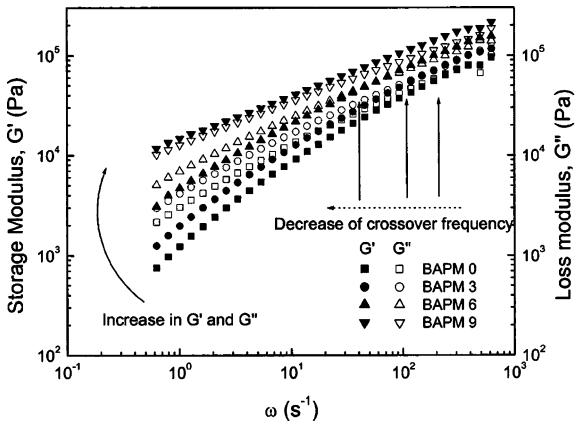

Fig. 7.20 G' (*filled symbols*) and G'' (*open symbols*) of nanocomposites with various clay loadings. Reproduced from Lim et al. [97] with permission

In the case of dynamic complex viscosity [$|\eta^*|(\omega)$], the master curves for the PBS/C_{18}-MMT, PBS/qC_{18}-MMT and PBS/qC16-SAP nanocomposites, based on linear dynamic oscillatory shear measurements, are also shown in Fig. 7.19. In the low-frequency region the neat PBS exhibited almost Newtonian behaviour, whereas all nanocomposites exhibited a very strong shear-thinning tendency. On the other hand, M_w and the polydispersity of neat PBS and various nanocomposites are almost same, thus the high viscosity of nanocomposites can be explained by the flow restrictions of polymer chains in the molten state due to the presence of clay particles. With an increase in clay content from 2 to 5.4 wt%, there was a remarkable increase of the magnitude of the dynamic complex viscosity of PBS/qC_{18}-MMT nanocomposites at low frequency values [81]. Similar trends were observed when the inorganic part of clay content in PBS/C_{18}-MMT nanocomposite had been increased from 1.7 to 2.8 wt% [23], when it was increased from 1.07 to 3.6 wt% [35]; and when the increase was from 1.04 to 3.84 wt% in the case of PBS/qC_{16}-SAP [35].

Lim et al. [97] and Lee et al. [98] studied solid-like transition of melt-intercalated biodegradable polymer (BAP)/clay nanocomposites. The BAP, going by the trade name Skygreen 2109, is closely related to the PBSA and is a synthetic copolymer made from the polycondensation reaction of diols (ethylene glycol and 1, 4 butanediol) and aliphatic dicarboxylic acids (succinic acid and adipic acid). The BAP/C25A nanocomposites were prepared with various organoclay contents and the samples abbreviated as BAPM3, BAPM6 and BAPM9, for nanocomposites with 3, 6 and 9 wt% organoclay, respectively. Rheological properties were determined with a rotational rheometer having parallel-plate geometry, 1.1 mm thick and 25 mm in diameter at 140 °C. In an oscillatory test mode, the frequency dependence of G' and G'' decreased monotonically with the increase in clay content as shown in Fig. 7.20.

At low frequencies, there was transition of the slopes to a flattened behaviour with an increase in the clay loading. As has already been discussed before in the case of PBS/clay nanocomposites, the slope and the higher absolute values of the

modulus imply a super-molecular structural formation in the nanocomposites. At low frequency values, the loss modulus is bigger than the storage modulus for the neat BAP and hence behaves like a liquid. On the other hand, the melt behaviour of BAP is solid-like ($G' > G''$) high frequency values. The authors defined the crossover frequency (ω_c) as G' (ω_c) = G'' (ω_c), and it is shifted toward a lower frequency with the clay content (see Fig. 7.20). At clay content of 9 wt% or higher, the G' was above G′throughout the frequency range, and hence there was no ω_c. Considering the mesoscopic structure at low clay concentrations, the authors suggested that beyond a critical volume fraction, the tactoids and individual layers are incapable of freely rotating, and are prevented from relaxing completely when subjected to shear. This incomplete relaxation due to physical jamming or percolation leads to the solid-like behaviour observed in both intercalated and exfoliated nanocomposites. Quite similar observation was made later on by Sinha Ray et al. [67], who also varied the clay content in PBSA nanocomposite from 3 to 9 wt%. In another study, Sinha Ray and Bousmina [63] related the extent of enthalpic between the clay surface and the PBSA backbones to rheological behaviour. The three nanocomposites were: PBSA/C30B; PBSA/C93A and PBSA/C15A. Their results showed that, upon increase in the favourable specific interactions between the surfactant and PBSA matrix, G' (ω) becomes a weak function of frequency and exhibits a pseudo–plateau in the terminal zone of the neat PBSA. The gradual change of behaviour from liquid-like to solid-like was mainly attributed to the extent of dispersion and distribution of the clay lamellae that form three dimensional percolating networks.

7.8.2 Steady Shear

The steady-shear rheological behaviour of neat PBS and a series of intercalated PBS/qC$_{18}$-MMT nanocomposites with 2, 3.6 and 5.4 wt% inorganic parts [85]. The shear viscosity of nanocomposites was enhanced considerably at all shear rates with time and increased monotonically with a decreasing shear rate. On the other hand, all the nanocomposites exhibited strong rheopexy behaviour, which became prominent at low shear rates (0.001 s^{-1}); whereas neat PBS exhibited a time-independent viscosity at all shear rates. As the shear rate increased, the shear viscosity attained a plateau after a certain time, and the time required to reach this plateau decreased with increasing shear rates. The authors attributed this behaviour to the planer alignment of the clay platelets toward the flow direction under shear. At low shear rate, the clay particles take longer time to attain a complete planar alignment along the direction of the flow. Whereas when the shear rate is high, shorter time is required for such an alignment. In Fig. 7.21, the shear-rate dependence of the viscosity of neat PBS and the nanocomposites measured at 120 °C is shown. The neat PBS shows a Newtonian behaviour, whereas the nanocomposites showed strong shear thinning within the measured shear rates, and this is analogous to the results obtained in the case of oscillatory-shear measurement.

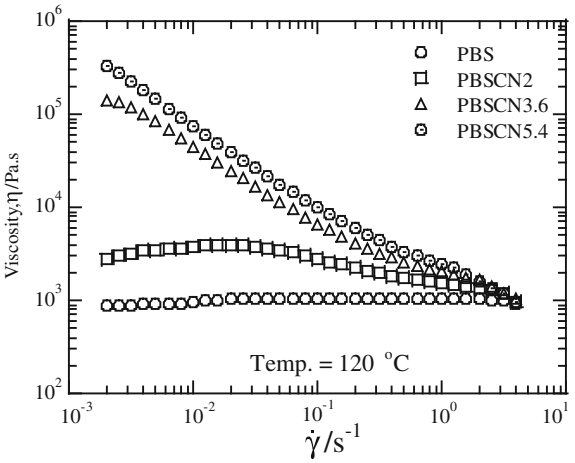

Fig. 7.21 η of neat PBS and various nanocomposites as a function of $\gamma(s^{-1})$. Reproduced from Sinha Ray et al. [81], with permission

However, for other systems [24, 35], at very low shear rates, the nanocomposites initially exhibited some shear thickening behaviour, and this corresponded to the rheopexy behaviour that had been observed in such systems at very low shear rates. In these systems, after the initial shear thickening, there was a very strong shear thinning behaviour. In addition, at very high shear rates, the steady-shear viscosities of the nanocomposites were comparable to that of neat PBS. This was attributed to the complete orientation of the clay particles in the direction of flow at high shear rates.

The PBS/clay nanocomposites discussed above displayed significant deviation from the Cox-Merz relation, whereas neat PBS obeyed the empirical Cox-Merz relation [99]. The relation requires that for $\gamma = \omega$ (where γ is the shear rate), the viscoelastic data should obey the relationship $\eta(\gamma) = |\eta|(\omega)$ (where η is the viscosity). Sinha Ray and co-workers [24, 35], attributed this to two reasons: first, the Cox-Merz rule is only applicable to homogeneous systems such as homopolymer melts, but nanocomposites are heterogeneous systems; and secondly, the structure formation is different when nanocomposites are subjected to dynamic oscillatory-shear and steady-shear measurements.

The steady shear measurements for PBSA/C30B, PBSA/C93A and PBSA/C15A have been carried out by Sinha Ray and and co-workers [63, 67]. Figure 7.22 represents the variation of the steady shear viscosity as a function of the shear rate for PBSA and the three nanocomposites. For comparison purposes, the small amplitude oscillatory shear viscosity is also reported on the figure. The steady shear viscosity and the dynamic viscosity overlapped very well for the neat PBSA at $\gamma = \omega$ (Cox-Merz rule holds). In contrast, for the nanocomposites, the rule fails and the steady shear viscosity becomes lower than the dynamic shear viscosity. At a high shear rate, the nanocomposites lose their solid-like behaviour and a rather classical Newtonian behaviour is observed for the three nanocomposites. The authors attributed this to the destruction of the percolating network and the alignment of the silicate layers in the direction of the flow.

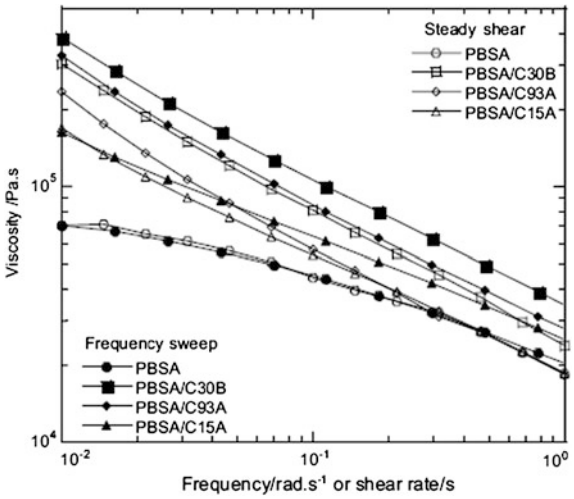

Fig. 7.22 Steady shear viscosity of neat PBSA and various nanocomposites as a function of shear rate. Reproduced from Sinha Ray and Bousmina [63] with permission

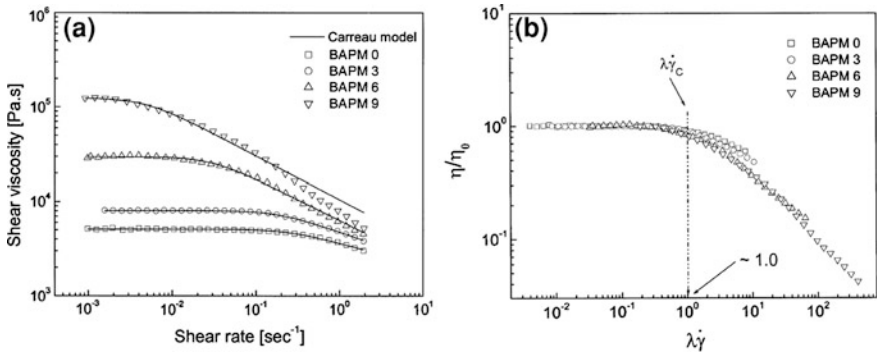

Fig. 7.23 **a** Steady shear viscosity of BAP and its nanocomposites as a function of the shear rate **b** Plot of $\eta/\eta o$ versus $\lambda\gamma$. Reproduced from Lim et al. [97] with permission

Lim et al. [56, 97], Lee et al. [98] analysed the relationship between steady shear viscosity and shear rate of BAP/C25A nanocomposites using the Carreau [100] model below:

$$\eta = \frac{\eta_o}{\left[1 + (\lambda\gamma)^2\right]^{(1-n)/2}} \tag{7.6}$$

where η_o is the zero shear rate viscosity, λ is the relation time (which characterises the onset point of shear thinning) and n is the power-law index. A typical model fit is as shown in Fig. 7.23a.

The degree of shear thinning (1–n) and λ was found to increase with clay loading. The authors attributed this observation to the alignment of the clay layers under shear, although the exact mechanism that causes the thinning, especially in presence of high clay loading is not known. The microstructure changed from a random structure to an ordered structure via shear-induced orientation. Figure 7.23b shows a Newtonian plateau at low shear rates and power-law behaviour at high shear rates. There is a strong correlation between λ and the critical shear rate (γ_c) for the nanocomposites. The γ_c measures crossover characteristics from a Newtonian plateau to a shear thinning region. It equates approximately to the inverse of the characteristic time for the nanocomposites. The authors postulated that $\lambda\gamma$ is a universal constant with a value of 1 while λ depends on the volume fraction and the structure of the nanocomposites.

7.9 Conclusions: Current Status and Future Prospects

The preparation, characterisation, and properties of nanocomposites based on PBS and PBSA has been discussed. Melt-intercalation has been shown to be particular a popular method for the preparation of the nanocomposites because of several advantages it has over the other methods. On the other hand, versatile characterisation methods have been applied to study the structure of the nanocomposites, and how that affects their properties. From these characterisation methods, one question that still lingers on is whether it is possible to have a truly complete exfoliation of the silicate layers in a polymer matrix. More studies into this and possible ways of achieving the true exfoliation, if it is possible, would go a long way in improving the properties of the nanocomposites.

Generally, there is improvement in the properties of the nanocomposites after incorporation of the silicate layers. Since the quantity of the clays used to achieve such improvement is normally lower than 5 wt%, the nanocomposites are far much lighter than the conventional composites, and this enhances their competitiveness with other materials for specific applications.

It has been shown that there is generally improvement in the dynamic mechanical properties of nanocomposites over those of neat polymers. This improvement is strongly dependent on the structure of the nanocomposite, processing procedure (like annealing) and the clay type and content used. Moreover, other mechanical properties such as tensile modulus of nanocomposites have also been shown to improve as compared with the neat polymers. This is probably due to the re-enforcement effect of the clays. However, elongation at beak and the tensile strength do not always improve with inclusion of layered silicate in the polymer matrices. Such changes in the tensile properties of the nanocomposites, whether improved or not, is dependent on, among other factors; the degree of dispersion of the silicate layers in polymer matrix, crystallinity, anisotropy and orientation of the dispersed clay particles.

The thermal stability of the nanocomposites is generally slightly higher than that of the neat polymers, although in certain instances, it is actually lower. The improvement in thermal stability is attributed to the ability of the clays to act as a superior insulator and mass transport barrier to the volatile products generated during decomposition.

In most instances, the gas barrier properties improve tremendously in the case of the nanocomposites, by creating a tortuous path for the gas molecules to diffuse through. On the other hand, biodegradation of the nanocomposites has also been shown to generally improve in most cases, whereas for a few others, it reduced. The rate of biodegradation of neat polymers and their nanocomposites is generally affected by the molecular weight, melting point, crystallinity, barrier properties of the samples.

In overall, the future prospects of the green nanocomposites based on PBS and PBSA look bright, especially in areas such as packaging. However, in order to realise the full potential of these green nanocomposites, ways have to be found to make them cost-effective and be widely accepted by the public. Governments all over the world are now introducing stringent laws aimed at protecting the environment and encouraging use of green products and technologies. Such initiatives are expected to drive up the demand for biopolymers like PBS and PBSA and their nanocomposites. It is expected therefore that more research will be done in future to make the nanocomposites more competitive. Even though moderate improvement in properties has been noted in the case of PBS and PBSA-based nanocomposites, further research work is needed to help come up with working formulations that will be easily processed and have lower or comparable financial cost to the conventional polymers. This would probably entail having research directed at establishing new approaches to tailor new environmental benign nanocomposite architectures that will result in even better improved. In food packaging industry for instance, barrier properties of the polymers needs to be improved. A challenge still exists on proper dispersion of the clay into polymer matrices so as to realise the required improvement in barrier property, among others.

Acknowledgments Authors would like to thank the Department of Science and Technology and the Council for Scientific and Industrial Research, both of South Africa, for financial support.

References

1. Chandra R, Rustgi R (1998) Biodegradable polymers. Prog Mater Sci 23:1273–1335
2. Sinha Ray S, Bousmina M (2005) Biodegradable polymers and their layered silicate nanocomposites: In greening the 21st century materials world. Prog Mater Sci 50:962–1079
3. Nair LS, Laurencin CT (2007) Biodegradable polymers as biomaterials. Prog Mater Sci 32:762–798
4. Siracusa V, Rocculi P, Romani S et al (2008) Biodegradable polymers for food packaging: a review. Trends Food Sci Tech 19:634–643
5. Kolybaba M, Tabil LG, Panigrahi S et al (2003) Biodegradable polymers: past, present, and future. In: The proceedings of American Society of Agricultural Engineers (ASAE) meeting, North Dakota, USA

6. Lenz RW (1995) Biodegradable polymers and plastics in Japan: research, development, and applications: International Technology Research Institute, US Department of Commerce. Report No.: PB95-199071
7. Mohanty AK, Misra M, Hinrichsen G (2000) Biofibres, biodegradable polymers and biocomposites: an overview. Macromol Mater Eng 276–277:1–24
8. Vaia RA, Teukolsky RK, Giannelis EP (1994) Interlayer structure and molecular environment of alkylammonium layered silicates. Chem Mater 6:1017–1022
9. Giannelis EP (1996) Polymer layered silicate nanocomposites. Adv Mater 8:29–35
10. Giannelis EP (1998) Polymer-layered silicate nanocomposites: synthesis, properties and applications. Appl Organomet Chem 12:675–680
11. Biswas M, Ray S (2001) Recent progress in synthesis and evaluation of polymer-montmorillonite nanocomposites. New Polymerization Techniques and Synthetic Methodologies. Springer, Berlin
12. Krishnamoorti R, Vaia RA, Giannelis EP (1996) Structure and dynamics of polymer-layered silicate nanocomposites. Chem Mater 8:1728–1734
13. LeBaron PC, Wang Z, Pinnavaia TJ (1999) Polymer-layered silicate nanocomposites: an overview. Appl Clay Sci 15:11–29
14. Vaia RA, Maguire JF (2007) Polymer nanocomposites with prescribed morphology: going beyond nanoparticle-filled polymers. Chem Mater 19:2736–2751
15. Sinha Ray S, Okamoto M (2003) Polymer/layered silicate nanocomposites: a review from preparation to processing. Prog Mater Sci 28:1539–1641
16. Bordes P, Pollet E, Avérous L (2009) Nano-biocomposites: biodegradable polyester/nanoclay systems. Prog Mater Sci 34:125–155
17. Yang K–K, Wang X-L, Wang Y-Z (2007) Progress in nanocomposite of biodegradable polymer. J Ind Eng Chem 13:485–500
18. Rossi A, Dahman S, Fischer S et al (2000) Nanocomposites: the latest developments. Plas Add Comp 2:34–36
19. Lee S-R, Park H-M, Lim H et al (2002) Microstructure, tensile properties, and biodegradability of aliphatic polyester/clay nanocomposites. Polymer 43:2495–2500
20. Maiti P, Yamada K, Okamoto M et al (2002) New polylactide/layered silicate nanocomposites: role of organoclays. Chem Mater 14:4654–4661
21. Ray SS, Yamada K, Ogami A et al (2002) New polylactide/layered silicate nanocomposite: nanoscale control over multiple properties. Macromol Rapid Commun 23:943–947
22. Sinha Ray S, Maiti P, Okamoto M et al (2002) New polylactide/layered silicate nanocomposites. 1. preparation, characterization, and properties. Macromolecules 35: 3104–3110
23. Sinha Ray S, Okamoto K, Maiti P et al (2002) New poly(butylene succinate)/layered silicate nanocomposites. 1: preparation and mechanical properties. J Nanosci Nanotechno 2: 171–176
24. Okamoto K, Sinha Ray S, Okamoto M (2003) New poly(butylene succinate)/layered silicate nanocomposites. II. Effect of organically modified layered silicates on structure, properties, melt rheology, and biodegradability. J Polym Sci B: Polym Phys 41:3160–3172
25. Zhu C, Zhang Z, Liu Q et al (2003) Synthesis and biodegradation of aliphatic polyesters from dicarboxylic acids and diols. J Appl Polym Sci 90:982–990
26. Fujimaki T (1998) Processability and properties of aliphatic polyesters, 'BIONOLLE', synthesized by polycondensation reaction. Polym Degrad Stabil 59:209–214
27. Ajioka M, Suizu H, Higuchi C et al (1998) Aliphatic polyesters and their copolymers synthesized through direct condensation polymerization. Polym Degrad Stabil 59:137–143
28. Wang G, Gao B, Ye H et al (2010) Synthesis and characterizations of branched poly(butylene succinate) copolymers with 1,2-octanediol segments. J Appl Polym Sci 117:2538–2544
29. Zhao J-H, Wang X-Q, Zeng J et al (2005) Biodegradation of poly(butylene succinate) in compost. J Appl Polym Sci 97:2273–2278

30. Chrissafis K, Paraskevopoulos KM, Bikiaris DN (2005) Thermal degradation mechanism of poly(ethylene succinate) and poly(butylene succinate): comparative study. Thermochim Acta 435:142–150
31. Ishii M, Okazaki M, Shibasaki Y et al (2001) Convenient synthesis of aliphatic polyesters by distannoxane-catalyzed polycondensation. Biomacromolecules 2:1267–1270
32. Han Y-K, Kim S-R, Kim J (2002) Preparation and characterization of high molecular weight poly(butylene succinate). Macromol Res 10:108–114
33. Kawasaki TY, Kamakura ET, inventors; Shower Highpolymer Co., Ltd., assignee (1995) polyester injection-molded articles. USA
34. Okamoto M (2006) Biodegradable polymer/layered silicate nanocomposites. In: Mallapragada S, Narasimhan B (eds) Handbook of biodegrdable polymeric materials and their applications. American Scientific Publishers, California
35. Sinha Ray S, Okamoto K, Okamoto M (2003) Structure-property relationship in biodegradable poly(butylene succinate)/layered silicate nanocomposites. Macromolecules 36:2355–2367
36. Montaudo G, Rizzarelli P (2000) Synthesis and enzymatic degradation of aliphatic copolyesters. Polym Degrad Stab 70:305–314
37. Cao A, Okamura T, Nakayama K et al (2002) Studies on syntheses and physical properties of biodegradable aliphatic poly(butylene succinate-co-ethylene succinate)s and poly(butylene succinate-co-diethylene glycol succinate)s. Polym Degrad Stabil 78:107–117
38. Papageorgiou GZ, Bikiaris DN (2007) Synthesis, co-crystallization, and enzymatic degradation of novel poly(butylene-co-propylene succinate) copolymers. Biomacromolecules 8:2437–2449
39. Nikolic MS, Djonlagic J (2001) Synthesis and characterization of biodegradable poly(butylene succinate-co-butylene adipate)s. Polym Degrad Stabil 74:263–270
40. Ahn BD, Kim SH, Kim YH et al (2001) Synthesis and characterization of the biodegradable copolymers from succinic acid and adipic acid with 1,4-butanediol. J Appl Polym Sci 82:2808–2826
41. Rizzarelli P, Puglisi C, Montaudo G (2004) Soil burial and enzymatic degradation in solution of aliphatic co-polyesters. Polym Degrad Stabil 85:855–863
42. Wang Y, Bhattacharya M, Mano JF (2005) Thermal analysis of the multiple melting behavior of poly(butylene succinate-co-adipate). J Polym Sci Pol Phys 43:3077–3082
43. Sato Y, Takikawa T, Sorakubo A et al (2000) Solubility and diffusion coefficient of carbon dioxide in biodegradable polymers. Ind Eng Chem Res 39:4813–4819
44. Eslami H, Grmela M, Dubois C et al (2009) Melt rheology of biodegradable poly[(butylene succinate)-co-adipate]: experimental and model predictions. J Polym Sci Pol Phys 48: 832–839
45. Ren M, Song J, Song C et al (2005) Crystallization kinetics and morphology of poly(butylene succinate-co-adipate). J Polym Sci Pol Phys 43:3231–3241
46. Zhao J-H, Wang X-Q, Zeng J et al (2005) Biodegradation of poly(butylene succinate-co-butylene adipate) by Aspergillus versicolor. Polym Degrad Stabil 90:173–179
47. Tserki V, Matzinos P, Pavlidou E et al (2006) Biodegradable aliphatic polyesters. Part II. Synthesis and characterization of chain extended poly(butylene succinate-co-butylene adipate). Polym Degrad Stabil 91:377–384
48. Hayase N, Yano H, Kudoh E et al (2004) Isolation and characterization of poly(butylene succinate-co-butylene adipate)-degrading microorganism. J Biosci Bioeng 97:131–133
49. Tomita K, Kuroki Y, Hayashi N et al (2000) Isolation of a thermophile degrading poly(butylene succinate-co-butylene adipate). J Biosci Bioeng 90:350–352
50. Fruzsina K, Százdi L, Fekete E et al (2006) Surface characteristics of layered silicates: influence on the properties of clay/polymer nanocomposites. Langmuir 22:7848–7854
51. Gilman JW, Morgan AB, Jr. RH et al (eds) (1999) Polymer layered-silicate nanocomposites: polyamide-6 polypropylene and polystyrene. New advances in flame retardant technology. Tucson, AZ. Fire Retardant Chemicals Association

52. Chen G, Yoon J-S (2005) Nanocomposites of poly[(butylene succinate)-co-(butylene adipate)] (PBSA) and twice-functionalized organoclay. P. Polym Int 54:939–945
53. Hwang SY, Ham MJ, Im SS (2010) Influence of clay surface modification with urethane groups on the crystallization behavior of in situ polymerized poly(butylene succinate) nanocomposites. Polym Degrad Stab 95:1313–1320
54. Alexandre M, Dubois P (2000) Polymer-layered silicate nanocomposites: preparation, properties and uses of a new class of materials. Mater Sci Eng: R: Rep 28:1–63
55. Ray SS, Okamoto M (2003) Polymer/layered silicate nanocomposites: a review from preparation to processing. Prog Polym Sci 28:1539–1641
56. Lim ST, Hyun YH, Choi HJ et al (2002) Synthetic biodegradable aliphatic polyester/montmorillonite nanocomposites. Chem Mater 14:1839–1844
57. Messersmith PB, Giannelis EP (1993) Polymer-layered silicate nanocomposites: in situ intercalative polymerization of e-caprolactone in layered silicates. Chem Mater 5: 1064–1066
58. Hwang SY, Yoo ES, Im SS (2009) Effect of the urethane group on treated clay surfaces for high-performance poly(butylene succinate)/montmorillonite nanocomposites. Polym Degrad Stab 94:2163–2169
59. Vaia RA, Jandt KD, Kramer EJ et al (1996) Microstructural evolution of melt intercalated polymer-organically modified layered silicates nanocomposites. Chem Mater 8:2628–2635
60. Vaia RA, Giannelis EP (1997) Lattice model of polymer melt intercalation in organically-modified layered silicates. Macromolecules 30:7990–7999
61. Vaia RA, Giannelis EP (1997) Polymer melt intercalation in organically-modified layered silicates: model predictions and experiment. Macromolecules 30:8000–8009
62. Pollet E, Delcourt C, Alexandre M et al (2006) Transesterification catalysts to improve clay exfoliation in synthetic biodegradable polyester nanocomposites. Eur Polym J 42: 1330–1341
63. Sinha Ray S, Bousmina M (2005) Poly(butylene sucinate-co-adipate)/montmorillonite nanocomposites: effect of organic modifier miscibility on structure, properties, and viscoelasticity. Polymer 46:12430–12439
64. Sinha Ray S (2009) Visualisation of nanoclay dispersion in polymer matrix by high-resolution electron microscopy combined with electron tomography. Macromol Mater Eng 294:281–286
65. Malwela T, Sinha Ray S (2011) Unique morphology of dispersed clay particles in a polymer nanocomposite. Polymer 52:1297–1301
66. Bandyopadhyay J, Sinha Ray S (2010) The quantitative analysis of nano-clay dispersion in polymer nanocomposites by small angle X-ray scattering combined with electron microscopy. Polymer 51:1437–1449
67. Sinha Ray S, Bousmina M, Okamoto K (2005) Structure and properties of nanocomposites based on poly(butylene succinate-co-adipate) and organically modified montmorillonite. Macromol Mater Eng 290:759–768
68. Bandyopadhyay J, Sinha Ray S (2010) Mechanism of enhanced tenacity in a polymer nanocomposite studied by small-angle X-ray scattering and electron microscopy. Polymer 51:4860–4866
69. Bandyopadhyay J, Maity A, Khatua BB et al (2010) Thermal and rheological properties of biodegradable poly[(butylene succinate)-co-adipate] Nanocomposites. J Nanosci Nanotechno 10:4184–4195
70. Sinha Ray S, Bandyopadhyay J, Bousmina M (2007) Thermal and thermomechanical properties of poly[(butylene succinate)-co-adipate] nanocomposite. Polym Degrad Stabil 92:802–812
71. Sinha Ray S, Bousmina M (2006) Crystallization behavior of poly[(butylene succinate)-co-adipate] nanocomposite. Macromol Chem Phys 207:1207–1219
72. Eslami H, Grmela M, Bousmina M (2009) Structure build-up at rest in polymer nanocomposites: flow reversal experiments. J Polym Sci Pol Phys 47:1728–1741

73. Chen G-X, Kim E-S, Yoon J-S (2005) Poly(butylene succinate)/twice functionalized organoclay nanocomposites: preparation, characterization, and properties. J Appl Polym Sci 98:1727–1732
74. Dean KM, Pas SJ, Yu L et al (2009) Formation of highly oriented biodegradable polybutylene succinate adipate nanocomposites: effects of cation structures on morphology, free volume, and properties. J Appl Polym Sci 113:3716–3724
75. Sinha Ray S (2010) A new possibility for microstructural investigation of clay-based polymer nanocomposite by focused ion beam tomography. Polymer 51:3966–3970
76. Shih Y-F, Wu T-M (2009) Enzymatic degradation kinetics of poly(butylene succinate) nanocomposites. J Polym Res 16:109–115
77. Ray SS (2010) A new possibility for microstructural investigation of clay-based polymer nanocomposite by focused ion beam tomography. Polymer 51:3966–3970
78. Shih Y, Wang T, Jeng R et al (2007) Biodegradable nanocomposites based on poly(butylene succinate)/organoclay. J Polym Environ 15:151–158
79. Shia D, Hui CY, Burnside SD et al (1998) An interface model for the prediction of Young's modulus of layered silicate-elastomer nanocomposites. Polym Compos 19:608–617
80. Someya Y, Nakazato T, Teramoto N et al (2004) Thermal and mechanical properties of poly(butylene succinate) nanocomposites with various organo-modified montmorillonites. J Appl Polym Sci 91:1463–1475
81. Sinha Ray S, Okamoto K, Okamoto M (2006) Structure and properties of nanocomposites based on poly(butylene succinate) and organically modified montmorillonite. J Appl Polym Sci 102:777–785
82. Makhatha ME, Ray SS, Hato J et al (2008) Thermal and thermomechanical properties of poly(butylene succinate) nanocomposites. J Nanosci Nanotechno 8:1679–1689
83. Shih YF, Wang TY, Jeng RJ et al (2008) Cross-linked and uncross-linked biodegradable nanocomposites. I. Nonisothermal crystallization kinetics and gas permeability. J Appl Polym Sci 110:1068–1079
84. Nielsen LE (1967) Models for the permeability of filled polymer systems. J Macromol Sci Pure 1:929–942
85. Ray SS, Okamoto K, Okamoto M (2006) Structure and properties of nanocomposites based on poly(butylene succinate) and organically modified montmorillonite. J Appl Polym Sci 102:777–785
86. Sinha Ray S, Yamada K, Okamoto M et al (2003) New polylactide/layered silicate nanocomposites. 5. designing of materials with desired properties. Polymer 44:6633–6646
87. Sinha Ray S, Bandyopadhyay J, Bousmina M (2008) Influence of degree of intercalation on the crystal growth kinetics of poly[(butylene succinate)-co-adipate] nanocomposites. Eur Polym J 44:3133–3145
88. Chen G-X, Yoon J-S (2005) Nonisothermal crystallization kinetics of poly(butylene succinate) composites with a twice functionalized organoclay. J Polym Sci Pol Phys 43:817–826
89. Avrami M (1939) Kinetics of phase change. I: general theory. J Chem Phys 7:1103
90. Avrami M (1940) Kinetics of phase change. II transformation-time relations for random distribution of nuclei. J Chem Phys 8:212
91. Avrami M (1941) Granulation, phase change, and microstructure kinetics of phase change. III. J Chem Phys 9:177
92. Ozawa T (1971) Kinetics of non-isothermal crystallization. Polymer 12:150–158
93. Liu T, Mo Z, Wang S et al (1997) Nonisothermal melt and cold crystallization kinetics of poly(aryl ether ether ketone ketone). Polym Eng Sci 37:568–575
94. Kuwabara K, Gan Z, Nakamura T et al (2002) Molecular mobility and phase structure of biodegradable poly(butylene succinate) and poly(butylene succinate-co-butylene adipate). Biomacromolecules 3:1095–1100
95. Krishnamoorti R, Yurekli K (2001) Rheology of polymer layered silicate nanocomposites. Curr Opin Colloid Int Sci 6:464–470

96. Sinha RS (2006) Rheology of polymer/layered silicate nanocomposites. J Ind Eng Chem 12:811–842
97. Lim ST, Lee CH, Choi HJ et al (2003) Solidlike transition of melt-intercalated biodegradable polymer/clay nanocomposites. J Polym Sci Pol Phys 41:2052–2061
98. Lee CH, Lim ST, Hyun YH et al (2003) Fabrication and viscoelastic properties of biodegradable polymer/organophilic clay nanocomposites. J Mater Sci Lett 22:53–55
99. Cox WP, Merz EH (1958) Correlation of dynamic and steady flow viscosities. J Polym Sci 28:619–622
100. Carreau PJ, Kee DCRD, Chhabra RP (1997) Rheology of polymeric systems—principles and applications. Hanser Publishers, New York
101. Ray SS, Bousmina M (2006) Crystallization behavior of poly[(butylene succinate)-co-adipate] nanocomposite. Macromol Chem Phys 207:1207–1219
102. Ray SS, Bandyopadhyay J, Bousmina M (2007) Thermal and thermomechanical properties of poly[(butylene succinate)-co-adipate] nanocomposite. Polym Degrad Stabil 92:802–812

Chapter 8
Clay Nano-Biocomposites Based on PBAT Aromatic Copolyesters

Eric Pollet and Luc Avérous

Abstract Despite the numerous studies reported on clay-based nano-biocomposites, only few articles concern works on PBAT/clay nano-biocomposites. However, in these studies, a large number of organo-clays has been tested to elaborate PBAT nano-biocomposites. Most of the reported works use the melt-intercalation route to elaborate such nanohybrids materials. According to the morphological analyses, nano-bio-composites with intercalated structures are mainly obtained and clay exfoliation seems difficult to reach in these systems. The best results in terms of clay dispersion and material properties are obtained with organo-clay bearing hydroxyl group and thus having better polarity matching with the matrix. For all intercalated structures, the clay addition has a limited beneficial effect on mechanical and thermal properties whereas the clay platelets dispersion seems to influence the PBAT crystallization with enhanced nucleation. Even if a large majority of the re-ported studies deals with montmorillonite clay, interesting results were also obtained with hectorite.

8.1 Main Characteristics of the Aliphatic-Aromatic Copolyesters

These copolyesters combine the biodegradability of aliphatic polyesters with the excellent properties imparted by aromatic polyesters. Indeed, while aliphatic polyesters are easily biodegradable, they usually lack thermal stability and mechanical properties which are required in many applications. On the other hand,

E. Pollet · L. Avérous (✉)
LIPHT-ECPM, EAc(CNRS) 4379, Université de Strasbourg 25 rue Becquerel,
67087 Strasbourg Cedex 2, France
e-mail: luc.averous@unistra.fr

L. Avérous and E. Pollet (eds.), *Environmental Silicate Nano-Biocomposites*,
Green Energy and Technology, DOI: 10.1007/978-1-4471-4108-2_8,

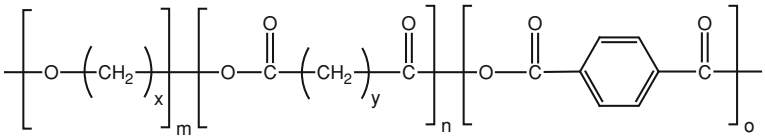

Fig. 8.1 General structure of aliphatic-aromatic copolyesters

aromatic polyesters provide excellent use properties (thermal and mechanical properties) but they are resistant to microbial attack under environmental conditions [1]. While the biological susceptibility of many aliphatic polyesters has been known for many years, aromatic polyesters such as polyethylene terephthalate (PET) or polybutylene terephthalate are considered as non-biodegradable [2]. Thus, to improve the use properties of aliphatic polyesters, attempts were made to include aromatic units in order to obtain novel aliphatic-aromatic copolyesters displaying good material performance while preserving the biodegradable character.

A wide range of copolyesters was synthesized by standard bulk polycondensation techniques from various aliphatic diols with a defined mixture of different aliphatic dicarboxylic acids and mainly terephthalic acid as the aromatic moiety. Copolyesters with molar masses in a range necessary for technical application were obtained [3, 4]. Among the aliphatic moieties, adipic, fumaric, sebacic and succinic acids were the main components to be copolymerized with propanediol, butanediol or ethylene glycol.

Random copolyesters composed of 1, 4-butanediol, terephthalic acid and adipic acid (BAT copolyesters) turned out to be the most promising materials for technical applications, not only for their degradation behaviour and their material properties, but also from the large availability of the monomers at a rather moderate price.

The main commercially available copolyesters obtained by modification of PBT (polybutylene terephthalate) with aliphatic dicarboxylic acids and diols are listed and presented hereafter.

Polybutylene adipate terephthalate (PBAT) is formed by the reaction of butanediol with adipic and terephthalic acids (Fig. 8.1). Both BASF and Eastman Chemicals developed and commercialized such copolyesters since the late 90s. Since then, the Eastar Bio technology from Eastman Chemicals has been sold in 2004 to Novamont who is now developing similar materials, partly obtained from renewable resources, under the Origo-Bi grades name.

Ecoflex (BASF) is a water resistant thermoplastic material claimed to be similar to LDPE but with better mechanical properties. The glass transition temperature (Tg) of Ecoflex is −30 °C and the melting temperature (Tm) range is 110–115 °C. It can be extruded to make tear-resistant and flexible films for packaging applications. Due to its moderate water vapour permeability it can be used to make breathable films. The content of terephthalic acid in the copolymer is approximately 42–45 mol% (with regard to the dicarboxylic monomers). A modification of the basic copolyester grade leads to a more flexible material which is especially suitable for film applications.

Eastar Bio (formerly commercialized by Eastman Chemicals) was a very similar material that could be processed on conventional polyethylene extrusion equipment and designed for blown and cast film extrusion, extrusion coating, and fibre or non-woven applications. The general purpose grade resin Eastar Bio GP had a glass transition temperature of −30 °C and a melting temperature of 108 °C. The high viscosity grade Eastar Bio Ultra copolyester with a Tg of −33 °C and a Tm range of 102–115 °C was mainly designed for blown film processing.

Accompanying the development of these materials, several studies were dedicated to the biodegradability of the PBAT copolyesters. Indeed, due to the complex structure of these copolyesters, which include components that may exhibit a very slow degradability, intensive investigations on the biodegradability and degradation mechanisms were necessary.

Degradation of PBAT under anaerobic conditions showed that copolyesters were attacked by some specific anaerobic microbial strains only if the terephthalic acid content was lower than 20 %. Thus, up to now there is no definite proof for the existence of anaerobic microorganisms able to depolymerise PBAT copolyesters having compositions suitable for technical applications (i.e. with terephthalic acid content around 40–50 %). The results reported so far indicate that a degradation of PBAT in anaerobic digestion plants will be difficult.

However, aerobic biodegradation behaviour in soil or under composting conditions showed much more positive results. The first biodegradation studies showed that only copolyesters with a quite high fraction of aliphatic units exhibited a significant biodegradability induced by lipase activity under composting conditions. The obtained results also demonstrated that the fraction of terephthalic acid in the copolymers predominantly determined the degradation behaviour whereas the type of diol monomer was of minor importance for the degradability of the material. According these studies, the key to biodegradability is the block length of the aromatic unit, which should preferably be no more than a trimer.

Witt et al. [5] have shown that the weight loss of copolyester films in soil (ambient temperature) is significantly lower than in compost at 60 °C. For a PBAT copolyester with about 40 mol% terephthalic acid in the acid component a weight loss of approximately 50 % was observed after 3 months while the same material degraded completely in compost within 3 months.

Moreover, when increasing the aromatic monomer to 50 mol%, no weight loss of PBAT films could be observed anymore in soil (at 60 °C and 60 % relative humidity) within the 3 months period whereas in compost (at the same temperature and humidity conditions) the test specimen exhibited a significant loss in molecular weight.

The biodegradation of Ecoflex was tested under composting conditions. After 100 days in a compost environment more than 90 % of the carbon in the polymer was converted to CO_2. Witt et al. [6] also performed a detailed investigation of the PBAT biodegradability and ecotoxicological impact. Results showed that metabolisation of more than 99 % could be obtained for Ecoflex using a thermophilic actinomycete strain and it can also be concluded that aromatic oligomers

Table 8.1 Structural characteristics of principal 2:1 layered silicates

Phyllosilicates	Octahedra occupancy	Interlayer cations	CEC (meq/100 g)	Aspect ratio
Smectites				
Montmorillonite (MMT)	Al (2/3)	Na^+, Ca^{2+}, Mg^{2+}	110	100–150
Hectorite (HEC)	Mg (3/3)	Na^+, Ca^{2+}, Mg^{2+}	120	200–300

are subject to biodegradation under such composting conditions. Ecotoxicological tests performed with *Photobacterium phosphorum* bacteria and *Daphnia magna* water fleas revealed no toxic effects induced by degradation intermediates. Ecotoxicity tests based on plants growth (such as oat, cress, radish, etc.) also demonstrated that degradation products are totally harmless to the tested plants [7]. Meeting the requirements, Ecoflex has thus been certified as compostable material.

Similar results were obtained when the biodegradation of Eastar Bio grades was tested under composting conditions since about 80 % of the polymer-carbon was released as CO_2 after 210 days of composting while another study showed that more than 90 % of metabolisation could be observed [8]. Risk assessments resulted in the conclusion that no toxic effects can be expected from composting PBAT copolyester.

It is worth noting that other aliphatic-aromatic copolyesters have been synthesized and even commercialized. For instance, the specific grade EnPol G8060 from Ire Chemicals is a PBAT copolyester but this products has not been used and studied for the elaboration of clay-based nano-biocomposites. Besides, poly(trimethylene terephthalate) (PTT), obtained by polycondensation of propanediol and terephthalic acid, is also often classified as an aliphatic-aromatic copolyester but this polyester is not biodegradable.

Nevertheless, new commercial grades of aliphatic-aromatic copolyesters could be produced in a near future. Indeed, while up to now the monomers were conventionally derived from petrochemical feedstocks, several companies have recently announced the production of bio-based monomers (such as succinic acid, propanediol or even more recently butanediol and adipic acid, etc.), opening the way for bulk production of biodegradable aliphatic-aromatic copolyesters from renewable resources.

However, as previously mentioned, the biodegradable character of these copolyesters is still observed only for limited contents of aromatic units. Thus, to further improve the thermal and mechanical properties of these copolyesters without increasing the aromatic content, the nanocomposites strategy has been developed. It consists in dispersing nanoscaled layered silicates such as montmorillonite (MMT) or organo-modified MMT (OMMT) into the matrix.

The characteristics of such layered silicates and details about the main nanoclays are presented in the following tables (Tables 8.1 and 8.2).

Table 8.2 Main organo-modified nanoclays and their characteristics

Supplier	Trade name	Code	Clay type	Organo-modifier type	Modifier content (meq/100 g)	Δw^a (%)	d-spacing (Å)
"Home-made" organoclays							
	NH_3^+(C12)		MMT	$NH_3^+(C_{12}H_{25})$	115.6	20.4	17.7
	NH_3^+(C18)		MMT	$NH_3^+(C_{18}H_{37})$	117.3	27.4	18.2
	$NH^+(EtOH)_2$(C12)		MMT	$NH^+(EtOH)_2(C_{12}H_{25})$	96.7	23.9	18.2
Southern Clay Products (USA)							
	Cloisite®Na	CNa	MMT	–	–	7	11.7
	Cloisite®20A	C20A	MMT	$N^+(Me)_2(tallow)_2$	95	38	24.2
	Cloisite®15A	C15A	MMT	$N^+(Me)_2(tallow)_2$	125	43	31.5
	Cloisite®30B	C30B	MMT	$N^+(Me)(EtOH)_2(tallow)$	90	30	18.5
Süd-Chemie (Germany)							
	Nanofil®804	N804	MMT	$N^+(Me)(EtOH)_2(tallow)$	N.A.	21	18
Laviosa Chimica Mineraria (Italy)							
	Dellite® 43B	D43B	MMT	$N^+(Me)_2(CH_2\text{-}\phi)(tallow)$	95	32–35	18.6
Elementis Specialties (UK)							
	Bentone 109	B109	HEC	$N^+(Me)_2(tallow)_2$	123	44	32

[a] % Weight loss on ignition tallow: ~65 % C_{18}; ~30 % C_16; ~5 % C_{14}

8.2 Preparation of Nano-Biocomposites Based on PBAT Aliphatic-Aromatic Copolyesters

The first study on PBAT nanocomposites was reported by Someya et al. [9] who prepared nano-biocomposites based on (O)MMT which were known to efficiently lead to intercalated structures with polybutylene succinate (PBS) [10], i.e., MMT-NH_3^+(C12), MMT-NH_3^+(C18), MMT-$NH^+(EtOH)_2$(C12). They investigated the morphology and the properties of PBAT/clay nano-biocomposites prepared by melt intercalation containing 3–10 wt% (O)MMT. Whatever the OMMT used, well intercalated structures were obtained for 5 and 10 wt% clay content. Thus, authors focused on the materials morphologies and properties obtained with 3 wt% of clay since this amount led to the best results in terms of clay dispersion quality [9]. Only very limited intercalation occurred with unmodified MMT whereas well intercalated structures were obtained in the case of MMT-NH_3^+(C12) and MMT-$NH^+(EtOH)_2$(C12). According to the authors, intercalation in addition to some partial exfoliation occurred with MMT-NH_3^+(C18), which was also more finely dispersed in the matrix. It was demonstrated that the mechanical properties were related to the clay content but also to the structure as well as the crystallinity of the nanocomposites. Increasing the clay content logically led to increased tensile modulus. Furthermore, dynamic viscoelastic analyses showed that the clay reinforcing effect is really effective above Tg, when the material is soft, with the storage modulus enhancement being due to restricted polymer chains motions. Tensile tests showed that the partially exfoliated PBAT/MMT-NH_3^+(C18) with 3 wt% of clay had the lowest modulus. This rather unexpected behaviour was explained by the presence of exfoliated clay platelets retarding the PBAT crystallization and thus lowering the crystallinity. However, one cannot exclude degradation of the matrix during processing that could be enhanced by such OMMT.

Biodegradability was evaluated by the aerobic biodegradation tests both in soil and in aqueous medium containing activated sludge [11]. Compared to neat PBAT, the microcomposite based on unmodified montmorillonite exhibited a higher weight loss after soil burial whereas the intercalated PBAT/MMT-NH_3^+(C18) nanocomposites showed reduced biodegradation compared to the neat matrix. The same trend was also observed for the biodegradation in aqueous medium evaluated by the biochemical oxygen demand. According to Someya et al. enhanced biodegradation observed with unmodified clay may be related to the highly hydrophilic character of the clay. These authors also explain that intercalated nano-biocomposites based on PBAT/MMT-NH_3^+(C18) show reduced biodegradation due to the more pronounced hydrophobic character of this organoclay as well as the finely dispersed platelets forming a more tortuous path hindering the enzymes or water diffusion in the material.

Pollet et al. [12] also reported on the melt blending elaboration of nano-biocomposites based on 3 wt% C30B and two PBAT grades, Ecoflex and EastarBio Ultra obtained respectively from BASF and Eastman Chemicals

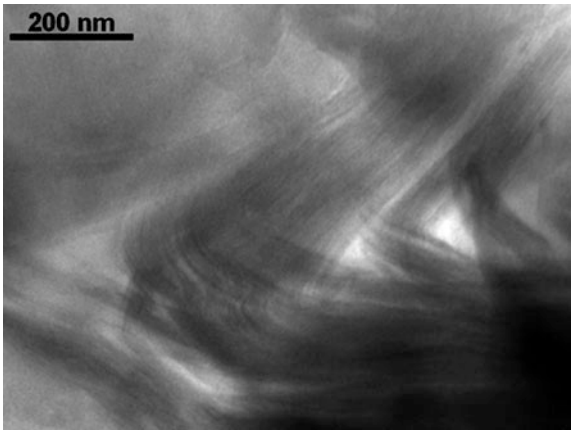

Fig. 8.2 Intercalated structure of PBAT/C20A nanocomposites [13]

(now commercialized by Novamont). The obtained materials showed intercalated morphology with only a very limited enhancement in their Young's modulus together with a slight decrease in elongation at break.

These early works were expanded by Chivrac et al. [13, 14] who tested various organoclays, such as C20A, D43B and N804 and compared the solvent and melt intercalation elaboration processes. The resulting materials structure and properties were compared to neat PBAT and to PBAT/MMT-Na, the composites with non-modified montmorillonite. This study revealed that higher intercalation degrees were obtained by solvent intercalation with C20A and D43B presenting better affinity with PBAT (see Figure 8.2). The thermal degradation behaviour has been examined by TGA. According to the recorded onset degradation temperatures, the highest improvements were observed for nano-biocomposites filled with 3 wt% of MMT-Na. However, a decrease of the onset degradation temperatures is observed for nano-biocomposites with higher clay contents, obtained from both the melt and solvent intercalations processes. This phenomenon can be explained by the clay acting as heat barrier and leading to char formation after thermal decomposition together with the fact that clay tactoids accumulate heat which could further be responsible of an accelerated decomposition reaction, as already described by Lim et al. [15]. No impact of the clay dispersion has been observed on the *T*g and *T*m values, whereas the crystallinity showed decreasing values when increasing the clay content for both unmodified and organomodified clays. Thus, authors investigated more in details the influence of the clay dispersion on the PBAT non-isothermal crystallization [14] and it was concluded that addition of a small amount of MMT enhances the PBAT nucleation mechanism, but also that the dispersed clay platelets hinder the crystallites growth. These two antagonist phenomena may lead to different PBAT crystallization behaviour depending on the clay dispersion.

Besides, tensile tests showed that the stiffness continuously increases with clay content [13]. This increased stiffness is due to strong interactions between PBAT

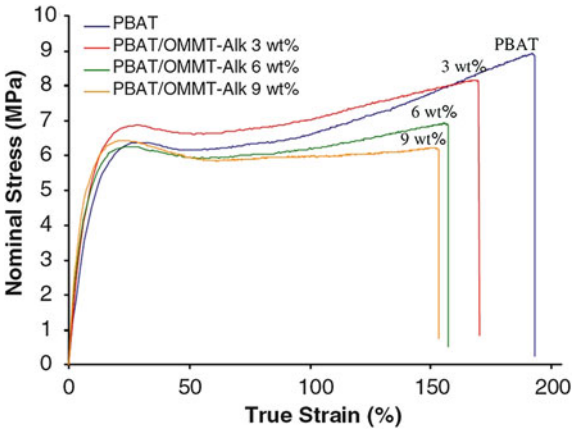

Fig. 8.3 Typical stress/strain curves of PBAT/C20A intercalated nanocomposites [13]

and nanofillers, particularly with C20A (see Fig. 8.3), since the crystallinity decreases with increasing clay content. Nevertheless, decreases of the strain at yield and at break have been observed due to more aggregated structures at higher clay contents.

Similar increase in stiffness for PBAT/C15A nano-biocomposites with intercalated morphology has also been reported by Shahlari et al. [16]. The nano-biocomposites obtained by melt blending with a twin screw extruder showed well intercalated structure and increasing elastic and flexural moduli with clay content. However, authors reported that the addition of nanoclay had no influence on the PBAT melting temperature, crystallization temperature or degree of crystallinity. In this study authors also looked at the influence of PLA addition on the nano-biocomposites properties. The results showed that additional increase in modulus is achieved by adding PLA and clay dispersion in the blends induces significant changes in the PLA melting and cold crystallization temperatures. Morphological characterization also showed that addition of clay decreased the PLA domains size as a result of enhanced compatibility between the blend components.

Recently, Mohanty et al. [17] reported on the melt intercalation elaboration of nano-biocomposites films based on PBAT and organo-modified clays using twin screw extruder and subsequent films blowing unit. According to the morphological analyses, well intercalated structures, with partial exfoliation, were obtained with organo-modified clays, whereas the unmodified one logically led to microcomposites without polymer intercalation between clay platelets. Among the organo-modified clays, C30B shows the highest intercalation due to strong interactions between carbonyl groups of PBAT and the OH groups of the organoclay.

Whatever the clay, both DSC and DMA results evidenced an increase in Tg and Tan δ peaks upon clay addition, the largest shift being observed for the highest intercalation extent due to greater interactions between the clay and the matrix. Meanwhile, a slight increase in crystallinity is observed with the addition of clay.

The fine clay dispersion is also evidenced by the thermogravimetric analyses displaying enhanced thermal stability for the nano-biocomposites obtained from organoclays. For instance, the PBAT/C30B and PBAT/B109 intercalated nanocomposites exhibit an initial degradation temperature shifted by more than 20 °C compared to the neat matrix. However, as expected, not noticeable improvement was observed for the microcomposites obtained from unmodified clay. The increase in thermal stability of the biopolymer matrix with the addition of layered silicates is primarily due to the clay nanoplatelets acting as heat barrier, thereby increasing the thermal stability of the system as well as assisting in char formation during thermal decomposition. For all nano-biocomposites a char residue was obtained which indicated improved flammability characteristic of the system.

The lack of improvement or even the negative impact observed for the microcomposites resulting from the use of unmodified clay is particularly noticeable when looking at the materials mechanical properties determined on the blown films (machine and transverse directions) [17]. In this case, the addition of unmodified clay results in decreased tensile strength and elongation at break while keeping constant the modulus. However, the fine dispersion of organo-modified clays in intercalated/exfoliated nanocomposites allows increasing the tensile modulus while keeping an almost constant elongation at break.

The nano-biocomposites prepared using B109 nanoclay, which is a hectorite layered silicate, exhibited the best performance as compared with the other nanocomposites. As commonly observed, this is likely due to the homogeneous distribution and dispersion of nanoclay leading to a well intercalated structure, with possible partial exfoliation, accomplished through shear stress during melt compounding. Furthermore, this hectorite clay has platelets with a higher aspect ratio which, once finely dispersed in the matrix, create more surface area and thus induce improved performances as compared with the organically modified montmorillonites.

Authors also noticed that in all the cases, the nanocomposite hybrids exhibited higher performance in the machine direction, which is likely due to the uniform alignment and improved interfacial adhesion of the clay nanoplatelets within the PBAT matrix.

Interestingly, authors also studied the influence of maleic anhydride (MA) as compatibilizer to improve interfacial interactions [17]. According the authors, addition of MA during reactive extrusion allowed compatibilization through grafting reaction between the organoclays and the matrix, as evidenced by FT-IR analyses. All the reported characterizations clearly demonstrate the compatibilizing effect brought by maleic anhydride grafting onto PBAT.

In case of MA-g-PBAT/C30B and MA-g-PBAT/B109 nano-biocomposites, the X-ray diffraction patterns show absence of peak which indicates exfoliation of clay platelets. This is due to the fact that MA acts as a compatibilizing reagent by diffusing into clay galleries and forming chemical linkage between the anhydride group of MA and PBAT and layered silicates. This further results in an increase in the gallery spacing allowing the polymer chains to easily enter and break the

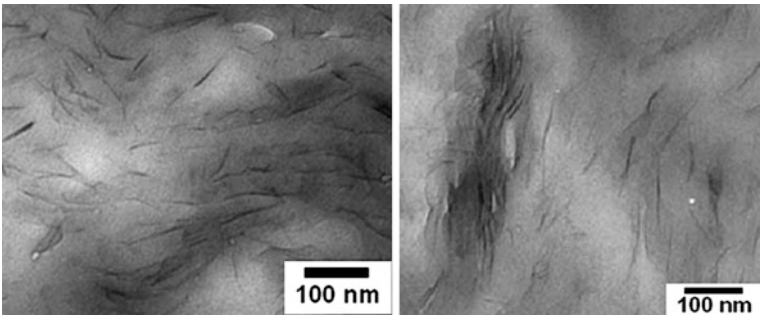

Fig. 8.4 TEM photographs of (*left*) MA-g-PBAT/C30B and (*right*) MA-g-PBAT/B109 nano-biocomposites showing clay exfoliation [17]

galleries during compounding resulting in exfoliated and improved dispersion (see Fig. 8.4).

As a result, nano-biocomposites based on MA-grafted PBAT display increased Tg and Tm values as well as markedly enhanced thermal stability. It is also observed that the grafted samples exhibited improved tensile modulus as compared with the ungrafted nano-biocomposites [17]. In case of MA-g-PBAT/C30B, the modulus increased of approximately 50 %. This is likely due to modification of interfacial region between PBAT matrix and C30B organoclay. MA acts as a bridge forming an ester linkage with the OH group of C30B while an intra molecular hydrogen bond is also formed between the carbonyl group of PBAT and hydroxyl groups of MA. Nanocomposites of B109, C20A with MA-g-PBAT also exhibited an increase in the Young's modulus which is probably due to the formation of inter molecular hydrogen bonding between hydrogenated tallow groups of these nanoclays and the MA-g-PBAT matrix. DMA results also evidenced that the grafted sample exhibited improved modulus as compared with the ungrafted nanocomposite hybrids. This further confirms improved interface between the nanofiller and the biopolymer matrix upon functionalization with MA.

The biodegradation behaviour under composting conditions has been studied for all the samples. The results confirmed that PBAT is a biodegradable polymer and that the incorporation of nanoclays does not hinder its inherent biodegradability [17]. It was observed that the rate of degradation of PBAT matrix increases with incorporation of unmodified nanoclay and marginally decreases for organo-modified nanoclays. The composites prepared using unmodified montmorillonite showed maximum biodegradation, which is probably due to hydrophilic nature of clay (see Fig. 8.5).

On the other hand, the rate of degradation decreased with organic modification of montmorillonite and grafting of PBAT matrix with MA. This could be due to the more hydrophobic nature of these nanoclays but may also result from the finely dispersed silicate layers. According to the authors, the fine dispersion in the PBAT matrix of clay platelets with large aspect ratio induces a more tortuous diffusion path

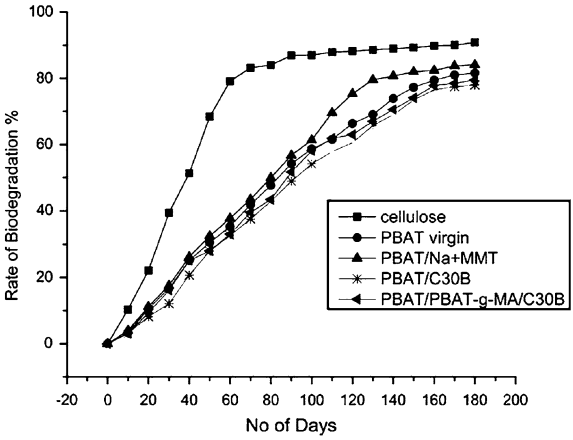

Fig. 8.5 Biodegradation rate of neat PBAT and corresponding nano-biocomposites [17]

for enzymes or water, resulting in a decreased biodegradation rate. Such results and explanation have also been reported by Someya et al. [11]. However, one cannot exclude that the clay organomodifiers (ammonium salts) may also contribute to the lower biodegradation rate due to their potential toxicity towards microorganisms.

Attempts to increase PBAT/OMMT nano-biocomposites biodegradability were also conducted by Nayak [18] who added to the blend 30 wt% of tapioca starch plasticized with water and glycerol. The influence of MA grafting compatibilization was also studied. Composting tests performed on these nano-biocomposites showed that the increase in biodegradation rate remains limited. However, the influence of thermo-plasticized starch (TPS) addition is markedly pronounced for the mechanical behaviour of the materials. Tensile tests revealed a 44 % increase in tensile modulus and a dramatic 776 % increase in elongation at break with the incorporation of 30 wt% TPS and C30B nanoclay. It is suggested that PBAT/TPS30 wt%/C30B3wt% shows maximum tensile modulus and elongation at break due to fine dispersion of silicate layers resulting from similarity in the surface polarity and interactions of C30B with TPS. Further grafting with MA also enhanced the mechanical properties, which was confirmed with improved morphology through SEM micrographs indicating reduction in the particulate size of TPS within the PBAT matrix with the addition of nanoclays. DMA and DSC analyses also confirmed the improved interactions between components leading to better morphology and enhanced properties for these nano-biocomposites.

Applying a similar strategy, Javadi et al. [19] prepared organoclay based nano-biocomposites from PBAT blended with PHBV and recycled wood fibres (RWF). Both solid and micro-cellular materials morphologies were obtained by melt blending and further injection molding. In these heterophasic systems the main improvements, in terms of mechanical properties, were brought by the addition of 10 wt% recycled wood fibres (with or without silane-based surface

treatment) to the neat PBAT:PHBV (weight ratio is 70:30) blend. The effects of adding 2 wt% nanoclay on the properties of PHBV/PBAT/silane-treated-RWF composites were also investigated. XRD analyses showed that the organo-modified clay led to nano-biocomposites exhibiting an intercalated structure. As far as microcellular foam-like materials are concerned, clay addition did not induce significant changes in the cell morphology (cell size and density). The well intercalated structure obtained from C30B did not lead to improved mechanical properties of the PHBV/PBAT/silane-treated-RWF composites. However, nanoclays dispersion did improve the thermal stability for both solid and microcellular materials with the first main degradation step (assigned to PHBV thermal degradation) being shifted by more than 10 °C on the TGA curves. Moreover, with the addition of organo-modified montmorillonite, the final ash content increased further since a major portion of nanoclay consists of silicates. As often observed and depicted, the increase in thermal stability induced by the addition of layered silicates in biopolymers arises from fact that nanoclays can act as a heat barrier, thereby increasing the thermal stability of the system.

Recently, Yang et al. [20] reported the elaboration of nano-biocomposites of PBAT and C30B by a solution-casting method. The effect of the clay loading on the crystallization behavior and physical properties of PBAT in PBAT/C30B nanocomposites was further investigated. As evidenced by the WAXD and TEM analyses, the nano-biocomposites films exhibited finely dispersed clay nanoplatelets with a very high degree of intercalation and substantial exfoliation at low clay contents (up to 5 wt%). As often depicted, higher clay contents led to intercalated clay aggregates remaining in the matrix with a less homogeneous dispersion. The DSC analyses showed that the glass-transition temperature (Tg) of PBAT remained almost unchanged despite the addition of C30B, whereas the melting temperature (Tm) slightly increased with increasing clay loadings in the nanocomposites. Globally, the basic thermal properties remained almost unchanged and, therefore, did not play a dominant role in the crystallization behavior of neat PBAT and its nanocomposites with different clay loadings. However, authors studied the non-isothermal crystallization, from the melt, of PBAT and the corresponding nano-biocomposites. The performed analyses combined to the different models applied demonstrated that C30B acted as a nucleating agent for the crystallization of PBAT. Moreover, the nucleation activity was first improved with increasing C30B contents when the clay loadings were <5 wt% and then decreased when the C30B loading further increased to 8 wt%. This was attributed to the better dispersion and higher intercalation degree observed at lower clay contents and to the clay agglomeration occurring at high loadings (i.e., 8 wt%), which decreased the nucleation effect of C30B. Such nucleating effect is consistent with previously reported results (Chivrac et al. [14]) and is also confirmed by the polarized optical microscopy (POM) observations (see Fig. 8.6).

The microphotographs showed that the PBAT spherulites became smaller and their density increased significantly with an increase in clay content as a

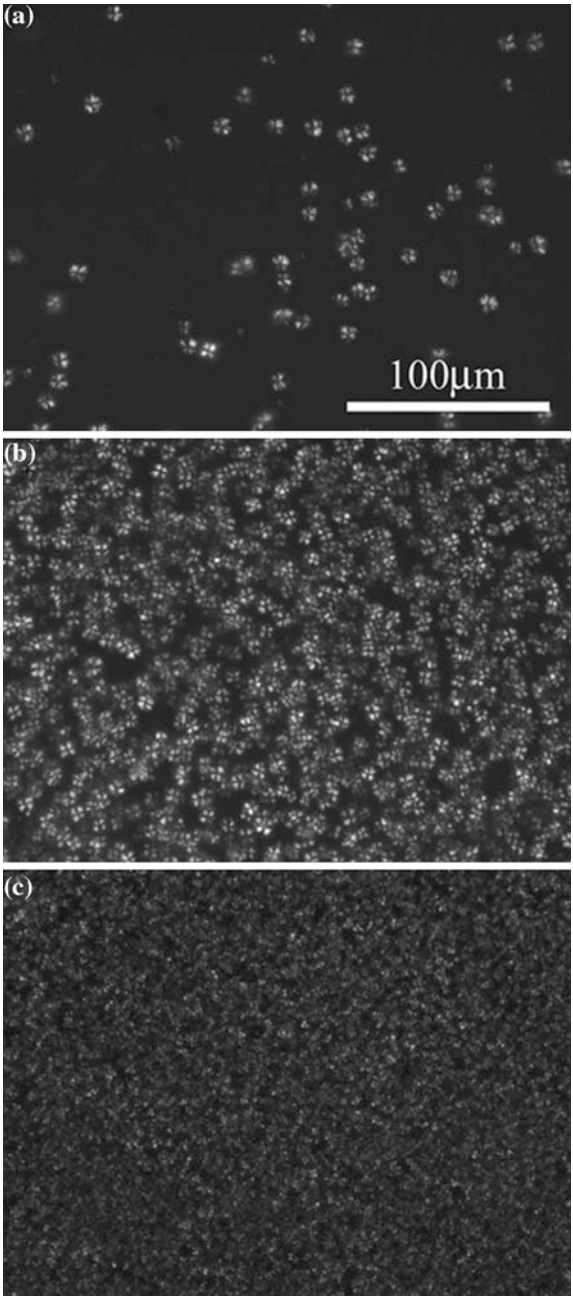

Fig. 8.6 POM images of **a** neat PBAT, **b** PBAT/C30B-2 wt% nanocomposite, and **c** PBAT/C30B-5 wt% nanocomposite crystallized at 120 °C for 30 min from the melt [20]

consequence of a heterogeneous nucleation effect of C30B. In conclusion, the addition of finely dispersed C30B in the PBAT matrix had a significant influence on the spherulitic morphology and overall crystallization process of PBAT [20].

The crystal structure of neat PBAT and PBAT/C30B nano-biocomposites with different clay loadings was investigated with WAXD. The presented diffraction patterns exhibited almost the same diffraction peaks at the same locations which indicated that the incorporation of C30B did not modify the crystal structure of PBAT.

Moreover, no positive effect on the PBAT thermal stability was observed upon clay addition. Indeed, the thermal stability of the PBAT/C30B nanocomposites decreased slightly versus that of neat PBAT, most likely because of C30B having a lower thermal stability. In addition, one cannot exclude thermal degradation of the matrix induced by the C30B organoclay.

As far as dynamic mechanical properties are concerned, it was observed a significant enhancement of E' for all the PBAT/C30B nanocomposites when the temperature was below Tg. However, the degree of enhancement of E' showed a different temperature dependence for these nano-biocomposites. Obviously, whatever the clay content in the nano-biocomposites, the increase in storage modulus is much more limited at temperatures above Tg.

As a conclusion, PBAT/C30B nanocomposites prepared by a solution-casting method from a chloroform solution led to intercalated morphologies with partial exfoliation. This resulted in high nucleating effect from the finely dispersed nanoclays and thus increased mechanical properties, as already reported in previous studies [14].

Thus, despite the numerous studies conducted so far on clay-based nano-biocomposites, only few articles report studies of PBAT/clay nano-biocomposites. According to the literature results, intercalated structure is the predominant materials morphology and clay exfoliation remains difficult to reach for PBAT nano-biocomposites based on commercial organoclays (see Table 8.3).

However, one has to notice the recent development of various studies on PBAT and nanoclays based materials used as a minor component in blends (either with biopolymers or with non biodegradable petroleum-based matrices such as PLA, PBS, PVC, etc.) to tune and control some of the material properties [21–25]. Since PBAT is only a minor constituent of these blends, these studies are not reported here.

Recently, Siva Kumar et al. [26] reported the synthesis, characterization and thermal studies of the random copolyester poly (butylene sebacate-co-butylene isophthalate) (PBSeI) and its nano-biocomposites, using organo-modified octadecyl ammonium-modified MMT clay by the solvent intercalation method. Here, the aliphatic-aromatic random copolyester has been synthesized by melt polycondensation using isophtalic acid, sebacic acid and butanediol, resulting in a copolyester having a slightly different structure compared to the commercially available PBAT (see Fig. 8.7).

The nanocomposites characterization showed that clay addition led to increased T_g, thermal stability and charring as a result of a mostly intercalated morphology.

One of the most interesting things in this study is that it opens the way for the elaboration of nano-biocomposites materials based on new aliphatic-aromatic copolyesters. Such perspective could represent a very interesting and promising

Table 8.3 Structure of the studied PBAT/clay nano-biocomposites

Process	System	Structure	References
Solvent intercalation	MMT-$N^+(Me)_2(tallow)_2$/chloroform	Intercalated	[13]
	MMT-$N^+(Me)_2(CH_2$-$\phi)$(tallow)/ chloroform	Intercalated	[13]
	MMT-$N^+(Me)(EtOH)_2$(tallow)/ chloroform	Intercalated/ exfoliated	[20]
Melt intercalation	MMT-$NH_3^+(C_{12})$	Intercalated	[9]
	MMT-$NH_3^+(C_{18})$	Intercalated/ exfoliated	[9]
	MMT-$NH^+(EtOH)_2(C_{12})$	Intercalated	[9]
	MMT-$N^+(Me)_2(tallow)_2$	Intercalated	[13, 16, 17]
	MMT-$N^+(Me)_2(CH_2$-$\phi)$(tallow)	Intercalated	[13]
	MMT-$N^+(Me)(EtOH)_2$(tallow)	Intercalated/ exfoliated	[12, 13, 17]
	HEC-$N^+(Me)_2(tallow)_2$	Intercalated	[17]
Melt intercalation with compatibilization	MMT-$N^+(Me)(EtOH)_2$(tallow)-g-PCL + PBAT	Intercalated	[12]
	MMT-$N^+(Me)(EtOH)_2$(tallow) + MA-g-PBAT	Exfoliated	[17]
	HEC-$N^+(Me)_2(tallow)_2$ + MA-g-PBAT	Exfoliated	[17]

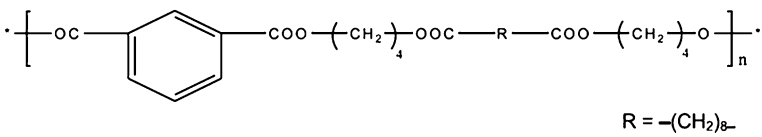

Fig. 8.7 Structure of poly(butylene sebacate-co-butylene isophthalate) (PBSeI) copolyester

field of investigations since one can expect in a near future the availability of bio-based monomers (or building blocks) such as diols and diacids obtained from the biomass, for the synthesis of renewable aliphatic-aromatic copolyesters.

8.3 Summary and Future Trends

As previously described, a large range of (organo-)clays has been tested to elaborate PBAT nano-biocomposites with the aim to improve mechanical and thermal properties of the polyester matrix while maintaining its biodegradability. Most of the reported studies use the melt-intercalation route to obtain such nanohybrids materials. According to the morphology of the obtained materials (see Table 8.3), intercalated structures are predominant and clay exfoliation seems

quite difficult to reach by simply using commercial organoclays. As often depicted for polyester-based nano-biocomposites, the best results in terms of clay dispersion and material properties are obtained with organo-clay bearing hydroxyl group and thus having better polarity matching with the matrix. As already observed in other systems, compatibilization through maleic anhydride grafting seems to facilitate the clay platelets exfoliation, resulting in further improved material properties. For all intercalated structures, slight increase in stiffness is observed but the influence of clay addition on thermal properties seems to be much more limited. Various studies report the impact of clay platelets dispersion on the PBAT crystallization with enhanced nucleation. Even if a large majority of the reported studies deals with montmorillonite clay, interesting results were also obtained with hectorite. Another interesting study concerns the elaboration of clay-based nanocomposites from original aliphatic-aromatic copolyesters. With the recent development of renewable bio-based alternatives for diacids and diols monomers (e.g. succinic acid, propanediol, etc.), one may expect future developments of bio-based aliphatic-aromatic copolyesters which properties could be further improved by the dispersion of mineral nanofillers.

References

1. Witt U, Müller R.-J, Augusta J, Widdecke H, Deckwer W.-D (1994) Synthesis, properties and biodegradability of polyesters based on 1,3-propanediol. Macromol Chem Phys 195(2): 793–802
2. Marten E, Muller R.-J, Deckwer W.-D (2005) Studies on the enzymatic hydrolysis of polyesters. II. Aliphatic-aromatic copolyesters. Polym Degrad Stab 88(3):371–381
3. Witt U, Muller R, Deckwer W (1997) Biodegradation behavior and material properties of aliphatic/aromatic polyesters of commercial importance. J Environ Polym Degrad 5(2):81–89
4. Muller RJ, Witt U, Rantze E, Deckwer WD (1998) Architecture of biodegradable copolyesters containing aromatic constituents. Polym Degrad Stab 59(1–3):203–208
5. Witt U, Muller R.-J, Deckwer W.-D (1995) New biodegradable polyester-copolymers from commodity chemicals with favorable use properties. J Environ Polym Degrad 3(4):215–223
6. Witt U, Einig T, Yamamoto M, Kleeberg I, Deckwer WD, Müller RJ (2001) Biodegradation of aliphatic-aromatic copolyesters: evaluation of the final biodegradability and ecotoxicological impact of degradation intermediates. Chemosphere 44(2):289–299
7. Rychter P, Kawalec M, Sobota M, Kurcok P, Kowalczuk M (2010) Study of aliphatic-aromatic copolyester degradation in sandy soil and its ecotoxicological impact. Biomacromolecules 11(4):839–847
8. Bastioli C (2005) Handbook of biodegradable polymers. Smithers Rapra Technology, UK
9. Someya Y, Sugahara Y, Shibata M (2005) Nanocomposites based on poly(butylene adipate-co-terephthalate) and montmorillonite. J Appl Polym Sci 95(2):386–392
10. Someya Y, Nakazato T, Teramoto N, Shibata M (2004) Thermal and mechanical properties of poly(butylene succinate) nanocomposites with various organo-modified montmorillonites. J Appl Polym Sci 91(3):1463–1475
11. Someya Y, Kondo N, Shibata M (2007) Biodegradation of poly(butylene adipate-co-butylene terephthalate)/layered-silicate nanocomposites. J Appl Polym Sci 106(2):730–736
12. Pollet E, Delcourt C, Alexandre M, Dubois P (2006) Transesterification catalysts to improve clay exfoliation in synthetic biodegradable polyester nanocomposites. Eur Polymer J 42(6):1330–1341

13. Chivrac F, Kadlecova Z, Pollet E, Averous L (2006) Aromatic copolyester-based nano-biocomposites: elaboration, structural characterization and properties. J Polym Environ 14(4):393–401
14. Chivrac F, Pollet E, Averous L (2007) Nonisothermal crystallization behavior of poly(butylene adipate-co-terephthalate)/clay nano-biocomposites. J Polym Sci B Polym Phys 45(13): 1503–1510
15. Lim ST, Hyun YH, Choi HJ, Jhon MS (2002) Synthetic biodegradable aliphatic polyester/ montmorillonite nanocomposites. Chem Mater 14(4):1839–1844
16. Shahlari M, Lee S (2008) Biodegradable polymer/clay nanocomposites based on poly(butylene adipate-co-terephthalate) and poly(lactic acid). In: AIChE annual meeting, conference proceedings, Philadelphia (USA), 16–21 Nov 2008
17. Mohanty S, Nayak SK (2010) Aromatic-aliphatic poly(butylene adipate-coterephthalate) bionanocomposite: Influence of organic modification on structure and properties. Polym Compos 31(7):1194–1204
18. Nayak SK (2010) Biodegradable PBAT/Starch nanocomposites. Polym Plast Technol Eng 49(14):1406–1418
19. Javadi A, Srithep Y, Lee J, Pilla S, Clemons C, Gong S, Turng L.-S (2010) Processing and characterization of solid and microcellular PHBV/PBAT blend and its RWF/nanoclay composites. Compos A Appl Sci Manuf 41(8):982–990
20. Yang F, Qiu Z (2011) Preparation, crystallization, and properties of biodegradable poly(butylene adipate-co-terephthalate)/organomodified montmorillonite nanocomposites. J Appl Polym Sci 119(3):1426–1434
21. Kumar M, Mohanty S, Nayak SK, Rahail Parvaiz M (2010) Effect of glycidyl methacrylate (GMA) on the thermal, mechanical and morphological property of biodegradable PLA/PBAT blend and its nanocomposites. Bioresour Technol 101(21):8406–8415
22. Jiang L, Liu B, Zhang J (2009) Properties of Poly(lactic acid)/Poly(butylene adipate-co-terephthalate)/Nanoparticle ternary composites. Ind Eng Chem Res 48(16):7594–7602
23. Chieng BW, Ibrahim NA, Wan Yunus WMZ (2010) Effect of organo-modified montmorillonite on poly(butylene succinate)/poly(butylene adipate-co-terephthalate) nanocomposites. Express Polym Lett 4(7):404–414
24. Ibrahim NA, Chieng BW, Wan Yunus WMZ (2010) Morphology, thermal and mechanical properties of biodegradable poly(butylene succinate)/poly(butylene adipate-co-terephthalate)/ clay nanocomposites. Polym Plast Technol Eng 49(15):1571–1580
25. Rahim M, Ibrahim N, Sharif J, Wan Yunus W (2010) Mechanical and thermal properties of poly(vinyl chloride)/poly(butylene adipate-co-terephthalate) clay nanocomposites. J Reinf Plast Compos 29(21):3219–3225
26. Siva Kumar G, Nanthini R (2010) Synthesis and characterization of aliphatic-aromatic random copolyester/clay nano-biocomposites. High Perform Polym 22(2):131–144

Chapter 9
Permeability in Clay/Polyesters Nano-Biocomposites

Andrea Sorrentino, Giuliana Gorrasi and Vittoria Vittoria

Abstract In this chapter we focus on the barrier properties of nanocomposite of biodegradable polyesters with layered inorganic fillers. First of all, to better understand the influence of the lamellar inorganic fillers on the permeability, the theory of permeation and the barrier models so far developed for polymer nanocomposites are reviewed. Afterwards the barrier properties of the most important biodegradable polyesters filled with inorganic lamellar solids, such as Polylactic acid (PLA), Polycaprolactone (PCL), Polyhydroxbutyrate (PHB), and Polybutylenesuccinate (PBS) are reviewed and the outstanding results enlightened. As a general trend, the best improvement of barrier properties is related to the exfoliation of clay platelets into the polymeric matrix, and this in turn is dependent on the chemical structure of the clay, the organic modification, the filler concentration and the processing procedure to prepare the composite. Where possible, all these parameters were reported and correlated with the final properties. Also the contrasting effect of clays on the two parameters determining the water permeability, that is sorption and diffusion, is reported in many cases.

A. Sorrentino (✉)
IMCB, National Research Council, P.le Enrico Fermi 1,
80055 Portici (Napoli), Italy
e-mail: asorrent@unisa.it

G. Gorrasi · V. Vittoria
DIIN, University of Salerno, via Ponte Don Melillo,
84084 Fisciano (Salerno), Italy
e-mail: ggorrasi@unisa.it

V. Vittoria
e-mail: vvittori@unisa.it

L. Avérous and E. Pollet (eds.), *Environmental Silicate Nano-Biocomposites*,
Green Energy and Technology, DOI: 10.1007/978-1-4471-4108-2_9,

9.1 Introduction

Bio-based polymers offer a sustainable alternative to traditional synthetic polymers, especially in short lifetime products such as packaging materials. Derived from natural organic resources, these types of polymers degrade under natural conditions in a time period ranging from several weeks to several months [1, 2].

Although most bio-based polymers have excellent properties, comparable to many oil-based plastics, these polymers, however, exhibit many undesirable physical properties, such as poor mechanical, thermal and barrier properties [1, 2]. In particular the barrier properties, especially to water, are to be improved to avoid loss of mechanical properties for exposition to humid environments [3, 4]. Therefore, the development of biodegradable polymeric materials with good barrier properties has become the focus of highly active research worldwide [5, 6].

One of the most promising routes in the current research is represented by the dispersion of inorganic nanofillers in the pristine polymers to prepare nanocomposites [7, 8].

Among the available nanometric fillers, particular interest has been raised up by organically modified layered silicate. The composites obtained with these fillers demonstrated so far significant enhancement, with respect to the starting polymer, including thermal stability, flammability resistance and barrier properties, without affecting or even increasing the rate of biodegradability [9, 10].

The key for nanocomposite technology is exfoliation of the clay into individual platelets, thereby achieving the greatest barrier properties as well as the lowest haze [8, 10, 11].

The interfaces between the organic and inorganic phases in the nanocomposites play the main role in the development of both the filler dispersion and the final properties. Due to the nanometric dimensions of the filler, the amount of these interfaces is enormous and characterizes all the composite properties. They, in fact, influence the load transfer between the organic and inorganic phases for the mechanical performance, the heat transfer for the heat resistance and the penetration of the molecules for the barrier resistance [8, 11].

The barrier properties, in particular, are very sensitive to the compatibility at the interface between the organic and inorganic phases. An incompatibility at the interface may lead to the generation of micro voids, leading to the higher extents of permeation through the composite materials as a function of filler volume fraction. The barrier properties may also be negatively impacted by the presence of small amount of low molecular weight compatibilizer which is generally added in the non-polar polymer composites to facilitate the nanoscale dispersion of the filler platelets in the high molecular weight polymer matrix. However, there are some experimental evidences that demonstrate how oxidized waxes or polyethylene are more efficient than higher molar mass maleic anhydride grafted PE to improve gas barrier properties of PE/montmorillonite systems [12, 13].

It is quite simple to obtain a nanocomposite in which mechanical properties are improved, but the barrier properties are strongly deteriorated with respect to the pristine material [10, 14–16].

9.2 Theory of Permeation

In a polymer film, the permeability coefficient, P, is defined as the flux of penetrant through the polymer, J, normalized by the film thickness, y, the sample surface area, S, the time t and the partial pressure difference between the upstream and downstream Δp (Eq. 9.1):

$$P = \frac{J \cdot y}{S \cdot t \cdot \Delta p} \tag{9.1}$$

The steady-state transport properties of water vapor in barrier polymers are characterized by water vapor transmission rate (WVTR) [15]. The dimensions of WVTR are quantity of water transmitted through a film times thickness divided by area and time.

The penetrant transport through polymers is characterized essentially by the molecules diffusion process that typically follows the Fick's law [17] (Eq. 9.2):

$$J = -D \cdot \frac{\partial C}{\partial x} \tag{9.2}$$

where D is the effective diffusion coefficient for the penetrant in the polymer and $\frac{\partial C}{\partial x}$ is the local concentration gradient of the penetrant. According to Eq. 9.2, the diffusion coefficient is a kinetic term characterizing the mass flux of penetrant through a polymer film in response to a concentration gradient [18]. When the downstream side penetrant concentration is negligible relative to that on the upstream face of the film, using Fick's law of diffusion (Eq. 9.2), permeability can be expressed as product of the effective diffusion coefficient D and the solubility coefficient S, which is the ratio of the equilibrium penetrant concentration in the polymer, C, divided by the penetrant partial pressure, p (Eq. 9.3):

$$P = D \cdot S \tag{9.3}$$

When the penetrants of interest are vapors or liquids, the partial pressure is often replaced by penetrant activity [19].

The permeability in polymers depends on many factors including system temperature and pressure, polymer matrix nature and morphology, penetrant molecules dimension and activity, etc. [20].

In biopolymers, deviations from Fickian behaviour often occur especially at relatively high activity [21]. These deviations are generally believed to arise as a consequence of the finite rate of polymer structure reorganization in response to penetrant-induced swelling during the sorption–diffusion process. An example of so-called non-Fickian diffusion behaviour is the penetrant sorbing into the polymer in two stages, an initial Fickian-like stage followed by a protracted, slow drift toward the final equilibrium sorption value [21–23].

Penetrant diffusivity, and hence permeability, can also be decreased by adding substituents to the polymer chain that reduce chain flexibility without increasing

the free volume fraction. Bulky side groups or rigid linkages such as aromatic groups decrease chain flexibility and hence reduce penetrant diffusion coefficients.

Also the crystallinity in a polymer generally affects both solubility and diffusion coefficients. For most polymers and penetrants of interest, crystalline regions, which are much more dense and well ordered than amorphous regions, preclude penetrant sorption, thereby reducing penetrant solubility. Additionally, the presence of impermeable crystallites in a polymer matrix acts as barriers to diffusion, increasing the path length for diffusion and, in some cases, increasing the amorphous interface chain rigidity [22–24].

The permeability of a polymer can be also influenced by the mechanical deformation and chain orientation. Impermeable polymer crystallites may become oriented into fibrous-like structures during deformation, and this process generally decreases penetrant diffusivity by increasing tortuosity. In addition, drawing of semicrystalline polymers can improve barrier properties through stress-induced crystallization and orientation of the remaining amorphous phase [25]. In some cases, a permeability increase was observed as consequence of microvoid development during orientation of the polymer chains after crystallinity was fully developed [26].

The absorption of water can increase, decrease, or have no effect on gas permeability of barrier polymers. Hydrophilic barrier polymers, generally, lose their barrier properties with increasing the relative humidity, RH. This is because water acts as a plasticizer and increases the free volume of the polymer [19, 20, 24].

9.3 Barrier Model in Polymer Nanocomposites

The effect of impermeable particles on the diffusion through polymer matrix can be expressed using the following model (Eq. 9.4):

$$D = \frac{D_m \cdot \beta}{\tau} \tag{9.4}$$

where D_m is the penetrant diffusion coefficient in the polymer matrix, τ is a geometric impedance (i.e, tortuosity) factor, and β is a factor that takes into account both, the chain immobilization and the interface formation due to the filler particles [27]. In particular, depending on the filler-penetrants interactions, β can be higher or lower than the unity. Impermeable particles force penetrants to follow a tortuous pathway through the permeable polymer regions. This effect is captured by the factor τ, which is the ratio of the average distance traveled by a penetrant molecule to the thickness of the sample. τ can be a complex function of particles content as well as particles size, shape, and orientation (Fig. 9.1). Its value can be derived by geometric considerations as shown in Fig. 9.1.

Heterogeneous particles can also restrict segmental mobility by acting as physical cross-links. This effect is taken into account by the factor β. In glassy polymers such as PET, the inherent rigidity of the chain backbone imposes more

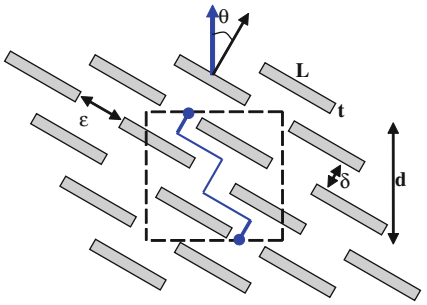

Fig. 9.1 Idealized model for the tortuosity factor calculation [10]

impedance to chain mobility than the particles and hence, β is one. A two-phase model is often used to describe penetrant solubility in a polymeric composite (Eq. 9.5) [20]:

$$S = S_m \cdot \chi_p \tag{9.5}$$

where S_m is solubility coefficient in the neat polymer matrix and $\varkappa_p$ is the polymer volume fraction. This model assumes that the solubility of penetrant within the filler particles is zero, and that the presence of particles does not change the amorphous phase solubility coefficient.

The simplest and most commonly used model for the effect of particles on steady-state permeability is based on the previous assumptions and is expressed by the following relationship (Eq. 9.6):

$$P = \left(S_m \cdot \chi_p\right) \times \left(\frac{D_m \cdot \beta}{\tau}\right) \tag{9.6}$$

The permeation of gases through mineral filled polymers was first dealt in model by Nielsen [28]. In this model, the gas permeability of the nanocomposites (P_c) is related to the permeability of the neat polymer (P_o) and the volume fraction (χ_p), length (L), and width of the clays (t), as in Eq. 9.7:

$$\frac{P_c}{P_0} = \left(1 + \frac{L}{2t}\chi_p\right)^{-1} \tag{9.7}$$

Fredrickson and Bicerano [29] found that in the dilute regime, (where the product of the aspect ratio α and volume fraction χ is small compared with unity), the "modified Nielsen" formula (Eq. 9.8) can be a useful approximation for randomly distributed disks with no spatial correlations:

$$\frac{D_c}{D_0} = \left(1 + \frac{\pi\alpha\chi}{2\ln\left(\frac{\alpha}{2}\right)}\right)^{-1} \tag{9.8}$$

The previous models assumed nanoplatelets of uniform size. For a continuous distribution of sizes, and constant thickness (t) Lape et al. [30] found (Eq. 9.9):

$$\frac{D_c}{D_0} = \left(1 + \frac{2\chi}{3 \cdot t \cdot \Lambda \cdot \left(\Lambda^2 + \psi^2\right)}\right)^{-1} \tag{9.9}$$

where Λ is the average size of the nanoplatelets and ψ is the deviation.

The previous model assumed that the sheets are placed perpendicular to the diffusive pathway. However, it is only an extreme condition with respect to all the physical situations. In order to overcome this problem, Bharadwaj [9] proposed to introduce the sheet orientation on the relative diffusivity model (Eq. 9.10):

$$\frac{D_c}{D_0} = \left(1 + \frac{2}{3}\alpha\chi \cdot \left(S + \frac{1}{2}\right)\right)^{-1} \tag{9.10}$$

where the order parameter (S) represents a conventional Hermans orientation factor defined by Eq. 9.11:

$$S = \frac{1}{2}\left\langle 3\cos^2\theta - 1\right\rangle \tag{9.11}$$

where θ represents the angle between the diffusion direction and the sheet normal vectors, the square bracket indicate the average value over all the system.

Sorrentino et al. [27] proposed a model that predicts effective diffusivity in heterogeneous systems with dispersed impermeable domains of variable orientation and distribution. In addition to the sinuous pathways formation, the model takes into account the formation of an interface region between the polymer bulk and the clay sheets that can influence the barrier properties of the composite. The relative diffusivity can be expressed by the following Eq. 9.12:

$$\frac{D_{eff}}{D_0} = \frac{(1-\phi)}{\left[(1-\phi) + \phi\left(1 + \frac{L\cos\theta \ + \ 2t\sin\theta}{L\sin\theta \ + \ 2t\cos\theta}\right)^2\right]} \cdot (1 + \phi \cdot \beta) \tag{9.12}$$

where, θ represents the orientation angle and β represents the ratio between the interface diffusivity and the bulk polymer diffusivity [27].

Several experimental results, discussed and interpreted with the aid of the previous models, have show that in addition to the aspect ratio and clay concentration, the polymer clay interactions as well as the sheets orientation are important factors controlling the barrier properties [27].

9.4 Polylactic Acid

PLA is the biodegradable polymer with the highest potential for a commercial scale production of commodity materials [31, 32]. This polymer, in fact, can provide similar mechanical properties as conventional polymers, while having a

lower environmental impact. However, PLA has also disadvantages, such as poor thermal stability, brittleness, and low gas and water vapor barrier properties. In particular, the permeability of currently available PLA is not adequate for applications that require high gas and water vapor barriers, or when long storage period are required.

A possible route for overcoming these limitations is to blend the polymer with nanoscale fillers. In fact, many authors have prepared and analyzed nanocomposites of PLA [33–37].

Sinha Ray et al. [36] prepared a series of PLA nanocomposites using melt extrusion. All nanocomposites exhibited remarkable improvements of material properties such as mechanical properties, flexural properties, oxygen gas permeability, with a simultaneous improvement in biodegradability. Intercalated nanocomposites show very high mechanical properties whereas disordered intercalated or near to exfoliated nanocomposites have very high gas barrier property.

Pluta et al. [38] prepared PLA nanocomposites by melt intercalation in the presence of a stabilizer. They found an improvement in the nanocomposite thermal stability under oxidative conditions in comparison to those for the microcomposite and unfilled PLA.

Thermal analysis revealed that the crystallization temperature of PLA in both PLA/clay and LLDPE toughened PLA/clay nanocomposites decreased with increasing content of organophilic clay, indicating nucleating effect of clay [35]. However, the glass transition temperature increases only slightly with increasing clay content. This may be due to the micro-composite structure rather than nanocomposite structure [39].

Rhim et al. [40] reported that the water vapor transmission rate of PLA was influenced by clay addition. In particular WVTR was reduced in nanocomposite films compounded with organically modified clays but was slightly increased in films with unmodified clay. These results were mainly attributed to the hydrophobicity of the organically modified clays.

An enhanced oxygen barrier capacity for PLA was obtained by silicate clay PLA [41, 42]. In particular, the barrier properties of PLA nanocomposites were found to depend both on the particle size and on the dispersion [42, 43].

Sinha Ray et al. [42] also investigated the effect of blending organically modified clays with PLA. A montmorillonite modified with trimethyl octadecylammonium cation was blended at different percentages with PLA by melt extrusion (Fig. 9.2). For all three nanocomposite films, these blends led to an increase in the oxygen barrier capacity. In Fig. 9.2, the authors report the theoretical curve predicted by Eq. 9.7, considering $L/2t = 275$. This value, calculated experimentally from TEM photographs, fit quite well all the experimental results [42].

Maiti et al. [43] reported that the chain length of the organic modifier phosphonium salt had an effect on the dispersing capacity of different types of clays such as montmorillonite, smectite, and mica in blends with PLA. Furthermore the layered structure and gallery spacing of organoclays and PLA nanocomposites show that, with a modifier of the same chain length, the gallery spacing of the organoclay was largest for mica and smallest for smectite. The higher

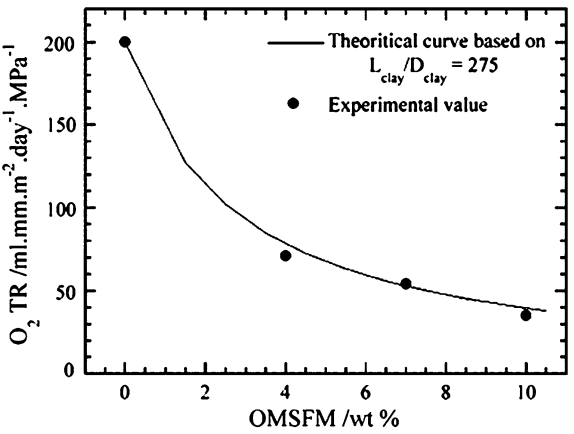

Fig. 9.2 Oxygen gas permeability of neat PLA and various PLA nanocomposites as a function of clay content at 20 °C and 90 % relative humidity. The filled circles represent the experimental data. Theoretical fits based on the Nelson tortuosity model [42]

ion-exchange capacity of mica and the physical jamming of the modifier likely caused a restricted conformation at the core part of the largest clay. The difference in the modulus between the nanocomposites and the PLA was larger in the case of smectite nanocomposites than for montmorillonite or mica nanocomposites, and this is due to the better dispersion in a smectite system for the same clay loading. As a well-dispersed system, smectite nanocomposites have better gas barrier properties than the montmorillonite or mica systems, which are larger in size but stacked in nature in their nanocomposites. In the well-dispersed smectite system, the intimate interaction between PLA and silicate layers may cause the local environment to be stiffer. As a result, both the modulus and barrier properties increase compared to those of the mica system.

Chowdhury [44] investigated the effect of clay aspect ratio and functional edge groups on the degree of order of two different montmorillonite clays and one fluoromica. Nanocomposites were compared with each other as well as with pure PLLA. X-ray diffraction and transmission electron microscopy results showed that both montmorillonite clays with a lower aspect ratio had better dispersion and a greater degree of disorder than fluoromica. Although the dimension of fluoromica was the highest among the three clays, the number of disks in a stack was higher (larger width) and its tactoid building blocks were ordered. Nanocomposites containing montmorillonite showed the highest oxygen barrier capacity.

In the Ref. [45], many types of organophilic clay was used as filler for the PLA. The oxygen permeabilities for all the nanocomposites with clay loadings up to 10 wt% were less than half of the corresponding values for neat PLA, regardless of the type of organoclay employed. For hybrid films, the tensile properties initially increased but afterwards decreased with the introduction of more inorganic phase.

Similarly, Thellen et al. [46] found that the oxygen and water vapor barrier properties of blown film processed PLA mixed with commercial modified clay

were higher than those of neat PLA films. Nanocomposite films showed a 48 % improvement in oxygen barrier and a 50 % improvement in water vapor barrier.

Ogata et al. [47] modified montmorillonite with distearyldimethylammonium chloride and blended it with PLA using chloroform as solvent. Results showed that the layers forming the clay were not individually dispersed in the PLA–clay blends. The clay, in the form of tactoids, formed a remarkable geometrical structure with their surfaces lay almost parallel to the film surface, and were stacked with the insertion of PLLA crystalline lamellae in the thickness direction of the film.

The authors [47] observed that this morphology allow the formation of plane-like voids during the drawing process of the film.

The use of nanoclays to improve the barrier properties of PLA blends was investigated by Plackett and Sodergard [48], who blended PLA with PCL and added nanoclays. They report a significant absorption of moisture for the PLA-PCL copolymer films. A significant reduction in oxygen was observed with the incorporation of nanoclays, but moisture absorption of the films also increased.

The incorporation of microcrystalline cellulose or bentonite, both at 5 wt%, was compared in PLA nanocomposites. The microcrystalline cellulose showed an improvement of tensile modulus without reducing the elongation at break, while the addition of bentonite resulted in reduced oxygen permeability [49]. The authors explain these differences suggesting that the bentonite material has theoretically twice the surface area of the microcrystalline cellulose. A larger surface area will allow the nanoreinforcement to interact with a larger amount of polymer chains and thereby having a larger effect on the mechanical and barrier properties.

The PLA/layered silicate nanocomposites, prepared by simple melt extrusion, exhibited remarkable improvement of material properties in both solid and melt states compared to the matrix without clay [50]. The oxygen permeability values for all the hybrids for clay loadings up to 10 wt% were less than half the corresponding values for pure PLA, regardless of the organoclay [51].

Koh et al. prepared PLA layered silicate nanocomposite membrane [52]. The authors reported that gas permeabilities of composites decreased with the increase of organoclay content. When compared to gas permeabilities of nanocomposites varying with types of organoclay, the barrier feature of nanocomposite with the better dispersion, as showed by X-ray diffraction patterns, was extremely outstanding. In other words, the nanocomposite membranes that had the largest d-spacing value resulted in a high gas barrier property give an estimation of the gas permeability decrease. [52, 53].

Cabedo et al. [54] reported the preparation of highly exfoliated nanocomposites of the PLA and PLA/PCL blends obtained by melt-mixing with a properly modified kaolinite. Raw PLA presents an oxygen permeability value of 1.125×10^{-18}(m^3 m)/(m^2 s Pa) and pristine PCL of 5.8×10^{-18} (m^3 m)/(m^2 s Pa). The addition of PCL to the PLA results in a significant decrease of the gas barrier properties, in the case of the blend containing 36 % PCL, the oxygen permeability has increased to 136 % with respect to the pure PLA. The decrease in the barrier properties is proportional to the amount of PCL added.

The nanocomposites showed enhanced gas barrier properties, due to the effect of the nanoplatelets on increasing the tortuosity factor across the film thickness. The oxygen permeability value of the PLA/Kaolinite is 6.25×10^{-19} (m^3 m)/(m^2 s Pa), while for the PCL/Kaolinite is 4.8×10^{-18} (m^3 m)/(m^2 s Pa), these values represent an increase in oxygen barrier of 43 and 17 % respectively. In the nanocomposite of the blend, the addition of the kaolinite nanofillers represent an increase of 27 %, being the actual value of 1.9×10^{-18} (m^3 m)/(m^2 s Pa). A blend of 20 % of PCL and 4 % kaolinite resulted in better processability, thermal stability and similar gas barrier properties as the neat PLA.

9.5 Poly(3-Hydroxybutyrate)

Poly(hydroxyalkanoates), PHA, constitute a group of biopolymers that is recently attracting much attention, due to their full biodegradability, biocompatibility and natural origin. Several applications have been proposed for these polymers in the fields of medicine, agriculture, and packaging.

The most studied and easily produced member of this family is poly(3-hydroxybutyrate), iPHB, an isotactic, high molecular weight polymer with a melting point around 172 °C, and a glass transition close to 0 °C. Produced by several microorganisms, iPHB can be used as a carbon and energy storage material. However, some drawbacks have prevented its introduction in the market as a valid alternative to the currently widespread non-degradable oil-based thermoplastics. Some of these drawbacks are its fragility, thermal degradability at temperatures not far above the melting point, and its high price.

Among the various strategies developed over the years to improve the properties of iPHB, copolymerization and blending have been so far used.

Several kinds of PHA copolymers have been described comprising structural units such as 3-hydroxyvalerate, 4-hydroxybutyrate, or 3-hydroxyhexanoate. These materials were explored to obtain an increased toughness by incorporating flexible units in the polymeric chain, as well as to improve the processability by reducing the melting temperature, so minimising the risk of thermal degradation [55–59].

The other main alternative to achieve better properties is blending with other polymers, both biodegradable and non biodegradable. Although many immiscible iPHB based blends have been described in the literature, it seems that little or no improvement in the physical properties is achieved in these cases, due to the incompatibility between iPHB and the second component. Some polymers that form immiscible blends with iPHB are ethylene-propylene rubber, ethylene -vinyl acetate copolymers, polystyrene, poly(methyl methacrylate), and polycaprolactone [60–64].

The water transport was also investigated in blends of PHB/LDPE in an effort to regulate the resistance to hydrolysis or (bio) degradation through the control of water permeability [65].

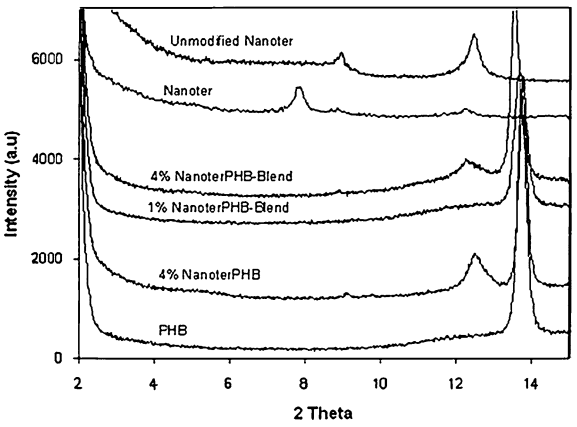

Fig. 9.3 X-ray diffractograms of the unmodified and modified kaolinite clays denoted unmodified Nanoter and Nanoter, respectively and of the various PHB nano-biocomposites [69]

Very recently the thermal, rheological, mechanical, and barrier properties of PHB with varying hydroxyvalerate content and different molecular weight were investigated. It was shown that the mechanical and barrier properties observed were greatly affected by the molecular weight of the polymers [66].

Recently, surface modified clays have been studied as advanced additives to improve or balance thermal, mechanical, fire resistance properties of nanocomposites because of high surface to volume ratios of clays and the subsequent intimate contact that they promote with the matrix at low filler additions. Aside from the enhancement in these properties, these clay platelets with very few nanometers (ideally one nanometer in fully exfoliated systems) in thickness have the potential to uniquely reduce the matrix permeability to gases and vapors, while maintaining largely unmodified interesting properties of the matrix such as toughness or transparency [67, 68].

Sanchez-Garcia et al. studied the morphological, thermal, and barrier properties of novel melt-mixed nano-biocomposites of PHB, poly(ε-caprolactones) (PCL), and layered phyllosilicates based on commercial organomodified kaolinite and montmorillonite clay additives [69].

They found that in the 4 % of phyllosilicate based on an organophilic surface modified kaolinite (Nanoter) in a PHB sample, blended with PCL, there was a better dispersion than in the 4 % Nanoter PBH sample, suggesting that a better dispersion of the organomodified clay may have been achieved through the use of the PCL component in the blends. From the SEM and the TEM results they considered reasonable to assume that a fraction of the clay has been, at the least, intercalated within the polymer matrix. Thus, they inferred that a better compatibilization of the organomodified clay with the PHB/PCL blend occurred [69].

Also the X-ray diffractograms, shown in Fig. 9.3, indicated that the blends seem to have a more favourable morphology in terms of dispersion than the organophilic surface modified kaolinite (indicated as Nanoter in figure) PHB samples.

Figure 9.4 shows, as an example, the oxygen transmission rate curves at 0 % RH of the 4 % NanoterPHB blend and of the unfilled PHB blend. From this figure, it is seen that the equilibrium transmission rate is higher in the unfilled blend than in the

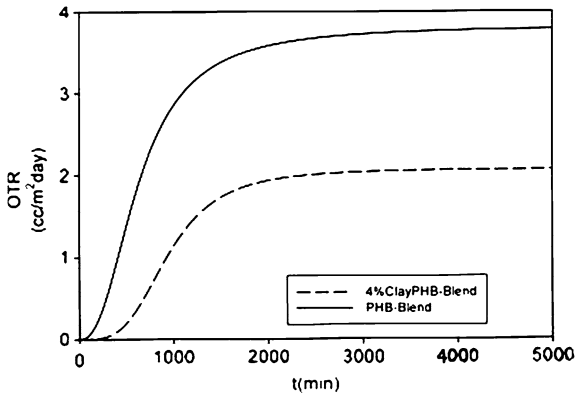

Fig. 9.4 Oxygen transmission rate curve of the PHB-Blend and of the 4 % NanoterPHB-Blend [69]

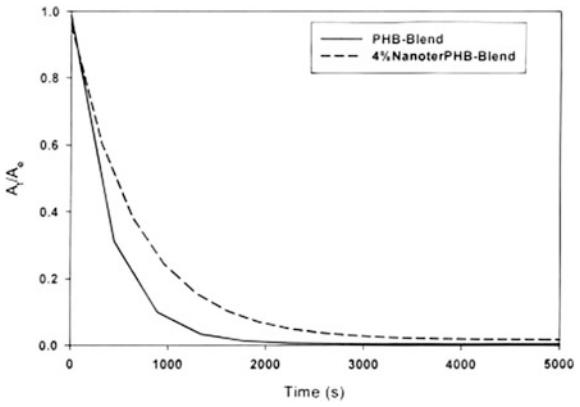

Fig. 9.5 Water desorption curves as follow by FTIR versus time for PHB-Blend and for 4 % NanoterPHB-Blend film specimens [69]

nanocomposite indicating that a lower permeability is reached in the nanocomposite systems, and that the diffusion appears faster in the unfilled blend.

Transport properties of water and limonene were investigated for the modified kaolinite composites, too. Figure 9.5 shows water desorption curves of unfilled and filled blends from equilibrium saturation conditions. From the data in Fig. 9.5, a diffusion coefficient was estimated and it resulted that the diffusion coefficient of water in the composite was reduced by about 70 % compared to the unfilled polymer blend during desorption. Nevertheless, the solubility was seen to increase in the composite blend. This means that the nanocomposite uptakes about 50 % more water than the unfilled blend due to likely the existing hydrophilic sites of the filler. On the whole, as the water permeability is the product of D and S, the reduction in diffusion is seen larger than the 50 % increase in solubility, determining a decrease of permeability.

Experimental results show that a reduction in permeability of 67 % and of 60 % in the diffusion coefficient is observed in the biocomposite for limonene. On the other hand, the limonene solubility shows the opposite behavior and increased in

the nanocomposite by 27 %. This is likely the result of the affinity of the organophilic sites of the filler for this less hydrophilic component.

9.6 Poly(Butylene Succinate)

Poly(butylene succinate), synthesized by the polycondensation of 1, 4-butanediol with succinic acid, has particularly attracted increasing commercial interest because of its many interesting properties, including biodegradability, melt processability, and thermal and chemical resistance [70–74].

In the past, the high price of petrochemically derived succinic acid has limited PBS acceptance into general use. Nowadays succinic acid can be obtained from the fermentation of sugars, and is becoming one of the most important value added chemicals from biomass from which many other industrially important chemicals can be derived [75–78].

PBS has physical and processing qualities in some respects similar to polyethylene making it more amenable to commercial adoption [79–81]. However, its softness and low gas-barrier properties have restricted further applications in many fields.

In spite of the importance of barrier properties for enhancing the properties, very few studies of these properties in PBS nanocomposites have been reported. Shih et al. presented a study of gas permeability in PBS nanocomposites [82]. Various nanocomposites of poly(butylene succinates) (PBS) with different ratios of organically modified layered silicates (OMLS) were prepared. Moreover, such PBS nanocomposites cross-linked by dicumyl peroxide (DCP) were also prepared in their work. OMLS were prepared by replacing Na + ions with cetyl pyridinium chloride (CPC) by means of ion exchange reactions. PBS (Bionolle) containing 1, 3, 5, 10 wt% of these OMLS (PBSMC1, PBSMC3, PBSMC5, PBSMC10, respectively) were prepared. Moreover, these nanocomposites were further cured by dicumyl peroxide to obtain cross-linked nanocomposites (PBSDMC1, PBSDMC3, PBSDMC5, and PBSDMC10).

WAXD indicated that the layers of clay were intercalated by the modifiers, and that the interlayer distance of OMLS in the nanocomposites could be expanded to about 2.96 nm, as shown in Figs. 9.6 and 9.7 for uncross linked and cross linked nanocomposites, respectively.

Gas permeability properties were investigated and the results of oxygen permeation test are shown in Fig. 9.8, in which the relative permeability is reported as a function of clay content for both the un-cross-linked (PB SMC) and crosslinked (PB SDMC) composites.

Oxygen relative permeability (P_o/P_p) is obtained by dividing the oxygen permeability coefficient of samples (P_o) with that of pristine PBS (P_p). The oxygen permeability coefficient was decreased with increases in the content of the organoclay, for both PBSMC and PBSDMC nanocomposites. When the content of organoclay reached 10 % (PBSMC10 and PBSDMC10), the decrement of the

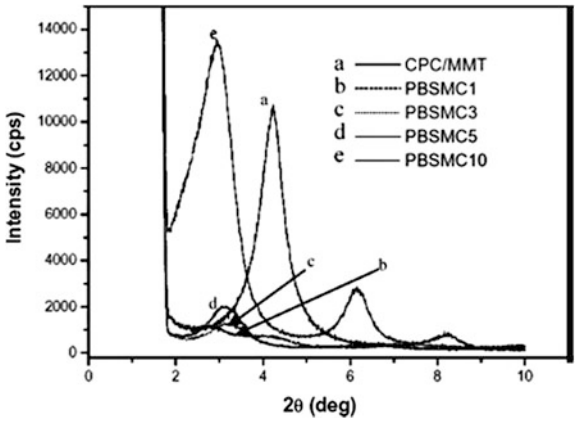

Fig. 9.6 WAXD Patterns of PBSMC composites [82]

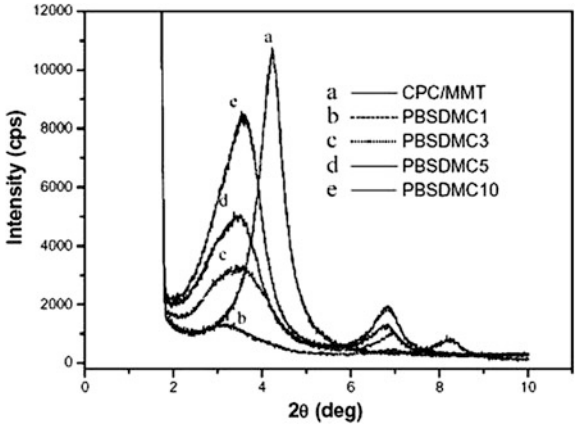

Fig. 9.7 WAXD Patterns of PBSDMC composites [82]

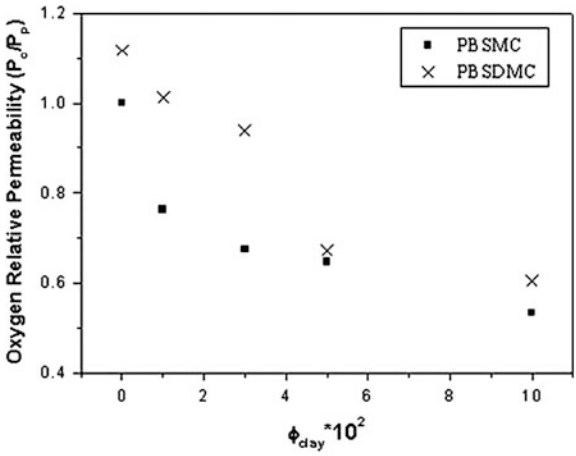

Fig. 9.8 Oxygen permeation rates of the nanocomposites as a function of the organoclay contents, for both un-cross linked (PB SMC) and cross-linked (PB SDMC) [82]

oxygen permeability coefficient reached about 46 % and 39 %, respectively. It is important to note that the cross-linked network structure was not able to enhance the barrier property of PBS. The oxygen permeability coefficient of cross-linked PBS1D was larger than that of the pristine PBS sample. Moreover, the decrements of oxygen permeability coefficient for the cross-linked PBSDMC nanocomposites also seemed smaller than those of un-cross-linked PBSMC ones. This was attributed to less homogeneity between the organoclay and cross-linked PBS, leading to a shorter path away from the cross-linked area. These results revealed that the gas permeability of PBS was effectively depressed by the addition of organoclay.

Organo-montmorillonite (OMMT)-filled poly(butylene succinate) (PBS) nanocomposites were recently prepared by a melt mixing process with internal mixer, at various loading levels (i.e., 2–10 wt%) of OMMT. The effects of clay loading towards the mechanical and thermal properties were investigated through various characterizations such as melt flow index (MFI), density, mechanical tests, X-ray diffraction (XRD), transmission electron microscopy (TEM), heat deflection temperature (HDT), and differential scanning calorimetry (DSC). The 2 wt% OMMT-filled PBS gave the highest strength among the rest due to higher degree of exfoliation of layered silicates in PBS matrix. Further increment in OMMT loading reduced the strength of nanocomposites, due to possible agglomerations. However, increment in clay loading enhanced the modulus of nanocomposites. Moisture absorption was studied in a large range of water activity and the results showed that higher OMMT loading and moisture level tend to increase the overall moisture uptake and also the diffusion coefficient [83].

Very recently PBS was blended with thermoplastic starch (TPS) to improve the mechanical properties and reduce water absorption of the resulting starch-based plastics. The miscibility between TPS and PBS was enhanced by reactive extrusion of TPS with functionalized PBS (RPBS). Hydrophobicity was enhanced and water absorption was reduced significantly in comparison with TPS [84]. In addition was found that the water absorption of the blend was significantly reduced with increasing RPBS content.

To improve PBS properties, beside the conventional method to blend PBS with other materials [85, 86], PBS-based nanocomposites are being developed as an emerging method to obtain better physical properties, and many PBS-based nanocomposites have recently been prepared for different applications [87–90].

9.7 Poly(ε-Caprolactone)

Poly(ε-caprolactone) (PCL) is a biodegradable aliphatic polyester that is currently being investigated for use in medical devices, pharmaceutical controlled release systems, and in degradable packaging. Preparation of PCL nanocomposites using silicates and/or organically modified silicates, maximizing their aspect ratios, has been demonstrated a satisfactory route for improving its physical and, in particular, barrier properties. The high permeability of pure PCL is an advantage when it is

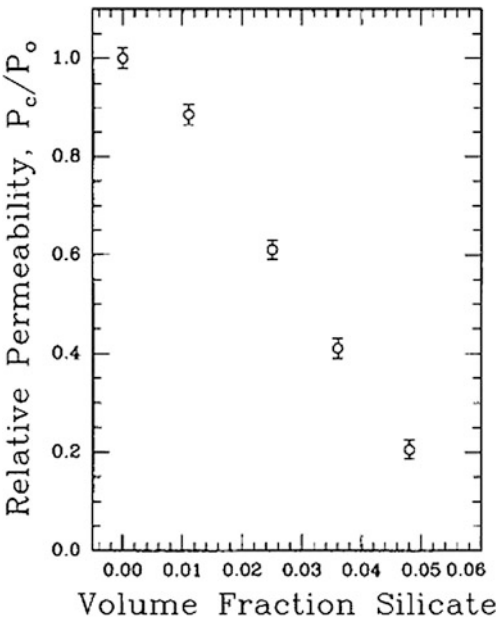

Fig. 9.9 Relative permeability versus volume fraction for nanocomposite films [91]

used as a biomedical material, but it is a drawback when applied to environmental fields. The barrier properties of PCL can be enhanced by introducing layered silicates into the matrix controlling the chemistry of the organic modifiers and the processing parameters for obtaining nanocomposites.

Messersmith and Giannelis [91] firstly reported the synthesis of PCL nanocomposite consisting of high aspect ratio layers of mica-type silicate embedded in a poly(ε-caprolactone) matrix. The nanocomposites were prepared by reacting a protonated amino acid-exchanged montmorillonite with ε-caprolactone monomer. Permeability to water at 75 % of relative humidity under steady state conditions was evaluated. It was reduced by nearly an order of magnitude at only 4.8 % silicate by volume. Figure 9.9 reports the relative permeability versus volume fraction of silicate.

The lowering of permeability in the nanocomposites was imputed to the presence of dispersed large aspect ratio silicate layers in the polymer matrix, whose orientation in-plane was favoured by the solvent casting technique, which created a tortuous pathway for the penetrating water molecules.

Gorrasi et al. [92] reported the preparation and analysis of barrier properties of different compositions of PCL and montmorillonite (MMT) obtained by melt blending or catalyzed ring opening polymerization of ε-caprolactone from Cloisite 30B, (MMT-$(OH)_2$). Microphase composites were obtained by direct melt blending of PCL and sodium montmorillonite (MMT-Na^+). Exfoliated nanocomposites were obtained by in situ ring opening polymerization of ε-caprolactone with an organo-modified montmorillonite (MMT-$(OH)_2$) by using dibutyltin dimethoxide as an initiator/catalyst. Intercalated nanocomposites were formed

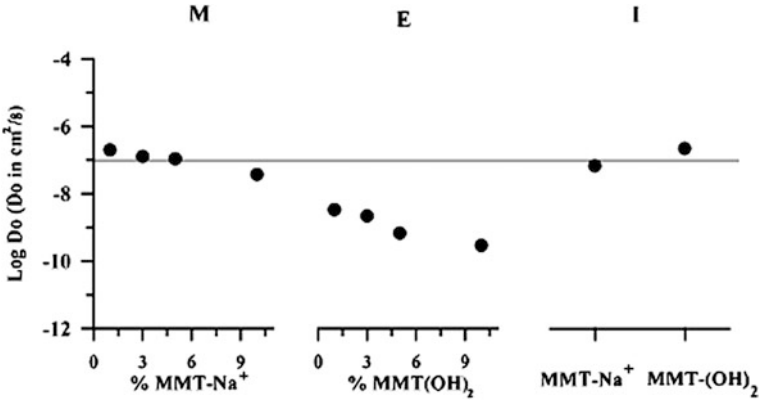

Fig. 9.10 Diffusivity to water vapor, as function of clay content for the micro-composite (M), the exfoliated nanocomposites (E) and the 3 wt% intercalated nanocomposites (I) [92]

either by melt blending with $MMT(OH)_2$ or in situ polymerization within $MMT\text{-}Na^+$. The sorption (S) and the thermodynamic diffusion parameter (D) were evaluated for water and dichloromethane vapors. Both microcomposites and intercalated nanocomposites showed diffusion parameters very near to PCL. Exfoliated nanocomposites showed much lower values, even for small MMT content. D parameters were compared to those of the parent PCL: both exfoliated and intercalated samples showed lower values, due to a more tortuous path for the penetrant molecules. The influence of the morphology on the diffusion parameter is illustrated in Fig. 9.10 where it is shown log D as a function of the MMT content for the microcomposites (M), the exfoliated nanocomposites (E), and the 3 wt% intercalated composites (I). The horizontal straight line represented the D of the pure unfilled PCL. Taking into account the logarithmic scale, the values for the microcomposites and intercalated nanocomposites are distributed around the PCL value, while the exfoliated nanocomposites strongly deviate, even at low montmorillonite content. The exfoliation of the inorganic component in the continuous PCL phase has been demonstrated to be a pre-requisite for improving the barrier properties of the material to the water vapor.

Authors suggested that in the micro-composite or in the intercalated samples, the ordered structure of the inorganic component did not constitute a barrier to the diffusion of the water molecules that can jump from one specific site to another. This diffusion mechanism is not possible when the structure is exfoliated, since there is no continuity in the inorganic phase. In the last case the inorganic platelets really do act as a barrier to the diffusion path.

Gorrasi et al. [93] reported nanocomposites based on PCL chains grafted onto montmorillonite modified by a mixture of nonfunctional ammonium salts and ammonium-bearing hydroxyl groups. The clay content was 3 wt%, whereas the hydroxyl functionality was 25, 50, 75, and 100 %, obtaining intercalated and exfoliated systems. Barrier properties were evaluated either to water or to

Table 9.1 Gas transport properties of the PCL and PCL nanocomposites films [94]

Sample	Preparation method	Permeability		
		He	H_2	CO_2
		$\left[10^{-19} \cdot \frac{m^2}{s} \cdot Pa\right]$		
PCL		2.33	2.48	10.43
PCL/(MMT-Na)	Melt blending	1.97	2.00	8.01
PCL/(MMT-$(OH)_2$)	Melt blending	1.22	1.28	4.58
PCL/(MMT-$(OH)_2$)	Two step	1.16	1.22	4.58
PCL/(MMT-$(OH)_2$)	In situ Polymerization	0.84	0.89	3.29

dichloromethane vapors. A lower sorption of water vapor was observed on increasing the hydroxyl content, up to the sample with 100 % hydroxyl content, which turned to be completely impermeable, even in liquid water. The sample with 75 % hydroxyl content showed a threshold relative humidity (R.H. = 40 %) below which it was impermeable to water vapor. The diffusion parameters decreased when the hydroxyl content increased, up to the 100 % sample, which showed not measurable diffusion. The diffusion parameters of dichloromethane, also exhibited a decreasing value on increasing the hydroxyl content in the nanocomposites.

Gain et al. [94] reported PCL/MMT nanocomposites with 3 wt% of inorganic using three different strategies: (i) melt blending, (ii) in situ polymerization initiated directly from the clay surface, (iii) two-step method (Table 9.1). This last method consisted of the in situ polymerization of ε-caprolactone in the presence of 32 wt% of clays to obtain a masterbatch, followed by the dispersion of this masterbatch in commercial PCL. Microcomposites and intercalated structures were obtained by melt blending and the two-step method, whereas clay delamination was achieved with in situ polymerization. The gas barrier properties (with respect to H_2; He and CO_2) proved the high dependence of such properties on the morphology, but also on the grafting density of the PCL chains onto the clay surface. The permeability and diffusion coefficients to CO_2 decreased going from microcomposites to intercalated structures. These transport parameters also became lower as the grafting density increased. The CO_2 solubility coefficients measured on the composites were equal or higher than the value determined for the neat PCL matrix and they were mostly related to the clay dispersion. For all composites, the variation of the diffusion coefficient was the main factor governing the transport properties and it was shown that it was possible with these composite series to tune up the transport properties and to decrease the initial gas permeability coefficients by a factor of three.

Di et al. [95] reported a study on PCL nanocomposites prepared by melt mixing using two different organoclays (Cloisite 30B and Cloisite 93A) and evaluated the barrier performance to air permeation. The effect of the organic modifiers strongly influenced the structure and, in turn, barrier performances of the samples. Microcomposites were obtained with Cloisite 93A, while nanocomposites were obtained with Cloisite 30B. The barrier performance of PCL/Cloisite 30B was

Table 9.2 The air permeability of PCL/organoclay hybrids [95]

Organoclay content (wt%)	Air permeability $\left[\frac{l}{m^2}\cdot s\right]$ [@ 200 Pa]	
0	7.99E−07	7.99E−07
2	5.21E−07	6.33E−07
5	4.03E−07	5.25E−07
10	3.43E−07	4.48E−07

Table 9.3 The air permeability of PCL/organoclay hybrids [95]

Material	Permeability $\left[\frac{g\cdot m}{s\cdot Pa\cdot m^2}\right]$		
	Water	Limonene	Oxygen
PCL	0.34×10^{-10}	5.05×10^{-10}	7.06×10^{-15}
PCL + 1 % AC11	0.16×10^{-10}	4.16×10^{-10}	5.48×10^{-15}
PCL + 5 % AC11	0.12×10^{-10}	2.58×10^{-10}	3.68×10^{-15}
PCL + 10 % AC11	0.12×10^{-10}	3.80×10^{-10}	3.67×10^{-15}

much more improved than pure PCL and PCL/Cloisite 93A. Table 9.2 reports the experimental data of permeability.

Such behavior was justified with a stronger interaction of the organic modifier of Cloisite 30B than the modifier of Cloisite 93A and an extra tortuous pathway for gas permeation caused by organoclay exfoliation.

Cava et al. [96] reported a comparative behavior between PET and biodegradable biopolymers such as PCL, PLA and PHBV and their nanobiocomposites, in terms of thermal and retorting resistance (thermal humid processes) and oxygen, water vapor, aroma and solvent barrier by means of time-resolved synchrotron radiation, FT-IR and permeation methods.

Sanchez-Garcia et al. [97] reported the preparation of PCL nanobiocomposites based on a natural mica modified with a food contact surfactant and 10 % of thymol as antimicrobial agent (AC11). Water, D-limonene and oxygen permeability were measured for nanocomposites. Table 9.3 shows the experimental data. Films with 5 wt% nanofiller content show the lowest permeability value. This observation indicated that there is a balance in the nanobiocomposites between the content of filler used (which has in itself barrier capacity) the morphology of the nanocomposite samples, and the possibility of a permeability deterioration that may be caused by filler agglomeration (clay solubility limit).

Shafiei Sabet et al. [98] prepared nanocomposites with enhanced biodegradability and reduced oxygen permeability via melt hybridization of organo-modified clay and poly (lactic acid) (PLA) as well as a PLA/polycaprolactone blend. The nanofiller was a montmorillonite modified with methyl tallow bis-(2-hydroxyethyl) ammonium (DK2). Two different PP-g-MAs were used as interfacial compatibilizers: Licocene with a maleic content of 7 % and and Polybond 3200 with a maleic content of 1 %.

From the reported results, it is evident that the inclusion of PCL in the PLA matrix resulted in increasing O_2 permeability, which can be attributed to the higher oxygen permeability of PCL versus to PLA. The incorporation of DK2 nanoclay into the PLA and PLA/PCL led to the decrease in the O_2 permeability. The PLA/DK2 and PLA/PCL/DK2 nanocomposites interfacially compatibilized by Polybond 3200 exhibited lower oxygen permeability. Longer and flocculated dispersed silicate layers enlarged the diffusing path, and this resulted in an improved barrier property of the nanocomposites based on Polybond 3200 as an interfacial compatibilizer. Although the inclusion of Licocene enhanced the separation of clay nanolayers, the higher permeability coefficient exhibited by the nanocomposites based on Licocene versus those of the corresponding uncompatibilized and compatibilized ones with Polybond 3200 was explained by the lubricating effect of low-molecular weight Licocene in the melt state, which can retard the packing of the PLA and PCL chains during the quenching process.

Vertuccio et al. [99] incorporated a sodium montmorillonite into a poly(ε-caprolactone)–starch blend by means of a ball mill. The structural organization and physical (mechanical, thermal and barrier) properties were analyzed and correlated with the milling conditions. The milling time strongly influenced the obtained structures (intercalated and/or exfoliated) and this is crucial in determining mechanical and barrier properties to water vapor. The exfoliation of the inorganic component in the continuous polymeric phase is a pre-requisite to improve the barrier properties of the material to the water vapor. In the micro-composites or in the intercalated samples the ordered structure of the inorganic component does not constitute an efficient barrier to the diffusion of the water molecules that can jump from one specific site to another. In contrast, this diffusion mechanism is not possible when the structure is exfoliated, since there is no continuity in the inorganic phase.

9.7.1 PCL/Clay Masterbatch

Benali et al. [100] reported the preparation and characterization of semi-intercalated, and semi-exfoliated poly(styrene-co-acrylonitrile)(SAN)/layered silicate nanocomposites using PCL-grafted organoclay nanohybrids as masterbatch to increase the degree of exfoliation. The PCL-grafted organoclay nanohybrids were added as masterbatches in SAN by melt blending. This two-step preparation of nanocomposites led to a well dispersed clay nanocomposites with 3 wt% of inorganics. Morphological (WAXD and AFM analyses) and solid state NMR spectroscopy measurements confirmed a more delaminated structure in SAN nanocomposites based on PCL-clay nanohybrid masterbatch (SAN/Cloisite 30B-PCL) while only an intercalated structure was found with the direct blend (SAN/Cloisite 30B). A strong improvement of both fire retardancy and gas barrier properties was recorded with the SAN/Cloisite 30B-PCL nanocomposite, which reflects the large superiority of the PCL-clay nanohybrid master batches strategy

over the direct blend for the SAN matrix. In comparison with SAN/Cloisite 30B, the SAN relative permeability of SAN/Cloisite 30B-PCL nanocomposite is lower but it depends on the gas nature. This result can be analyzed taking into account two main combined effects: clay dispersion degree and presence of PCL. The higher clay exfoliation observed in SAN/Cloisite 30B-PCL in comparison with SAN/Cloisite 30B leads to a higher decrease of the permeability. Furthermore, owing to PCL, the SAN relative permeability properties of SAN/Cloisite 30B-PCL nanocomposite depend on the gas nature. So, the larger decrease of permeability coefficient is measured with helium (∼67 %), followed by the decrease with carbon dioxide (∼59 %) and with oxygen (∼43 %).

9.7.2 Barrier Properties of Nanocomposites PCL/LDHs

Layered double hydroxides (LDHs) constitute a very attractive class of lamellar inorganic host solids for producing inorganic–organic intercalation compounds. They exhibit anion-exchange properties, therefore a wide possibility of manipulation. These layered hosts, also known as "anionic clays" or "hydrotalcite-like compounds", have the general formula: [MII(1-x)MIII x(OH)2](An-x/n) ·mH2O where MII is a divalent cation such as Mg, Ni, Zn, Cu, or Co and MIII is a trivalent cation such as Al, Cr, Fe, or Ga with An- an anion of charge n. The x value generally ranges between 0.2 and 0.4 and determines the positive-layer charge density and the anion-exchange capacity. The interlayer anions can be exchanged by other inorganic, organic, or metallo-organic anions and even by biomolecules containing ionisable acidic groups to obtain novel materials of interest in the fields of photophysics and photochemistry, electrochemistry, catalysis, drug storage and release, pharmaceutical care, and environmental protection. Moreover, the obtained intercalated compounds can be used to prepare polymeric composites having the peculiar properties of the filler. The active molecular anions, fixed by ionic bonds to the inorganic layers, not only can improve the compatibility with the polymer matrix but also can be released with controlled kinetics in particular environments.

Sorrentino et al. [101] reported the preparation and characterization of PCL-modified LDH (LDH intercalated with 12-hydroxydodecanoate anion (HDA)) nanocomposites at different filler loadings. Barrier properties of water vapor, in terms of diffusion, showed dependence from the nanocomposite composition and from the morphological organization of the filler. Figure 9.11 shows the diffusional results.

The improvement of the barrier properties, in terms of decrease of diffusion at zero vapor concentration, is maximum for sample loaded with 2.8 wt% of inorganic, whereas at higher inorganic content the diffusion coefficient value increases, even though it remains lower that of the pure PCL. The decrease of Do values was ascribed to the presence of the inorganic filler. The presence of the filler increases to a large extent the tortuosity of the system, leading to an expected large decrease

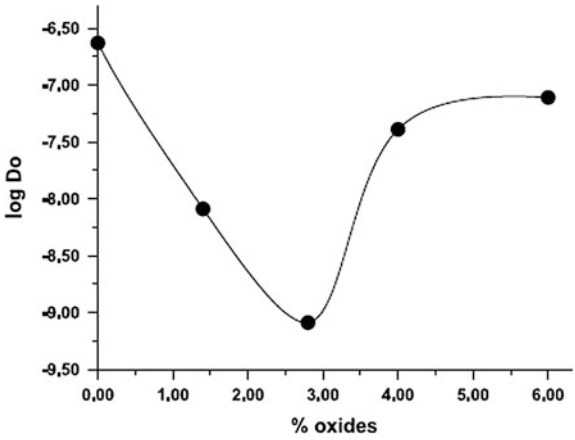

Fig. 9.11 The thermodynamic diffusion coefficient, D_0, as a function of the inorganic content [101]

in the value of the diffusion coefficient. Exfoliation of the layered solid into individual lamellae led to a remarkable increase of the developed surface of the filler with a consequent increase in the barrier improvement, also in the presence of very low inorganic content. In the present case, an increase of the filler content led or leads to a lower dispersion and exfoliation of the layered filler, with a decrease in the amount of organic/inorganic interfaces.

Bugatti et al. [102] reported the preparation and characterization of PCL-based nano-hybrids composed of ZnAl-LDH intercalated with benzoate (Bz) and benzoate derivatives as 2, 4-dichlorobenzoate (BzDC), p-hydroxybenzoate (p-BzOH) and o-hydroxybenzoate (o-BzOH), all having antimicrobial properties. The effect of both nature and position of the aromatic ring substituents on the arrangement of the guest species into interlamellar region of LDH was investigated. The barrier properties were investigated, measuring the sorption isotherms and the diffusion of water vapor for all the composites. The composites isotherms follow the same trend of PCL, although showing a higher sorption in all the activity range, due to the higher hydrophilicity of the inorganic lamellae. At variance, the thermodynamic diffusion parameter, at zero vapor concentration, was significantly lower and decreased on increasing the inorganic concentration for all the composites. The most effective reduction of diffusion was found for the exfoliated samples.

9.8 Conclusions and Future Trends

Nanocomposites concept represents a stimulating route for creating new and innovative materials, also in the area of the biodegradable polyesters. In the previous pages, several examples of bio-composites with a large variety of properties have been reported, and even more works on that kind of materials are due to be realized. Biopolymers-based nanocomposites are even able to compete, both in

price and in performance, with synthetic polymeric materials in several applications such as food packaging (containers and wrapping films), hard coating, interior and exterior panels in constructions and automotive industry.

The barrier properties, in particular, can be modulated by adding appropriate nano-particles and promoting the dispersion within the polymer matrix. The improvement of the permeability for the hybrids is maximally due to the decreasing of the diffusion coefficient. The correlation between diffusivity and clay particle dispersion is so strict that can be used for characterizing the composites morphologies even at level which may be insensitive to the other techniques.

In few years, probably, we will be able to use biodegradable polyesters for a number of applications that require severe storage and environmental conditions. A better explanation of the mechanism that controls the transport properties of these composites and how it can be modified by suitable thermal, mechanical or chemical treatments will make possible the development of materials with permeation properties that will be more advantageous for a given application and tunable in dependence of many controllable parameters.

References

1. Kaplan DL (1998) Biopolymers from renewable resources. Springer, New York
2. Fakirov S, Bhattacharya D (2007) Engineering biopolymers: homopolymers, Blends and Composites. Hanser Gardner Pubns, Munchen
3. Van de Velde K, Kiekens P (2002) Biopolymers: overview of several properties and consequences on their applications. Polym Testing 21:433–442
4. Bordes P, Pollet E, Averous L (2009) Nano-biocomposites: biodegradable polyester/nanoclay systems. Prog Polym Sci 34(2):125–155
5. Pan P, Inoue Y (2009) Polymorphism and isomorphism in biodegradable polyesters. Prog Polym Sci 34(7):605–640
6. Siracusa V, Rocculi P, Romani S, Dalla Rosa M (2008) Biodegradable polymers for food packaging: a review. Trends Food Sci Technol 19(12):634–643
7. Alexandre M, Dubois P (2000) Polymer-layered silicate nanocomposites preparation, properties and uses of a new class of materials. Mater Sci Eng 28:1–11
8. Sinha Ray S, Okamoto M (2003) Polymer/layered silicate nanocomposites: a review from preparation to processing. Prog Polym Sci 28:1539–1641
9. Bharadwaj RK (2001) Modeling the barrier properties of polymer-layered silicate nanocomposites. Macromolecules 34:9189–9192
10. Sorrentino A, Tortora M, Vittoria V (2006) Diffusion behaviour in polymer-clay nanocomposites. J Polym Sci B Polym Phys 44(2):265–274
11. Oya A, Kurokawa Y, Yasuda H (2000) Factors controlling mechanical properties of clay mineral/polypropylene nanocomposites. J Mater Sci 35:1045–1050
12. Picard E, Vermogen A, Gérard JF, Espuche E (2008) Influence of the compatibilizer polarity and molar mass on the morphology and the gas barrier properties of polyethylene/clay nanocomposites. J Polym Sci B Polym Phys 46(23):2593–2604
13. Durmus A, Woo M, Kasgoz A, Macosko CW, Tsapatsis M (2007) Intercalated linear low density polyethylene (LLDPE)/clay nanocomposites prepared with oxidized polyethylene as a new type compatibilizer: structural, mechanical and barrier properties. Eur Polym J 43(9):3737–3749

14. Giannelis EP (1996) Polymer layered silicate nanocomposites. Adv Mater 8(1):29–35
15. Vieth WR (1991) Diffusion in and through polymers: principles and applications. Hanser, New York
16. Lucian AL, Orlando JR (2009) The nanoscience and technology of renewable biomaterials. Wiley, Chichester
17. Frisch HL, Rogers CE (1966) Transport in polymers. J Polym Sci C 12:297–315
18. Cussler EL (1997) Diffusion: mass transfer in fluid systems. Cambridge University Press, New York
19. Frisch HL (1980) Sorption and transport in glassy polymers: a review. Polym Eng Sci 20(1):2–13
20. Peterlin A (1975) Dependence of diffusive transport on the morphology of crystalline polymers. J Macromol Sci Phys B11(1):57–87
21. Comyn J (1985) Polymer permeability. Elsevier Appl Sci, London
22. Vieth WR, Amini MA (1974) In: Hopfenberg HB (ed) Permeability of plastic films and coatings. Plenum Press, London
23. Soney CG, Sabu T (2001) Transport phenomena through polymeric systems. Prog Polym Sci 26(6):985–1017
24. Hedenqvist M, Gedde UW (1996) Diffusion of small-molecule penetrants in semicrystalline polymers. Prog Polym Sci 21(2):299–333
25. Shastri R, Roehrs HC, Brown CN, Dollinger SE (1990) Permeability of competitive oxygen-barrier resins: orientability and effect of orientation. In: Barrier polymers and structures ACS symposium series, vol. 423, pp 239–251, ISBN: 9780841212794 Chap. 12
26. Tabatabaei SH, Carreau PJ, Ajji A (2008) Microporous membranes obtained from polypropylene blend films by stretching. J Membr Sci 325(2):772–782
27. Sorrentino A, Gorrasi G, Tortora M, Vittoria V (2006) Barrier properties of polymer/clay nanocomposites. In: Mai Y-W, Yu Z-Z (eds.) Polymer nanocomposites, "Woodhead Publishing Ltd", Cambridge, pp 273–292 Chap. 11
28. Neilsen LE (1967) Models for the permeability of filled polymers. J Macromol Sci (Chem) A1(5):929–942
29. Fredrickson GH, Bicerano J (1999) Barrier properties of oriented disk composites. J Chem Phys 110:2181–2188
30. Lape NK, Nuxoll EE, Cussler EL (2004) Polydisperse flakes in barrier films. J Membr Sci 236:29–37
31. Lim L-T, Auras R, Rubino M (2008) Processing technologies for poly(lactic acid). Prog Polym Sci 33(8):820–852
32. Garlotta D (2001) A literature review of poly(lactic acid). J Polym Environ 9(2):63–84
33. Sinha Ray S, Yamada K, Ogami A, Okamoto M, Ueda K (2002) New polylactide/layered silicate nanocomposite: nanoscale control over multiple properties. Macromol Rapid Commun 23(16):943–947
34. Ozkoc G, Kemaloglu S, Quaedflieg M (2010) Production of poly(lactic acid)/organoclay nanocomposite scaffolds by microcompounding and polymer/particle leaching. Polym Compos 31(4):674–683
35. Sinha Ray S, Okamoto K, Yamada K, Okamoto M (2002) Novel porous ceramic material via burning of polylactide/layered silicate nanocomposite. Nano Lett 2(4):423–425
36. Sinha Ray S, Yamada K, Okamoto M, Fujimoto Y, Ogami A, Ueda K (2003) New polylactide/layered silicate nanocomposites. 5. Designing of materials with desired properties. Polymer 44(21):6633–6646
37. Sinha Ray S, Yamada K, Okamoto M, Ueda K (2002) Polylactide-layered silicate nanocomposite: a novel biodegradable material. Nano Lett 2(10):1093–1096
38. Pluta M, Galeski A, Alexandre M, Paul M-A, Dubois P (2002) Polylactide/montmorillonite nanocomposites and microcomposites prepared by melt blending: structure and some physical properties. J Appl Polym Sci 86(6):1497–1506

39. Balakrishnan H, Hassan A, Wahit M-U, Yussuf AA, Razak SBA (2010) Novel toughened polylactic acid nanocomposite: mechanical, thermal and morphological properties. Mater Des 31(7):3289–3298
40. Rhim J-W, Hong S-I, Ha C-S (2009) Tensile, water vapor barrier and antimicrobial properties of PLA/nanoclay composite films. LWT–Food. Sci Technol 42(2):612–617
41. Cava D, Cabedo L, Gimenez E, Gavara R, Lagaron JM (2006) The effect of ethylene content on the interaction between ethylene-vinyl alcohol copolymers and water: (I) Application of FT-IR spectroscopy to determine transport properties and interactions in food packaging films. Polym Testing 25(2):254–261
42. Sinha Ray S, Yamada K, Okamoto M, Ogami A, Ueda K (2003) New polylactide/layered silicate nanocomposites. 3. high-performance biodegradable materials. Chem Mater 15(7):1456–1465
43. Maiti P, Yamada K, Okamoto M, Ueda K, Okamoto K (2002) New polylactide/layered silicate nanocomposites: role of organoclays. Chem Mater 14(11):4654–4661
44. Chowdhury SR (2008) Some important aspects in designing high molecular weight poly(L-lactic acid)—clay nanocomposites with desired properties. Polym Int 57(12):1326–1332
45. Chang J-H, An YU, Sur GS (2003) Poly(lactic acid) nanocomposites with various organoclays. I. Thermomechanical properties, morphology, and gas permeability. J Polym Sci B Polym Phys 41(1):94–103
46. Thellen C, Orroth C, Froio D, Ziegler D, Lucciarini J, Farrell R, D'Souza NA, Ratto JA (2005) Influence of montmorillonite layered silicate on plasticized poly(L-lactide) blown films. Polymer 46(25):11716–11727
47. Ogata N, Jimenez G, Kawai H, Ogihara T (1997) Structure and thermal/mechanical properties of poly(l-lactide)-clay blend. J Polym Sci B Polym Phys 35(2):389–396
48. Plackett D, Sodergard A (2005) Polylactide-based biocomposites. In: Mohanty AK, Misra M, Drzal LT (eds) Natural fibers, biopolymers, and biocomposites. CRC Press, Boca Raton, pp 579–598
49. Petersson L, Oksman K (2006) Biopolymer based nanocomposites: comparing layered silicates and microcrystalline cellulose as nanoreinforcement. Compos Sci Technol 66(13):2187–2196
50. Sinha Ray S, Maiti P, Okamoto M, Yamada K, Ueda K (2002) New polylactide/layered silicate nanocomposites. 1. Preparation, characterization, and properties. macromolecules 35(8):3104–3110
51. Pandey JK, Kumar AP, Misra M, Mohanty AK, Drzal LT, Singh RP (2005) Recent advances in biodegradable nanocomposites. J Nanosci Nanotechnol 5(4):497–526
52. Koh HC, Park JS, Jeong MA, Hwang HY, Hong YT, Ha SY, Nam SY (2008) Preparation and gas permeation properties of biodegradable polymer/layered silicate nanocomposite membranes. Desalination 233(1–3):201–209
53. Park H-M, Ha C-S (2010) Barrier properties biodegradable nanocomposites. Barrier properties of polymer clay nanocomposites, pp 231–256
54. Cabedo L, Feijoo JL, Villanueva MP, Lagaron JM, Giménez E (2006) Optimization of biodegradable nanocomposites based on PLA/PCL blends for food packaging applications. Macromol Symp 233:191–197
55. Yano K, Usuki A, Okada A (1997) Synthesis and properties of polyimide-clay hybrid films. J Polym Sci A Polym Chem 35(11):2289–2294
56. Holmes PA (1985) Applications of PHB—a microbially produced biodegradable thermoplastic. Phys Technol 16(1):32–36
57. Pouton CW, Akhtar S (1996) Biosynthetic polyhydroxyalkanoates and their potential in drug delivery. Adv Drug Deliv Rev 18(2):133–162
58. Byrom D (1993) The synthesis and biodegradation of polyhydroxyalkanoates from bacteria. Int Biodeterior Biodegradation 31(3):199–208
59. Inoue Y, Yoshie N (1992) Structure and physical properties of bacterially synthesized polyesters. Prog Polym Sci 17(4):571–610

60. Doi Y (1995) Microbial synthesis, physical properties, and biodegradability of polyhydroxyalkanoates. Macromol Symp 98:585–599
61. Verhoogt H, Ramsay BA, Favis BD (1994) Polymer blends containing poly(3-hydroxyalkanoate)s. Polymer 35(24):5155–5169
62. Miguel O, Egiburu JL, Iruin JJ (2001) Blends of bacterial poly(3-hydroxybutyrate) with synthetic poly(3-hydroxybutyrate) and poly(epichlorohydrin): transport properties of carbon dioxide and water vapor. P Polym 42(3):953–962
63. Abe H, Matsubara I, Doi Y, (1995) Physical properties and enzymic degradability of polymer blends of bacterial Poly[(R)-3-hydroxybutyrate] and Poly[(R,S)-3-hydroxybutyrate] stereoisomers. Macromolecules 28(4):844–853
64. Gonzalez A, Iriarte M, Iriondo PJ, Iruin JJ (2002) Miscibility and carbon dioxide transport properties of blends of bacterial poly(3-hydroxybutyrate) and a poly(vinylidene chloride-co-acrylonitrile) copolymer. Polymer 43(23):6205–6211
65. Pankova YN, Shchegolikhin AN, Iordanskii AL, Zhulkina AL, Ol'khov AA, Zaikov GE (2010) The characterization of novel biodegradable blends based on polyhydroxybutyrate: the role of water transport. J Mol Liq 156:65–69
66. Modi S, Koelling K, Vodovotz Y (2011) Assessment of PHB with varying hydroxyvalerate content for potential packaging applications. Eur Polymer J 47:179–186
67. Lagaron JM, Catala R, Gavara R (2004) Structural characteristics defining high barrier properties in polymeric materials. Mater Sci Technol 20(1):1–7
68. Lagaron JM, Cabedo L, Cava D, Feijoo JL, Gavara R, Gimenez E (2005) Improving packaged food quality and safety. Part 2: Nanocomposites. Food Addit Contam 22(10):994–998
69. Sanchez-Garcia MD, Gimenez E, Lagaron JM (2008) Morphology and barrier properties of nanobiocomposites of poly(3-hydroxybutyrate) and layered silicates. J Appl Polym Sci 108(5):2787–2801
70. Song J, Ren M, Song C, Wang S, Zhang H, Mo Z (2004) The effect of 60Co y-rays on the crystal structure, melting and crystallization behavior of poly(butylene succinate). Polym Int 53(11):1773–1779
71. Fujimaki T, Harigaya N (1993) Development of biodegradable plastics Bionolle. Seikei Kako 5(1):36–41
72. Ishioka D (2002) Biopolymers, polyesters III. applications and commercial products, vol. 4. Wiley-VCH Verlag Gmbh, Weinheim, p 275
73. Nikolic MS, Djonlagic J (2001) Synthesis and characterization of biodegradable poly(butylene succinate-co-butylene adipate)s. Polym Degrad Stab 74(2):263–270
74. Fujimaki T (1998) Processability and properties of aliphatic polyesters, "Bionolle", synthesized by polycondensation reaction. Polym Degrad Stab 59(1–3):209–214
75. Werpy T, Frye J, Holladay J (2006) Succinic acid e a model building block for chemical synthesis from renewable resources. In: Kamm JB, Gruber PR, Kam M (eds) Biorefineries e industrial processess and products: status quo and future directions, vol 1. WileyeVCH, Weinheim
76. Song H, Lee SY (2006) Production of succinic acid by bacterial fermentation. Enzym Microb Technol 39(3):352–361
77. Dornburg V, Hermann BG, Patel MK (2008) Scenario projections for future market potentials of biobased bulk chemicals. Environ Sci Technol 42(7):2261–2267
78. Caesar B (2008) Industrial biotechnology: more than just ethanol—factors driving industry growth. Ind Biotechnol 4(1):50–54
79. Huang X, Li C, Zheng L, Zhang D, Guan G, Xiao Y (2009) Synthesis, characterization and properties of biodegradable poly(butylene succinate)-block-poly(propylene glycol) segmented copolyesters. Polym Int 58(8):893–899
80. Papageorgiou GZ, Bikiaris DN (2005) Crystallization and melting behavior of three biodegradable poly(alkylene succinates). comp study Polym 46(26):12081–12092

81. Liu Y, Ranucci E, Lindblad MS, Albertsson A-C (2001) New biodegradable polymers from renewable sources: polyester-carbonates based on 1,3-propylene-co-1,4-cyclohexanedimethylene succinate. J Polym Sci A Polym Chem 39(14):2508–2519
82. Shih YF, Wang TY, Jeng RJ, Wu JY, Wuu DS (2008) Crosslinked and uncross-linked biodegradable nanocomposites. I. Nonisothermal crystallization kinetics and gas permeability. J Appl Polym Sci 110(2):1068–1079
83. Phua YJ, Chow WS, Ishak ZAM (2011) Poly(butylene succinate)/Organo-montmorillonite nanocomposites: effects of the organoclay content on mechanical, thermal, and moisture absorption properties. J Thermoplast Compos Mater 24(1):133–151
84. Zenga J-B, Jiao L, Li Y-D, Srinivasan M, Li T, Wanga Y-Z (2011) Bio-based blends of starch and poly(butylene succinate) with improved miscibility, mechanical properties, and reduced water absorption. Carbohydr Polym 83:762–768
85. Dean K, Yu L, Bateman S, Wu DY (2007) Gelatinized starch/biodegradable polyester blends: processing, morphology, and properties. J Appl Polym Sci 103(2):802–811
86. John J, Mani R, Bhattacharya M (2002) Evaluation of compatibility and properties of biodegradable polyester blends. J Polym Sci A Polym Chem 40(12):2003–2014
87. Okamoto K, Sinha Ray S, Okamoto M (2003) New poly(butylene succinate)/layered silicate nanocomposites. Part II. Effect of organically modified layered silicates on structure, properties, melt rheology, and biodegradability. J Polym Sci B Polym Phys 41(24):3160–3172
88. Chen G-X, Kim H-S, Yoon J-S (2007) Synthesis and characterization of poly(butylene succinate)/epoxy group functionalized organoclay. Polym Int 56(9):1159–1165
89. Chen G-X, Yoon J-S (2005) Nonisothermal crystallization kinetics of poly(butylene succinate) composites with a twice functionalized organoclay. J Polym Sci B Polym Phys 43(7):817–826
90. Chen G-X, Kim E-S, Yoon J-S (2005) Poly(butylene succinate)/twice functionalized organoclay nanocomposites: preparation, characterization, and properties. J Appl Polym Sci 98(4):1727–1732
91. Messersmith PB, Giannelis EP (1995) Synthesis and barrier properties of poly(ε-Capro1actone)-layered silicate nanocomposites. J Polym Sci A Polym Chem 33:1047–1057
92. Gorrasi G, Tortora M, Vittoria V, Pollet E, Lepoittevin B, Alexandre M, Dubois P (2003) Vapor barrier properties of polycaprolactone montmorillonite nanocomposites: effect of clay dispersion. Polymer 44:2271–2279
93. Gorrasi G, Tortora M, Vittoria V, Pollet E, Alexandre M, Dubois P (2004) Physical properties of poly(ε-caprolactone) layered silicate nanocomposites prepared by controlled grafting polymerization. J Polym Sci B Polym Phys 42:1466–1475
94. Gain O, Espuche E, Pollet E, Alexandre M, Dubois P (2005) Gas barrier properties of poly(ε-caprolactone)/clay nanocomposites: influence of the morphology and polymer/clay interactions. J Polym Sci B Polym Phys 43:205–214
95. Di Y, Iannace S, Sanguigno L, Nicolais L (2005) Barrier and mechanical properties of poly(caprolactone)/orgnoclay nanocomposites. Macromol Symp 228:115–124
96. Cava D, Giménez E, Gavara R, Lagaron JM (2006) Comparative performance and barrier properties of biodegradable thermoplastics and nano bio composites versus PET for food packaging applications. J Plast Film Sheeting 22(4):265–274
97. Sanchez-Garcia MD, Ocio MJ, Gimenez E, Lagaron JM (2008) Novel Polycaprolactone nanocomposites containing thymol of interest in antimicrobial film and coating applications. J Plast Film Sheeting 24:3–4
98. Shafiei Sabet S, Katbab AA (2009) Interfacially Compatibilized Poly(lactic acid) and Poly(lactic acid)/Polycaprolactone/Organoclay nanocomposites with improved biodegradability and barrier properties: effects of the compatibilizer structural parameters and feeding route. J Appl Polym Sci 111:1954–1963
99. Vertuccio L, Gorrasi G, Sorrentino A, Vittoria V (2009) Nano clay reinforced PCL/starch blends obtained by high energy ball milling. Carbohydr Polym 75:172–179
100. Benali S, Olivier A, Brocorens P, Bonnaud L, Alexandre M, Bourbigot S, Espuche E, Gouanve F, Lazzaroni R, Dubois P (2008) Fire and gas barrier properties of poly(styrene-

co-acrylonitrile) nanocomposites using polycaprolactone/clay nanohybrid based-masterbatch. Adv Mater Sci Eng Article ID 394235, p 11 doi:10.1155/2008/394235
101. Sorrentino A, Gorrasi G, Tortora M, Vittoria V, Costantino U, Marmottini F, Padella F (2005) Incorporation of Mg-Al hydrotalcite into a biodegradabile poly(ε-caprolactone) by high energy ball milling. Polymer 46:1601–1608
102. Bugatti V, Costantino U, Gorrasi G, Nocchetti M, Tammaro L, Vittoria V (2010) Nano-hybrids incorporation into poly(e-caprolactone) for multifunctional applications: mechanical and barrier properties. Eur Polymer J 46:418–427

Chapter 10
Flammability and Thermal Stability in Clay/Polyesters Nano-Biocomposites

Sergio Bocchini and Giovanni Camino

Abstract In these years we are witnessing the growth of the biopolymers durable application markets such as buildings, transportation, electronic equipments etc. Thus, the fire retardancy issue is becoming important and it is expected that in the next future more and more research will be devoted to the subject. So far, a limited number of papers reports on flame retardant properties of biopolyesters and they are mainly on polylactide. Most of the papers published on this topic regarding biopolyesters, concern polyesters fire retarded by traditional fire retardants developed for oil sourced polymers, especially polyesters such as polyethylene terephthalate or other polymers such as polycarbonate. The recently developed use of nanoclays to fire retard polymers has proved to be beneficial also for polyesters from renewable resources. This chapter reviews the studies published on thermal and fire behaviour of polylactide nanocomposites based on clays. Indeed, PLA is the most important commercial plastic from renewable resources (RRP) polyester for which durable applications are being developed and fire retardant aspects are investigated.

10.1 Introduction

First applications of biopolyesters were designed for disposable materials (e.g. packaging) where flame retardancy is not required. In the last years the bioplastics are experiencing a rapid growth with 38 % annual average growth rate

S. Bocchini (✉) · G. Camino
Politecnico di Torino, Dipartimento di Scienza dei Materiali
e Ingegneria Chimica, Viale Teresa Michel, 5-15121 Alessandria, Italy
e-mail: sergio.bocchini@polito.it

G. Camino
e-mail: giovanni.camino@polito.it

L. Avérous and E. Pollet (eds.), *Environmental Silicate Nano-Biocomposites*,
Green Energy and Technology, DOI: 10.1007/978-1-4471-4108-2_10,

between 2003 and 2007 [1]. The companies directly involved are expecting even a more rapid growth with a worldwide increase from 0.36 in 2007 to 2.33 in 2013 and 3.45 Mt in 2020. Even if for reasons such as economic barriers (especially production costs and capital availability), technical challenges in the scale-up, short term availability of bio-based feedstocks, it will be impossible to substitute in a short term, all petrochemical polymer counterparts consumed worldwide (300 Mt including fibres in 2007), the technical substitution potential of bio-based polymers is estimated at 270 Mt, or 90 % of the total. In these years we are witnessing the growth of the biopolymers durable application markets such as buildings, transportation, electronic equipments etc. Thus, the fire retardancy issue is becoming important and it is expected that in the next future more and more research will be devoted to the subject. So far, a limited number of papers reports on flame retardant properties of plastics from renewable resources (RRP) and there are mainly on polylactide (PLA).

Organic polymeric materials may originate or propagate fire because they decompose under the action of heat, evolving combustible products. Combustion begins when the heat from an external source to which the polymer may accidentally be exposed, leads to volatile combustion products whose concentration is within the flammability limits and an ignition source such as a flame or a spark originates the flame. In case of heating in absence of ignition source, ignition occurs only when autoignition temperature is reached. The combustion, which is a radical chain thermal oxidation process, producing heat and light, proceeds then as long as the heat supplied by the flame to the polymer is sufficient to sustain its thermal degradation at a rate exceeding that required to feed the flame. Otherwise the flame extinguishes. Flame retardants interfere with combustion during one or more of the steps involved in combustion, e.g. polymer decomposition, ignition, flame spread, etc. with the ultimate target of lowering the heat fraction of the flame which is fed back to the polymer, below the self-sustaining limit, which would lead to flame extinguishment. There are many types of fire retardants that act in the solid phase and/or in the gaseous phase with different mechanisms, such as flame poisoning, formation of an insulation char on the polymer surface, etc. [2].

Most of the papers published on this topic regarding RRP polyesters, concern polyesters fire retarded by traditional fire retardants developed for oil sourced polymers, especially polyesters such as PET or other polymers such as polycarbonate. The recently developed use of nanoclays to fire retard polymers has proved to be beneficial also for polyesters from renewable resources.

This chapter reviews the studies published on thermal and fire behaviour of PLA nanocomposites based on clays. Indeed, PLA is the most important commercial RRP polyester for which durable applications are being developed and fire retardant aspects are investigated.

10.2 Thermal Degradation of Clays and Organoclays

The thermal stability of the clays, especially of their organic compatibilising treatment, becomes an important issue for nanocomposites preparation and in their thermal and fire retardant properties. Indeed, when preparing clay nanocomposites by melt blending processing, elevated temperatures are required. If the processing temperature is greater than the thermal stability of the organic treatment of the clays, its decomposition will occur, altering the interface between the filler and the polymer. As a consequence, the mechanical properties of the nanocomposite are affected as well as its combustion behaviour. Furthermore, during the combustion of the clay nanocomposites, besides the barrier effect due to the ablative reassembling of the silicate layers on the specimen surface, the formation of strongly acidic proton sites created during the thermal decomposition of organo-modifier plays an important role in delaying heat release because of the formation of a stable char residue by their catalysis [3, 4]. Thus, it is very important to know which kind of mechanism controls the degradation of the organic molecules intercalated in the clays galleries.

The most commonly used layered silicates belong to the family of phyllosilicates, their crystal structure is made of two dimensional layers (thickness $\sim$1 nm), constituted of two modular units: tetrahedral and octahedral sheets. In the 2:1 layered silicates two tetrahedral sheets of silica are fused with an edge-shared octahedral sheet of alumina (montmorillonite) or magnesia (hectorite) [5]. Stacking of the layered silicates leads to regular van der Waals gap between the layers called interlayer or gallery. One of the most important chemical characteristics, which can strongly affect the final properties of the nanocomposite, such as the combustion behaviour, is the clay acidity. In fact hydroxyl groups, weakly acidic SiOH and strongly acidic hydroxyl groups bridging two silicon atoms, present at the layer edges act as Brønsted acid sites. Lewis acid centres, instead, arise from the isomorphic substitutions with ions such as Fe^{2+} and Fe^{3+} and from crystallographic defect sites within the layers. They can act as catalytic sites accepting electrons from donor molecules with low ionization potential, coordinating organic radicals, abstracting electrons from vinyl monomers or, in the case of transition metals, working as peroxide decomposers [6–9]. Moreover, the morphology and degree of aggregation of the clays affect the rate of products and reactants transfer within the pseudo-two-dimensional galleries, greatly modifying the kinetics of reactions [10].

The thermal stability of pristine layered silicates (i.e. sodium salts), depends on clays chemistry. For example, sodium montmorillonite (and generally all layered silicates containing hydroxyl groups) below 400 °C evolves free water and interlayered water without modification of the layered structure. Then, between 500 and 1,000 °C, dehydroxylation occurs with the modification of the lattice structure. In Fig. 10.1, the thermogravimetry of sodium montmorillonite in nitrogen atmosphere is reported, which is identical to that in air because of the complete absence of organic oxidable moieties.

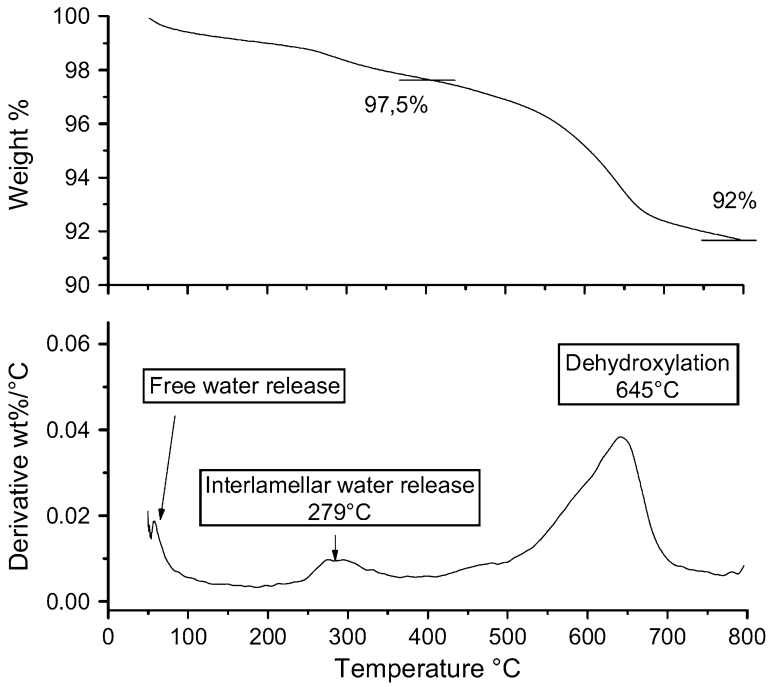

Fig. 10.1 Thermogravimetry (TG) and differential thermogravimetry (DTG) of sodium montmorillonite performed in nitrogen. From Bellucci et al. [11] Reproduced with kind permission from ©Elsevier (2007)

Isomorphic substitution of cations within the layers by metal cations bearing a lower charge generates negative charges on the lamellae that are counter balanced by interlayer exchange cations such as Na^+, Ca^{2+}, and Mg^{2+}. This type of layered silicate is characterized by a moderate surface charge known as cation exchange capacity (CEC). The interlayer cations do not belong to the crystal structure, thus they can be exchanged with other cations and/or molecules. In order to achieve better interaction of clay surface with a polymeric matrix modifications of clay surface are required. Typically, ion exchange of the interlayer cations by alkylammonium ions converts the clay interlayer from hydrophilic to hydrophobic characteristics (organoclay), also reducing the physical or electrostatic bonding force between clay layers and increases the interlayer distance. This facilitates the diffusion of polymer chains between the clay layers to give intercalated or exfoliated nanocomposites depending on whether the clay platelets stacking is kept or lost to a disordered clay layers distribution in the polymer matrix [12–15]. In other words, organoclays can be viewed as clay-rich intercalated nanocomposites.

Once organic modifiers are included into the clay layers, the thermal behaviour of the layered silicates is modified, showing four main temperature regions for

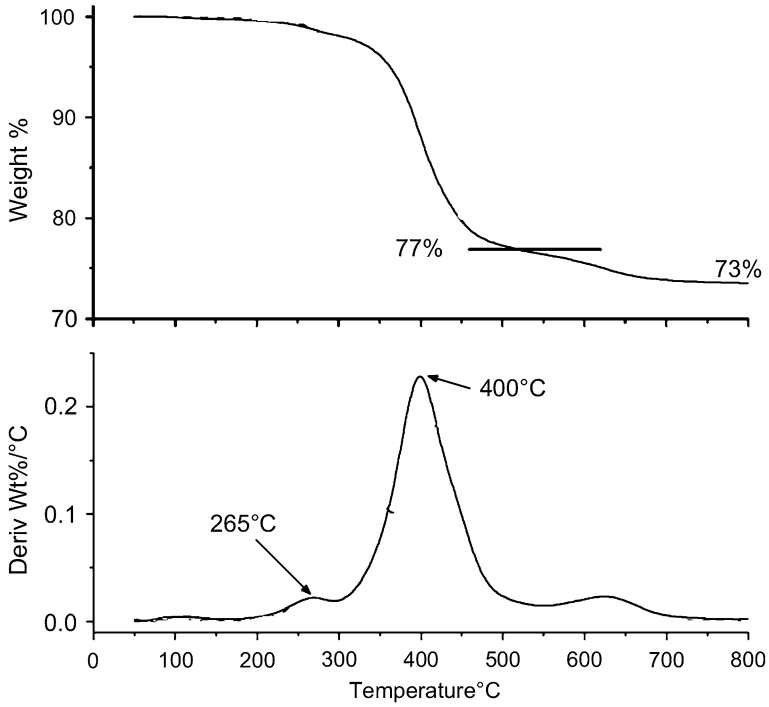

Fig. 10.2 Thermogravimetry (TG) and derivative thermogravimetry (DTG) performed in nitrogen of montmorillonite made organophilic by ion exchange with octadecylammonium. From Bellucci et al. [16] Reproduced with kind permission from ©Elsevier (2007)

thermal degradation. The evolution of absorbed water and volatile impurities occurs below 180 °C, organic moieties evolve from 200 to 500 °C then, between 500 and 800 °C the dehydroxylation of the aluminosilicate structure occurs and finally there is evolution of products associated with organic carbonaceous residue between 700 and 1,000 °C. Although conventional nanocomposites in the service environment would not include temperatures over 500 °C, the complete degradation behaviour of the organoclays at these extreme temperatures has implications for the utilization as flame retardants.

Usually the organic modifiers of layered silicates are alkylammonium salts which thermal degradation takes place in one step in a short temperature range (250–350 °C) [17], whereas Fig. 10.2 shows that the alkylammonium ions intercalated between the clay layers, decompose to volatile compounds in more than one step and in a larger temperature range (e.g. 200–500 °C) [10, 11, 17–19]. These differences are explained by the interaction clay-organic compound and they help in understanding the thermal behaviour of clay-organic polymer nanocomposites.

The degradation onset temperatures of alkylammoniums intercalated in the clay interlayer space are usually lower than those of the pure alkylammonium salt.

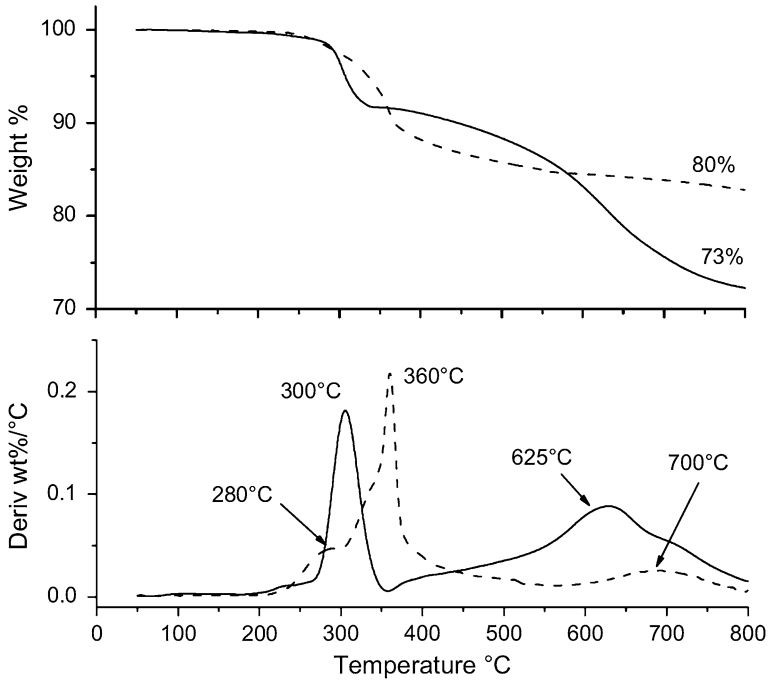

Fig. 10.3 Thermogravimetry (TG) and differential thermogravimetry (DTG) in air of montmorillonite (solid line) and fluorohectorite (dotted line) ion exchanged with octadecylammonium. From Bellucci et al. [20] Reproduced with kind permission from ©Elsevier (2007)

The first event of decomposition is usually due to the unconfined fraction of alkylammonium, that consists of alkylammonium surfactant which has not undergone the ion exchange reaction and is either complexed on the outer surface of the clay or within void spaces between primary particles or inside the interlayer space but in a peripheral position [10, 17–19]. This behaviour shows that the Lewis and/or Brønsted acid sites behave as catalytic sites affecting the initial stage of decomposition of the alkylammonium molecules accelerating the carbon–carbon bond scission at high temperature.

The further degradation steps regard the alkylammonium molecules that have undergone ion exchange, which weight loss is delayed by the barrier effect of the clay layers to the diffusion of the volatile compounds formed by thermal degradation of the organic moiety.

In Fig. 10.3 the thermogravimetry in air of montmorillonite and fluorohectorite ion exchanged with the same octadecylammonium ion, is reported. In such thermal degradation under oxidative conditions the clays promote the charring of the organic modifier with the formation of a stable char residue which decomposes at higher temperature with the production of CO_2 [17].

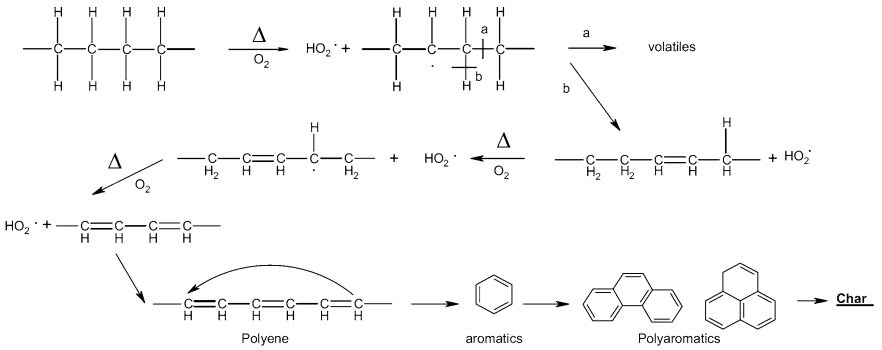

Fig. 10.4 Degradation mechanism of the alkyl chains in oxidative atmosphere. From Bellucci et al. [21] Reproduced with kind permission from ©Elsevier (2007)

Charring is due to oxygen initiated pyrolysis of alkyl groups of the alkylammonium ions which leads to char through oxidative dehydrogenation which is in competition with volatilisation, as shown in Fig. 10.4.

The char yield of octadecylammonium chloride decomposed in the same conditions of Fig. 10.3 is 20 wt% [17]. Thus taking into account the content of octadecyl ammonium ions in the clays, by heating in air the organo-modified montmorillonite or fluorohectorite the char yields should be respectively the 44 and 70 wt% whereas 60 and 80 wt% are respectively obtained in Fig. 10.3. The extrapolated char yields of octadecylammonium decomposition are thus respectively 60 and 32.5 wt% for montmorillonite and fluorohectorite.

This effect is due to a catalytic action which depends on the type of clay. Indeed acidity of montmorillonite, due to the presence of −OH groups at the edges of clay lamellae [22] promotes charring catalysis more effectively than fluorohectorite, in which a large portion of edge −OH groups are substituted by fluorination.

The clays catalytic action shown here, for the organic modifier, is obviously occurring also on heating polymer nanocomposites and affects their behaviour in combustion. Indeed, charring of the polymer matrix in nanocomposites combustion is widely reported.

10.3 Thermal Evolution of Nanocomposites

Since the first studies about thermal degradation and fire behaviour [23, 24], it was pointed out that the behaviour of the different clay nanocomposites was quite similar: once exposed to forced combustion (e.g. cone calorimeter studies) well dispersed clays reduce the heat release rate (HRR) as a consequence of a lower fuel feed rate often without substantial modifications of the polymer bulk degradation pathway. It is generally accepted that such behaviour is related to the formation of a physical shield built up by coalescence of the inorganic nanoparticles mixed with

polymer char, left behind by polymer ablation, which acts as a barrier, slowing down the release of generated gas fuel. However, often more complex phenomena can take place in the region near the surface during nanocomposite burning, affecting the accumulation of inorganic particles and their interaction with the polymer while the building of a surface structured inorganic phase takes place.

The currently available knowledge on the mechanisms for the formation of the physical shield during clay nanocomposite burning is the result of many years of work from different groups and went through the accumulation of evidences on re-organization of the clay nanoparticles inside the polymer during thermal degradation/combustion. Fundamental mechanisms of physical thermal evolution in nanocomposites are reviewed in this paragraph. Kashiwagi et al. [24–26] were the first to examine the fire behavior of exfoliated polyamide 6 (PA6)-clay nanocomposites, showing that PA6/clay nanocomposites significantly reduced the heat release rate in combustion, compared to neat PA6 and explained this result with the formation of protective floccules on the sample surface acting as a thermal insulation layer. The analysis of the protective floccules evidenced that they are mainly formed by clay particles, in which lamellae are stacked with a d-spacing larger than the original clay without organic modifier. This higher interlayer distance was explained by the presence of thermally stable organic components possibly with graphitic-like structure, probably formed by the organic molecules entangled during clay re-assembling with a catalytic charring mechanism.

Two mechanisms were proposed for accumulation of the initially well-dispersed clay particles. The first is the classical accumulation of clay particles on the surface of the burning material by polymer ablation. De-wetted clay lamellae, left behind by polymer pyrolysis, tend to aggregate and stack against each other because the degradation of the organic modifier of the lamellae surface makes them more hydrophilic and less compatible with the polymer matrix. The second mechanism involves the thermal degradation of the clay organic treatment in the molten polymer and subsequent aggregation in particles stacks. These aggregates of nanoparticles may be moved to the surface by the rising bubbles of volatile products obtained by organic modifier/polymer degradation and/or convection flow in the high temperature melt. Lewin [27] pointed out that the clay platelets inside the nanocomposites can migrate also at lower temperatures because of the thermal decomposition of the organic modifier and subsequent migration to the surface, driven by surface energy minimization.

Pastore et al. [28] demonstrated a high temperature structural rearrangement of intercalated clay nanocomposites based on poly[ethylene-co-(vinyl acetate)] (EVA), using in situ high temperature X-ray diffraction. Below 225 °C migration of the layered silicate towards the nanocomposite surface and an increase of the interlayer distance were found both under nitrogen or air. At higher temperatures (up to 350 °C) inert or oxidizing atmosphere differently affect the structural modification of the nanocomposite. Indeed, de-intercalation and the corresponding decrease of the silicate interlayer space were found under nitrogen as a consequence of thermal degradation of the organic modifier, whereas increase of the silicate interlayer space and exfoliation were the main processes found under air.

It was proposed that at high temperature the role of the organic modifier lost by thermal decomposition is played under oxidative atmosphere by polar groups such as ketones and esters created by surface polymer oxidation. This will drive the platelets in intimate contact of the polymer on the oxygen-rich high polar surface of burning polymer nanocomposites. Thus the main factor affecting the thermal behaviour of nanocomposites under fire combustion is the clay/polymer interaction. The same results were obtained by Wang et al. [29] on studying polystyrene-clay nanocomposites either intercalated or exfoliated in which an accumulation and coalescence of alumino-silicate on the surface of burning specimens was found whereas there was no surface structured accumulation in the case of corresponding microcomposites.

On the other hand, it has to be pointed out that the dispersion of nanoparticles, assessed in the bulk of the polymer matrix at room temperature, is not necessarily retained at the temperatures reached by the surface of the composite during burning. Indeed, the chemical interaction between the nanoclay and the thermally degrading polymer melt, which control the clay dispersion, may be significantly different from the interactions taking place with the polymer in the processing step at lower temperatures. In a series of articles on PP/nanoclay and PA6/nanoclay Lewin and co-workers accumulated evidence for the formation of the surface clay-rich barrier for which they proposed a mechanism [30–33]. Taking into account the morphology changes that take place when the nanocomposite temperature increases, it was proved that the organophilic layered silicate particles migrate and accumulate to the surface of the molten polymer at temperatures even far below pyrolysis temperature. The causes of the migration were identified in the temperature and viscosity gradients of the melt. The organo-modified layered silicates were propelled to the surface by gas bubbles from the decomposing surfactant and polymer and/or by the difference in surface free energy between the polymer and the polymer/clay interface. The migration depends not only on temperature and time as expected for a diffusion process, but also on the extent of exfoliation of clay particles. In absence of polymer clay interaction as in the case of PP/nanoclay, the more exfoliated the structure, the more significant the migration effects, whereas in PA6, a polymer highly interacting with nanoclays, there are more factors that influence migration.

Since the annealing in the presence of oxygen decreases migration in PA6, it was proposed that the presence of oxygen accelerated the degradation of the surfactant producing acidic clay that can strongly interact with PA6 by protonation and formation of strong linkages lowering clay mobility. Moreover, migration extent increases in the temperature range 250–275 °C whereas a further increase in temperature reduces the extent of migration. This phenomenon, which is contrary to expectations, is explained by the gradual conversion of the nanocomposite to a microcomposite due to an acceleration of organic modifier decomposition. The microcomposite, which is not a colloid, it is not subject to surface potential forces and does not migrate. Instead, it aggregates in larger sediments and either stays suspended, or precipitates [32]. On the other hand it was shown by Frache et al. [34] that

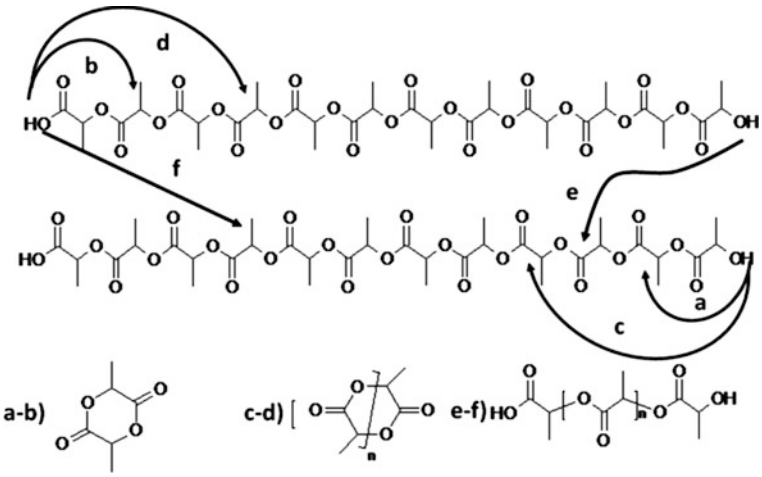

Fig. 10.5 PLA degradation: intra and intermolecular alcoholysis/acidolysis **a** Intramolecular alcoholysis: lactide formation **b** Intramolecular acidolysis: lactide formation **c** Intramolecular alcoholysis: higher cyclic oligomers formation **d** Intramolecular acidolysis: higher cyclic oligomers formation **e** Intermolecular alcoholysis: linear oligomers formation alcoholysis **f** Intermolecular acidolysis: linear oligomers formation alcoholysis

clay intercalation and exfoliation are essentially controlled by the polymer–clay affinity, since they can take place in shear less, static conditions [35].

10.4 Polylactide Thermal Degradation and Thermal Oxidation

On the basis of literature, the main PLA pyrolysis mechanism involves the intra- and intermolecular ester alcoholysis/acidolysis of polylactide ester groups of the chain (Fig. 10.5) [36–39]. This dominant reactions pathway in the case of intramolecular reaction, leads to the formation of lactide and cyclic oligomers. Linear oligomers are formed instead by intermolecular alcoholysis/acidolysis reactions which may volatilise depending on their molecular weight.

If the alcoholysis reaction involves the ester of the same monomer unit, acetaldehyde plus carbon monoxide are produced (Fig. 10.6) and the original OH end structure is regenerated [36, 37, 40]. In this case the process is similar to an unzipping depolymerization. The lower the molecular weight, the more concentrated are the terminal hydroxyl groups, which accelerate the unzipping depolymerization and alcoholysis reactions.

PLA chain scission by ester bonds β-elimination also occurs (Fig. 10.7) but it is a minor reaction. Even at high temperature, only a small amount of acrylic acid

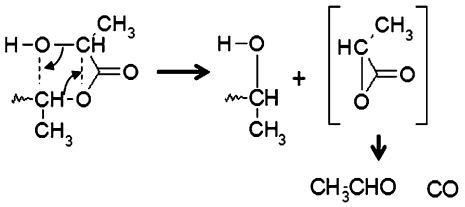

Fig. 10.6 Unzipping depolymerisation

and acrylic oligomers (<5 % in weight) are produced [41, 42] which however are important because the acid groups which they bear, contribute to PLA degradation by acidolysis of the ester groups of the chain.

The condensation reaction of lactic acid, one of the methods used to produce PLA, is an equilibrium reaction, thus residual moisture causes hydrolysis of PLA into lactic acid at elevated temperatures [43], also in this case the hydroxyl groups generated increase the rate of pyrolysis reaction.

Finally, it has been demonstrated that the various kinds of metals which can be found in the polymer (e.g. as contaminants or catalysts) such as Sn, Zn, Al and Fe catalyze the intra- and intermolecular alcoholysis/acidolysis and depolymerization reactions at high temperature [44, 45]. In the case of residual catalysts the more selective is the catalyst the less efficient is its depolymerization effect at high temperature.

As for many polyesters, the thermal stability of PLA in air is similar to that under inert atmosphere. However there are some minor effects such as the decrease of about 3–5 °C of the onset temperature and of the temperature of maximum degradation during themogravimetry [36]. This small difference is an indirect confirmation that the main thermal degradation mechanism of PLA is not a radical mechanism. Then the role of oxygen is probably limited to a minor increase in the fragmentation of PLA by a peroxide radical chain mechanism below 250 °C or a hydrogen abstraction and radical chain fragmentation over about 250 °C as usually happens for compounds containing alkylic fragments [46]. No detailed studies on the thermal oxidation of PLA are available except for the studies of Gupta et al. [47, 48] and Liu et al. [40]. A thermal oxidation mechanism was not proposed and the only conclusions were a small increase of degradation rate and the formation of carboxylic groups probably by thermal oxidation.

10.5 Thermal Behavior of Clay/Polylactide Nanobiocomposites

Among the clays used to prepare PLA micro and nano-composites one of the most used is montmorillonite particularly organomodified montmorillonite. Most research on the thermal stability of PLA and its micro- and nanocomposites has focused on the use of thermogravimetric analysis (TGA) under both air and nitrogen [49–52].

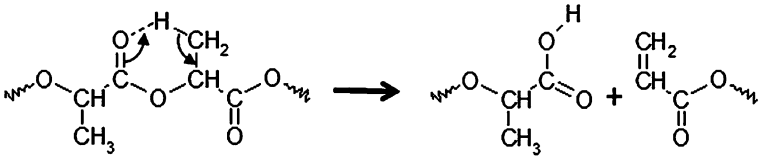

Fig. 10.7 PLA β-elimination mechanism

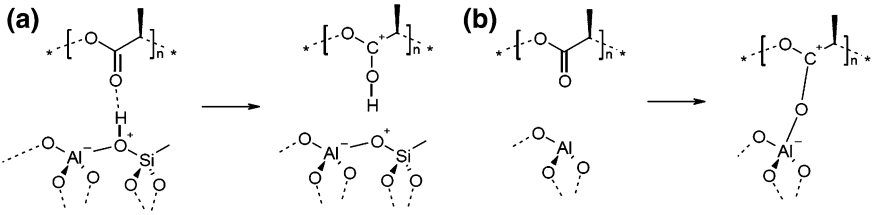

Fig. 10.8 Sodium montmorillonite: **a** Brønsted acid sites and **b** Lewis acid sites proposed to catalyze PLA degradation [54]

Unmodified clay, such as sodium montmorillonite was tested for the first time by Pluta et al. [49], 3 wt% of the clay was dispersed at micrometric level and the results were a small decrease of thermal stability in helium atmosphere. Similar results were obtained by Paul et al. [50] describing the data of TGA degradation under nitrogen of plasticized PLA filled with sodium montmorillonite: by increasing the filler content there was a substantial continuous decrease in thermal stability. The temperature of maximum degradation rate of TGA continuously decreased from about 370 to 325 °C while the level of sodium montmorillonite increased from 1 to 10 wt%. The authors explained this behaviour by the presence of water hydrating the sodium cations intercalated in the clay: at high temperature this water is released, therefore hydrolysis of ester groups is more pronounced and responsible for the increase of the chain scission rate. However it is not yet clear if this effect is due to hydrolysis occurring during melt blending process which creates reactive chain ends as shown above or during thermal degradation. Probably it is a combination of both effects. These results were confirmed by Zhou and Xanthos [53] who assumed also a catalytic effect by montmorillonite Brønsted and Lewis acids groups (Fig. 10.8) as previously described by Okamoto et al. [54].

The nanocomposites obtained by melt blending, using either montmorillonite modified by dimethyl 2-ethylhexyl hydrogenated tallow ammonium cation [49] or bis-(2-hydroxyethyl) methyl hydrogenated tallow ammonium [55] show a slight increase (about 10 °C) in temperature of maximum degradation rate. A systematic study of the effect of clay organic modifier by Zhou and Xanthos showed that in melt blending prepared nanocomposites, the effect of organic modifier is generally negligible [53]. On the other hand Chang et al. [56] found that PLA nanocomposites prepared from solution casting using hexadecyl-amine montmorillonite or dodecyl-trimethyl-amine montmorillonite or Cloisite 25A have a decreased

thermal stability under nitrogen as compared to PLA. The TGA onset temperature of these nanocomposites decreases linearly increasing the amount of organoclay in the range from 2 to 8 wt%. It could be supposed that the lower thermal stability of PLA nanocomposites prepared by solution casting method was due to the organic modifiers decomposition that acts as an initiator for thermal degradation of PLA. Indeed, on the contrary of what is obtained for PLA nanocomposites prepared by melt blending, organoclay of nanocomposites prepared by solvent casting are heated for the first time during the TGA analyses. Thus, the thermally unstable organic modifier adsorbed on the peripheral position of clay layers, that usually decomposes during processing in melt blending [57], is still present and decomposes at lower temperature in TGA when solvent casting is used. This effect depends on the type of used organic modifier since in the case of ammonium bromide–montmorillonite, the onset temperature of PLA weight loss had nearly constant values regardless of the clay loading even if prepared by solvent casting [56].

In thermal oxidative conditions, PLA-clay microcomposites decompose as pure PLA, whereas nanocomposites show a relevant stabilization effect [49, 50, 53, 55]. Pluta et al. [49] reported that an increase by 25 °C of the temperature of maximum degradation rate was observed under air for a PLA/organo-modified MMT (PLA/OMMT) as compared to PLA. Paul et al. [50] showed an increase of the thermal stability of PLA when filled with an amount of OMMT as low as 3 wt%. This effect was more or less pronounced depending on the organic modifier substituted ammonium cation (length of the alkyl chain, functionality of the ammonium cation etc.) and is independent from its thermal stability. The most effective stabilizing organoclay is Cloisite 30B that is the most PLA compatible and the one that forms the largest fraction of exfoliated structure which is the main factor influencing the oxidative thermal degradation of PLA.

This is confirmed by the dependence of PLA thermal stability on Cloisite 30B concentration. Indeed, an increase in thermal stability with the Cloisite 30B content is observed by TGA, with a maximum at 5 wt% clay loading. A further increasing of the filler content involves a decrease in thermal stability. Such a behaviour was explained by the relative extent of exfoliation/delamination in function of the amount of organoclay [50]. At low filler content, exfoliation dominates but the amount of exfoliated silicate layers is not sufficient to promote any significant improvement of the thermal stability. Increasing the filler content leads to relatively more exfoliated individual particles, and increases the thermal stability of the nanocomposites. At filling content above ca. 5 wt%, complete exfoliation of such high aspect ratio silicate layers is more and more hindered because of geometrical constraints within the limited space remaining available in the polyester matrix and no more increase in thermal stability is detected.

Zhou and Xanthos [53] have thoroughly investigated the thermal oxidation behaviour of PLA/MMT micro- and nanocomposites both in dynamic and isothermal conditions (200 °C). This last is the really sound chemical approach to study kinetics of chemical processes which in addition avoids overlapping of different reactions typical of dynamic runs. Also in these conditions, the degradation

rate of nanocomposites is significantly lower than that of unfilled PLA and of micro-composites, due to the good dispersion of the nanofillers in the polymer matrix.

As discussed above for other polymers, at these temperatures the major function of the silicate platelets is to act as a barrier against oxygen diffusion towards the bulk of the polymer.

10.6 Effect of Clays on Fire Behaviour of PLA

The described phenomena occurring during thermal degradation and thermal oxidation of nanocomposites directly affect the results of fire tests carried out on them. On the other hand, performance of polymer materials and nanocomposites in a fire test strongly depends on test scenario i.e. on the fire model. At present, the fire retardance scientific community takes advantage of basically three different fire tests, namely vertical UL94, Limiting Oxygen Index (LOI) and Oxygen Consumption Calorimeter ("Cone Calorimeter"). UL94 and LOI are generally referred to as flammability tests, in which the material behaviour exposed to a small flame is addressed, in terms of capability to ignite and to self-sustain a flame, thus representing a scenario in which the material is at the origin of a fire. Cone calorimeter test is representative of a forced combustion, in which the material is forced to burn under controlled heat flux. This test addresses the ignition time, the rate of combustion and the total heat released, modelling the contribution of the material to a fire started on other items. Moreover, these flammability and combustion tests also differ for the specimen positioning, the formers being vertical tests (bottom ignition for UL94 and top ignition for LOI) the latter most often being an horizontal test, despite vertical configuration is even provided by the standard methods [58, 59]. Considered these differences, it is certainly reasonable to expect different performances of a given fire retarded formulation compared with the reference material, when testing in different fire tests, expected to be representative of different fire scenarios. With polymer nanocomposites, the differences in performance obtained in flammability and forced combustion tests are usually very significant, this having caused an ongoing discussion on the actual effectiveness of nanoparticles as fire retardants [60, 61]. The consequence of these facts is twofold: the relevance of different fire tests to real fire scenarios becomes crucial for the final application of polymer nanocomposites and, on the other hand, the scientific significance of standard tests must be carefully evaluated.

Only a few papers are devoted to the flame retardancy of polyesters from renewable resources and even less of clay/polyester nanobiocomposites [62], these papers essentially concern PLA nanobiocomposites and combination of flame retardants/fillers with clays. The reason is that the first applications of biopolyesters were designed for disposable materials (e.g. packaging) which do not need flame retardancy. Now the markets turns to more durable materials and bio-based polymers are expected to substitute commodity plastics in sectors such as

transportation and electrical/electronic applications. In those sectors, the fire hazard is a relevant issue and flame retardancy is required. In this section the use of clay to improve fire resistance and as co-adjuvant for fire retardants is reviewed.

The addition of a small amount of well dispersed clay (exfoliated/intercalated) has been shown to reduce the rate of combustion in forced combustion test (cone calorimeter: reduction of maximum heat release rate, pHRR) in the case of many thermoplastic polymers [63–65] including PLA [66]. A pHRR reduction by 40 % is obtained when about 3–5 wt% of clay platelets are well dispersed inside PLA [67, 68]. Similar results were obtained also in the presence of a plasticizer for PLA multifilaments nanocomposites with the incorporation of 4 wt% of organo-modified clay. The knitted fabric made with the PLA/clay nanocomposites exhibits a reduction of about 40 % in pHRR compared to the virgin one [69]. It is reported that a smooth char layer is formed at the surface of the nanocomposites leaving a black char residue at the end of the experiments while on the contrary pure PLA burns completely with vigorous bubbling and no residue is left at the end of the experiment. Thus the suggested mechanism by which clay nanocomposites act as fire retardants, involves the formation of a char that serves as a potential barrier to both mass and energy transport. Fukushima et al. [55] reported that from a well-dispersed PLA-organo-modified montmorillonite nanocomposite, charring of UL94 specimens was observed confirming the hypothesis concerning the formation of the carbonized inorganic protective surface layer during burning. The SEM micrographs obtained for the nanocomposite residue (Fig. 10.9) show a continuous carbon layer rich in silicon and oxygen according to EDS analysis (Si: 19 wt% as compared to 1.3 wt% in original sample), which was explained by accumulation of silicate layers at the sample surface. This is also qualitatively appreciable by the lighter shade of gray for the surface when using a backscattered electron detector due to the higher atomic weight of silicon Si compared to C (carbon), which directly influences the intensity of backscattered electron signal (Fig. 10.9). The silica accumulation was confirmed by the comparison of infrared spectra of the surface and of the interior of the same fragment: the infrared of the surface shows only the signal typical of MMT. The internal part instead shows the typical signals of pure PLA clay nanocomposites, confirming that the bulk material was protected from combustion.

Thus the mechanism of protection of well dispersed nanoclays is due to the formation of a protective layer which increases resistance to fire.

Despite the formation of an extended inorganic-char structure [55], this mechanism alone is not generally sufficient to meet some commercial testing requirements such as UL94. This is the reason why nanoclays had been used as an additive to promote synergistically the effects of fire retardants.

In order to obtain PLA composites characterized by specific end-use flame retardant properties, the addition of gypsum was considered for PLA-OMMT nanocomposites [70]. Gypsum was selected because it is a by-product of lactic acid fabrication process. The use of gypsum anhydrite II (AII) form preserved PLA molecular weight and key properties during processing of the composite products [70]. Co-addition of AII and OMMT leads to PLA nanocomposites characterized

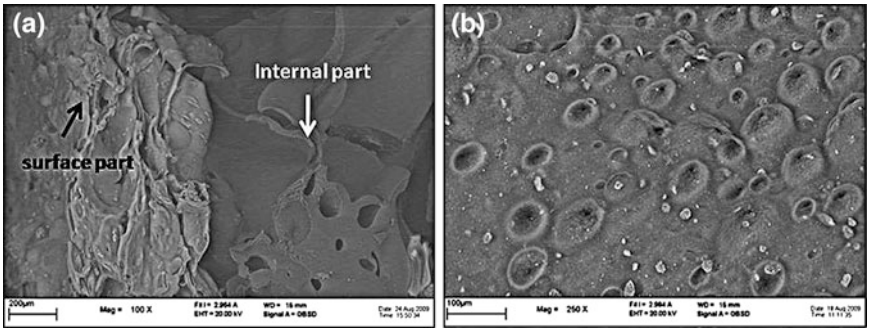

Fig. 10.9 SEM micrographs of residual material from PLA with 3 wt% of organic modified montmorillonite-after UL94 V test: **a** in the sample fracture zone and **b** on the surface part from **a** From Fukushima et al. [55], reproduced with kind permission from ©Elsevier 2010

by good (nano) filler dispersion, thermal stability and adequate mechanical resistance. The cone calorimetry showed significant increase in the ignition time compared to neat PLA and a decrease of pHRR, i.e. ca. 40 %, typical of well dispersed PLA nanocomposites. Moreover, the UL94 horizontal burning test (UL94 HB) was successfully passed revealing non-dripping effect and extensive char formation.

PLA based-nanocomposites obtained by co-addition of expanded graphite and OMMT show considerable improvements in the thermal, mechanical and fire retardant properties of PLA, thus they are potentially interesting for engineering applications when black colour is acceptable [55]. The ternary systems reveal advanced flame retardant properties. The horizontal burning test (UL94 HB) is successfully passed showing anti-dripping properties and the formation of char, as well as lower burning rate as compared to neat PLA and to binary systems. This phenomenon could be related to the excellent co-dispersion of the nanofillers and to the occurrence of their interactions in the polymer matrix. Interesting flame retardant properties attributed to formation of an inorganic/carbonaceous surface layer during burning were achieved mainly by the ternary compositions in the vertical burning test (UL94 VB). Especially at high amount of graphite (6–9 wt%) and by co-addition of clay (3 wt%), the ternary compositions showed the formation of an extensive compact char together with a significant reduction of the vertical combustion rate and advanced anti-dripping properties.

Intumescence which involves formation of a blown multi-cellular surface protecting char during combustion, is a method used to limit the flammability of polymers. Fontaine and Bourbigot [71] reported the combination of ammonium polyphosphate (APP) with melamine (MEL) in an appropriate ratio (5–1, respectively) as efficient intumescent for PLA at a loading as low as 10 wt%. The incorporation of an additional nanofiller such as organo-modified montmorillonite, shows a large synergistic effect on PLA fire behaviour either in cone calorimeter, oxygen index and UL94 (reaching the highest ranking, V-0). These high performances

were explained by the increase of the thermal stability of the formulation with the montmorillonite, according to previous results on other polymers with the same intumescent formulation by Bourbigot et al. [72, 73], assuming that montmorillonite reacts with APP to form alumino- and silico-phosphates stabilizing the intumescent structure at high temperature.

10.7 Conclusions

Clay nanoparticles can enhance the thermal stability of organic molecules with which they are in molecular contact, by the physical containment of the fragments created by chain bonds thermal scission which delays their volatilization. In the case of polymers which thermal degradation can be initiated by oxygen, the barrier effect of clay layers to oxygen diffusion slows down the volatilization process. Moreover, depending on the kind of clay, a role is played by its catalytic action that effectively promotes charring catalysis on heating polymer nanocomposites (e.g. by oxidative dehydrogenation) and reduces their combustion rate even at low clay loading (e.g. 2–3 wt%).

Although the rate reduction be generally relevant, nanocomposites may fail to meet the requirements of some fire retardancy tests designed for commercial use. While studies are being carried out to make nanocomposites perform satisfactorily in all fire retardant tests, combination of nanoparticles and fire retardants is being used when reaching required prescriptive rankings cannot be met just by nanoparticles. This generally results in a synergic behaviour leading to the reduction of the overall amount of additives which is beneficial from environmental point of view.

In this chapters it is shown that clays nanodispersed in polymers from renewable resources can improve thermal and fire retardance properties as in the case of oil derived polymers. Although available literature data mostly concern PLA, it is to be expected a similar behaviour for the upcoming new bio-based polymers.

References

1. Shen L, Haufe J, Patel MK (2009) Product overview and market projection of emerging biobased plastics (PROBIP 2009). Commissioned by European Polysaccharide Network of Excellence (EPNOE) and European Bioplastics. Group Science, Technology and Society (STS), Copernicus Institute for Sustainable Development and Innovation, Utrecht University Utrecht, the Netherlands, June 2009. Report No: NWS-E-2009-32
2. Horrocks AR, Price D (2001) Fire retardant materials. CRC Press, Boston
3. Vaia RA, Ishii H, Giannelis EP (1993) Synthesis and properties of two-dimensional nanostructures by direct intercalation of polymer melts in layered silicates. Chem Mater 5(12):1694–1696
4. Zanetti M, Camino G, Mülhaupt R (2001) Combustion behaviour of EVA/fluorohectorite nanocomposites. Polym Degrad Stab 74(3):413–417

5. Brindely GW, Brown G (1980) Crystal structure of clay minerals and their X-ray identification. Mineralogical Society, London
6. Solomon DH, Hawthorne DG (1991) Chemistry of pigments and fillers. Krieger, Malabar
7. Sposito G, Skipper NT, Sutton R, Park SH, Soper AK, Greathouse JA (1999) Surface geochemistry of the clay minerals. Proc Natl Acad Sci USA 96:3358–3364
8. Sherman JD (1996) Synthetic zeolites and other microporous oxide molecular sieves. Proc Natl Acad Sci USA 96:3471–3478
9. Bocchini S, Fukushima K, Di Blasio A, Fina A, Frache A, Geobaldo F (2010) Polylactic acid and Polylactic acid-based nanocomposites photooxidation. Biomacromolecules 11(8): 2919–2926
10. Xie W, Gao Z, Pan W, Hunter D, Singh A, Vaia R (2001) Thermal degradation chemistry of alkyl quaternary ammonium montmorillonite. Chem Mater 13(9):2979–2990
11. Bellucci F, Camino G, Frache A, Sarra A (2007) Catalytic charring-volatilization competition in organoclay nanocomposites. Polym Degrad Stab 92(3):425–436 Figure 1 in
12. Akelah A, Moet A (1996) Polymer-clay nanocomposites: free-radical grafting of polystyrene on to organophilic montmorillonite interlayers. J Mater Sci 31(13):3589–3596
13. Agag T, Takeichi T (2000) Polybenzoxazine-montmorillonite hybrid nanocomposites: synthesis and characterization. Polymer 41(19):7083–7090
14. Chen TK, Tien YI, Wie KH (2000) Synthesis and characterization of novel segmented polyurethane/clay nanocomposites. Polymer 41(4):1345–1353
15. Cho JW, Paul DR (2001) Nylon 6 nanocomposites by melt compounding. Polymer 42(3):1083–1094
16. Bellucci F, Camino G, Frache A, Sarra A (2007) Catalytic charring-volatilization competition in organoclay nanocomposites. Polym Degrad Stab 92(3):425–436 Arranged from Figure 8 in
17. Bellucci F, Camino G, Frache A, Sarra A (2007) Catalytic charring-volatilization competition in organoclay nanocomposites. Polym Degrad Stab 92(3):425–436
18. Davis RD, Gilman JW, Sutto TE, Callahan JH, Trulove PC, De Long HC (2004) Improved thermal stability of organically modified layered silicates clays. Clay Miner 52(2):171–179
19. Bellucci F, Camino G, Frache A, Ristori V, Sorrentino L, Iannace S, Bian X, Guardasole M, Vaccaro S (2006) Effect of organoclay impurities on mechanical properties of EVA-layered silicate nanocomposites e-Polymers n°14
20. Bellucci F, Camino G, Frache A, Sarra A (2007) Catalytic charring-volatilization competition in organoclay nanocomposites. Polym Degrad Stab 92(3):425–436 Arranged from Figure 9
21. Bellucci F, Camino G, Frache A, Sarra A (2007) Catalytic charring-volatilization competition in organoclay nanocomposites. Polym Degrad Stab 92(3):425–436 Scheme 1 in
22. Park SJ, Seo DI, Lee JR (2002) Surface modification of montmorillonite on surface Acid-base characteristics of clay and thermal stability of epoxy/clay nanocomposites. J Coll InterfSci 251(1):160–165
23. Gilman JW, Kashiwagi T (1997) Nanocomposites: a revolutionary new flame retardant approach. SAMPE J 33:40–46
24. Kashiwagi T, Gilman JW, Nyden MR, Lomakin SM (1998) Polymer combustion and new flame retardants. In: Le Bras M, Camino G, Bourbigot S, Delobel R (eds.) Fire retardancy of polymers: the use of intumescence, The Royal Society of Chemistry, Cambridge
25. Gilman JW, Kashiwagi T, Giannelis EP, Manias E, Lomakin S, Lichtenhan JD, Jones P (1998) Nanocomposites: radiative gasification and vinyl polymer flammability. In: Le Bras M, Camino G, Bourbigot S, Delobel R (eds.) Fire retardancy of polymers: the use of intumescence, The Royal Society of Chemistry, Cambridge
26. Kashiwagi T, Harris RH, Zhang X, Briber RM, Cipriano BH, Raghavan SR, Awad WH, Shields JR (2004) Flame retardant mechanism of polyamide 6-clay nanocomposites. Polymer 45(3):881–891
27. Lewin M (2003) Some comments on the modes of action of nanocomposites in the flame retardancy of polymers. Fire Mater 27(1):1–7

28. Pastore HO, Frache A, Boccaleri E, Marchese L, Camino G (2004) Heat induced structure modifications in polymer-layered silicate nanocomposites. Macromol Mater Eng 289(9): 783–786
29. Wang J, Du J, Zhu J, Wilkie CA (2002) An XPS study of the thermal degradation and flame retardant mechanism of polystyrene-clay nanocomposites. Polym Degrad Stab 77(2): 249–252
30. Tang Y, Lewin M, Pearce EM (2006) Effects of annealing on the migration behavior of PA6/ Clay nanocomposites. Macromol Rapid Comm 27(18):1545–1549
31. Hao J, Lewin M, Wilkie CA, Wang J (2006) Additional evidence for the migration of clay upon heating of clay/polypropylene nanocomposites from X-ray photoelectron spectroscopy (XPS). Polym Degrad Stab 91(10):2482–2485
32. Tang Y, Lewin M (2007) Maleated polypropylene OMMT nanocomposite: annealing, structural changes, exfoliated and migration. Polym Degrad Stab 92(1):53–60
33. Lewin M, Tang Y (2008) Oxidation-migration cycle in polypropylene-based nanocomposites. Macromolecules 41(1):13–17
34. Frache A, Monticelli O, Ceccia S, Brucellaria A, Casale A (2008) Preparation of nanocomposites based on PP and PA6 by direct injection moulding. Polym Eng Sci 48(12): 2373–2381
35. Ceccia S, Bellucci F, Monticelli O, Frache A, Traverso G, Casale A (2010) The effect of annealing conditions on the intercalation and exfoliation of layered silicates in polymer nanocomposites. J Polym Sci Pol Phys 48(23):2476–2483
36. Mcneill IC, Leiper HA (1985) Degradation studies of some polyesters and polycarbonates 1 polylactide: general features of the degradation under programmed heating conditions. Polym Degrad Stab 11(3):267–285
37. Mcneill IC, Leiper HA (1985) Degradation studies of some polyesters and polycarbonates 2 polylactide: degradation under isothermal conditions, thermal degradation mechanism and photolysis of the polymer. Polym Degrad Stab 11(4):309–326
38. Wachsen O, Reachert KH, Kruger RP, Much H, Schulz G (1997) Thermal decomposition of biodegradable polyesters—III studies on the mechanisms of thermal degradation of oligo-L-lactide using SEC LACCC and MALDI-TOF-MS. Polym Degrad Stab 55(2):225–231
39. Fan YJ, Nishida H, Hoshihara S, Shirai Y, Tokiwa Y, Endo T (2003) Pyrolysis kinetics of poly(L-lactide) with carboxyl and calcium salt end structures. Polym Degrad Stab 79(3): 547–562
40. Liu X, Zou Y, Li W, Cao G, Chen W (2006) Kinetics of thermo-oxidative and thermal degradation of poly(D, L-lactide) (PDLLA) at processing temperature. Polym Degrad Stab 91(12):3259–3265
41. Kopinke FD, Mackenzie K (1997) Mechanistic aspects of the thermal degradation of poly(lactic acid) and poly(b-hydroxybutyric acid). J Anal Appl Pyrol 40–41:43–53
42. Kopinke FD, Remmler M, Mackenzie K, Moder M, Wachsen O (1996) Thermal decomposition of biodegradable polyesters—II Poly(lactic acid). Polym Degrad Stab 53(3): 329–342
43. Gogolewski S, Jovanovic M, Perren S, Dillon J, Hughes M (1993) The effect of melt-processing on the degradation of selected polyhydroxyacids: polylactides, polyhydroxybutyrate, and polyhydroxybutyrate-co-valerates. Polym Degrad Stab 40(3):313–322
44. Jamshidi K, Hyon S, Ikada Y (1988) Thermal characterization of polylactides. Polymer 29(12):2229–2234
45. Cam D, Marucci M (1997) Influence of residual monomers and metals on poly (L-lactide) thermal stability. Polymer 38(8):1879–1884
46. Bensons SW, Nangia PS (1979) Some unresolved problems in oxidation and combustion. Accounts Chem Res 12(7):223–228
47. Gupta MC, Deshmukh VG (1982) Thermal oxidative degradation of poly-lactic acid Part I: activation energy of thermal degradation in air. Coll Polym Sci 260(3):308–311

48. Gupta MC, Deshmukh VG (1982) Thermal oxidative degradation of poly-lactic acid Part II: molecular weight and electronic spectra during isothermal heating. Coll Polym Sci 260(5): 514–517
49. Pluta M, Galeski A, Alexandre M, Paul MA, Dubois P (2002) Polylactide/montmorillonite nanocomposites and microcomposites prepared by melt blending: structure and some physical properties. J Appl Polym Sci 86(6):1497–1506
50. Paul MA, Alexandre M, Degee P, Henrist C, Rulmont A, Dubois P (2003) New nanocomposite materials based on plasticized poly(L-lactide) and organo-modified montmorillonites: thermal and morphological study. Polymer 44(2):443–450
51. Marras S, Zuburtikudis I, Panayiotou C (2007) Nanostructure vs. microstructure: morphological and thermomechanical characterization of poly(L-lactic acid)/layered silicate hybrids. Eur Polym J 43(6):2191–2206
52. Chen G, Yoon J (2005) Morphology and thermal properties of poly(L-lactide)/poly (butylene succinate-co-butylene adipate) compounded with twice functionalized clay. J Polym Sci Polym Phys 43(5):478–487
53. Zhou Q, Xanthos M (2009) Nanosize and microsize clay effects on the kinetics of the thermal degradation of polylactides. Polym Degr Stab 94(3):327–338
54. Okamoto K, Toshima K, Matsumura S (2005) Degradation of poly(lactic acid) into repolymerizable oligomer using montmorillonite K10 for chemical recycling. Macromol Biosci 5(9):813–820
55. Fukushima K, Murariu M, Camino G, Dubois P (2010) Effect of expanded graphite/layered-silicate clay on thermal, mechanical and fire retardant properties of poly(lactic acid). Poly Degr Stab 95(6):1063–1076
56. Chang J, An Y, Sur G (2003) Poly(lactic acid) nanocomposites with various organoclays I Thermomechanical properties, morphology and gas permeability. J Polym Sci Polym Phys 41(1):94–103
57. Lee JW, Lim YT, Park OO (2000) Thermal characteristics of organoclay and their effects upon the formation of polypropylene/organoclay nanocomposites. Polym Bull 45(2):191–198
58. ISO standard 5660 (2002)
59. ASTM standard E 1354 (2003)
60. Bourbigot S, Duquesne S (2007) Fire retardant polymers: recent developments and opportunities. J Mater Chem 17(22):2283–2300
61. Bartholmai MM, Schartel B (2004) Layered silicate polymer nanocomposites: new approach or illusion for fire retardancy? Investigations of the potentials and the tasks using a model system. Polym Adv Technol 15(7):355–364
62. Bourbigot S, Fontaine G (2010) Flame retardancy of polylactide: an overview. Polym Chem 1(9):1413–1422
63. Zanetti M, Kashiwagi T, Falqui L, Camino G (2002) Cone calorimeter combustion and gasification studies of polymer layered silicate nanocomposites. Chem Mat 14(2):881–887
64. Gilman JW, Jackson CL, Morgan AB, Harris R, Manias E, Giannelis EP, Wuthenow M, Hilton D, Phillips SH (2000) Flammability properties of polymer—layered-silicate nanocomposites polypropylene and polystyrene nanocomposites. Chem Mat 12(7): 1866–1873
65. Bocchini S, Frache A, Camino G, Costantini E, Ferrara G, Fatinel F (2006) Poly-1-Butene/ Clay nanocomposite effect of compatibilisers on thermal and fire retardant properties. Polym Adv Technol 17(4):246–254
66. Bourbigot S, Fontaine G, Bellayer S, Delobel R (2008) Processing and nanodispersion: A quantitative approach for polylactide nanocomposites. Polym Test 27(1):2–10
67. Bourbigot S, Fontaine G, Duquesne S, Delobel R (2008) PLA nanocomposites: quantification of clay nanodispersion and reaction to fire. Int J Nanotechnol 5(6/7/8):683–692
68. Murariu M, Bonnaud L, Yoann P, Fontaine G, Bourbigot S, Dubois P (2010) New trends in polylactide (PLA)-based materials: "Green" PLA-Calcium sulfate (nano) composites tailored with flame retardant properties. Polym Degrad Stab 95(3):374–381

69. Solarski S, Mahjoubi F, Ferreira M, Devaux E, Bachelet P, Bourbigot S, Delobel R, Coszach P, Murariu M, Da Silva FA, Alexandre M, Degee P, Dubois P (2007) Plasticized Polylactide/clay nanocomposite textile: thermal, mechanical, shrinkage and fire properties. J Mater Sci 42(13):5105–5117
70. Murariu M, Da Silva Ferreira A, Bonnaud L, Dubois P (2009) Calcium sulfate as high-performance filler for polylactide (PLA) or how to recycle gypsum as by-product of lactic acid fermentation process. Compos Interf 16(2–3):65–84
71. Fontaine G, Bourbigot S (2009) Intumescent polylactide: A nonflammable material. J Appl Polym Sci 113(6):3860–3865
72. Bourbigot S, Le Bras M, Delobel R, Decressain R, Amoureux JP (1996) Synergistic effect of zeolite in an intumescence process: study of the carbonaceous structures using solid-state NMR. J Chem Soc Faraday T 92(1):149–158
73. Bourbigot S, Le Bras M, Dabrowski F, Gilman JW, Kashiwagi T (2000) PA-6 clay nanocomposite hybrid as char forming agent in intumescent formulations. Fire Mater 24(4):201–208

Chapter 11
Starch/Clay Nano-Biocomposites

Analía Vazquez, Viviana P. Cyras, Vera A. Alvarez and Juan I. Moran

Abstract The aim of this chapter is to describe the main studies and results on starch-based nanocomposites reinforced with clay particles. This particular combination leads to the formation of a nanocomposite material with novel properties. However, a good knowledge about starch (structure, type, chemical and physical modification) and its rheological behaviour is necessary for developing these nanocomposites. Many factors and processing parameters affect the final properties of the starch based nano-biocomposites. The main factors which influence the mechanical properties of the nano-biocomposites will be analyzed such as the type of clay, the chemical modification of clay, the type of plasticizer, the water humidity test conditions, the use of chemically modified starches, the thermal stability and water absorption. In addition, the influence of different processing techniques and mixing methods will be studied.

11.1 Starch as a Matrix for Nano-Biocomposites

The term nanocomposite refers to those materials manufactured using a reinforcement with at least one dimension in the range of the nanometer (10–9 m). The first efforts to use nanometer-sized reinforcements date back to 1976, with the work of Fujiwara and Sakamoto [1]. In 1989, researchers from Toyota reported the first nanocomposite made from nylon 6 and montmorillonite [2–4] displaying

A. Vazquez (✉)
INTECIN, University of Buenos Aires, Buenos Aires, Argentina
e-mail: avazquez@fi.uba.ar

V. P. Cyras · V. A. Alvarez · J. I. Moran
INTEMA, National University of Mar del Plata, Buenos Aires, Argentina

L. Avérous and E. Pollet (eds.), *Environmental Silicate Nano-Biocomposites*, Green Energy and Technology, DOI: 10.1007/978-1-4471-4108-2_11,

exceptional mechanical properties. Since then, numerous research groups have worked on the development of polymer nanocomposites [5–7]. The most common nanoparticles used to reinforce polymeric materials are layered silicates. The use of montmorillonites and bentonites is very interesting due to environmental and economic reasons [8]. In addition, their natural abundance, and their mechanical and chemical resistances makes them very useful as polymeric material reinforcements. Finally, a new challenge is the production of biodegradable nanocomposites using for example a biodegradable polymer matrix and reinforcing it with a nanoscale material.

Natural biodegradable polymers appear as an attractive solution to the problems associated with the production, use and disposal of conventional non-degradable plastics. Starch is a very attractive source for the development of biodegradable nanocomposites. Starch is one of the most economical biodegradable materials currently available in the global market and is a very versatile biopolymer with great potential for applications in non-food industries [9, 10]. The price of starch is currently much lower than that of polyethylene and other commodities [10, 11].

Starch is obtained mainly from cereals (corn, wheat, etc.), and to a lesser extent from tubers such as potatoes and cassava. World production of starch has increased significantly over the past 30 years, reaching 70 million tons in 2010. The U.S. is the world's leading producer of starch. However, the production of corn starch in China is growing at a rate close to 15 % per year, competing directly with producers in Europe and the U.S. [12].

The main sources of starch are maize, cassava, wheat and potato. The starch from cereals is the most important with 81 % global market share (73 % and 8 % for corn and wheat, respectively). The second most important sources of starch are the tubers and roots which account for 18 % of world production (14 % cassava, 4 % potato) [12–14]. Starch from cassava is grown mainly in tropical and subtropical regions. The cassava starch market is divided primarily between Asia (90 %) and Latin America (10 %). Thailand and Brazil are the countries with the largest producers respectively. On the other hand, Europe is the largest producer of potato starch accounting for more than 80 % of the world production (The Netherlands, France, Belgium, Germany and Switzerland) [13].

The preponderance of cereal starch in the market is attributed to an easier and faster extraction process due to its lower moisture content (Table 11.1). The extraction of starch from roots and tubers consume a large amount of water during the washing, grinding and sedimentation steps. This water must be carefully treated before returning it to the environment, which makes the process more expensive. Even after the extraction process, the moisture content in this type of starch is about 40 %. Therefore, additional costs are incurred in order to complete the drying process [15]. Despite the major difficulties associated with the extraction process, the root and tuber starches have particular physical and rheological properties that make them attractive for use in specific products.

Starch is used in food industries, as thickening, binding, and filling agent. Starch is commonly used in canned soups, instant desserts, ice creams, processed meats, sauces, bakery products, and production of sugar. However, starch is being

Table 11.1 Composition of starch by source [11]

	Fibre	Lipids	Protein	Moisture	Starch
Maize	2, 5	3, 5	11	18	65
Wheat	3	2	14	15	66
Cassava	0, 75	0, 25	1	71	27
Potato	0, 5	0, 5	2	79	18

used in several non-food applications such as textile, paper, plywood, adhesives and pharmacology industries.

The use of starch for non-food applications is still a discussion topic due to the global rise in food prices. Using food for other purposes is reasonably controversial. However, there are different industries which produce starch-rich residues (i.e. production of fried potatoes or rice), and their use in other applications could add value to the whole process and contribute solving the waste accumulation concern.

It is clear that the use of starch as a matrix in the fabrication of nanobiocomposites can be an interesting way to add value to this material for food and non-food applications.

11.2 Starch Structure

Starch is the most important form of energy storage in plants [16]. Starch can be found in the form of discrete semi-crystalline particles called granules, whose size, shape, morphology and composition depend on the botanical origin [17–21]. The structural differences arise from the variation in activity levels of enzymes that synthesize starch within the plant [22, 23].

The starch granules are partially crystalline and are composed mainly of two glucopyranose homopolymers: amylose and amylopectin. Starch granules are insoluble in water. The properties of starch depend largely on the content of amylose and amylopectin as well as the shape and size of the granules. The presence of numerous hydroxyl groups determines the hydrophilic nature of starch.

Amylose is an essentially linear polymer composed of D-glucopyranose units linked by α−1,4 links (Fig. 11.1a) [22, 24]. Some amylose molecules have a small number of branches (between 0.3 and 0.5 %) caused by unusual α-1,6 type links [22, 25]. The degree of polymerization of amylose molecules depends on the botanical origin of the starch granules. In rice starch, the number of glucopyranose units forming amylose molecules is about 900−1,100 [26]. In corn starch, it is about 900–1300 units, and in potato and tapioca starch, it is about 2,500–5,000 units [26, 27]. Generally, the amylose content in starch is 15–30 %, depending mainly on its botanical origin [18–20, 28–33]. However, there are different types of genetically altered starches that have amylose contents between 0 and 80 %.

On the other hand, amylopectin is a highly branched polysaccharide. Amylopectin consists in thousands of D-glucopyranose units linked by α-1,4 links

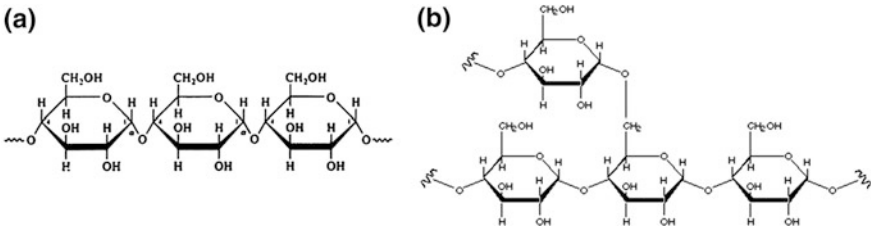

Fig. 11.1 Chemical structure of **a** amylose and **b** amylopectin

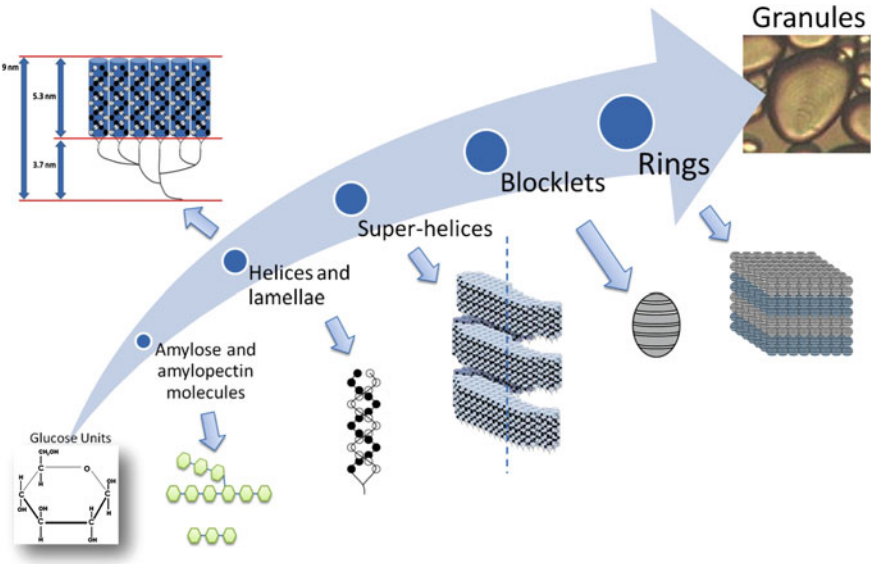

Fig. 11.2 Starch structure at different levels of organization

(Fig. 11.1b). The ramifications are produced by the formation of a small amount (4–5 %) of α−1,6 links [34]. The average degree of polymerization is between 4×10^5 and 4×10^7 anhydroglucose units. Individual chain segments are between 10 and 100 glucose units [20, 22].

During the last decades, significant progress was made in order to reveal the fine structure of the molecules that make up the starch granules. However, many details still remain unexplained [20, 29, 35, 36]. Starch has a very complex hierarchical structure, which may be described better if divided into different levels of organization [20, 22, 29, 35–38].

Starch complex hierarchical structure is sketched in Fig. 11.2.

In the superstructure of starch granules, amylopectin gives rise to the creation of superstructures with different levels of organization, while amylose is distributed in the amorphous regions. For this reason, the description of the hierarchical structure is concentrated mainly in the superstructures formed by amylopectin chains.

- Structure in the range 0.1–1 nm—amylopectin molecules:

Peat et al. [39] described the basic structure of amylopectin in terms of three types of chains (A, B, and C). They form a tree like structure. A type chains are linked through their reducing ends to B chains, which are also linked to C type chains. The reducing end of C type chains grows from the center of the granule (hilum).

- Structure in the range 1–10 nm—semi-crystalline lamellae:

A type chains and the linear region of B type chains are arranged in double helices in a structure similar to DNA. The helical structure is interrupted at the point where branching occurs. A complete turn of each single helix consists of 6 units of glucose (2.1 nm). The chain length between branches (CL) depends on the origin, age and growing conditions of the plant. Furthermore, the double helices are grouped in parallel crystalline regions (crystalline lamellae). Each lamella is attached to another one by highly branched amylopectin chains, forming an amorphous region of 3–4 nm thick (amorphous lamellae). Amylose molecules are distributed in the latter region. The lamellae are laterally associated into units called clusters [22, 40, 41].

- Structure in the range 10–100 nm—super-helices and blocks:

The spatial arrangement of clusters gives rise to a succession of crystalline and amorphous regions. The association of lamellae is not flat, but it generates a superstructure known as super-helix. This super-helix has a thickness of 4–5 helices, a width of approximately 18–40 double helices and a separation between levels of the order of 9 nm. Several super-helices form spherical blocklets. The length of the blocklets is about 10 full turns of the super-helix (approximately 100 nm). Each blocklet is formed by amorphous and crystalline regions.

- Structure in the range 100–1,000 nm—Growth rings:

The relation between amorphous and crystalline regions in the blocklets depends on the degree of branching of amylopectin chains. A greater proportion of branches hinder the parallel arrangement of amylopectin double helices, leading to a lower degree of crystallinity. Throughout its growth, the starch granules experience different environmental conditions. Growing conditions vary periodically, during some periods the growth of crystalline blocklets is favored. Afterward, the opposite happens and the formation of highly amorphous blocklets prevails. This sequence of blocklets types gives rise to the so-called growth rings [22, 40, 41].

- Structure in the range 1–100 μm: Granules:

Starch granules are formed by 2–200 concentric growth rings. The observation of starch granules under cross polarized light in an optical microscope shows the Maltese cross, typical of the radial orientation of macromolecules [34].

These granules have a diameter ranging from 1 to 100 μm and can be present in different regular or irregular shapes (spherical, oval, prismatic, lenticular).

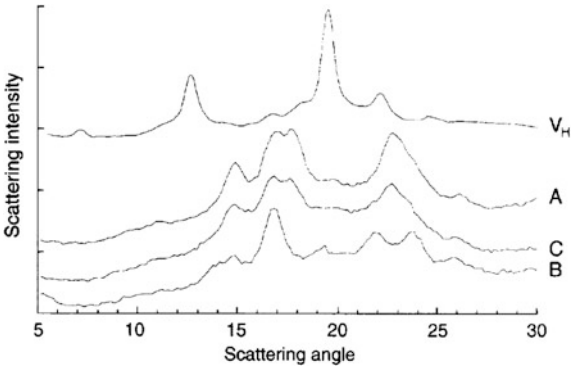

Fig. 11.3 XRD patterns of different starch types: A, B, C, and V_H. Reproduced from van Soest J.J.G. and Vliegenthart J.F.G. [45] with kind permission from ©Elsevier 1997

The crystalline domains within the starch granule can present two allomorphic structures that are characterized by distinctive diffraction patterns (A and B). The diffraction pattern 'A' is typical of corn starch. In contrast, the 'B' pattern corresponds to starches derived from tubers and roots. The pattern 'C' is an intermediate pattern between the 'A' and 'B', but does not correspond to a specific crystalline structure [19]. The differences between crystal types 'A' and 'B' are related to the packing of double helices in the unit cell and the number of water molecules that stabilize these helices. In the 'A' type structure packing is monoclinic with four water molecules per unit cell. In contrast, the 'B' type structure has an hexagonal packing, which leaves room for an interior channel that can hold up to 36 water molecules per unit cell [29]. The crystal structure in the starch granule is determined by the chain length between branches of amylopectin molecules [42, 43]. If the chain length is less than 19.7 anhydroglucose units, the granule will show an 'A' type pattern. If the length is increased to 21.6 units, it will show the most common type 'B' pattern. However, for intermediate values, the granule will show the type 'C' pattern. Finally, another crystalline form associated to the amylose fraction can be observed. Pattern V is usually observed in high amylose starches and correspond to a single left handed amylose helix [44]. The X-ray diffraction patterns corresponding to all types of starch crystals are shown in Fig. 11.3.

The type of X-ray diffraction pattern, morphology and average size of the granules of starches derived from different botanical sources are shown in Table 11.2.

11.3 Starch Modification

While it is possible to produce plastics from native starch, these are not suitable for use as packaging material due to its poor mechanical properties and high moisture susceptibility. As a result, numerous physical and chemical modification methods have been developed to enhance starch's positive characteristics, reduce its undesirable qualities and add new attributes [15, 25, 35, 44, 50–53]. The main limitations associated with the use of native unmodified starch are its very high viscosity

Table 11.2 Size, morphology and X-Ray pattern of starch from different botanical sources [19, 21, 46–49]

Source	Average Size	Morphology	X-ray pattern
Corn	5–30	Round, polygonal	A
Rice	1–6	Polygonal	A
Wheat	1–45	Round, lenticular	A,B
Potato	1–100	Oval, spherical	B
Sweet potato	10–30	Round, polygonal	A
Cassava	1–40	Round, polygonal	A

for low solid concentrations (which makes it difficult to process) and its high susceptibility to retrogradation (starch gels become opaque and release water).

The modification of starch can act on the following attributes [46]: susceptibility to humidity/moisture; swelling capacity; solubility; resistance (thermal, mechanical, chemical); characteristics of starch gels and pastes (clarity, rheology, temperature characteristics); compatibility (interaction with other substances); enzymatic degradation susceptibility; ability to act as emulsifying agent; ability to stabilize suspensions; ability to encapsulate particles; and interaction with charged particles.

There are basically two methods for the modification of starch: physical and chemical. The physical modification of starch promotes structural changes within the starch granules in order to alter their behaviour. The starch granules are subjected to the action of temperature, humidity and/or mechanical stress in order to induce partial or complete gelatinization and thereof, the loss of crystallinity. It is achieved by independent or simultaneous application of heat and shear. The properties of physically modified starch strongly depend upon several factors, including its botanical origin, the treatment temperature, heating time, and shear intensity among others. But the most important parameter is the moisture content during the treatment (which determines the degree to which gelatinization occurs). Physical modification of starch is important because it allows obtaining starch with different properties without the use of chemical reagents [50]. The physical modification of starch granules leads to starch with different solubility in cold water [51, 54–84].

Chemical modification of starch is carried out by the reaction or treatment of native starch with chemical reagents to introduce new functional groups, induce the cleavage of molecular chains, promote oxidation of molecules or induce molecular rearrangement [25]. Several factors affect the extent of the chemical reactions during starch modification (composition, morphology and structure of starch granules, reaction conditions, among others) [15, 25, 35, 50, 85–87]. The main methods of chemical modification can be divided into conversion and derivatization.

Conversion refers to the partial or complete depolymerization of starch. The high viscosity of starch blends and pastes originates from its high molecular weight and swelling capacity. Certain applications (especially those requiring high concentrations of starch) need to use lower molecular weight products because they exhibit a low viscosity, facilitating their processing [46]. The main starch conversion processes are acid hydrolysis [25, 46, 52], oxidation [50], dextrinization or pyroconversion [25, 46, 52] and enzymatic hydrolysis [88, 89].

Table 11.3 Different clays and their composition

Phyllosilicate	General formula	CEC (meq/100 g)
Montmorillonite (MMT)	$M_x(Al_{4-x}\ Mg_x)Si_8O_{20}(OH)_4$	119
Hectorite	$M_x(Al_{6-x}\ Mg_x)Si_8O_{20}(OH)_4$	55
Saponite	$M_x\ Mg_6(Si_{8-x}\ Al_x)O_{20}(OH)_4$	100

M = monovalent cation; x = isomorphic substitution degree (between 0.5 and 1.3)

Derivatization refers to the modification of starch by reaction of the hydroxyl groups, replacing them with other groups with the desired functionality. Many types of derivatized starch can be obtained. The main derivatization methods are grouped together according to the type of substituent used: stabilization [25, 50, 90, 91], crosslinking [25, 90, 92, 93], cationization [94–99] and grafting [100, 101]. Most derivatization reactions are carried out in suspensions with high starch content (30/40 %) with constant stirring and controlled temperature and acidity [46].

11.4 Clays and Clay Modification

Clay is a naturally occurring aluminium silicate composed primarily of fine-grained minerals. Clay has a crystalline structure consisting of bi-dimensional layers where a central octahedral layer of either alumina or magnesia is joined to two external tetrahedrons of silica in such a way that the oxygen ions of the octahedral layer also belong to the tetrahedral layers [102, 103]. Clay is a subtype of phyllosilicate minerals.

There are different types of alumino-silicates depending on the content of each compound: alumina, magnesia, silica. This type of clay is characterized by a moderate negative charge (known as cation exchange capacity, CEC, and expressed in meq/100 g [104, 105] (Table 11.3).

In order to obtain a nanocomposite material with the desired properties, a key point is the dispersion of the silicate layered particles in the polymeric matrix. The diffusion of the polymer molecules can lead to different degrees of layer penetration. Intercalated structure is the physical process by which the polymer goes into the galleries formed between two clay layers. In this case, the clay layers stacking remains and the width of the gallery (d_{001}, also called *d-spacing*) is not much higher than initially. However, the best properties can be obtained only when a totally exfoliated structure is achieved [106]. Complete exfoliation means that the silicate layers are completely individually dispersed in a continuous polymeric matrix. Nevertheless, the tendency of the particles to agglomerate is very important and difficult to overcome. Thus, the nature of the clay interlayer gallery is the crucial factor that affects the exfoliation process necessary for the delamination of the clay platelet stacks into individual silicate layers [107].

Due to the presence of exchangeable cations within the clay's galleries, they usually show a hydrophilic nature. In contrast, polymers are generally hydrophobic. Therefore, it is necessary to make a previous treatment to the clay or to the

polymer in order to increase the polymer/clay compatibility. The most popular method consists on converting these hydrophilic silicates to organophilic ones via an ionic exchange reaction [103, 108, 109]. During this reaction, the hydrated Na^+ cations that are situated in the interlayer (which are not structural) are replaced by other positively charged surfactants such as alkyl ammonium or phosphonium cations with long alkyl chains [103, 108, 109]. Depending on the functionality, the packing density, and the length of the modifiers, the organically modified clay could be able to optimize the compatibility with a given polymer [110]. In addition, the basal spacing of the layers increases, giving more space for the polymeric chains to enter between clay galleries [111]. The obtained modified clays have lower surface energy than unmodified clays and result more compatible with hydrophobic polymers. Thus, polymers will be able to introduce inside the galleries under defined processing conditions [103, 112].

As it has been previously explained, modifications are generally performed by exchanging the inorganic cations of the clay by ammonium or phosphonium cations (quaternary salts). Some of the most common quaternary-ammonium salts are summarized on Table 11.4.

The quantity of modifier is related to the clay's CEC. The mass of organic cation and clay needed can be determined using the following equation [113]:

$$M_c = f.CEC.X.PMc.10^{-3} \tag{11.1}$$

where: M_c is the mass of organic cation (g); f is the fraction of CEC satisfied by the organic cation; CEC is the cation exchange capacity of the clay (meq/g clay); X is the mass of clay (g); and PMc is the gram molecular weight of the organic cation (g/mol).

Different organically modified clays are commercially available. Different degrees of hydrophobicity are achieved. Therefore care must be taken prior to selecting the appropriate clay for each polymer to be reinforced. The highest the compatibility, the highest level of intercalation/exfoliation achieved. Figure 11.4 shows the most common types of organically modified clays ordered by increasing polymer/monomer hydrophobicity and increasing surface hydrophobicity [114].

However, starch is hydrophilic due to the presence of several hydroxyl groups within its structure. As a consequence, natural unmodified clays (or with high Na^+ content) should be more compatible. Moreover, hydrophobic clays can also be employed in order to improve other properties, such water absorption or thermal stability.

The mechanism of intercalation by diffusion of starch molecules into the clay galleries was discussed by Zhang et al. [115]. An increase in the d-spacing of the organically modified clays was attributed to the intercalation with starch molecules, while the increase of the d-spacing of the native clays was mainly caused by the intercalation with glycerol (Fig. 11.5). Molecular weight and polar interactions between the clay and the polymer can influence the intercalation of the polymer. The organically modified clay provides a much larger d-spacing than the size of starch molecules. Organically modified clays are immiscible with hydrophilic biomacromolecules such as starch. Therefore, the use of hydrophilic modified clays may be a promising way to further enhance the exfoliation of the clay.

Table 11.4 Quaternary ammonium salts used to modifiy clays-characteristic of the Southern clay products sorted from the highest to the lowest hydrophilicity

Clay	Organic modifier	Modifier concentration (meq/100 g clay)	Specific gravity (g/cm^3)	d_{001} (Å)
Montmorillonite (C Na +)	None	–	2.86	14.0
Closite 30B (C30B)	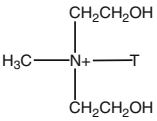	90	1.98	18.8
Closite 10A (C10A)	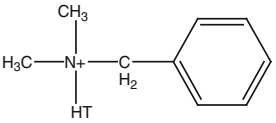	125	1.90	20.0
Cloisite 20A (C20A)	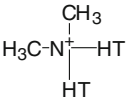 Cloisite 20A	95	1.77	24.2
Cloisite 25A (C25A)	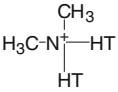	95	1.87	18.6
Cloisite 15A (C15A)	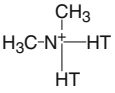 Cloisite15A	125	1.66	31.5
Cloisite 93A (C93A)	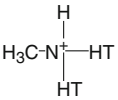 Cloisite 93A	90	1.88	23.6

HT is hydrogenated tallow (≅65 % C18, ≅30 % C16, ≅5 %C14)

Fig. 11.4 Commercially available organically-modified clays order by increasing hydrophobicity [114]

11.5 Rheology of Starch

The use of starch as a base material for the manufacture of bioplastics requires the disruption of the granular structure. This is achieved through the process of gelatinization [116, 117]. When heated in the presence of water, starch granules

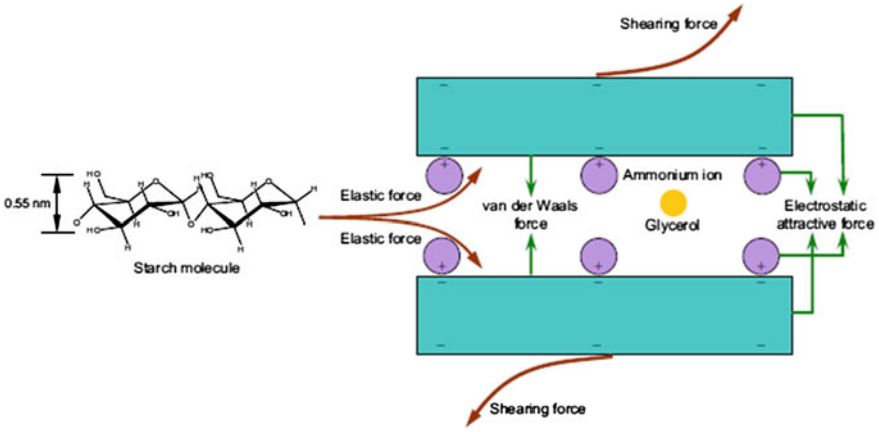

Fig. 11.5 Schema of process of the increase of d-spacing of clay (reprinted from [115] with permission of ©Elsevier Ltd 2007)

Table 11.5 Properties of starch from different botanical sources: amylose content %, swelling capacity, solubility, gelatinization temperature, gelatinization heat [19, 21, 46–49]

Starch source	Amylose content (%)	Swelling capacity (g/g) at 95 °C	Solubility (%) at 95 °C	Tgel (°C)	ΔHgel (J/g)
Normal corn	22,4–32,5	22	22	62,3–84,3	12,0–14,0
Waxy corn	1,4–2,7	–	–	64,3–84,3	13,7–15,4
High amylose corn	42,6–67,8	6,3	12,4	66,8–73,3	13,7
Normal rice	5,0–28,4	23–30	11,0–18,0	57,7–97,5	8,2–13,2
Waxy rice	0,0–2,0	45–50	2,3–3,2	66,1–78,8	7,7–12,1
Normal wheat	18–30	18,3–26,6 (100 °C)	1,55	46,0–76,0	9,0–17,9
Normal potato	21,1–31,0	1159	82	57,0–80,3	12,55–17,4
Sweet potato	19,1	80 (90 °C)	68	64,6–84,6	12,9
True yam	10,0–30,0	17–23	8–17	63,5–74,8	19,2
Cassava tapioca	18,6–23,6	51	26	57,0–84,1	4,8–12,9

swell, increasing its size several times. When the temperature reaches a critical value, usually between 60 and 70 °C, the swelling degree reaches a maximum and the structure of the granules brakes irreversibly, leading to a starch paste [118–122]. Amylose molecules tend to re associate forming small crystalline domains in a process called retrogradation [123].

Highly branched amylopectin molecules require longer times to reorganize [15]. Some properties of the swelling and gelatinization process for different starch sources are summarized in Table 11.5.

Gelatinized starch is usually referred of as thermoplastic starch. This material is the basis for the manufacture of bioplastics. Thermoplastic starch can be obtained by the application of energy in the form of heat or mechanical stress. Moreover, both types of energy can be applied simultaneously during extrusion processing [119, 120, 122].

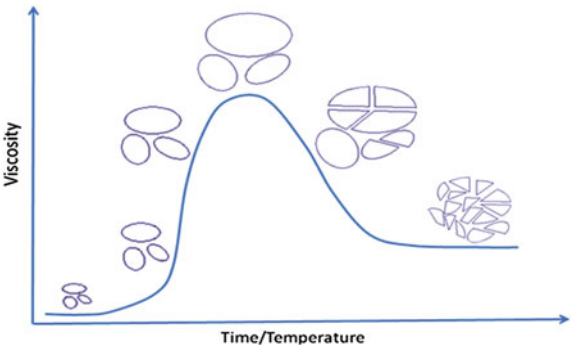

Fig. 11.6 Evolution of starch paste viscosity during heating in excess water. Reproduced from Chivrac, Pollet, Dole & Avérous with kind permission from ©Elsevier Ltd 2010

Detailed knowledge of the rheological behaviour of starch pastes is of critical importance for the development of appropriate extrusion dies and injection molds. Proper viscosity/shear rate functions within relevant shear rates range are needed [124]. The study of the rheological behaviour of starch pastes and suspensions can be divided into two stages. Firstly, the behaviour of starch granules during swelling and gelatinization is studied. Secondly, the rheological behaviour of thermoplastic starch is studied.

As shown in previous section, starch granules swell during continuous heating in presence of excess water. The viscosity of a suspension of particles strongly depends on the concentration [48, 125]. Swelling results in an apparent increase in the concentration of suspended particles, since they take a larger portion of the available volume. Accordingly, a great evolution in the viscosity is observed while heating a starch suspension. After reaching the maximum degree of swelling, the starch granules start breaking apart, leading to a suspension of granule fragments in an amylose-water solution, reducing the apparent viscosity of the paste (Fig. 11.6). If shear is simultaneously applied to the system, the structure of the grain disappears completely resulting in the formation of thermoplastic starch.

11.6 Thermoplastic Starch Rheological Behavior

The transformation of native starch into thermoplastic starch leads to the formation of a re-meltable material that can be processed by extrusion or injection moulding. The destructurization of native starch can be achieved by using a suitable twin screw extruder with additives (water and glycerol) and appropriate operating parameters [124].

The generalization of starch rheology is not an easy task. Many studies can be found on specific literature, but results are fairly dissimilar. This is essentially because too many different formulations are being studied, depending on the final use of the starch based material. One of the variables of the formulation is the starch concentration, as well as the type and quantity of plasticizer being used. Highly concentrated dispersions of poorly swollen granules at temperatures lower than the gelatinization one often show dilatant (the viscosity increases with shear

stress) or shear thickening behaviour (the viscosity decreases with the shear stress), while more diluted suspensions of highly swollen granules at temperatures higher than the gelatinization one show the characteristic pseudo-plastic or shear thinning behaviour [126].

Different authors have studied the influence of several factors on the rheological behaviour of plasticized starch [127–137], such as starch structure [138], chemical modification [139, 140], glycerol content [124], moisture content [141, 142], among others [143].

11.7 Rheology of Starch-Clay Nanocomposites

Chiou et al. [144] studied several types of starch and nanoclays. They investigated wheat, potato and waxy corn starch combined with Cloisite (C) nanoclays: CNa^+, C30B, C10A, and C15A. Dynamic rheological properties of the starch-clays mixtures were measured in a rheometer using plate–plate configuration. The studies were carried out during the gelatinization of starch. The combination of wheat starch and CNa^+ (heated at 95 °C), showed the highest modulus. This behaviour was attributed to two factors: the interaction between the clay and the amylose leached during the gelatinization; and the formation of a material with a gel-like structure. However, when they analyzed the X-ray diffraction patterns, the position of the diffraction peaks did not change, indicating that the platelets of the clay remained in a stacked configuration, and the interaction with starch molecules takes place at the surface level. The addition of the other clays did not produce a significant increase in the modulus due to their hydrophobic character. Wheat and corn starch show a similar modulus. However, potato starch and waxy corn starch show a decrease in the modulus at higher temperatures. In the case of potato starch, this effect has been attributed to the production of a softer material due to the higher swelling. In the case of waxy corn starch, this behaviour has been explained by its low amylose content, which restricts the formation of entanglements, reducing the extent of the gel-like structure.

11.8 Processing Starch/Clay Nanocomposites

The preparation of starch/clays mixtures can be achieved by different processing routes. However, the most important processing techniques (casting, intensive mixing, and extrusion) rely on two different mechanisms of mixing the clay particles and the starch molecules. Mixing of clay with starch should be analyzed by the quality of the mixing. The quality of mixing is related to how well dispersed and distributed are the clay nanoparticles within the natural polymer matrix.

Distributive and dispersive are different mixing mechanisms and their schematic illustration is shown in Fig. 11.7. Dispersive mixing refers to the reduction in size or break-up of the minor component (i.e. clay) of a mixture into smaller size

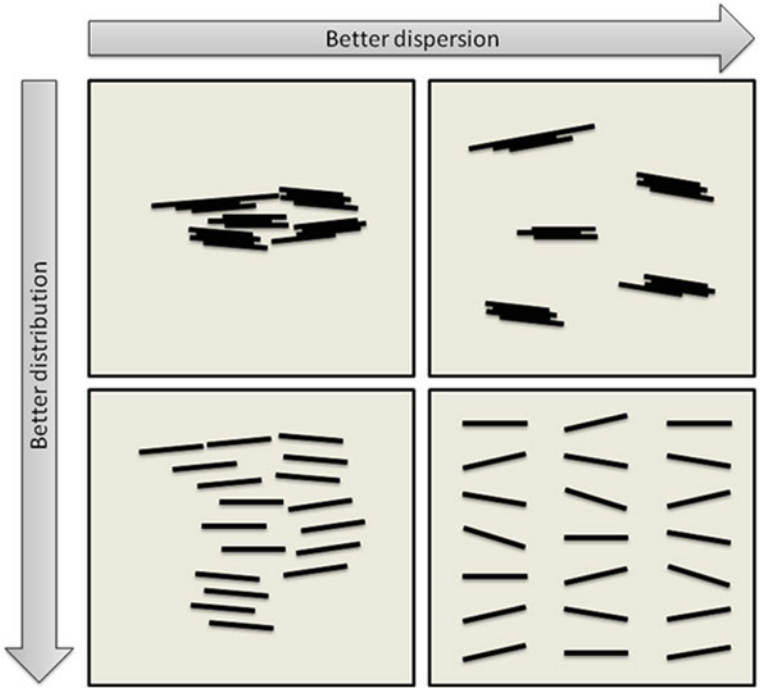

Fig. 11.7 Schematic illustration of dispersive and distributive mixing mechanism. Reproduced from Manas-Zloczower I. and Cheng H [145] with kind permission from ©Elsevier Ltd

particles, whereas distributive mixing leads to a homogenous spatial distribution of the minor component (i.e. clay) into the polymer matrix [145]. In dispersive mixing cohesive resistance has to be overcome to achieve higher levels of dispersion. Dispersive mixing is also called intensive mixing. Distributive mixing aims to improve the spatial distribution of the clay in the starch without cohesive resistance playing a role and is also called extensive mixing.

The selection of an appropriate processing technique greatly influences the final mechanical properties of the bio-nanocomposites [146]. During mixing, voids formation and thermal degradation can take place, affecting the properties of the obtained material.

11.8.1 Solvent Casting

This technique aims to produce intercalation/exfoliation of the layered silicate particles into single layers by using a compatible solvent in which the polymer is also soluble. Layered silicate particles can be easily dispersed, and the weak forces that join the layers together can be easily overcome. The polymer then adsorbs

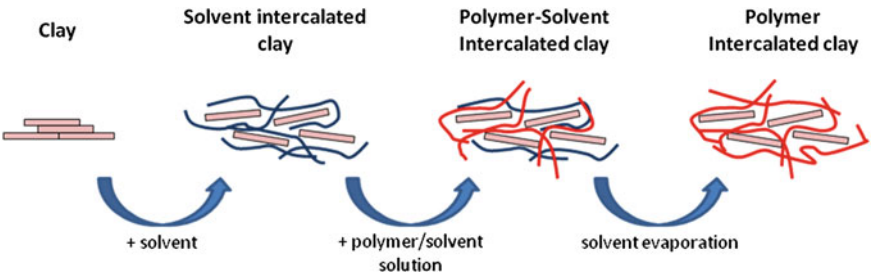

Fig. 11.8 Scheme of exfoliation-adsorption process to produce nanocomposites

onto the delaminated sheets and when the solvent is evaporated, the sheets reassemble, sandwiching the polymer to form an ordered multilayer structure (Fig. 11.8). On a lab scale, starch/clay nanocomposites are usually prepared by solvent casting. This technique is frequently used for investigating the effect of plasticizer content and type as well as clay content and type on the mechanical, thermal and barrier properties of nanocomposites. This processing method requires low temperatures, is relatively simple to set up and leads to well dispersed intercalated/exfoliated nanocomposites. The critical parameters to be taken into account in this technique are the type of solvent (degree of polymer dissolution, swelling of clay) and evaporation conditions (time and temperature). Additionally, some authors have applied ultrasonic waves to facilitate the intercalation/exfoliation of the clay particles, finding that this action also influences the final structure (depending of the time and temperature at which it is applied) [147].

However, this process shows some disadvantages. For instance, it is restricted to thin films due to the formation of blisters and cracks during solvent evaporation. In addition, it is usually a discontinuous and time-consuming process. This technique also requires intercalation/exfoliation of the clay prior to adding it to the gelatinized starch. Consequently, good levels of intercalation/exfoliation are achieved together with a good dispersion of the particles within the matrix.

11.8.2 Intensive Mixing Intercalation

This processing technique aims to produce intercalation/exfoliation of clay platelets by the action of shear forces. The polymer and the clay are mixed together, and shear forces separate the clay particles (Fig. 11.9). The polymer viscosity can be very high because the mixers usually have high power for rotating. The conditions under which dispersive mixing occurs are determined by the balance between the cohesive forces holding agglomerates together and the disruptive hydrodynamic forces. The chemical structure of the clay surface is one of the key factors because if the clay is compatible with starch polymer the dispersion of the clay will be better.

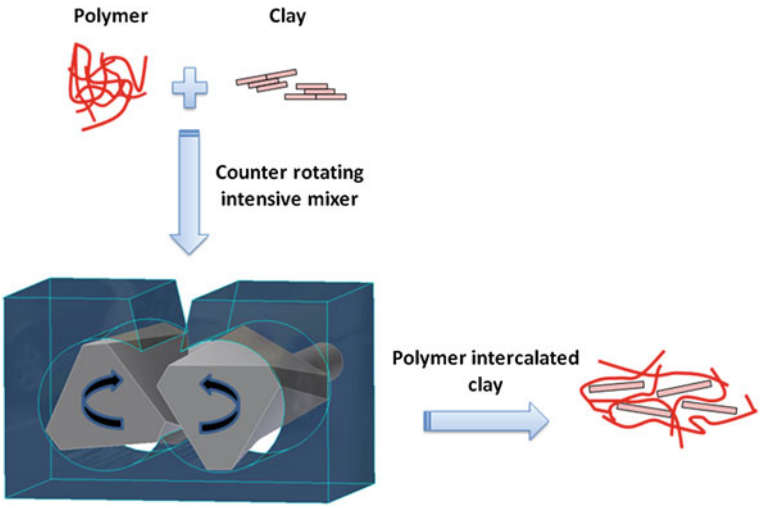

Fig. 11.9 Scheme of melt-intercalation process to produce nanocomposites. Reproduced from Chivrac, Angellier-Coussy, Guillard,Pollet and Luc Avérous with kind permission from ©Elsevier 2010

However, the processing machine used for mixing will also influence the quality of mixing. A minimum shear stress value needs to be reached in order to break apart the clay agglomerates. Elongational flow together with shear flow is much more efficient than shear flow to produce dispersive mixing. Therefore, single screw extruders (and injection molding equipments) are rather inefficient as dispersive mixers because the polymer flow is mainly shear flow. Twin screw extruders (and Brabender like intensive mixers) are preferred when dispersive mixing is required [148, 149]. During this process, the polymer is melt and intercalation/exfoliation of the clay particles takes place (*melt intercalation*).

Figure 11.10 shows a scheme of a twin-screw extruder with the different steps performed for the addition of the different components. In the figure, nylon pellets are added to the extruder. However, this can be adapted to the case of starch granules aqueous suspension. First the starch/water mixture is gradually added into the extruder from the hooper. The feeding zone of the extruder is used for the gelatinization of starch granules. When starch granules are completely gelatinized, a small pump is used for the addition of the clay slurry. The excess of water should be vented to the atmosphere in order to decrease the pressure into the machine. The continuous product is then pelletized and nanocomposite pellets of thermoplastic starch and clay are obtained at the end of the process.

However, the process becomes quite complicated. Therefore, thermoplastic starch pellets are previously prepared and then the normal melt intercalation route is followed.

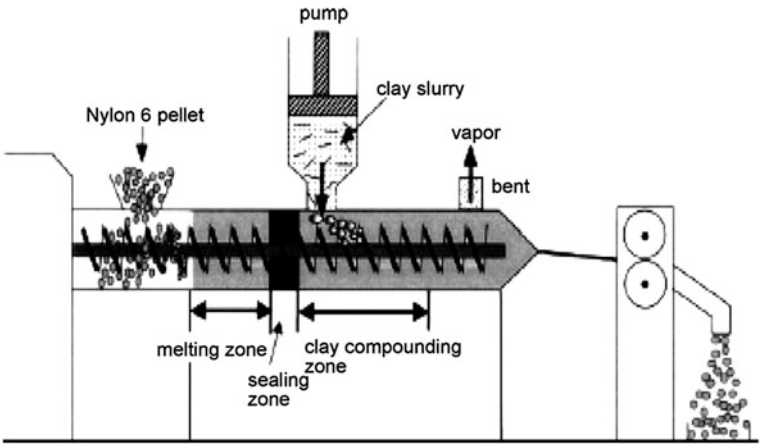

Fig. 11.10 Compounding process for the preparation of clay nanocomposites (reprinted from [150] with permission of Elsevier Ltd 2003)

11.8.3 In Situ Polymerization

This name was used for thermosetting polymer obtained with the clay included during the reaction. If the gelatinization is carried out during the extrusion process and the clay is intercalated/exfoliated at the same time, the process could be called In situ *polymerization.*

If chemical modification of the polymer is needed, the process is called *Reactive extrusion*. In addition, starch can also be gelatinized during the same extrusion process with the addition of clay in some step of the extruder.

11.9 The Influence of the Addition of Clays to the Properties of Thermoplastic Starch

Starch has poor water resistance and relatively poor mechanical properties. In order to improve starch properties, the addition of natural clays to produce nanocomposites have been investigated. Such combination retains starch biodegradation properties, and therefore environmental acceptability, and improves barrier [151], mechanical [152–154], and heat resistance properties [155].

All conditions affect the performance of the final films obtained. The structures obtained depend on: amount of clay and plasticizer, type of starch, plasticizer and clay, glycerol/clay ratio, pH, dispersion methodologies, and processing conditions [156]. In general, an optimum content of plasticizer and/or clay for each system needs to be found in order to produce starch films with the highest levels of exfoliation and best improvement in the properties [157–161].

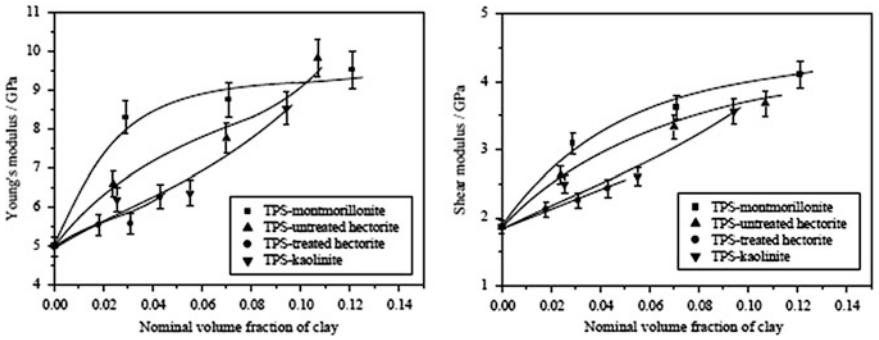

Fig. 11.11 Young's modulus and shear modulus of thermoplastic starch–clay composites (reprinted from [152] with permission of ©Elsevier Ltd 2005)

11.10 Effect of Different Clay Types on the Mechanical Properties

Chen and Evans prepared glycerol-plasticized starch based nanocomposites using different types of clays by intensive mixing processing. They used natural smectite clay, montmorillonite, kaolinite, hectorite, and treated hectorite. The hectorite was modified with 2 methyl, 2 hydrogenated tallow quaternary ammonium chloride.

The presences of clay increased Young's and shear modulus for all the clays. The montmorillonite and unmodified hectorite provided a significantly higher increase than kaolinite and treated hectorite (Fig. 11.11). The treated-hectorite nanocomposites had similar elastic modulus to those composites prepared from kaolinite. Hectorite particles have a lower aspect ratio and larger surface area than montmorillonite. The former factor tends to give a smaller increase in modulus and the latter gives a greater increase in modulus. At low clay volume fraction, montmorillonite caused a higher Young's modulus increase than hectorite but at higher clay fractions, reinforcement ability deteriorated. For nanocomposites, montmorillonite generally provided a slightly greater improvement in the modulus than untreated hectorite.

Figure 11.12 shows the TEM micrographs of the treated hectorite and the glycerol-plasticized starch–treated hectorite composite. The treated hectorite (the hectorite intercalated with quaternary ammonium chloride) showed exfoliated and intercalated structures. The TPS–treated hectorite composite also has these two structures. However, TEM images showed large dark regions, which were attributed to thick large particles, suggesting the formation of clay agglomerates in the nanocomposites. This indicates that the highly hydrophilic starch molecules are not able to interact with the clay and the clay particles cannot disperse well.

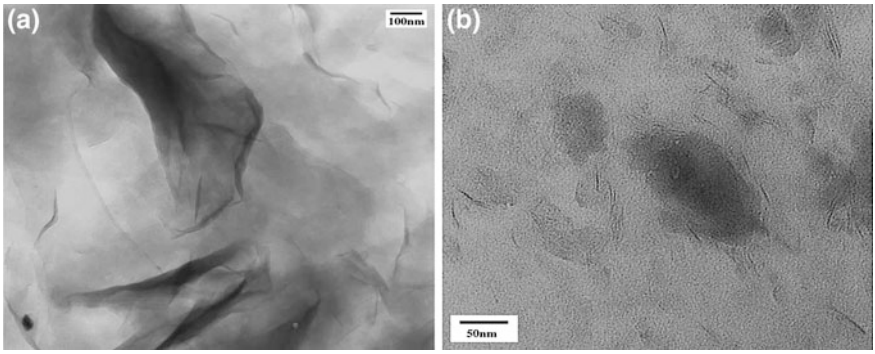

Fig. 11.12 TEM micrographs of **a** treated hectorite, and **b** TPS–treated hectorite composites containing 3 wt% clay platelets (reprinted from [152] with permission of ©Elsevier Ltd 2005)

11.11 Effect of Plasticizer Nature

Chivrac et al. [162] analyzed the effect of the plasticizer nature on the clay exfoliation process in wheat starch composites. The nano-hybrids materials have been elaborated by melt blending starch with glycerol, sorbitol or glycerol/sorbitol mixture. Intercalated/aggregated and exfoliated morphologies were obtained with sodium montmorillonite (MMT-Na) and cationic starch organo-modified montmorillonite (OMMT-CS) respectively. Thermo-mechanical analysis revealed the occurrence of phase separation between plasticizer rich and poor domains induced by the high plasticizer content of the starch formulations. Two relaxations peaks are observed, one for each component. The main relaxation (T_α) is attributed to the plasticized starch glass transition and the second relaxation (T_β) is consistent with the plasticizer glass transition and occurs at lower temperature. This behavior is related to higher plasticizing efficiency of glycerol compared with sorbitol as well as a higher water absorption of glycerol. Table 11.6 shows that T_β changes slightly with the clay content. This may be because the platelets have no effect on the Tg of the plasticizer rich domains. On the other hand, an increase in T_α versus clay content is observed, for all plasticizers. The better the dispersion is, the greater the clay/matrix interface area is, and a higher, than expected Tα was observed for the WS/OMMT-CS samples. Moreover, an increase in T_β as a function of the clay content is observed for all plasticizers. The same effect is found for wheat starch/MMT-CS composites. A portion of the plasticizer is immobilized on the clay platelets. Immobilized plasticizer cannot plasticize the starch matrix, explaining the higher T_α obtained for the wheat starch/MMT. These results were also related to previous observations from TEM analyses, basing such assumption on the high affinity between the clay platelets and the glycerol [163].

Water humidity test conditions

Avella et al. [153] obtained starch/clay nanocomposite films by homogeneously dispersing montmorillonite nanoparticles in different starch-based materials via

Table 11.6 T_α and T_β versus clay clay inorganic content for starch nano-biocomposites plasticized with glycerol, glycerol/sorbitol mixture and sorbitol (reprinted from [162] with permission of Elsevier Ltd)

	T_α (°C)			T_β(°C)		
	Gly	Polysorb	Sorb	Gly	Polysorb	Sorb
WS	11.7	31.7	35.3	−54.6	−23.6	−6.1
WS/MMT-Na 3 wt%	15.7	36.5	41.7	−54.9	−22.9	−6.0
WS/MMT-Na 6 wt%	23.9	38.5	49.8	−50.56	−21.1	−6.0
WS/OMMT-CS 3 wt%	14.9	35.2	41.8	−53.56	−22.9	−6.7
WS/OMMT-CS 3 wt%	21.7	38.4	47.1	−51.6	−22.2	−4.9

Table 11.7 Mechanical analysis of the samples (reprinted from [153] with permission of Elsevier Ltd)

Sample Conditioned at	Clay (%)	Young modulus (MPa)	Stress at peak (MPa)	Strain at break (%)
15 % relative humidity	0	979	19	3
	4	1135	22	4
60 % relative humidity	0	610	9	9
	4	830	10	2
Without conditioning	0	219	6	25
	4	450	6	10

polymer melt processing techniques. Table 11.7 shows the results of mechanical properties of samples containing 65 wt% starch: 20 wt% water: 15 wt% glycerol and their nanocomposites with 4 wt% of clay.

It is known that water can also act as a plasticizer of the polymer and that this effect is also affected by the presence of clay. It was found that the higher the plasticizer content, the lower the elastic modulus and the higher the strain at break resulted. The total amount of plasticizer (water + glycerol) should be high enough to prevent brittleness. A good dispersion of starch into clay interlayer galleries showed an increase of mechanical parameters, such as modulus and tensile strength (dispersed and exfoliated/intercalated).

11.12 Use of Chemical Modified Starches with Clay

Tomasik et al. [164] used modified corn starches with succinic, maleic and phthalic anhydrides to form starch esters. In this case, the esterification reactions were carried out within the extrusion process under the process called reactive extrusion. After esterification, more hydrophobic anionic starch resulted as a product of the reaction of starch with cyclic anhydrides in alkaline medium. The process was undertaken in the presence of water and relatively high temperature (130 °C), which results in a very difficult process.

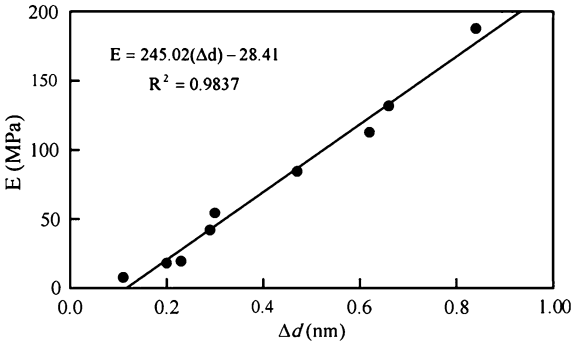

Fig. 11.13 Correlation between Young's modulus and gallery spacing (Δd) of nanocomposites with 5 wt% of various clays (reprinted from [166] with permission of ©Elsevier Ltd 2010)

Recently, Narayan et al. [165] presented a patent claim for the fabrication of chemically modified starch nano-biocomposites reinforced with clays as nanofiller. The chemical modification reaction and plasticizer used defines the chemically modified plasticized starch (CMPS) [165]. The CMPS was prepared by reacting starch with an organic dibasic acid or an anhydride of the acid in the presence of a plasticizer and using optionally free radical initiators. During the extrusion process, it is necessary to extract the water being evaporated from the mixture by means of appropriate venting valves in the extruder. The nanoclays (0.5–25 wt%) can also be incorporated during the reactive extrusion process. This reaction conducts to less hydrophilic starch with a low degree of substitution, which is more compatible with chemically modified clays. The chemically modified thermoplastic starch has lower viscosity than the native thermoplastic starch. The present patent covers the fabrication of pellets of nano-biocomposites based on modified starch.

11.13 Comparison Between some Mechanical Properties of Different Clay/Starch Nanocomposites

As it was stated, the mechanical properties are strongly influenced by the clay type, the glycerol and clay content, the clay's gallery spacing in the intercalated/exfoliated state into the nanocomposite, and the clay mixing mode [144, 153, 166–168].

The Young's modulus increases linearly with the gallery spacing (Fig. 11.13). A greater gallery spacing is representative of more starch molecules that have diffused into the space between the layers and thus promoting more interfacial interactions that lead to more intensive reinforcing effects [166].

The most common technique used to determine the dispersion of the clay into the starch is the Wide Angle X-ray scattering (WAXS). The position of the main peak for the nanocomposite is related to the position of the peak of the pristine clay. This is a way to identify the nanocomposite structure (intercalated or exfoliated).

The spacing of the clay can be determined from Bragg′s law which is given below:

$$n.\lambda = 2.d.\ \sin\theta \quad (1)$$

where: n is an integer indicating the peak number, λ is the wavelength of the X-rays, θ is the angle of incidence of the X-ray beam and d is the spacing between clay layers.

Table 11.8 summarizes different authors' results for uniaxial tensile tests corresponding to different starch/clay nanocomposites.

Chivrac et al. [169] studied plasticized wheat starch reinforced with sepiolite and montmorillonite. Wheat starch/sepiolite nanocomposites showed a higher Young's modulus and stress at break values than the corresponding wheat starch/montmorillonite. This effect was attributed mainly to the better affinity between the sepiolite nanofiller and the polysaccharide chains, and partly to the new crystal structure induced by the dispersion of sepiolite, which increases the overall crystallinity of starch [169, 170].

Chung et al. [164] studied the mechanical properties of corn starch films and the nanocomposites with MMT. Nanocomposites showed an improvement in Young's modulus and tensile strength compared to the pure matrix. The important increase in modulus and strength was attributed to the good dispersion of the clay within the starch matrix [154].

Cyras et al. [155] performed micro-tensile tests on potato starch/glycerol nanocomposites films finding a significant improvement in the Young modulus up to 500 % for the nanocomposite containing 5 wt% of MMT. The authors related this improvement to the stronger interfacial interaction between the matrix and layered silicate due to the vast surface exposed by the clay layers [155].

11.14 Thermal Stability

The thermal stability of starch-based nanocomposites can be evaluated by thermogravimetric analysis. Thermal decomposition of starch involves desorption of physically absorbed water, removal of structural water, depolymerization accompanied by the rupture of C–O and C–C bonds resulting in formation of CO, CO_2 and H_2O, and finally the formation of graphitic carbon structures [160, 174]. On the other hand, pure montmorillonite exhibit mass loss in the temperature range between 100 and 300 °C due to the loss of water (free and from the interlayer water region) and then, the dehydroxylation of bounded hydroxyl groups of the structural water in the temperature range 500–1000 °C. However, the onset decomposition temperature of the organically modified silicates is approximately 200 °C. It has been proposed that the organically modifiers begins to degrade earlier.

The incorporation of clay into the polymer matrix was found to enhance its thermal stability. The degree of nano-scaled dispersion determines the thermal resistance of the nanocomposite. The clay acts as a heat barrier improving the overall thermal stability of the system. When a good interfacial interaction exists in an organic–inorganic composite, the inorganic phase can act as restriction sites

Table 11.8 Mechanical properties of different starches and clays

Reference	Sample	Young modulus (MPa)	Stress at peak (MPa)	Strain at break (%)
Chivrac et al. 2010 [169]	Wheat starch	28.3 ± 1.8	2.24 ± 0.04	31.7 ± 1.5
	Wheat starch + 3 wt% MMT-Na	35.6 ± 0.6	2.32 ± 0.08	27.3 ± 0.6
	Wheat starch + 6 wt% MMT-Na	39.2 ± 1.4	1.90 ± 0.06	21.0 ± 0.8
	Wheat starch + 3 wt% SEP-Na	45.3 ± 1.8	2.91 ± 0.06	36.5 ± 2.1
	Wheat starch + 6 wt% SEP-Na	67.3 ± 2.3	2.99 ± 0.04	31.0 ± 1.0
Cyras et al. 2008 [155]	Potato starch	29.8 ± 4.4	3.3 ± 0.4	62.6 ± 10.1
	Potato starch + 2 wt% of MMT	29.6 ± 12.1	3.1 ± 0.3	55.1 ± 17.2
	Potato starch + 3 wt% of MMT	150.5 ± 25.6	3.2 ± 0.7	37.6 ± 14.5
	Potato starch + 5 wt% of MMT	195.6 ± 38.6	5.2 ± 0.8	46.8 ± 19.2
Chung et al. 2010 [154]	Corn starch	840 ± 61	11.82 ± 0.57	4.62 ± 1.06
	Corn starch + 5 wt% of MMT (conditioned at 43 %RH)	1390 ± 166	15.49 ± 0.67	4.34 ± 1.15
Huang et al. 2004 [171]	Corn starch	38.15	5.51	85.32
	Corn starch + 30 wt% of MMT (conditioned at 39 %RH)	206.74	27.34	17.82
Majdzadeh-Ardakani et al. 2010 [166]	Corn starch + 20 wt% glycerol + 5 wt% MMT (conditioned at 39 %RH)	131.5	9.2	25.2
	Corn starch + 20 wt% glycerol + 5 wt% 30B-MMT (conditioned at 39 %RH)	7.5	2.0	73.3
	Potato starch + 20 wt% glycerol + 5 % MMT (conditioned at 39 %RH)	19.1	2.4	84.8
	Potato starch + 20 wt% glycerol + 5 % 30B-MMT (conditioned at 39 %RH)	41.7	2.5	76.6
Carvalho et al. 2001 [172]	Corn starch (28 % amylose) + 30 wt% glycerol	125 ± 4	5.0 ± 1.0	31 ± 11
	Corn starch (28 % amylose) + 30 wt% glycerol 10 % Kaolin	163 ± 3	5.3 ± 0.3	26 ± 5
	Corn starch (28 % amylose) + 30 wt% glycerol + 30 % Kaolin	200 ± 12	5.9 ± 0.4	18 ± 3
	Corn starch(28 % amylose) + 30 wt% glycerol + 60 % Kaolin	254 ± 22	6.0 ± 0.8	12 ± 3
Wilhelm et at 2003 [173]	Cará roots starch + 20 wt% glycerol	815 ± 90	11 ± 3	–
	Cará roots starch + 20 wt% glycerol + 10 wt% Hectorite	829 ± 50	8 ± 1	–
	Cará roots starch +20 wt% glycerol + 20 wt% Hectorite	850 ± 60	9 ± 3	–
	Cará roots starch +20 wt% glycerol + 30 wt% Hectorite	1046 ± 50	5 ± 1	–

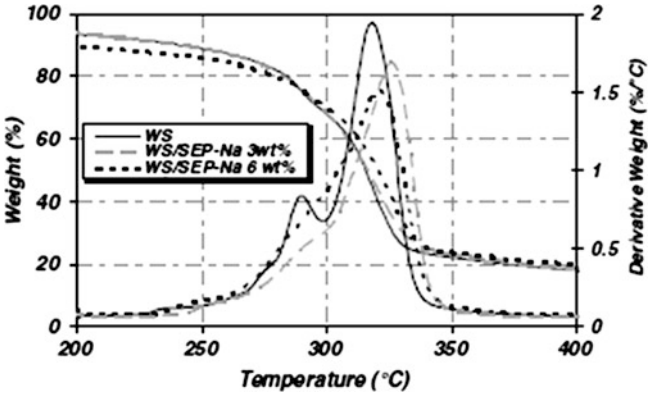

Fig. 11.14 TG and DTG curves for WS, WS/SEP-Na 3 wt% and 6 wt% (reprinted from [169] with permission of ©Elsevier Ltd 2010)

for the movement of polymer chains, which typically increase the degradation temperature. Also, the presence of the filler assists the char formation, during the thermal decomposition [115, 175].

A typical thermogram for wheat starch/glycerol (WS) is showed in Fig. 11.14. It shows three different steps of weight loss at 292, 318 and 526 °C. The first step corresponds to the glycerol plasticizer volatilization. The two others weight losses correspond to the starch amylose and amylopectin thermal degradation. The wheat starch maximum degradation temperature is shifted towards higher temperatures in the nanocomposites and is correlated to the natural sepiolite content (SEP-Na). It has been mainly attributed to an increase in the tortuosity of the diffusion pathway induced by the clay dispersion, which limits the diffusion of the pyrolysis gases to the material surface. While using MMT as clay, a decrease in thermal stability of starch was observed [169].

Thermograms of potato starch/glycerol films usually show three weight losses (Fig. 11.15). The first one between 50 and 180 °C corresponds to water loss, the second between 100 and 260 °C corresponding to the volatilization of the plasticizer, and the last one at around 300 °C corresponds to starch decomposition. No significant difference was found in the thermal stability of starch in presence of glycerol or/and after the incorporation of the montmorillonite (MMT) [176].

Cyras et al. studied glycerol-plasticized potato starch/clay nanocomposites films using from montmorillonite (MMT) as filler. The films were prepared by solvent casting and the clay nanolayers formed an intercalated structure. The thermogravimetric curves showed an initial peak in the temperature range from 30 to 200 °C that represents the evaporation of water and the glycerol. At about 291 °C the starch decomposition was observed. This peak shifted to higher temperatures in the nanocomposites, indicating that the introduction of clay improve the thermal stability of starch (Fig. 11.16) [155].

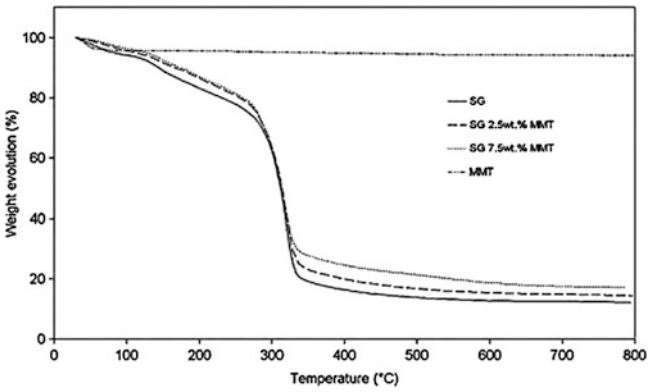

Fig. 11.15 Thermogravimetric curves of MMT powder, starch/glycerol, starch/glycerol 2.5 wt% MMT and starch/glycerol 7.5 wt% MMT films (reprinted from [176] with permission of ©Elsevier Ltd 2010)

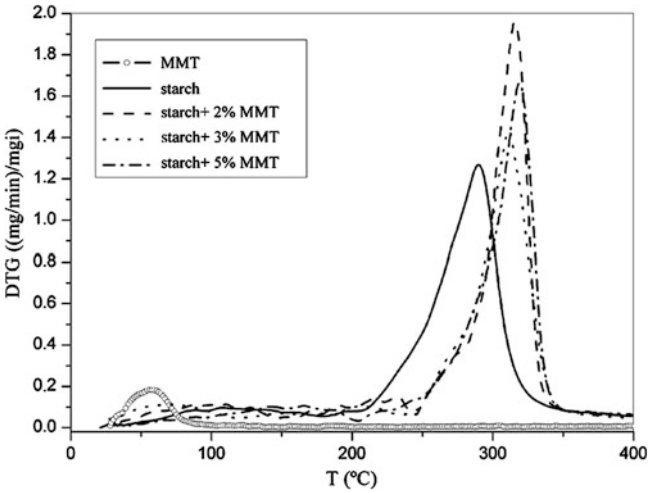

Fig. 11.16 Thermogravimetric curves of films of starch, MMT and its nanocomposites (reprinted from [155] with permission of ©Elsevier Ltd 2008)

11.15 Water Vapour Permeability

The addition of nanoclays has been thought as an interesting approach for reducing the water absorption of starch. However, different results can be found in the specific literature, ranging from significant decrease to slight reduction of water absorption [151, 155, 161, 177, 178].

Table 11.9 Water vapour permeability at 20 °C for a relative humidity difference of 0–100 % for native wheat starch films and related nano-biocomposites with high percentage of glycerol (reprinted from [163] with permission of Elsevier Ltd)

Sample	WVP (mol m^{-1} s^{-1} Pa^{-1})
Wheat starch	2.6×10^{-11}
Wheat starch/3wt% MMT	2.7×10^{-11}
Wheat starch/3wt% MMT-CS	2.8×10^{-11}
Wheat starch/6wt% MMT	2.2×10^{-11}
Wheat starch/6wt% MMT-CS	3.1×10^{-11}

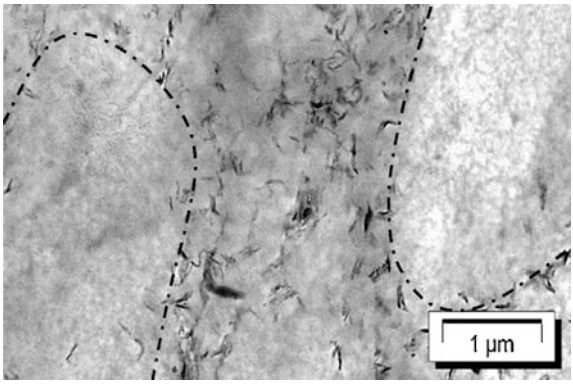

Fig. 11.17 TEM picture of wheat starch/MMT-CS 3 wt% highlighting the phase separation phenomenon (reprinted from [163] with permission of ©Elsevier Ltd 2010)

Chivac et al. [163] studied the water vapour permeability of native wheat starch films (plasticized with 23 wt% glycerol) and wheat starch films (plasticized with 23 wt% glycerol) filled with different contents of montmorillonite (MMT) and organically modified montmorillonite with cationic starch (MMT-CS). The bio-nanocomposites was tested for a 0–100 % relative humidity difference (Table 11.9). The addition of montmorillonite or organically modified montmorillonite did not improve the moisture barrier properties of glycerol-plasticized wheat starch materials. TEM observations showed phase separation among the domains rich in clay platelets and domains without nanofillers (Fig. 11.17). The authors concluded that glycerol rich domains represented a preferred route for water transport and that nanoparticles are preferentially located in starch rich domains.

11.16 Summary

The properties of nano-biocomposites based on starch and clay strongly depend on several factors, such as type of starch and clay, processing method and conditions, moisture content, aspect ratio and degree of dispersion of clay and chemical modification of both starch and clay.

In order to make more hydrophobic starch chemical derivatization is undertaken by reaction of the OH groups, increasing the compatibility with organically-modified clays.

The aspect ratio of the clay (length to width ratio) is also an important factor for the mechanical properties. For higher aspect ratios, lower critical lengths and less nanoparticle contents are necessary to reach the percolation level. Moreover, the higher degree of interlaminar separation achieved (d) the higher will the elastic modulus result. The degree of intercalation and exfoliation depends mainly on the chemical modification of the clay and its compatibility with the starch molecules.

Rheology of starch depends on the type of starch and its chemical modification. The swelling capacity of starch during the gelatinization produces high pressure into the processing equipment, and the final viscosity of the thermoplastic starch also influences the shear flow. The knowledge of the rheology of starch is necessary for determining the processing conditions in order to be able to produce TPS and nanocomposites in an industrial scale. Only a limited number of studies related to the rheological behavior of starch/clay nano-biocomposites have been found [144].

The processing method adopted for the fabrication of nanocomposites plays an important role in their mechanical properties. The most used equipment for producing nanocomposites is the twin-screw extruder due to the combination of shear and elongational flow. However, this processing technique combined with calendering or blow molding will introduce an extra elongation to the extrusion process. In this way, nanoclay particles could be also oriented in one particular direction [179].

The mechanical properties should be measured in the same humidity conditions in order to be able to compare the mechanical properties of different nanobiocomposites. In addition, starch undergoes retrogradation to some extent, depending on the type of starch and their chemical modification. As a consequence, the films properties should be measured after two weeks of fabrication. Mechanical properties depend on the starch and clay type, the chemical modification of starch and/or clay, the processing method and filler content, and on the plasticizer type and amount. The water or humidity absorption of the nanobiocomposite strongly depends on the glycerol content, due to their high degree of hydrophilic character. High glycerol content produces high water absorption. Starch water content influences the results of the mechanical tests.

Acknowledgments The authors kindly thank to the Consejo Nacional de Investigaciones Científica y Técnicas (CONICET).

References

1. Fujiwara S, Sakamoto T (1976) Unichika K.K Japan. Patent Application No. 109998 Japanese Kokai, Japan
2. Okada A, Fukushima Y, Kawasumi M, Inagaki S, Usuki A, Sugiyama S, Kurauch T, Kamigaito O (1988) Toyota Motor Co. Japan. United States Patent No. 4739007. United States Patent and Trademark Office, USA

3. Kawasumi M, Kohzaki M, Kojima Y, Okada A, Kamigaito O (1989) Toyota Motor Co. Japan. United States Patent No. 4810734 United States Patent and Trademark Office, USA
4. Usuki A, Mizutani T, Fukushima Y, Fujimoto M, Fukumori K, Kojima Y, Sato N, Kurauch T, Kamigaito O (1989) Toyota Motor Co. Japan. United States Patent No. 4889885. United States Patent and Trademark Office, USA
5. Thomas S, Zaikov GE, Valsaraj SV (eds) (2008) Recent advances in polymer nanocomposites. Nova Science Publishers, Inc, New York, p 528
6. Valea A, Miguez JC, Mondragón I, González ML (2007) Preparación de nanocomposites de poliamida. Anales de Mecánica de la Fractura 1:359–363
7. Fischer H (2003) Polymer nanocomposites: from fundamental research to specific applications. Mater Sci Eng, C 23(6–8):763–772
8. Zampori L, Gallo Stampino P, Dotelli G, Botta D, Natali Sora I, Setti M (2008) Interlayer expansion of dimethyl ditallowylammonium montmorillonite as a function of 2-chloroaniline adsorption. Appl Clay Sci 41(3–4):149–157
9. Mathew AP, Dufresne A (2002) Morphological investigation of nanocomposites from sorbitol plasticized starch and tunicin whiskers. Biomacromolecules 3(3):609–617
10. Shen L, Haufe J, Patel MK (2009) PRO-BIP2009: Product overview and market projection of emerging bio-based plastics, Group Science, Technology and Society (STS); Copernicus Institute for Sustainable Development and innovation, Utrecht University, Utrecht
11. International Starch Institute (2010) Available www.starch.dk
12. Röper H, Elvers B (2008) Starch economic aspects, in Ullmann's encyclopedia of industrial chemistry (7th edn). Wiley, New York, pp 21–22
13. FAO (2010) Food Outlook-global market analysis. Global information and early warning system, Food and Agriculture Organization of the United Nations, Rome
14. Bertolini AC (2010) Trends in starch applications. In: Bertolini AC (ed) Starches: characterization, properties, and applications. CRC Press, Boca Raton
15. Bertolini AC (ed) (2010) Starches: characterization, properties, and applications. CRC Press, Boca Raton, p 288
16. Stevens ES (2002) Green plastics an introduction to the new science of biodegradable plastics. Princeton University Press, New Jersey
17. Hizukuri S, Takeda Y, Maruta N, Juliano BO (1989) Molecular structures of rice starch. Carbohydr Res 189:227–235
18. Zobel HF (1988) Molecules to granules: a comprehensive starch review. Starch-Stärke 40(2):44–50
19. Hoover R (2001) Composition, molecular structure, and physicochemical properties of tuber and root starches: a review. Carbohydr Polym 45(3):253–267
20. Bertoft E, Blennow A (2009) Structure of potato starch. In: Jaspreet S, Lovedeep K (eds) Advances in potato chemistry and technology. Academic Press, San Diego, pp 83–98
21. Hoover R, Hughes T, Chung HJ, Liu Q (2010) Composition, molecular structure, properties, and modification of pulse starches: a review. Food Res Int 43(2):399–413
22. Vandeputte GE, Delcour JA (2004) From sucrose to starch granule to starch physical behaviour: a focus on rice starch. Carbohydr Polym 58(3):245–266
23. Shannon JC, Garwood DL, Boyer CD, Genetics (2009) Physiology of starch development. In: Bemiller JN, Whistler B (eds) starch: chemistry and technology. Academic Press, New York, p. 879
24. Gérard C, Barron C, Colonna P, Planchot V (2001) Amylose determination in genetically modified starches. Carbohydr Polym 44(1):19–27
25. Wurzburg OB (ed) (1986) Modified starches : properties and uses. CRC Press, Boca Raton
26. Takeda Y, Hizukuri S, Juliano BO (1986) Purification and structure of amylose from rice starch. Carbohydr Res 148(2):299–308
27. Champagne ET (1996) Rice starch composition and characteristics. Cereal Foods World 41(11):833–838
28. Cheetham NWH, Tao L (1998) Variation in crystalline type with amylose content in maize starch granules: an X-ray powder diffraction study. Carbohydr Polym 36(4):277–284

29. Imberty A, Buléon A, Tran V, Péerez S (1991) Recent advances in knowledge of starch structure. Starch-Stärke 43(10):375–384
30. Bates FL, French D, Rundle RE (1943) Amylose and amylopectin content of starches determined by their iodine complex formation1. J Am Chem Soc 65(2):142–148
31. Mestres C, Matencio F, Pons B, Yajid M, Fliedel G (1996) A rapid method for the determination of amylose content by using differential-scanning calorimetry. Starch-Stärke 48(1):2–6
32. Rundle RE, Foster JF, Baldwin RR (1944) On the nature of the starch—iodine complex. J Am Chem Soc 66(12):2116–2120
33. Yu X, Houtman C, Atalla RH (1996) The complex of amylose and iodine. Carbohydr Res 292:129–141
34. Buléon A, Colonna P, Planchot V, Ball S (1998) Starch granules: structure and biosynthesis. Int J Biol Macromol 23(2):85–112
35. Singh J, Kaur L, McCarthy OJ (2009) Potato starch and its modification. In: Jaspreet S, Lovedeep K (eds) Advances in potato chemistry and technology, Academic Press, San Diego, pp 273–318
36. Angellier-Coussy H, Putaux JL, Molina-Boisseau S, Dufresne A, Bertoft E, Perez S (2009) The molecular structure of waxy maize starch nanocrystals. Carbohydr Res 344(12): 1558–1566
37. Pérez S, Baldwin PM, Gallant DJ (2009) Structural features of starch granules I. In: Bemiller JN, Whistler B (eds) Starch: Chemistry and technology, Academic Press: New York, p. 879
38. Jane J (2009) Structural features of starch granules II. In: Bemiller JN, Whistler B (eds) Starch: chemistry and technology, Academic Press, New York, p 879
39. Peat S (1956) The enzymic synthesis and degradation of starch. Part XXII. Evidence of multiple branching in waxy-maize starch: a correction. J Chem Soc, 3025–3030
40. Gomand SV, Lamberts L, Derde LJ, Goesaert H, Vandeputte GE, Goderis B, Visser RGF, Delcour JA (2010) Structural properties and gelatinisation characteristics of potato and cassava starches and mutants thereof. Food Hydrocoll 24(4):307–317
41. Jenkins JPJ, Cameron RE, Donald AM (1993) A universal feature in the structure of starch granules from different botanical sources. Starch Starke 45(12):417–420
42. Hizukuri S, Kaneko T, Takeda Y (1983) Measurement of the chain length of amylopectin and its relevance to the origin of crystalline polymorphism of starch granules. Biochimica et Biophysica Acta (BBA)—General Subjects, 760(1):188–191
43. Hizukuri S (1985) Relationship between the distribution of the chain length of amylopectin and the crystalline structure of starch granules. Carbohydr Res 141(2):295–306
44. BeMiller JN, Whistler RL (eds) (2009) Starch: chemistry and technology. In: Taylor SL (ed) Food science and technology international series, Academic Press: New York, 879
45. van Soest JJG, Vliegenthart JFG (1997) Crystallinity in starch plastics: consequences for material properties. Trends Biotechnol 15(6):208–213
46. Thomas DJ, Atwell WA (eds) (1999) Starches. Eagan Press, St. Paul, P 94
47. Singh N, Singh J, Kaur B, Singh Gill L, Singh Sodhi N (2003) Morphological, thermal and rheological properties of starches from different botanical sources. Food Chem 81(2): 219–231
48. Srichuwong S, Sunarti TC, Mishima T, Isono N, Hisamatsu M (2005) Starches from different botanical sources II: contribution of starch structure to swelling and pasting properties. Carbohydr Polym 62(1):25–34
49. Srichuwong S, Sunarti TC, Mishima T, Isono N, Hisamatsu M (2005) Starches from different botanical sources I: Contribution of amylopectin fine structure to thermal properties and enzyme digestibility. Carbohydr Polym 60(4):529–538
50. Huber KC, BeMiller JN (2010) Modified starch chemistry and properties. In: Bertolini AC (ed) Starches characterization properties and applications. CRC Press, Boca Raton FL, pp 145–203

51. Tester RF, Debon SJJ (2000) Annealing of starch—a review. Int J Biol Macromol 27(1): 1–12
52. Van Beynum GMA, Roels JA (1985) Starch conversion technology1985. CRC Press, Boca Raton, P 363
53. Whistler RL, BeMiller JN (eds) (1993) Industrial gums: polysaccharides and their derivatives, 3rd edn. Academic Press, San Diego, p 642
54. Anastasiades A, Thanou S, Loulis D, Stapatoris A, Karapantsios TD (2002) Rheological and physical characterization of pregelatinized maize starches. J Food Eng 52(1):57–66
55. Takahashi R, Ojima T (1969) Pregelatinization of wheat starch in a drum drier. Starch-Stärke 21(12):318–321
56. Doublier JL, Colonna P, Mercier C (1986) Extrusion cooking and drum drying of wheat starch. II. Rheological characterization of starch pastes. Cereal Chem 63:240–246
57. Colonna P, Doublier JL, Melcion JP, de Monredon F, Mercier C (1984) Extrusion cooking and drum drying of wheat starch. I. Physical and macromolecular modifications. Cereal Chem 61:538–543
58. Eastman JE, Moore CO (1984) Cold-water-soluble granular starch for gelled food compositions, A. E. Staley Manufacturing Company, Decatur
59. Rajagopalan S, Seib PA (1992) Properties of granular cold-water-soluble starches prepared at atmospheric pressure. J Cereal Sci 16(1):29–40
60. Singh J, Singh N (2003) Studies on the morphological and rheological properties of granular cold water soluble corn and potato starches. Food Hydrocoll 17(1):63–72
61. Chen B, Jane J (1994) Preparation of granular cold-water-soluble starches by alcoholic-alkaline treatment. Cereal Chem 71(6):618–622
62. Chen J, Jane J (1995) Effectiveness of granular cold-water-soluble starch as a controlled release matrix. Cereal Chem 72(3):265–268
63. Chen J, Jane J (1994) Properties of granular cold-water-soluble starches prepared by alcoholic-alkaline treatment. Cereal Chem 71(6):623–626
64. Jackowski R, Czuchajowska Z, Baik B-K (2002) Granular cold water gelling starch prepared from chickpea starch using liquid ammonia and ethanol. Cereal Chem 79(1):125–128
65. Baik BK, Jackowski R (2004) Characteristics of granular cold-water gelling starches of cereal grains and legumes prepared using liquid ammonia and ethanol, vol. 81, American Association of Cereal Chemists, St. Paul, p 6
66. Morrison WR, Tester RF (1994) Properties of damaged starch granules IV. Composition of ball-milled wheat starches and of fractions obtained on hydration. J Cereal Sci 20(1):69–77
67. Morrison WR, Tester RF, Gidley MJ (1994) Properties of damaged starch granules II. Crystallinity, molecular order and gelatinisation of ball-milled starches. J Cereal Sci 19(3): 209–217
68. Huang Z-Q, Lu J-P, Li X-H, Tong Z-F (2007) Effect of mechanical activation on physico-chemical properties and structure of cassava starch. Carbohydr Polym 68(1):128–135
69. Hoover R, Vasanthan T (1994) The flow properties of native, heat-moisture treated, and annealed starches from wheat, oat, potato and lentil. J Food Biochem 18:67–82
70. Jacobs H, Eerlingen RC, Clauwaert W, Delcour JA (1995) Influence of annealing on the pasting properties of starches from varying botanical sources. Cereal Chem 72(5):480–487
71. Lan H, Hoover R, Jayakody L, Liu Q, Donner E, Baga M, Asare EK, Hucl P, Chibbar RN (2008) Impact of annealing on the molecular structure and physicochemical properties of normal, waxy and high amylose bread wheat starches. Food Chem 111(3):663–675
72. Kiseleva VI, Genkina NK, Tester R, Wasserman LA, Popov AA, Yuryev VP (2004) Annealing of normal, low and high amylose starches extracted from barley cultivars grown under different environmental conditions. Carbohydr Polym 56(2):157–168
73. Tester RF, Debon SJJ, Sommerville MD (2000) Annealing of maize starch. Carbohydr Polym 42(3):287–299
74. Waduge RN, Hoover R, Vasanthan T, Gao J, Li J (2006) Effect of annealing on the structure and physicochemical properties of barley starches of varying amylose content. Food Res Int 39(1):59–77

75. Jayakody L, Hoover R (2008) Effect of annealing on the molecular structure and physicochemical properties of starches from different botanical origins—a review. Carbohydr Polym 74(3):691–703
76. Kawabata A, Takase N, Miyoshi E, Sawayama S, Kimura T, Kudo K (1994) Microscopic observation and X-ray diffractometry of heat/moisture-treated starch granules. Starch-Stärke 46(12):463–469
77. Jacobs H, Delcour JA (1998) Hydrothermal modifications of granular starch, with retention of the granular structure: a review. J Agr Food Chem 46(8):2895–2905
78. Varatharajan V, Hoover R, Liu Q, Seetharaman K (2010) The impact of heat-moisture treatment on the molecular structure and physicochemical properties of normal and waxy potato starches. Carbohydr Polym 81(2):466–475
79. Gunaratne A, Hoover R (2002) Effect of heat-moisture treatment on the structure and physicochemical properties of tuber and root starches. Carbohydr Polym 49(4):425–437
80. Hoover R, Manuel H (1996) The effect of heat-moisture treatment on the structure and physicochemical properties of normal maize, waxy maize, dull waxy maize and amylomaize v starches. J Cereal Sci 23(2):153–162
81. Hoover R, Manuel H (1996) Effect of heat–moisture treatment on the structure and physicochemical properties of legume starches. Food Res Int 29(8):731–750
82. Miyazaki M, Morita N (2005) Effect of heat-moisture treated maize starch on the properties of dough and bread. Food Res Int 38(4):369–376
83. Chiu CW, Schiermeyer E, Thomas DJ, Shah MB (1998) Thermally inhibited starches and flours and process for their production, National Starch and Chemical Investment Holding Corporation, Wilmington
84. Chiu C-W, Shi Y-C, Sedam M (1999) Process for producing amylase resistant granular starch. National Starch and Chemical Investment Holding Corporation, Wilmington
85. Jane J (1995) Starch properties, modifications, and applications. J Macromol Sci Part A Pure Appl Chem 32(4):751–757
86. Huber KC, BeMiller JN (2010) Modified starch: chemistry and properties. In: Bertolini AC (ed) Starches: Characterization, properties, and applications, CRC Press, Boca Raton
87. Singh J, Kaur L, McCarthy OJ (2007) Factors influencing the physico-chemical, morphological, thermal and rheological properties of some chemically modified starches for food applications–a review. Food Hydrocoll 21(1):1–22
88. Kaper T, van der Maarel MJEC, Euverink GJW, Dijkhuizen L (2004) Exploring and exploiting starch-modifying amylomaltases from thermophiles. Biochem Soc Trans 32(Pt 2): 279–282
89. van der Maarel MJEC, van der Veen B, Uitdehaag JCM, Leemhuis H, Dijkhuizen L (2002) Properties and applications of starch-converting enzymes of the [alpha]-amylase family. J Biotechnol 94(2):137–155
90. Rutenberg MW, Solarek D (1984) Starch derivatives: production and uses. In: Whistler RL BeMiller JN Paschall EF (eds) Starch: chemistry and technology, Academic Press, London. p. 77
91. Cyras V, Tolosa Zenklusen M, Vazquez A (2006) Relationship between structure and properties of modified potato starch biodegradable films. J Appl Polym Sci 101(6):4313–4319
92. Woo K, Seib PA (1997) Cross-linking of wheat starch and hydroxypropylated wheat starch in alkaline slurry with sodium trimetaphosphate. Carbohydr Polym 33(4):263–271
93. Carmona-Garcia R, Sanchez-Rivera MM, Méndez-Montealvo G, Garza-Montoya B, Bello-Pérez LA (2009) Effect of the cross-linked reagent type on some morphological, physicochemical and functional characteristics of banana starch (Musa paradisiaca). Carbohydr Polym 76(1):117–122
94. Kweon MR, Sosulski FW, Bhirud PR (1997) Cationization of waxy and normal corn and barley starches by an aqueous alcohol process. Starch-Stärke 49(2):59–66
95. Kweon MR, Sosulski FW, Han HS (1997) Effect of aqueous ethanol cationization on functional properties of normal and waxy starches. Starch-Stärke 49(5):202–207

96. Yook C, Sosulski F, Saskatoon PRB (1994) Effects of cationization on functional properties of pea and corn starches. Starch-Stärke 46(10):393–399
97. Radosta S, Vorwerg W, Ebert A, Begli AH, Grülc D, Wastyn M (2004) Properties of low-substituted cationic starch derivatives prepared by different derivatisation processes. Starch-Stärke 56(7):277–287
98. Siau CL, Karim AA, Norziah MH, Wan Rosli WD (2004) Effects of cationization on DSC thermal profiles, pasting and emulsifying properties of sago starch. J Sci Food Agr, 84(13): 1722–1730
99. Han HL, Sosulski FW (1998) Cationization of potato and tapioca starches using an aqueous alcoholic-alkaline process. Starch-Stärke 50(11–12):487–492
100. Fanta GF,Doane WM (1986) Grafted starches. In: Wurzburg OB (ed) Modified starches : properties and uses, CRC Press, Boca Raton, pp 149–178
101. Willett JL (2009) Starch in polymer compositions, In: Whistler B, BeMiller JN (eds) Starch: chemistry and technology, Academic Press, New York
102. Alexandre M, Dubois P (2000) Polymer-layered silicate nanocomposites: preparation, properties and uses of a new class of materials. Materials Science and Engineering: R: Reports 28(1–2):1–63
103. Picard E, Gauthier H, Gérard JF, Espuche E (2007) Influence of the intercalated cations on the surface energy of montmorillonites: consequences for the morphology and gas barrier properties of polyethylene/montmorillonites nanocomposites. J Colloid Interface Sci 307(2): 364–376
104. Mandalia T, Bergaya F (2006) Organo clay mineral-melted polyolefin nanocomposites Effect of surfactant/CEC ratio. J Phys Chem Solids 67(4):836–845
105. He H, Duchet J, Galy J, Gérard J-F (2006) Influence of cationic surfactant removal on the thermal stability of organoclays. J Colloid Interface Sci 295(1):202–208
106. Roelofs JCAA, Berben PH (2006) Preparation and performance of synthetic organoclays. Appl Clay Sci 33(1):13–20
107. Capková P, Pospísil M, Valásková M, Merínská D, Trchová M, Sedláková Z, Weiss Z, Simoník J (2006) Structure of montmorillonite cointercalated with stearic acid and octadecylamine: modeling, diffraction, IR spectroscopy. J Colloid Interface Sci 300(1):264–269
108. Xie W, Xie R, Pan W-P, Hunter D, Koene B, Tan L-S, Vaia R (2002) Thermal stability of quaternary phosphonium modified montmorillonites. Chem Mater 14(11):4837–4845
109. Xi Y, Frost RL, He H (2007) Modification of the surfaces of Wyoming montmorillonite by the cationic surfactants alkyl trimethyl, dialkyl dimethyl, and trialkyl methyl ammonium bromides. J Colloid Interface Sci 305(1):150–158
110. Xie W, Gao Z, Pan W-P, Hunter D, Singh A, Vaia R (2001) Thermal degradation chemistry of alkyl quaternary ammonium montmorillonite. Chem Mater 13(9):2979–2990
111. Xi Y, Ding Z, He H, Frost RL (2004) Structure of organoclays–an X-ray diffraction and thermogravimetric analysis study. J Colloid Interface Sci 277(1):116–120
112. Drown EK, Mohanty AK, Parulekar Y, Hasija D, Harte BR, Misra M, Kurian JV (2007) The surface characteristics of organoclays and their effect on the properties of poly(trimethylene terephthalate) nanocomposites. Compos Sci Technol 67(15–16):3168–3175
113. Upson RT, Burns SE (2006) Sorption of nitroaromatic compounds to synthesized organoclays. J Colloid Interface Sci 297(1):70–76
114. Southern Clay Products I (2011) www.nanoclay.com. Accessed 2011
115. Zhang Q-X, Yu Z–Z, Xie X-L, Naito K, Kagawa Y (2007) Preparation and crystalline morphology of biodegradable starch/clay nanocomposites. Polymer 48(24):7193–7200
116. Mohanty AK, Misra M, Drzal LT (eds) (2006) Natural fibers, biopolymers, and biocomposites. Polymer international, CRC Press, Taylor & Francis Group, Boca Raton, p 896
117. Sugih AK (2008) Synthesis and properties of starch based biomaterials. Netherlands, University of Groningen p, Gronigen, p 155
118. Donovan JW (1979) Phase transitions of the starch-water system. Biopolymers 18(2): 263–275

119. Lelievre J (1974) Starch gelatinization. J Appl Polym Sci 18(1):293–296
120. Lelievre J (1976) Theory of gelatinization in a starch-water-solute system. Polymer 17(10): 854–858
121. Svensson E, Eliasson A-C (1995) Crystalline changes in native wheat and potato starches at intermediate water levels during gelatinization. Carbohydr Polym 26(3):171–176
122. Tako M, Hizukuri S (2002) Gelatinization mechanism of potato starch. Carbohydr Polym 48(4):397–401
123. Vazquez A, Alvarez VA (2008) Starch/cellulose fibres. In: Long Y (ed) Biodegradable polymer blends and composites from renewable resources. Wiley, New York, p 488
124. Aichholzer W, Fritz H-G (1998) Rheological characterization of thermoplastic starch materials. Starch-Stärke 50(2–3):77–83
125. Achayuthakan P, Suphantharika M (2008) Pasting and rheological properties of waxy corn starch as affected by guar gum and xanthan gum. Carbohydr Polym 71(1):9–17
126. Bagley EB, Christianson DD (1982) Swelling capacity of starch and its relationship to suspension viscosity-effect of cooking time, temperature and concentration. J Texture Stud 13(1):115–126
127. Doublier JL (1987) A rheological comparison of wheat, maize, faba bean and smooth pea starches. J Cereal Sci 5(3):247–262
128. Härröd M (1989) Time-dependent flow behavior of starch pastes, with food process applications. J Food Process Eng 11(4):297–309
129. Djakovic LJ, Sovilj V, Miloscaronevi S (1990) Rheological behaviour of thixotropic starch and gelatin gels. Starch-Stärke 42(10):380–385
130. Dintzis FR, Bagley EB, Felker FC (1995) Shear-thickening and flow-induced structure in a system of DMSO containing waxy maize starch [sup a)]. J Rheol 39(6):1399–1409
131. Ortega-Ojeda FE, Larsson H, Eliasson A-C (2004) Gel formation in mixtures of high amylopectin potato starch and potato starch. Carbohydr Polym 56(4):505–514
132. Núñez-Santiago MC, Bello-Pérez LA, Tecante A (2004) Swelling-solubility characteristics, granule size distribution and rheological behavior of banana (Musa paradisiaca) starch. Carbohydr Polym 56(1):65–75
133. Cai W, Diosady LL (1993) Model for gelatinization of wheat starch in a twin-screw extruder. J Food Sci 58(4):872–875
134. Benbow J, Bridgwater J (1993) Paste flow and extrusion.clarendon, Press: Oxford Series on Advanced Manufacturing
135. Xue T, Yu L, Xie F, Chen L, Li L (2008) Rheological properties and phase transition of starch under shear stress. Food Hydrocoll 22(6):973–978
136. Martin O, Averous L, Della Valle G (2003) In-line determination of plasticized wheat starch viscoelastic behavior impact of processing. Carbohydr Polym 53(2):169–182
137. Yu L, Kealy T (2006) Study of starch gelatinization in a flow field using simultaneous rheometric data collection and microscopic observation. Int Polym Proc 4:379–385
138. Della Valle G, Buleon A, Carreau PJ, Lavoie PA, Vergnes B (1998) Relationship between structure and viscoelastic behavior of plasticized starch. J Rheol 42(3):507–525
139. Morán JI, Cyras VP, Giudicessi S, Erra-Balsells R, Vázquez A (2011) Influence of glycerol content and temperature on the rheology of native and acetylated potato starch during and after gelatinization. J Appl Polym Sci 120(6):3410–3420
140. Morán JI, Cyras VP, Vázquez A, Foresti L (2011) Characterization of chemically modified potato starch films through enzymatic degradation. J Polym Environ 19(1):217–224
141. Rodriguez-Gonzalez FJ, Ramsay BA, Favis BD (2004) Rheological and thermal properties of thermoplastic starch with high glycerol content. Carbohydr Polym 58(2):139–147
142. Willett JL, Jasberg BK, Swanson CL (1995) Rheology of thermoplastic starch: effects of temperature, moisture content, and additives on melt viscosity. Polym Eng Sci 35(2): 202–210
143. Xie F, Yu L, Su B, Liu P, Wang J, Liu H, Chen L (2009) Rheological properties of starches with different amylose/amylopectin ratios. J Cereal Sci 49(3):371–377

144. Chiou B-S, Yee E, Glenn GM, Orts WJ (2005) Rheology of starch-clay nanocomposites. Carbohydr Polym 59(4):467–475
145. Manas-Zloczower I, Cheng H (1996) Analysis of mixing efficiency in polymer processing equipment. Macromol Symp 112(1):77–84
146. Plackett D, Vazquez A (2004) Biopolymers and biocomposites. In: Baille C (ed) Green composites: polymer composite and the environment, Woodhead Publishers, Boca Raton, Cambridge
147. Vazquez A, Alvarez VA, Cyras VP, Pérez J, Ludueña L (2007) Starch based/montmorillonite nanocomposites, in BIOPLASTIC2007, Montreal, Canadá
148. Rauwendaal CJ, Osswald TA, Gramann PJ, Davis B (1998) New dispersive mixers for single screw extruders, in 56th SPE ANTEC
149. Luduena L, Bálzamo V, Vazquez A, Alvarez VA (2009) Evaluation of methods for stiffness predictions of polymer based nanocomposites: theoretical background and examples of applications (PCL-clay nanocomposites). In: Silva VCAR (ed) Nanomaterials: properties, preparation and processes, Nova Publishers, New York
150. Hasegawa N, Okamoto H, Kato M, Usuki A, Sato N (2003) Nylon 6/Na-montmorillonite nanocomposites prepared by compounding Nylon 6 with Na-montmorillonite slurry. Polymer 44(10):2933–2937
151. Park H-M, Lee W-K, Park C-Y, Cho W-J, Ha C-S (2003) Environmentally friendly polymer hybrids Part I Mechanical, thermal, and barrier properties of thermoplastic starch/clay nanocomposites. J Mater Sci 38:909–915
152. Chen B, Evans JRG (2005) Thermoplastic starch-clay nanocomposites and their characteristics. Carbohydr Polym 61(4):455–463
153. Avella M, De Vlieger JJ, Errico ME, Fischer S, Vacca P, Volpe MG (2005) Biodegradable starch/clay nanocomposite films for food packaging applications. Food Chem 93(3): 467–474
154. Chung Y-L, Lai H-M (2010) Preparation and properties of biodegradable starch-layered double hydroxide nanocomposites. Carbohydr Polym 80(2):525–532
155. Cyras VP, Manfredi LB, Ton-That M-T, Vázquez A (2008) Physical and mechanical properties of thermoplastic starch/montmorillonite nanocomposite films. Carbohydr Polym 73(1):55–63
156. Vazquez A, Alvarez VA (2009) Biodegradable nanocomposites based on starch, pcl and their blends. In: Mancini L, Espósito C (eds) Nanocomposites: preparation, properties and performance, Nova Publisher, New York. p 133–164
157. Dean K, Yu L, Wu DY (2007) Preparation and characterization of melt-extruded thermoplastic starch/clay nanocomposites. Compos Sci Technol 67(3–4):413–421
158. Liu H, Chaudhary D, Yusa S-I, Tadé MO (2011) Glycerol/starch/Na+ montmorillonite nanocomposites: A XRD, FTIR, DSC and 1H NMR study. Carbohydr Polym 83(4):1591–1597
159. Magalhães NF, Andrade CT (2009) Thermoplastic corn starch/clay hybrids: effect of clay type and content on physical properties. Carbohydr Polym 75(4):712–718
160. Singh B, Sharma DK, Kumar R, Gupta A (2009) Controlled release of the fungicide thiram from starch-alginate-clay based formulation. Appl Clay Sci 45(1–2):76–82
161. Tang X, Alavi S, Herald TJ (2008) Effects of plasticizers on the structure and properties of starch-clay nanocomposite films. Carbohydr Polym 74(3):552–558
162. Chivrac F, Pollet E, Dole P, Avérous L (2010) Starch-based nano-biocomposites: plasticizer impact on the montmorillonite exfoliation process. Carbohydr Polym 79(4):941–947
163. Chivrac F, Angellier-Coussy H, Guillard V, Pollet E, Avérous L (2010) How does water diffuse in starch/montmorillonite nano-biocomposite materials? Carbohydr Polym 82(1): 128–135
164. Tomasik P, Wang YJ, Jane J-L (1995) Facile route to anionic starches succinylation, maleination and phthalation of corn starch on extrusion. Starch Stärke 47(3):96–99
165. Narayan R, Balakrishnan S, Nabar Y, Shin B, Dubois P, Raquez J (2006) Chemically modified plasticized starch compositions by extrusion processing, U.S.P. Office (ed), Board of Trustees of Michigan State University, Michigan

166. Majdzadeh-Ardakani K, Navarchian AH, Sadeghi F (2010) Optimization of mechanical properties of thermoplastic starch/clay nanocomposites. Carbohydr Polym 79(3):547–554
167. Huang M, Yu J, Ma X (2006) High mechanical performance MMT-urea and formamide-plasticized thermoplastic cornstarch biodegradable nanocomposites. Carbohydr Polym 63(3):393–399
168. Mondragón M, Hernández EM, Rivera-Armenta JL, Rodríguez-González FJ (2009) Injection molded thermoplastic starch/natural rubber/clay nanocomposites: morphology and mechanical properties. Carbohydr Polym 77(1):80–86
169. Chivrac F, Pollet E, Schmutz M, Avérous L (2010) Starch nano-biocomposites based on needle-like sepiolite clays. Carbohydr Polym 80(1):145–153
170. Chivrac F, Pollet E, Schmutz M, Avérous L (2008) New approach to elaborate exfoliated starch-based nanobiocomposites. Biomacromolecules 9(3):896–900
171. Huang M-F, Yu J-G, Ma X-F (2004) Studies on the properties of montmorillonite-reinforced thermoplastic starch composites. Polymer 45(20):7017–7023
172. Carvalho AJF, Curvelo AAS, Agnelli JAM (2001) A first insight on composites of thermoplastic starch and kaolin. Carbohydr Polym 45(2):189–194
173. Wilhelm HM, Sierakowski MR, Souza GP, Wypych F (2003) Starch films reinforced with mineral clay. Carbohydr Polym 52(2):101–110
174. Parikh A, Madamwar D (2006) Partial characterization of extracellular polysaccharides from cyanobacteria. Bioresour Technol 97(15):1822–1827
175. de Carvalho AJF, Curvelo AAS, Agnelli JAM (2001) A first insight on composites of thermoplastic starch and kaolin. Carbohydr Polym 45(2):189–194
176. Masclaux C, Gouanvé F, Espuche E (2010) Experimental and modelling studies of transport in starch nanocomposite films as affected by relative humidity. J Membr Sci 363(1–2): 221–231
177. Mondragón M, Mancilla JE, Rodríguez-González FJ (2008) Nanocomposites from plasticized high-amylopectin, normal and high-amylose maize starches. Polym Eng Sci 48(7): 1261–1267
178. Zeppa C, Gouanvé F, Espuche E (2009) Effect of a plasticizer on the structure of biodegradable starch/clay nanocomposites: thermal, water-sorption, and oxygen-barrier properties. J Appl Polym Sci 112(4):2044–2056
179. Ludueña LN, Vazquez A, Kenny JM, Alvarez VA (2010) The effect of processing technique on the performance of PCL/clay nanocomposite, In: Frontiers in polymer science—second international symposium. Lyon

Chapter 12
Protein/Clay Nano-Biocomposites

Hélène Angellier-Coussy and Emmanuelle Gastaldi

Abstract In the current context, protein-based materials might be considered as an alternative to the petroleum-based plastics since fully biodegradable and characterized by remarkable functional properties that can be exploited in a wide range of non-food applications. To improve their performances that are often restricted by high water sensitivity and low mechanical properties, a relevant strategy consisted in the development of protein/clay nanocomposite. For this purpose, several examples of protein-based nano-biocomposites were presented with a special attention for the methods used for the incorporation of layered silicates (organically modified or not) into the matrices and the ultimate functional properties exhibited by the resulting materials. In terms of mechanical properties, the addition of nanoclays leads to a significant improvement of material performance with an increase of Young's modulus and tensile strength ranging between 1.5 and 2 times. As regards as barrier properties, the improvement appeared quite moderate in spite of a rather good dispersion of layered silicates that would be expected to result in a tortuous pathway limiting diffusion of gases molecules. Thus, a two-fold reduction in water vapour permeability was obtained, and the same or no effect in the case of permeability toward O_2 and CO_2.

List of Abbreviations

DSC	Differential scanning calorimetry
FTIR	Fourrier transformed infrared
MMT	Montmorillonite
OMMT	Organically modified montmorillonite
RH	Relative humidity

H. Angellier-Coussy (✉) · E. Gastaldi
UMR IATE, Université Montpellier II, CC023, pl. E. Bataillon,
34095 Montpellier Cedex, France
e-mail: helene.coussy@univ-montp2.fr

L. Avérous and E. Pollet (eds.), *Environmental Silicate Nano-Biocomposites*,
Green Energy and Technology, DOI: 10.1007/978-1-4471-4108-2_12,

SEM	Scanning electron microscopy
SPI	Soy protein isolate
TEM	Transmission electron microscopy
TGA	Thermogravimetric analysis
WG	Wheat gluten
WPI	Whey protein isolate
WVP	Water vapour permeability
XRD	X-ray diffraction

12.1 Introduction

Among agricultural products, proteins have long and empirically been used as raw materials in a wide range of non-food applications such as adhesives, glues, paints, leather finishes, textile fibers, paper coatings, photographic supports and various moulded plastic items (buttons, door handles, jewellery…). However, in the 1960s the competition with synthetic plastics led the interest for protein-based materials to markedly decrease until a recent renewal of interest for renewable and biodegradable materials, over the last two decades, in response to raising awareness on environmental issues. Owing to their good film-forming properties, several proteins stemming from animal (casein, whey proteins, gelatin, collagen, egg white, keratin and fish myofibrillar proteins) and vegetable (soy proteins, wheat gluten, corn zein and pea protein isolates) sources have received attention for production of films or coatings. Proteins can be defined as natural polymers able to form amorphous three-dimensional structures mainly stabilized by non-covalent interactions. In contrary to most other biodegradable polymers, they are heteropolymers constituted of different amino acids and characterized by specific levels of structure ensuring various interactions and bindings differing in position, type, and energy. Protein-based materials can be prepared using either a solvent process also called casting or a common thermoplastic process such as extrusion or thermomolding. Their formulation often requires the addition of plasticizers to allow their thermo-processability and impart film flexibility. Resulting protein-based materials are characterized by remarkable functional properties that are highly dependant on structural heterogeneity, especially on interactions between polypeptide chains, thermal sensitivity, and hydrophilic behaviour of proteins. Protein-based materials are fully biodegradable without toxic products release. However serious concerns remain regarding their performance, mainly including their high water sensitivity and low mechanical properties.

As largely described in the literature, the incorporation of layered silicates at the nanoscale level into a polymeric matrix often results in significant enhancement of mechanical, barrier and thermal properties. The high affinity of clays to proteins and amino acids bearing neutral, positive, and even negative charges were

initially noted in soils and already largely used in winemaking for protein precipitation, which hints the possibility to prepare protein-based nanocomposite materials. This strategy has begun to be explored in the field of protein-based materials for gelatin less than ten years ago (first publications in 2002). The development of protein/clay nano-biocomposites has been yet devoted to almost all proteins previously mentioned with the intention of mainly improving mechanical and barrier properties. Protein-based nano-biocomposites are also developed for the controlled release of active agents, for example for antimicrobial applications.

After a short presentation of the protein structure, which is at the root of the properties of protein-based materials, the second part of the chapter will be devoted to the possible processing routes to prepare protein-based nano-biocomposites. The third part will focus on the structure/properties relationships of proteins (gelatin, milk proteins, soy proteins, corn zein and wheat gluten)/clay nano-biocomposites.

12.2 Structure of Proteins

Proteins are heteropolymers constituted of 20 different amino acids and characterized by different levels of structure that permit various interactions and bindings differing in position, type, and energy. The functionalities of proteins-based materials mainly depend on the composition of the amino acids constituting their primary sequence and more precisely on the chemical reactivity of the amino acids lateral groups i.e., polar or hydrophobic, ionised or not, acid or basic, aromatic or aliphatic (Table 12.1). According to the chemical specificity of the amino acids constituting proteins, different types of interactions could be established leading to intra and inter-polypeptidic chain linkages. Among them, the most representative are non-covalent bonds since considered as critical in stabilizing protein three-dimensional structure that can be described at four levels i.e., from primary structure to secondary, tertiary and quaternary structure [1]. The secondary structure of proteins corresponds to the spatial arrangement of the polypeptide chains, which results from the establishment of periodic hydrogen bindings involving carbonyl and amine groups (CO–NH) of peptide bonds. We distinguish the α-helix and the β-sheets structures. Proteins containing a relatively large proportion of proline and hydroxyproline may be less prone to adopt an ordered structure due to the disruptive effect of these amino acid residues on typical secondary structure. The tertiary structure of proteins results from diverse interactions (hydrogen, hydrophobic, electrostatic, covalent…) between amino acids belonging to the same polypeptide chain but being not neighbours. Finally, the quaternary structure generally results from non-covalent interactions between polypeptide chains. This latter structure is closely related to the functional properties of the final protein-based materials.

Table 12.1 Characteristics of the main proteins used to prepare protein/clay nano-biocomposites

Proteins	Amino acid ratios				Sub-units		
	Ionized polar[a]	Non- ionized polar[a]	Apolar[a]	Cysteine involved in disulphide bonds	Name	Rate (%)	Molecular weight (kDa)
Gelatine [46, 47]	29.1	27.6	43.3	0			3–200
Whey proteins [48, 49]	28.5	25	42.5	4	α-lactalbumin	60	14
					β − lactoglobulin	20	18
Soy proteins [50]	47	16.7	35	1.3	Glycinin	40	350
					β-conglycinine	35	185
Wheat gluten [51]	18	41	38.3	2.7	Gliadin	45	30–80
					Glutenin	45	200–2000
Corn zein [51]	15	38	45	2	α-zein	80	23–27

[a] Ionized polar: Glu, Asp, Lys, Arg, His; Non-ionized polar: Gly, Asn, Gln, Ser, Thr, Tyr; Apolar: Ala, Val, Leu, Ileu, Pro, Phe, Met, Trp

Amino acids are generally classified in groups depending on their ability to establish interactions via either hydrogen bonds (involving non-ionized polar amino acids, 8–40 kJ.mol^{-1} [1]), ionic interactions (implying ionized polar amino acids, 42–84 kJ.mol^{-1} [1]), hydrophobic interactions (between apolar amino acids, 4–12 kJ.mol^{-1} [1]) or covalent linkages (amino acids involved in disulphide bonds, 330–380 kJ.mol^{-1} [1]) (Table 12.1). Although the non-covalent bonds are weak chemical forces ranging from 4 to 30 kJ.mol^{-1} [1], they impart stability to the structures generated by their collective action. Van der Waals forces (involving both polar and apolar non-ionised amino acids, 0.4-4 kJ.mol^{-1} [1]) are also implicated but their effect on protein structure is minor. Their highly heterogeneous structure characterized by the absence of repeating units along the polypeptide chains render ineffective Van der Waals interactions that mainly act at short distance with a very low energy input. In aqueous medium proteins generally adopt a conformation in which polar amino acids are located at the interface with solvent whereas the hydrophobic parts of the polypeptide chains tend to avoid solvent by burying within the structure. Depending on the polarity, pH and ionic force of the solvent used, the respective contributions of these interactions can be modified. In pH conditions far from its isoelectric point, proteins are stabilized in the medium since the interactions established between protein and solvent are greater than those formed between amino acids. In addition to non-covalent interactions, covalent disulphide bonds formed by oxidation of two thiol groups also play an important role in the stability of the proteins containing cysteine residues.

The functional properties of the final materials will depend on the respective contribution of these different kinds of interactions that are closely related to the characteristics of the protein raw material but that can also be modulated by the conditions used to process and store the protein-based materials. Furthermore, this heterogeneous structure offers many opportunities for cross-linking or chemical grafting.

12.3 Preparation of Protein-Based Nano-Biocomposites

The formation of a macromolecular network from proteins requires three steps: first the rupture of low-energy intermolecular bonds that stabilize polymers in the native state, secondly the arrangement and the orientation of polymer chains (shaping), and finally the formation of a three-dimensional network stabilized by new interactions and bonds after the agent that breaks intermolecular bonds is removed [2]. Due to the high glass transition temperature of proteins (above their temperature of degradation), their formulation often requires the addition of plasticizers to allow their thermo-processability and impart material flexibility. Besides water molecules that could be considered as the natural plasticizer of most proteins, the most usual plasticizers are polyols (glycerol, sorbitol), mono-, di-, and oligo-saccharides, and fatty acids.

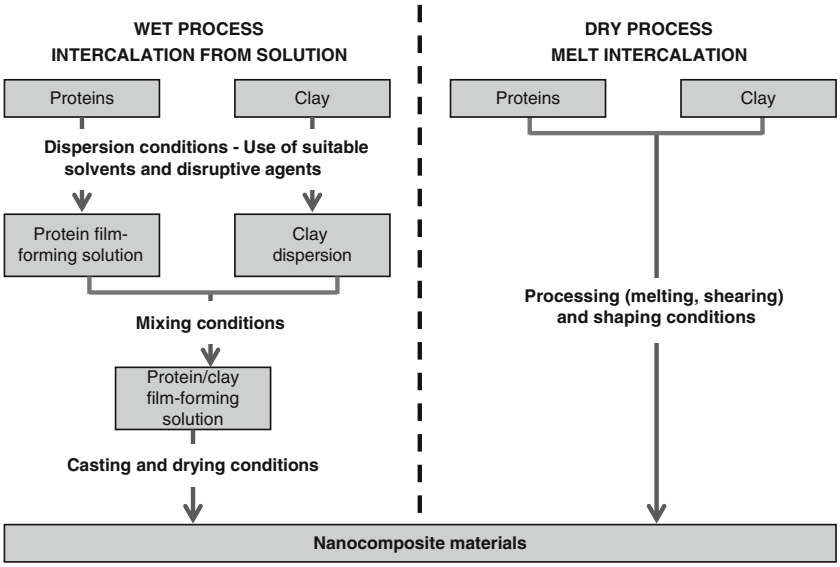

Fig. 12.1 Schematic representation of the two main technological processes used to prepare protein/clay nano-biocomposite materials

Several methods have been considered to prepare polymer/layered silicate nanocomposites with an optimal dispersion state of nanofillers [3]. Two of them are compatible with the production of protein-based materials: (1) the intercalation of proteins from solution, which is compatible with the preparation of protein-based materials via a wet process, commonly called casting, based on the dispersion or solubilisation of proteins in a solvent, and (2) the melt-intercalation technique, which is compatible with the preparation of protein-based materials via a dry, that is, thermo-mechanical process based on the thermoplastic properties of some proteins. These two processes are schematically represented on Fig. 12.1.

12.3.1 Wet Process/Intercalation from Solution

The wet process is suitable for all proteins. The solvents used to prepare protein film-forming solutions are generally based on water and ethanol, and occasionally acetone. Proteins are required to unfold and realign before a new three-dimensional network can be formed, and then stabilized by new inter- and intra-molecular interaction. Depending on the amino acid sequence, dispersing proteins in solution may involve the addition of solvents, disruptive agents, pH adjustment by the addition of acids or bases, or ionic strength control by electrolyte addition [2]. Then, the functional properties of protein-based films prepared by casting depend on protein concentration in solution, pH, additives, solvent polarity, drying rate and

Table 12.2 Main proteins used as polymeric materials to develop agromaterials: tested methods to obtain nano-biocomposites

Proteins	Solution intercalation via casting	Solution intercalation followed by solvent evaporation, then shaping of the material using a dry process (thermoforming or extrusion)	Melt intercalation using a thermo-mechanical process (thermoforming or extrusion)	Melt intercalation using a thermo-mechanical process, then shaping via casting
Gelatine	[10–16]	–	–	–
Whey proteins	[19–21]	–	–	–
Soy proteins	[26]	[27, 30]	–	[28, 29]
Corn zein	[31]	[31]	–	–
Wheat gluten	[39, 40, 41, 44]	[52]	[33, 42]	–

temperature [2]. Ideally, layered silicates are exfoliated into single layers using a solvent in which the proteins are easy to disperse. Proteins then adsorb onto the delaminated surfaces of clay and when the solvent is evaporated, the sheets reassemble, sandwiching proteins (Fig. 12.1). To facilitate introduction of proteins into clay galleries, it is possible to play on the pH value of the film-forming solution to positively increase the protein net charge in favour of electrostatic interactions established with the negatively charged clay surfaces. To prepare optimized film-forming solutions, the conditions are retained in such a way to favour proteins unfolding together with a minimal viscosity. So far, the intercalation of layered silicates from solution was largely preferred for making protein-based nano-biocomposites (Table 12.2) for several reasons, including the non-necessity to use plasticizers, the easiness of processing and the possibility to achieve well exfoliated nanocomposite structures due to the capacity of layered silicates to swell in an appropriate solvent (such as water). In some cases, solution intercalation followed by solvent evaporation (often by freeze-drying) is only considered as a preliminary step allowing obtaining good nanoclay dispersion, the resulting dried powders being then shaped using a dry process (Fig. 12.1, Table 12.2).

12.3.2 Dry Process/Melt-Intercalation

Thermoplastic properties of proteins mainly depend on the type and the density of intermolecular interactions. Extrusion requires the formation of a homogeneous protein melt implying processing temperature above the protein softening point. The fact that proteins contain a wide range of inter-molecular interactions reduces chain mobility, increases viscosity and results in a high glass transition temperature often above the decomposition temperature. Furthermore, the heat sensitivity of some proteins that aggregate and cross-link upon heating restricts the window of feasible

processing conditions. Because chain mobility is a key parameter to achieve successful extrusion, protein/protein interactions can become unfavourable and should thus be controlled during processing. For this purpose, chemical additives, such as sodium sulphite, sodium dodecyl sulphate and urea, known to disrupt covalent and non-covalent bonds are often used as processing aids in combination with plasticizers [4]. Although most of proteins are suitable for the extrusion process, to date, only wheat gluten and soy proteins have led to nano-biocomposites by using a dry process, such as extrusion, roller milling or thermo-molding (Table 12.2). To prepare nanocomposite materials, layered silicates are mixed with the protein matrix in the molten state under heating and shearing (Fig. 12.1). In the case of proteins containing cysteine residues (such as soy and wheat gluten) the thermal treatment not only allows polymer melting but also induces cross-linking reactions between thiol groups (from rather low temperatures; 70°C in the case of wheat gluten [5], for instance). Thus, extrusion conditions (temperature and shearing) should be optimised in order to limit the temperature-induced cross-linking and favour the shear-induced alignment of polymer chains preventing the viscosity increase and allowing processability. When clay layers surface is sufficiently compatible with the protein, polypeptide chains can crawl into the galleries and lead to either an intercalated or exfoliated nanocomposite structure depending on the degree of penetration of the polymer into the clay interlayer. According to Vaia and Giannelis [6], interplay of entropic and energetic factors determines the outcome of polymer intercalation. Exfoliation or complete layer separation depends on the establishment of very favourable interactions between polymer and clay surfaces to overcome the entropy loss associated with polymer confinement and penetration between the clay layers. In the case of clays modified with alkylammonium, the increased conformational freedom of the surfactant chain induced by the clay layers separation might compensate additionally the entropy decrease associated with the polymer chain penetration between the clay. The kinetic of intercalation of the polymer chains between the clay layers also depends on the polymer mobility that is related with the temperature difference between the processing temperature and the polymer glass temperature [7]. Although still too little used to prepare protein-based nanocomposites, the polymer melt intercalation is considered as a more efficient and environmentally–benign alternative than the polymer intercalation from solution since requiring no solvent. Moreover, dry processes are all available at the industrial scale and commonly used in plastics processing.

12.4 Structure/Properties Relationships of Protein-Based Nano-Biocomposites

12.4.1 Gelatine-Based Nano-Biocomposites

Gelatine is a protein resulting from partial thermal or chemical hydrolysis of collagen polypeptide chains stemming from animal skin, bones and cartilages. For commercial production of gelatine, two processes are mainly used differing by the

pH conditions; type A gelatine involves an acid extraction whereas type B gelatine is obtained by an alkaline lime followed by a solubilisation at near neutral pH at 60–90°C [8]. Gelatine was one of the first food protein to be used as raw material not only for food applications but also in the pharmaceutical and photographic film industries due to large availability, low production cost (between 1 and 5 €/kg depending on the animal origin and the targeted application, food or non-food uses) and excellent film forming ability. Gelatine has been successfully used to form, by casting, films that are transparent, flexible, water-resistant and impermeable to oxygen [2]. Although gelatine can be used as a valuable biopolymer in tissue engineering, its poor mechanical properties, especially in the wet state, and its high water sensitivity, revealed by a high water swelling, restrict its application as a structural biomaterial such as osteosynthetic devices. The development of gelatine/clay nano-biocomposites provided some new opportunities to overcome these limitations and widen end-uses. They are considered as the first group of nano-biocomposites deliberately created from the assembling of a natural polymer and a layered solid. Gelatine/clay nanocomposites can only be prepared using a solvent intercalation based on an ion exchange process. In this manner, the control of pH is crucial because it is required to protonate the amino groups, in order to intercalate positively charged gelatine by replacing the interlayer cation when the pH of the solution is kept below the isoelectric point of the protein [9].

Zheng et al. first prepared gelatine/sodium MMT nano-biocomposites using a solution intercalation method [10] and MMT contents up to 20 wt%. The work mainly focused on thermal and mechanical properties. XRD results revealed that an intercalated or partially exfoliated structure was achieved. DSC and TGA results indicated that thermal properties of gelatine were significantly improved (the onset thermal decomposition temperature is 40°C higher than that of the pure gelatine for a filler content of 30 wt%), as later confirmed by Martucci et al. [11]. The tensile strength and Young's modulus were also improved (Table 12.3), reaching maximum values for MMT content of 17 wt%. The wet mechanical strength was also significantly improved, which was mainly attributed to the nano-dispersion of MMT within the gelatine matrix and the barrier effect of MMT sheets to solvent. A significant enhancement of both the Young's modulus and the tensile strength by about a factor 2 without sacrificing toughness was further confirmed by many authors for other sources of gelatine at a low MMT loading (5 wt%) [12–14] (Table 12.3).

Concerning barrier properties, several studies showed that the introduction of MMT led to a significant reduction in the water sensibility and oxygen permeability of gelatine due to the creation of an exfoliated nanocomposite structure (Table 12.4). Li et al. first showed that the incorporation of natural MMT led to a significant decrease of both the swelling rate and the maximum solvent uptake [15]. Then, Bae et al. [13] and Martucci and Ruseckaite [16] showed that water vapour permeability could be reduced by about a factor 2 for a 5 wt% MMT filler content. The effect of clay on the oxygen barrier properties is not so pronounced, probably due to an already very low permeability of the neat matrix (Table 12.4).

Table 12.3 Mechanical properties of gelatine/clay nano-biocomposites: Young's modulus (E), tensile strength (TS) and deformation at break (ε)

Sample	E (GPa)	TS (MPa)	ε (%)	Ref
Bovine skin gelatine (type B) (25 wt% glycerol)	0.9	49.3	–	[10, 15]
−5 wt% Na + MMT	1.6	78.9	–	
−17 wt% Na + MMT	2.0	89.1	–	
Gelatine (type 4) (no plasticizer)	3.3	88.9	9.6	[12][a]
−5 wt% Cloisite Na+	5.9	97.4	3	
−10 wt% Cloisite Na+	8.3	110.8	0.9	
Bloom fish gelatine (20 wt% glycerol)	–	30.3 ± 2.4	48 ± 4	[13][b]
−5 wt% Cloisite Na+	–	40.9 ± 5.3	38 ± 3	
Porcine skin gelatine (type A)	2.1 ± 0.2	–	3.3	[14]
−5 wt% sepiolite	3.3 ± 0.1	–	2.5	

[a] Mechanical properties evaluated at 50 %RH
[b] Mechanical properties and P_{O2} measured at 50 % RH

Table 12.4 Barrier properties of gelatine/clay nano-biocomposites: Water vapour permeability (WVP), oxygen permeability (PO2) and maximum water uptake (W)

Sample	WVP (mol/(m.s.Pa)	P_{O2} (mol/(m.s.Pa)	W (%)	Ref
Bloom fish gelatine (20 wt% glycerol)	17.3×10^{-12}	2.08×10^{-18}	–	[13][b]
−5 wt% Cloisite Na+	7.6×10^{-12}	9.8×10^{-19}	–	
−5 wt% sepiolite	–	–	–	[14]
Bovine hide gelatine (type B)	13.7×10^{-12}	6.87×10^{-17}	–	[16][c]
−5 wt% Na + MMT	7.7×10^{-12}	5.58×10^{-17}	–	

[b] Mechanical properties and P_{O2} measured at 50 % RH
[c] WVP measured between 0 and 65 % RH and P_{O2} at 65 % RH. Such details were not specified for other data

12.4.2 Milk Proteins-Based Nano-Biocomposites

Milk has a protein content of about 33 $g.L^{-1}$ and contains two main types of proteins: caseins which represent about 80 % of total milk protein and whey proteins (20 % of total) that principally consist of β-lactoglobulin, α-lactalbumin and serum albumin. Caseins are proteins of major importance in the food industry due to their key role in the cheese making process. Whey proteins are by-products of the cheese or casein manufacture that remain in milk serum after pH/rennet-induced casein coagulation. Increased production of whey because of expanding cheese manufacture has led to identify new uses for whey proteins. This also involves that whey proteins are available at lower price than caseins. The film-forming properties of milk proteins have been indirectly demonstrated by films formed on processing equipment surfaces and at air–water interfaces during heating of non-fat milk [2]. Caseins and whey proteins have been used to produce transparent, flexible, colourless and odourless edible films and coatings displaying excellent oxygen, aroma and oil barrier properties at low RH, but poor moisture barrier properties as related to their high

hydrophilicity and water solubility. To remedy this drawback, several attempts have been made through the incorporation of hydrophobic materials such as lipids in whey and casein film formulation [17, 18]. However, phase separation often occurs and limits the efficiency of lipids addition demonstrating the need to develop other strategies to improve water resistance. The creation of a nanocomposite structure via the incorporation of layered silicate fillers in film formulation can be considered as a convenient way to reach this goal. Though, up to date, very few studies have been reported on whey protein/clay nanocomposite materials and not any on casein/clay nanocomposite materials. This is probably due to the high nutritional values and sensory acceptance of casein and whey protein that render them more suitable for edible purposes. In fact, edible applications are not compatible with the nanocomposite route.

Among studies already published on whey protein based nanocomposites, the works of Sothornvit et al. [19, 20] and Hedenqvist et al. [21] constitute the only available data reporting the effect of clay on the transport properties of whey-based materials. In all studies, nanocomposite films were obtained by the casting process from solutions in which whey protein isolates (WPI) were dispersed in water and heat denatured at temperature above 73°C [22] to allow unfolding of their globular native structure and unmasking of most of the hydrophobic and sulfhydryl groups hidden in the core of the structure. WPI film forming solutions were then mixed with a water suspension of montmorillonites.

In Sothornvit et al. studies, different types of MMT were tested; an unmodified clay (Cloisite Na^+) and two organically modified MMT (Cloisite 30B and Cloisite 20A) with a clay loading of 5 wt% [19] or up to 20 wt% [20]. In spite of the lack of morphological and structural analysis provided by the authors, the fact that mechanical properties (tensile strength and elongation at break) of nanocomposites were either unchanged (Cloisite Na^+ and Cloisite 30B) or decreased (Cloisite 20A) as compared to the neat matrix drops hints that a composite rather than a nanocomposite structure was achieved [19]. In the case of nanocomposite films prepared with Cloisite 30B, other results showed a dramatic decrease in tensile properties for clay loadings higher than 5 wt% [20]. The MMT effect on the water vapour permeability (WVP) indicated a small but significant decrease of a 1.4 and 1.6 factor with Cloisite Na^+ at 5 wt% and Cloisite 30B at 20 wt% respectively, whereas no effect was observed with Cloisite 30B and 20A at 5 wt%. According to the authors, the improvement of the WVP could be directly related to the hydrophilicity of the nanoclays that largely influences their compatibility with the WPI matrix and the level of dispersion.

In the work reported by Hedenqvist et al. [21] the montmorillonites used were previously intercalated with poly(vinylidene pyrrolidone) which is water soluble and acts as surfactant by easily adsorbing onto the MMT Na^+ surface. Clay filler loadings tested were up to 4.8 vol% MMT as expressed in inorganic content. This study mainly focused on the effect of clay content on the methanol diffusion through the films in relation to the morphology of the composite and the thermal properties of the polymer matrix. Thermal analysis confirmed that the polymer matrix was influenced by the presence of the nanoparticles as evidenced by a reduction of the glass

transition temperature indicating a reduction of the segmental mobility in the nanocomposite. They also noted that the absence of a significant increase in relaxed rubber modulus in the nanocomposites suggests that the reinforcing effect of the filler was limited, due to an incomplete exfoliation of clay nanoparticles, as confirmed by TEM analysis. Finally, a small but significant reduction (by almost two orders of magnitude) in the average methanol diffusivity was obtained for the highest MMT content (4.8vol%). According to these authors, the effect of nanoclays on the penetrant diffusivity was due to a reduction of the segmental mobility that reflects interactions between the filler particles and the polymer matrix and the tortuosity induced by MMT that extends the diffusion pathway of the penetrant molecules.

Beside evaluating the effect of nanoclays on mechanical and transport properties, Sothornvit et al. also studied the antimicrobial properties of WPI films reinforced with Cloisite Na^+, Cloisite 30B and Cloisite 20A [19, 20]. Results obtained showed that WPI/Cloisite 30B nanocomposite films exhibited a significant bacteriostatic effect against Gram-positive bacteria (*L. monocytogenes*) and no effect on Gram-negative bacteria (*E. coli* O157:H7) whereas, no antimicrobial activity was observed with WPI films reinforced with Cloisite Na^+ and Cloisite 20A. According to another study focusing on the antimicrobial activity of nanoclays alone [23], this antimicrobial effect was mainly ascribed to the quaternary ammonium group carried by the organically modified clays that might be able to disrupt bacterial cell membranes to cause cell lysis. This hypothesis is supported by the fact that among the different unmodified and organically modified clays studied, the unmodified one was the only clay to display no antimicrobial activity [23].

12.4.3 Soy-Based Nano-Biocomposites

Most of the proteins in soybean can be classified as globulin. Protein in the form of meal is one of the typical end products from soybean industrial processing. Protein meal can further be concentrated for the production of commercially available soy protein concentrates and isolates. Because soy protein isolates (SPI) are a highly refined class of soybean proteins that contains more than 90% protein and 18 different amino acids, they became the favourite choice of researchers. The film-forming properties of soy proteins have been traditionally used in Asia to obtain edible films by collecting the lipo-proteic skin formed after boiling soya milk [2]. Soy-based materials can be prepared using either a wet or a dry process (Table 12.1). In the casting process, heating up to 80°C is essential for unfolding proteins and unmasking sulfhydryl groups and hydrophobic side chains that will be involved in the resulting protein network [24]. The concentration of total solids should not exceed 9 %, to avoid gelation and thickening upon heating, and film formation is favoured in slightly basic conditions. SPI-based films alone possess poor flexibility. Therefore, plasticizers are usually used to overcome the brittleness, leading unavoidably to a significant decrease in their tensile strength [25].

Table 12.5 Mechanical properties (Young's modulus (E), tensile strength (TS), deformation at break (ε)) and water vapour permeability (WVP) of soy protein isolate (SPI)/clay nano-biocomposites

Sample	E (MPa)	TS (MPa)	ε (%)	WVP (mol/(m.s.Pa))	Reference
SPI (glycerol)	–	7.4	68	17×10^{-11}	[26][a]
−10 wt% Na^+ MMT	–	5.7	16	20×10^{-11}	
−10 wt% OMMT	–	9.4	54	16×10^{-11}	
−10 wt% bentonite	–	9.7	58	8.4×10^{-11}	
SPI (30 wt% glycerol)	180	8.7	88	–	[27][b]
−4 wt% Na^+ MMT	260	10.3	63	–	
−8 wt% Na^+ MMT	340	12.2	32	–	
−12 wt% Na^+ MMT	420	14	15	–	
−16 wt% Na^+ MMT	540	15.4	8	–	
−20 wt% Na^+ MMT	587	14.5	6	–	
SPI (30 wt% glycerol)	180	6.8	108	–	[30][b]
−4 wt% rectorite	360	9	57	–	
−8 wt% rectorite	450	11.8	21	–	
−12 wt% rectorite	560	12.8	12	–	
−16 wt% rectorite	620	10	8	–	
−20 wt% rectorite	580	9.4	7	–	
SPI (15 wt% glycerol)	–	2.3 ± 0.5	11.8 ± 0.4	$5.85 \pm 0.17 \times 10^{-11}$	[28][c]
−5 wt% Na + MMT	–	6.3 ± 0.9	65 ± 5	$4.56 \pm 0.15 \times 10^{-11}$	
−10 wt% Na + MMT	–	12.6 ± 0.6	24 ± 5	$3.85 \pm 0.12 \times 10^{-11}$	
−15 wt% Na + MMT	–	15.6 ± 1.7	18 ± 3	$3.34 \pm 0.09 \times 10^{-11}$	
SPI (15 wt% glycerol)	–	2.3 ± 0.5	11.8 ± 0.4	$5.85 \pm 0.17 \times 10^{-11}$	[29][c]
−5 wt% Cloisite 30B	–	15.1 ± 0.9	82 ± 3	$4.75 \pm 0.08 \times 10^{-11}$	
−10 wt% Cloisite 30B	–	16.2 ± 0.8	104 ± 5	$4.11 \pm 0.12 \times 10^{-11}$	
−15 wt% Cloisite 30B	–	18.6 ± 0.3	55 ± 3	$3.59 \pm 0.14 \times 10^{-11}$	

[a] Mechanical properties measured on films stored at 50 %RH and WVP according to the ASTM Method E 96–95

[b] Mechanical properties measured on films stored at 0%RH

[c] mechanical properties measured at 65 %RH and WVP between 65 and 100 %RH

Furthermore, they display high water vapour permeability due to the hydrophilic nature of proteins. Several authors succeeded in improving these latter properties by introducing unmodified montmorillonites [26–28], organically modified montmorillonites (OMMT) [26, 29] or rectorite [30] (Table 12.5).

Whatever the type of MMT used and the MMT loading (from 5 to 15 wt%), highly exfoliated and intercalated structures have been successfully prepared either via a solution intercalation process in a neutral aqueous media without any special aid [26, 27, 30] or via melt extrusion [28, 29]. In fact, in most studies, both the dry and the wet processes were used; the first one with the objective to exfoliate clays in the SPI matrix, and the second to obtain ultimate nanocomposite materials [27–30]. According to Chen and Zhang [27], the high affinity between soy proteins and the MMT layers was due to two types of interactions: hydrogen bonding between the –NH and Si–O groups and electrostatic interactions between the positive-charge-rich domains of soy protein and the negatively charged MMT

layers as evidenced by zeta-potential measurements and FTIR analysis. In spite of the negative charge of soy proteins at neutral pH, the heterogeneous distribution of the surface positive charges provided the possibility for soy proteins to intercalate and exfoliate negatively charged MMT layers [27]. However, structures and properties were shown to strongly depend on the filler content used. An increase in the filler content up to 12 wt% led to a significant increase in both the Young's modulus and the tensile strength (Table 12.5).

It is accompanied by a drop in the deformation at break due to the restricted segmental motion of soy proteins and the establishment of favourable interactions between the clay sheets and the protein chains. For filler content as high as 12–16 wt%, all the mechanical properties were degraded, due to phenomenon of MMT aggregation leading to a phase separation that occurred in the soy protein matrix [27, 30].

The introduction of clay led to a small but significant reduction of the water vapour permeability (Table 12.5). However, filler contents higher than 10 wt% are required to get a decrease of about a factor 2. Authors classically attribute this effect to the creation of a tortuous pathway for water vapour to diffuse [28, 29].

12.4.4 Corn Zein-Based Nano-Biocomposites

Zein is the major corn protein fraction (prolamin fraction) commercially produced from corn gluten meal, a by-product of corn wet-milling processing. Corn gluten meal contains about 55–60 % proteins and is available at relatively low price; 600–700 dollar/metric ton depending on the grade (food or not). Zein-based materials can be formed by different processes including casting and thermoplastic processing. Due to its low content in polar amino acids and high amount of apolar amino acids, zein-based films are not water-soluble and exhibit remarkable grease-resistance properties [2]. However, zein-based materials although less water sensitive than other biopolymers still show high water vapour permeability and low tensile strength when compared with commodity polymers. As it was the case for other proteins, its inherent brittleness may be improved by the use of plasticizers, which, on the other hand, further decrease water vapour and gas barrier properties.

To our knowledge, only one article has been recently published on the development of nano-biocomposite materials to improve the properties of zein-based films [31]. In this study, zein/organically-modified MMT nano-biocomposite films were successfully produced from two different processes, (i) solvent casting and (ii) blown extrusion involving precipitating zein protein from solution into zein resin and blowing into zein balloon, which resembled the melt intercalation method. Both techniques resulted in partially exfoliated structures, as demonstrated by XRD analysis and TEM observations. The introduction of nanoclays did not affect the translucency and the yellow colour of the films. The thermal stability of zein-based films was significantly improved for films prepared using the blown technique since a loading of only 5 wt% led to a delay of about 10°C of the temperature corresponding

to a 20% weight loss. However, the improvement of mechanical and barrier properties of the zein-based films did not evolve linearly with the MMT content. Luecha et al. showed that for the solvent casting technique, critical MMT contents of 5 wt% and 3 wt% resulted in optimal improvement of tensile strength and water vapour barrier properties, respectively [31]. The limitation of the blown technique was the restriction to use very low filler contents (below 3 wt%).

12.4.5 Wheat Gluten-Based Nano-Biocomposites

Wheat gluten (WG) has been widely investigated as a protein source because it is annually renewable and readily available at a reasonable cost (from 1 to 1.3 €/kg). Wheat gluten proteins consist of monomeric gliadins with a molecular weight ranging from 15000 to 85000 and a mixture of glutenin polymers with a molecular weight between about 80000 to several million (Table 12.1). WG proteins can undergo disulphide interchange upon heating, which leads to the formation of a covalent three-dimensional macromolecular network. The reactivity of the WG proteins toward chemical and temperature allows preparing WG-based materials by using two technological approaches: either a solvent-based process or a common thermo-mechanical process based on the thermoplastic properties of WG. With respect to its unique viscoelastic and film-forming properties, WG is an interesting raw material that can be used as a food packaging material. WG based-films present an attractive combination of strength and flexibility [32, 33], a high gas (oxygen and carbon dioxide) permeability in dry condition and a significant gas perm-selectivity at high relative humidity [34–36], and good grease [36] and aroma barrier properties [37] which are key functional properties for food quality preservation. They also are translucent [33] and can be heat-sealed [38]. A downside to the use of WG-based materials is their *per se* reactivity and thus lower inertia than most conventional petrochemical-based plastics. As mentioned above for soy proteins-based films, WG-based films are sensitive towards water due to the hydrophilic nature of many amino acids constituting the protein chains and to the need for adding hydrophilic plasticizer. As a consequence, their mechanical properties and water vapour barrier properties in high moisture conditions are relatively poor as compared to synthetic films such as low-density polyethylene.

The development of nanocomposite structures has been recently applied to WG-based materials to improve moisture resistance and mechanical properties [39–42] as well as to create antimicrobial delivery systems [43, 44]. All the studies devoted to WG-based nanocomposites involve the use of both unmodified and organically modified montmorillonites. The properties of these nanocomposite materials are directly related to their structure and, in this respect, the state of dispersion (intercalation/exfoliation) of the inorganic phase seems to be a key parameter [45]. The level of exfoliation highly depends on the nature of the montmorillonites. Almost fully exfoliated structures were obtained in the case of unmodified sodium MMT (Nanofil EXM 757 from Süd-Chemie (from [40]) or

Table 12.6 Mechanical properties (Young's modulus (E), tensile strength (TS), deformation at break (ε)) and water vapour permeability (WVP) of wheat gluten/clay nano-biocomposites

Sample	E (MPa)	TS (MPa)	ε (%)	WVP (mol/(m.s.Pa))	Reference
WG (10 wt% glycerol)	3.7	1.9	58	1.4×10^{-11}	[40][a, e]
−2.5 wt% Na^+ MMT	5.6	2.4	55	1.4×10^{-11}	
−5 wt% Na^+ MMT	10.6	4.7	16	6.6×10^{-12}	
−7.5 wt% Na^+ MMT	11.4	3.6	15	7.2×10^{-12}	
WG (12 wt% water/15 wt% glycerol)	65.4	5.8	106	–	[41][b]
−3 wt% C30B	91.8	9	78	–	
WG (T = 120°C; 37.2 wt% glycerol)	6.5	1.6	86	–	[33][c]
−2 wt% Na + MMT	9.5	1.8	70	–	
−5 wt% Na + MMT	23.6	2.5	42	–	
WG (T = 80°C; 37.2 wt% glycerol)	1.1	0.31	33	–	[33][c]
−2 wt% Na + MMT	1.7	0.32	30	–	
−5 wt% Na + MMT	6.4	0.66	23	–	
WG (no plasticizer)	737	48	–	–	[52][d]
−3 wt% attapulgite	691	50	–	–	
−7 wt% attapulgite	773	59	–	–	
−10 wt% attapulgite	783	57	–	–	
−20 wt% attapulgite	770	49	–	–	

Mechanical properties evaluated at [a] 70 %RH
[b] 50 %RH
[c] 75 %RH
[d] 53 %RH
[e] WVP measured between 0 and 100 % RH

Cloisite Na^+ from Southern Clay Products, Inc (from [39]). Contrarily, the presence of both stacks on TEM pictures and a d_{001} peak characteristic of an intercalated structure on XRD patterns evidenced that organically modified montmorillonites (Cloisite 10A [39] and Cloisite 30B [41]) were not well exfoliated. This highlighted that the affinity between wheat proteins and nanoclays is a key parameter governing the state of dispersion of the nanoclays. The use of unmodified MMT, which are naturally hydrophilic and thus, compatible with proteins seems to be more appropriate.

All studies demonstrated that the introduction of MMT nanoparticles in WG-based materials resulted in significant improvement in tensile strength and Young's modulus with a simultaneous decrease in deformability due to increased interfacial interactions (Table 12.6). An optimal filler content of around 5 wt% was required to achieve the greatest improvement of mechanical properties, due to the possibility of layered silicates to form a tridimensional network (Table 12.6). In the case of organically modified MMT, the presence of quaternary alkylammonium might act as a plasticizer in the WG matrix, which would play a negative role in achieving higher strength enhancement in the nanocomposites [41].

According to other studies, the moisture sensitivity of WG materials was efficiently reduced when wheat gluten proteins were combined with unmodified MMT [39, 40, 42]. For example, the liquid water uptake in cast WG-based nanocomposite films and liquid water diffusivity in thermoformed films were both divided by a factor 2 for respectively 10 wt% and 21.9 wt% of unmodified MMT [40, 42]. A decrease in WVP from 1.6×10^{-11} to 0.6×10^{-11} $mol.m^{-1}.s^{-1}.Pa^{-1}$ between the neat matrix and the nanocomposite (from 5 to 10 wt% of MMT) might be related to the establishment of hydrophilic interactions between gluten proteins and nanoclays, which resulted in a lower availability of the hydrophilic sites for water vapour. As regards to O_2 and CO_2 permeability (evaluated at 25°C and 80–90 % RH), no significant effect was observed for WG cast films over the range of studied MMT contents (up to 10 wt%) [40]. However, increased barrier properties towards 2-heptanone were also obtained for MMT contents $\geq$5 wt%. This decrease in permeability was ascribed to a tortuosity effect liable for a significant diffusivity decrease while increasing MMT contents [40].

Besides the improvement of protein based materials performance, the addition of clays could also be use to control the release of active compound. In this context, an antimicrobial delivery system based on WG as matrix, unmodified MMT as structuring agent and carvacrol as antimicrobial compound have been investigated [44, 45]. In the presence of 5 wt% MMT, particle size measurements and microscopic observations pointed out large aggregated structures that were supposed to entrap carvacrol molecules. Such structures could be responsible for the increased carvacrol retention as exhibited by both WG film-forming solutions and cast films. Further indications of this assumption were provided by wide angle X-ray analysis that confirmed the establishment of specific interactions between MMT, carvacrol and WG. The effect of MMT on the carvacrol release from wheat gluten coated papers was studied under controlled humidity from 40 to 100 % RH in a second part of this study [44]. Results indicated an increase of the carvacrol diffusivities while increasing RH and this RH-induced effect was accentuated in the presence of 5 wt% of MMT. As evidenced by scanning electron microscopy (SEM) and TEM, specific aggregated structures were formed in the presence of carvacrol and 5 wt% MMT creating a preferential pathway for carvacrol diffusion. The antimicrobial efficiency of the MMT-WG-coated papers toward *Escherichia coli* was assessed and showed that the antimicrobial effect was related to the carvacrol diffusivity. The diffusivity coefficients were utilized to optimize the packaging characteristics required to develop an efficient anti-microbial system and were finally validated against *Botrytis cinerea*.

12.5 Conclusion

In the current context, societal concerns and growing environment awareness have triggered the search for new products and processing that could be considered as an alternative to the existing petroleum-based plastics. In this chapter, several

examples of protein-based nano-biocomposites have been presented with a special attention for the methods used for the incorporation of layered silicates (organically modified or not) into the biodegradable matrices and the ultimate functional properties exhibited by these new kind of materials. The majority of the studies are devoted to the influence of filler content on mechanical properties, with very few data concerning other properties such as barrier properties.

One of the advantages of layered silicates as nanofiller is to ensure polymeric material reinforcement in two dimensions without requiring a special process to prepare the materials. Whatever the protein used, unmodified clays which are naturally hydrophilic and thus, compatible with proteins seem to be fully appropriate for the preparation of protein-based nano-biocomposites displaying both a good level of clay dispersion and a low environmental impact. The rather good dispersion of layered silicates leads to the formation of an expected tortuous path limiting the diffusion of small gases molecules, and thus to a significant decrease of permeability towards gases (oxygen, water vapour) and aroma compounds. The addition of nanoclays also leads to a significant improvement of material performance in terms of mechanical properties. The improved properties reported above are generally attained at low silicates contents ($\approx$5 wt%) as compared to that of conventional composites. However, although nanoclays are well dispersed within the protein matrix, the resulting improvement of barrier properties is quite moderate and does not exceed a two-fold reduction in the case of water vapour, and the same effect or even no effect in the case of 0_2 and $C0_2$. Concerning the effect on mechanical properties, the relative increase in Young's modulus and in tensile strength range between 1.5 and 2 times, with often a dramatic decrease in elongation for filler contents of 5 wt% and 50 %RH.

It seems that it would be more relevant to develop the "nano-biocomposite" strategy for other purposes than the improvement of mechanical and barrier properties of protein-based materials. The introduction of nanoclays in protein-based matrices could provide new additional functionalities such as UV protection or controlled delivery of active agents (antimicrobial compounds, agrochemicals, fertilizers or drugs). These properties are highly demanded in polymers in general, and all the more in the case of bio-sourced polymers with interests in a wide range of applications such as packaging, medicine and agriculture.

References

1. Garrett RH and Grisham CM (1996) Part I: Molecular components of cells. In: Thomson Brooks/Cole (ed), Biochemistry 3rd edn. Harcourt Brace Custom Publishers, Belmont, pp 1–375
2. Cuq B, Gontard N, Guilbert S (1998) Proteins as agricultural polymers for packaging production. Cereal Chem 75(1):1–9
3. Alexandre M, Dubois P (2000) Polymer-layered silicate nanocomposites: preparation, properties and uses of a new class of materials. Mat Sci Eng R 28:1–63
4. Verbeek CJR, Van den Berg LE (2010) Extrusion processing and properties of protein-based thermoplastics. Macromol Mater Eng 295:10–21

5. Schofield JD, Bottomley RC, Timms MF, Booth MR (1983) The effect of heat on wheat gluten and the involvement of sulfydryl-disulfide interchange reactions. J Cereal Sci 1(4): 241–253
6. Vaia RA, Giannelis EP (1997) Lattice model of polymer melt intercalation in organically-modified layered silicates. Macromolecules 30:7990–7999
7. Vaia RA, Jandt KD, Kramer EJ, Giannelis EP (1995) Kinetics of polymer melt intercalation. Macromolecules 28:8080–8085
8. Arvanitoyannis I (2002) Formation and properties of collagen and gelatin films and coatings. In: Gennadios A (ed) Protein based films and coatings. CRC Press, pp 275–304
9. Darder M, Ruiz AI, Aranda O et al (2006) Bio-Nanohybrids based on layered inorganic solids: gelatin nanocomposites. Curr Nanosci 2:231–241
10. Zheng JP, Li P, Ma YL, Yao KD (2002) Gelatin/montmorillonite hybrid nanocomposite. I. Preparation and properties. J Appl Polym Sci 86:1189–1194
11. Martucci JF, Vazquez A, Ruseckaite RA (2007) Nanocomposites based on gelatin and montmorillonite Morphological and thermal studies. J Therm Anal Calorim 89(1):117–122
12. Rao YQ (2007) Gelatin-clay nanocomposites of improved properties. Polymer 48:5369–5375
13. Bae HJ, Park HJ, Hong SI et al (2009) Effect of clay content, homogeneization RPM, pH, and ultrasonication on mechanical and barrier properties of fish gelatin/montmorillonite nanocomposite films. LWT—Food. Sci Technol 42:1179–1186
14. Fernandes FM, Ruiz AI, Darder M et al (2009) Gelatin-clay bio-nanocomposites: structural and functional properties as advanced materials. J Nanosci Nanotechnol 9:221–229
15. Li P, Zheng JP, Ma YL, Yao KD (2003) Gelatin/Montmorillonite Hybrid nanocomposite. II Swelling behaviour. J Appl Polym Sci 88:322–326
16. Martucci JF, Ruseckaite RA (2010) Biodegradable three-layer film derived from bovine gelatin. J Food Eng 99:377–383
17. McHugh TH, Krochta JM (1994) Water vapor permeability properties of edible whey protein-lipid emulsions films. JAOC 71:301–312
18. Krochta JM, Pavlath AE, Goodman N (1990) Edible films from casein-lipid emulsions for lightly processed fruits and vegetables. In: Spiess WEL, Schubert H (eds) Engineering and food—Preservation processes and related techniques, vol 2. Elsevier Applied Science, London, pp 329–340
19. Sothornvit R, Rhim J-W, Hong S-I (2009) Effect of nano-clay type on the physical and antimicrobial properties of whey protein isolate/clay composite films. J Food Eng 91: 468–473
20. Sothornvit R, Hong S-I, An DJ, Rhim J-W (2010) Effect of clay content on the physical and antimicrobial properties of whey protein isolate/organo-clay composite films. LWT-Food Sci Technol 43:279–284
21. Hedenqvist MS, Backman A, Gällstedt M et al (2006) Morphology and diffusion properties of whey/montmorillonite nanocomposites. Compos Sci Technol 66(13):2350–2359
22. Perez-Gago MB, Krochta JM (2002) Formation and properties of whey protein films and coatings. In: Gennadios A (ed) Protein based films and coatings. CRC Press, london, pp 159–180
23. Hong SI, Rhim JW (2008) Antimicrobial activity of organically modified nanoclays. J Nanosci Nanotechno 8:5818–5824
24. Gennadios A, McHugh TH, Weller CL, Krochta JM (1994) Edible coating and films based on proteins. In Krochta JM, Baldwin EA, Nisperos-Carriedo MO (eds) Edible coatings and films to improve food quality. Technomic Publishing Co inc, Lancaster, pp 201–277
25. Wang S, Sue HJ, Jane J (1996) Effects of polyhydric alcohols on the mechanical properties of soy protein plastics. J Macromol Sci-Part A 33(5):557–569
26. Rhim J-W, Lee J-H, Kwak H-S (2005) Mechanical and water barrier properties of soy protein and clay mineral composite films. Food Sci Biotechnol 14(1):112–116
27. Chen P, Zhang L (2006) Interaction and properties of highly exfoliated soy protein/montmorillonite nanocomposites. Biomacromolecules 7:1700–1706

28. Kumar P, Sandeep KP, Alavi S et al (2010) Preparation and characterization of bio-nanocomposite films based on soy protein isolate and montmorillonite using melt extrusion. J Food Eng 100:480–489
29. Kumar P, Sandeep KP, Alavi S et al (2010) Effect of type and content of modified montmorillonite on the structure and properties of bio-nanocomposite films based on soy protein isolate and montmorillonite. J Food Sci 75(5):46–56
30. Yu J, Cui G, Wei M, Huang J (2007) Facile exfoliation of rectorite nanoplatelets in soy protein matrix and reinforced bionanocomposites thereof. J Appl Polym Sci 104:3367–3377
31. Luecha J, Sozer N, Kokini JL (2010) Synthesis and properties of corn zein/montmorillonite nanocomposite films. J Mater Sci 45(13):3529–3537
32. Cuq B, Boutrot F, Redl A, Lullien-Pellerin V (2000) Study of the temperature effect on the formation of wheat gluten network: influence on mechanical properties and protein solubility. J Agr Food Chem 48:2954–2959
33. Angellier-Coussy H, Torres-Giner S, Morel MH et al (2008) Functional properties of thermoformed wheat gluten/montmorillonite materials with respect to formulation and processing conditions. J Appl Polym Sci 107:487–496
34. Gontard N, Thibault R, Cuq B, Guilbert S (1996) Influence of relative humidity and film composition on oxygen and carbon dioxide permeabilities of edible films. J Agr Food Chem 44:1064–1069
35. MujicaPaz H, Gontard N (1997) Oxygen and carbon dioxide permeability of wheat gluten film: effect of relative humidity and temperature. J Agr Food Chem 45:4101–4105
36. Guillaume C, Pinte J, Gontard N, Gastaldi E (2010) Wheat gluten-coated papers for bio-based food packaging: structure, surface and transfer properties. Food Res Int 43(5): 1395–1401
37. Chalier P, Peyches-Bach A, Gastaldi E, Gontard N (2007) Effect of concentration and relative humidity on the transfer of alkan-2-ones through paper coated with wheat gluten. J Agr Food Chem 55:867–875
38. Cho SW, Ullsten H, Gallstedt M, Hedenqvist MS (2007) Heat-sealing properties of compression-molded wheat gluten films. J Biobased Mater Bio 1:56–63
39. Olabarrieta I, Gallstedt M, Ispizua I et al (2006) Properties of aged montmorillionite-wheat gluten composite films. J Agr Food Chem 54:1283–1288
40. Tunc S, Angellier H, Cahyana Y et al (2007) Functional properties of wheat gluten/montmorillonite nanocomposite films processed by casting. J Membrane Sci 289:159–168
41. Zhang X, Do MD, Dean K et al (2007) Wheat gluten-based natural polymer nanoparticle composites. Biomacromolecules 8:345–353
42. Angellier-Coussy H, Gastaldi E, Correa F et al. (submitted) Nanoparticle size aspect ratio and liquid water sorption kinetic in agropolymer-based nanocomposite films. J Membrane Sci
43. Mascheroni E, Chalier P, Gontard N, Gastaldi E (2010) Designing of a wheat gluten/montmorillonite based system as carvacrol carrier: rheological and structural properties. Food Hydrocoll 24:406–413
44. Mascheroni E, Guillard V, Gastaldi E et al. (2011) Anti-microbial effectiveness of relative humidity-controlled carvacrol release from wheat gluten/montmorillonite coated papers. Food Control, (In press)
45. Ray SS, Bousmina M (2005) Biodegradable polymers and their layered silicate nanocomposites: in greening the 21st century materials world. Progress Mater Sci 50: 962–1079
46. Rose PI (1987) Gelatin. In: Mark HF, Bilakes NM, Overberger CG, Menges G (eds) Encyclopedia of polymer science and engineering, vol 7. Wiley, New York, pp 488–513
47. FAO (Food and Agriculture Organization of the United Nations) (1981) Amino acid content of foods and biological data on proteins. www.fao.org/DOCREP/005/…/AC854T00.htm
48. Braunitzer G, Chen R, Schrank B, Stangl A (1972) Automatische sequenzanalyse eines protein (β lactoglobulin AB). Hoppe-Seyler's Physiol Chem 353:832–834
49. Vanaman TC, Brew K, Hill RL (1970) The disulfide bonds of bovine α lactalbumin. J Biol Chem 245:4583–4590

50. Boldwell CE, Hopkins DT (1985) In: Altschul AM, Wilcke HL (eds) New Protein Foods, vol 2. Academic Press Inc, Orlando, p 152
51. Solsuski FW, Imafidon GI (1990) Amino acid composition and nitrogen-to-protein conversion factors for animal and plant foods. J Agric Food Chem 38:1351–1356
52. Yuan Q, Lu W, Pan Y (2010) Structure and properties of biodegradable wheat gluten/attapulgite nanocomposite sheets. Polym Degrad Stabil 95:1581–1587

Chapter 13
Analysis of Protein/Clay Nano-Biocomposites Systems

Xiaoqing Zhang and Katherine Dean

Abstract Plant protein-based clay nano-biocomposites were analyzed through a series of material characterization technologies including x-ray diffraction (XRD), transmission electron microscopy (TEM), dynamic mechanical analysis (DMA), differential scanning calorimetry (DSC) and high-resolution solid-state nuclear magnetic resonance (NMR) spectroscopy. Efficient dispersion of nano-clay in soy proteins or wheat gluten matrix was achieved via ultra-sonication treatment of the clay nanoparticles in plasticizers or using chemically modified clay nano particles. The dispersion status of the nanoclay in the composites were examined by XRD and TEM respectively and correlated to the changes in molecular motions and glass transitions of the protein matrixes to explore the effect derived from the nanoclay particles. High-resolution solid-state NMR further provides the interaction between the nanoclay and each component in the wheat gluten matrix, and the whole phase structures of the protein matrix. To correlate these results to the physical properties of the nanocomposites is fundamental to understand the performance of the systems and design new protein clay nanocomposites.

X. Zhang · K. Dean (✉)
CSIRO Materials Science and Engineering,
Gate 5, Normanby Road, Clayton VIC 3168, Australia
e-mail: Katherine.Dean@csiro.au

X. Zhang
e-mail: Xiaoqing.Zhang@csiro.au

L. Avérous and E. Pollet (eds.), *Environmental Silicate Nano-Biocomposites*,
Green Energy and Technology, DOI: 10.1007/978-1-4471-4108-2_13,

13.1 Introduction

Development of renewable polymer materials from agriculture feedstocks such as proteins, starch and cellulose has become a great challenge for material scientists due to increasing environmental concerns and diminishing petrochemical resources. A significant amount of research has been undertaken to develop a thorough understanding of biodegradable polymers and their potential applications [1–8]. Plant proteins including chickpea and soy protein isolates [2, 9–14], wheat proteins [15–19], zein [20, 21], pistachio [22], sunflower [23] and pea proteins [24] have also been used to produce biodegradable polymer materials.

These plant proteins consist of various combinations of amino acid units as derived from different plant sources and thus exhibit different properties [25]. In general, they have good viscoelastic properties, strong tensile strength when no plasticizers are used, and excellent gas barrier properties. However, it is normally difficult to thermally process the proteins directly due to strong inter- and intramolecular interactions in conjunction with some extent of crosslinking among the protein macromolecules [26]. Large amounts of plasticizers are usually required in the process to reduce the strong inter-/intra-molecular interactions and increase the mobility of the protein chains to reach sufficient flexibility and extensibility of the materials. Such plasticization significantly weakens the material strength. Therefore, enhancement of the mechanical performance of plasticized natural protein-based materials plays a key role in extending the application of the materials.

Chemical modification including crosslinking and polymer grafting has been widely applied to modify the structures and properties of plant protein-based materials [2, 27–33]. Formation of clay nanocomposites is another way to achieve a significant improvement in many aspects of the performance of polymers with a very low dosing amount of the nanoparticles [34–43]. The main reason for such property improvement as compared to pure polymers or conventional composites (micro- or macro-composites), is due to the significantly strengthened interfacial interactions between the polymer matrix and the clay nanoparticles (layer thickness of the order of 1–2 nm, diameter of 30–2000 nm) when such particles are well dispersed in the polymer matrix. Layered silicates such as montmorillonite, hectorite and saponite are frequently used [40]. Generally two types of polymer/layered clay nanocomposites are achievable and described on the basis of the particle dispersion: *intercalated* and *exfoliated* nanocomposites [35], although a *flocculated* model was also mentioned [40]. The clay nanocomposites can be produced through in situ polymerization, solvent intercalation/exfoliation and melt intercalation/exfoliation.

A series of plant protein-based clay nanocomposites have been studied and have shown many aspects of enhancement of material performance including tensile strength, stiffness, toughness, modulus, barrier properties and so on. Various advanced material characterization technologies have been applied not only to examine the property improvement of the nanocomposites, but also to explore the interactions between the protein matrix and clay nanoparticles, dispersion status of

the nanoclay particles, molecular motions of the matrix, nanoclay effect to each component of the protein systems and phase structures of the whole protein matrixes. This chapter will focus on the analysis of the protein-based clay nanocomposites to correlate the structural information with material properties thus providing an inside understanding of the performance of the clay nanocomposites.

13.2 Analytical Methodologies

Polymer nanocomposites generally consist of nano-scale layered clay dispersed within a polymer matrix. In an intercalated nanocomposite often a single polymer chain will be driven between the clay silicate layers, but the system still remains quite well ordered in a stacked type of arrangement. In an exfoliated nanocomposite the silicate layers are completely delaminated from each other and are individually well dispersed in the polymer matrix. These exfoliated nanocomposites have shown to exhibit the most significant improvement in physical properties [34, 44].

The degree of intercalation and exfoliation of layered silicates in protein nanocomposites can be quantified using x-ray diffraction (XRD) and transmission electron microscopy (TEM). Generally, layered silicates have a defined interlayer spacing basal reflection corresponding to the d_{001} spacing in an X-ray diffractogram. When such layered silicates are dispersed in protein matrixes and an intercalated system is formed, the d-spacing values will be increased resulting in the reflection peak shifting to lower 2θ value direction in the X-ray diffractogram. The formation of an exfoliated system can significantly increase the d-spacing value until the point where no coherent X-ray diffraction can be observed [37, 38, 42, 45]. TEM is a complimentary technique to XRD where an image of the dispersion of the silicate within a polymer matrix can be directly visualized and analyzed both qualitatively and quantitatively [37, 38, 42, 46].

Dynamic mechanical analysis (DMA) is also usually applied in studying protein-based clay nanocomposites since the result provides both dynamic mechanical performance of the nanocomposites and the information of molecular motions and phase transitions of the protein matrix in the nanocomposites. The storage modulus decreased significantly at glass transition in conjunction with the appearance of a loss tangent peak (tan δ). The methodology is complimentary to glass transition analysis of the nanocomposites through conventional differential scanning calorimetry (DSC) measurement. In addition, secondly transitions are also detected in the DMA measurement. As a result, DMA has been applied in many protein-based polymer materials including their clay nanocomposites [38, 42].

The performance of protein clay nanocomposites have been examined through mechanical property testing [47], surface hydrophobicity and wettability evaluation [48], optical measurement [47], permeability to gas or water–vapor analysis [45, 47–49] and thermal stability [48].

Fourier transform infrared (FT-IR) and near-infrared (NIR) are sensitive to the secondary structures of proteins especially the random coil/helix and beta-sheet structures, thus the methods are widely used to examine the structural transition of proteins and intermolecular interactions in protein clay nanocomposites [45, 50–54].

Solid-state nuclear magnetic resonance (NMR) spectroscopy is a powerful technique to explore both chemical structural and molecular motions of polymer materials [55, 56]. Many protein-based polymer systems are also multi-component/multi-phase systems due to various components (such as plasticizers, lipid, other carbohydrate impurities, crosslinkers and other additives) that would co-exist. High-resolution solid-state NMR has made it possible to study the chemical structure changes of such systems in conjunction with the molecular motions of each component/phase and interactions among these components. The cross-polarization (CP) method under magic angle spinning (MAS) condition is sensitive to the rigid components/phases where strong dipolar interactions in the system allow the polarization transfer from protons to nearby carbons, thus efficiently enhancing the carbon intensities. On the other hand, a single 90 ° pulse excitation (SPE) method under MAS is sensitive to mobile components/phases when a short repetition time is used. Therefore, by using different pulse sequences, protein components/phases with different mobility can be selectively examined [55–57].

Molecular motions, intermolecular interactions among different components and phase structures of the protein systems can be examined via measurements of various NMR relaxation times including spin–spin (T_2), spin–lattice (T_1) and spin–lattice relaxation time in rotation frame ($T_{1\rho}$), chemical shift changes, spin-diffusion interactions and so on [16, 28, 30, 32, 42, 58, 59]. When clay nanoparticles are dispersed into polymer matrix, their paramagnetic impurity Fe^{3+} ions exert a sizable influence on the nuclear spin near the clay surface. If the distance between the Fe^{3+} and the studied nuclei is close enough, significant signal weakening and linewidth broadening will occur for these nuclei. Remarkable shortening ^1H T_1 or even ^1H $T_{1\rho}$ values of the polymer matrix may also be observed because such effects can penetrate into the protons farther away from the clay surface due to strong proton spin diffusion interactions among the polymer matrix. The paramagnetic effect on the ^1H spin–lattice relaxation times of polymer matrix should be correlated to the surface-to-volume ratio of the clay nanoparticles, thus reflecting the clay dispersion in the matrix [60–63]. Examination of the ^1H spin–lattice relaxations of protein clay nanocomposites provides a bulk analytical method to characterize the clay dispersion in the nanocomposites.

By a combination of these characterization techniques, the chemical structures, molecular motions, the morphology of protein matrixes, the dispersion status of nanoclay particles and the interactions between the nanoclay and protein chains can be investigated and correlated to the material performance of the nanocomposites. A good understanding of the correlation between the structures and properties of the protein-based clay nanocomposites is fundamentally important for development of advanced materials from natural protein-based resources.

13.3 Clay Nanocomposites of Plant Proteins

13.3.1 Soy Protein-Based Clay Nanocomposites

Commercially available soy products include soy isolate, soy concentrate and soy flours [10, 13]. Soy protein isolates are generally used in the preparation of soy-based plastics due to their high protein content (approximately 90 %) [13]. Extruded soy protein is generally plasticised with glycerol and water, and the resulting properties depend on the amount of plasticizer used in the extruded soy protein [38].

Soy protein-based clay nanocomposites were produced by dispersing unmodified sodium montmorillonite clay (Cloisite Na^+, supplied by Southern Clay Products) in a solution of glycerol and water (1:1 in wt.) in a high-powered sonifier, then mixing the Cloisite Na^+ solution to a water-soluble soy protein isolate (Profam 974, from Archer Daniels Midland) in a high-speed mixer, and finally extruded using a twin extruder (Theysohn 30). The contents of Cloisite Na^+ and plasticizers in the nanocomposites were 3 and 38.8 wt% respectively.

Sufficient intercalation and exfoliation of the clay and plasticizers were achieved under the sonication treatment as examined by XRD measurements (Brüker D8 Diffractometer operating at 40 kV, 40 mA, Cu Kα radiation monochromatised with a graphite sample monochromator). The X-ray diffractograms for Cloisite Na^+:glycerol:H_2O (ratio 1:10:10 in wt) are illustrated in Fig. 13.1. After initial mixing a broad peak was observed, corresponding to the d_{001} spacing or interlayer clay spacing of $\sim$18.3 Å. The broadness of this particular peak may give an indication of the different states ranging from separations of 15.6–19.9 Å (corresponding to the outer edges of this XRD peak). After 5 min of ultrasonic treatment this broad peak reflecting a spacing of $\sim$18.3 Å had disappeared and a peak at 2 theta angle 1.8° (corresponding to a spacing of around 64 Å) could be seen. This higher peak was still visible after ultrasonic treatment for 20 min, but disappeared after 25 and 30 min of the treatment, indicated good dispersion or exfoliation of clay particles in the glycerol/water system. The main mechanism for the expansion of the clay layers was due to interactions between the sodium ion of the Cloisite Na^+ and the dipole of the water/glycerol [64, 65].

XRD and TEM were used for assessing the dispersion of clays in the soy protein nanocomposites as shown in Fig. 13.2. The X-ray diffractogram for the untreated protein/glycerol/water/Cloisite Na^+ sample (Fig. 13.2 left) indicates a range of clay configurations, observed as a broad series of peaks corresponding to interlayer clay spacing from 10 Å to 60 Å. However, the diffractogram for the ultrasonically treated protein/glycerol/water/Cloisite Na^+ sample shows the disappearance of the broad series of peaks, indicating the nanocomposite formed was exfoliated. The result was further confirmed by the TEM images (Fig. 13.2 right), indicating a range of clay configurations including large clay agglomerates in the untreated nanocomposites, while exfoliated structures with only some smaller

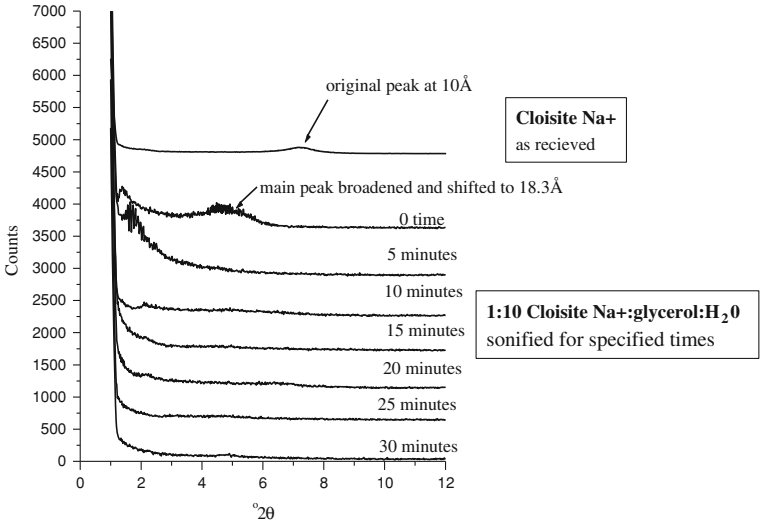

Fig. 13.1 XRD traces of Cloisite Na^+ in glycerol and H_2O (1:10:10 in wt) sonicated for varying periods of time. Reproduced from Dean K, Yu L [38] with kind permission from ©Woodhead Publishing 2005

tactoids of silicates (5–20 particles) were present in the ultrasonically treated nanocomposite sample.

DMA results (observed at a Perkin-Elmer Pyris Diamond DMA in tension mode after conditioning at RH = 50 %, room temperature) of the soy protein nanocomposites are shown in Fig. 13.3. The variation in storage modulus (E′) for the neat protein, the untreated and the treated nanocomposites over the temperature range clearly showed that the ultrasonically treated sample exhibited a higher storage modulus throughout the whole range, reconfirming the positive structure/property relationship due to exfoliation of the clay particles.

The neat protein/glycerol/water sample shows a tan δ peak corresponding to glass transition temperature T_g at 108.5 °C while the secondary (or β) relaxation was situated at –52.0 °C (Fig. 13.3) due to the motion of the hydrated soy protein side groups, or the crankshaft motion of the main chain as described previously [11]. The tan δ peak of the untreated nanocomposites sample was shifted to a high temperature (at 112.5 °C) due to the restriction in molecular motion of the protein by the dispersion of the nanoclay, while the secondary (or β) relaxation was situated at –55 °C (3 °C lower than in the neat protein). This lowering of the β relaxation may be due to the disruption of the protein side groups due to the large agglomerates of clay particles in the system [11]. The ultrasonic-treated nanocomposite sample displayed an even higher T_g (tan δ peak at 118.0 °C), suggesting the further restriction in molecular motion of the protein by the predominantly exfoliated dispersion of the nano-clay. The secondary (or β) relaxation in the treated sample was situated at –51 °C, similar to that of the neat protein/glycerol/

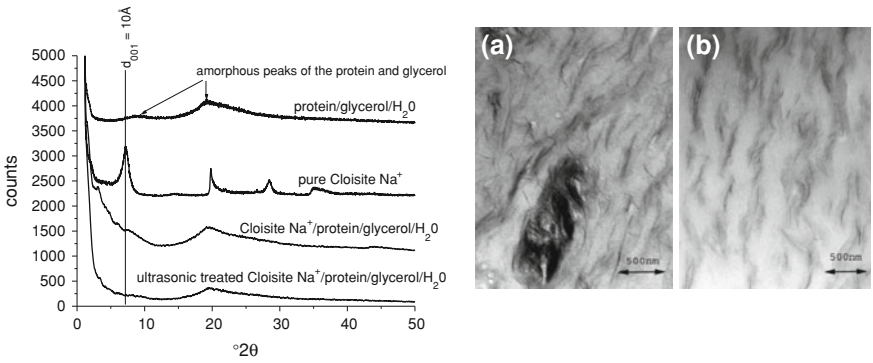

Fig. 13.2 XRD traces (*left*) of neat soy protein/glycerol, neat Cloisite Na^+ and the nanocomposites, and TEM images (*right*) of the untreated nanocomposites (**a**) and ultrasonic-treated nanocomposites sample (**b**). Reproduced from Dean K, Yu L [38] with kind permission from ©Woodhead Publishing 2005

water sample, indicating that the finely dispersed clay particles did not significantly affect the motion of the protein side groups or crankshaft motion of the main chain as previously described [11] in protein systems.

The T_g values of the nanocomposites were also measured using differential scanning calorimetry (Perkin-Elmer DSC-7) in scanning mode (20 °C/min) after the conditioning. The T_gs obtained from the DSC (using the midpoint method) showed similar trends to the maximum in tan δ from the DMA (Fig. 13.3). The neat protein/glycerol/water sample had a T_g of 51 °C, the untreated nanocomposite sample had a slightly higher T_g of 53 °C and the ultrasonically treated sample had a T_g of 58 °C. Despite similarities in trends, the values of T_g from the DSC were significantly lower than the temperatures where tan δ peaks were detected in DMA. The difference is mainly due to the mechanisms of the two different testing methods. The DMA samples in tension may have lost moisture (despite their silicone oil coating), hence reducing the mobility of the protein chains, which would be observed as an increase in the T_g that was actually measured. Note that the onset temperatures of tan δ increases corresponding to their T_g appear at a similar temperature range of the T_g values as observed in DSC testing.

A significant improvement in modulus (84 % compared with the neat protein/glycerol/water sample) is observed in the ultrasonically treated nanocomposites sample [38]. An improvement (23 % or 47 %) in tensile strength was also observed for untreated or treated nanocomposite sample, respectively [38]. As is expected from the inclusion of a hard silicate into a polymeric material, the break elongation for both nanocomposites is reduced moderately [38].

This study has illustrated that clean ultrasonic energy does promote the intercalation and exfoliation of unmodified montmorillonite clays, and when melt blended in particular combinations with soy protein and plasticisers produces a biodegradable nanocomposite polymer film with significant improvement in

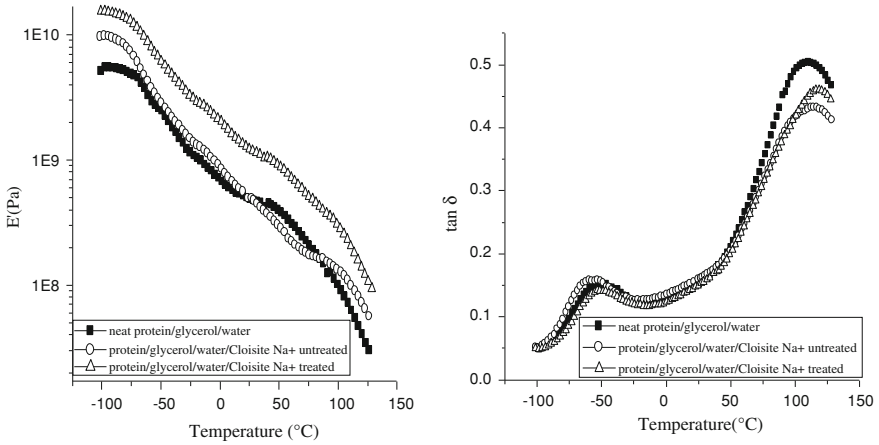

Fig. 13.3 The storage modulus (E′) (*left*) and tan δ (*right*) traces of neat soy proteins, untreated and ultrasonic-treated nanocomposites. Reproduced from Dean K, Yu L [38] with kind permission from ©Woodhead Publishing 2005

mechanical properties. The complete exfoliation of clay silicates without the use of chemical modification is significant both in terms of cost and biodegradability.

13.3.2 Wheat Protein-Based Clay Nanocomposites

As one of the cheapest plant protein derived from the second largest cereal crop wheat (after maize), wheat proteins (WP) and wheat gluten (WG) also have excellent properties (like soy proteins) in viscoelastic performance, tensile strength and gas-barrier performance. However, a large amount of plasticizers (normally glycerol and water) are required in thermal processing, the same as in processing soy protein-based materials, to interrupt the strong self-association among protein segments, to increase the mobility of the protein chains and thus to improve the flexibility and extensibility of the materials. Such plasticization results in high moisture sensitivity and low strength of the materials. Formation of clay nanocomposites has been studied for achieving strength enhancement of the WP or WG-based materials.

Cloisite® 30B (C-30B) from Southern Clay Products Inc, a natural montmorillonite modified with methyl tallow bis-2-hydroxyethyl quaternary ammonium chloride, 3 wt%, was dispersed into plasticized WG (WG-1), or WG/polyvinyl alcohol (PVOH) = 90/10 blend (WG-2), or WG/PVOH = 90/10 blend with 1 wt% of glyoxal as crosslinker (WG-3) via high-speed mixing and then compression moulding to form corresponding clay nanocomposites (WG-1 N, -2 N or -3 N) at 130 °C. 12 wt% water and 15 wt% glycerol were used as plasticizers in all of these samples. The X-ray diffractograms (Brüker D8 Diffractometer) of pure

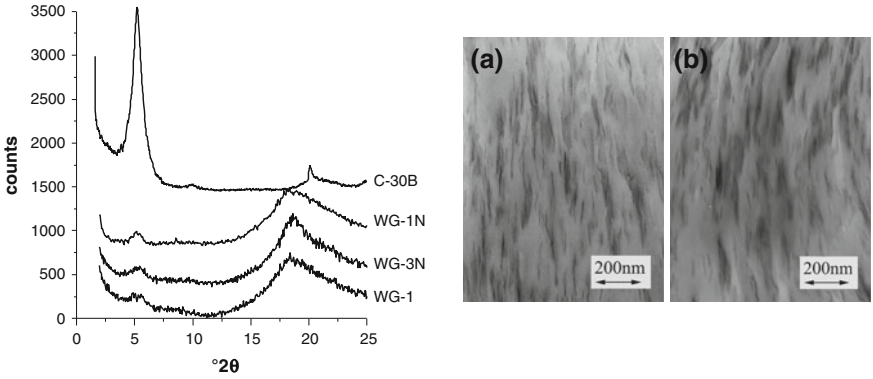

Fig. 13.4 The XRD traces (*left*) of samples WG-1, WG-1 N, WG-2 N and C-30B and TEM images (*right*) of WG-1 N (**a**) and WG-2 N (**b**). Reproduced from Zhang X et al. [42] with kind permission from ACS Publications (2007)

C-30B, WG-1, WG-1 N and WG-3 N and TEM images of WG-1 N and -3 N are shown in Fig. 13.4. The strong diffraction peak of C-30B at 5.2° (2θ) corresponding to an averaged interlayer clay spacing of 17.5 Å, was significantly reduced in intensity and the diffractogram showed a similar pattern to that of WG without any C-30B (WG-1), indicating that intercalated/exfoliated dispersion of the nanoclay was achieved in these nanocomposites. The TEM images of WG-1 N and WG-3 N confirmed the XRD result, showing that smaller tactoids (3–5 particles) were the predominant structure in the nanocomposites, but no large agglomerates were visible in the systems. Significant improvement in mechanical strength for the nanocomposites sample was obtained under relative humidity of 50 and 85 % [42].

The DMA behaviour (observed at a Perkin-Elmer Pyris Diamond DMA in bending mode) for the WG clay nanocomposites after conditioning at RH = 50 %, room temperature was similar to those of plasticized WG [16] as shown in Fig. 13.5. As temperature increased, the storage modulus (E′) decreased slowly and then dropped markedly at a typical temperature due to glass transition, while a strong tan δ peak was observed corresponding to the transitions. At a temperature range of -60– -50 °C, a minor tan δ peak was obtained in conjunction with an E′ onset due to β transitions of the protein matrix. These β-transitions were not influenced by the dispersion of the nanoclay. Although a certain amount of water ($\sim$12 wt%) was present in the systems, a transition due to ice melting was not observed at around 0 °C, indicating the water molecules were strongly hydrogen bonded with protein macromolecules and did not exist as free water as described in previous reports. Comparison of the results of WG with their nanocomposites showed that the E′ data in the low temperature range were similar for all WG systems, but the nanocomposites samples displayed a relatively high E′ at high temperatures especially above the T_g.

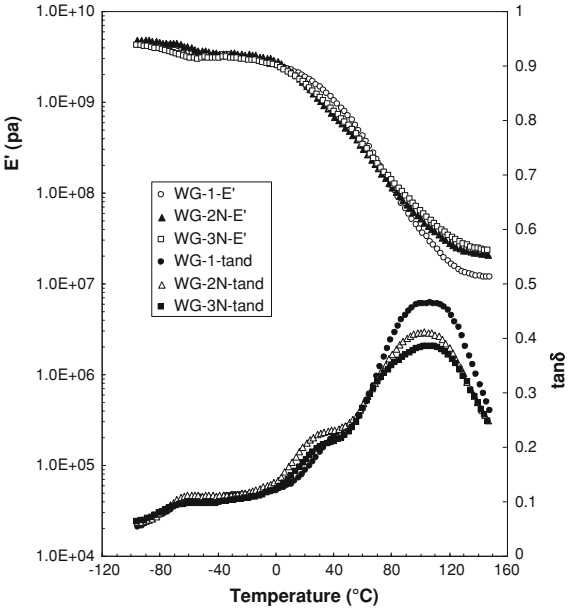

Fig. 13.5 The DMA results of WG and their nanocomposites samples. Reproduced from Zhang X et al. [42] with kind permission from ACS Publications (2007)

Table 13.1 Key DMA data of WG nanocomposites [42]

Samples	Tan δ-β (°C)	Tan $\delta - \alpha_2$ (°C)	Tan $\delta - \alpha_1$ (°C)	Tan δ max (α_1)
WG-1	-55	31	104	0.463
WG-1 N	-53	33	107	0.424
WG-2	-60	31	102	0.444
WG-2 N	-60	32	104	0.409
WG-3	-60	32	105	0.405
WG-3 N	-57	33	107	0.402

[1] error bar of 3–5 %

Best fitting the results of the tan δ curves suggested two T_g transitions (α transitions) for all of the systems as listed in Table 13.1. The relatively weak peaks (tan $\delta - \alpha_2$) appeared at a lower temperature around 26–33 °C should be attributed to the T_g of the plasticized matrixes/phases. Although the dispersion of clay nanoparticles caused the T_g transition to start at lower temperatures for the matrix, it only broadened the tan $\delta - \alpha_2$ peaks but did not shift the maximum of these peaks significantly. The major tan δ peaks (tan $\delta - \alpha_1$) shifted slightly to higher temperatures for nanocomposite samples, the maximum values of tan δ peaks were significantly reduced. The WG-3 N displayed the highest E′ and lowest tan δ maximum, corresponding to the highest modulus and motional restriction due to a combination effect of blending, crosslinking and interactions with the nanoclay particles.

Table 13.2 ^{1}H spin–spin relaxation time T_2 values (μs) and their proportions (%) obtained via analysis of ^{1}H FID signals[1] for WG nanocomposites [42]

Samples	T_{2S} (μs)	A_{2S} (%)	T_{2M} (μs)	A_{2M} (%)	T_{2L} (μs)	A_{2L} (%)
WG-1	11.1	46	103	29	980	25
WG-1 N	11.3	45	65	36	619	19
WG-2	9.1	55	118	25	501	20
WG-2 N	9.6	53	53	30	488	17
WG-3	9.7	56	109	28	751	16
WG-3 N	10.4	55	59	37	539	8

[1] error bar of 3–5 %

Normally exfoliation of nanoparticles in a polymer matrix results in an increase in T_g due to interactions between polymer chains and the nanoparticles [38]. The minor change in T_g of WG/C-30B nanocomposites is possibly due to the mobile organics (ca. 30 wt% of methyl tallow bis-2-hydroxyethyl quaternary ammonium chloride) used for modification of the nanoparticles, that the nanoclay could have both motional restriction effect (interactions between nanoparticles and mobility enhancement effect (additional plasticization) simultaneously, but the motional restriction effect was more pronounced above T_g (the decrease in tan δ max) for most of the nanocomposites.

The broad tan δ peaks corresponding to T_g transitions of these nanocomposites are due to the presence of a series of complicated phase structures in conjunction with their different interactions with the nanoclay particles. In addition, multi-components such as proteins, starch, lipid, polymer additives (PVOH) and plasticizers co-exist in the systems and their interactions with the nanoparticles would also behave differently. High-resolution solid-state NMR techniques were applied to investigate these plasticizing, blending and crosslinking effects on each component in the nanocomposites and intermolecular interactions between different components.

^{1}H spin–spin relaxation (T_2) data (observed at a Bruker Minispec PC120 spectrometer at 20 MHz, listed in Table 13.2) showed three phase components in the WG-nanocomposites. The dispersion of nanoclay particles into these plasticized protein systems caused a significant reduction in T_2 values of T_{2M} (intermediate phase) and T_{2L} (mobile phase), suggesting motional restriction in these mobile phases of nanocomposites. No significant influence on T_{2S} phases (rigid phase) was observed, except the T_{2S} proportions decreased slightly. Higher T_{2S} proportions obtained in WG-2 and WG-3 systems were attributed to the blending with PVOH (PVOH mainly remained in the rigid phase) and the crosslinking with glyoxal [28, 58]. The high proportion of rigid phases in the WG systems would contribute to their higher tensile strength and modulus. Usually DMA provides motional information of polymer components over a scale of 20–100 nm whilst ^{1}H T_2 is very sensitive to local dipolar interactions at the molecular level (a scale below 1 nm). The two methodologies provide information of motional dynamics of a material on different scales.

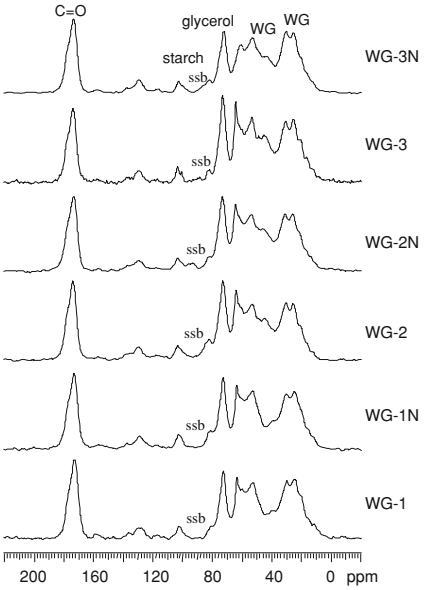

Fig. 13.6 ^{13}C CP/MAS NMR spectra of WG-1, WG-2, WG-3 and their nano composites WG-1 N, WG-2 N and WG-3 N (ssb: spinning-side bands). Reproduced from Zhang X et al. [42] with kind permission from ACS Publications (2007)

The CP/MAS ^{13}C NMR spectra of WG and their nanocomposites (observed at a Varian Unity plus spectrometer at 300 MHz for ^{1}H and 75 MHz for ^{13}C) are shown in Fig. 13.6 in conjunction with the assignment. Two sharp peaks at 64 and 74 ppm are due to the plasticizer glycerol in all cases. Examination of ^{1}H T_2 measured via high-resolution solid-state NMR technique can provide the motional information of each component in such multi-component systems. The ^{13}C CP/MAS NMR spectra of WG-2 N observed with varied CP delay times (τ) are shown in Fig. 13.7 (left), where the intensity changes following ^{1}H T_2 decay [28]. Most of the proteins and starch resonances decayed rapidly as τ time increased, and when τ reached 30 μs, the only signals remained were glycerol at 73 and 64 ppm. The behaviors of the other WG systems were similar, suggesting the rigid phases (T_{2S}) in the nanocomposites were still corresponding to proteins and starch components, while the T_{2M} could be due to plasticized proteins and starch. Plasticizers such as water and glycerol were present in all three phases and interact with different components mainly via hydrogen bonding interactions. Their distribution in the three phases depends on the nature of the plasticizers and the amount of plasticizers used. In the cases studied in this work, the major proportion of plasticizers existed in the intermediate (T_{2M}) and mobile (T_{2L}) phases.

The presence of mobile components in the system has also made it possible to observe high-resolution solid-state ^{1}H NMR spectra by MAS technique under a low spinning rate at around 7 kHz. Only mobile components such as lipid and plasticizers can be obtained by this method while the rigid phases would be missed as a broad baseline. Figure 13.7 (right) shows the ^{1}H spectra of a nanocomposite WG-1 N observed by Carr-Purcel-Meiboom-Gill (CPMG) pulse sequence using

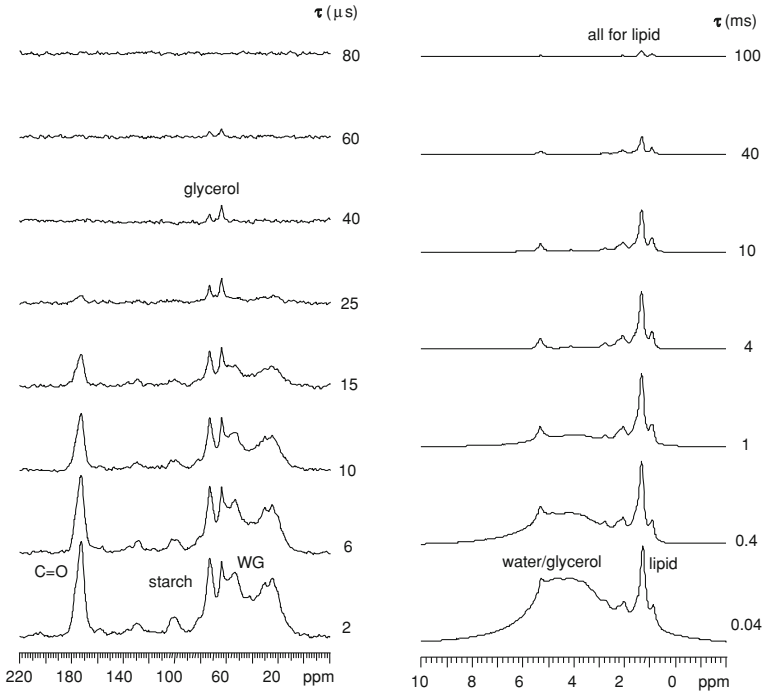

Fig. 13.7 ^{13}C CP/MAS NMR spectra (*left*) of WG-1 N measured with varied CP delay times (τ) where the intensity decay follows ^{1}H T_2 decay and ^{1}H NMR spectra (*right*) of WG-1 N observed by CPMG pulse sequence under MAS (**B**) with varied τ delay times. Reproduced from Zhang X et al. [42] with kind permission from ACS Publications (2007)

typical τ times at which the nth echo appeared under MAS conditions. These narrow peaks at 0.9, 1.3, 2.0, and 5.2 ppm were all assigned to lipid resonances while the broad peak at around 4.0 ppm was due to water and glycerol. The minor amount of resonances of proteins (if existing) might be overlapping with these strong resonances. As the τ time increased, the intensity of the water/glycerol peak (4.0 ppm) decayed much faster than these lipid resonances. At τ above 10 ms, only lipid resonances were observed, indicating that lipid was the most mobile component in the nanocomposites.

The study of ^{1}H spin–lattice T_1 relaxations of each component in a multi-component system can explore not only the molecular motions at MHz range but also the homo- or heterogeneity of the whole systems on a scale of ca. 20–30 nm, which is the effective spin-diffusion length during the T_1 relaxation times [66–68]. ^{1}H T_1 data of the WG nanocomposites were observed either via ^{13}C resonances through CP/MAS (mainly the rigid phases/components) or via their ^{1}H MAS spectra (the mobile components/phases) and are listed in Table 13.3.

The ^{1}H T_1 data of protein components observed at 174 ppm and 30–25 ppm via ^{13}C CP/MAS spectra were quite similar in most of samples indicating a strong

Table 13.3 ^{1}H spin–lattice relaxation time T_1 values (s) of difference components of WG matrixes obtained via difference methods [42]

Samples	Via ^{13}C CP/MAS Spectra			Via ^{1}H MAS Spectra	
	Proteins	Starch	Glycerol	Lipid	Water/Glycerol
WG-1	0.63	0.82	0.64	0.59	0.65
WG-1 N	0.23	0.38	0.28	0.35	0.29
WG-2	0.42	0.78	0.38	0.37	0.39
WG-2 N	0.22	0.72	0.23	0.33	0.24
WG-3	0.37	0.88	0.37	0.40	0.36
WG-3 N	0.19	0.71	0.21	0.31	0.23

[1] error bar of 3–5 %

spin-diffusion interaction among the components, thus, their averaged values are shown in Table 13.3 as the T_1 value of the protein component in each sample. The T_1 data detected at 103 ppm reflected the behaviour of the starch component, while those of glycerol were detected from the narrow line at 64 ppm. For those obtained via ^{1}H MAS spectra, the T_1 data for lipid were measured at 1.3 ppm (the -CH_2-) while those of the water/glycerol plasticizers were detected at 4.0 ppm.

For all WG samples the T_1 of the starch component was quite different from those of proteins, lipid and plasticizers, indicating that the starch was not mixed intimately with the other components at the scale of 20–30 nm. When clay nanoparticles were dispersed into the systems, the T_1 data decreased for all the cases. It seemed that the nanoparticles also enhanced the miscibility between starch and other components in WG-1 N, the T_1 data became much closer to each other in the nanocomposite. However, when blending PVOH and crosslinking were applied in the systems (WG-2 N and WG-3 N), such effect disappeared; the T_1 of the starch component did not decrease as much as that in WG-1 N, although the nano clay still generated a similar T_1 decrease to all other components in the nanocomposites. The polymer matrixes of these nanocomposites were heterogeneous at a scale of 20–30 nm, which could be the reason for multiple T_g transitions observed in DMA measurements. Note that the ^{1}H T_1 data of all WG nanocomposites samples were reduced as compared to the WG systems without nanoclay particles. Such change reflects the interaction between WG and clay platelets as reported previously [60–62].

Naturally occurring montmorillonite clays usually contain 2–5 wt% of paramagnetic Fe^{3+} ions mainly substituted into the octahedral Al^{3+} sites. These Fe^{3+} ions have no influence on the embedded charge, but exert a sizable influence on the nuclear spin near the clay surface. As the clay layer is only about 1 nm, the polymer chains directly interacting on the clay surface would be influenced by the Fe^{3+}. When the amount of Fe^{3+} is sufficient and the distance between the Fe^{3+} and the studied nuclei is close enough, remarkable shortening in their ^{1}H T_1 would occur for these nuclei. Through strong proton spin diffusion interactions among the polymer matrix, such effect can penetrate into the protons further away from the clay surface. When the clay content is constant, a more shortened ^{1}H T_1 would

be observed for an exfoliated nanocomposite since the exfoliation of the clay sheets would result in a high clay-polymer interfacial area, short average distance between clay platelets, and a short spin-diffusion pathway in the polymer matrix. Thus, the decrease in ^{1}H T_1 of the WG matrix can be used as a measure for the quality of clay dispersion in the nanocomposites.

The observed ^{1}H T_1 value of the polymer matrix in a nanocomposite is attributed to several factors as listed below:

$$(1/T_1) = \left(1/ T_{1(0)}\right) + \left(1/ T_{1para}\right) \tag{13.1}$$

where $T_{1(0)}$ is the value for the polymer without dispersing nano-clay and T_{1para} is the effect due to the interactions with paramagnetic Fe^{3+} ions in the clay, and should be correlated to the surface-to-volume ratio reflecting the clay dispersion in the polymer matrix.

$$S_{clay}/V_{starch} \propto 1/T_{1para} \tag{13.2}$$

For a polymer/clay system with given clay concentration, the higher the clay/starch interfacial area, the shorter the average distance between clay platelets ($<\bar{D}>$) within the polymer matrix, and then the shorter the T_{1para} value of the WG matrix. Therefore,

$$<\bar{D}> \propto T_{1para} \tag{13.3}$$

This correlation between T_{1para} and the separation of clay platelets ($<\bar{D}>$) provides a simple bulk analytical method to characterize the clay dispersion or a degree of exfoliation for polymer nanocomposites, reflecting an average result of all samples in the MAS rotor ($\sim$100 mg), rather than a very small specific area of the sample as detected by TEM or XRD which has been commonly used in the study on nanocomposites. On the other hand, the clay dispersion observed from TEM pictures can be overestimated when clay platelets are not oriented directly parallel to the electron beam because multiple clay platelets may be observed in the TEM image [46].

For WG nanocomposites studied here, the clay was modified with 30 wt% of methyl tallow bis-2-hydroxyethyl quaternary ammonium chloride which acted as an additional plasticizer to WG matrix, thus, the variation of T_1 values of the nanocomposites could be due to a combination of the plasticizing effect and the paramagnetic effect, therefore, to quantify the paramagnetic effect would be difficult. At room temperature, which is below the T_g of the nanocomposites, both effect should reduce the ^{1}H T_1 value. Overall, the larger reduced ^{1}H T_1 value, the stronger the interaction between protein matrix and nanoclay particles.

WG-1 N sample displayed the strongest interaction between WG matrix and nanoclay particles since the T_1 values of most components in WG-1 N were reduced by 55–65 %. The interactions between lipid and nano clay was slightly weaker as only 40 % of T_1 reduction was observed possibly due to its hydrophobic nature. A similar behaviour was obtained for WG-2 N and -3 N samples where the

T_1 values of the proteins, water and glycerol components were decreased by 40–50 %, while those of starch and lipid were reduced only by 10–20 %. This result is consistent with what was observed in starch/clay nanocomposites [33] where the addition of PVOH additives also decreased the clay exfoliation in starch matrix due to molecular motions of PVOH acting as a driving force to reach a more stable interaction between PVOH chains and clay platelets, thus reducing the interactions between nano clay and starch matrix.

13.4 Conclusion

Two plant proteins (soy and wheat proteins)-based clay nano-biocomposite systems were studied through a series of modern material characterization technologies. The results have demonstrated the characterization methodologies of nanoclay dispersion in protein matrixes and the effect on the properties of the nanocomposites. These methodologies have provided powerful tools to study the relationship between composite performance and key structural information of nanocomposites, such as nanoparticle dispersion status, interactions between the nanoparticles and protein matrixes, molecular motions and phase structures of the matrixes, and nano-additive effects on different components of the protein matrixes. The results also indicated that efficient dispersion of nanoclay in soy proteins or wheat gluten was achieved via ultra-sonication treatment of the clay nanoparticles in plasticizers or using chemically modified clay nano particles. Such exfoliation – intercalation of the clay nanocomposites generated a series of changes in molecular motions and glass transitions of the protein matrixes. The mechanical properties of the proteins were enhanced while other material performances were also modified. Understanding the correlation between these structural and property results of proteins-based nanocomposites is fundamental to design new biodegradable nanocomposites for various applications from agriculture feedstocks.

References

1. Otaigbe JU, Goel H, Babcock T, Jane J (1999) Processability and properties of biodegradable plastics made from agricultural biopolymers. J Elastom Plast 31:56–71
2. Salmoral EM, Gonzalez ME, Mariscal MP, Medina LF (2000) Comparison of chickpea and soy protein isolate and whole flour as biodegradable plastics. Ind Crop Prod 11:227–236
3. Mohanty AK, Misra M, Hinrichsen G (2000) Biofibres, biodegradable polymers and biocomposites: an overview. Macromol Mat Eng 276–277:1–24
4. Yu L, Christie G (2001) Measurement of starch thermal transitions using differential scanning calorimetry. Carbohyr Polym 46:179–184
5. Vaz CA, Mano JF, Fossen M, Tuil RFv, Graaf LAd, Reis RL, et al (2002) Mechanical, dynamic-mechanical and thermal properties of soy protein-based thermoplastics with potential biomedical applications. J Macromol Sci Phys 41:33–46

6. Vaz CM, de Graaf LA, Reis RL, Cunha AM (2003) Effect of crosslinking, thermal treatment and UV irradiation on the mechanical properties and in vitro degradation behavior of several natural proteins aimed to be used in the biomedical field. J Mater Sci Mater Med 14:789–796
7. Hernandez-Izquierdo VM, Krochta JM (2008) Thermoplastic processing of proteins for film formation—a review. J Food Sci 73:30–39
8. Yu L (ed) (2009) Biodegradable polymer blends and composites from renewable resources. Wiley, Hoboken
9. Cho SY, Rhee C (2002) Sorption characteristics of soy protein films and their relation to mechanical properties. LWT-Food Sci Tech 35:151–157
10. Kumar R, Choudhary V, Mishra S, Varma IK, Mattiason B (2002) Adhesives and plastics based on soy protein products. Ind Crop Prod 16:155–172
11. Zhang J, Mungara P, Jane J (2001) Mechanical and thermal properties of extruded soy protein sheets. Polymer 42:2569–2578
12. Achouri A, Zhang W, Shiying X (1998) Enzymatic hydrolysis of soy protein isolate and effect of succinylation on the functional properties of resulting protein hydrolysates. Food Res Int 31:617–623
13. Paetau I, Chen C-Z, Jane J-l (1994) Biodegradable plastic made from soybean products. 1. effect of preparation and processing on mechanical properties and water absorption. Ind Eng Chem Res 33:1821–1827
14. Sue HJ, Wang S, Jane JL (1997) Morphology and mechanical behaviour of engineering soy plastics. Polymer 38:5035–5040
15. Kunanopparat T, Menut P, Morel M-H, Guilbert S (2008) Plasticized wheat gluten reinforcement with natural fibers: effect of thermal treatment on the fiber/matrix adhesion. Composites Part A 39:1787–1792
16. Zhang X, Burgar I, Do MD, Lourbakos E (2005) Intermolecular interactions and phase structures of plasticized wheat proteins materials. Biomacromolecules 6:1661–1671
17. Mangavel C, Rossignol N, Perronnet A, Barbot J, Popineau Y, Gueguen J (2004) Properties and microstructure of thermo-pressed wheat gluten films: a comparison with cast films. Biomacromolecules 5:1596–1601
18. Pommet M, Redl A, Guilbert S, Morel M-H (2005) Intrinsic influence of various plasticizers on functional properties and reactivity of wheat gluten thermoplastic materials. J Cereal Sci 42:81–91
19. Shewry PR, Popineau Y, Lafiandra D, Belton P (2000) Wheat glutenin subunits and dough elasticity: findings of the EUROWHEAT project. Trends Food Sci Tech 11:433–441
20. Sessa DJ, Woods KK, Mohamed AA, Palmquist DE (2011) Melt-processed blends of zein with. polyvinylpyrrolidone 33:57–62
21. Woods KK, Selling GW (2008) Melt reaction of zein with glyoxal to improve tensile strength and reduce solubility. J Appl Polym Sci 109:2375–2383
22. Ma Z, Morgan DP, Felts D, Michailides TJ (2002) Sensitivity of Botryosphaeria dothidea from California pistachio to tebuconazole. Crop Protect 21:829–835
23. Orliac O, Rouilly A, Silvestre F, Rigal L (2003) Effects of various plasticizers on the mechanical properties, water resistance and aging of thermo-moulded films made from sunflower proteins. Ind Crop Prod 18:91–100
24. Gueguen J, Viroben G, Noireaux P, Subirade M (1998) Influence of plasticizers and treatments on the properties of films from pea proteins. Ind Crop Prod 7:149–157
25. McGrath K, Kaplan D (1997) Protein-based materials. In: Maskarinec SA, Tirrell DA (eds) Chemical synthesis of peptides and polypeptides. Birkhauser, Boston, pp 3–37
26. Verbeek CJR, van den Berg LE (2010) Extrusion processing and properties of protein-based thermoplastics. Macromol Mat Eng 295:10–21
27. Mezgheni E, Vachon C, Lacroix M (2000) Bacterial use of biofilms cross-linked by gamma irradiation. Radiat Phys Chem 58:203–205
28. Zhang X, Hoobin P, Burgar I, Do MD (2006) Chemical modification of wheat protein-based natural polymers: cross-linking effect on mechanical properties and phase structures. J Agri Food Chem 54:9858–9865

29. Kurniawan L, Qiao GG, Zhang X (2007) Chemical modification of wheat protein-based natural polymers: grafting and cross-linking reactions with poly (ethylene oxide) diglycidyl ether and ethyl diamine. Biomacromolecules 8:2909–2915
30. Zhang X, Do MD, Bilyk A (2007) Chemical modification of wheat-protein-based natural polymers: formation of polymer networks with alkoxysilanes to modify molecular motions and enhance the material performance. Biomacromolecules 8:1881–1889
31. Kurniawan L, Qiao GG, Zhang X (2009) Formation of wheat-protein-based biomaterials through polymer grafting and crosslinking reactions to introduce new functional properties. Macromol Biosci 9:93–101
32. Zhang X, Do MD (2009) Plasticization and crosslinking effects of acetone-formaldehyde and tannin resins on wheat protein-based natural polymers. Carbohydr Res 344:1180–1189
33. Zhang X, Dean K, Burgar IM (2010) A high-resolution solid-state NMR study on starch-clay nanocomposites and the effect of aging on clay dispersion. Polym J 42:689–695
34. Giannelis EP (1998) Polymer-layered silicate nanocomposites: synthesis, properties and applications. Appl Organomet Chem 12:675–680
35. LeBaron PC, Wang Z, Pinnavaia TJ (1999) Polymer-layered silicate nanocomposites: an overview. Appl Clay Sci 15:11–29
36. Schmidt D, Shah D, Giannelis EP (2002) New advances in polymer/layered silicate nanocomposites. Curr Opin Solid State Mater Sci 6:205–212
37. Ray SS, Bousmina M (2005) Biodegradable polymers and their layered silicate nanocomposites: In greening the 21st century materials world. Prog Mat Sci 50:962–1079
38. Dean K, Yu L (2005) Biodegradable protein-nanoparticles composites. In: Smith R (ed) Biodegradable polymers for industrial applications. Woodhead Publishing Ltd, Cambridge, pp 289–312
39. Rhim J-W, Ng PKW (2007) Natural biopolymer-based nanocomposite films for packaging applications. Crit Rev Food Sci Nutr 47:411–433
40. Sinha Ray S, Okamoto M (2003) Polymer/layered silicate nanocomposites: a review from preparation to processing. Prog Polym Sci 28:1539–1641
41. Fischer H (2003) Polymer nanocomposites: from fundamental research to specific applications. Mat Sci Eng 23:763–772
42. Zhang X, Do MD, Dean K, Hoobin P, Burgar IM (2007) Wheat-gluten-based natural polymer nanoparticle composites. Biomacromolecules 8:345–353
43. Angellier-Coussy H, Torres-Giner S, Morel M-H, Gontard N, Gastaldi E (2008) Functional properties of thermoformed wheat gluten/montmorillonite materials with respect to formulation and processing conditions. J Appl Polym Sci 107:487–496
44. Vaia RA, Giannelis EP (1997) Polymer melt intercalation in organically-modified layered silicates: model predictions and experiment. Macromolecules 30:8000–8009
45. Guilherme MR, Mattoso LHC, Gontard N, Guilbert S, Gastaldi E (2010) Synthesis of nanocomposite films from wheat gluten matrix and MMT intercalated with different quaternary ammonium salts by way of hydroalcoholic solvent casting. Composites Part A 41:375–382
46. Bertmer M, Wang M, Kruger M, Blumich B, Litvinov VM, van Es M (2007) Structural changes from the pure components to nylon 6-montmorillonite nanocomposites observed by solid-state NMR. Chem Mater 19:1089–1097
47. Sothornvit R, Rhim J-W, Hong S-I (2009) Effect of nano-clay type on the physical and antimicrobial properties of whey protein isolate/clay composite films. J Food Eng 91:468–473
48. Tunc S, Angellier H, Cahyana Y, Chalier P, Gontard N, Gastaldi E (2007) Functional properties of wheat gluten/montmorillonite nanocomposite films processed by casting. J Membr Sci 289:159–168
49. Olabarrieta I, Gallstedt M, Ispizua I, Sarasua J-R, Hedenqvist MS (2006) Properties of aged montmorillonite-wheat gluten composite films. J Agri Food Chem 54:1283–1288
50. Georget DMR, Belton PS (2006) Effects of temperature and water content on the secondary structure of wheat gluten studied by FTIR spectroscopy. Biomacromolecules 7:469–475

51. Mangavel C, Barbot J, Popineau Y, Gueguen J (2001) Evolution of wheat gliadins conformation during film formation: a fourier transform infrared study. J Agri Food Chem 49:867–872
52. Mo C, Wu P, Chen X, Shao Z (2009) The effect of water on the conformation transition of Bombyx mori silk fibroin. Vib Spectrosc 51:105–109
53. Wellner N, Mills ENC, Brownsey G, Wilson RH, Brown N, Freeman J et al (2004) Changes in protein secondary structure during gluten deformation studied by dynamic fourier transform infrared spectroscopy. Biomacromolecules 6:255–261
54. Yuan Q, Lu W, Pan Y (2010) Structure and properties of biodegradable wheat gluten/attapulgite nanocomposite sheets. Polym Degrad Stab 95:1581–1587
55. McBrierty V, Packer K (1993) Nuclear magnetic resonance in solid polymers. Cambridge University Press, Cambridge
56. Saito H, Ando I, Naito A (2006) Solid state NMR spectroscopy for biopolymers: principles and applications: Springer. The Netherlands, Dordrecht
57. Axelson DE, Russell KE (1985) Characterization of polymers by means of 13C NMR spectroscopy : (a) Morphology by Solid-State NMR (b) End-Group Studies. Prog Polym Sci 11:221–282
58. Zhang X, Burgar I, Lourbakos E, Beh H (2004) The mechanical property and phase structures of wheat proteins/polyvinyl alcohol blends studied by high-resolution solid-state NMR. Polymer 45:3305–3312
59. Zhang X, Do MD, Hoobin P, Burgar I (2006) The phase composition and molecular motions of plasticized wheat gluten-based biodegradable polymer materials studied by solid-state NMR spectroscopy. Polymer 47:5888–5896
60. VanderHart DL, Asano A, Gilman JW (2001) NMR measurements related to clay-dispersion quality and organic-modifier stability in nylon-6/clay nanocomposites. Macromolecules 34:3819–3822
61. VanderHart DL, Asano A, Gilman JW (2001) Solid-state nmr investigation of paramagnetic nylon-6 clay nanocomposites. 1. crystallinity, morphology, and the direct influence of $Fe3^{+}$ on nuclear spins. Chem Mater 13:3781–3795
62. VanderHart DL, Asano A, Gilman JW (2001) Solid-state nmr investigation of paramagnetic nylon-6 clay nanocomposites. 2. measurement of clay dispersion, crystal stratification, and stability of organic modifiers. Chem Mater 13:3796–3809
63. Bourbigot S, VanderHart DL, Gilman JW, Awad WH, Davis RD, Morgan AB et al (2003) Investigation of nanodispersion in polystyrene–montmorillonite nanocomposites by solid-state NMR. J Polym Sci Pt B Polym Phys 41:3188–3213
64. Kozak M, Domka L (2004) Adsorption of the quaternary ammonium salts on montmorillonite. J Phys Chem Solids 65:441–445
65. Wilhelm HM, Sierakowski MR, Souza GP, Wypych F (2003) Starch films reinforced with mineral clay. Carbohydr Polym 52:101–110
66. Dickinson LC, Yang H, Chu CW, Stein RS, Chien JCW (1987) Limits to compatibility in poly(x-methylstyrene)/poly(2,6-dimethylphenylene oxide) blends by NMR. Macromolecules 20:1757–1760
67. Havens JR, VanderHart DL (1985) Morphology of poly(ethylene terephthalate) fibers as studied by multiple-pulse proton NMR. Macromolecules 18:1663–1676
68. Zhang X, Takegoshi K, Hikichi K (1993) Molecular motion in a blend of poly(vinylphenol) and poly(ethylene oxide) as studied by high-resolution solid-state carbon-13 NMR spectroscopy. Macromolecules 26:2198–2201

Chapter 14
Chitosan-Clay Bio-Nanocomposites

Margarita Darder, Pilar Aranda and Eduardo Ruiz-Hitzky

Abstract The present review chapter includes an overview on the current state-of-art of chitosan-clay based bio-nanocomposites. In the same way than conventional nanocomposites, these biohybrid materials also exhibit both structural and functional properties together with biocompatibility and biodegradability, which can be of great interest for different applications. Four main areas of interest have been identified showing examples of applications as green nanocomposites, bio-nanocomposites addressed to biomedical purposes (tissue engineering and drug delivery), environmental remediation and electroanalytical devices. Finally, examples of bio-nanocomposites based on chitosan assembled to other inorganic solids have been introduced to show the versatility of this biopolymer for development of diverse type of advanced functional materials.

14.1 Introduction

The importance of biopolymers assembly to nanoparticles like clays and related inorganic solids has been recently remarked in reviews focusing aspects from bio-nanocomposites synthetic approaches to applications in different fields [1–17]. The term bio-nanocomposite was probably introduced for the first time to design nanocomposites based on layered double hydroxides (LDHs) assembled to alginate

M. Darder · P. Aranda · E. Ruiz-Hitzky (✉)
Instituto de Ciencia de Materiales de Madrid, ICMM-CSIC,
c/Sor Juana Inés de la Cruz 3, 28049 Madrid, Spain
e-mail: eduardo@icmm.csic.es

M. Darder
e-mail: darder@icmm.csic.es

P. Aranda
e-mail: aranda@icmm.csic.es

L. Avérous and E. Pollet (eds.), *Environmental Silicate Nano-Biocomposites*,
Green Energy and Technology, DOI: 10.1007/978-1-4471-4108-2_14,

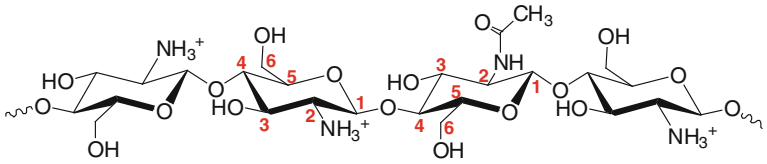

Fig. 14.1 Chemical structure of chitosan

and other biopolymers [18]. The use of such a term became more employed than other related names including nano-biocomposites although both terms coexist for referring to that type of nanomaterials.

Assembling of polysaccharides, proteins and other polymers of natural origin to inorganic micro- or nano-particulate solids with emphasis in layered clay minerals can be driven by diverse mechanisms, such as electrostatic and hydrogen bonding, van der Waals forces and water bridges [10]. General procedures for preparation of bio-nanocomposites based on ion-exchange reactions, sol–gel processes, self-assembly, and layer-by-layer (LbL) adsorption using the concept of supramolecular chemistry, biomimetics, and biomineralization were reported [3, 9, 10]. In this way, soluble biopolymers mainly present as hydrogels can be easily assembled to nanoparticulate inorganic solids by direct adsorption from aqueous solutions. In this situation, layered clay minerals (smectites such as montmorillonite, saponite, hectorite, stevensite, etc.) are swollen and may intercalate positively charged biopolymers, as for instance chitosan and gelatin, by ion-exchange reactions giving rise to intercalated compounds or even delaminated composites [6, 19]. Sepiolite and palygorskite microfibrous clays can also interact through hydrogen bonding and water bridges with neutral and charged biopolymers [20, 21]. Apart from the abovementioned procedures involving biopolymers in aqueous solutions, certain modified polymers, such as some derivatives of cellulose and starch, can be thermally compounded with clays by adding plasticizers and other additives [7].

Chitin, a linear homopolysaccharide composed of N-acetylglucosamine residues in $\beta(1 \rightarrow 4)$ linkage, is the main constituent of the hard exoskeletons of crustaceans and insects and the second most abundant polysaccharide in nature after cellulose [22]. Chitosan (Fig. 14.1), poly-α(1,4)-2-amino-2-deoxy-D-glucose, exists naturally only in a few species of fungi and it is usually derived from chitin by partial deacetylation through basic treatment with concentrated alkali solutions at high temperature [23]. Chemically, both can be regarded as derivatives of cellulose with a substitution of the C-2 hydroxyl group by an acetamide group or a free amine group. Deacetylation of chitin is never complete and the polysaccharide with a deacetylation degree (DD) higher than 75 % is known as chitosan, composed of glucosamine and *N*-acetylglucosamine units (Fig. 14.1). Free amine groups located in the C-2 position of the glucose residues show acid–base behavior, with a pK_a value of 6.3 [24]. While chitin is hydrophobic and insoluble in water and most organic solvents, chitosan dissolves readily in dilute organic acids, providing clear, homogeneous, and viscous solutions. Most of the applications of chitosan are based on its polyelectrolytic nature and on the chelating ability of the amine group, being

these properties mainly governed by the acidity of the $-NH_3^+$ group. It shows interesting properties of hydrophilicity, biocompatibility, biodegradability, non-toxicity, adsorption, film formation ability as well as antimicrobial properties, which allow the use of chitosan for a wide number of applications including food and nutrition, cosmetics, water treatment, tissue engineering and drug delivery among other purposes [25]. Pioneering works on chitosan-clay materials were published by the Ruiz-Hiztky's group using chitosan polysaccharide as a cationic polyelectrolyte in slightly acidic aqueous media [20, 26, 27].

14.2 The Assembling of Chitosan to Clays

Biopolymers interact with clays and other soil components as silica, metal oxides, carbonates and phosphates, as widely reviewed by Theng [28]. In fact, soils comprise organic components coming from the microbial degradation of dead matter such as lignin. Among them, humic substances are the major organic constituents of soils and their interaction with clay minerals leads to the formation of organo-mineral complexes and composites [29]. The comprehension of the interaction mechanisms between clay minerals and those organic components, with biopolymers amongst them, is a crucial factor to understand physico-chemical and biological properties, i.e. life in soils. Thus, the study on the adsorption pathways of biopolymers on the surface of soil minerals began to be addressed by many researchers several decades ago. Special emphasis was put on smectites, expanding 2:1 type layer silicates (Fig. 14.2a), which are of great interest because of their ability to intercalate a wide variety of organic compounds. Those studies were also focused on other clay minerals such as kaolinite or the fibrous clays sepiolite and palygorskite. Both types of clays have interesting industrial application related to the fabrication of paper, in which kaolinite is used as filler and coating agent [30], and the clarification of wine, cider and vinegar, being the fibrous clays the mainly employed clay minerals due to their strong tendency to associate proteins [31].

One of the first attempts to form an organo-mineral complex involving chitosan was carried out by Clapp and Emerson [32]. For this purpose, they made use of homoionic smectites (Ca-montmorillonite) and found that the positively charged chitosan was adsorbed at the same extent as the most strongly adsorbed neutral species. The mechanisms that control smectite-biopolymer interactions depend on the nature of both the involved biopolymers and the clay mineral hosts. Given that diluted acid solutions are required to dissolve chitosan, this biopolymer behaves in solution as a positively charged polyelectrolyte, being able to intercalate montmorillonite and other smectites by ion-exchange reactions [19, 26, 33]. The intercalation mechanism is mainly driven by electrostatic interaction of the positively charged amino groups in the chitosan chains with the negatively charged sites in the clay mineral layers. Besides, hydrogen bonding and other types of interaction may contribute to the adsorption mechanism. Depending on the synthesis conditions, nanocomposites with one, two or more layers of intercalated

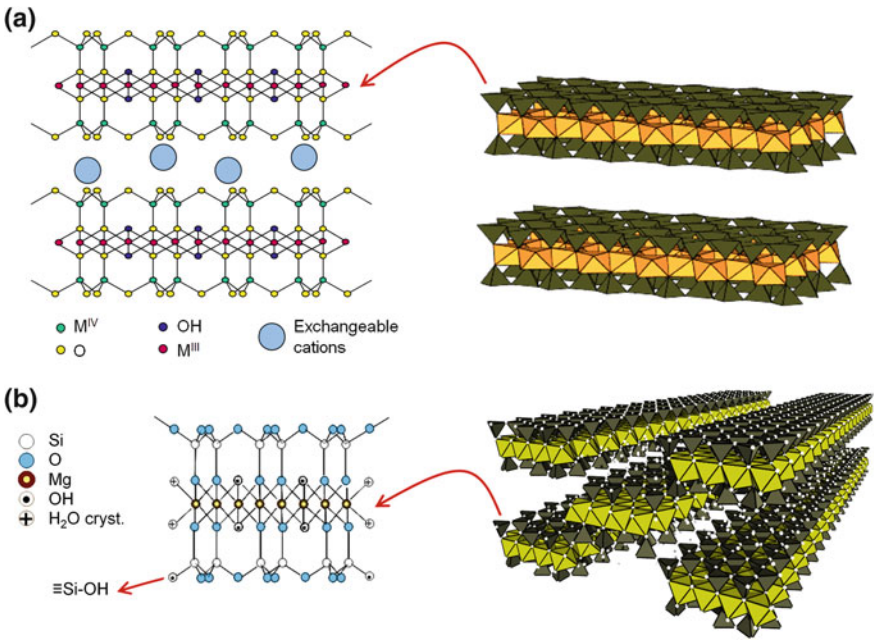

Fig. 14.2 Typical structures of **a** 2:1 smectite clay and **b** the microfibrous silicate sepiolite

polymer may be obtained, reaching to exfoliated structures in some cases. When the starting amount of chitosan is lower than the cationic exchange capacity (CEC) of the clay, the intercalation of chitosan in Na-montmorillonite takes place in monolayer configuration, in agreement with an observed increase of the basal spacing (d_{00l}, from 1.2 to 1.5 nm) corresponding to the thickness of one polysaccharide chain. The strong interaction between the chitosan chains and the clay layers is confirmed by FTIR, as those bands related to the deformation vibrations of protonated amino groups (δ_{NH_3}) are shifted towards lower wavenumber, which points out to a perturbation provoked by the host–guest interactions [26]. In contrast, the use of high amounts of polysaccharide exceeding the CEC may lead to the uptake of two or more chitosan chains. The uptake of chitosan in a bilayer configuration was reported in the case of Na-montmorillonite, showing a basal spacing of $d_{00l} = 2.1$ nm. In this configuration, hydrogen bonding and water bridges between the chitosan chains and the clay mineral interface also contribute to the adsorption mechanism. It is also confirmed the entrapment of counter-ions in the interlayer space in order to compensate the excess of positively charged groups of chitosan that do not interact electrostatically with the clay mineral lamellae. This fact introduces new properties, as the initial CEC of the clay is reversed to an anion-exchange capacity (AEC) in the resulting bio-nanocomposite, as revealed by ^{13}C solid state NMR spectroscopy [27]. This technique confirmed that acetate ions, coming from the chitosan solution and initially acting as counter-ions of the free $-NH_3^+$ groups, could be replaced by other anions after treatment of the

bio-nanocomposite with salt solutions such as sodium nitrate. This new ability to act as anion exchangers allows the application of these biohybrids for several purposes, from removal of pollutants to active phase in electrochemical sensors.

Depending on the synthesis conditions, other arrangements of chitosan chains and clay platelets can be found in addition to intercalated structures. Thus, for high amounts of chitosan, Wang and coworkers [19, 33] observed the coexistence of both intercalated and exfoliated structures by means of XRD and TEM techniques. This type of arrangement is beneficial in the preparation of nanocomposites with improved mechanical properties and thermal stability. It has been confirmed the increase of the hardness and the elastic modulus with increasing the amount of montmorillonite, due to the good dispersion of the clay platelets within the chitosan matrix [19]. Such an arrangement contributes to increase the barrier properties of the resulting nanocomposite towards the passage of gases and water vapor, due to the tortuous way imposed by the dispersed clay layers.

Chitosan and montmorillonite have been also used to produce biomimetic materials such as artificial nacre. Yao et al. [34] reported recently an attempt to mimic the structure of nacre using chitosan and montmorillonite as components. The novelty of this work was the procedure used to prepare this artificial nacre by self-assembly of chitosan-clay hybrid building blocks, followed by vacuum filtration or water evaporation for processing as films, instead of usually employed layer-by-layer methods. The resulting films showed exceptional mechanical properties, high transparency as well as fire resistance properties.

Sepiolite is a microfibrous hydrated magnesium silicate with the theoretical half unit-cell formula $Si_{12}O_{30}Mg_8(OH,F)_4(OH_2)_4{\cdot}8H_2O$ [35, 36], being structurally built up by blocks formed by an octahedral sheet of magnesium oxide/hydroxide packed between two tetrahedral silica layers (Fig. 14.2b). The periodic inversion of the SiO_4 tetrahedra determines a regular discontinuity of the sheets, being the origin of the structural cavities (*tunnels*) extended along the c axis, i.e. the axis of the microfibers [35], as well as the presence of silanol groups (Si–OH) [37, 38]. This clay mineral shows high specific surface area (>300 m^2/g) and large pore volume ($\sim$0.4 cm^3/g) that together with its cationic exchange capacity ($\sim$15 meq/100 g) and the involvement of its surface silanol groups make it prone to assemble many different type of compounds [38, 39]. Such environment is quite appropriate to assemble biopolymers of different nature [21, 40–44]. Palygorskite is a parent silicate also showing fibrous habit that can be also assembled to natural polymers following the same approaches than those used for sepiolite [39].

Chitosan-sepiolite bio-nanocomposite materials were prepared by Darder et al. [20] following a similar approach than the one above indicated for smectite clays, i.e. using acidic media conditions where the amino groups of chitosan are protonated. In these conditions this polysaccharide turns into a cationic polymer electrolyte able to compensate the negatively charged sepiolite surface. Here also, the interaction mechanism can be mainly attributed to hydrogen bonding between the surface silanol groups of sepiolite and the hydroxyls and amino groups of the assembled biopolymer. Adsorption isotherm shows the high affinity between the sepiolite substrate and the chitosan adsorbate that determines the almost quantitative polymer

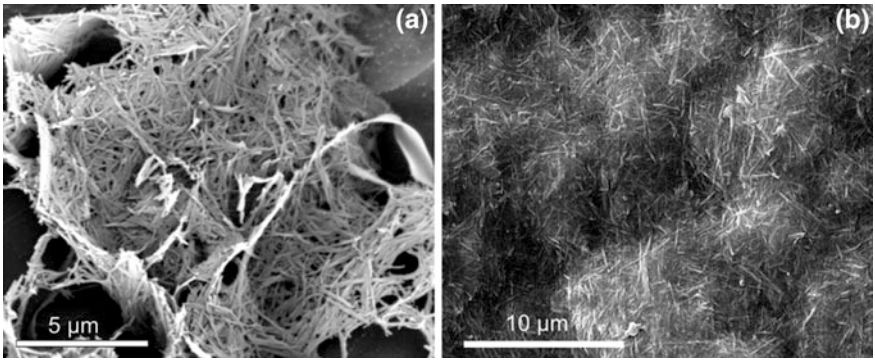

Fig. 14.3 **a** Low-temperature SEM image of a chitosan-sepiolite mixture and **b** SEM image of the surface of a chitosan-sepiolite bio-nanocomposite film prepared by solvent casting

adsorption from dilute solutions, i.e. at the low equilibrium concentrations [20]. A multilayer coverage of chitosan on the sepiolite surface is observed at high equilibrium concentrations where the biopolymer forms aggregates that can be directly adsorbed [20]. The formation of chitosan-chitosan layer aggregates is explained by the high tendency of this polysaccharide to interact through intermolecular hydrogen bonding, and perhaps also through water bridges, trapping water molecules due to its hygroscopic tendency. Upon washing these last bio-nanocomposites, the sepiolite surface remains covered by only a few layers of chitosan that still overpass the cited exchange capacity value of about 15 meq/100 g.

Spectroscopy techniques (FTIR and ^{13}C NMR) support the proposed mechanisms and low-temperature SEM images of sepiolite-chitosan layers show a texture in which the biopolymer acts as a binder of the clay fibers (Fig. 14.3) [20]. Such assembling is also observed when samples are prepared using freeze-drying processes giving rise to "cellular structures" (foam-like materials) as described below.

As the sepiolite is strongly integrated within the biopolymer structure, the chitosan-sepiolite bio-nanocomposites are provided of great compactness and can be conformed as well-ordered self-supporting films with good mechanical properties forming nacre-like materials [20]. It is noteworthy that they show a clear improvement in the mechanical properties (elastic modulus) with respect to both pure starting components as determined by dynamic mechanical analysis. These results corroborate the typical synergistic behavior found in conventional clay mineral-based polymer nanocomposites, in which the mechanical properties of the components associated at the nanometer level are superior to those of the components measured separately.

Another interesting characteristic of chitosan-sepiolite bio-nanocomposites is their improved thermal stability, also observed in other sepiolite-based bio-nanocomposites [43, 45]. The temperature required for thermal decomposition of chitosan increases upon association with sepiolite, which has a significant role in the protection towards pyrolysis and combustion of the assembled biopolymer [20]. Actually, pyrolysis of clay-based bio-nanocomposites conducted under oxygen-free

atmosphere results in graphene-like materials supported on clays, exhibiting good electrical conductivity together with elevated specific surface area [46, 47].

14.3 Properties and Applications of Chitosan-Clay Composites

14.3.1 Chitosan Bio-Nanocomposites as Green Plastics

The substitution of petroleum-based polymers by bio-based products is of growing interest in the so-called "green nanocomposites" or "bioplastics" [1, 4, 12]. In this context much research is devoted to bioplastic derived from bacterial sources such as polycaprolactone (PCL), polylactic acid (PLA), and polyhydroxyalkanoates biodegradable polymers. Polysaccharides, especially starch and cellulose, and in less extent chitosan, are abundant natural resources also investigated for this purpose [48–51]. As these biopolymers do not present enough mechanical properties and show drawbacks in their potential use as bioplastics due to their low barrier properties and high hydrophilic character compared to conventional plastics, a strategy to overcome these problems consists in their assembly to clay nanofillers. In addition, bio-nanocomposites offer the advantage that the inorganic nanoparticles can be used as carrier of antimicrobials and other additives, which is of crucial importance for their use in food packaging applications. In the case of chitosan-based nanocomposites an additional advantage concerns the anti-microbial properties exhibited by this polysaccharide that can be profited in this field of applications [52].

Improvement of the mechanical properties and preservation of the film formation ability of chitosan in their assembly to clays is determinant in view to applications, not only in food packaging but also as membranes for diverse applications, such as gas separations and components of electrochemical devices (fuel-cells, potentiometric sensors). Chitosan-sepiolite bio-nanocomposites represent an illustrative example for the preparation of reinforced self-supporting films from aqueous suspensions [20]. The use of layered clays is potentially of great interest in the conformation of chitosan bio-nanocomposite as films. In these cases, composites with a mixed exfoliated-intercalated structure, in which the hardness and elastic modulus are gradually enhanced with the content of clay, are obtained [19]. Not only the mechanical properties are affected by the assembly of chitosan to clays, but also the water vapor barrier properties of these bio-nanocomposite films are strongly affected by the clay content [53, 54].

Two strategies are addressed to improve the mechanical and barrier properties of chitosan-clay bio-nanocomposites: (i) modification of chitosan to decrease its high affinity to water molecules, and (ii) use of modified clays (organo-clays), mainly referred to smectites exchanged with cationic surfactants. In this way, derivatives of chitosan such as carboxymethyl- and trimethyl-chitosan have been assembled to montmorillonite giving rise to highly exfoliated bio-nanocomposites [33]. Derivatives of the intercalated chitosan by grafting of polydimethyl siloxane

assisted by UV irradiation have been used to prepare flexible films in order to modulate the water barrier properties of the bio-nanocomposites [55]. Graft copolymerization of butylacrylate onto chitosan assisted by gamma irradiation results in bio-nanocomposites based on organo-montmorillonite containing triacetadecylmethylammonium ions [56]. On the other hand, taking into account that chitosan is a highly hydrophilic biopolymer it is difficult to assemble it to organo-clays, such as Cloisite 30B. Xu and co-workers observed that exfoliated bio-nanocomposites are formed using Na-montmorillonite up to 5 % in weight, but microcomposites are formed when the Cloisite 30B organophilic montmorillonite is used [57]. More recently, it has been reported the exfoliation of Cloisite 10A by assembling to chitosan, improving mechanical and water barrier properties [58]. Other authors reported the preparation of chitosan-Cloisite 30B bio-nanocomposite films with improved tensile, water vapor barrier and water resistance properties as well as superior antimicrobial activity in comparison to chitosan-montmorillonite films using chitosan/glycerol mixtures [59]. Similarly, the use of glycerol associated to chitosan favors the films formation in hydrophilic Na-montmorillonite [60]. Alternatively, chitosan has been used to compatibilize montmorillonite and starch introducing a reinforcement of mechanical properties and improving the hydrophobicity of the resulting composite films [61].

14.3.2 Membranes Based on Chitosan Bio-Nanocomposites

Chitosan-clay bio-nanocomposites conformed as films open way to new applications besides food package plastics as above discussed. Barrier properties can be used for development of membranes. For instance, quaternized chitosan by reaction of chitosan with an excess of methyl iodide can be intercalated into Na-montmorillonite giving rise to different delamination degree as a function of the clay content [62]. These bio-nanocomposites conformed as films were tested as membranes for the pervaporation dehydration of isopropanol, showing that incorporation of montmorillonite results in the highest separation selectivity with a relatively high permeation flux [62]. Incorporation of carbon nanotubes (CNTs) together with the clay component results in a synergistic reinforcement effect in the resulting ternary bio-nanocomposites [63] and produces a significant improvement in barrier properties towards benzene vapors, which can be of interest for future development of pervaporation membranes [64].

Chitosan bio-nanocomposites based on chitosan assembling to inorganic solids such as silica, alumina, magnesia, titania and mordenite have been studied as membranes showing enhanced proton conductivity in comparison with Nafion membranes of interest in fuel cell devices [65]. The corresponding bio-nanocomposites based on clays can be used as fillers of Nafion to develop polyelectrolyte membranes for direct methanol fuel cells. It has been observed that the incorporation of chitosan-montmorillonite considerably improves the membrane selectivity and reduces methanol crossover while adequately maintains the proton conductivity properties [66, 67].

14.3.3 Environmental Remediation

Chitosan has been applied for metal capture from wastewater and sorption of dyes from textile mill effluents due to its adsorbent properties [25], which are due to the presence of hydroxyl groups and anion-exchange sites in its chemical structure. Given that clay minerals also offer interesting adsorption properties, the use of chitosan-clay nanocomposites as biosorbents for the removal of water pollutants is experiencing a huge growth [68]. Numerous examples found in literature report the application of chitosan-based nanocomposites for removal of dyes, heavy metal ions and other pollutants. Thus, chitosan-montmorillonite was successfully tested in the uptake of negatively charged compounds such as tannic acid [69], the dye Congo Red [70], and anionic species of tungsten [71] or As(V) and Cr(VI) species [72]. Due to the anionic charge of these compounds, uptake may occur through electrostatic interaction at low pH, at which the amine groups of chitosan are protonated. Above pH 7, other mechanisms are proposed including chemisorption, which is suggested to take place in the uptake of Congo Red [70]. Similarly, chitosan-bentonite composites showed good adsorption properties, being successful sorbents not only for the removal of pollutants from water, including harmful dyes like tartrazine [73], but also in the uptake of pollutants in gas phase, such as mercury vapor (Hg°) [74], although in this case the sorbent required a previous modification with iodine to enhance the adsorption. Maghemite (γ-Fe_2O_3) nanoparticles have been incorporated in a chitosan-kaolinite composite in order to enlarge the adsorption of an anionic azo dye, methyl orange, due to enhanced electrostatic interaction [75]. The new functionality related to the magnetic behavior of these nanoparticles could be profited for an easy recovery of the adsorbent beads after removal of the dye by applying a magnetic field, but this possibility was not evaluated in the reported study. Other works were focused on the recovery of the biosorbent after the pollutant uptake. For instance, a strategy for this purpose was the use of an activated clay that enhances the agglomeration of chitosan, allowing the preparation of chitosan-clay beads with reduced swelling. This property facilitates their separation from solution after removal of methylene blue and other pollutants [76].

Chitosan-clay materials can be combined with a hydrophilic polymer such as polyacrylic acid in an approach to prepare improved superabsorbent materials for environmental applications. For this purpose, the anion-exchange capacity of chitosan-montmorillonite composites was profited for the uptake of acrylic acid, which was then polymerized resulting in a nanocomposite provided with superabsorbent properties in water and improved photostability [77]. Alternatively, a similar material was prepared in a one-step route in which chitosan was intercalated in montmorillonite forming superabsorbent nanocomposites through in situ graft-polymerization with acrylic acid [78]. The resulting material showed high efficiency in the removal of methylene blue from aqueous solution [79].

Besides layered silicates, other clay minerals showing different morphologies were also employed in the development of chitosan-based superabsorbent materials.

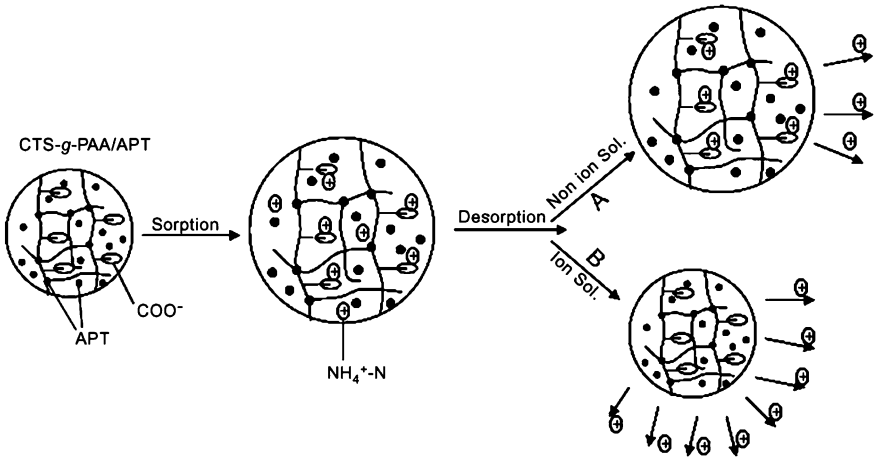

Fig. 14.4 Chitosan-g-poly(acrylic acid)/palygorskite nanocomposite (CTS-g-PAA/APT) applied in the removal of ammonium nitrogen (NH_4^+–N). Regeneration of the superabsorbent material is carried out by treatment with appropriate solutions: (*A*) treatment with non-ionic solution as distilled water produces release of physically adsorbed ions; (*B*) treatment with ion solutions including 0.1 mol/L HCl, NaOH or NaCl produces the release of both the physically adsorbed and the electrostatically adsorbed NH_4^+–N to the carboxylic groups of PAA. Reprinted from Ref. [82] with permission from © Elsevier Ltd 2009

Among them, the microtubular clay halloysite was embedded within a polymeric network of poly(acrylic acid) grafted to chitosan, contributing to enhance the uptake of ammonium ions in a pH-independent process [80]. Microfibrous clays like sepiolite and palygorskite, also known as attapulgite, have been also incorporated in this type of superabsorbent composites. The chitosan-g-poly(acrylic acid) network was synthesized in the presence of sepiolite by free-radical graft polymerization, using N,N′-methylenebisacrylamide as crosslinker and ammonium persulfate as initiator, and FTIR revealed that both chitosan and sepiolite participated in the grafting reaction with acrylic acid [81]. The best properties of water absorbency and swelling rate were achieved when using acid-activated and cation-exchanged sepiolite rather than raw sepiolite. Following a similar copolymerization process in aqueous solution, chitosan-g-poly(acrylic acid)/palygorskite hydrogels were prepared. The resulting superabsorbent composites showed high capacity for removal of diverse pollutants, such as ammonium nitrogen (NH_4^+–N) [82], but they were mainly applied in the uptake of heavy metal ions like Hg(II), Cd(II) or Cu(II) [83–85]. In all these examples, the superabsorbent material showed high adsorption efficiency and the spontaneous and endothermic adsorption processes reached the equilibrium in few minutes.

An additional advantage was the possibility to regenerate and reuse this type of superabsorbent material, as shown in Fig. 14.4.

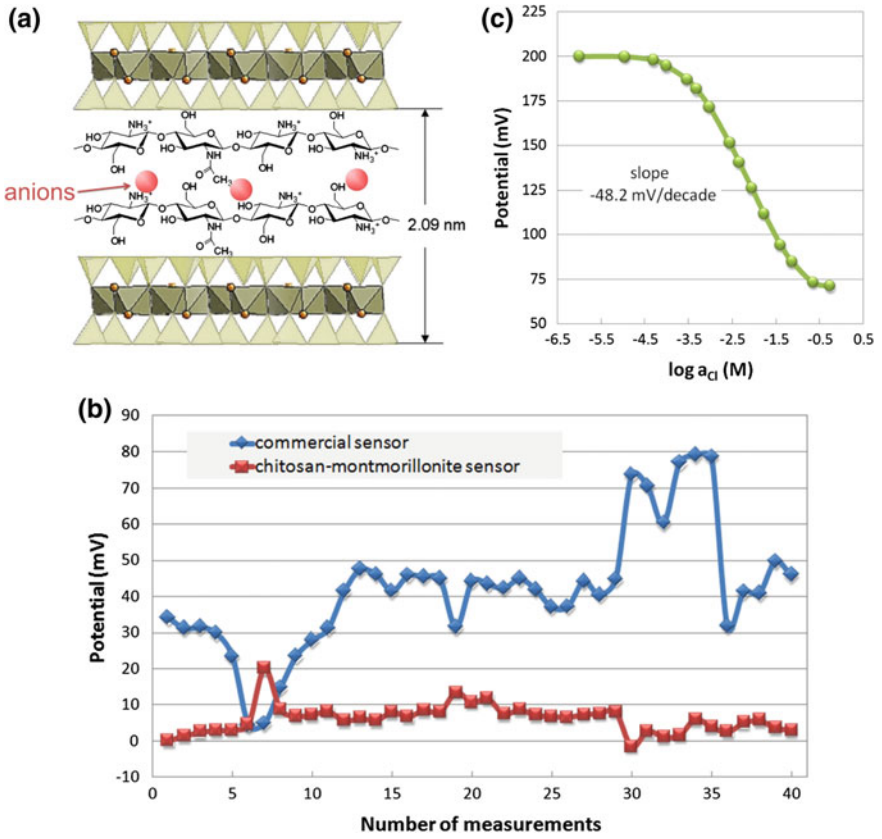

Fig. 14.5 **a** Schematic view of chitosan intercalation as a bilayer in smectites, showing anion-exchange property. **b** Potentiometric response towards chloride ions of the homemade sensor based on the chitosan-montmorillonite nanocomposite with 173.8 mEq of adsorbed chitosan/100 g clay. **c** Long-term stability, in the measurement of nitrate ions, of the same homemade sensor integrated in the four sensor-array of an electronic tongue device, in comparison with a commercial ion-selective electrode (ISE) for nitrate operating in the same configuration

14.3.4 Electroanalytical Applications

Chitosan-clay nanocomposites can be also employed in the development of sensors for electroanalytical applications. It has been reported their use as active phase of potentiometric sensors, profiting from the presence of protonated amino groups in the chitosan structure. As mentioned above, the intercalation of chitosan in smectites can be carried out in controlled conditions that lead to the transformation of the cationic exchange capacity (CEC) of the pristine clay into an anionic exchange capacity in the hybrid material (Fig. 14.5a). Thus, the positively charged amino groups behave as anion-exchange sites, allowing the use of these bio-nanocomposites as active phase in potentiometric sensors for the determination of

anions [27]. For this application, it is also important to mention the mechanical properties and stability offered by chitosan-montmorillonite materials. These bio-nanocomposites are very stable materials, without apparent desorption of the biopolymer when exposed to aqueous salt solutions for extended periods of time. The construction of modified electrodes commonly requires the use of polymeric matrices (epoxides, polysiloxanes…) that bind together the sensing and the conducting particles and confer tough mechanical properties. In contrast, these binders are not required in sensors based on chitosan-montmorillonite nanocomposites, as they can be produced with enough robustness and high long-term stability under certain synthesis conditions. Thus, their use as electrode material only requires the addition of graphite powder before the drying step in order to afford electronic conductivity. In this way, the resulting materials work simultaneously as the electronic collector and as the sensing phase of these eco-friendly potentiometric sensors.

The electroanalytical response of these electrodes was evaluated by means of direct potentiometry, taking into account the relationship between the potential of the electrode in solutions of increasing concentration and the logarithm of the ion activity, as described by the Nernst equation [86]. As mentioned in Sect. 14.2, the observed cation or anion exchange properties are strongly influenced by the presence of intercalated chitosan in monolayer or bilayer disposition, respectively [26]. Thus, when measuring a set of NaCl solutions, those sensors based on the bio-nanocomposite integrating chitosan as a bilayer showed a potential decrease as the concentration of NaCl solutions was increased, with a negative slope around −50 mV/decade (Fig. 14.5b). This behavior indicates the response of the sensors towards the anions present in solution [27]. In contrast, the sensors based on the material with chitosan in a monolayer configuration, which still retain cationic exchange capacity, showed the opposite behavior. Given the great interest in developing ion-selective electrodes for anions, especial emphasis was put in the study of the chitosan-montmorillonite material acting as anion-exchanger. The sensor based on this material showed good potentiometric responses to different anions, demonstrating lack of specificity towards a unique analyte. However, it exhibits a significant selectivity towards monovalent anions in comparison to di- or tri-valent anions, as shown in the following sequence:

$$NO_3^- \approx CH_3COO^- \approx Cl^- \approx F^- \ggg SO_4^{2-} \approx Cr_2O_7^{2-} \gg Fe(CN)_6^{3-}$$

This behavior was attributed to the special arrangement of the chitosan chains in the clay interlayer space [26, 27], since it was not observed in surface modified electrodes based on non-modified chitosan, which consists of a film of pristine chitosan deposited on the surface of a graphite electrode. Due to this partial selectivity, also known as “cross-sensitivity”, this sensor was incorporated in an array of potentiometric sensors controlled by means of the artificial intelligence method known as Case Based Reasoning (CBR) [87]. This electronic tongue was applied in the evaluation of the multicomponent solutions used for fertigation in greenhouse crops. Important features of the homemade chitosan-clay sensor were its good response towards nitrate, the main component in fertigation solutions, and

the long-term stability, which was even better than that shown by a commercial nitrate selective sensor operating under the same conditions (Fig. 14.5c).

In a similar way to smectites, the positively charged chitosan chains were also assembled to the fibrous clay sepiolite, modifying its CEC and even reversing it depending on the amount of associated chitosan [20]. Due to this functionality, the chitosan-sepiolite nanocomposites were also used in the construction of potentiometric sensors. However, their robustness was not as high as that of chitosan-montmorillonite materials and a binder was required in the construction of the modified electrodes. In addition, the sensors lacked the stability required for electroanalytical purposes. Thus, the application of the resulting sensors was mainly conceived as a simple and fast procedure for a quick evaluation of the ion-exchange capacity of the biohybrid material.

Chitosan has been also applied for the immobilization of enzymes and other biological species, as it provides a biocompatible and hydrophilic environment that helps to preserve the activity of those biologicals [88]. The presence of hydroxyl and amino groups in the chitosan structure can be profited for covalent immobilization of enzymes, generally using glutaraldehyde or similar cross-linkers. However, the low mechanical strength of the biopolymer limits the potential industrial uses of enzyme-immobilized chitosan materials. This disadvantage may be overcome by using chitosan-based composites with improved mechanical resistance instead of the raw biopolymer, being clay minerals good candidates for this purpose [89]. The enzymes can be also cross-linked to the chitosan-clay materials due to available anchoring sites from the biopolymer. Different examples that follow this strategy have demonstrated the increased thermal and pH stability of the immobilized enzymes, together with relative activities higher than those of free enzymes.

The good stability of enzymes immobilized in chitosan-clay composites allows the application of these functional bio-nanocomposites in the development of electrochemical biosensors. For instance, several works found in literature report the use of the synthetic nanoclay laponite in the preparation of chitosan-based composites for immobilization of the enzymes glucose oxidase [90] and horseradish peroxidase (HRP) [91]. In both examples, the use of the cross-linker glutaraldehyde was avoided as the enzymes were incorporated in the nanocomposite films by using step-by-step self-assembly. In a similar way, a biosensor based on the co-immobilization of chitosan and LDH with polyphenol oxidase (PPO) was also prepared in absence of crosslinker [92]. The combination of chitosan and the LDH enhances the biocompatibility, the adhesion and the mechanical strength of the immobilization host matrix, and the use of glutaraldehyde can be avoided thanks to the strong association between the enzyme and the LDH in this co-precipitation method.

In addition to layered hosts, halloysite nanotubes assembled to chitosan were also employed as support for enzyme immobilization [93]. The tubular structure, high specific surface area, and good biocompatibility of this clay seem to be responsible for the preservation of the biocatalytic activity, as well as for the direct electron transfer between the HRP and the support during the enzymatic reaction.

Chitosan bio-nanocomposites used as support for immobilization of enzymes have been also proposed for application as bioreactors [94–97]. Enzymes such as

ß-glycosidase and acid phosphatase have been immobilized on chitosan bionanocomposites based on acid activated montmorillonite for this purpose [95–97]. For instance, the bioreactor based on composite beads constituted by cuttlebone chitosan and activated clay entrapping acid phosphatase [95] showed enhanced thermal and pH stabilities of the enzyme, and its activity was well preserved upon continuous use, keeping 90 % of the original activity after 50 times of reuse. Bioreactors containing protease have been developed using chitosan-kaolinite and chitosan-starch granulate composites processed as beads [94]. It should be noted that kaolinite unlike montmorillonite and other smectites is a non-swelling clay and therefore its interaction mechanism with chitosan is completely different. Thus, the incorporation of starch granules allowed the preparation of beads enhancing both the stiffness and the functionality of these systems.

14.3.5 Chitosan-Clay Composites as Scaffolds in Tissue Engineering

The use of chitosan in biomedical applications started several decades ago profiting from the biocompatibility, non-toxicity and antibacterial properties of this biopolymer. Among them, tissue engineering involving the production of resorbable scaffolds is an interesting area of application of this biopolymer [98], and other common uses of chitosan within this field include its application as artificial skin, wound-dressings or drug carriers [25]. Nowadays, biopolymers and biopolymer-based nanocomposites are replacing synthetic polymers and their composites for biomedical applications because of the cytocompatibility of natural polymers as well as non-toxicity of their degradation products [99]. Thus, chitosan nanocomposites involving diverse inorganic solids, mainly hydroxyapatite (HAP), have been studied as scaffolds for bone regeneration [100], profiting from both the valuable characteristics of this biopolymer and the mechanical stability of the reinforced nanocomposites. On the other hand, clay minerals have been also widely employed for biomedical purposes, including the development of scaffolds for tissue engineering, given their well-known beneficial effect on health, null toxicity, high specific surface area, high sorptive capacity, rheological properties, and cation or anion exchange capacity [101]. However, few examples of the application of chitosan-clay nanocomposites as scaffolds for bone repair are found in literature, and most of them are focused on three-component systems that incorporate an additional polymer or another type of inorganic solid together with chitosan and clay. Among them, an interesting work reported the preparation of a nanocomposite involving chitosan, montmorillonite and the structural protein gelatin [102]. It was confirmed that the clay platelets not only enhanced the mechanical properties of the resulting material, acting as physical crosslinking sites, but also had a strong influence on the biodegradation rate. This behavior was attributed to the protection exerted by the clay platelets on the biopolymers against the action of lysozyme present in body fluids. The cytocompatibility and the good adhesion properties of these nanocomposites

processed as films were confirmed by in vitro studies, with the attachment and proliferation of rat stromal cells [102]. Similarly, a third component can be included through modification of chitosan by grafting reaction, as in the case of chitosan-g-lactic acid/montmorillonite nanocomposites [103]. In this example, the beneficial effect of the clay for cell proliferation was also confirmed, as well as its influence on the reduced swelling of the polymer, which contributed to reduce the loss of mechanical integrity of the material. In addition, the clay acted as a physical barrier retaining the moisture in the nanocomposite for longer time.

The synthetic clay laponite was also used in the preparation of bioactive implants for bone repair, forming a ternary system with chitosan and poly(ethylene oxide) (PEO), in which the clay served as crosslinker of PEO [104]. Chitosan endowed the laponite-PEO nanocomposites with new functionalities, as it increased cell adhesion and afforded antimicrobial properties, improving at the same time the structural integrity of the nanocomposite. The influence of chitosan together with the bioactive silicate on osteoblast cells spreading and cytoskeleton organization was also assessed.

An alternative strategy in the production of chitosan-montmorillonite implants for bone repair, as suitable scaffolds for osteoblast cells proliferation, has evaluated the combination of these components with HAP [99]. The mechanical properties of the resulting ternary system were better than those of chitosan-clay and chitosan-HAP nanocomposites, and the material offered biocompatibility and improved cell proliferation rate, confirming it as a good candidate for application in bone tissue engineering.

Although the preliminary studies to check in vitro the suitability of these materials for bone regeneration are usually carried out on materials processed as films, bioresorbable scaffolds for in vivo studies require a three-dimensional structure with interconnected macropores that mimics the organization of bone. Such an opened structure is necessary to accommodate the proliferating cells and to allow the passage of nutrients as well as the removal of metabolic wastes. Several strategies are commonly employed for processing polymers and composites as porous materials or foams, and they include for instance freeze-drying, supercritical CO_2 drying, solvent casting and particulate leaching, gas foaming as well as fibre knitting [105, 106]. Among them, freeze-drying is the most usually employed technique for removing the solvent (water) when materials involve natural polymers, using the ice crystals as the porogen. This technique was applied for instance to process the gelatin-chitosan-montmorillonite material mentioned above as scaffolds of high porosity, in which the mechanical properties and the degradation rate can be controlled by adjusting the amount of montmorillonite [107].

14.3.6 Chitosan-Clay Composites as Drug Delivery Systems

An important application of diverse type of bio-nanocomposites in the biomedicine field is related to controlled drug delivery systems (DDS). In this way,

different biodegradable and biocompatible polymers including chitosan [108], are appropriate drug carriers that can be released at a constant, predetermined rate and even, targeted to a certain location in the body [48]. The incorporation of bioactive species in inorganic solids, such as LDHs or clay minerals, improves their protection allowing in some cases a better controlled release [109].

Bio-nanocomposites prepared by assembly of chitosan in montmorillonite and other clay minerals are able to incorporate different types of drugs as the nature and extent of the electrical charge (positive or negative) depends on the chitosan intercalation degree [4]. Assays carried out using a derivative of chitosan intercalated in montmorillonite incorporating BSA as a protein drug model, shows that this type of bio-nanocomposites can be used as DDS [110].

Recent examples of chitosan-clay based DDS explore alternative methodologies for preparing more efficient systems. In some cases the positively charged drug, for instance the chemotherapeutic doxorubicin hydrochloride (DOX), can be incorporated to a clay suspension in ethanol and then treated with a chitosan water solution at pH 5.5 and conformed as pellets after freeze-drying process. The resulting material liberates DOX in a controlled manner, the release being determined by mechanisms of swelling and pH media that produces degradation of the nanocomposite particle carrier into its individual components [111]. Another example is the intercalation of the drug, for instance the anti-arrhythmic procainamide hydrochloride in montmorillonite, and then conformed as beads by compounding with alginate and further assembled with chitosan [112].

Negatively charged drugs, such as the anti-inflammatory 5-aminosalicylic acid (5-ASA) require alternative strategies for incorporation of chitosan-clay composites. In this way, Viseras and co-workers [113] developed a new approach consisting in the treatment of water suspensions of chitosan-montmorillonite placed into a dialysis cellulose membrane, with a 5-ASA solution allowing to diffuse that system at pH 5 for 2 days. Interestingly, the drug release in acidic medium is practically linear with time, being slower than DDS based on the association of the active drug with either chitosan or montmorillonite alone. Diclofenac is a non-steroidal anti-inflammatory negatively charged drug that has been also incorporated to chitosan-based bio-nanocomposites. In this DDS, the drug is incorporated to chitosan modified with polyacrylic acid assembled to vermiculite in aqueous media, being further processed as beads using $CaCl_2$ as crosslinking agent [114].

Non-charged drugs are more difficult to be incorporated into clay-chitosan systems. Doxycycline is a non-charged antibiotic belonging to the tetracycline family that has recently been incorporated to chitosan composites incorporating an organoclay [115]. The only objection of these DDS systems can be related to the use of organoclays that contain toxic alkylammonium species (cationic surfactants), which can produce mild skin and respiratory irritation or anaphylactic reactions amongst other health effects.

Due to the film forming properties of chitosan, this type of bio-nanocomposites have been recently proposed as coatings of tablets for modulating drug release due to the different diffusion mechanism for positively and negatively charged species [116]. The ability of clay-chitosan bio-nanocomposites to form films showing

electrostimulus deformation and volume recovery behaviour [117], appears as an attractive property to develop new DDS.

Chitosan-clay bio-nanocomposites have been also used for assembling DNA in order to develop alternative systems for non-viral gene therapy. In this context, using chitosan-rectorite bio-nanocomposites Wang et al. have applied this biocompatible substrate for DNA adsorption, giving DNA-composites that have been tested in vitro as non-viral vectors for gene transfection [118, 119]. Although these last systems show a limited efficiency in transfection assays, they constitute a model for the use of clay-based bio-nanocomposites as vectors for gene therapy, opening the way to further research in this line for enlarging their applications.

14.4 Functional Bio-Nanocomposites Based on Chitosan

Above we have introduced a series of examples of chitosan-clay nanocomposites giving rise to a great variety of functional biohybrid materials. The main objective of this chapter focuses on clay-chitosan interactions but it is worthy to note a short reference to chitosan bio-nanocomposites based on other solids mainly present as nanoparticles (NPs) [2, 4, 120]. In this way, chitosan has been also employed to develop bio-nanocomposites based on nanoparticulate inorganic solids alone (Table 14.1) or in combination with clays in ternary systems.

Concerning the ternary systems, i.e. those built up by the assembly of chitosan to clay and comprising simultaneously other type of NPs, they may result in synergistic reinforcing effects together with functional behaviour. Montmorillonite and HAP can be combined to chitosan giving improved composites with respect to the corresponding binary systems. For instance, biocompatibility is enhanced and these biohybrids show interest for applications in bone tissue engineering [99]. Other interesting ternary system involves the incorporation of multiwall carbon nanotubes (MWCNTs) resulting in synergistic reinforcement effect due to the combination of 2D (clay) and 1D (CNT) nanofillers [63]. Reinforced films for bioplastics and biomedical uses, as well as conducting composite materials can be envisaged as special applications of this type of ternary systems (Fig. 14.6).

14.5 Concluding Remarks

Chitosan-clay bio-nanocomposites exhibit interesting properties due to the characteristics of both the silicate (swelling and ion-exchange ability, nano- and microparticulate nature, morphology enhancing the mechanical properties, …) and the biopolymer (biocompatibility, functionality related to amino groups, film-forming ability…). Several examples detailing the application of these materials in four main areas of interest have been introduced in this chapter in order to illustrate the versatility of this biopolymer for developing a wide variety of advanced functional

Table 14.1 Representative examples of bio-nanocomposites based on the assembly of chitosan and different nanoparticulated inorganic solids

Inorganic particles	Characteristics/applications	References
Ca-carbonates	Artificial nacre. Crystallization of $CaCO_3$ as thin films Silk fibroin based composites	Diaz-Dosque et al. [121] Wu et al. [122]
Ca-phosphates	$CaHPO_4$, $Ca_3(PO_4)_2$, $Ca_4(PO_4)_2O$ and HAP. Films and scaffolds for bone repair using chitosan and chitosan-gelatin	Rusu et al. [123], Liu et al. [124], Kong et al. [125], Liu et al. [126], Xu et al. [127, 128], Kim et al. [129], Li et al. [130, 131], Gutiérrez et al. [132], Teng et al. [133], Mohamed and Mostafa [134], Katti et al. [99]
Zr-phosphate	Nanofiller for film reinforcement	Liu et al. [135]
Silica based	Combination with silica NPs, silica matrix generated from alkoxysilanes for applications as sensors, adsorbents, tissue engineering and regioselective catalysis	Rashidova et al. [136], Zhang and Dong [137], Shirosaki et al. [138], Corma et al. [139]
Iron oxides (magnetics)	Combination with iron oxide nanoparticles already formed or in situ generated for applications in biomedicine, environmental remediation, etc.	Li et al. [140], Hu et al. [141], Zhu et al. [142]
Au and quantum dots	CdS semiconductor nanoparticles. Au NPs for biosensor applications	Li et al. [143], dos Santos et al. [144], Kulys and Stupak [145]
Carbon nanotubes	Improvement of mechanical properties	Wang et al. [146], Liu et al. [147], Shieh et al. [148], Spinks et al. [149], Shieh and Yang [148], Tang et al. [63]
	Providing of electrical conductivity. Electrodes and electrochemical sensors	Luo et al. [151], Zhang et al. [150], Zhai et al. [152], Chakraborty et al. [153], Gutiérrez et al. [154], Wu et al. [122], Galandova et al. [155]
	Scaffolds for tissue engineering	Gutiérrez et al. [156, 157], Lau et al. [158]

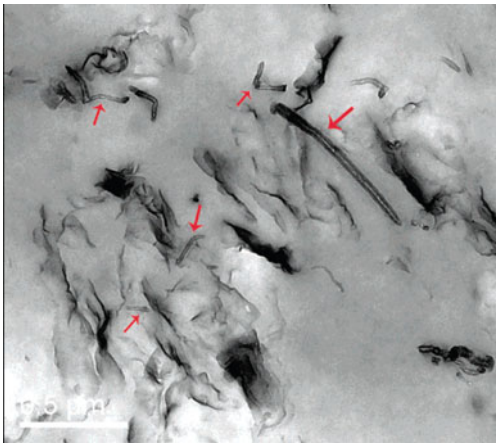

Fig. 14.6 TEM image of a chitosan-montmorillonite-CNTs bio-nanocomposite (3 % clay/0.4 % CNTs). (Reprinted with permission from Ref. [63]. © American Chemical Society 2001.)

materials. Amongst them, the production of green plastics involving chitosan and clays is a remarkable topic, given the current efforts to reduce the use of synthetic plastics derived from petroleum and to minimize plastic waste. Special emphasis is also made in biomedical and pharmaceutical purposes due to the non-cytotoxicity and antimicrobial properties afforded by this biopolymer and its derived clay-based composites. Examples on the application of chitosan-clay systems as scaffolds for tissue engineering or as vectors for controlled drug delivery are also introduced in this chapter in order to illustrate the important role of these materials in health related fields. Biocompatibility of chitosan-clay nanocomposites can be also profited for preserving the biological activity of enzymes, affording the development of biosensors and bioreactors with increased long-term stability. Adsorbent properties and ion-exchange capacity of chitosan-clay based materials are also attractive properties for environmental remediation, being these systems used for recovery of harmful chemical compounds from azo dyes to heavy metal ions. In addition, the possibility of tuning the ion-exchange capacity of the bio-nanocomposite material by varying the amount of chitosan in the preparation of the bio-nanocomposites has been also reviewed, showing a novel application of chitosan-clay materials as active phase of potentiometric sensors as well as the possibility to include them in an electronic tongue device.

Future research could profit from the facility of chitosan to assemble with other entities from nanoparticles of different nature, functional or structural polymers and biopolymers and even more complex systems including biological fragments or entire bodies (bacteria, algae, viruses…). This amazing versatility of chitosan and chitosan-based composites is a very attractive feature allowing and promising new developments in this research area.

Acknowledgments The authors are grateful for funding from CICYT (Spain), project MAT2009-09960 and from CSIC-Academie Hassan II, project 2010MA0003.

References

1. Darder M, Aranda P, Ruiz-Hitzky E (2007) Bionanocomposites: a new concept of ecological, bioinspired, and functional hybrid materials. Adv Mater 19:1309–1319
2. Ruiz-Hitzky E, Aranda P, Darder M (2009) Polymer and biopolymer-layered solid nanocomposites: organic–inorganic assembling in two-dimensional hybrid systems. In: Ariga K, Nalwa HS (eds) Bottom up nanofabrication. American Scientific Publishers, Stevenson Ranch
3. Ruiz-Hitzky E, Aranda P, Darder M, Ogawa M (2011) Hybrid and biohybrid silicate based materials: molecular vs. block-assembling bottom-up processes. Chem Soc Rev 40:801–828
4. Ruiz-Hitzky E, Darder M, Aranda P (2010) Progress in bionanocomposite materials. In: Cao G, Zhang Q, Brinker CJ (eds) Annual review of nanoresearch. World Scientific Publishing, Singapore
5. Ruiz-Hitzky E, Darder M, Aranda P, Ariga K (2010) Advances in biomimetic and nanostructured biohybrid materials. Adv Mater 22:323–336
6. Ruiz-Hitzky E, Darder M, Aranda P (2005) Functional biopolymer nanocomposites based on layered solids. J Mater Chem 15:3650–3662
7. Rhim JW (2007) Potential use of biopolymer-based nanocomposite films in food packaging applications. Food Sci Biotechnol 16:691–709
8. Chivrac F, Pollet E, Averous L (2009) Progress in nano-biocomposites based on polysaccharides and nanoclays. Mater Sci Eng R Rep 67:1–17
9. Ruiz-Hitzky E, Ariga K, Lvov YM (2008) Bio-inorganic hybrid nanomaterials strategies syntheses, characterization and applications. Wiley-VCH, Weinheim
10. Ruiz-Hitzky E, Aranda P, Darder M (2008) Bionanocomposites. In: Kirk-Othmer encyclopedia of chemical technology. Wiley, Hoboken
11. Ray SS, Okamoto M (2003) Polymer/layered silicate nanocomposites: a review from preparation to processing. Prog Polym Sci 28:1539–1641
12. Pandey JK, Kumar AP, Misra M, Mohanty AK, Drzal LT, Singh RP (2005) Recent advances in biodegradable nanocomposites. J Nanosci Nanotechnol 5:497–526
13. Bordes P, Pollet E, Averous L (2009) Nano-biocomposites: biodegradable polyester/nanoclay systems. Prog Polym Sci 34:125–155
14. Rhim JW, Ng PKW (2007) Natural biopolymer-based nanocomposite films for packaging applications. Crit Rev Food Sci Nutr 47:411–433
15. Zhao RX, Torley P, Halley PJ (2008) Emerging biodegradable materials: starch- and protein-based bio-nanocomposites. J Mater Sci 43:3058–3071
16. Mittal V (2011) Nanocomposites with biodegradable polymers. Synthesis, properties, and future perspectives. Oxford University Press, New York
17. Darder M, Aranda P, Ruiz AI, Fernandes FM, Ruiz-Hitzky E (2008) Design and preparation of bio-nanocomposites based on layered solids with functional and structural properties. Mater Sci Technol 24:1100–1110
18. Darder M, Lopez-Blanco M, Aranda P, Leroux F, Ruiz-Hitzky E (2005) Bio-nanocomposites based on layered double hydroxides. Chem Mater 17:1969–1977
19. Wang SF, Shen L, Tong YJ, Chen L, Phang IY, Lim PQ, Liu TX (2005) Biopolymer chitosan/montmorillonite nanocomposites: preparation and characterization. Polym Degrad Stabil 90:123–131
20. Darder M, Lopez-Blanco M, Aranda P, Aznar AJ, Bravo J, Ruiz-Hitzky E (2006) Microfibrous chitosan-sepiolite nanocomposites. Chem Mater 18:1602–1610
21. Fernandes FM, Ruiz AI, Darder M, Aranda P, Ruiz-Hitzky E (2009) Gelatin-clay bio-nanocomposites: structural and functional properties as advanced materials. J Nanosci Nanotechnol 9:221–229
22. Nelson DL, Cox MM (2008) Lehninger principles of biochemistry, 5th edn. W H Freeman, New York
23. Agboh OC, Qin Y (1996) Chitin and chitosan fibers. Polym Adv Technol 8:335–365

24. Muzzarelli R (1978) Modified chitosans and their chromatographic performances. In: Muzzarelli R, Pariser ER (eds) Proceedings of the first international conference on chitin/chitosan. Massachusetts Institute of Technology, Boston
25. Ravi Kumar MNV (2000) A review of chitin and chitosan applications. React Funct Polym 46:1–27
26. Darder M, Colilla M, Ruiz-Hitzky E (2003) Biopolymer-clay nanocomposites based on chitosan intercalated in montmorillonite. Chem Mater 15:3774–3780
27. Darder M, Colilla M, Ruiz-Hitzky E (2005) Chitosan-clay nanocomposites: application as electrochemical sensors. Appl Clay Sci 28:199–208
28. Theng BKG (1979) Formation and properties of clay-polymer complexes. Elsevier, New York
29. Ohashi H, Nakazawa H (1996) The microstructure of humic acid-montmorillonite composites. Clay Miner 31:347–354
30. Murray HH (2000) Traditional and new applications for kaolin, smectite, and palygorskite: a general overview. Appl Clay Sci 17:207–221
31. Robertson RHS (1957) Sepiolite—a versatile raw material. Chem Ind 1492–1495
32. Clapp CE, Emerson WW (1972) Reactions between Ca-montmorillonite and polysaccharides. Soil Sci 114:210–216
33. Wang SF, Chen L, Tong YJ (2006) Structure-property relationship in chitosan-based biopolymer/montmorillonite nanocomposites. J Polym Sci Pol Chem 44:686–696
34. Yao HB, Tan ZH, Fang HY, Yu SH (2010) Artificial nacre-like bionanocomposite films from the self-assembly of chitosan-montmorillonite hybrid building blocks. Angew Chem Int Ed 49:10127–10131
35. Brunauer K, Preisinger A (1956) Struktur und Entstehung des Sepioliths. Miner Petrol 6:120–140
36. Santaren J, Sanz J, Ruiz-Hitzky E (1990) Structural fluorine in sepiolite. Clays Clay Miner 38:63–68
37. Ahlrichs JL, Serna C, Serratosa JM (1975) Structural hydroxyls in sepiolites. Clays Clay Miner 23:119–124
38. Ruiz-Hitzky E (2001) Molecular access to intracrystalline tunnels of sepiolite. J Mater Chem 11:86–91
39. Ruiz-Hitzky E, Aranda P, Alvarez A, Santarén J, Esteban-Cubillo A (2011) Advanced materials and new applications of sepiolite and palygorskite. In: Galán E, Singer A (eds) Developments in palygorskite-sepiolite research a new outlook of these nanomaterials. Elsevier B.V., Oxford
40. Perez-Castells R, Alvarez A, Gavilanes J, Lizarbe MA, Martinez Del Pozo A, Olmo N, Santaren J (1987) Adsorption of collagen by sepiolite. In: Schultz LG, van Olphen H, Mumpton FA (eds) Proceedings of the international clay conference Denver, 1985. The Clay Minerals Society, Bloomington
41. Ruiz-Hitzky E, Darder M, Aranda P, Martin del Burgo MA, del Real G (2009) Bionanocomposites as new carriers for influenza vaccines. Adv Mater 21:4167–4171
42. Wicklein B, Darder M, Aranda P, Ruiz-Hitzky E (2010) Bio-organoclays based on phospholipids as immobilization hosts for biological species. Langmuir 26:5217–5225
43. Alcântara ACS, Darder M, Aranda P, Ruiz-Hitzky E (2008) Interacciones de zeína con minerales de la arcilla. Macla 9:25–26
44. Fernandes FM, Manjubala I, Ruiz-Hitzky E (2011) Gelatin renaturation, a new approach to filler role in bionanocomposites. Phys Chem Chem Phys 13:4901–4910
45. Ruiz-Hitzky E, Fernandes FM (2010) Uso de arcillas fibrosas como coadyuvantes para mejorar la estabilidad coloidal de nanotubos y nanofibras de carbono en medios hidrofílicos. Spanish Patent P200931135ES
46. Ruiz-Hitzky E, Fernandes FM (2011) Composición de material carbonoso obtenible por carbonización de un biopolímero soportado sobre arcilla. Spanish Patent ES-P201130835
47. Fernandes FM (2011) On the structural and functional properties of sepiolite in polymer-clay nanocomposites and materials derived thereof. PhD dissertation, Autonomous University of Madrid

48. Chandra R, Rustgi R (1998) Biodegradable polymers. Prog Polym Sci 23:1273–1335
49. Gross RA, Kalra B (2002) Biodegradable polymers for the environment. Science 297: 803–807
50. Tharanathan RN (2003) Biodegradable films and composite coatings: past, present and future. Trends Food Sci Technol 14:71–78
51. Siracusa V, Rocculi P, Romani S, Dalla Rosa M (2008) Biodegradable polymers for food packaging: a review. Trends Food Sci Technol 19:634–643
52. Han YS, Lee SH, Choi KH, Park I (2010) Preparation and characterization of chitosan-clay nanocomposites with antimicrobial activity. J Phys Chem Solids 71:464–467
53. Rhim JW (2006) The effect of clay concentration on mechanical and water barrier properties of chitosan-based nanocomposite films. Food Sci Biotechnol 15:925–930
54. Casariego A, Souza BWS, Cerqueira MA, Teixeira JA, Cruz L, Diaz R, Vicente AA (2009) Chitosan/clay films' properties as affected by biopolymer and clay micro/nanoparticles' concentrations. Food Hydrocolloids 23:1895–1902
55. Depan D, Kumar B, Singh RP (2008) Preparation and characterization of novel hybrid of chitosan-g-PDMS and sodium montmorillonite. J Biomed Mater Res B 84B:184–190
56. Li Y, Liu L, Zhang WA, Fang YE (2004) A new hybrid nanocomposite prepared by graft copolymerization of butyl acrylate onto chitosan in the presence of organophilic montmorillonite. Radiat Phys Chem 69:467–471
57. Xu YX, Ren X, Hanna MA (2006) Chitosan/clay nanocomposite film preparation and characterization. J Appl Polym Sci 99:1684–1691
58. Oguzlu H, Tihminlioglu F (2010) Preparation and barrier properties of Chitosan-layered silicate nanocomposite films. Polychar-18 World Forum Adv Mater 298:91–98
59. Rhim JW, Hong SI, Park HM, Ng PKW (2006) Preparation and characterization of chitosan-based nanocomposite films with antimicrobial activity. J Agric Food Chem 54: 5814–5822
60. Lavorgna M, Piscitelli F, Mangiacapra P, Buonocore GG (2010) Study of the combined effect of both clay and glycerol plasticizer on the properties of chitosan films. Carbohyd Polym 82:291–298
61. Kampeerapappun P, Aht-Ong D, Pentrakoon D, Srikulkit K (2007) Preparation of cassava starch/montmorillonite composite film. Carbohyd Polym 67:155–163
62. Choudhari SK, Kariduraganavar MY (2009) Development of novel composite membranes using quaternized chitosan and Na^+-MMT clay for the pervaporation dehydration of isopropanol. J Colloid Interface Sci 338:111–120
63. Tang CY, Xiang LX, Su JX, Wang K, Yang CY, Zhang Q, Fu Q (2008) Largely improved tensile properties of chitosan film via unique synergistic reinforcing effect of carbon nanotube and clay. J Phys Chem B 112:3876–3881
64. Tang CY, Chen NX, Zhang Q, Wang K, Fu Q, Zhang XY (2009) Preparation and properties of chitosan nanocomposites with nanofillers of different dimensions. Polym Degrad Stabil 94:124–131
65. Ramirez-Salgado J (2007) Study of basic biopolymer as proton membrane for fuel cell systems. Electrochim Acta 52:3766–3778
66. Hasani-Sadrabadi MM, Dashtimoghadam E, Majedi FS, Kabiri K (2009) Nafion®/bio-functionalized montmorillonite nanohybrids as novel polyelectrolyte membranes for direct methanol fuel cells. J Power Sour 190:318–321
67. Hasani-Sadrabadi MM, Dashtimoghadam E, Majedi FS, Kabiri K, Mokarram N, Solati-Hashjin M, Moaddel H (2010) Novel high-performance nanohybrid polyelectrolyte membranes based on bio-functionalized montmorillonite for fuel cell applications. Chem Commun 46:6500–6502
68. Ngah WSW, Teong LC, Hanafiah M (2011) Adsorption of dyes and heavy metal ions by chitosan composites: a review. Carbohyd Polym 83:1446–1456
69. An JH, Dultz S (2007) Adsorption of tannic acid on chitosan-montmorillonite as a function of pH and surface charge properties. Appl Clay Sci 36:256–264

70. Wang L, Wang AQ (2007) Adsorption characteristics of Congo Red onto the chitosan/montmorillonite nanocomposite. J Hazard Mater 147:979–985
71. Gecol H, Miakatsindila P, Ergican E, Hiibel SR (2006) Biopolymer coated clay particles for the adsorption of tungsten from water. Desalination 197:165–178
72. An JH, Dultz S (2008) Adsorption of Cr(VI) and As(V) on chitosan-montmorillonite: selectivity and pH dependence. Clays Clay Miner 56:549–557
73. Ngah WSW, Ariff NFM, Hanafiah M (2010) Preparation, characterization, and environmental application of crosslinked chitosan-coated bentonite for tartrazine adsorption from aqueous solutions. Water Air Soil Pollut 206:225–236
74. Zhang AC, Sun LS, Xiang J, Hu S, Fu P, Su S, Zhou YB (2009) Removal of elemental mercury from coal combustion flue gas by bentonite–chitosan and their modifier. J Fuel Chem Technol 37:489–495
75. Zhu HY, Jiang R, Xiao L (2010) Adsorption of an anionic azo dye by chitosan/kaolin/gamma-Fe_2O_3 composites. Appl Clay Sci 48:522–526
76. Chang MY, Juang RS (2004) Adsorption of tannic acid, humic acid, and dyes from water using the composite of chitosan and activated clay. J Colloid Interface Sci 278:18–25
77. Qiu HX, Yu JG, Zhu JL (2005) Polyacrylate/(chitosan modified montmorillonite) nanocomposite: water absorption and photostability. Polym Polym Compos 13:167–172
78. Zhang JP, Wang L, Wang AQ (2007) Preparation and properties of chitosan-g-poly(acrylic acid)/montmorillonite superabsorbent nanocomposite via in situ intercalative polymerization. Ind Eng Chem Res 46:2497–2502
79. Wang L, Zhang JP, Wang AQ (2008) Removal of methylene blue from aqueous solution using chitosan-g-poly (acrylic acid)/montmorillonite superadsorbent nanocomposite. Colloid Surf B Biointerfaces 322:47–53
80. Zheng YA, Wang AQ (2010) Enhanced adsorption of ammonium using hydrogel composites based on chitosan and halloysite. J Macromol Sci A Pure Appl Chem 47:33–38
81. Xie YT, Wang AQ, Liu G (2010) Superabsorbent composite XXII: effects of modified sepiolite on water absorbency and swelling behavior of chitosan-g-poly(acrylic acid)/sepiolite superabsorbent composite. Polym Compos 31:89–96
82. Zheng Y, Zhang JP, Wang AQ (2009) Fast removal of ammonium nitrogen from aqueous solution using chitosan-g-poly(acrylic acid)/attapulgite composite. Chem Eng J 155:215–222
83. Wang XH, Zheng Y, Wang AQ (2009) Fast removal of copper ions from aqueous solution by chitosan-g-poly(acrylic acid)/attapulgite composites. J Hazard Mater 168:970–977
84. Wang XH, Wang AQ (2010) Adsorption characteristics of chitosan-g-poly(acrylic acid)/attapulgite hydrogel composite for Hg(II) ions from aqueous solution. Sep Sci Technol 45:2086–2094
85. Wang XH, Wang AQ (2010) Removal of Cd(II) from aqueous solution by a composite hydrogel based on attapulgite. Environ Technol 31:745–753
86. Brett CMA, Brett AMO (1993) Electrochemistry principles methods and applications. Oxford University Press, Oxford
87. Darder M, Valera A, Nieto E, Colilla M, Fernandez CJ, Romero-Aranda R, Cuartero J, Ruiz-Hitzky E (2009) Multisensor device based on case-based reasoning (CBR) for monitoring nutrient solutions in fertigation. Sens Actuator B Chem 135:530–536
88. Krajewska B (2004) Application of chitin- and chitosan-based materials for enzyme immobilizations: a review. Enzyme Microb Technol 35:126–139
89. Chang MY, Juang RS (2005) Activities, stabilities, and reaction kinetics of three free and chitosan-clay composite immobilized enzymes. Enzyme Microb Technol 36:75–82
90. Shi QF, Li QB, Shan D, Fan Q, Xue HG (2008) Biopolymer-clay nanoparticles composite system (Chitosan-laponite) for electrochemical sensing based on glucose oxidase. Mater Sci Eng C Biomimetic Supramol Syst 28:1372–1375
91. Shan D, Li QB, Ding SN, Xu JQ, Cosnier S, Xue HG (2010) Reagentless biosensor for hydrogen peroxide based on self-assembled films of horseradish peroxidase/laponite/chitosan and the primary investigation on the inhibitory effect by sulfide. Biosens Bioelectron 26:536–541

92. Han E, Shan D, Xue HG, Cosnier S (2007) Hybrid material based on chitosan and layered double hydroxides: characterization and application to the design of amperometric phenol biosensor. Biomacromolecules 8:971–975
93. Sun XM, Zhang Y, Shen HB, Jia NQ (2010) Direct electrochemistry and electrocatalysis of horseradish peroxidase based on halloysite nanotubes/chitosan nanocomposite film. Electrochim Acta 56:700–705
94. Sangeetha K, Abraham TE (2008) Investigation on the development of sturdy bioactive hydrogel beads. J Appl Polym Sci 107:2899–2908
95. Chang MY, Juang RS (2004) Stability and catalytic kinetics of acid phosphatase immobilized on composite beads of chitosan and activated clay. Process Biochem 39:1087–1091
96. Chang MY, Juang RS (2007) Use of chitosan-clay composite as immobilization support for improved activity and stability of beta-glucosidase. Biochem Eng J 35:93–98
97. Chang MY, Kao HC, Juang RS (2008) Thermal inactivation and reactivity of beta-glucosidase immobilized on chitosan-clay composite. Int J Biol Macromol 43:48–53
98. Muzzarelli RAA (2009) Chitins and chitosans for the repair of wounded skin, nerve, cartilage and bone. Carbohyd Polym 76:167–182
99. Katti KS, Katti DR, Dash R (2008) Synthesis and characterization of a novel chitosan/montmorillonite/hydroxyapatite nanocomposite for bone tissue engineering. Biomed Mater 3:art. #034122
100. Muzzarelli RAA (2011) Chitosan composites with inorganics, morphogenetic proteins and stem cells, for bone regeneration. Carbohyd Polym 83:1433–1445
101. Ruiz-Hitzky E, Aranda P, Darder M, Rytwo G (2010) Hybrid materials based on clays for environmental and biomedical applications. J Mater Chem 20:9306–9321
102. Zhuang H, Zheng J, Gao H, De Yao K (2007) In vitro biodegradation and biocompatibility of gelatin/montmorillonite-chitosan intercalated nanocomposite. J Mater Sci Mater Med 18:951–957
103. Depan D, Kumar AP, Singh RP (2009) Cell proliferation and controlled drug release studies of nanohybrids based on chitosan-g-lactic acid and montmorillonite. Acta Biomater 5:93–100
104. Gaharwar AK, Schexnailder PJ, Jin Q, Wu CJ, Schmidt G (2010) Addition of chitosan to silicate cross-linked PEO for tuning osteoblast cell adhesion and mineralization. ACS Appl Mater Interfaces 2:3119–3127
105. Gibson LJ, Ashby MF (1997) Cellular solids: structure and properties, 2nd edn. Cambridge University Press, Cambridge
106. Darder M, Aranda P, Ferrer ML, Gutiérrez MC, del Monte F, Ruiz-Hitzky E (2011) Progress in bionanocomposite and bioinspired foams. Adv Mater 23:5262–5267
107. Zheng JP, Wang CZ, Wang XX, Wang HY, Zhuang H, De Yao K (2007) Preparation of biomimetic three-dimensional gelatin/montmorillonite-chitosan scaffold for tissue engineering. React Funct Polym 67:780–788
108. Dash M, Chiellini F, Ottenbrite RM, Chiellini E (2011) Chitosan—a versatile semi-synthetic polymer in biomedical applications. Prog Polym Sci 36:981–1014
109. Alcantara ACS, Aranda P, Darder M, Ruiz-Hitzky E (2010) Bionanocomposites based on alginate-zein/layered double hydroxide materials as drug delivery systems. J Mater Chem 20:9495–9504
110. Wang XY, Du YM, Luo JW (2008) Biopolymer/montmorillonite nanocomposite: preparation, drug-controlled release property and cytotoxicity. Nanotechnology 19:art. #065707
111. Yuan Q, Shah J, Hein S, Misra RDK (2010) Controlled and extended drug release behavior of chitosan-based nanoparticle carrier. Acta Biomater 6:1140–1148
112. Kevadiya BD, Joshi GV, Bajaj HC (2010) Layered bionanocomposites as carrier for procainamide. Int J Pharm 388:280–286
113. Aguzzi C, Capra P, Bonferoni C, Cerezo P, Salcedo I, Sanchez R, Caramella C, Viseras C (2010) Chitosan-silicate biocomposites to be used in modified drug release of 5-aminosalicylic acid (5-ASA). Appl Clay Sci 50:106–111
114. Wang Q, Xie XL, Zhang XW, Zhang JP, Wang AQ (2010) Preparation and swelling properties of pH-sensitive composite hydrogel beads based on chitosan-g-poly (acrylic

acid)/vermiculite and sodium alginate for diclofenac controlled release. Int J Biol Macromol 46:356–362
115. Sahoo S, Sasmal A, Sahoo D, Nayak P (2010) Synthesis and characterization of chitosan-polycaprolactone blended with organoclay for control release of doxycycline. J Appl Polym Sci 118:3167–3175
116. Khunawattanakul W, Puttipipatkhachorn S, Rades T, Pongjanyakul T (2010) Chitosan-magnesium aluminum silicate nanocomposite films: physicochemical characterization and drug permeability. Int J Pharm 393:219–229
117. Liu KH, Liu TY, Chen SY, Liu DM (2007) Effect of clay content on electrostimulus deformation and volume recovery behavior of a clay-chitosan hybrid composite. Acta Biomater 3:919–926
118. Wang XY, Pei XF, Du YM, Li Y (2008) Quaternized chitosan/rectorite intercalative materials for a gene delivery system. Nanotechnology 19:art. #375102
119. Wang XY, Strand SP, Du YM, Varum KM (2010) Chitosan-DNA-rectorite nanocomposites: effect of chitosan chain length and glycosylation. Carbohyd Polym 79:590–596
120. Ruiz-Hitzky E, Darder M, Aranda P (2008) An introduction to bio-nanohybrid materials. In: Ruiz-Hitzky E, Ariga K, Lvov YM (eds) Bio-inorganic hybrid nanomaterials strategies, syntheses, characterization and applications. Wiley-VCH, Weinheim
121. Diaz-Dosque M, Aranda P, Darder M, Retuert J, Yazdani-Pedram M, Arias JL, Ruiz-Hitzky E (2008) Use of biopolymers as oriented supports for the stabilization of different polymorphs of biomineralized calcium carbonate with complex shape. J Cryst Growth 310: 5331–5340
122. Wu ZG, Feng W, Feng YY, Liu Q, Xu XH, Sekino T, Fujii A, Ozaki M (2007) Preparation and characterization of chitosan-grafted multiwalled carbon nanotubes and their electrochemical properties. Carbon 45:1212–1218
123. Rusu VM, Ng CH, Wilke M, Tiersch B, Fratzl P, Peter MG (2005) Size-controlled hydroxyapatite nanoparticles as self-organized organic-inorganic composite materials. Biomaterials 26:5414–5426
124. Liu TY, Chen SY, Li JH, Liu DM (2006) Study on drug release behaviour of CDHA/chitosan nanocomposites—effect of CDHA nanoparticles. J Control Release 112:88–95
125. Kong LJ, Gao Y, Lu GY, Gong YD, Zhao NM, Zhang XF (2006) A study on the bioactivity of chitosan/nano-hydroxyapatite composite scaffolds for bone tissue engineering. Eur Polym J 42:3171–3179
126. Liu H, Li H, Cheng WJ, Yang Y, Zhu MY, Zhou CR (2006) Novel injectable calcium phosphate/chitosan composites for bone substitute materials. Acta Biomater 2:557–565
127. Xu HHK, Burguera EF, Carey LE (2007) Strong, macroporous, and in situ-setting calcium phosphate cement-layered structures. Biomaterials 28:3786–3796
128. Xu HHK, Weir MD, Simon CG (2008) Injectable and strong nano-apatite scaffolds for cell/growth factor delivery and bone regeneration. Dent Mater 24:1212–1222
129. Kim HS, Kim JT, Jung YJ, Ryu SC, Son HJ, Kim YG (2007) Preparation of a porous chitosan/fibroin-hydroxyapatite composite matrix for tissue engineering. Macromol Res 15:65–73
130. Li J, Chen Y, Yin Y, Yao F, Yao K (2007) Modulation of nano-hydroxyapatite size via formation on chitosan-gelatin network film in situ. Biomaterials 28:781–790
131. Li JJ, Dou Y, Yang J, Yin YJ, Zhang H, Yao FL, Wang HB, Yao KD (2009) Surface characterization and biocompatibility of micro- and nano-hydroxyapatite/chitosan-gelatin network films. Mater Sci Eng C Biomimetic Supramol Syst 29:1207–1215
132. Gutierrez MC, Jobbagy M, Ferrer ML, del Monte F (2008) Enzymatic synthesis of amorphous calcium phosphate—Chitosan nanocomposites and their processing into hierarchical structures. Chem Mater 20:11–13
133. Teng SH, Lee EJ, Yoon BH, Shin DS, Kim HE, Oh JS (2009) Chitosan/nanohydroxyapatite composite membranes via dynamic filtration for guided bone regeneration. J Biomed Mater Res A 88:569–580

134. Mohamed KR, Mostafa AA (2008) Preparation and bioactivity evaluation of hydroxyapatite-titania/chitosan-gelatin polymeric biocomposites. Mater Sci Eng C Biomimetic Supramol Syst 28:1087–1099
135. Liu CH, Wu HX, Yang YJ, Zhu LN, Teng YL (2011) The structure and properties of a novel nanocomposite films from chitosan and layered zirconium phosphonate. J Appl Polym Sci 120:1106–1113
136. Rashidova SS, Shakarova DS, Ruzimuradov ON, Satubaldieva DT, Zalyalieva SV, Shpigun OA, Varlamov VP, Kabulov BD (2004) Bionanocompositional chitosan-silica sorbent for liquid chromatography. J Chromatogr B 800:49–53
137. Zhang LH, Dong SJ (2006) Electrogenerated chemiluminescence sensors using Ru(bpy)(3)(2+) doped in silica nanoparticles. Anal Chem 78:5119–5123
138. Shirosaki Y, Okayama T, Tsuru K, Hayakawa S, Osaka A (2008) Synthesis and cytocompatibility of porous chitosan-silicate hybrids for tissue engineering scaffold application. Chem Eng J 137:122–128
139. Corma A, Concepcion P, Dominguez I, Fornes V, Sabater MJ (2007) Gold supported on a biopolymer (chitosan) catalyzes the regioselective hydroamination of alkynes. J Catal 251: 39–47
140. Li BQ, Jia DC, Zhou Y, Hu QL, Cai W (2006) In situ hybridization to chitosan/magnetite nanocomposite induced by the magnetic field. J Magn Magn Mater 306:223–227
141. Hu QL, Wu J, Chen FP, Shen JC (2006) Biomimetic preparation of magnetite/chitosan nanocomposite via in situ composite method. Potential use in magnetic tissue repair domain. Chem Res Chin U 22:792–796
142. Zhu HY, Jiang R, Xiao L, Li W (2010) A novel magnetically separable gamma-Fe_2O_3/crosslinked chitosan adsorbent: preparation, characterization and adsorption application for removal of hazardous azo dye. J Hazard Mater 179:251–257
143. Li Z, Du YM, Zhang ZL, Pang DW (2003) Preparation and characterization of CdS quantum dots chitosan biocomposite. React Funct Polym 55:35–43
144. dos Santos DS, Goulet PJG, Pieczonka NPW, Oliveira ON, Aroca RF (2004) Gold nanoparticle embedded, self-sustained chitosan films as substrates for surface-enhanced Raman scattering. Langmuir 20:10273–10277
145. Kulys J, Stupak R (2008) Glucose biosensor based on chitosan-gold and Prussian blue-gold nanoparticles. Open Nanosci J 2:34–38
146. Wang SF, Shen L, Zhang WD, Tong YJ (2005) Preparation and mechanical properties of chitosan/carbon nanotubes composites. Biomacromolecules 6:3067–3072
147. Liu YY, Tang J, Chen XQ, Xin JH (2005) Decoration of carbon nanotubes with chitosan. Carbon 43:3178–3180
148. Shieh YT, Yang YF (2006) Significant improvements in mechanical property and water stability of chitosan by carbon nanotubes. Eur Polym J 42:3162–3170
149. Spinks GM, Shin SR, Wallace GG, Whitten PG, Kim SI, Kim SJ (2006) Mechanical properties of chitosan/CNT microfibers obtained with improved dispersion. Sens Actuator B Chem 115:678–684
150. Zhang MG, Smith A, Gorski W (2004) Carbon nanotube-chitosan system for electrochemical sensing based on dehydrogenase enzymes. Anal Chem 76:5045–5050
151. Luo XL, Xu JJ, Wang JL, Chen HY (2005) Electrochemically deposited nanocomposite of chitosan and carbon nanotubes for biosensor application. Chem Commun 2169–2171
152. Zhai XR, Wei WZ, Zeng JX, Gong SG, Yin J (2006) Layer-by-layer assembled film based on chitosan/carbon nanotubes, and its application to electrocatalytic oxidation of NADH. Microchim Acta 154:315–320
153. Chakraborty S, Raj CR (2007) Mediated electrocatalytic oxidation of bioanalytes and biosensing of glutamate using functionalized multiwall carbon nanotubes-biopolymer nanocomposite. J Electroanal Chem 609:155–162
154. Gutierrez MC, Hortiguela MJ, Amarilla JM, Jimenez R, Ferrer ML, del Monte F (2007) Macroporous 3D architectures of self-assembled MWCNT surface decorated with Pt nanoparticles as anodes for a direct methanol fuel cell. J Phys Chem C 111:5557–5560

155. Galandova J, Ziyatdinova G, Labuda J (2008) Disposable electrochemical biosensor with multiwalled carbon nanotubes—Chitosan composite layer for the detection of deep DNA damage. Anal Sci 24:711–716
156. Gutierrez MC, Garcia-Carvajal ZY, Hortiguela MJ, Yuste L, Rojo F, Ferrer ML, del Monte F (2007) Biocompatible MWCNT scaffolds for immobilization and proliferation of *E. coli*. J Mater Chem 17:2992–2995
157. Hortiguela MJ, Gutierrez MC, Aranaz I, Jobbagy M, Abarrategi A, Moreno-Vicente C, Civantos A, Ramos V, Lopez-Lacomba JL, Ferrer ML, del Monte F (2008) Urea assisted hydroxyapatite mineralization on MWCNT/CHI scaffolds. J Mater Chem 18:5933–5940
158. Lau C, Cooney MJ, Atanassov P (2008) Conductive macroporous composite chitosan-carbon nanotube scaffolds. Langmuir 24:7004–7010

Chapter 15
Nano-Biocomposites for Food Packaging

Alfonso Jiménez and Roxana A. Ruseckaite

Abstract The main directions in food packaging research are targeted towards improvements in food quality and safety. For this purpose, food packaging providing longer product shelf-life, as well as the monitoring of safety and quality based upon international standards, is desirable. New active packaging strategies represent a key area of development in new multifunctional materials. Nanotechnology can help to address these requirements and also with other packaging functions, such as food protection and preservation, marketing and smart communication to consumers. The use of nano-biocomposites for food packaging combines two of the most active research areas on materials in contact with food. Thus, applications of nano-biocomposites could help to provide new food packaging materials with improved mechanical, barrier, antioxidant and antimicrobial properties. From the food industry standpoint, concerns such as the safety and risk associated with nanomaterials, migration properties, possible ingestion considering mechanisms for nanoparticles to interact with the human body and regulations on the use of nanotechnology need to be considered. The latest innovations in food packaging and the use of nano-biocomposites are reviewed in this chapter. Legislative issues related to the use of nanomaterials in food packaging systems are also discussed.

A. Jiménez (✉)
Department of Analytical Chemistry Nutrition and Food Sciences,
University of Alicante, 03690 San Vicente del Raspeig, Spain
e-mail: alfjimenez@ua.es

R. A. Ruseckaite (✉)
University of Mar del Plata/INTEMA, Juan B. Justo 4302,
7600 Mar del Plata, Argentina
e-mail: roxana@fi.mdp.edu.ar

L. Avérous and E. Pollet (eds.), *Environmental Silicate Nano-Biocomposites*,
Green Energy and Technology, DOI: 10.1007/978-1-4471-4108-2_15,

15.1 Introduction

A food package has traditionally been considered as a container to transport food from the place where it has been produced to the retail outlet and then on to the consumer. Since the main function of packaging is preservation of food from external contamination, other important features such as retardation of deterioration, extension of shelf-life and maintenance of quality and safety of packaged food should be taken into account. Packaging can protect food from environmental influences such as heat, moisture, oxygen, enzymes, loss of aromas, unpleasant odor components, as well as the attack from micro and macroorganisms. Besides all these technological functions, the packaging can also help in marketing and distribution. Furthermore, the global market is becoming more demanding and is continuously in need of novel and stable products which at the same time could retain the natural properties of the food. In summary, the demand for new packaging materials and food packaging functionalities is increasing.

Among the wide variety of materials currently used in food packaging, polymers have taken a major share because of their versatility and advantageous cost/performance ratio. However, most polymers used for food packaging are not biodegradable or compostable and therefore represent an increasingly serious end-of-life disposal and environmental problem worldwide. These drawbacks of the use of common polymers in food packaging are getting an important issue in the design of attractive systems for the general public distribution. Although food package stability during the shelf-life of the product is an advantage, it turns into a disadvantage when the packages enter the post-use phase. In consequence, the use of polymeric materials obtained from non-renewable resources (which are usually non-biodegradable) in food packaging applications presents important environmental impact and waste generation issues. Packaging waste accounted for 71.6 million tons or 29.5 % of the total municipal solid waste (MSW) in 2009 in the USA [1] and 56.3 million tons or 25 % in 2006 in Europe [2]. Currently, landfilling is the dominant method of packaging waste disposal, followed by recycling, incineration, and composting. Even though recovery methods such as reuse, recycling and/or composting are encouraged as a way of reducing packaging waste disposal, there is still much work to do to substantially reduce the quantity of plastic present in MSW [3].

Some alternative packaging materials, obtained from renewable resources, such as poly(lactic acid), PLA, poly(hydroxyalkanoates) (PHAs), starch or proteins, have been proposed as alternatives to non-biodegradable polymers in food packaging applications [4–7]. PLA in particular has been considered for such applications and indeed is already in use in some markets because of its transparency and relatively good mechanical properties. PLA is therefore a strong environmentally-sound contender in the food packaging market since it fulfills all the environmental concerns (i.e. it is derived from renewable raw materials and compostable) [8].

One of the most important features in the still incipient commercial uses of bio-based polymers in food packaging is the development of some of these

materials (e.g., PLA, PHAs) for rigid containers [9]. Their current production is in fact mainly focused on packaging applications (approximately 70 % of the total) but, even if packaging will remain a major outlet, producers foresee new and important applications for these polymers in the next decade [9]. Commercial biopolymers show some limitations in terms of performance (thermal resistance, poor barrier and brittleness) as well as relatively high prices, which are limiting their current applications.

The present situation is such that the cost of bio-plastics is generally higher and performance is equal to or even lower than that of conventional plastics. The development of nano-biocomposites in fields where unique performance or raw material characteristics show an added technological value (for instance sourced from renewable materials, biodegradability, water barrier, antimicrobial properties, aroma barrier) or marketing-wise (e.g., green or sustainability image) is both a challenge and an opportunity for the food packaging industries.

Nanotechnology has potential applications in all aspects of the food chain including storage, quality monitoring, food processing, and food packaging. Therefore, nanotechnology applications in these fields range from intelligent packaging to creation of on-demand interactive packaging that allows consumers to modify food, depending on nutritional needs and tastes. Surprisingly the application of nanotechnologies to materials for food packaging is still in the early stages of development, but the field is growing rapidly and much research work has been recently published.

The use of nano-biocomposites, their advantages and shortcomings for food packaging applications, has been the subject of numerous recent studies, showing that the interest in such formulations is continuously increasing. Several review articles [10–14] highlight the need for further research and development in fields such as processing, characterization, determination of functional properties, and risk assessment. The resulting knowledge from such research will be necessary for the full industrial implementation of nano-biocomposites in food packaging materials, either in monolayers or multilayer film systems.

Nano-biocomposites are hybrid nanostructured materials with improved mechanical, thermal and gas barrier properties [15–17]. The use of nano-biocomposites for food packaging may not only protect foodstuff and increase shelf-life, but may also be viewed as an environmentally friendly solution to the increasing problem of food packaging waste disposal on a global scale [18–20].

An interesting approach to nano-biocomposites involves the use of layered silicates. These hybrid composites improve stability of the resulting nano-biocomposites and their biodegradability can be tuned by varying the amount of other components in their formulations [16]. This is particularly important for the modulation of mechanical properties but can also be used to adjust another important property of food packaging materials (i.e., its ability to act as a barrier to mass transfer from and to a food product). Permeation of gases, such as oxygen and carbon dioxide, as well as water vapour, is critical in many food packaging applications, such as modified atmosphere packaging (MAP) and can also be a key consideration for carbonated beverage packaging. In addition to the improvement

in terms of novel applications (e.g., extension of their use to high moisture content foods), barrier functions may potentially be provided by incorporation of polysaccharides and/or lipids and, so far, some studies have investigated the possible incorporation of nanoparticles in packaging with the aim to improve the physico-chemical and barrier properties of such films [21–23].

15.2 Biodegradable Polymers in Food Packaging Applications

Bio-derived and biodegradable thermoplastics which can be processed on conventional equipment are gaining increasing attention. The most widely studied thermoplastic biopolymers are starch, PLA and PHAs. Among these, starch and PLA are the most interesting for food packaging since they have become commercially available, have an interesting balance of properties and are produced on an industrial scale. For instance, PLA shows excellent transparency and relatively good water resistance [24–26]. Its high stiffness is usually reduced by the addition of plasticizers [27–29] but these additives also lead to a decrease in oxygen barrier and thermal resistance [30, 31]. It is therefore of great industrial interest to enhance the barrier properties of PLA while maintaining its inherently good properties such as transparency and biodegradability. This is one of the main challenges at present in the development of nano-biocomposites for food packaging.

There are other biomaterials with a high potential in food packaging and which can be directly extracted from biomass, such as gluten, zein, prolamine obtained from corn and chitosan which is typically obtained from crustaceous chitin. These materials generally have excellent oxygen barrier under dry conditions. However, their main drawbacks are their inherent high rigidity, difficulties in processing using conventional equipment and strong water sensitivity arising from their hydrophilic character, which leads to plasticization affecting mechanical and barrier properties [32, 33]. Nevertheless, chitosan and zein biopolymers exhibit two very interesting characteristics. Chitosan has antimicrobial properties [34, 35] and the unusual water resistance of zein makes this biopolymer potentially useful for multilayer food packaging applications [36].

All biopolymers with commercial interest can show excellent gas barrier properties in their optimum formulations, although their barrier performance is dramatically reduced in the presence of moisture and/or other plasticizers, necessary to get materials adequate for processing. Other biopolymers like PHAs, show very high water barrier properties. So, in principle, the use of multilayer systems where an inner layer of plasticized chitosan could be sandwiched between PHA layers could be an interesting possibility. However, these materials normally suffer from relatively high production costs, which means that competition with conventional thermoplastics is problematic.

In summary, modification of biopolymers through innovative technologies, such as nanotechnology, is an important challenge for material scientists. The formulation of nano-biocomposites is an effective way to enhance their properties while improving renewability and biodegradability in order to reduce the carbon footprint and the participation of packaging materials in the MSW.

15.3 Nano-Biocomposites with Layered Silicates for Food Packaging

Within the polymer/clay nanocomposites, the case of nano-biocomposites containing biopolymers and clays is one of the most outstanding and novel developments in food packaging technologies. The main biodegradable polymers normally used for monolayer and some multilayer applications are PLA, PHAs, starch and poly(ε-caprolactone), PCL. Although having well known advantages, these materials have shortcomings in their barrier, mechanical and thermal performance when compared to conventional thermoplastics. The use of nanoclays to improve their performance, particularly barrier properties, is one of the most active areas of current research and this section pays special attention to the current status of the literature regarding enhancement in the properties of thermoplastic biocomposites by the addition of layered silicates.

In one of the first studies on barrier properties in nanocomposites, Maiti et al. [37] reported that the barrier properties of non-interacting gases in nanocomposites primarily depend on two factors: 1) the layered silicate particle aspect ratio, and 2) the extent of dispersion of the silicate within the polymer matrix. When the degree of dispersion of the layered organoclay is maximised (and consequently a fully exfoliated morphology is attained) the barrier properties solely depend on the particles' aspect ratio. This is the case when nanoclays are used at moderate levels (4–7 wt%) and correctly processed. In most cases, the reduction in oxygen permeability through incorporation of organoclays falls in the 50–60 % range. Sinha Ray et al. [38] claimed reductions in oxygen permeability up to 65 % for PLA + 4 wt% of synthetic fluorine mica prepared by melt mixing. Nano-biocomposites with similar contents, but different kinds of clay showed lower levels of oxygen permeability reduction, from 6 to 56 % [39–41]. In the case of plasticized PLA for film manufacturing, Martino et al. [42] reported a reduction of ~35 % in oxygen transmission rate (OTR) at a 5 wt% addition of commercial montmorillonite (Cloisite®30B). In summary, in the case of PLA-based nano-biocomposites, the barrier properties strongly depend upon clay type, clay organomodifier, aspect ratio, addition level and dispersion.

In the case of PHAs, researchers have mainly focused their interest on the lower melting temperature copolymers of poly(3-hydroxybutyrate), PHB, such as poly(3-hydroxybutyrate-co-3-hydroxyvalerate), PHBV, with improved chemical stability and good physical properties, but poor barrier performance [43, 44].

Nano-biocomposites of PHBV with montmorillonites have been investigated and good dispersion and barrier properties were obtained [45].

PCL shows a wide melt processing window and adequate final properties for using in food packaging applications [46–48]. The barrier properties of nano-biocomposites based on PCL have been studied. For instance, Gorrasi et al. [49] reported interesting results for water vapour permeability (WVP) for PCL–MMT biocomposites. Although WVP increased with increasing MMT content, the diffusion parameters of the samples showed much lower values in exfoliated systems. Other authors reported that nano-biocomposites based on PCL and mica-type silicates exhibited a significant reduction in WVP and a linear dependence on silicate content [50]. Gain et al. [51] presented an interesting study in which PCL/montmorillonite nano-biocomposites were prepared by melt blending and maintaining a constant inorganic content. This approach involved in situ polymerization of ε-caprolactone in the presence of organo-modified clays, and initiation of ε-caprolactone polymerization from the silicate layer with appropriate organomodified montmorillonites. The highest barrier properties were obtained for an exfoliated morphology and the highest grafting density. In all cases the significant decrease in WVP observed for PCL-based nano-biocomposites is of significance when considering their use in food packaging applications, particularly as protective coatings and in other systems where efficient polymeric barriers are necessary. This significant improvement as well as the better mechanical properties for PCL-nanocomposites could be attributed to the fine dispersion state of organoclay in the PCL matrix and the strong interaction between the organic modifier and the matrix.

Starch-based nano-biocomposites are conditioned by the high sensitivity of starch towards water sorption, so the first challenge in these materials is to improve this property. Park et al. [52, 53] prepared starch-organoclay nanocomposites by melt intercalation with different commercial montmorillonites as well as organo-modified MMT. The water vapour barrier properties were improved compared to pure starch. In general, for the preparation of starch-based nano-biocomposites by solution casting the addition of a plasticizer has been considered a necessary requirement. Kampeerapappun et al. [54] prepared starch/MMT films by casting, using chitosan as a compatibilizing agent in order to disperse the clay in the starch matrix. Other starch nanocomposites were prepared via different plasticizer and MMT addition sequences and solvent casting. The resulting nano-biocomposites exhibited reduced hydrophilicity. In terms of mechanical properties, the addition of an organically modified layered silicate in a polymer matrix generally results in significant improvements in Young modulus, as has been reported in many studies [55–57]. In the case of nano-biocomposites for food packaging, Pucciarello et al. [58] reported an increase in modulus from 216 to 390 MPa for a PCL nanocomposite containing 10 wt% of an organo-modified MMT. However, in some cases a different behaviour was observed. For instance, a decrease in modulus with increasing clay content was found in crosslinked polyester/MMT nano-biocomposites [57]. Authors explained this phenomenon by suggesting that the intercalation and exfoliation of the clay in the polyester resin serves to effectively reduce the number of crosslinks in the macromolecular structure.

15.4 Cellulose-Based Nanoreinforcements

Cellulose, the structural polymer in plant cell walls, is a highly strong natural polymer. Cellulose nanofibers (NFs) and/or nanocrystals (NCs) are potentially a low cost and widely available material. Moreover, these nanofillers are environmentally friendly and they can be easily recycled by combustion. With appropriate technology development, these nanofillers can be produced with relatively low energy consumption. All of this makes cellulose nanofibers and nanocrystals an attractive class of nanomaterials for elaboration of low cost, light-weight, and high-strength nano-biocomposites [59]. Basically two types of nanoreinforcements can be obtained from cellulose: microfibrils and whiskers [60]. In plants or animals the cellulose chains are synthesized to form microfibrils (or nanofibers), which are bundles of molecules that are elongated and stabilized through hydrogen bonding [60, 61]. The microfibrils have nanosized diameters (2–20 nm, depending on the origin), and lengths in the micrometer range. Each microfibril in the plant is formed by aggregation of elementary fibrils, which are made up of crystalline and amorphous parts. The crystalline parts, which can be isolated by several treatments, are the whiskers, also known as nanocrystals, nanorods, or rod-like cellulose microcrystals [62, 63], with lengths ranging from 500 nm up to 1–2 μm, and about 8–20 nm or less in diameter, resulting in high aspect ratios.

In the case of nano-biocomposites reinforced with nanocelluloses for food packaging, some key properties could be improved by their use. For instance, starch-based materials have been extensively investigated as a product which can improve the biodegradability of a variety of plastics. However, the brittleness of starch requires the use of plasticizers such as polyols or glycerol, which improve starch flexibility but, on the other hand, decrease its thermomechanical properties. The addition of cellulose whiskers to starch systems enhances their thermomechanical properties, reduces water sensitivity, and maintains biodegradability. Several studies have reported the effects of cellulose nanoreinforcements on the performance of starch. Some authors [64] reported that cellulose nanofiber addition increased the T_g of starch. This reinforcing effect depends strongly on the formation of a cellulose microfibrillar network within the matrix, resulting from hydrogen bonds which are formed during the solvent evaporation step. Water uptake by starch films decreases linearly or almost linearly with increasing cellulose whisker content [65].

The moisture barrier properties of polymer films have been improved by cellulose nanoreinforcements [66–68]. The presence of crystalline fibers is thought to increase the tortuosity in the materials leading to slower diffusion processes and, hence, to lower permeability. The barrier properties are enhanced if the filler is less permeable, has good dispersion in the matrix and a high aspect ratio. However, one challenge for the effective inclusion of nanocelluloses in biopolymer matrices lies in the difference in hydrophilicity between the components. This drawback should be overcome before mixing and it is not an easy task. Some research is currently on-going to increase compatibility between nanocelluloses and hydrophobic biopolymers, such as PLA. One of the technologies that could be used to overcome

this problem is the grafting of polymer precursors onto cellulose (e.g., L-lactide). This strategy has been used to improve the compatibility of cellulose nanofibers in organic solvents and consequently their compatibility with the polymer matrix. This approach permits an increase in the non-polar character of the cellulose surface through grafting with agents having a reactive terminal group and a compatible tail [69]. Most of these studies have been carried out with PCL, since this polymer is capable of forming chemical bonds with the cellulose nanocrystals. Habibi et al. [70] processed nano-biocomposites by grafting PCL onto ramie NCs (NC–g–PCL), using an isocyanate-based approach. The comparison between NC–g–PCL and non-modified NC showed a lower modulus and a significant increase in deformation at break after mixing and preparation of films. This unusual behavior was attributed to the reticulation of percolation networks produced by hydrogen bonds, although after the PCL grafting the structural and morphological integrity of the NCs was not affected. A similar study was carried out using cellulose microfibrils (MFC), in which case PCL was used for grafting on the surface of fibers by means of ring-opening polymerization (ROP) [71].

The study of grafting of nanocelluloses and PLA has not been widely investigated. Löngberg et al. [72] used L-lactide to obtain PLA by ROP on the surface of cellulose fibers. In another work, cellulose fibers were modified by using lactic acid as monomer, an aluminum catalyst and glycerol. The polymerization of PLA on the surface of the fibers was also carried out by ROP [73]. Other authors proposed the grafting of PCL chains on the NC surface [74, 75]. These modified nanoparticles were further mixed in the PLA matrix by casting with dichloromethane. PLA films with 5 wt% of these nanoparticles showed an increase in the elongation at break and in the tensile strength. These findings presumably arise because PCL chains grafted to the cellulose surface improve the association between PLA matrix and the NCs.

15.5 Nano-Biocomposites with Nanotubes

Nanotechnology has already led to several innovations in the food packaging area, including the use of nanotubes [76, 77]. A nanotube is a nanometer-scale wire-like structure, most frequently composed of carbon. Nanotubes can be incorporated into polymer structures (liquids, solutions, melts, gels, amorphous and crystalline matrices) to increase their tensile strength and elasticity [78].

A very interesting example in the development of nano-biocomposites of particular relevance to the food sector is the possibility to obtain nanotubes from milk protein (α-lactalbumin) by partial hydrolysis. These nanotubes are able to increase viscosity owing to their high aspect ratio (i.e., large surface area) and stiffness, which requires lower amounts of protein [79, 80]. In addition, α-lactalbumin nanotubes show cavities of 8 nm in diameter in their structure, which might permit the immobilization and controlled release of food components, such as vitamins or enzymes, potentially leading to active packaging systems. These cavities could also be used to encapsulate and protect nutraceuticals or to mask undesirable flavor or

aroma compounds [80]. Since these nanotubes consist of milk protein, they are considered food-grade materials, which should make their introduction into the market relatively easy and might facilitate widespread applications in nanoencapsulating of nutrients, supplements and pharmaceuticals.

15.6 Antimicrobial Nano-Biocomposites

The incorporation of antimicrobial compounds into food packaging materials has received considerable attention during the last few years. Films with antimicrobial activity could help to control the growth of pathogenic and spoilage microorganisms. An antimicrobial nano-biocomposite film is particularly desirable due to its acceptable structural integrity and barrier properties imparted by the nanocomposite matrix, and the antimicrobial properties provided by natural antimicrobial agents impregnated within [81]. Materials in the nanoscale range have a higher surface-to-volume ratio when compared with their microscale counterparts. This allows nanomaterials to encapsulate more biological molecules, conferring greater efficiency [82].

The most common nano-biocomposites used as antimicrobial films for food packaging could be based on silver, which is well known for its strong toxicity to a wide range of microorganisms [83], with high temperature stability and low volatility [84]. Some mechanisms have been proposed for the antimicrobial property of silver nanoparticles (Ag-NPs), including adhesion to cell surfaces, degradation of lipopolysaccharides [85]; penetration inside bacterial cells, damaging DNA [86], and releasing antimicrobial Ag^+ ions by Ag-NP dissolution [87]. The latter mechanism is consistent with findings by Kumar and Münstedt [84], who affirmed that the antimicrobial activity of silver-based polymers depends on releasing of Ag^+, which binds to electron donor groups in biological molecules containing sulphur, oxygen or nitrogen.

Silver nanocomposites have been produced by several researchers, and their antimicrobial effectivity has usually been reported. Damm, Münstedt, and Rösch [88], comparing the efficiency of polyamide 6/silver-nano- and micro-composites, reported that nanocomposites with low silver content presented an increased antimicrobial efficiency against *Escherichia coli* than microcomposites with a much higher silver content. The same authors reported that polyamide 6 filled with 2 wt% Ag-NPs was effective against *E. coli*, even after immersion in water for 100 days [89].

15.7 Risk Assessment and Safety Issues in the Use of Nanomaterials in Food Packaging

The development of new strategies for the use of nanocomposites in food packaging materials has been the object of many studies. Reviewing the whole food manufacturing chain, nanotechnologies used in food processing are currently

more abundant than those used in food packaging and therefore risk assessment problem should cover the whole process and not only materials for food packaging. However, the focus is on packaging materials since most people and policy makers are still unsure of the safety of nanomaterials to be used in direct contact with food. An examination of risk assessment and safety issues in this area is important in order to get an insight about the use of nanomaterials in this field.

The main risk of consumer exposure to nanomaterials from food packaging is likely to be through their potential migration into the packaged food. However, migration experimental data for nanoparticles in food contact materials are still relatively scarce and few studies have been published. Difficulties in characterizing nanomaterials in composites and the lack of methods for qualitative and quantitative analysis are responsible for this limited research on migration in nanocomposites. However, recent reviews have stressed this issue and it is likely that on-going and future work will provide the necessary data [90]. A recent example of research on nanocomposite characterization and nanoparticle migration has been published by Schmidt et al. [91].

A theoretical study by Simon et al. [92] looked at migration in the context of physico-chemical properties of both, nanoparticles and packaging polymers, such as the density of the polymer, the size of the nanoparticles, their density in the polymer macromolecular structure and the average distance of nanoparticles from the polymer surface. It was reported that the smaller size of nanoparticles and lower polymer density resulted in higher migration and that nanoparticles as small as 1 nm might need to be present for significant migration to occur.

The main risk for human health associated to the use of nanocomposites for food packaging systems would come from the oral uptake from food with added nanoparticles, and any migration from the nanocomposite. The digested nanomaterials would temporarily remain and accumulate in the gastrointestinal tract, and could be then absorbed by the intestinal epithelium to be transported to other body systems and organs [93, 94]. Some studies have gone into details on the effect of the ingestion of nanomaterials in laboratory rats and authors concluded that those effects are multiple and should be taken into account before using nanocomposites in food packaging applications [95, 96]. The outline presented there suggests the potential use of layered double hydroxides (LDHs) to prepare polymer nanocomposites because LDHs are soluble at low pH, as occurs in the human stomach. The use of LDHs in polymer nanocomposites has recently been reviewed [97].

The potential migration of nanoparticles from packaging materials to packaged food raises public concern, and may be corroborated by animal oral administration and in vitro cell experiments. In general, two types of mechanisms can be adopted to explain the toxicity effects on humans. One is that the toxicity is independent of the nanoparticle structure, and could be realized by generating reactive oxygen species (ROS) within the cells. Another approach is based on the hypothesis that the toxicity has a strong relationship with the chemical components of nanomaterials. For example, the crystallization and recrystallization of some metals or metal oxides at the nanoscale will modify the secondary or tertiary conformation of the proteins. While other types of nanoparticles, such as the metal alloy,

or single-wall carbon nanotubes (SWNT) or multi-wall carbon nanotubes (MWNT) might result in direct or indirect gene toxicity.

In summary, much work is still necessary to get the final conclusions regarding risk and health issues associated with the use of nanocomposites (or nano-biocomposites) in food packaging systems. Recently, the U.S. Department of Agriculture and Food and Drug Administration (FDA) conducted a brief assessment on nanoparticles and nanomaterials applied in various areas of medical and food technologies [98]. The relatively scarce scientific data on migration, exposure sources and toxicities indicate the difficulties and problems in properly understanding the nature of the interactions between materials at the nanoscale and the human body [99]. The following problems were identified and need to be resolved:

1. More and effective separation and determination techniques are needed to develop and establish the matrix for nano-biocomposites to be used in food packaging.
2. Comprehensive physico-chemical characteristics of the applied nanoparticles should be established. These data would include size, size distribution, inherent crystal structure, morphologies, surface ligand properties, surface charge, surface reactivity and aggregation behaviour under different pH conditions.
3. Establishment of the relationships between particle size, purity and toxicity.
4. A methodology needs to be established for determining and assessing the migration potential of nanoparticles from food contact materials into packaged food.
5. Development of an understanding of toxicity following oral intake of a wide range of nanomaterials for which there is likely human exposure.
6. Generation of information on the toxico-kinetic properties of nanoparticles after oral exposure and appropriate dose metrics in relation to their toxicity. Correlation of these data with the physico-chemical characteristics of nanoparticles in order to generate information on the bioavailability from food for a range of nanomaterials and to investigate the potential accumulation and transport through different body organs.
7. To develop, improve and validate in vitro and in vivo test methodologies to assess the toxicity of nanoparticles and their interaction with human cells.

15.8 Conclusions

In summary, a great amount of work has been recently and is currently carried out to propose new nano-biocomposites for food packaging with the aim of improving food shelf-life and preservation and to reduce waste generation from food packaging systems. However, despite the fact that there are many studies in the literature that report barrier enhancements in polymer and biopolymer matrices, it is clear from the modeling results that the expected improvements are not yet experimentally attained or reproducible at large scale. This is the result of several

factors that could be summarized by the lack of (1) complete exfoliation of the nanofiller, (2) good compatibility between nanofiller and matrix and/or (3) good purification and appropriate selection of raw materials and surface modifications. In general there is still a need for a better understanding of the composition-structure-processing-properties relationships in nano-biocomposites for food packaging, both at the laboratory and industrial scale. Moreover, since many of the studies related to this issue have been carried out using very few nanomaterials (mostly nanoclays), there is still a lot of room for variation and maturation in the development of nano-biocomposites for application in food packaging.

References

1. http://www.epa.gov/osw/nonhaz/municipal/pubs/msw2009-fs.pdf. Accessed June 2011
2. http://www.waste-management-world.com/index/display/article-display/304406/articles/waste-management-world/volume-8/issue-4/features/msw-management-in-europe.html. Accessed June 2011
3. Jamshidian M, Tehrany EA, Imran M et al (2010) Poly-lactic acid: production, applications, nanocomposites, and release studies. Compr Rev Food Sci Food Saf 9:552–571
4. Martucci JF, Ruseckaite RA (2010) Biodegradable three-layer film derived from bovine gelatin. J Food Eng 99:377–383
5. Kechichian V, Ditchfield C, Veiga-Santos P et al (2010) Natural antimicrobial ingredients incorporated in biodegradable films based on cassava starch. LWT—Food Sci Technol 43:1088–1094
6. Arzu AB, Tulay O, Oya IS et al (2010) The utilisation of microbial poly-hydroxy alkanoates (PHA) in food industry. Res J Biotechnol 5:76–79
7. Ahmed J, Varshney SK (2011) Polylactides-chemistry, properties and green packaging technology: a review. Intern J Food Prop 14:37–58
8. Auras R, Harte B, Selke S (2004) An overview of polylactides as packaging materials. Macromol Biosci 9:835–864
9. Shen L, Haufe J, Patel MK (2009) Product overview and market projection of emerging bio-based plastics PRO-BIP2009, Utrecht University
10. Sorrentino A, Gorrasi G, Vittoria V (2007) Potential perspectives of bionanocomposites for food packaging applications. Trends Food Sci Technol 18:84–95
11. de Azeredo HMC (2009) Nanocomposites for food packaging applications. Food Res Int 42:1240–1253
12. Neethirajan S, Jayas DS (2011) Nanotechnology for the food and bioprocessing industries. Food Bioprocess Technol 4:39–47
13. Sozer N, Kokini JL (2010) Nanotechnology and its applications in the food sector. Trends Biotechnol 27:82–89
14. Lagaron JM, López-Rubio A (2011) Nanotechnology for bioplastics: opportunities, challenges and strategies. Trends Food Sci Technol. doi:10.1016/j.tifs.2011.01.007
15. Alexandre M, Degee P, Henrist C et al (2001) Preparation and properties of layered silicate nanocomposites based on ethylene vinyl acetate copolymers. Macromol Rapid Commun 22:643–646
16. Li X (2001) Preparation and characterization of poly (butyleneterephthalate) organoclay nanocomposites. Macromol Rapid Commun 22:1306–1312
17. Khare A, Deshmukh S (2006) Studies toward producing eco-friendly plastics. J Plastic Film Sheeting 22:193–211

18. Bordes P, Pollet E, Averous L (2009) Nano-biocomposites: biodegradable polyester/nanoclay systems. Prog Polym Sci 34:125–155
19. Suyatma NE, Copinet A, Tighzert L et al (2004) Mechanical and barrier properties of biodegradable films made from chitosan and poly (lactic acid) blends. J Polym Environ 12:1–6
20. Tharanathan RN (2003) Biodegradable films and composite coatings: past, present and future. Trends Food Sci Technol 14:71–78
21. Kaynak C, Tasan C (2006) Effects of production parameters on the structure of resol type phenolic resin/layered silicate nanocomposites. Eur Polym J 42:1908–1921
22. Pereira de Abreu DA, Paseiro-Posada P, Angulo I et al (2007) Development of new polyolefin films with nanoclays for application in food packaging. Macromol Nanotechnol 43:2229–2243
23. Martino VP, Ruseckaite RA, Jiménez A et al (2010) Correlation between composition, structure and properties of poly(lactic acid)—polyadipate based nano-biocomposites. Macromol Mat Eng 295:551–558
24. Park ES, Kim MN, Yoon JS (2002) Grafting of polycaprolactone onto poly(ethylene-*co*-vinyl alcohol) and application to polyethylene-based bioerodable blends. J Polym Sci Part B Polym Phys 40:2561–2569
25. Tsuji H, Yamada T (2003) Blends of aliphatic polyesters. VIII. Effects of poly(L-lactide-co-ε-caprolactone) on enzymatic hydrolysis of poly(L-lactide), poly(ε-caprolactone), and their blend films. J Appl Polym Sci 87:412–419
26. Chen CC, Chueh JY, Tseng H et al (2003) Preparation and characterization of biodegradable PLA polymeric blends. Biomaterials 24:1167–1173
27. Martin O, Averous L (2001) Poly(lactic acid): plasticization and properties of biodegradable multiphase systems. Polymer 42:6209–6219
28. Ljungberg N, Wesslén B (2002) The effects of plasticizers on the dynamic mechanical and thermal properties of poly(lactic acid). J Appl Polym Sci 86:1227–1234
29. Ljungberg N, Wesslén B (2003) Tributyl citrate oligomers as plasticizers for poly (lactic acid): thermo-mechanical film properties and aging. Polymer 44:7679–7688
30. Courgneau C, Domenek S, Guinault A et al (2011) Analysis of the structure–properties relationships of different multiphase systems based on plasticized poly(lactic acid). J Polym Environ 19:362–371
31. Martino VP, Ruseckaite RA, Jiménez A (2009) Ageing of poly(lactic acid) films plasticized with commercial polyadipates. Polym Int 58:437–444
32. Rogovina SZ, Alexanyan CV, Prut EV (2011) Biodegradable blends based on chitin and chitosan: Production, structure, and properties. J Appl Polym Sci 121:1850–1859
33. Anderson TJ, Lamsa BP (2011) Zein extraction from corn, corn products, and coproducts and modifications for various applications: a review. Cereal Chem 88:159–173
34. Aider M (2010) Chitosan application for active bio-based films production and potential in the food industry: review. LWT-Food Sci Technol 43:837–842
35. Campos CA, Gerschenson LN, Flores SK (2011) Development of edible films and coatings with antimicrobial activity. Food Bioprocess Technol 4:849–875
36. Wang Y, Padua GW (2004) Zein adsorption to hydrophilic and hydrophobic surfaces investigated by surface plasmon resonance. J Agric Food Chem 52:3100–3105
37. Maiti P, Yamada K, Okamoto M et al (2002) New polylactide/layered silicate. Nanocomposites: role of organoclay. Chem Mater 14:4654–4661
38. Ray SS, Yamada K, Okamoto M et al (2003) New polylactide/layered silicate nanocomposites. 5. Designing of materials with desired properties. Polymer 44:857–866
39. Petersson L, Oksman K (2006) Biopolymer based nanocomposites: Comparing layered silicates and microcrystalline cellulose as nanoreinforcement. Comp Sci Technol 66:2187–2196
40. Zenkiewicz M, Richert J (2008) Thermoforming of polylactide nanocomposite films for packaging containers. Polym Test 27:835–840
41. Rhim JW, Hong SI, Ha CS (2009) Tensile, water barrier and antimicrobial properties of PLA/nanoclay composite films. LWT Food Sci Technol 42:612–617

42. Martino VP, Jiménez A, Ruseckaite RA et al (2011) Structure and properties of clay nanobiocomposites based on poly(lactic acid) plasticized with polyadipates. Polym Adv Technol 22:2206–2213
43. Choi WM, Kim TW, Park OO et al (2003) Preparation and characterization of tapioca starch-poly(lactic acid)-Cloisite Na nanocomposite foams. J Appl PolymSci 90:525–529
44. Wang SF, Song CJ, Chen GX et al (2005) Characteristics and biodegradation properties of poly(3-hydroxybutyrate-*co*-3-hydroxyvalerate)/organophilic montmorillonite (PHBV/OMMT) nanocomposite. Polym Degrad Stab 87:69–76
45. Cabedo L, Plackett D, Giménez E et al (2009) Studying the degradation of polyhydroxybutyrate-co-valerate during processing with clay-based nanofillers. J Appl Polym Sci 112:3669–3676
46. González I, Eguizabal JI, Nazabal J (2006) New clay-reinforced nanocomposites based on a polycarbonate/polycaprolactone blend. Polym Eng Sci 46:864–873
47. Cabedo L, Feijoo JL, Villanueva MP et al (2006) Optimization of biodegradable nanocomposites based on PLA/PCL blends for food packaging. Macromol Symp 233:191–197
48. Chen BQ, Evans JRG (2006) Poly(ε-caprolactone)-clay nanocomposites: Structure and mechanical properties. Macromolecules 39:747–754
49. Gorrasi G, Tortora M, Vittoria V et al (2004) Physical properties of poly(ε-caprolactone) layered silicate nanocomposites prepared by controlled grafting polymerization. J Polym Sci Part B Polym Phys 42:1466–1475
50. Messersmith PB, Giannellis EP (1993) Polymer-layered silicate nanocomposites: in situ intercalative polymerrization of poly(ε-caprolactone). Chem Mat 5:1064–1066
51. Gain O, Espuche E, Pollet E et al (2005) Gas barrier properties of poly(ε-caprolactone)/clay nanocomposites: Influence of the morphology and polymer/clay interactions. J Polym Sci Part B Polym Phys 43:205–214
52. Park HM, Li X, Jin CZ et al (2002) Preparation and properties of biodegradable thermoplastic starch/clay hybrids. Macromol Mat Eng 287:553–558
53. Park HM, Lee WK, Park CY et al (2003) Environmentally friendly polymer hybrids. Part I Mechanical, thermal, and barrier properties of thermoplastic starch/clay nanocomposites. J Mat Sci 38:909–915
54. Kampeerapappun P, Ath-ong D, Pentrakoon D et al (2007) Preparation of cassava starch/montmorillonite composite film. Carbohydrate Polym 67:155–163
55. Finnigan B, Martin D, Halley P et al (2004) Morphology and properties of thermoplastic polyurethane nanocomposites incorporating hydrophilic nanoparticles. Polymer 45:2249–2260
56. Peeterbroeck S, Alexandre M, Jerome R et al (2005) Poly(ethylene-co-vinyl acetate)/clay nanocomposites: effect of clay nature on properties. Polym Degrad Stab 90:288–294
57. Almasi H, Ghanbarzadeh B, Entezam AA (2010) Physicochemical properties of starch-CMC-nanoclay biodegradable films. Int J Biol Macromol 46:1–5
58. Pucciariello R, Villani V, Gorrasi G et al (2005) Phase behavior of blends of poly(ε-caprolactone) and a modified montmorillonite-poly(ε-caprolactone) nanocomposite. J Macromol Sci 44:79–92
59. Podsiadlo P, Choi SY, Shim B et al (2005) Molecularly engineered nanocomposites: layer-by-layer assembly of cellulose nanocrystals. Biomacromolecules 6:2914–2918
60. Azizi Samir MAS, Alloin F, Dufresne A (2005) Review of recent research into cellulosic whiskers, their properties and their application in nanocomposites field. Biomacromolecules 6:612–626
61. Wang B, Sain M (2007) Isolation of nanofibers from soybean source and their reinforcing capability on synthetic polymers. Comp Sci Technol 67:2521–2527
62. Azizi Samir MAS, Alloin F, Sanchez JY et al (2004) Cellulose nanocrystals reinforced poly(oxyethylene). Polymer 45:4149–4157
63. Dujardin E, Blaseby M, Mann S (2003) Synthesis of mesoporous silica by sol-gel mineralisation of cellulose nanorod nematic suspensions. J Mat Chem 13:696–699
64. Alemdar A, Sain M (2008) Biocomposites from wheat straw nanofibers: morphology, thermal and mechanical properties. Comp Sci Technol 68:557–565

65. Lu Y, Weng L, Cao X (2005) Biocomposites of plasticized starch reinforced with cellulose crystallites from cotton-seed linter. Macromol Biosci 5:1101–1107
66. Paralikar SA, Simonsen J, Lombardi J (2008) Poly(vinyl alcohol)/cellulose nanocrystal barrier membranes. J Membr Sci 320:248–258
67. Sanchez-Garcia MD, Gimenez E, Lagaron JM (2008) Morphology and barrier properties of solvent cast composites of thermoplastic biopolymers and purified cellulose fibers. Carbohydrate Polym 71:235–244
68. Svagan AJ, Hedenqvist MS, Berglund L (2009) Reduced water vapour sorption in cellulose nanocomposites with starch matrix. Comp Sci Technol 69:500–506
69. Dufresne A (2010) Processing of polymer nanocomposites reinforced with polysaccharide nanocrystals. Molecules 15:4111–4128
70. Habibi Y, Dufresne A (2008) Highly filled bionanocomposites from functionalized polysaccharide nanocrystals. Biomacromolecules 9:1974–1980
71. Chen G, Dufresne A, Huang J et al (2009) A Novel Thermoformable Bionanocomposite Based on Cellulose Nanocrystal-graft-Poly(ε-caprolactone). Macromol Mat Eng 294:59–65
72. Löngberg H, Fogelström L, Samir MASA et al (2008) Surface grafting of microfibrillated cellulose with poly(ε-caprolactone)—synthesis and characterization. Eur Polym J 44:2991–2997
73. Löngberg H, Zhou Q, Brumer H et al (2006) Grafting of cellulose fibers with poly(ε-caprolactone) and poly(L-lactic acid) via ring-opening polymerization. Biomacromolecules 7:2178–2185
74. Funabashi M, Kunioka M (2005) Biodegradable composites of poly(lactic acid) with cellulose fibers polymerized by aluminum triflate. Macromol Symposia 224:309–321
75. Lin N, Chen G, Huang J et al (2009) Effects of polymer-grafted natural nanocrystals on the structure and mechanical properties of poly(lactic acid): a case of cellulose whisker-graft-polycaprolactone. J Appl Polym Sci 113:3417–3425
76. Weiss J, Takhistov P, McClements DJ (2006) Functional materials in food nanotechnology. J Food Sci 71:107–116
77. Elkin T, Jiang X, Taylor S et al (2005) Immuno carbon nanotubes and recognition of pathogens. ChemBioChem 6:640–643
78. Ruoff RS, Lorents DC (1995) Mechanical and thermal properties of carbon nanotubes. Carbon 33:925–930
79. Ipsen R, Otte J (2007) Self-assembly of partially hydrolysed α-lactalbumin. Biotechnol Adv 25:602–607
80. Graveland-Bikker JF, de Kruif CG (2006) Unique milk protein based nanotubes: food and nanotechnology meet. Trends Food Sci Technol 17:196–203
81. Rhim JW, Ng PKW (2007) Natural biopolymer-based nanocomposite films for packaging applications. Crit Rev Food Sci Nutr 47:411–433
82. Luo PG, Stutzenberger FJ (2008) Nanotechnology in the detection and control of microorganisms. In Laskin AI, Sariaslani S, Gadd GM (eds). Adv Appl Microbiol 63:145–181. Elsevier, London
83. Liau SY, Read DC, Pugh WJ et al (1997) Interaction of silver nitrate with readily identifiable groups: relationship to the antibacterial action of silver ions. Lett Appl Microbiol 25:279–283
84. Kumar R, Munstedt H (2005) Silver ion release from antimicrobial polyamide/silver composites. Biomaterials 26:2081–2088
85. Sondi I, Salopek-Sondi B (2004) Silver nanoparticles as antimicrobial agent: a case study on *E. coli* as a model for Gram-negative bacteria. J Colloid Interface Sci 275:177–182
86. Li Q, Mahendra S, Lyon DY et al (2008) Antimicrobial nanomaterials for water disinfection and microbial control: potential applications and implications. Water Res 42:4591–4602
87. Morones JR, Elechiguerra JL, Camacho A et al (2005) The bactericidal effect of silver nanoparticles. Nanotechnology 16:2346–2353
88. Damm C, Munstedt H, Rosch A (2008) The antimicrobial efficacy of polyamide 6/silver-nano- and microcomposites. Mat Chem Phys 108:61–66
89. Damm C, Munstedt H, Rosch A (2007) Long-term antimicrobial polyamide-6/silver-nanocomposites. J Mat Sci 42:6067–6073

90. Wei H, YanJun Y, NingTao L et al (2011) Application and safety assessment for nano-composite materials in food packaging. Chinese Sci Bull 56:1216–1225
91. Schmidt B, Petersen JH, Koch CB et al (2009) Migration of nanosized layered double hydroxide platelets from polylactide nanocomposite films. Food Addit Contam 26:1619–1627
92. Šimon P, Qasim C, Dušan B (2008) Migration of engineered nanoparticles from polymer packaging to food. A physicochemical view. J Food Nutr Res 47:105–113
93. Hoet PH, Bruske-Hohlfeld I, Salata OV (2004) Nanoparticles-known and unknown health risks. J Nanobiotechnology 2:12–27
94. Fievez V, Garinot M, Schneider IJ et al (2006) Nanoparticles as potential oral delivery systems of proteins and vaccines: a mechanistic approach. J Control Release 116:1–27
95. Kim YS, Kim JS, Cho HS et al (2008) Twenty-eight-day oral toxicity, genotoxicity, and gender-related tissue distribution of silver nanoparticles in Sprague-Dawley rats. Inhal Toxicol 20:575–583
96. Günter O, Eva O, Jan O (2005) Nanotoxicology: an emerging discipline evolving from studies of ultrafine particles. Environ Health Persp 113:823–839
97. Costantino U, Nocchetti M, Gorrasi G et al (2011) Hydrotalcites in nanobiocomposites. In: Lagaron JM (ed) Multifunctional and reinforced polymers for food packaging. Woodhead Publishing Ltd, Cambridge
98. http://www.fda.gov/MedicalDevices/ScienceandResearch/ucm-221171.htm. Accesed June 2011
99. Bawa R (2008) Nanoparticle-based therapeutics in humans. A survey. Nanotechnol Laws Bus 5:1–21

Chapter 16
Biodegradation and Applications of Nanobiocomposites

Melissa A. L. Nikolić, Katherine Dean and Peter J. Halley

Abstract This chapter summarizes the state of the art in biodegradation and applications of nanobiocomposites. Specifically we examine the biodegradation of various biopolymer nanocomposite classes (starch, PLA, PCL and PHA matrix polymers) in various environments (soil, compost, marine) and then discuss the development of new biodegradation standards. We then examine applications and research focused to new applications for the same range of materials, before focusing on some key application areas. It is clear that development of nanobiocomposites in a systematic, tailored fashion increases the application areas whilst maintaining biodegradability in various environments for a range of biopolymer matrices.

16.1 Biodegradation

Biodegradation is a process of degradation, which is initiated or propagated by microorganisms such as fungi and bacteria. For a polymer to be labeled biodegradable, it is important that polymer fractions are assimilated by microorganisms and completely mineralized into carbon dioxide, water and biomass, without

M. A. L. Nikolić
School of Chemistry, Physics and Mechanical Engineering,
Cooperative Research Centre for Polymers,
Queensland University of Technology, Brisbane 4001, Australia

K. Dean
CSIRO Materials Science and Engineering, Private Bag 33,
Clayton South MDC, VIC 3168, Australia

P. J. Halley (✉)
Australian Institute for Bioengineering and Nanotechnology,
The University of Queensland, Brisbane, Qld 4072, Australia
e-mail: p.halley@uq.edu.au

L. Avérous and E. Pollet (eds.), *Environmental Silicate Nano-Biocomposites*,
Green Energy and Technology, DOI: 10.1007/978-1-4471-4108-2_16,

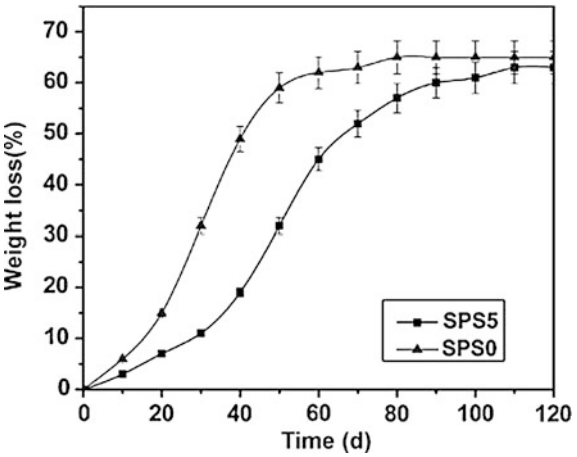

Fig. 16.1 The weight loss of starch/PVA/nano-SiO_2 with 0 wt% of SiO_2 (SPS0) and 5 wt% SiO_2 (SPS5) after 120 days incubation. Reproduced from Tang et al. [2] with permission from ©Elsevier Ltd. 2008

leaving any toxic residue. Biodegradation testing follows inoculation of test materials in environmental samples such as soil, compost, sewage, fresh or marine water under simulated or real-time exposure conditions [1].

16.2 Biodegradation of Nanobiocomposites in Different Environments

16.2.1 Starch

A number of authors have investigated the effects of different nanoparticles on the biodegradation rates of the starch nanocomposites they form. The results were shown to vary depending on the biodegradation environment, nanoparticle type and loading.

16.2.1.1 Soil

Tang et al. [2] studied several starch/polyvinyl alcohol (PVA)/nano-silicon dioxide (SPS) biodegradable blend films prepared by a solution casting method. The soil burial test showed that the addition of 5 wt.% nano-SiO_2 had no significant influence on the biodegradability of the films in soil—see (Fig 16.1).

16.2.1.2 Compost

Nayak et al. [3] have investigated the biodegradation of thermoplastic starch/polybutylene adipate-co-terephthalate (TPS/PBAT) blends at various TPS contents (10, 20, 30 & 40 wt.%) with two different organically modified nanoclays: Cloisite

20A (C20A) and Cloisite 30B (C30B) at 1, 3 & 5 wt.% respectively. To improve the interfacial adhesion properties, the interfacial region between the polymer and nanoclay were modified by grafting maleic anhydride (MA) with PBAT chains during melt blending via a two stage reactive extrusion process, followed by solvent casting to form thin films of these materials. The PBAT/TPS30wt.%/C30B3wt.% formulation showed the maximum tensile modulus and elongation at break, which the authors attributed to the intercalation of silicate layers resulting from similarity in the surface polarity and interactions of C30B with TPS. WAXD and SEM techniques were used to study the morphology of the PBAT/TPS30wt.%/C30B3wt.% formulation. These results showed an improvement in intercalation and dispersion of starch within PBAT by the incorporation of nanoclay C30B. The biodegradability of the following film samples were evaluated in controlled compost at 58 °C: PBAT, TPS/PBAT, PBAT/TPS/C30B and TPS/MA-g-PBAT/PBAT, with cellulose being used as the positive reference and polyethylene as the negative control in the experiment. Beyond the incubation time of 130 days, only a slight increase in the rate of biodegradation could be observed for the TPS/PBAT/C30B formulation. Therefore, it was observed that the rate of degradation of PBAT matrix increased with the incorporation of TPS/nanoclay.

16.2.1.3 Marine and Freshwater

Spiridon et al. [4] studied the role of α-amylase in biodegradation of PVA/starch blends containing different nanoparticles. A range of montmorillonite (MMT) silicate nanoparticles (Nanocor I28, Bentonite, Peruvian nanoclay) were incorporated into PVA/starch blends from 1–5 wt.%. The individual diameter of the nanoclay platelets was approximately 1 μm with an aspect ratio of 1000:1. The Bentonite was a smectic MMT with chemical formulae $Al_2.4SiO_2.H_2O$ and the Peruvian nanoclay was surface modified with inorganic cations. The amount of non-degraded residual blends containing nanoparticles suggests the possibility to optimize the material degradability by incorporation of nanoparticles. It has been established that biodegradation was mainly controlled by dissolution/erosion, while enzymatic degradation of starch also occurred. The biodegradation behavior of films depended on both the type and content of nanoparticles. The susceptibility of nanocomposite films to enzymatic degradation varied in the following order: PVA/starch/NanocorI28 > PVA/starch/Bentonite > PVA/starch/Peruvian nanoclay, as also supported by the water adsorption capacity, which is one of the main conditions for biodegradation. Figures 16.2, 16.3, 16.4 illustrate the key mass loss results for these materials.

During surface erosion, the α-amylase molecules agglomerate on the surface and scission of the α (1–4) glucose units occurs while, in the second stage, diffusion in the bulk takes place, indicative of advanced enzymatic degradation.

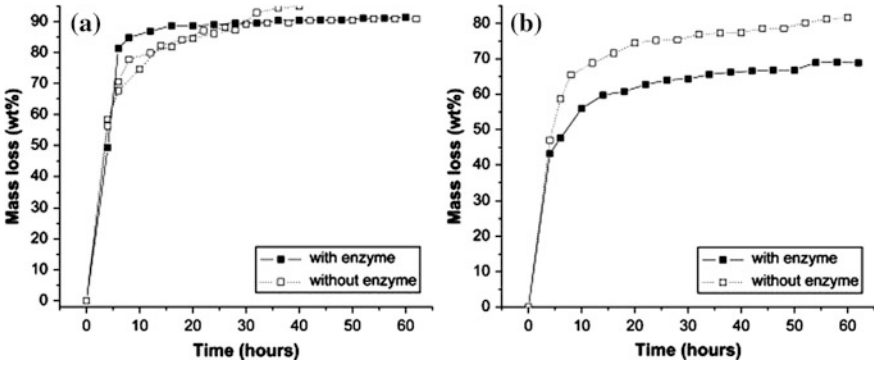

Fig. 16.2 Mass loss versus incubation time for **a** PVA/starch/1wt.% NanocorI28; **b** PVA/starch/5wt.% NanocorI28 nanocomposites. Reproduced from Spiridon et al. [4] with permission from ©Elsevier Ltd. 2008

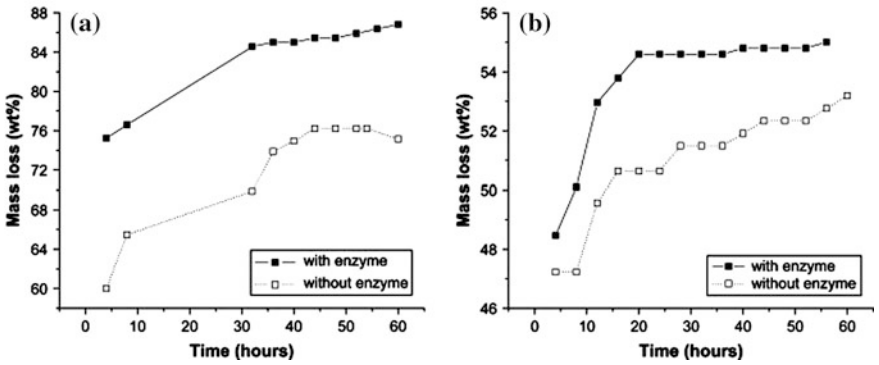

Fig. 16.3 Mass loss versus incubation time for **a** PVA/starch/1wt.% Bentonite; **b** PVA/starch/5wt.% Bentonite nanocomposites. Reproduced from Spiridon et al. [4] with permission from ©Elsevier Ltd. 2008

16.2.2 Polylactic Acid

A number of authors have reported how the inclusion of nanoparticles has affected the biodegradation rate of polylactic acid (PLA) [5–11], these typically report that the inclusion of nanoparticles (typically those which are more hydrophilic than the PLA itself) lead to enhanced rates of biodegradation.

16.2.2.1 Soil

A thorough but not exhaustive review of the literature found no information on the biodegradation of PLA/nanobiocomposites in soil.

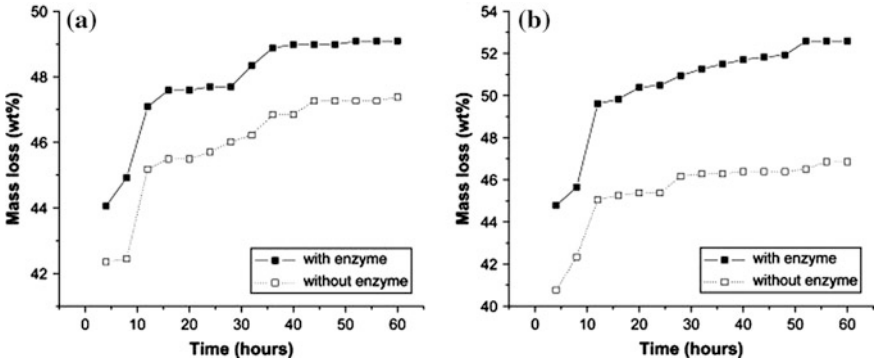

Fig. 16.4 Mass loss versus incubation time for **a** PVA/starch/1wt.% Peruvian nanoclay; **b** PVA/Starch/5wt.% Peruvian nanocomposites. Reproduced from Spiridon et al. [4] with permission from ©Elsevier Ltd. 2008

16.2.2.2 Compost

In a study by Ozkoc and Kemalogluthis [6], PLA and polyethylene glycol (PEG)-plasticized PLA nanocomposite films including 0, 3, and 5 wt.% montmorillonite nanoclay (Cloisite 30B) were prepared by melt intercalation using a laboratory scale compounder. The increase in the rate of biodegradation in a composting medium was found in the order of PLA > PLA/PEG >3wt.%Nanoclay/PLA/PEG >5wt.%Nanoclay/PLA/PEG >3wt.%Nanoclay/PLA.

Sinha Ray et al. [7, 12] also investigated the biodegradability of PLA nanocomposites containing different types of layered silicates (OMLS). They found that the biodegradability of neat PLA was enhanced significantly after incorporation of the layered silicate and was strongly dependent on the nature of the pristine layered silicates and the surfactant used to modify the layered silicate. Figure 16.5 shows the progression of biodegradation via carbon dioxide evolution and loss of molecular weight of PLA and various PLA/OMLS nanocomposites. The biodegradation of the PLA component in PLA/4wt.% fluromica with a dipolyoxyethylene alkyl (coco) methylammonium cation (MEE4) or PLA/4wt.% saponite modified with hexadecyltributylphosphonium cation (SAP4) was significantly enhanced. On the other hand, PLA/4wt.% montmorillonite modified with octadecylammonium cation (ODA4) showed only a marginal increase in biodegradation rate, while the rate of degradation of pure PLA and PLA/4wt.% montmorillonite modified with octadecyltrimethyl ammonium cation (SBE4) was almost the same. Sinha Ray et al. [12] suggested that different types of OMLS may thus cause a different mode of attack on the PLA component, further suggesting this might be due to the different ammonium salts used to organically modify the nanoclay.

Fukishima et al. [8] investigated the biodegradation of PLA containing two different organically modified montmorillonites, Cloisite 30B and Nanofil 804 at 5wt.% loading in a commercial compost. The addition of montmorillonites was found to increase the PLA degradation rate, particularly for Cloisite 30B due to its improved dispersion compared to Nanofil 804 within the PLA matrix.

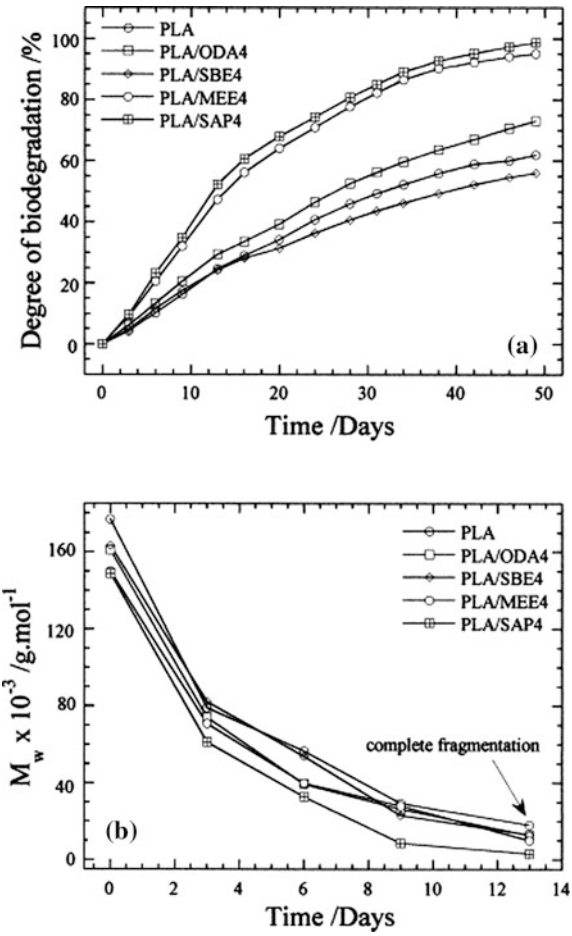

Fig. 16.5 **a** Degree of biodegradation (i.e. CO_2 evolution) and **b** change of matrix M_w of pure PLA and PLA with various nanocomposites investigated in compost. Reproduced from Sinha Ray et al. [12] with permission from ©Elsevier Ltd. 2003

Biodegradation by microorganisms isolated from the compost showed that bacterium *Bacillus licheniformis* was responsible for PLA biodegradation in compost. It was also found that nanoclays can influence the polymer bacterial degradation depending on their chemical structure and affinity of the bacterium towards the nanoclay [8].

Sangwan et al. [10] completed a more comprehensive study of the changes in microbial community structure and population during degradation of PLA/OMLS nanocomposites. Cloned gene sequences belonging to members of the phyla *Actinobacteria* and *Ascomycota* were the most dominant groups of microorganisms during biodegradation of PLA/OMLS nanocomposites. Due to their numerical abundance, members of these microbial groups are likely to play an important role during biodegradation process. Sangwan et al. [10] used novel molecular ecological techniques for in situ identification of new microorganisms involved in biodegradation of these PLA nanocomposite materials.

Sabet et al. [13] have studied the biodegradability of PLA and a PLA/PCL blend loaded with 3wt.% nanoclay (montmorillonite modified with methyl tallow bis-(2-hydroxyethyl) ammonium, commercial name DK2) in compost at 58 °C [13]. The results from this studied clearly showed that the incorporation of a nanoclay, increased the rate of hydrolytic degradation of PLA and the PLA/PCL blended material, compared to neat PCL and PLA/PCL with no nanoclay. However, the results indicate a longer induction time and rate of biodegradation for all the PLA/PCL/nanoclay nanocomposite materials in comparison with their counterpart PLA/nanoclay nanocomposites. This effect is observed due to the lower rate of PCL biodegradation dispersed throughout the PLA matrix. Sabet et al. [13] also concluded that blending PLA with PCL weakens the oxygen gas-barrier property, impacting on the rate of biodegradation, even though optimization of mechanical properties was obtained.

16.2.2.3 Marine and Freshwater

Paul et al. [11] studied the hydrolytic degradation of polymer layered silicate nanocomposites based on a PLA matrix and OMLA in phosphate buffer solution for more than 5 months. Three difference OMLS systems were incorporated into the PLA matrix at a 3wt.% loading: a natural unmodified montmorillonite/Na^+ nanoclay (Cloisite Na^+), montmorillonite organo-modified either by 2-ethylhexyl (hydrogenated tallow alkyl) ammonium cations (Cloisite 25A) and Cloisite 30B. Cloisite Na^+ led to the formation of a microcomposite, whereas intercalated nanocomposites were obtained with Cloisite 25A and Cloisite® 30B in the PLA matrix. The most rapid rate of PLA hydrolysis was observed for the PLA/Cloisite Na^+ composite, due to the higher hydrophilicity of the nanoclay compared to Cloisite 25A and Cloisite 30B. At the end of the hydrolytic study, the PLA chains extracted from the PLA/Cloisite Na^+ composite exhibited a 93.1 % decrease in their initial chain length. During the hydrolytic degradation study, all PLA composites turned white and became extremely brittle, particularly the PLA/Cloisite Na^+ composite. The crystallinity of the unfilled PLA sample was consistent throughout the hydrolytic study, however the degree of crystallinity was greatest for the PLA/Cloisite Na^+ nanobiocomposite, followed by PLA/Cloisite 30B. PLA/Cloisite 25A exhibited the lowest degree of crystallinity, due to the decrease in the water diffusion throughout the PLA matrix. Overall, the relative hydrophilicity of the nanoclay layers was shown to play a key role in the hydrolytic degradation of the PLA chains.

16.2.3 Polycaprolactone

PCL/nanobiocomposites provide significant overall improvements in the processability, thermal, mechanical moisture barrier and gas permeability properties, in comparison to neat polycaprolactone (PCL) [14–19].

Several authors have investigated the biodegradability PCL containing nanocomposites such as organo-nanoclays, in diverse biodegradation environments. These research findings have been summarized in the sections below.

16.2.3.1 Soil

A thorough but not exhaustive review of the literature found very limited information on the biodegradation of PCL/nanobiocomposites in soil. The paragraph below summarizes the findings that were obtained on this topic.

Ratto et al. [20] have investigated the biodegradability of a range of PCL/nanoclay nanocomposite materials in soil, where the amount of nanoclay was varied from 5 to 25wt.%. The biodegradability results showed that mineralization reached 50 % in 50 days for PCL/nanoclay combinations, whereas after the same duration, neat PCL had only reached 10 %. No change in glass transition temperature of the PCL was identified with the addition of nanoclay from Dynamic Mechanical Analysis; however X-ray diffraction patterns demonstrated varying degrees of intercalation in the silicate layers of the nanoclay. Farrell et al. [21] have also investigated the rate of biodegradation of co-extruded nanocomposites, comprised of PCL and an organically modified nanoclay nanocomposite in soil, compost and marine environments. PCL of molecular weight's 83,000 and 43,000 Da were mixed with synthetically modified montmorillonite nanoclay at 2 and 5wt.%, followed by extrusion in a twin screw extruder into pellets. A multi-layering technology was used to co-extrude the pellets into 15-inch wide films from a 256 and 1024 layer die multiplier configuration. The biodegradation results of these materials investigation in soil showed that the rate of biodegradation was significantly accelerated with the incorporation of selective nanocomposites into the PCL.

16.2.3.2 Compost

Fukushima et al. [9] have evaluated the biodegradation of PCL/sepiolite in compost. The PCL/sepiolite material was prepared by melt mixing the components in an internal mixer at 75 °C for 5 min, manually extracted from the mixer and then air cooled then milled into a fine powder using a rotary mill. Films of thickness 0.6 mm were obtained by compression molding at 120 °C for 5 min.

During the compost biodegradation study of PCL/sepiolite composites (dimensions 20 × 6 × 0.6 mm^3), the temperature was kept constant at 40 °C and relative humidity 50–70 %. At pre-determined time intervals, samples were extracted from the compost, which was composed of pruning residues, wood chips, dried leaves and straw, washed with water to remove compost material and then dried at room temperature until constant sample weight was obtained. Several methods and techniques were used to evaluate the overall biodegradation of the PCL/sepiolite materials, such as optical microscopy, Fourier Transform Infrared

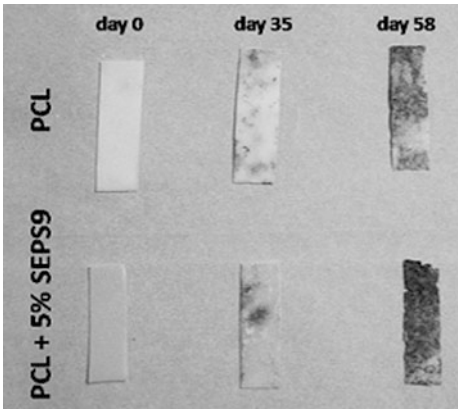

Fig. 16.6 The change in physical morphology for neat PCL and PCL/sepiolite (PCL/SEPS9) film, after burial in compost for 0, 35 and 58 days. Reproduced from Fukushima et al. [9] with permission from ©Elsevier Ltd. 2010

Spectroscopy (FTIR), Size Exclusion Chromatography (SEC) and Differential Scanning Calorimetry (DSC). Figure 16.6 illustrates the change in physical morphology for neat PCL and PCL/sepiolite film, after burial in compost for 0, 35 and 58 days. The optical microscopy results indicated that the PCL/sepiolite and neat PCL showed preferential inhomogeneous surface degradation.

As shown here in Fig. 16.7, measurement of the residual sample mass as a function of degradation time in compost, indicated that approximately 50 % weight loss of PCL and PCL/sepiolite samples was achieved after 100 days in compost. The rate and extent of PCL degradation was not significantly affected by the addition of sepiolite at 5wt.% to the PCL.

More recently, Fukushima et al. investigated the biodegradation of melt-blended PCL based nanocomposites, by the addition of three different types of fumed silica [22]. Fumed silica was used as a filler to improve the UV resistance as well as the thermal and rheological properties of the polymer. The residual mass data for PCL and PCL fumed silica samples, indicate that the presence of fumed silica did not significantly impact on the rate of PCL degradation. This result is evident from the interpretation of Fig. 16.8.

Previous investigations by Fukushima et al. [9] on the biodegradability of PCL/nanocomposites in compost were performed by comparing two commercial modified montmorillonite nanoclays Cloisite 30B and Nanofil804.

The results from this study, reproduced here as Fig. 16.9, indicate that the presence of these modified montmorillonite nanoclays does not significantly affect the rate of polymer degradation. Additionally, the data presented in Fig. 16.9 suggests that the rate and extent of PCL degradation is significantly reduced after 6 weeks burial in compost. The authors have indicated that the data obtained after 6 weeks burial is not as reliable, due to the difficulty to accurately remove all degraded material after this point [9].

In most cases, the biodegradability of PCL blends containing a nanobiocomposite has not been evaluated. Predominantly, investigations on PCL blends with nanobiocomposite have focused on the optimization of the mechanical, thermal and gas barrier properties [23–27].

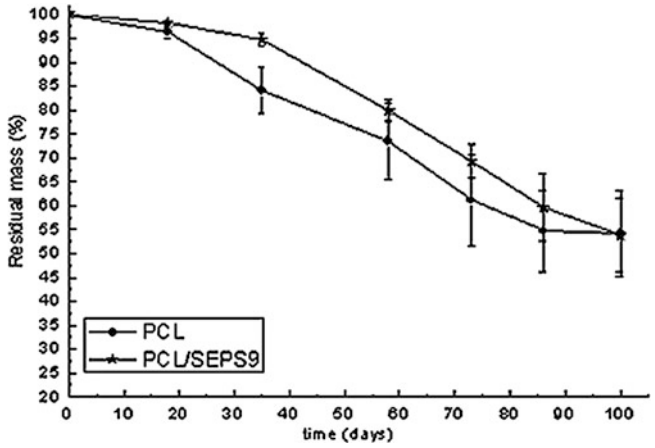

Fig. 16.7 Residual mass for neat PCL and PCL/sepiolite as a function of burial time in compost. Reproduced from Fukushima [9] with permission from ©Elsevier Ltd. 2010

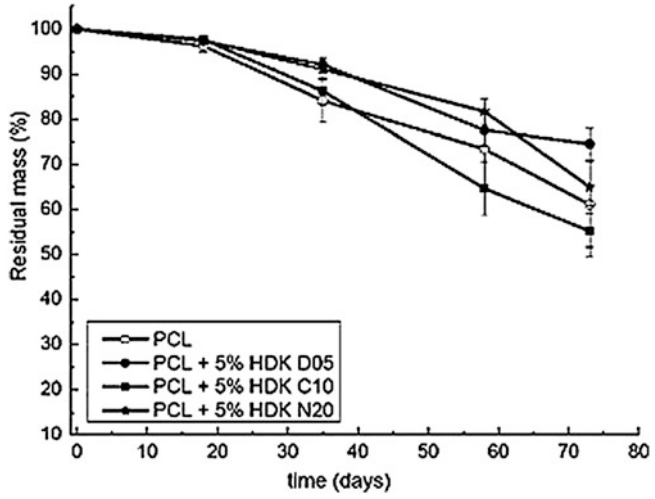

Fig. 16.8 Residual mass of PCL and PCL/fumed silica nanocomposite samples, as a function of burial time in compost. Reproduced from Fukushima [22] with permission from ©Elsevier Ltd. 2011

16.2.3.3 Marine and Freshwater

Farrell et al. investigated the biodegradation of PCL/nanoclay (a synthetically modified montmorillonite nanoclay) in marine conditions containing natural populations of microbes at 22 °C [21].

Prior to the biodegradation study, films of neat PCL (80 kDa) and PCL/5wt.% nanoclay were prepared and dried. Films were then placed in triplicate flasks

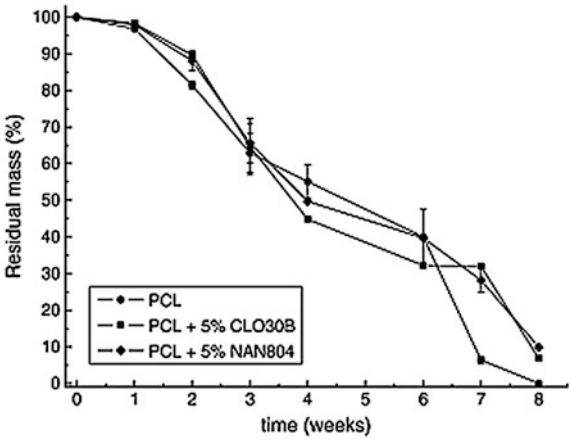

Fig. 16.9 Residual mass of neat PCL, PCL/5 % Cloisite30B and PCL/NANOFIL804 materials as a function of degradation time in compost. Reproduced from Fukushima [9] with permission from ©Elsevier Ltd. 2010

containing aerated natural seawater, where the seawater remained aerobic throughout the incubation period. The films were evaluated under two nutrient conditions: (a) unsupplemented and (b) supplemented with 5.0 mg/L nitrogen (as NH4Cl) and 1.0 mg/L phosphorous (as KH_2PO_4). For the neat PCL films of an initial thickness of 25.4 μm, 90 % weight loss was observed after 8 days whilst being agitated at 200 rpm. The 76.2 μm thick neat PCL sample exhibited 60 % weight loss after 8 days incubation. Films that were not agitated during incubation exhibited a considerably lower mass loss as expected. The same trend was observed between agitated and non-agitated degradation studies for the PCL/5wt.%nanoclay system. After a 2-day incubation period, the PCL/5wt.%nanoclay film of approximately 25 μm in thickness exhibited an 80 % weight loss—significantly higher than that observed for neat PCL of the same thickness after 2 days incubation period.

After conducting the biodegradation study for approximately 30 days, the percentage of overall biodegradation was marginally higher for the PCL/nanoclay material compared to neat PCL.

16.2.4 Polyhydroxyalkanoates

Many studies have been reported on the use of nanobiocomposites to improve the mechanical, permeability to gases and liquids, crystallization and thermal properties of polyhydroxyalkanoates (PHAs), such as poly(3-hydroxybutyrate-co-3-hydroxyvalerate) (PHBV) [28–35] and polyhydroxybutyrate (PHB) [28, 31, 36–53]. However, there is limited literature available on the biodegradation of PHA based nanocomposites in various degradation environments. Within this section, investigations that have been performed on the biodegradation of PHA-based nanobiocomposites are summarized.

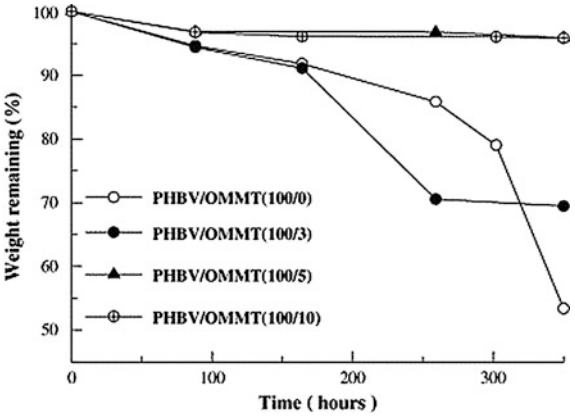

Fig. 16.10 Sample mass remaining of PHBV and PHBV/OMMT nanocomposites after biodegradation trials in a soil suspension. Reproduced from Wang et al. [54] with permission from ©Elsevier Ltd. 2005

16.2.4.1 Soil

Wang et al. [54] have investigated the biodegradability of PHBV based organophilic montmorillonite (PHBV/OMMT) nanocomposites in a soil suspension. The PHBV/OMMT mixtures were prepared using a solution intercalation method, using chloroform as the solvent to make the final PHBV/OMMT solutions at weight ratios of 100/0, 100/1, 100/3, 100/5, 100/7, 100/10 respectively. Dispersion of the OMMT in the PHBV was further developed using ultrasonication for 3 h followed by aging for 4 days with periodic stirring and final heating at 60 °C for 1 h. The PHBV/OMMT films were cast into a glass dish and dried under constant vacuum at 40 °C, where the final thickness of the film was 0.6–0.8 mm.

A soil sample was taken from the topsoil of a farm site in China, where there was no previous history of PHBV exposure to the soil, followed by combination and dispersion with a salt solution. Each PHBV/OMMT sample was placed in the soil suspension, repeated in triplicate and incubated at 28 °C under aerobic conditions. Once samples were removed from the soil suspension, the films were washed with 75 % ethanol in water, to prevent the continuation of microbial attack to the material and then dried to constant weight under vacuum. Dried films were weighed and morphological changes were observed using SEM. Additionally, a bacterial count on the number of PHBV-degrading microorganisms in the soil was performed.

The results from this study, adapted here as Fig. 16.10, have shown that after exposing PHBV/OMMT samples to the soil suspension for up to 350 h, the weight loss of neat PHBV was 46.62 % and for PHBV/OMMT samples 100/3, 100/5 and 100/10 were 30.53, 4.12 and 4.18 % respectively. These results indicate that the rate and extent of PHBV biodegradability in a soil suspension decreased significantly as the amount of OMMT in the PHBV matrix was added at 5 and 10wt.%.

SEM micrographs of samples 100/0, 100/3 and 100/5 before and after biodegradation in the soil suspension, adapted here as Fig. 16.11, show smoother film topography with increased loading of OMMT in the PHBV. The SEM micrographs and mass loss data are in agreement, suggesting that the addition of OMMT

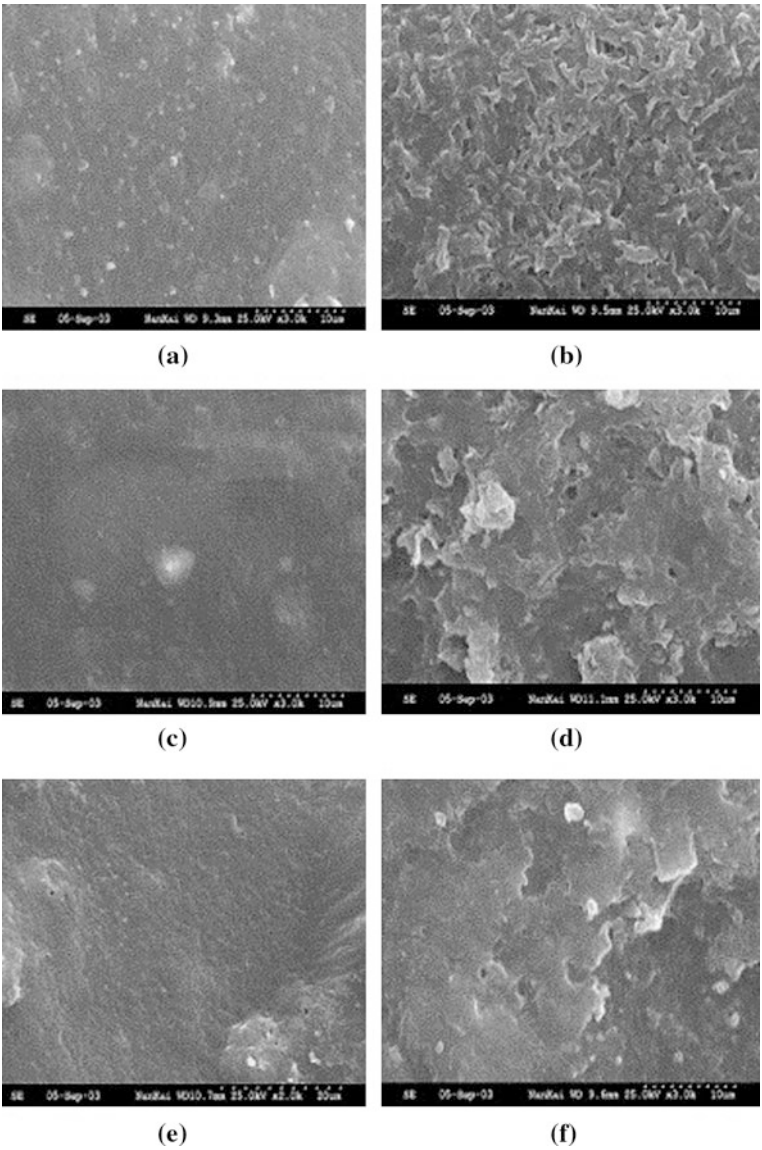

Fig. 16.11 Scanning electron micrograph of PHBV and PHBV/OMMT nanocomposites before and after biodegradation. **a** 100/0 before biodegradation; **b** 100/0 after biodegradation for 350 h; **c** 100/3 before biodegradation; **d** 100/3 after biodegradation for 350 h; **e** 100/5 before biodegradation; **f** 100/5 after biodegradation for 350 h. Reproduced from Wang et al. [54] with permission from ©Elsevier Ltd 2005

nanocomposites hindered the biodegradation of the PHBV. The proliferation of PHBV-degrading bacteria increased during the biodegradation of PHBV/OMMT materials in the soil suspension. Initially, the number of PHBV-degrading bacteria

in the soil suspension was the same for PHBV and PHBV/OMMT (100/3) nanocomposite trials at 5.28×10^3 counts/mL. After biodegradation of these materials in the soil suspension for 350 h, the number of PHBV-degrading bacteria increased by orders of magnitude to 1.40×10^9 counts/mL for neat PHBV and 2.30×10^8 counts/mL for PHBV/OMMT sample 100/3. These results exemplified that the proliferation of PHBV degrading bacteria and extent of PHBV biodegradation correlated, where higher numbers of PHBV-degrading bacteria on the composite sample resulted in a higher extent of PHBV biodegradation.

16.2.4.2 Compost

A conclusive but not exhaustive search of the literature found very little available literature on the biodegradation of PHB/nanocomposites in compost. However, Maiti et al. [55] investigated the biodegradation of melt extruded PHB with the incorporation of a tallow organically modified fluoromica nanoclay at 2wt.%, (referred to as PHBCN2 in the publication) in compost. Post melt extrusion PHB/organonanoclay samples were compression molded followed by rapid quenching in liquid nitrogen to maximize the amorphous content of the polymer, then cut into square samples of dimensions $30 \times 30 \times 1$ mm^3. The biodegradation of the neat PHB and PHB/CN2 was investigated at two different temperatures; room temperature and 60 °C, in a sealed chamber at constant humidity of approximately 85 % in compost manure. The progression of polymer degradation was monitored by measuring the mass loss of the polymer, morphological changes with SEM and changes in the spherulite size with biodegradation.

The rate and extent of PHB biodegradation in compost was significantly increased with the incorporation of the tallow organically modified layered silicate (Fig. 16.12) with close to 100 % biodegradation at room temperature within 7 weeks for PHB/CN2. Additionally, the degradation profile of neat PHB compared to PHB/CN2 are different, where there is a far more pronounced initial lag phase for the biodegradation of neat PHB compared to PHB/CN2 where the initial rate of biodegradation is close to a linear relationship.

Additionally, the temperature has a significant effect on the biodegradation of PHB/organonanoclay materials under compost conditions. It is important to note that the T_g of PHB with nanocomposites is approximately 16 °C. At 60 °C, the rate of biodegradation of PHB and PHB/CN2 is much slower, attributed to the lower concentration of microorganisms that may be present at 60 °C. The rate of biodegradation at 60 °C decreased 2–3 times compared with biodegradation of identical samples at room temperature.

As part of the same biodegradation study, Maiti et al. [55] investigated the impact of crystallinity on the biodegradation, by crystallizing samples at two different temperatures of 100 and 125 °C before burial of the nanobiocomposites in compost. From these results, it was clear that when the neat PHB and PHB/CN2 were crystallized at 100 °C, the spherulites of PHB/CN2 were much smaller than those of neat PHB crystallized at the same temperature. It was evident from these results that the nanoclay improved nucleation of the crystal spherulites.

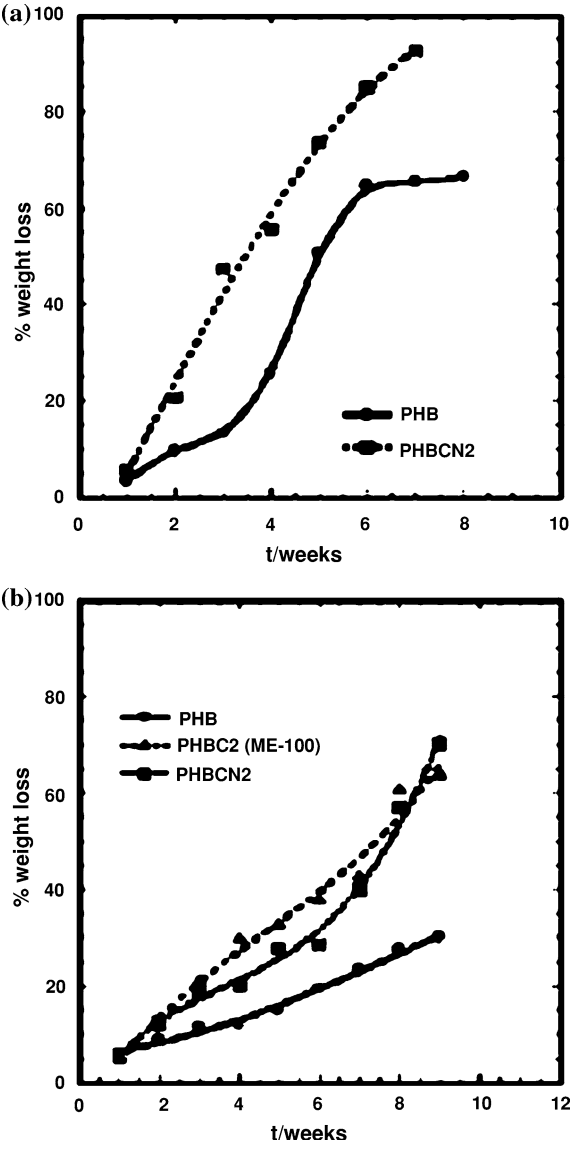

Fig. 16.12 Percentage weight loss during biodegradation in the compost media **a** at room temperature (RT) and **b** at 60 °C. Reproduced from Maiti et al. [55] with permission from ©American Chemical Society, 2007

Figure 16.13 shows the polarized optical images demonstrating the difference in spherulite size for PHB and PHB/CN2 crystallized at 100 °C, before and after 6 weeks biodegradation in compost. It is also evident from examination of Fig. 16.13 that sample PHB/CN2 was significantly more biodegraded compared with neat PHB under the same conditions. The spherulite morphology of neat PHB appears to remain intact. Therefore, the more rapid rate of biodegradation of PHB/CN2 is attributed to the smaller spherulites and higher interspherulitic area.

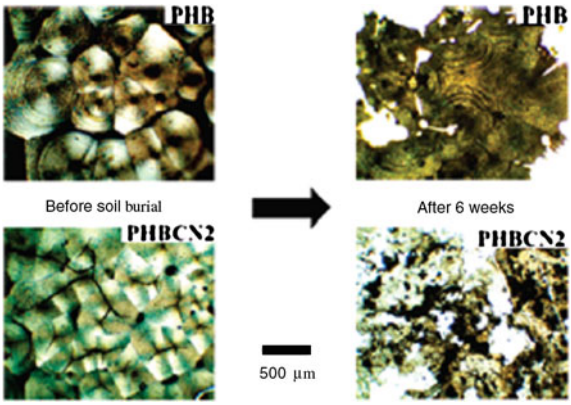

Fig. 16.13 Polarizing optical images of PHB and PHB/CN2 before and after 6 weeks of biodegradation in a compost medium. The samples were crystallized at 100 °C prior to composting. Reproduced from Maiti et al. [55] with permission from the ©American Chemical Society, 2007

For neat PHB and PHB/CN2 crystallized at the higher temperature of 125 °C, the spherulite size in both samples was much larger compared to effects observed at 100 °C. After exposing neat PHB and PHB/CN2 crystallized at these conditions to compost for 8 weeks, the spherulite morphology remained intact, apart from some cracking of PHB/CN2 spherulites, due to mechanical distortion in compost, shown here in Fig. 16.14. Therefore, Maiti et al. concluded that the rate of biodegradation of PHB/organonanoclay materials may be tailored by modifying the temperature of crystallization.

16.3 Biodegradation Standards Development

There are several standard test methods and drafts available (Table 16.1), which are frequently used to assess biodegradability of polymers by measuring molecular weight and molecular weight distribution, tensile properties, weight loss, extent of fragmentation, enzyme assays, biochemical oxygen demand, carbon dioxide production and ecotoxicity. A combination of test procedures can be used during evaluation to confirm that biodegradation has actually occurred. The selection of test methodology should be based on potential fields of application of the test polymer and its fate at the end i.e. compost, soil, fresh or marine water. Some of the widely used standards are: AS4736; ASTM D5338; ASTM D6002; EN 13432; ISO 14855 (for compost exposure), ASTM D5988; ISO 17556 (for soil exposure) and ASTM D6691; ASTM D6692; ISO 15314; ISO 16221 (for marine exposure).

The European standard for biodegradability is EN 13432. This norm standard is a reference point for all European producers, authorities, facility managers and consumers. The standard specifies requirements and procedures to determine the compostability of plastic packaging materials based on four main areas, biodegradability; disintegration during biological treatment; effect on the biological treatment process; and effect on the quality of the resulting compost. This standard can apply to other packaging materials in addition to polymers, and incorporates following tests and standards, ISO 14855; ISO 14852; ASTM D5338-92; ASTM

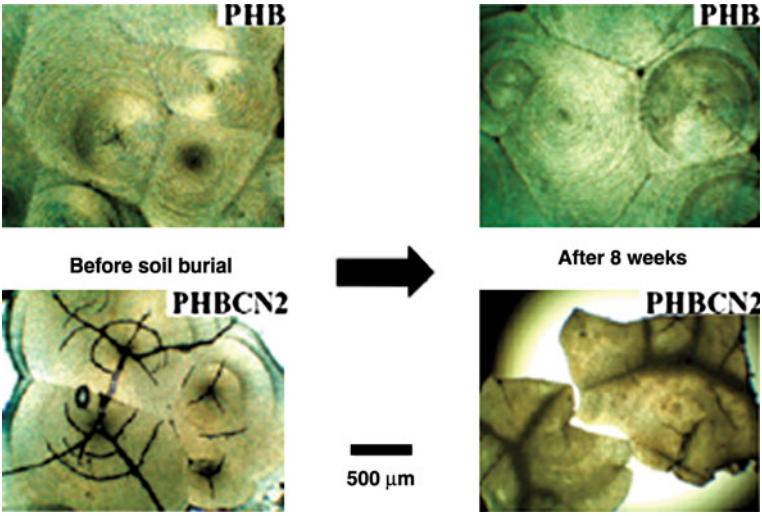

Fig. 16.14 Polarizing optical images of PHB and PHB/CN2 before and after 8 weeks of biodegradation in a compost medium. The samples were crystallized at 125 °C prior to composting. Reproduced from Maiti et al. [55] with permission from the ©American Chemical Society, 2007

D5511-94; ASTM D5152-92; ASTM E1440-91; modified OECD 207; and CEN TC 261/SC4/WG2.

In this test procedure polymers are exposed to environments in standard biometric test methods to measure the rate and degree of biodegradation. After this biodegradation stage, the end-residues are subjected to aquatic and terrestrial toxicity tests (E1440, OCED guideline 207 and OCED guideline 208) to ensure that they are environmentally benign and not persistent. Each degradation stage is independently evaluated to allow a combined evaluation of a polymer's environmental performance under controlled laboratory setting. According to the standard, the results of laboratory exposure cannot be directly extrapolated to estimate absolute rate of deterioration by the environment because the acceleration factor is material dependent and can be significantly different for each material and for different formulations of the same material. However, exposure of a similar material of known outdoor performance (a control) at the same time as the test specimens, allows comparison of the durability relative to that of the control under the test conditions.

16.4 Application Areas of Nanobiocomposites

The drive toward more sustainable and low carbon footprint polymer materials has seen the development of bio-based polymers. However the inherent drawbacks of bio-based polymers have been found such as poor stability, mechanical properties and barrier properties, which have limited their use in wider applications. At the

Table 16.1 Selected list of published standards for biodegradation

Standard	Description
AS 4736–2006	Biodegradable plastics—biodegradable plastic suitable for composting and other microbial treatment
ASTM D6954–04	Standard guide for exposing and testing plastics that degrade in the environment by a combination of oxidation and biodegradation
ASTM D5209–92	Standard test method for determining the aerobic biodegradation of plastic materials in the presence of municipal sewage sludge
ASTM D5338–98	Standard test method for determining aerobic biodegradation of plastic materials under controlled composting conditions
ASTM D5526–94	Standard test method for determining anaerobic biodegradation of plastic materials under accelerated landfill conditions
ASTM D5951–96 (2002)	Standard practice for preparing residual solids obtained after biodegradability standard methods for plastics in solid waste for toxicity and compost quality testing
ASTM D5988–03	Standard test method for determining aerobic biodegradation in soil of plastic materials or residual plastic material after composting
ASTM D6002–96	Standard guide for assessing the compostability of environmentally degradable plastics
ASTM D6340–98	Standard test methods for determining aerobic biodegradation of radiolabeled plastic materials in an aqueous or compost environment
ASTM D6400–99	Standard specifications for compostable plastics
ASTM D6691–01	Standard test method for determining aerobic biodegradation of plastic materials in the marine environment by a defined microbial consortium
ASTM D6692–01	Standard test method for determining biodegradability of radiolabeled polymeric plastic materials in seawater
ASTM D7081–05	Standard specifications for non-floating biodegradable plastics in the marine environment
DIN V 54900–2	Testing of compostability of plastics—part 2: testing of the complete biodegradability of plastics in laboratory tests
EN 13432:2000	Requirements for packaging recoverable through composting and biodegradation—Test scheme and evaluation criteria for the final acceptance of packaging
EN 14045:2003	Packaging—evaluation of the disintegration of packaging materials in practical oriented tests under defined composting conditions
EN 14046:2003	Packaging—evaluation of the ultimate aerobic biodegradability of packaging materials under controlled composting conditions—method by analysis of released carbon dioxide
EN 14047:2002	Packaging—determination of the ultimate aerobic biodegradability of packaging materials in an aqueous medium—method by analysis of evolved carbon dioxide
EN 14048:2002	Packaging—determination of the ultimate aerobic biodegradability of packaging materials in an aqueous medium—method by measuring the oxygen demand in a closed respirometer
EN 14806:2005	Packaging—preliminary evaluation of the disintegration of packaging materials under simulated composting conditions in a laboratory-scale test

(continued)

Table 16.1 (continued)

Standard	Description
ISO 14851:1999	Determination of the ultimate aerobic biodegradability of plastic materials in an aqueous medium—method by measuring the oxygen demand in a closed respirometer
ISO 14852:1999	Determination of the ultimate aerobic biodegradability of plastic materials in an aqueous medium—method by analysis of evolved carbon dioxide
ISO 14855:1999	Determination of the ultimate aerobic biodegradability and disintegration of plastic materials under controlled composting conditions—method by analysis of evolved carbon dioxide
ISO 14593:1999	Water quality—evaluation of the ultimate aerobic biodegradability of organic compounds in aqueous medium—method by analysis of inorganic carbon in sealed vessels (CO_2 headspace test)
ISO 16221:2001	Water quality—guidance for the determination of biodegradability in the marine environment
ISO 16929:2002	Plastics—determination of the degree of disintegration of plastic materials under defined composting conditions in a pilot-scale test
ISO 17556:2003	Plastics—determination of the ultimate aerobic biodegradability in soil by measuring the oxygen demand in a respirometer or the amount of carbon dioxide evolved
ISO 20200:2004	Plastics—determination of the degree of disintegration of plastic materials under simulated composting conditions in a laboratory-scale test
CEN/TR 15822	Plastics—biodegradable plastics in or on soil—Recovery, disposal and (under approval) related environmental issues

same time polymer nanocomposite materials have been developed that offer improved functionality and properties, such as improved barrier properties, strength, elasticity, optical clarity and antimicrobial properties. Thus it is clear why much new exciting research and development has focused on the development of nanocomposite bio-based and/or biodegradable materials (nanobiocomposites) to overcome the inherent drawbacks of pure biopolymers and widen application areas for nanobiocomposites.

This section will review key advances in specific types of nanobiocomposites—highlighting key property advances that will lead to new applications—and then the specific application areas that will be attractive to nanobiocomposites will be described.

16.4.1 Starch Nanobiocomposite Advances

Starch is an inexpensive and abundant natural material and currently much research on nanobiocomposites focuses on starch nanobiocomposites. Native starch is a mixture of linear amylose and a highly branched amylopectin macromolecules, and its mechanical and physical properties are poor. However the incorporation of plasticizers and the application of heat and shear produce thermoplastic starch (TPS) which has improved properties and enables its processability via extrusion, injection molding, film blowing and blow molding material, similar to many conventional synthetic thermoplastic polymers. However, TPS can still have limitations such as high water-sensitivity and poor mechanical and barrier properties at high moisture contents [56, 57], limiting their use in biodegradable packaging applications.

The addition of nanoparticles has been shown to modify the crystallization kinetics, the crystalline morphology, the crystal form, and the crystallite size, which in turn significantly changed the overall mechanical and physical properties of the material [58], improving their potential use in biodegradable packaging applications.

The addition of nanoclays exhibiting good exfoliation in the TPS matrix, have been shown to result in materials with significantly improved mechanical properties [59–66], however as pointed out by Pandey et al. [66], overall all TPS nanobiocomposites were very brittle compared to conventional plastics used in packaging applications. Additionally, an improvement in moisture barrier properties for starch nanobiocomposites has been observed [67–76].

16.4.2 PLA Nanocomposite Advances

Historically PLA was first produced in 1845, and recently (2002) a 140 t/yr PLA production plant was developed by Natureworks, USA. PLA has been processed via injection molding, film blowing and blow molding but initial formulations

reported poor impact strength and heat resistance, poor mechanical properties and high moisture sensitivity, which restricted applications to flexible packaging. Recent developments have seen an increase in PLA blended with proteins, starch and PHA (Cereplast), with PCL and ethylene vinyl alcohol and very recently in research areas with nanocomposites. Whilst there are currently no commercial PLA nanocomposite products on the market, PLA nanobiocomposites have a high potential for use as renewable packaging.

Rhim et al. [77] examined a range of PLA-based composite films for potential use in packaging applications, with different types of nanoclays such as Cloisite Na^+, Cloisite 30B and Cloisite 20A and found that the tensile strength and elongation at break decreased, depending on the type of nanoclay used. Among the nanoclay types used, Cloisite 20A was the most effective in improving the water vapor barrier property while sacrificing tensile properties the least. The PLA/Cloisite 30B composite film showed a bacteriostatic function against *Listeria monocytogenes*. Sanchez-Garcia and Lagaron [78] examined PLA nanocomposites prepared using cellulose nanowhiskers (CNW) for food packaging applications also. The results indicated that the CNW nanofiller was well dispersed in the PLA matrix and did not impair the thermal stability but induced the formation of transcrystallinity. Interestingly, the water permeability of nanobiocomposites based on PLA decreased with the addition of CNW, that were prepared by freeze drying by up to 82 % and the oxygen permeability by up to 90 %. Optimum barrier enhancement was found for composites containing loadings of CNW below 3wt.%. From the results, CNW exhibit novel significant potential in coatings, membranes and food agro-based packaging applications.

Recently Singh and Sinha Ray reviewed PLA nanocomposites research [79] focusing on nano-materials such as carbon nanotubes, cellulose nanowhiskers, hydroxyapatite, and layered silicates. The potential of PLA for biomedical applications, industrial applications, food packaging and other areas were also reviewed.

In one of the first studies of the potential applications of PLA nanobiocomposites, Sinha Ray et al. [80] and Sinha Ray et al. [81] examined PLA/OMLS nanocomposites, and reported intercalated stacked and disordered/exfoliated mica layers coexist in the nanocomposite. The nanocomposite showed improved materials properties and crystallization behavior with a simultaneous improvement in biodegradability, compared to neat PLA.

In terms of industrial film applications Katiyar et al. [82] highlighted the use of nanoclays to improve barrier properties in PLA films. PLA-magnesium aluminium layered double hydroxides (LDH) nanocomposites were formed by ring-opening polymerization to give good dispersion of LDH in the polymer. It was seen that PLA/LDH nanobiocomposites exhibited higher degradation onset temperatures however, the molecular weight of the PLA was significantly reduced when polymerized in situ in the presence of the LDHs. This result suggests chain termination via LDH surface hydroxyl groups and/or metal-catalyzed degradation has occurred.

Potschke et al. [83] has examined melt spun PLA/multi-walled carbon nanotube (MWNT) composites for potential use as electrically conductive fibers. Enhanced orientation of MWNT along the fiber axis was seen. In context with the targeted

application of leakage detection, fibers with low MWNT amount and low draw down ratio (as extruded fibers with 2wt.% MWNT) were found suitable for electronic applications.

Strange et al. [84] examined polymer photovoltaic devices prepared by an L-PLA substrate loaded with nanoclay in an attempt to improve the thermal properties and possibly reduce permeation of water and oxygen. It was found that L-PLA as a substrate holds potential, but there are several challenges (such as the planarity of the L-PLA surface, the mechanical stresses induced by the extrusion process, the limitation in processing temperature, and the limitation in the available range of solvents for solution processing) which must be met before general application within this field can be envisaged.

El-Kady et al. [85] examined the potential biomedical application of sol–gel derived bioactive glass (SG) nanoparticles in PLA/nanocomposites as bone engineering scaffolds. Results showed that by increasing the glass content in the scaffolds, the water absorption decreased, the weight loss increased and the cumulative ion concentrations released from them also increased, indicating the possibility of modulating the degradation rate by varying the glass/polymer ratio and enhancing their in vitro bioactivity. Ozkoc et al. [15] examined organonanoclay reinforced PLA/PVA blend porous nanocomposite scaffolds. It is seen that PVA acts as a polymeric porogen that enhances the state of dispersion of nanoclay particles resulting in an exfoliated structure. The porosities of all the scaffolds are higher than 70 % and the pores are well interconnected. The addition of nanoclay to the scaffolds also improves the compressive modulus and these nanocomposites are seen as good candidates for production of polymeric scaffolds for tissue engineering applications.

16.4.3 PCL Nanobiocomposite Advances

PCL is obtained by Ring Opening Polymerization of ε-caprolactone and is widely used as a PVC solid plasticizer, for polyurethane applications, as a carrier for controlled release of drugs and for soft compostable packaging. Different commercial grades are produced by Perstorp (CAPA™) or by Union Carbide (Tone®). Commercial PCL nanocomposite materials do not exist but the following summarizes possible future application areas, based on recent research advances.

Bugatti et al. [86] examined High Energy Ball Milling (HEBM) of nanomaterials into PCL. It was found that the nature and the position of the aromatic ring substituents to the nano-materials affect the value of the interlayer distance and the hydrogen bonds of the nano-hybrids. Exfoliation improved the mechanical and barrier properties and release kinetic of the benzoate-antimicrobial anions bound to LDH highlighted very good perspectives in the field of controlled release of active species (which was further extended in more recent work [87]).

Campbell et al. [18] highlighted pharmaceutical application potential for paracetamol loaded PCL with layered silicates (nanoclays) from using hot-melt extrusion.

The paracetamol crystals and layered silicates formed both intercalated and partially exfoliated nanocomposite morphologies depending on composition. The dissolution and initial burst effect were retarded slightly by the nanoclay. The highly dispersed nano-platelets hindered the mobility of PCL chains and alter the crystallization behavior of PCL.

Lee et al. [88] developed a method to produce homogeneous carbon nanotubes CNT/PCL nanocomposites with various and controllable CNT concentrations using an ionically-modified multi-walled CNT. The physicochemical and mechanical properties of the resultant nanocomposites were examined and the biological usefulness was highlighted.

In terms of foam packaging and biomedical applications, Liu et al. [89] examined biodegradable PCL/calcium carbonate ($CaCO_3$) nanocomposite foams. It was seen that cellular structure of nanocomposite foams changes with different $CaCO_3$ loading, that mean cell size achieved the minimum value at 5wt.% $CaCO_3$ loading, and cell wall thickness increased with $CaCO_3$ content. The changes in cellular structure and improvement of mechanical properties also enhanced the mechanical properties of PCL/$CaCO_3$ nanocomposite foams. Liu et al. [90] has recently extended this work to PCL/nanoclay nanocomposite foams, where the presence of the nanoclay enhanced several properties of the foam. The nanoclay used in the study was a montmorillonite modified by methyl tallow bis-2-hydroxyethyl ammonium. DSC results revealed that a maximum crystallinity was achieved with a 5wt.% loading of the nanoclay in the PCL, above which, the mobility of the PCL chains was reduced and the crystallization was hindered. The rheological properties of the PCL/nanoclay composites were investigated at the foaming temperature of 200 °C and the results revealed that a nanoclay loading up to 10wt.% showed a slight shear rate dependence, indicative of crosslinking behavior. Whereas at higher nanoclay loadings (>10wt.%), the shear rate dependence became more obvious. The loss modulus was almost unchanged for up to 10wt.% nanoclay in PCL and increased at 20 and 30wt.% loadings of the nanoclay in PCL. A rapid decline in the ductility of PCL/nanoclay was observed at nanoclay loadings greater than 10wt.%, due to a greater amount of intercalation and dispersion of the nanoclay or that there is a reduced gel fraction at higher nanoclay loadings. The compressive modulus of the PCL/nanoclay foams was measured and it was found that it increased until 10wt.% nanoclay and was maintained at higher nanoclay loadings of 20 and 30wt.%.

Roohani-Esfahani et al. [91] examined biomedical potential for a composite biphasic calcium phosphate (BCP) scaffold by coating a nanocomposite layer, consisting of hydroxyapatite (HA) nanoparticles and PCL, over the surface of BCP. Micro-computerized tomography studies showed that the prepared scaffolds were highly porous (similar to 91 %) with large pore size (400–700 μm) and an interconnected porous network of similar to 100 %. Needle shaped coated HA/PCL particles induced the differentiation of primary human bone derived cells, with significant up-regulation of osteogenic gene expression (Runx2, collagen type I. osteocalcin and bone sialoprotein) and alkaline phosphatase activity compared to other groups. These properties are essential for enhancing bone

ingrowth in load-bearing applications. The developed composite scaffolds possessed superior physical, mechanical, elastic and biological properties rendering them potentially useful for bone tissue regeneration. In terms of electrical and biomedical applications, Xiao et al. [92] examined electroactive shape memory nanocomposites from cross-linked PCL and conductive MWNT. The effect of MWNT functionalization was examined. Results showed that these nanocomposites could perform favorable shape memory recovery both in hot water and in electric fields. In addition, functionalized MWCT nanocomposites possessed more favorable properties such as mechanical, biocompatible, and electroactive shape memory functions.

16.4.4 PHA Nanobiocomposite Advances

PHAs were first discovered in 1926 and are a natural energy storage polymer of bacteria and plants. In the 1980s ICI developed Biopol (a polyhydroxybutyrate) via bioreactors. Biopol was sold to Monsanto in 1996, which was then sold to Metabolix in 1998. A joint venture Telles was formed in 2006 to develop PHB-based biopolymers under the name Mirel, where a 50,000 t/yr production plant opened in 2009. PHAs have traditionally has been used from flexible coatings to stiff packaging depending on the type of copolymer used. Currently no products have been commercialized with PHA nanocomposites, but the following review of advances in PHA nanocomposite research will give a preview of potential application areas.

Araujo et al. [93] examined PHB nanocomposites with modified polyaniline nanofibers. It was shown that both semi-conductivity and biodegradability properties were seen, and that these properties were maintained after gamma irradiation. This new material was seen to have many potential applications in biological science, engineering, and medicine.

Cai and Yang [38] developed a biocompatible polymeric nanocomposite by incorporating bacterial cellulose (BC) into a PHB matrix. The transparency of the PHB/BC nanocomposite was high due to the homogeneous nano-sized spherulite and nanofibril of PHB and BC, which are smaller than the wavelength of visible rays. The thermal stability of PHB in the nanocomposite film was also improved. An increase in the mechanical properties was observed by incorporating the BC into the PHB matrix. This PHB/BC nanocomposite can be considered for various applications, such as display devices, tissue engineering scaffold, and food packaging, because of its improved mechanical properties along with biodegradability and biocompatibility (as shown in [39]).

Chen [94] examined a nanocomposite based on bioresorbable polymer PHBV and nano-sized hydroxyapatite (nano-HA). The results indicated that the storage modulus (E') of PHBHV was considerably improved with the introduction of nano-HA. The in vitro investigation indicated that the nanocomposite has an improved bioactivity over the conventional one.

Choi et al. [43] examined PHBV/organonanoclay nanocomposites using Cloisite 30B. An intercalated microstructure was formed and finely distributed in the PHBV copolymer matrix because PHBV has a strong hydrogen bond interaction with the hydroxyl group in the organic modifier of Cloisite 30B. The nano-dispersed organonanoclay also acts a nucleating agent, increasing the temperature and rate of crystallization of PHBV; therefore, the thermal stability and tensile properties of the organonanoclay-based nanocomposites are enhanced.

Duan et al. [95] examined biomaterials based on PHBV microspheres and calcium phosphate (Ca–P)/PHBV nanocomposite microspheres. The microspheres with suitable sizes were then used as raw materials for scaffold fabrication via selective laser sintering (SLS), which is a mature rapid prototyping technique. Optimized PHBV scaffolds and Ca–P/PHBV scaffolds were fabricated using the optimized values of SLS parameters.

In terms of membrane applications, Ong et al. [45] attempted to align PHB/functionalized multi-walled carbon nanotubes (MWCNT) into a chitosan matrix. The MWCNTs were first functionalized with PHB and aligned into a membrane filter template through a filtration process. A solution casting technique was then applied to cast the chitosan onto the template to form PHB/MWCNT/chitosan nanocomposite membranes. The presence of the PHB functional moieties helped to improve the dispersion and compatibility of the MWCNTs in the chitosan matrix. When the PHB/MWCNT/chitosan nanocomposite membranes were used in the pervaporation process of 1,4-dioxane dehydration, the nanocomposite membrane showed a relatively high permeation flux and selectivity towards water, compared to existing membrane.

In terms of biomedical applications, Tang et al. [96] examined the water transport properties and solubility of a nano-biomaterial incorporating PHBHV and nano-HA modified with a silane coupling agent. Compared to those for the base resin, the diffusion coefficients for the nanocomposite decrease, whereas the sorption coefficients and the solubility increase.

Ten et al. [32] examined bacterial polyester PHBV reinforced with CNW. It was demonstrated that CNW was an effective PHBV nucleation agent. Tensile strength, Young's modulus and toughness of PHBV increased with the increasing concentration of CNW. DMA results showed an increased tan delta peak temperature and broadened transition peak, indicating restrained PHBV molecular mobility in the vicinity of the CNW surface. These results indicated that the CNW could substantially increase the mechanical properties of PHBV and this increase could be attributed to the strong interactions at the interphase.

Wang et al. [54] examined PHBV/OMMT nanocomposites. Results showed that the nanocomposite's melting temperature and enthalpy were decreased, small-sized PHBV spherulites were formed, crystallinity of PHBV reduced, and the range of the processing temperature enlarged with increasing amount of OMMT in the nanocomposite. The biodegradability of PHBV/OMMT nanocomposites in soil suspension also decreased with increasing amount of OMMT.

Xu and Qiu [52] investigated the electrical potential of PHB/functionalized multi-walled carbon nanotubes (f-MWNTs) nanocomposite. A homogeneous

distribution of f-MWNTs in the PHB matrix was found and the presence of f-MWNTs enhances the crystallization of PHB due to the heterogeneous nucleation effect of f-MWNTs. Moreover, the incorporation of a small quantity of f-MWNTs apparently improves the thermal stability of the PHB/f-MWNTs nanocomposite with respect to neat PHB.

16.4.5 Specific Application Area Opportunities for Nanobiocomposites

16.4.5.1 Food Packaging

Packaging materials to minimize food losses and provide safe, fresh, high quality food products has been the focus of food packaging. The potential for use of bio-nanocomposites for food packaging applications is high, because the materials would be able to provide these functionalities as well as offer a solution to packaging waste and disposal problems.

Specifically bio-nanocomposites can exhibit the following advantages for food packaging [97, 98].

- Enhanced organoleptic characteristics of food, such as appearance, odor, and flavor
- Reduced packaging volume, weight, and waste
- Extended shelf life and improved quality of usually non-packaged items
- Control over inter-component
- Individual packaging of small particulate foods, such as nuts and raisins
- Function as carriers for antimicrobial and antioxidant agents
- Controlled release of active ingredients
- Renewable resource materials
- Biodegradability

These unique characteristics of nanobiocomposites may lead to new product development in the food industry, such as individual packaging of particulate foods, carriers for functionally active substances, and nutritional supplements.

16.4.5.2 Agricultural Applications

The world consumption of plastic materials in agriculture amounts yearly to 6.5 million tons in order to improve crop production and protect agricultural products after harvesting, in the form of solarization films, greenhouse films, mulch films, silage films and bale wraps [99, 100]. Consequently there is a large amount of plastics discarded into the environment, buried in the soil or burnt by farms releasing harmful substances.

One solution to this problem can be the introduction in agriculture of nanobiocomposite films, which can be disposed directly into the soil or into a composting system at the end of their lifetime. Some examples of nanobiocomposite agricultural films have been prepared with nanomaterial additives such as TiO_2 and montmorillonite layered silicates [101, 102] and have resulted in the following advantages:

- Biodegradation in the soil due to the action of microorganisms such as bacteria, fungi and algae
- Degradation by sunlight and water
- Control release of active substance, such as pesticides or insecticides
- Controlled degradation for optimal crop development
- Enhanced durability and properties, under ultraviolet, visible and infrared radiation
- Renewable resource materials

Several degradable or biodegradable materials have been extensively tested in field trials in different countries and for different crops such as in maize, melon, strawberries and cotton [99, 103]. In summary, use of nanobiocomposites in agriculture can promote sustainable and environmentally friendly cultivation reducing the contamination of the soil, enhancing the protection of optimal soil conditions, and increasing the use of renewable raw materials.

16.4.5.3 Other Industrial Applications

Recently Ruiz-Hitzky et al. [104] reviewed a large range of nanobiocomposites utilizing biopolymers such as polysaccharides (cellulose, sucrose, starch, chitosan), many peptides and proteins, nucleic acids (DNA), and mixed and modified biopolymers, with natural and synthetic nanoparticles. The diverse range of possible novel applications included clothes, conductive polymers, bone repair, drug delivery, gene repair, super-adsorbent materials, drinking water purification, oxygen barrier films and green packaging applications. They noted a key consideration for product development was that care must be given to processing soft biomolecules and polymers at relatively moderate temperatures and pressures (such as spin coating and supercritical gas-aided (lower temperature) processing) as well as the use of chemically modified nano-materials that are capable of intercalation and exfoliation and can carrying targeted biomolecules and biochemicals.

White et al. [105] has reported the use of cellulose/montmorillonite and modified nanoclay nanocomposites as fire retardants, due to the increased thermal stability by the presence of the nanoclay. Chitosan/hydroxyapatite/silica nanocomposites have potential use for bone repair as the porosity and morphology can be controlled to result in the optimal structure required for the application [106–108]. Chitosan nanocomposites chitosan/montmorillonite and chitosan/sepiolite have been reported as potential use as electrochemical sensors and hybrid membranes [109–111]. Cellulose ethers such as hydroxyethyl cellulose and

hydroxypropyl cellulose have been processed with smectites, sepiolite and palygorskite for use in the building industry to improve sag resistance and control setting behavior [112]. Park et al. [113] has successfully incorporated Cloisite 30B into cellulose acetate (CA) that has been plasticized with triethyl citrate (TEC). Maintaining the balance between processability, optimal impact strength and stiffness in the CA/TEC/Cloisite 30B nanobiocomposite is important for possible use in the transportation industry. Cellulose acetate/20wt.%TEC/5wt.%Cloisite 30B showed the most improved intercalation and exfoliated structure compared to cellulose acetate/30–40wt.%TEC [113].

For further reading on potential and application areas, Yang et al. [33] reviews recent developments related to the preparation, characterization, properties, and applications of nanocomposites based on biodegradable polymers (including PLA, PCL, poly(*p*-dioxanone) (PPDO), poly(butylene succinate) (PBS), PHAs such as PHB, PHBV and natural renewable polymers such as starch, cellulose, chitin, chitosan, lignin, and proteins). In this review the nanoparticles that have been also utilized to fabricate the nanocomposites include inorganic, organic, and metal particles such as nanoclays, nanotubes, magnetites, Au and Ag, hydroxyapatite, cellulose, chitin whiskers and lignin.

16.5 Conclusions

The biodegradation of polymer/nanobiocomposites systems based on starch, PLA, PCL and PHAs in various degradation environments, such as soil and compost have been reviewed and discussed. Many authors have found that the inclusion of nanobiocomposites has improved the processability, mechanical, thermal, gas permeability and crystallization properties of the polymer. In instances where the biodegradability of these polymer/nanobiocomposites was evaluated, the rate and/or extent of polymer biodegradation was accelerated [7, 8, 20, 22, 55, 114, 115], decreased [22, 54] or showed no impact whatsoever on the biodegradation of the polymer [9, 22].

The application prospects of biodegradable polymers has broadened and advanced significantly, by the advancement in functionalities and properties of biodegradable polymer/nanobiocomposites [5, 38, 39, 56–60, 80, 81, 86, 91, 93]. These developments have led to the increased application potential of biobased plastic/nanobiocomposite materials into the food packaging industry, as these functionalities offer a solution to packaging and disposal waste problems [97, 98].

The potential use of biobased polymer/nanobiocomposites in the agriculture industry has increased, as a way to improve crop production and protection by using truly biodegradable and renewable plastics, compared to traditionally used plastics such as the polyolefins [99, 100]. Additionally, application areas such as the textile and biomedical industries have been positively impacted upon by the improved functionality and properties of biobased plastic/nanobiocomposites [104].

As this area continues to flourish, the inherent drawbacks of pure biobased plastics will continue to improve significantly and the potential use of these materials in new application areas will continue to emerge.

References

1. Ammala A, Bateman S, Dean K, Petinakis E, Sangwan P, Wong S et al (2011) An overview of degradable and biodegradable polyolefins. Prog Polym Sci 36:1015–1049
2. Tang S, Zou P, Xiong H, Tang H (2008) Effect of nano-SiO2 on the performance of starch/polyvinyl alcohol blend films. Carbohydr Polym 72:521–526
3. Nayak SK (2010) Biodegradable PBAT/Starch nanocomposites. Polym-Plast Technol Eng 49:1406–1418
4. Spiridon I, Popescu MC, Bodârlau R, Vasile C (2008) Enzymatic degradation of some nanocomposites of poly(vinyl alcohol) with starch. Polym Degrad Stab 93:1884–1890
5. Maiti P, Yamada K, Okamoto M, Ueda K, Okamoto K (2002) New polylactide/layered silicate nanocomposites: role of organoclays. Chem Mater 14:4653–4661
6. Ozkoc G, Kemaloglu S (2009) Morphology, biodegradability, mechanical, and thermal properties of nanocomposite films based on PLA and plasticized PLA. J Appl Polym Sci 114:2481–2487
7. Ray SS, Yamada K, Okamoto M, Ueda K (2003) Control of biodegradability of polylactide via nanocomposite technology. Macromol Mat Eng 288:203–208
8. Fukushima K, Abbate C, Tabuani D, Gennari M, Camino G (2009) Biodegradation of poly(lactic acid) and its nanocomposites. Polym Degrad Stab 94:1646–1655
9. Fukushima K, Tabuani D, Abbate C, Arena M, Ferreri L (2010) Effect of sepiolite on the biodegradation of poly(lactic acid) and polycaprolactone. Polym Degrad Stab 95:2049–2056
10. Sangwan P, Way C, Wu D-Y (2009) New insight into biodegradation of polylactide (PLA)/Clay nanocomposites using molecular ecological techniques. Macromol Biosci 9:677–686
11. Paul MA, Delcourt C, Alexandre M, Degée P, Monteverde F, Dubois P (2005) Polylactide/montmorillonite nanocomposites: study of the hydrolytic degradation. Polym Degrad Stab 87:535–542
12. Sinha Ray S, Yamada K, Okamoto M, Fujimoto Y, Ogami A, Ueda K (2003) New polylactide/layered silicate nanocomposites: 5. Designing of materials with desired properties. Polymer 44:6633–6646
13. Sabet SS, Katbab AA (2009) Interfacially Compatibilized Poly(lactic acid) and Poly(lactic acid)/Polycaprolactone/Organoclay nanocomposites with improved biodegradability and barrier properties: effects of the compatibilizer structural parameters and feeding route. J Appl Polym Sci 111:1954–1963
14. Di Y, Iannace S, Di ME, Nicolais L (2003) Nanocomposites by melt intercalation based on polycaprolactone and organoclay. J Polym Sci Part B Polym Phys 41:670–678
15. Ozkoc G, Kemaloglu S, Quaedflieg M (2010) Production of Poly(lactic acid)/Organoclay nanocomposite scaffolds by microcompounding and Polymer/Particle leaching. Polym Comp 31:674–683
16. Di ME, Iannace S, Sorrentino L, Nicolais L (2004) Isothermal crystallization in PCL/clay nanocomposites investigated with thermal and rheometric methods. Polymer 45:8893–8900
17. Singh S, Gupta RK, Ghosh AK, Maiti SN, Bhattacharya SN (2010) Poly (L-Lactic Acid)/Layered silicate nanocomposite blown film for packaging application: thermal, mechanical and barrier properties. J Polym Eng 30:361–375
18. Campbell K, Qi S, Craig DQM, McNally T (2009) Paracetamol-Loaded Poly(epsilon-Caprolactone) layered silicate nanocomposites prepared using hot-melt extrusion. J Pharma Sci 98:4831–4843

19. Pantoustier N, Alexandre M, Degree P, Calberg C, Jerome R, Henrist C et al (2001) Poly(caprolactone) layered silicate nanocomposites: effect of clay surface modifiers on the melt intercalation process. E-Polym: Paper No. 9
20. Ratto JA, Steeves DM, Welsh EA, Powell BE (1999) A study of polymer clay nanocomposites for biodegradable applications. Antec ′99: Plastics bridging the Millennia, conference proceedings, Soc Plastics Engineers, New York, pp 1628–1632
21. Farrell R, Goodwin S, Wirsen C, Lucciarini J, Martinez M, Ratto JA (2000) A biodegradation study of co-extruded nanocomposites conisisting of polycaprolactone and organically modified clay. Antec 2000: society of plastics engineers technical papers, conference proceedings, Vols. 1–3. Technomic Publ Co Inc., Lancaster pp 2796–2800
22. Fukushima K, Tabuani D, Abbate C, Arena M, Rizzarelli P (2011) Preparation, characterization and biodegradation of biopolymer nanocomposites based on fumed silica. Euro Polym Jl 47:139–152
23. Cabedo L, Feijoo JL, Lagaron JM, Saura JJ, Gimenez E (2005) Development and characterization of thermoplastic biodegradable nanocomposites. Annu Tech Conf Soc Plast Eng 63:1300–1304
24. Cabedo L, Feijoo JL, Villanueva MP, Lagaron JM, Gimenez E (2006) Optimization of biodegradable nanocomposites based on aPLA/PCL blends for food packaging applications. Macromol Symp 233:191–197
25. Kalambur S, Rizvi SSH (2005) Biodegradable and functionally superior starch-polyester nanocomposites from reactive extrusion. J Appl Polym Sci 96:1072–1082
26. Kalambur S, Rizvi SSH (2008) Starch-polycaprolactone nanocomposites from reactive extrusion: synthesis, characterization and properties. 235th ACS National Meeting New Orleans, LA, American Chemical Society: AGFD-027, USA
27. Liu Q, Chen D (2008) Viscoelastic behaviors of poly(caprolactone)/attapulgite nanocomposites. Eur Polym J 44:2046–2050
28. Cabedo L, Plackett D, Gimenez E, Lagaron JM (2009) Studying the degradation of polyhydroxybutyrate-co-valerate during processing with clay-based nanofillers. J Appl Polym Sci 112:3669–3676
29. Dagnon KL, Chen HH, Innocentini-Mei LH, D′Souza NA (2009) Poly[(3-hydroxybutyrate)-co-(3-hydroxyvalerate)]/layered double hydroxide nanocomposites. Polym Int 58:133–141
30. Ma PM, Wang RY, Wang SF, Zhang Y, Zhang YX, Hristova D (2008) Effects of fumed silica on the crystallization behavior and thermal properties of poly(hydroxybutyrate-co-hydroxyvalerate). J Appl Polym Sci 108:1770–1777
31. Sanchez-Garcia MD, Lagaron JM (2010) Novel clay-based nanobiocomposites of biopolyesters with synergistic barrier to UV light, gas, and vapor. J Appl Polym Sci 118: 188–199
32. Ten E, Turtle J, Bahr D, Jiang L, Wolcott M (2010) Thermal and mechanical properties of poly(3-hydroxybutyrate-co-3-hydroxyvalerate)/cellulose nanowhiskers composites. Polymer 51:2652–2660
33. Yang KK, Wang XL, Wang YZ (2007) Progress in nanocomposite of biodegradable polymer. J Ind Eng Chem 13:485–500
34. Zhang Q, Zhao Y, Chen L (2009) Effect of PHBV content on the transparency and swelling behavior of polymer/hectorite nanocomposite hydrogel. Int J Mod Phys B 23:1365–1370
35. Choi WM, Kim TW, Park OO, Chang YK, Lee JW (2003) Preparation and characterization of poly(hydroxybutyrate-co-hydroxyvalerate)-organoclay nanocomposites. J Appl Polym Sci 90:525–529
36. Achilias DS, Panayotidou E, Zuburtikudis I (2011) Thermal degradation kinetics and isoconversional analysis of biodegradable poly(3-hydroxybutyrate)/organomodified montmorillonite nanocomposites. Thermochim Acta 514:58–66
37. Bordes P, Pollet E, Bourbigot S, Averous L (2008) Structure and properties of PHA/clay nano-biocomposites prepared by melt intercalation. Macromol Chem Phys 209:1473–1484
38. Cai ZJ, Yang G (2011) Optical nanocomposites prepared by incorporating bacterial cellulose nanofibrils into poly(3-hydroxybutyrate). Mater Lett 65:182–184

39. Cai ZJ, Yang GA, Kim J (2011) Biocompatible nanocomposites prepared by impregnating bacterial cellulose nanofibrils into poly(3-hydroxybutyrate). Curr Appl Phys 11:247–249
40. das GdS-VM, Wang SH, Wiebeck H, Valenzuela-Diaz FR (2010) Nanocomposite microcapsules from powders of polyhydroxybutyrate (PHB) and smectite clays. Mater Sci Forum 660–661:794–798
41. Erceg M, Kovacic T, Klaric I (2009) Poly(3-hydroxybutyrate) nanocomposites: Isothermal degradation and kinetic analysis. Thermochim Acta 485:26–32
42. Erceg M, Kovacic T, Perinovic S (2010) Isothermal degradation of poly(3-hydroxybutyrate)/organically modified montmorillonite nanocomposites. Polym Compos 31:272–278
43. Lim ST, Hyun YH, Lee CH, Choi HJ (2003) Preparation and characterization of microbial biodegradable poly(3-hydroxybutyrate)/organoclay nanocomposite. J Mater Sci Lett 22:299–302
44. Ohashi E, Drumond WS, Zane NP, Barros PWdF, Lachtermacher MG, Wiebeck H et al (2009) Biodegradable poly(3-hydroxybutyrate) nanocomposite. Macromol Symp 279: 138–144
45. Ong YT, Ahmad AL, Zein SHS, Sudesh K, Tan SH (2011) Poly(3-hydroxybutyrate)-functionalised multi-walled carbon nanotubes/chitosan green nanocomposite membranes and their application in pervaporation. Sep Purif Tech 76:419–427
46. Parulekar Y, Mohanty AK, Imam SH (2007) Biodegradable nanocomposites from toughened polyhydroxybutyrate and titanate-modified montmorillonite clay. J Nanosci Nanotech 7:3580–3589
47. Parulekar YS, Mohanty AK (2005) Novel green nanocomposites from toughened polyhydroxyalkanoate and titanate modified montmorillonite clay. Annu Tech Conf Soc Plast Eng 63:1305–1309
48. Sanchez-Garcia MD, Gimenez E, Lagaron JM (2008) Morphology and barrier properties of nanobiocomposites of poly(3-hydroxybutyrate) and layered silicates. J Appl Polym Sci 108:2787–2801
49. Wu T-M, Hsu S-F, Shih Y-F, Liao C-S (2008) Thermal degradation kinetics of biodegradable poly(3-hydroxybutyrate)/layered double hydroxide nanocomposites. J Polym Sci Part B Polym Phys 46:1207–1213
50. Xu C, Qiu Z (2009) Isothermal melt crystallization kinetics study of biodegradable poly(3-hydroxybutyrate)/multiwalled carbon nanotubes nanocomposites. Polym J (Tokyo, Japan) 41:888–892
51. Xu C, Qiu Z (2009) Nonisothermal melt crystallization and subsequent melting behavior of biodegradable poly(hydroxybutyrate)/multiwalled carbon nanotubes nanocomposites. J Polym Sci Part B Polym Phys 47:2238–2246
52. Xu CL, Qiu ZB (2011) Crystallization behavior and thermal property of biodegradable poly (3-hydroxybutyrate)/multi-walled carbon nanotubes nanocomposite. Polym Adv Technol 22:538–544
53. Zuburtikudis I, Marras SI, Tornikidou K, Tsimpliaraki A, Panayotidou E, Cristofidou G (2008) Enhanced thermal stability of biodegradable poly(3-hydroxybutyrate)/layered silicate nanocomposites. AIChE Annual Meeting Philadelphia PA: American Institute of Chemical Engineers: 908/901-908/907
54. Wang SF, Song CJ, Chen GX, Guo TY, Liu J, Zhang BH et al (2005) Characteristics and biodegradation properties of poly(3-hydroxybutyrate-co-3-hydroxyvalerate)/organophilic montmorillonite (PHBV/OMMT) nanocomposite. Polym Degrad Stab 87:69–76
55. Maiti P, Batt CA, Giannelis EP (2007) New biodegradable polyhydroxybutyrate/layered silicate nanocomposites. Biomacromolecules 8:3393–3400
56. Ollett AL, Parker R, Smith AC (1991) Deformation and fracture-behavior of wheat-starch plasticized with glucose and water. J Mater Sci 26:1351–1356
57. Slade L, Levine H (1993) Water relationships in starch transitions. Carbohydr Polym 21:105–131
58. Okamoto M, Nam PH, Maiti P, Kotaka T, Hasegawa N, Usuki A (2001) A house of cards structure in polypropylene/clay nanocomposites under elongational flow. Nano Lett 1:295–298

59. Wilhelm HM, Sierakowski MR, Souza GP, Wypych F (2003) Starch films reinforced with mineral clay. Carbohydr Polym 52:101–110
60. Wilhelm HM, Sierakowski MR, Souza GP, Wypych F (2003) The influence of layered compounds on the properties of starch/layered compound composites. Polym Int 52: 1035–1044
61. Qiao XY, Jiang WB, Sun K (2005) Reinforced thermoplastic acetylated starch with layered silicates. Starch-Starke 57:581–586
62. Chen BQ, Evans JRG (2005) Thermoplastic starch-clay nanocomposites and their characteristics. Carbohydr Polym 61:455–463
63. Bagdi K, Muller P, Pukanszky B (2006) Thermoplastic starch/layered silicate composites: structure, interaction, properties. Compos Interf 13:1–17
64. Dean K, Yu L, Bateman S, Wu DY (2007) Gelatinized starch/biodegradable polyester blends: processing, morphology, and properties. J Appl Polym Sci 103:802–811
65. Dean K, Yu L, Wu DY (2007) Preparation and characterization of melt-extruded thermoplastic starch/clay nanocomposites. Compos Sci Technol 67:413–421
66. Pandey J, Singh R (2005) Green nanocomposites from renewable resources: effect of plasticizer on the structure and material properties of clay-filled starch. Starch/Starke 57:8
67. Park HM, Lee WK, Park CY, Cho WJ, Ha CS (2003) Environmentally friendly polymer hybrids—Part I—mechanical, thermal, and barrier properties of thermoplastic starch/clay nanocomposites. J Mater Sci 38:909–915
68. Park HM, Li XC, Jin CZ, Park CY, Cho WJ, Ha CS (2002) Preparation and properties of biodegradable thermoplastic starch/clay hybrids. Macromol Mater Eng 287:553–558
69. Chiou BS, Yee E, Wood D, Shey J, Glenn G, Orts W (2006) Effects of processing conditions on nanoclay dispersion in starch-clay nanocomposites. Cereal Chem 83:300–305
70. Chen M, Chen BQ, Evans JRG (2005) Novel thermoplastic starch-clay nanocomposite foams. Nanotechnology 16:2334–2337
71. Dufresne A, Cavaille JY (1998) Clustering and percolation effects in microcrystalline starch-reinforced thermoplastic. J Polym Sci Part B Polym Phys 36:2211–2224
72. Liao H-T, Wu C-S (2005) Synthesis and characterization of polyethylene-octene elastomer/ Clay/biodegradable starch nanocomposites. J Appl Polym Sci 97:397–404
73. Kvien I, Sugiyama J, Votrubec M, Oksman K (2007) Characterization of starch based nanocomposites. J Mater Sci 42:8163–8171
74. Averous L, Boquillon N (2004) Biocomposites based on plasticized starch: thermal and mechanical behaviours. Carbohydr Polym 56:111–122
75. Averous L, Fringant C, Moro L (2001) Plasticized starch-cellulose interactions in polysaccharide composites. Polymer 42:6565–6572
76. Averous L, Moro L, Dole P, Fringant C (2000) Properties of thermoplastic blends: starch-polycaprolactone. Polymer 41:4157–4167
77. Rhim JW, Hong SI, Ha CS (2009) Tensile, water vapor barrier and antimicrobial properties of PLA/nanoclay composite films. Lwt-Food Sci Tech 42:612–617
78. Sanchez-Garcia M, Lagaron J (2010) On the use of plant cellulose nanowhiskers to enhance the barrier properties of polylactic acid. Cellulose 17:987–1004
79. Singh S, Ray SS (2007) Polylactide based nanostructured biomaterials and their applications. J Nanosci Nanotech 7:2596–2615
80. Ray SS, Yamada K, Ogami A, Okamoto M, Ueda K (2002) New polylactide/layered silicate nanocomposite: nanoscale control over multiple properties. Macromol Rap Comm 23: 943–947
81. Ray SS, Yamada K, Okamoto M, Ueda K (2002) Polylactide-layered silicate nanocomposite: a novel biodegradable material. Nano Lett 2:1093–1096
82. Katiyar V, Gerds N, Koch CB, Risbo J, Hansen HCB, Plackett D (2010) Poly L-lactide-layered double hydroxide nanocomposites via in situ polymerization of L-lactide. Polym Degrad Stab 95:2563–2573

83. Potschke P, Andres T, Villmow T, Pegel S, Brunig H, Kobashi K et al (2010) Liquid sensing properties of fibres prepared by melt spinning from poly(lactic acid) containing multi-walled carbon nanotubes. Compos Sci Technol 70:343–349
84. Strange M, Plackett D, Kaasgaard M, Krebs FC (2008) Biodegradable polymer solar cells. Sol Ener Mat Sol C 92:805–813
85. El-Kady AM, Ali AF, Farag MM (2010) Development, characterization, and in vitro bioactivity studies of sol-gel bioactive glass/poly(L-lactide) nanocomposite scaffolds. Mat Sci Eng C Mat Bio 30:120–131
86. Bugatti V, Costantino U, Gorrasi G, Nocchetti M, Tammaro L, Vittoria V (2010) Nanohybrids incorporation into poly(epsilon-caprolactone) for multifunctional applications: Mechanical and barrier properties. Euro Polym J 46:418–427
87. Bugatti V, Gorrasi G, Montanari F, Nocchetti M, Tammaro L, Vittoria V (2011) Modified layered double hydroxides in polycaprolactone as a tunable delivery system: in vitro release of antimicrobial benzoate derivatives. Appl Clay Sci 52:34–40
88. Lee HH, Shin US, Jin GZ, Kim HW (2011) Highly homogeneous carbon nanotube-polycaprolactone composites with various and controllable concentrations of ionically-modified-MWCNTs. B Kor Chem Soc 32:157–161
89. Liu H, Han CY, Dong LS (2010) Preparation and characterization of Poly(epsilon-caprolactone)/Calcium Carbonate nanocomposites and nanocomposite foams. Polym Compos 31:1653–1661
90. Liu H, Han CY, Dong LS (2010) Study of the biodegradable Poly(epsilon-caprolactone)/Clay Nanocomposite Foams. J Appl Polym Sci 115:3120–3129
91. Roohani-Esfahani SI, Nouri-Khorasani S, Lu ZF, Appleyard R, Zreiqat H (2010) The influence hydroxyapatite nanoparticle shape and size on the properties of biphasic calcium phosphate scaffolds coated with hydroxyapatite-PCL composites. Biomaterials 31: 5498–5509
92. Xiao Y, Zhou SB, Wang L, Gong T (2010) Electro-active shape memory properties of Poly(epsilon-caprolactone)/functionalized multiwalled carbon nanotube nanocomposite. ACS Appl Mater Interf 2:3506–3514
93. Araujo PLB, Ferreira C, Araujo FS (2011) Biodegradable conductive composites of poly(3-hydroxybutyrate) and polyaniline nanofibers: preparation, characterization and radiolytic effects. Expr Polym Lett 5:12–22
94. Chen DZ, Tang CY, Chan KC, Tsui CP, Yu PHF, Leung MCP et al (2007) Dynamic mechanical properties and in vitro bioactivity of PHBHV/HA nanocomposite. Comp Sci Tech 67:1617–1626
95. Duan B, Cheung WL, Wang M (2011) Optimized fabrication of Ca-P/PHBV nanocomposite scaffolds via selective laser sintering for bone tissue engineering. Biofabrication 3:015001/015001-015001/015013
96. Tang CY, Chen DZ, Yue TM, Chan KC, Tsui CP, Yu PHF (2008) Water absorption and solubility of PHBHV/HA nanocomposites. Comp Sci Tech 68:1927–1934
97. Rhim JW, Ng PKW (2007) Natural biopolymer-based nanocomposite films for packaging applications. Crit Rev Food Sci Nutr 47:411–433
98. Fowler PA, Hughes JM, Elias RM (2006) Biocomposites: technology, environmental credentials and market forces. J Sci Food Agric 86:1781–1789
99. Bonora M, De Corte D (2003) Additives for controlled degradation of agricultural plastics: ENVIROCARE (TM). Macromol Symp 197:443–453
100. Jouet J (2001) Plastics in the World. Plasticulture 120:108
101. Jana T, Roy BC, Maiti S (2001) Biodegradable film 6. Modification of the film for control release of insecticides. Eur Polym J 37:861–864
102. Yew SP, Tang HY, Sudesh K (2006) Photocatalytic activity and biodegradation of polyhydroxybutyrate films containing titanium dioxide. Polym Degrad Stabil 91:1800–1807
103. Scarascia-Mugnozza G, Schettini E, Vox G, Malinconico M, Immirzi B, Pagliara S (2006) Mechanical properties decay and morphological behaviour of biodegradable films for agricultural mulching in real scale experiment. Polym Degrad Stabil 91:2801–2808

104. Ruiz-Hitzky ER, Darder M, Aranda P (2005) Functional biopolymer nanocomposites based on layered solids. J Mater Chem 15:3650–3662
105. White LA (2004) Preparation and thermal analysis of cotton–clay nanocomposites. J Appl Polym Sci 92:2125–2131
106. Yamaguchi I, Tokuchi K, Fukuzaki H, Koyama Y, Takakuda K, Monma H et al. (2000) Preparation and microstructure analysis of chitosan/hydroxyapatite nanocomposites. J Biomed Mater Res 55:20–27
107. Retuert J, Quijada R, Arias V, Yazdani-Pedram M (2003) Porous silica derived from chitosan-containing hybrid composites. J Mater Res 18:487–494
108. Fuentes S, Retuert PJ, Gonzalez G, Ruiz-Hitzky E (1997) Chitosan based films. Synthesis and crystalline properties of nanocomposites with amine propyl siloxane. Electrochimica Acta 35:61–70
109. Aranda P, Darder M, Fernández-Saavedra R, López-Blanco M, Ruiz-Hitzky E (2006) Relevance of polymer—and biopolymer–clay nanocomposites in electrochemical and electroanalytical applications. Thin Solid Films 495:104–112
110. Darder M, Colilla M, Ruiz-Hitzky E (2003) Biopolymer-Clay nanocomposites based on chitosan intercalated in montmorillonite. Chem Mater 15:3774–3780
111. Darder M, Colilla M, Ruiz-Hitzky E (2005) Chitosan-clay nanocomposites: application as electrochemical sensors. Appl. Clay Sci 28:199–208
112. Glatthor A Construction chemistry: the chemistry of building materials. http://www.baustoffchemie.de/en/additives/cellulose-ether/modified.html
113. Park H-M, Misra M, Drzal LT, Mohanty AK (2004) "Green" nanocomposites from cellulose acetate bioplastic and clay: effect of eco-friendly triethyl citrate plasticizer. Biomacromolecules 5:2281–2288
114. Sinha Ray S, Okamoto M (2003) Biodegradable polylactide/layered silicate nanocomposites: open a new dimension for plastics and composites. Macromol Rap Comm 24:815–840
115. Sinha Ray S, Okamoto M, Yamada K, Ueda K (2003) New polylactide/layered silicate nanocomposites: concurrent improvement of materials properties and biodegradability. Proceedings of Nanocomposites, San Diego

Index

L. Avérous and E. Pollet (eds.), *Environmental Silicate Nano-Biocomposites*, Green Energy and Technology, DOI: 10.1007/978-1-4471-4108-2,